BNL-NCS-50681
ERDA/NDC-11/L
NEANDC(US)-202/L
INDC(USA)-78/L

SYMPOSIUM ON NEUTRON CROSS-SECTIONS FROM 10 TO 40 MEV

HELD AT
BROOKHAVEN NATIONAL LABORATORY,
UPTON, NEW YORK 11973
MAY 3-5, 1977.

Edited by
M.R. BHAT AND S. PEARLSTEIN

JOINTLY SPONSORED BY THE DIVISIONS
OF MAGNETIC FUSION ENERGY
AND PHYSICAL RESEARCH
OF THE U.S. ENERGY RESEARCH
AND DEVELOPMENT ADMINISTRATION

July 1977

INFORMATION ANALYSIS CENTER REPORT

NATIONAL NUCLEAR DATA CENTER
BROOKHAVEN NATIONAL LABORATORY
UPTON, NEW YORK 11973

MASTER

DISTRIBUTION OF THIS DOCUMENT IS UNLIMITED

BNL-NCS-50681
ERDA/NDC-11/L
NEANDC(US)-202/L
INDC(USA)-78/L
(Physics-Nuclear - TID-4500)

SYMPOSIUM ON NEUTRON CROSS-SECTIONS FROM 10 TO 40 MEV

HELD AT
BROOKHAVEN NATIONAL LABORATORY
UPTON, NEW YORK 11973
MAY 3-5, 1977

Edited by
M.R. BHAT AND S. PEARLSTEIN

NOTICE
This report was prepared as an account of work sponsored by the United States Government. Neither the United States nor the United States Department of Energy, nor their employees, nor any of their contractors, subcontractors, or their employees, makes any warranty, express or implied, or assumes any legal liability or responsibility for the accuracy, completeness or usefulness of any information, apparatus, product or process disclosed, or represents that its use would not infringe privately owned rights.

July 1977

JOINTLY SPONSORED BY THE DIVISIONS OF MAGNETIC FUSION ENERGY AND PHYSICAL RESEARCH
OF THE UNITED STATES ENERGY RESEARCH AND DEVELOPMENT ADMINISTRATION

NATIONAL NUCLEAR DATA CENTER
BROOKHAVEN NATIONAL LABORATORY
ASSOCIATED UNIVERSITIES, INC.
UNDER CONTRACT NO. EY-76-C-02-0016 WITH THE
UNITED STATES ENERGY RESEARCH AND DEVELOPMENT ADMINISTRATION

DISTRIBUTION OF THIS DOCUMENT IS UNLIMITED

TABLE OF CONTENTS

		Page
PROLOGUE		1
WELCOMING ADDRESS		
H. Kouts		3
LIST OF ATTENDEES		4
WORKSHOP REPORTS		5
A. SESSION II	INTENSE HIGH ENERGY NEUTRON SOURCES AND THEIR CHARACTERISTICS	
Chairman:	C.D. Bowman	7
B. SESSION III	DIFFERENTIAL DATA AND EXPERIMENTAL TECHNIQUES	
Chairman:	F.G. Perey	15
C. SESSION IV	MATERIALS DAMAGE STUDIES	
Chairman:	A.N. Goland	29
D. SESSION V	INTEGRAL EXPERIMENTS AND DATA TESTING	
Chairman:	B.R. Leonard, Jr.	36
E. SESSION VI	DATA EVALUATION AND NUCLEAR MODEL CODES	
Chairman:	P.G. Young	41
REVIEW AND CONTRIBUTED PAPERS		
SESSION I INTRODUCTORY		
Chairman: S.L. Whetstone		49
1. The Program for Alloy Development for Irradiation Performance in Fusion Reactors-Review J.O. Stiegler and T.C. Reuther		51
2. Review of Magnetic Fusion Energy Neutron Cross-Section Needs: Neutronics Viewpoint-Review D.J. Dudziak and D.W. Muir		59
SESSION II INTENSE HIGH ENERGY NEUTRON SOURCES AND THEIR CHARACTERISTICS		
Chairman: G.A. Bartholomew		77
1. Intense Fast Neutron Source Re. tions-Review M.A. Lone		79
2. Thick Target Neutron Yields from the d-Be Reaction at E_d = 15.6, 29.9 and 49.0 MeV R.G. Graves, J.B. Smathers, N. Hertel, V.A. Otte, P.R. Almond and W. Grant		117

Page

3. Neutron Spectra from Deuteron and Proton Bombardment of Thick Lithium Targets
C.E. Nelson, F.O. Purser, P. Von Behren and H.W. Newson 125

4. Neutron Spectra from 30-MeV Deuterons on A Thick Beryllium Target
D.R. Nethaway, R.A. Van Konynenburg, M.W. Guinan and L.R. Greenwood 135

5. Neutron Spectra and Basic Data Requirements for (d,Li) and (d,Be) Target Systems
P.J. Persiani, W. Becker and J. Donahue 151

6. Fluence Mapping of RTNS-I by Helium Accumulation and Foil Activation Methods
H. Farrar IV, D.W. Kneff, R.A. Britten and R.R. Heinrich 175

7. Neutron Spectra Characteristics for the Intense Neutron Source, INS
M. Battat, R. Dierckx and C.R. Emigh 185

SESSION III DIFFERENTIAL DATA AND EXPERIMENTAL TECHNIQUES
Chairman: A.B. Smith 199

1. Review of Neutron Data: 10 to 40 MeV - Review
R.C. Haight 201

2. Differential and Integral Neutron Standards for High Energy Neutrons
O.A. Wasson 225

3. Neutron Cross Section Programs in the Energy Region from 1 to 24 MeV at the LASL Van de Graaff Facilities
G.F. Auchampaugh, D.M. Drake and L.R. Veeser 231

4. A Facility for Neutron-Induced Charged Particle Reactions in the Energy Range E_n = 20-60 MeV
J.L. Romero, T.S. Subramanian, F.P. Brady, N.S.P. King, and J.F. Harrison 247

5. Neutron Scattering Measurements at Ohio University in the Energy Range 7-26 MeV
J. Rapaport, R.W. Finlay, D.E. Bainum, J.D. Carlson and T.S. Cheema 257

Page

6. An Evaluation of the Neutron-Induced Reaction Cross Sections on Carbon from 10 to 20 MeV
G. Haouat, J. Lachkar, J.P. Delaroche, Y. Patin and J. Sigaud 277

7. Nuclear Emulsion Techniques and Data Needs for Fast Neutron Angular Spectrometry
J.H. Roberts and R. Gold 287

8. Development of a Spectrometer for the Measurement of (n,xp), (n,xd) and (n,xα) Cross Sections, Angular Distributions and Spectra at E_n = 15 MeV
S.M. Grimes, R.C. Haight, J.D. Anderson, K.R. Alvar and R.R. Borchers 297

9. Cross Sections for the Nb(n,xn) and Nb(n,xγ) Reactions between 1 and 20 MeV
G.L. Morgan and F.G. Perey 305

SESSION IV MATERIALS DAMAGE STUDIES
Chairman: T.C. Reuther, Jr. 319

1. MFE Damage Analysis Program Nuclear Data Needs-Review
D.G. Doran, R.R. Heinrich, L.R. Greenwood, and H. Farrar IV 321

2. Neutron Dosimetry at the Intense Neutron Source (INS)
R. Dierckx 351

3. Initial Damage Rates in Nb, V and Mo from 30 MeV d-Be Neutrons
M.W. Guinan and C.E. Violet 361

SESSION V INTEGRAL EXPERIMENTS AND DATA TESTING
Chairman: R.J. Howerton 373

1. Integral Experiments for CTR Nuclear Data-Review
C.W. Maynard 375

2. Integral Testing of Neutron Activation Cross Sections Using the ^{9}Be(d,n) Reaction at 14-16 MeV
L.R. Greenwood and R.R. Heinrich 391

3. Differential Integral Experiments for Testing Cross Section Evaluations for Fusion Reactors
L.F. Hansen, J.D. Anderson, C. Wong and T. Komoto 403

Page

4. An Integral Measurement to Test Evaluated Neutron Cross Sections for Carbon
G.L. Morgan 413

SESSION VI DATA EVALUATION AND NUCLEAR MODEL CODES
Chairman: A. Prince 433

1. Neutron Evaluation at High Energies- Problems and Prospects -Review
L. Stewart and E.D. Arthur 435

2. Multi-Step Hauser-Feshbach Codes with Pre-Compound Effects: A Brief Review of Current and Required Developments and Applications up to 40 MeV - Review
C.Y. Fu 453

3. Cross Sections in the Energy Range from 10 to 40 MeV Calculated with the GNASH Code
E.D. Arthur and P.G. Young 467

4. He Production- An Example of Hauser-Feshbach Calculations
F.M. Mann and R.E. Schenter 485

5. Neutron, Proton and Deuteron Induced Reaction Products in the 10-40 MeV Range
M. Divadeenam 491

6. The Intranuclear-Cascade-Evaporation Model for Nonelastic Nuclear Collisions and Its Application in Biomedical and MFE Research
T.A. Gabriel and R.G. Alsmiller, Jr. 515

7. Multi-Step Direct Reaction Approach to Fit Continuous Spectra of Nuclear Reactions
T. Tamura and T. Udagawa 533

8. JULIAN. A Monte-Carlo Hauser-Feshbach Program For Evaporation from Compound Nuclei
M. Hillman and Y. Eyal 539

CINDA INDEX 549

PROLOGUE

This symposium was organized under the auspices of the Division of Magnetic Fusion Energy (DMFE) and the Division of Physical Research (DPR) of the U.S. Energy Research and Development Administration (ERDA) to consider in detail the present state of neutron cross sections in the energy range 10-40 MeV and indicate future directions to pursue in order to effectively use intense high energy neutron sources such as the d-Li source expected to be operational in the near future. Although the main concern of the symposium was the immediate data needs of the DMFE program, topics from other fields overlapping in technology such as the following were also considered appropriate:

(i) applications of intense high energy neutron sources for medicine,

(ii) problems of acquiring differential data and related experimental techniques,

(iii) dosimetry measurements at high energies,

(iv) use and validation of nuclear model codes to supplement experimental data, and

(v) data evaluation and testing.

With these objectives in mind the symposium was divided into six sessions under the following subjects:

1. Introductory - consisting of two review talks broadly outlining the data needs.

2. Intense High Energy Neutron Sources and Their Characteristics.

3. Differential Data and Experimental Techniques.

4. Materials Damage Studies.

5. Integral Experiments and Data Testing.

6. Data Evaluation and Nuclear Model Codes.

In each of the sessions, there was a review which summarized the present status of the subject under consideration. This was followed by contributed papers which reflected the present level of support and was indicative of the activity in the particular field. In addition, each session had a workshop where as a result of active participation by representatives from different laboratories, a report evaluating the present status of the subject under discussion and indicating future directions for development and including specific recommendations to funding agencies was prepared. These workshop reports are reproduced in these proceedings.

The editors gratefully acknowledge the fine cooperation received from the Symposium sponsors and participants.

M. R. Bhat and S. Pearlstein

WELCOMING ADDRESS

H. Kouts

Let me begin by welcoming you here. I know most of you; most of you know me, from my being on the receiving end of cross section data for many years.

The welcoming address is supposed to say how happy we are that you have come to this most important workshop, and the coffee will be available at the breaks, and so on. These are of course true statements. What I can say more interesting is a few remarks about the singular importance of this meeting, which constitutes a start of concentration on new areas of cross-section data.

The immediate reason for this start is the need for better comprehension of the nuclear processes that will be encountered in magnetic fusion machines of the future, so that these can be designed better than we could do so with present knowledge. The data needed fall in several ranges, some covered by this workshop, and some that perhaps will be taken up in future ones. These involve processes in the plasma, reactions in the walls of the vacuum chamber, including damage mechanisms and methods of reducing damage and activation, and processes in the blanket and in the magnet structure themselves. The neutron-induced reactions are of course of principal importance, because of the problems of deep penetration, and the damage mechanisms. At a second level is the need to analyze and interpret bulk experiments on radiation damage that will come with the advent of new intense neutron sources. Since these experiments will generally be done with neutron spectra differing from those in magnetic fusion devices, a lot of analysis and interpretation will be needed to convert to the circumstances of interest. To make use of radiation damage induced by a D-Li source will involve neutron reactions over the whole range to be discussed at this workshop; and this is one of the principal reasons for the workshop.

I would like to indicate something further. The interest I have in this meeting stems more broadly from a host of new opportunities generated by modern developments in linear accelerator technology, of which the use for radiation damage experiments with a D-Li source is only a forerunner. It is now possible to build linear accelerators with power in the beam approaching that of a nuclear power reactor. This leads to the possibility of a number of new applications: heavy-particle-induced fusion, linear accelerator induced breeding of fissionable material, accelerator-driven reactors. Analysis of all of these involves cross-sections in ranges that break from the old limits of fission neutrons. The need for precise neutron-induced and charged-particle cross sections is undertaking a quantum jump. It is a pleasure to welcome you all to this first manifestation of that transition.

LIST OF ATTENDEES

R.G. Alsmiller, Jr., ORNL
E.D. Arthur, LASL
G. Auchampaugh, LASL
D. Bainum, Ohio University
G.A. Bartholomew, CRNL
M.R. Bhat, BNL
C.D. Bowman, NBS
T.W. Burrows, BNL
R.E. Chrien, BNL
H. Conde', NDRI, Sweden
J.J. Coyne, NBS
R. Dierckx, LASL/ISPRA
M. Divadeenam, BNL
D.G. Doran, HEDL
C.R. Emigh, LASL
H. Farrar, IV, AI
R.W. Finlay, Ohio University
C.Y. Fu, ORNL
T.A. Gabriel, ORNL
P.M. Garvey, CRNL
A.N. Goland, BNL
R. Graves, Texas A&M Univ.
L.R. Greenwood, ANL
M. Guinan, LLL
R.C. Haight, LLL
L. Hansen, LLL
G. Haouat, Bruyeres-le-Chatel
R.R. Heinrich, ANL
G. Herling, Naval Res. Lab/DC
M. Hillman, BNL
N.E. Holden, BNL
R.J. Howerton, LLL
W.Y. Kato, BNL
R.R. Kinsey, BNL
H. Kouts, BNL
R.O. Lane, Ohio University
B. Leonard, BNW
R.A. Lindgren, Naval Res. Lab/DC
M.A. Lone, CRNL
B.A. Magurno, BNL
F.M. Mann, HEDL
C. Maynard, Univ. of Wisconsin
V.L. McLane, BNL
M.S. Moore, LASL
G.L. Morgan, ORNL
S.F. Mughabghab, BNL
A. Namenson, Naval Res. Lab/DC
C. Nelson, Duke University
S. Pearlstein, BNL
F.G. Perey, ORNL
P.J. Persiani, ANL
A. Prince, BNL
J. Rapaport, Ohio University
H.W. Rief, ISPRA
T.C. Reuther, Jr., DMFE, ERDA
J.L. Romero, U. Calif. at Davis
P.F. Rose, BNL
R.S. Sanna, US ERDA (NYC, NY)
A.B. Smith, ANL
J.O. Stiegler, ORNL
L. Stewart, LASL
H. Takahashi, BNL
T. Tamura, University of Texas
G. Thompson, BNL
J.K. Tuli, BNL
B. Twining, DMFE, ERDA
O.A. Wasson, NBS
S.L. Whetstone, DPR, ERDA
C. Whitehead, AERE, Harwell
P.G. Young, LASL

WORKSHOP REPORTS

INTENSE HIGH ENERGY NEUTRON SOURCES AND THEIR CHARACTERISTICS

C. D. Bowman, NBS - Chairman
D. Bainum, Ohio U.
G. A. Bartholomew, AECL
T. W. Burrows, BNL
R. Dierckx, LASL/EURATOM ISPRA
D. G. Doran, HEDL
R. Graves, Texas A&M
L. R. Greenwood, ANL
R. C. Haight, LLL
R. R. Heinrich, ANL
R. A. Lindgren, NRL
M. A. Lone, AECL
M. S. Moore, LASL
C. E. Nelson, Duke U.
S. Pearlstein, BNL
P. L. Persiani, ANL
C. Whitehead, AERE/Harwell

1. Introduction

In order to approach the source characterization in an orderly way, the workshop focused first on the objective of the measurement program - to provide data for the study of materials damage from high-energy neutrons. The damage itself is a complex matter which may involve DPA (displacements per atom), PKA (primary knock-on atom), activation*, gas production, etc. Ultimately, there will be cross sections or other damage functions which are energy dependent. Therefore, the ultimate aim of this meeting in the workshop's view, was to plan the measurement system by which the detailed neutron intensities and energy distributions could be specified in whatever irradiation facility that might be used for damage studies. The workshop's view of the measurement system follows.

The approach to the measurement system took two parallel avenues. In the first, a complete specification of the neutron intensity and energy distribution is obtained from a distribution of

*Henceforth, the term activation will refer to any reaction leading to cumulative reaction products which can be measured after completion of the irradiation.

"activation" foil packets spread throughout the measurement volume. The measurement system relies on the accurate cross-section measurement and unfolding methods from a sufficient set of activation foils. The source characterization is therefore limited only to that necessary to measure these activation cross sections accurately. The damage facility can be arranged as desired, essentially free of source properties.

The second approach relies on detailed calculational techniques to compute the neutron intensity and energy distributions throughout the measurement volume. This, of course, requires the detailed characterization of the source and an adequate knowledge of cross sections necessary to properly handle the neutron transport.

While in principle either approach might stand alone, the workshop recommended that it would be most prudent to follow both the activation and calculational approaches with the intent of bringing them into confrontation in specific damage experiments. The first approach of measuring the accurate activation cross sections can make use of the d-T, d-Li and other sources. We begin a discussion of the first approach considering the d-T source.

II. d-T and t-D Source Characterizations

This source may be used in two ways which might be considered distinct. First, neutrons may be produced with deuterons or tritons in the 200-400 keV range in which case the distribution is nearly isotropic, the energy relatively constant and restricted to a rather narrow range. It appears that the current state of the

art for this source as determined by comparison of 14-MeV cross-section measurements for specific materials does not exceed ± 7%. The workshop recommends that neutron fields for the d-T and/or T-d sources be established by comparing the associated particle and the proton-recoil technique. An accuracy of 2% or better should be possible. Further, the workshop recommends that collaborative efforts be taken to avoid effects of energy uncertainty by carefully establishing the neutron energy of the d-T source.

The energy of neutrons from the d-T reaction can be varied over a wide range for activation cross-section measurements. The useful energy limits might be 12.8 to about 25 MeV. Several problems appear at higher energies. One encounters break-up problems which give rise to a low-energy tail, the angular distribution effects become more pronounced, and the source has not been calibrated with sufficient accuracy since detection calibrations have not been carried out at higher energies. In addition, one must contend with deuterium build up in the target and with neutron scattering in the environment, deuterons stopping upstream of the target -- all of which give rise to low-energy neutron contamination.

III. d-Li* Source Characterizations

The d-Li source is a more intense source of neutrons than the d-T reaction with generally a larger number of low-energy neutrons and with higher-energy neutrons distributed over a wide energy

*In this report d-Li and d-Be are used interchangeably.

range. The fraction of lower-energy neutrons depends on the target thickness through the effects of scattering of the neutrons before they leave the target. The lower energy neutrons have not been measured carefully and thoroughly documented. The continuous nature of the spectrum makes it exceedingly difficult to use this reaction for activation measurements in the higher energy region except for reactions with very large negative Q values. The high energy portion of the spectrum has not been measured with an accurately calibrated neutron detector.

For the purpose of activation cross-section measurement, the workshop recommends that the low-energy component of the neutron spectrum be measured accurately. In addition, the high-energy d-Li continuum should be measured with a well calibrated neutron detector. It does not appear that this reaction can play a primary role in activation cross section measurement. Rather, the workshop recommends that the calibrated d-Li source be used as an integral test of activation cross section measurements obtained from the d-T or other reactions.

IV. Other Reactions

The measurement of the activation cross sections will perhaps require other sources besides the d-T reaction in the energy range above 25 MeV. The most promising reactions appear to be p-T and p-^{7}Li in the forward direction. The neutron spectrum from these reactions also should be measured by time-of-flight with a well defined solid angle about the forward direction. Such measurements will permit the necessary correction for removal of the low-energy

background contribution to the excitation functions. The t-D reaction also should be considered owing to the favorable effect of the higher incoming momentum.

V. Detection Sandwich Testing

Upon completing the measurement of suitable activation cross sections, a sandwich of detectors can be assembled for absolute calibration of the neutron field in intensity and energy spectrum. The workshop recommends that well characterized standard fields be established to confirm the usefulness of the sandwich of activation foils. At least three such fields should be established. The standard fields recommended include the monoenergetic 14 MeV field created with 200-400 keV deuterons, a moderated 14 MeV field, and a higher energy field based on the d-Li source probably using 40 MeV deuterons. These fields should possess a stable beam spot position, well calibrated deuteron energy, and a stable angular distribution. The workshop recommends spectrum accuracy with maximum uncertainty of 4 to 5% from 0.5 to 30 MeV and 5 to 10% from 30 to 40 MeV.

Throughout the discussion a calibrated neutron detector has played a major role in the measurement of activation cross sections and in characterizing standard fields. There are several characteristics which the detector should have for maximum usefulness. It should have fast-time response to permit its use in neutron time-of-flight work. Pulse shape discrimination against γ-rays would be helpful. It should be physically small enough to permit easy measurement of angular distributions. It should have an effi-

ciency at least as high as 1%. A suitable scintillator should meet these criteria. The workshop recommends that a suitable neutron detector be calibrated with an associated particle, recoil telescope, or other appropriate means to an accuracy of 2 to 4% from 0.5 to 30 MeV and 4 to 8% from 30-40 MeV.

VI. Calculational Approach

The calculational approach probably can be taken with either the d-T source at 14 MeV, or with the d-Li source. Probably the d-T source characteristics and related information are already sufficiently well known, with the exception of the absolute neutron intensity, to permit the required calculations now. However, for the d-Li source, a very complete series of absolute measurements are required. The workshop recommends that the 4π-thin-target yields of the d-Li source be accurately measured. The angular distribution should be measured from 0° - 150° over the neutron energy range from 100 keV to 40 MeV. These measurements should be performed as a function of deuteron energy. Any unknown neutron transport cross section should be measured to the required accuracy.

VII. Summary

Both the activation package and the calculational method appear to be a feasible means to establish completely the characterization of any field suitable for damage irradiations. Each approach has its merits; the problems of both appear to be manageable. The workshop recommends that the required measurements and calculations be given the same priority as the detailed accelerator

design to assure that the facility is planned for maximum usefulness and to assure that the tools for damage studies will be at hand as soon as the facility becomes operational.

VIII. Summary of Recommendations

1. Follow both the foil activation and calculational methods of specifying neutron intensities and energy distributions with the intent of bringing them into confrontation in specific damage experiments.

2. Neutron fields for the d-T and/or T-d sources should be established by comparing results obtained by the associated particle and the proton-recoil techniques. Collaborative efforts should be taken to carefully establish the neutron energy of the d-T source to avoid effects of energy uncertainty.

3. The low-energy component of the d-Li neutron spectrum should be measured accurately and the high-energy continuum measured with a well calibrated neutron detector.

The 4π-thin-target yields of the d-Li source should be accurately measured. The angular distribution should be measured from 0 - 150 degrees over the neutron energy range from 100 keV to 40 MeV. These measurements also should be performed as a function of deuteron energy.

For d-Li source calculations unknown neutron transport cross sections should be measured to the accuracy required.

4. The calibrated d-Li source should be used to integrally test activation cross sections obtained from d-T or other reactions.

5. Well characterized fields should be established to confirm the usefulness of the sandwich of activation foils. At least 3 such fields should be established that include the monoenergetic 14-MeV field created by 200 - 400 keV deuterons, a moderated 14-MeV field, and a higher energy field based on the d-Li source probably using 40-MeV deuterons.

6. A suitable neutron detector should be calibrated with an associated particle, recoil telescope, or other appropriate means to an accuracy of 2 to 4% from 0.5 to 30 MeV and 4 to 8% from 30 - 40 MeV.

7. The required measurements and calculations mentioned above should be given the same priority as the detailed accelerator design to assure that the irradiation facility is planned for maximum usefulness and to assure that the tools for damage studies will be at hand as soon as the facility becomes operational.

DIFFERENTIAL DATA AND EXPERIMENTAL TECHNIQUES

F. G. Perey, ORNL - Chairman
D. Rainum, Ohio U.
H. Condé, NDRI, Sweden
F. W. Finlay, Ohio U.
R. C. Haight, LLL
G. Haouat, B.le C., France
R. J. Howerton, LLL
R. O. Lane, Ohio U.
V. McLane, BNL
M. S. Moore, LASL
G. L. Morgan, ORNL
C. Nelson, Duke U.
J. Rapaport, Ohio U.
A. B. Smith, ANL
O. A. Wasson, NBS

I. Introduction

As we have heard from R. C. Haight in his review talk there is a fair amount of data above 10 MeV but most of it is below 14 MeV. This current situation reflects both the interest of the physicists in obtaining data to study particular phenomena and technological applications which until now have mostly involved neutrons of energies below 14 MeV.

It is doubtful if much more data in the range above 14 MeV is going to be generated for its fundamental interest because we are entering a regime of mechanisms of nuclear reactions where many competing channels are open. From what we have heard at this conference on the needs of some applications, particularly in the area of radiation damage using intense neutron sources based upon the (d,Li^6) reaction, a large body of cross section data will be needed all the way to 40 MeV and it is unlikely that most of those data will be supplied from measurements in the near future. In certain areas, particularly for neutron energies below 15 MeV, most of the needs can be met through measurements. In other areas such as for gas production and damage energies a great

reliance will have to be placed upon calculations anchored by measurements.

Our report is divided into two parts. In Part I we consider the areas where the data will be used mostly to assist the calculations such as transmutation reactions and other reactions contributing to the specific damage. In Part II we consider the area of dosimetry where most of the data will have to come from measurements.

II. Part I - TRANSMUTATION AND SPECIFIC DAMAGE CROSS SECTIONS

A. Present Programs

As we have seen from reports to this conference some facilities and experimental techniques are available today to make measurements of some of the cross sections of interest. It is in large part due to the ability of model calculations to fit those data that we derive some of the confidence that model calculations will be very useful in satisfying the needs in the energy range 15 to 40 MeV.

Examples of data which are presently obtainable have been presented at this conference.

1. Hydrogen, Helium, Charged-Particle Production and Other Transmutation Cross Sections

The hydrogen and helium produced by neutron bombardment of materials are being measured with mono-energetic neutrons near 14 MeV and at 50 MeV. At the lower energy, a wide spectrum of materials of DMFE interest is being investigated, whereas at 50 MeV the targets are those of medical interest, in particular car-

bon, oxygen and nitrogen. Near 14 MeV, the helium production cross sections are measured by a mass spectrographic determination of the helium accumulation or by a measurement of the alpha particles. For helium production at 50 MeV and for hydrogen production at both energies, the measurements are made only by detecting the protons, deuterons and tritons.

In addition to the integrated production cross sections, the charged particle spectra and angular distributions are being measured as they provide more stringent tests of nuclear model calculations. They also provide data directly for the evaluations of recoil spectra and of KERMA (Kinetic Energy Released in biological systems.

The other transmutation products for reactions induced by neutrons between 10 and 40 MeV are generally not known, and no measurement program is currently active. For a few cases and for neutrons below 15 MeV, the transmutation cross section can be deduced from activation cross sections or from the hydrogen and helium production cross sections. The need for cross sections appear to be somewhat less urgent than for the hydrogen and helium production cross sections.

2. Other Cross Sections

These cross sections consist of total cross sections, elastic scattering, inelastic scattering, neutron emission, and (n,xn) cross sections. Many of these cross sections have not been measured over the complete energy range from 10 to 40 MeV.

For some of them it would be a straight forward matter to perform the measurements over the complete energy range using existing techniques. For others there are currently limitations in neutron source strengths and techniques.

B. Status of Measurements

1. Hydrogen, Helium, Charged-Particles Production and Other Transmutation Cross Sections

Already a significant number of helium accumulation and charged particle production cross sections have been measured near 14 MeV. Within the next two years the results at this energy will be extended to most of the highest priority materials for DMFE. The data on carbon and oxygen at 50 MeV neutron energy will be completed.

At other neutron energies between 14 and 50 MeV, some additional cross sections will be measured by detecting the charged particles directly. Because the neutron sources are not mono-energetic above 20 MeV, the time-of-flight techniques will be required in general to select the incident neutron energy. Measurement of the helium accumulation will give only spectrum averaged cross sections in this energy range for the same reason.

The present techniques likely will be improved in the next two years are better electronic timing, larger solid angles for detecting the charged particles, better thin detectors, and more intense sources all of which seem likely in the near term.

Other laboratories not presently involved in these measurements could add to this program of measurements if they have rather intense neutron sources and the manpower, and are willing to use newly developed or improved techniques.

C. Other Cross Sections

Total cross sections, elastic scattering, inelastic scattering, neutron emission, gamma ray emission and (n,xn) cross sections can be measured. For many of the elements of interest adequate techniques and standards are available.

D. Recommendations

Our main recommendation is that the bulk of the data required for applications should not come from measurements, but be obtained from model calculations which have been validated by some experimental data. We recognize that model calculations may not be applicable to light nuclides and that for those the experimental data have to be generated. The specific recommendations we make are:

1. Hydrogen, Helium, Charged-Particle Production and Other

a) The likely improvements to the existing programs of measurements should be carried out.

b) The measurements near 14 MeV and at 50 MeV should cover the materials of both DMFE and medical interest.

c) These measurements should also be used to validate model codes as well as to improve evaluated data files.

d) Measurements of the charged particle production cross sections, spectra and angular distributions should be made on selected isotopes at a few energies between 15 and 50 MeV. The isotopic data should be used to check nuclear model calculations.

e) For carbon, oxygen and nitrogen, more measurements should be made at more energies in the 15 to 50 MeV range. The nuclear models may not be appropriate for these light elements which are of crucial importance in neutron therapy.

f) The feasibility of and need for measurements of other transmutation cross sections should be assessed.

g) Pulsed white neutron sources between 15 and 40 MeV in the measurement of the charged particle production cross sections should be considered. These sources would offer the possibility of measuring the cross sections over the entire energy range.

2. Other Cross Sections

a) Total cross sections should be measured over the complete energy range and be reproduced by model calculations.

b) Elastic scattering measurements be made at selected energies from 15 to 40 MeV. To establish the systematics of the optical model parameters used in calculations and obtain reference reaction cross sections which should be reproduced by model calculations. The extensive data base for charged particle scattering should be used with the neutron data to establish the optical model parameters.

c) Multiple particle emission data such as (n,xn) should be obtained, particularly for the specific nuclides of interest in applications, in order to check the model calculations.

d) Inelastic cross sections, neutron and gamma ray emission spectra should be obtained in order to check the model calculations.

e) Charged particle data should also be used to validate the model calculations.

f) The experimental program should be strongly coordinated with the model calculations and evaluation effort. The CSEWG seems an adequate forum where interaction between measurers, evaluators and users should take place to have an effective program.

III. Part II - DOSIMETRY CROSS SECTIONS[a]

A. Needs - Objectives

Dosimetry needs are probably the best defined, most quantitative and the most experimentally oriented differential data requirements discussed at this meeting. These data have a wide impact on and are critical to:

1. MFE damage programs

Essential to spectral-field definition

Essential to practical utilization of radiation facilities

[a]Primarily based on discussions among A. Smith (Leader), M. Moore, O. Wasson, H. Conde and R. Howerton.

2. Bio-Med. applications of high energy neutrons

Essential to source definition, dose determination, etc.

3. Essentially any bulk-media applications of fast neutron excesses, e.g., design of shield of medium energy accelerators. Mastery of the dosimetry area is explicitly essential to the effective utilization of large rad-damage facilities such as the proposed MFE-LiD machine.

B. Character and Scope of the Problem

The broad outlines of the problem area are reasonably evident:

1. $E_n \leq 14$ MeV

Precise needs (5-10%)

Required precision experimental measurement

Theory will have minor impact, confined primarily to interpolation between 11-14 MeV.

2. $E_n = 14-30$ MeV

Modest accuracies (10-20%)

Measurements difficult but feasible

Theory will play a useful interpolation role

3. $E_n = 30-50$ MeV

Qualitative accuracies (30-50%)

Reliance on theory extrapolating upward in energy from experimental values primarily at the lower extreme.

4. By the very application nature, the reactions of interest are simple and relatively easy to observe. The observ-

able is the objective (not necessarily the underlying physical reaction).

5. A complicating feature is the broad energy scope requiring attention to energy-dependent reaction shapes at or near both the threshold region and the transition region marked by the onset of strong channel competition. This is in contrast to the fission-reactor need which is generally confined to within a "one-neutron's-binding energy" of the threshold.

6. Some potentially useful reactions are subject to perturbation due to channel competition and others have proven historically difficult to measure (e.g., (n,γ) processes above 10 MeV). Careful selection of reaction type is warranted in the context of microscopic measurement theory and user application.

C. Status and Capability

1. The ENDF dosimetry effort has provided ~ 40 reaction types to energies of 20 MeV. A number have been extensively validated using fission benchmark tests. However, it is doubtful that the above 5-8% accuracy goal has been achieved in few, if any, cases--and probably never achieved above 20 MeV. However, the ENDF dosimetry file should be the basis for future extensions in energy reaction type and accuracy.

2. Measured values are sparse and of marginal accuracy above 20 MeV. The few good quality results have generally been obtained for studies of "explosive devices."

3. Measurements are generally feasible, particularly below 30 MeV and results could impact on need within a short time span (i.e., $\leq$ 2 yrs).

4. A few measurement groups are active at a modest level. These have developed and proven the essential experimental analytical techniques. Their performance is, in principle, assured. Measurement programs should proceed in conventional and proven channels, or equivalent, in a correlated manner. Specifically to be avoided is a fragmented or uncorrelated effort.

5. Requirements are for mono-energetic sources. Suitable performance is readily available at several facilities for energies to 25-30 MeV. Capabilities for producing > 30 MeV neutrons are not as suitable but still should meet the overall need, particularly in the near term. Precision measurements will require associated studies of source properties (distribution in angle and energy). However, there appears to be no requirements for extensive new source facilities.

6. For a successful program above energies of fission-reactor interest (e.g., 8 MeV) it is essential that modest operational support be given to existing measurement efforts in a correlated manner. Without such support, the higher energy measurements will not be done and even the retention existing competence will be in doubt.

D. Procedures and Practices

1. At once a special selected study group of measurers-users-evaluator/theorists should be formed to specifi-

cally define 10-15 critical reaction types optimizing the capabilities of all three parties. Subsequently, the measurement effort should focus on these reactions. The Cross Section Evaluation Working Group provides a suitable vehicle for organizing such a group.

2. Uniform guidelines should be established for the proper correlation of measurement programs including:

a) Definition of coverage and responsibility (E_n and reaction type)

b) Use of reference standards (see below)

c) Data handling and correction procedures

d) Associated theoretical calculations

3. Definition of reference standards and data representation should be established including:

a) Explicit requirement for direct reporting of ratio values.

b) Specific statement of secondary reference standard used. They should be consistent with a limited (~4) generally accepted secondary standards.

c) Specification of energy scale relevant to Nuclear Energy Agency Nuclear Data Committee recommended values.

d) Continued intensive effort to determine the secondary standards to ≲ 3% relative to the primary H(n;n) standard.

It is noted that default in the standard area has been a major cause of uncertainty in previous measurements.

The above program can be well defined, is well within current technical capability and with modest support can provide results essential to near term applied needs (e.g., MFE source). This is illustrated by the following milestone chart which provides for critical needs within a 2 year time frame at a level of effort estimated at 10-15 man/yrs. The goal appears relatively realistic and a cost that is a very small portion of the primary program it supports.

E. Summary of Recommendations

1. The ENDF dosimetry file should be the basis for future extensions in energy reaction type and accuracy.

2. Measurement programs should proceed in conventional proven channels, or equivalent, in a correlated manner. Specifically to be avoided is a fragmented or uncorrelated effort.

3. There appears to be no requirement for extensive new source facilities.

4. It is essential that modest operational support be given to existing measurement efforts in a correlated manner.

5. A special selected study group of measurers-users-evaluator/theorists should be formed to specifically define 10-15 critical reaction types optimizing the capabilities of all three parties. Subsequently, the measurement effort should focus on these reactions.

6. Uniform guidelines should be established for the proper correlation of measurement programs.

7. Definitions for reference standards and data representations should be established.

F. Schedule

Task	Calendar Years			
	1/2	1	1½	2
A. Detailed specification of 10-20 reaction types	●			
B. Implement ratio measurements to 20 MeV, < 5% values			●	
C. Provide calculational base for extrapolation			●	
D. Derive first-pass evaluated set				●
E. Start Benchmark tests				●
F. Provide 3% secondary standard				●
G. Initiate measurements above 20 MeV		●		

MATERIALS DAMAGE STUDIES

A. N. Goland, BNL - Chairman
D. G. Doran, HEDL
R. R. Heinrich, ANL
L. Greenwood, ANL
M. Guinan, LLL
T. A. Gabriel, ORNL
L. Stewart, LASL
B. Magurno, BNL
R. Dierckx, EURATOM/ISPRA
S. Pearlstein, BNL

I. Objectives of Materials Damage Studies

The primary goals of materials damage studies are to correlate or predict physical property changes induced by neutron irradiations performed in diverse sources. In order to achieve these objectives, materials scientists require adequate characterization of the radiation environment, e.g. flux, spectrum and temperature, as initial input. This information is used for the subsequent calculation of primary-atom recoil spectra, displacement cross sections and other defect parameters. Determination of these quantities is required for irradiations in neutron spectra extending to 40 MeV. In addition, it is necessary to determine transmutation-product production rates over the same energy range because materials behavior is known to be very sensitive to gaseous products and to trace amounts of other transmutants.

II. Status of Research

The existing ENDF/B dosimetry file[1] was established to meet the needs of the breeder reactor program. Although it now extends to 20 MeV, little data testing has been done above 10 MeV. Reliable methods for extending the file data to 40 MeV should be standardized; for example, an appropriate nuclear model could be used for this purpose. New dosimetry reactions especially for energies above 20 MeV need to be selected, and techniques such as helium

accumulation fluence monitoring and solid-state track recording should be pushed to higher energies.

At present, calculations of PKA (primary knock-on atom) spectra are believed to be adequate for neutron energies below 15 MeV although analysis of uncertainties arising from errors in ENDF/B has not been completed. Calculations of PKA spectra are generally performed assuming an equalibrium evaporation model with isotropic particle emission to describe charged-particle-out reactions. They usually neglect emission subsequent to the first particle emitted. The validity of this procedure can not be ascertained from ENDF/B data that do not distinguish between the particles. The ENDF/B format permits inclusion of angular and energy distribution data for particle emission, and some of these data are available in the files for (n,p) reactions. However, this kind of information is generally absent from the files.

Minor radiation-induced changes in composition may have major impacts on the properties of materials. Determination of transmutation products that are important to the alloy is underway. The gaseous impurities, He and H, are already known to be important, and recent experiments have shown that dilute concentrations of certain other elements can suppress swelling in ternary alloys. A special application file for gas production has already been initiated. Moreover, a continuous need exists for reaction cross section and decay data to permit estimates of induced radioactivity in reactor materials.

III. Recommendations

1. Dosimetry Reactions

For characterization of the neutron environment in which materials studies will be conducted over the next ten years extension of absolute cross section data above 15 MeV for the following primary dosimetry reactions listed in Table I is needed:

Table I. Primary Dosimetry Reactions

Reaction	Energy Range (MeV)
$^{23}Na(n,2n)^{22}Na$	12 - 30
$^{27}Al(n,\alpha)^{24}Na$	8 - 30
$^{54}Fe(n,\alpha)^{51}Cr$	1 - 25
$^{54}Fe(n,p)^{54}Mn$	3 - 25
$^{58}Ni(n,p)^{58}Co$	2 - 25
$^{60}Ni(n,p)^{60}Co$	3 - 30
$^{58}Ni(n,2n)^{57}Ni$	12 - 40
$^{58}Ni(n,3n)^{56}Ni$	22 - 40
$^{59}Co(n,p)^{59}Fe$	4 - 25
$^{59}Co(n,2n)^{58}Co$	10 - 35
$^{59}Co(n,3n)^{57}Co$	20 - 40
$^{59}Co(n,4n)^{56}Co$	30 - 40

Table I. Primary Dosimetry Reactions (Cont'd)

Reaction	Energy Range (MeV)
$^{93}Nb(n,2n)^{92}Nb$	9 - 25
$^{90}Zr(n,2n)^{89}Zr$	12 - 35
$^{90}Zr(n,3n)^{88}Zr$	22 - 40
$^{90}Zr(n,p)^{90m}Y$	3 - 25
$^{89}Y(n,2n)^{88}Y$	12 - 35
$^{89}Y(n,3n)^{87}Y$	22 - 40
$^{107}Ag(n,2n)^{106m}Ag$	10 - 35
$^{107}Ag(n,3n)^{105}Ag$	18 - 40
$^{169}Tm(n,2n)^{168}Tm$	8 - 35
$^{169}Tm(n,3n)^{167}Tm$	15 - 40
$^{169}Tm(n,4n)^{166}Tm$	26 - 40
$^{197}Au(n,2n)^{196}Au$	8 - 30
$^{197}Au(n,3n)^{195}Au$	15 - 35
$^{197}Au(n,4n)^{194}Au$	23 - 40
$^{197}Au(n,5n)^{193}Au$	35 - 40
$^{238}U(n,2n)^{237}U$	6 - 25

This extension should be in the energy range of importance, including the threshold energy. It is possible that these cross sections will have to be determined to an accuracy of 10-20% in the energy region of primary response. Absolute accuracy requirements for these cross sections can not be established without some sensitivity studies (see 4 below), and further data testing. However, accuracies of 5-10% may be needed in the energy ranges of primary response, including reaction threshold regions, below 25-35 MeV. Lower accuracies may suffice above 35 MeV.

2. Materials Studies Cross Sections

a) as a start, desired cross sections (including angular and energy distributions) of the following materials should be provided: Fe, Cr, Ni, Mn, V, Nb, Mo, Ti, Al, Pb, Zr, C, Cu, Sn, Si.

b) partial cross sections up to 40 MeV are needed for damage calculations; the required detail and accuracy should be determined by preliminary sensitivity studies. Cross sections for gaseous reaction products are especially important because of the role of gases in affecting properties of materials.

c) elemental evaluations are adequate for use in damage calculations, but isotopic evaluations are necessary for dosimetry and transmutation product determinations.

3. Reference Spectra

It is necessary to establish well characterized reference spectra for 14-MeV and deuteron-stripping sources so that

materials scientists can correlate their experimental results. Correlation will require integral testing of nuclear data to establish uniform dosimetry practices. This step is needed to permit accurate comparisons of experimental data obtained in different irradiation facilities. It is likely that an intense 14-MeV source, such as the RTNS,[2] and a d-Be source at an existing cyclotron will be suitable as reference spectra in the high-energy neutron range.

4. Sensitivity Studies

Broad-based sensitivity studies intended to determine the sensitivity of materials damage parameters to variations in cross-section data and nuclear models should be carried out. These would not require complex error analysis or the creation of correlation parameter files by evaluators. However, the studies would require close collaboration between materials scientists and cross-section evaluators.

5. Special Purpose Files

Existing special purpose files should be extended to 40 MeV, e.g. total gas production and dosimetry files. Charged particle energy spectra which are often calculated but not used should be retained in a file. At present the ENDF/B format is adequate for the needs of materials damage calculations. However, reassessment should be made periodically as the files are extended to 40 MeV.

A damage cross section file could be established, and consideration should be given to the creation of an accepted PKA

spectra file. If special purpose files of this type are to be widely used, they should be endorsed by an official group, such as the Damage Analysis and Fundamental Studies Task Group of the Division of Magnetic Fusion Energy (ERDA).

6. Charged-Particle Irradiations

Protons, deuterons and alpha particles are being used in radiation damage studies at energies of 10-20 MeV/amu. Primary recoil spectra and gas production rates are needed. Recommendation 2. applies to these particles as well as to neutrons.

References

1. B. A. Magurno, Editor, ENDF/B-IV Dosimetry File, BNL-NSC-50446 (ENDF-216), April 1975.

2. R. S. Booth, Nucl. Instrum. Methods 120, 353 (1974).

INTEGRAL EXPERIMENTS AND DATA TESTING

B. R. Leonard, Jr.	BNW	Chairman
R. G. Alsmiller	ORNL	
H. Farrar	AI	
L. Hansen	LLL	
R. J. Howerton	LLL	
C. W. Maynard	U. Wisc.	
P. Rose	BNL	

I. Status

The Proceedings of the Magnetic Fusion Energy Blanket and Shield Workshop (ERDA-76/117/1, CONF-760343) contains a Compendium of 14 MeV neutron source experiments (B. R. Leonard, Jr., pp. 66-76). These were known experiments using near monoenergetic 14 MeV neutron sources which could be considered in the assessment of integral results and microscopic nuclear data. These experiments were integral in either multiple target reactions or experimental observables, or both.

At this Symposium, Professor C. W. Maynard, U. Wisc., presented a paper "Integral Experiments for CTR Nuclear Data." This paper also contained a similar compilation of 14 MeV neutron source experiments. These compilations are identical in the identification of the majority of experiments.

The comparison of theoretical analysis of these experiments with integral results remains unchanged: the primary disagreements are at many mean free paths in the detecting media where the "deep penetration" of near 14 MeV neutrons is underestimated analytically. These experimental results and analyses led to the ongoing DMFE Program at ORNL of 14 MeV source neutron experiments in bulk media. These experiments, of utmost practical importance

in fusion reactor design and analytical implications, are considered to have an impact primarily on calculational methods, and probably have little impact on the validity of microscopic neutron data.

There are now new integral experimental results which have an impact on the testing of microscopic nuclear data. These are:

A. Improved experimental data with the Lawrence Livermore Laboratory pulsed-source 15 MeV experiments. (Reported by L. Hansen, et al., Paper this Symposium.)

B. Total helium production experiments using the RTNS near-14 MeV neutron source. (Reported by H. Farrar, et al., Paper this Symposium.)

C. Secondary neutron emission spectrum measurements using ORELA. (Reported by G. L. Morgan, Paper this Symposium.)

D. The qualification of neutron spectra by multiple foil techniques (Reported by L. Greenwood, et al., ANL, Paper this Symposium.)

II. Problems to be Solved

The interpretation of experiments in bulk media is still inadequate. It presently seems that this is a calculational problem, as opposed to an experimental or nuclear data problem. The ORNL program results expected this year should give insight into this problem.

The newer evaluations (ENDF/B-IV) are in much better agreement with the results of the LLL pulsed sphere experiments. In particular, the LLL experiments were of value in producing strong

evidence of the physical process - pre-equilibrium emission of neutrons. The experimental results, however, indicate an apparently persistent problem in that the calculated neutron distributions differ from the observed secondary neutron energy yield for energies below some 8 MeV and differ systematically below 5 MeV. These results should be studied further to determine if these are isolated data problems. The problem could relate possibly to ENDF/B conventions.

III. Recommendations

14-15 MeV Source Experiments

A. Total helium production experimental results, such as those by Farrar, et al., using the RTNS, should be given priority consideration in studying nuclear data evaluation problems. The measurements completed and in progress are shown on Table 1. The results of these experiments should be used in the evaluation of microscopic nuclear data.

B. Neutron emission experimental data, such as that produced at ORNL, should be considered in data evaluations. This type of experiment should be extended to materials other than those of ORNL evaluations.

C. Multiple foil neutron spectra results, such as those reported by Greenwood, et al., should be considered in microscopic neutron data evaluation. These experiments seem to be deficient in defining the spectra below ∿5 MeV. This problem arises because threshold reactions which are used to define fission spectra in this range do not apply in broad spectra. New reactions or new

techniques, e.g., subtraction of reactions of differing threshold energies are needed.

D. Apparent systematic problems for $E_n < 5$ MeV in the interpretation of the LLL pulsed sphere experiments should receive further study.

Data Needs in Support of D, Be and D, Li Neutron Source Radiation Damage Experiments

A. Pulsed sphere experiments, such as those performed at LLL, should be evaluated to see if meaningful data can be obtained with the use of higher-energy DT neutron sources.

B. Neutron emission experiments, such as those performed at ORELA, should be evaluated with regard to using LINAC-produced neutrons in the energy range greater than 20 MeV for neutron emission spectra experiments.

C. The planned experiments of Farrar, et al., using 30 MeV d, Be source neutrons to take place in the summer of 1977, are strongly endorsed.

TABLE

Elements and Isotopes that have been or will be Integrally Tested in RTNS-I for Total Helium Production

Helium

Samples Irradiated and already analyzed for helium	Samples Irradiated and awaiting helium analysis	
C	^{6}LiF	^{61}Ni
Al	^{7}LiF	^{62}Ni
Ti	^{10}B	^{64}Ni
V	^{11}B	^{63}Cu
Fe	Si	^{65}Cu
Ni	Mn	^{92}Mo
Cu	Cr	^{94}Mo
Zr	^{54}Fe	^{95}Mo
Nb	^{56}Fe	^{96}Mo
Mo	^{58}Fe	^{97}Mo
Au	^{58}Ni	^{98}Mo
Pt	^{60}Ni	^{100}Mo

DATA EVALUATION AND NUCLEAR MODEL CODES

P. G. Young, LASL – Chairman
M. Hillman, BNL
A. Prince, BNL
T. Tamura, U. of Texas
E. D. Arthur, LASL
M. Divadeenam, BNL
C. Y. Fu, ORNL
G. H. Herling, NRL
F. M. Mann, HEDL
H. Takahashi, BNL
R. G. Alsmiller, Jr., ORNL
J. J. Coyne, NBS
R. Finlay, Ohio U.

I. Introduction

The above group met on May 4 and 5, 1977, in conjunction with the Symposium on Neutron Cross Sections 10-40 MeV to discuss problems associated with nuclear data evaluation and model code calculations required for analysis of materials damage studies in the neutron energy range 10-40 MeV. The remainder of this report summarizes discussions by the group regarding (1) present status of evaluations and nuclear models, (2) problem areas in model calculations, and (3) recommendations and conclusions regarding future work.

II. Status of Nuclear Data to 40 MeV

A. Evaluations

Formal nuclear data evaluations now exist primarily for neutron energies below 20 MeV, for example, the ENDF/B system. While isolated efforts have been made to extend evaluated data beyond 20 MeV, they have either not been very comprehensive in scope or have been based on relatively incomplete studies. Additionally, because of previous lack of interest in nuclear data past 15 MeV for fission, fusion, and weapons application, some of the ENDF/B data from 15 to 20 MeV are based on relatively crude extrapolations from lower energies.

B. Model Codes

The primary nuclear models applicable to nuclear data problems in the range 10-40 MeV are multi-step Hauser-Feshbach, precompound, direct reaction, and intranuclear-cascade-evaporation models. Several computer codes that implement one or more of these models are described in the symposium proceedings, and we include in Appendix I a summary of the status and availability of these codes.

III. Deficiencies in Model Calculations

A general problem concerning nuclear model calculations at energies between 15 and 40 MeV is the serious lack of relevant experimental data for parameter and model verification. More specific problems are:

A. Level Densities

Considerable uncertainty exists in the effect of different level density representations and parameterizations on calculations of such quantities as neutron, charged-particle, and gamma-ray emission spectra and angular distributions.

B. Non-compound Effects

As pointed out in the symposium, present treatments of pre-compound do not include spin and parity effects, which might be important for some calculations. In addition, present models do not include angular distribution effects, and direct and pre-compound contributions are frequently not considered in a consistent manner.

C. Optical Model Parameters

Reliable optical model parameters, which are required for calculation of transmission coefficients, are not always available. Particularly lacking are reliable energy-dependent alpha-particle parameters. In addition, in spite of several past studies, confusion still exists regarding the accuracy of certain routines used to compute transmission coefficients from optical model parameters.

D. Gamma-ray Strength Functions

Reliable parameters for estimating γ-ray strength functions are frequently difficult to obtain. These are important for estimating gamma-ray competition near particle thresholds.

E. Isospin Effects

Many of the nuclear model codes do not include isospin effects. These effects should be incorporated for proper utilization of proton-induced data in determining model parameters.

IV. Recommendations and Conclusions

Because of the sparsity of experimental data at neutron energies between 15 and 40 MeV, the group concluded that nuclear model calculations must play an important role in meeting the data requirements for damage studies at these energies. Much progress has been made in the last several years in developing calculational tools that can be useful for this purpose. In particular, the multi-step Hauser-Feshbach/pre-compound models appear to be capable of providing much of the required data up to 40 MeV, provided that sufficient experimental data exist to val-

idate model parameters for the important nuclides and data of interest. The group also noted that the multi-step direct reaction approach offers promise to provide a very useful supplement for the Hauser-Feshbach calculations.

The following specific recommendations are made:

A. The nuclear models subcommittee of the Cross Section Evaluation Working Group (CSEWG) should strengthen its code comparison effort to ensure accuracy and consistency in calculations performed with the various model codes. In addition, the specific problems outlined in Section III should be addressed by the subcommittee, with particular emphasis on establishing their effect on calculations of hydrogen and helium production cross sections, emitted neutron energy and angular distributions, etc. Recommendations from the subcommittee regarding possible standardization of optical model subroutines, mass tables, energy level tables, etc., would also be most useful.

B. Nuclear model calculations for light elements are relatively more difficult than for medium mass nuclei. In particular, global parameterizations are not as reliable, and special care should be taken to ensure the appropriateness of models and parameters for nuclei lighter than ^{27}Al. This conclusion implies, of course, a more extensive measurement program for important light nuclei.

C. The models and techniques discussed here can be validated and parameters obtained from proton-induced measurements as well as from incident-neutron experiments. Therefore, the group

recommends that available proton data be utilized in model studies when possible. In addition, we encourage charged-particle experimenters to consider measurements of such quantities as alpha and proton production cross sections, spectra, and angular distributions induced by protons up to 40 MeV, as well as proton elastic scattering and emission spectra.

D. Authors of nuclear model codes are urged to provide documentation of their codes. Documentation should include a theoretical description and, if the code is to be generally available, user instructions.

E. The neutron-induced measurements that are most essential for providing the required data evaluations up to 40 MeV are neutron total cross sections, elastic scattering angular distributions*, hydrogen and helium production cross sections, and important dosimetry and activation cross sections. While we can provide estimates of these quantities with model codes now, experimental data at a few energies for important materials would greatly improve the overall accuracy of the calculations. Additionally, measurements of secondary neutron and charged-particle emission spectra at a few angles and incident energies are needed to verify calculations of Primary Knock-on Atom (PKA) spectra.

F. Once a firm decision is reached to build a D-Li source, a "working library" of evaluated nuclear data to 40 MeV should be derived for the few most important materials on a relatively short

*Mainly needed for verification of model parameters.

time scale (∿ 2 years). The purpose of this library would be to provide at an early point data that can be used in preliminary sensitivity analyses, experiment design studies, etc. The library should be in ENDF/B format (with modifications, as needed), but should not be part of the official general purpose files. Rather, it should be a working library so that it can be updated more frequently as the need and new data justify.

APPENDIX I

SUMMARY OF MODEL CODES DESCRIBED AT SYMPOSIUM

Program	Authors	Location	Type	Documentation	Availability
TNC	C. Y. Fu	ORNL	Multi-step Hauser-Feshbach with pre-compound.	No	Exportable if potential users spend a few days at ORNL under tutelage of the author.
GNASH	E. D. Arthur P. G. Young	LASL	Multi-step Hauser-Feshbach with pre-compound	Report is in preparation	Available from authors. Presently operating on CDC computers.
HAUSER	F. M. Mann	HEDL	Multi-step Hauser-Feshbach.	Yes	HAUSER-4 is available and has run on CDC and IBM computers. HAUSER-5 is in test stage.
ALICE	M. Blann	U. of Rochester	Multi-step Weisskopf-Ewing Evaporation with pre-compound.	Yes	Available from author.
NMTC	R. G. Allsmiller, Jr. T. A. Gabriel	ORNL	Inter-nuclear cascade plus Evaporation.	Yes	Available from the Radiation Shielding Information Center at Oak Ridge.
ORION-1	T. Tamura T. Udagawa	U. of Texas	Multi-step direct reaction with possibility of linking to Hauser-Feshbach codes.	No	Code is presently in test stage. Authors hope to have it available for general use by the end of summer, 1977.
JULIAN	M. Hillman Y. Eyal	BNL Weizmann Inst.	Monte Carlo Hauser-Feshbach.	Extensive comments in program and sample problem available.	Available from authors. Presently operating on CDC and IBM machines.

SESSION I

INTRODUCTORY

Chairman: S. L. Whetstone, DPR, ERDA

CONF-770523-10

The Program for Alloy Development for Irradiation Performance in Fusion Reactors*

J. O. Stiegler
Oak Ridge National Laboratory, Metals and Ceramics Division,
Oak Ridge, Tennessee 37830

T. C. Reuther
U. S. Energy Research and Development Administration
Division of Magnetic Fusion Energy, Washington, D.C. 20545

The Division of Magnetic Fusion Energy of ERDA is about to embark on the most ambitious alloy development program in history — the identification and perfection of a material to withstand the hostile environment of the first wall of a fusion reactor. For a neutronic wall loading of ~ 3 MW/m^2, atoms will be displaced from their lattice positions at rates equivalent to those in current fast fission reactors, but because of the current of 14 MeV neutrons born in the d-t fusion process, damaging transmutation products, especially helium, will be produced at rates orders of magnitude higher. A comparison of critical damage parameters is given in Table 1.

Table 1

A Comparison of Displacement Damage and Helium Production in Fast Fission and Fusion Reactors for Stainless Steel

	Damage Accumulated in One Year of Operation	
	Displacements per Atom	Parts per Million Helium
Fusion Reactor (3 MW/m^2)	36	525
EBR-II	35	10

Core components in fast breeder reactors are designed for a service life of about two years. Replacement or repair of a fusion reactor first wall is expected to be a significantly more difficult task, so a longer life, in the range of five to ten years, will be required for economical generation of electricity. This will result in a cumulative damage level well above that of fast reactors.

*Research sponsored by the Energy Research and Development Administration under contract with Union Carbide Corporation.

In Table 1 displaced atoms and helium are identified as the principal components of damage. Experiments in which these have been studied independently have demonstrated their capability for degrading properties. Other transmutation products, hydrogen as well as solids, also may be harmful, but except in special cases the evidence is not conclusive.

The biggest obstacle in the path of development of an alloy for fusion reactor use is lack of a testing facility with a neutron flux and spectrum that matches fusion reactor conditions. Fusion neutron sources available or authorized for construction, RTNS I and II and INS, have fluxes and experimental volumes that are much too low for use in testing large numbers of specimens to end of life exposures necessary for design of structural components. It is important to recognize that it is a combination of flux and volume that must be available for alloy development. Fluxes must be high enough to allow testing at damage rates close to those expected in reactor operation. A capability for accelerated testing clearly would be desirable. Development and eventual qualification of an alloy for reactor service will require an experimental volume in the range of ten liters. Thus, a testing facility for alloy development and qualification testing must satisfy simultaneously both flux and volume requirements.

The requirements of a large number of test specimens seems surprising at first glance. The reason for this is that there are several potential failure mechanisms that must be investigated. Fatigue and crack growth studies involve large numbers of large specimens, for results are sensitive to specimen geometry, temperature, mean stress level, stress variations and hold times as well as irradiation and environmental parameters. Additionally, since the expected damage levels are well beyond our present experience, we are unable to identify with assurance even a class of materials that will provide the best solution to the problem. This means that multiple materials options must be incorporated into the test matrix.

The fusion reactor is not unique in that early machines will have to be constructed without complete irradiation testing in the proper environment. The first fission reactors, for example, were built under this condition, but they did not suffer from significant damage to structural components. In the case of fusion reactors we know from experience with the Breeder Reactor program that the first wall will suffer from void swelling and irradiation-induced embrittlement.

To repeat, the real problem is lack of a suitable fusion environment testing facility. This is not a simple consequence of a lack of funding, since serious technical difficulties stand in the way of developing such a facility. Furthermore, structural components of a test reactor will certainly suffer from radiation effects themselves. In any case such a device likely will not be available for at least ten to fifteen years, and it as well as early fusion reactors will have to be designed on the basis of data from non-fusion irradition experiments.

The flux-volume requirement discussed previously limits our current choice of existing irradiation facilities to fission reactors. As can be seen in Table 1, fast reactors provide only a partial solution to the testing dilemma; atoms are displaced at the proper rate, but helium is generated much too slowly. Nature, which usually conspires against us, has given us a partial solution to this problem. Nickel-58 undergoes a two step reaction with thermal neutrons to produce helium via the sequence

$$^{58}Ni + n \longrightarrow {}^{59}Ni$$

$$^{59}Ni + n \longrightarrow {}^{56}Fe + {}^{4}He \ .$$

In mixed (fast/thermal) spectrum research reactors currently available atoms can be displaced by fast neutrons and helium generated by thermal neutrons (for materials containing nickel). Cross sections for both processes are high enough that damage levels close to those given in Table 1 for fusion reactors can be produced in existing reactors. The situation is complicated by the two step reaction for the production of helium. As a consequence of this, helium is generated at an accelerating rate, but displacements are produced by the fast neutrons at a constant rate. This deficiency can be overcome in some reactors by varying the ratio of thermal to fast fluxes during the irradiation. For materials that contain nickel, therefore, an acceptable approach exists for approximating the damage expected in fusion reactors. For other materials the situation is far less satisfactory. There is a possibility that fast reactor irradiations may be useful if the irradiation temperature is maintained below the range where helium effects are important, but this remains to be demonstrated by experiments. For a material like vanadium that might correspond to temperatures below about 600°C and for austenitic stainless steel to temperatures of 450–500°C or less.

The intent of this discussion is to show that in the near future only fission reactors can provide the basis for irradiation testing of structural materials to generate engineering data and that there is reason to believe that under certain conditions fission reactors may provide a reasonable approximation of the effects of the fusion environment. The program plan prepared by the Division of Magnetic Fusion Energy to address the alloy development task rests on this premise. It recognizes as well that this by itself is insufficient to guarantee a reliable structural material. Important considerations such as differences in the primary recoil spectra and differences in rates of production of other transmutation products such as hydrogen between the fission and fusion reactor neutron spectra also must be considered. In the DMFE program a separate task group on Damage Analysis and Fundamental Studies has been established to examine quantitatively the relationships between damage produced in different neutron sources. The damage analysis technique, which develops energy dependent damage cross sections, has been used successfully in

fission reactor programs by interpolating between known spectra. Although combined displacement and helium effects present a more complicated situation, there is reason to believe that such techniques founded on a fundamental understanding of the relevant physical processes can be applied to fusion reactor problems. An essential requirement is that data be available from spectra that overlap the spectrum for which property estimates are required. For the fusion reactor application fission reactor data alone are not sufficient. Additional data covering the energy range between fission reactor energies and 14 MeV are required. Such a source must have a flux high enough to reach the damage levels of interest on a limited number of specimens.* A Li (d,n) source having a useful volume of several hundred cubic centimenters meets this need. Such a source also will provide information on the effects of large amounts of hydrogen on properties and will allow a test of the idea that helium effects can be neglected in low temperature irradiations. It also will permit flux cycling experiments that can not be performed easily in fission reactors. It is not intended that this type of source will be used to generate statistical engineering data but rather that it be used for specialized experiments that allow interpretation and projection of data generated in fission reactors for fusion environments. Its purpose is to tell us how to use those data. Of course, high energy cross section data are needed to tell us how to use the Li (d,n) source.

The DMFE Materials Radiation Effects Program is organized around four Task Groups as shown in Table 2. The Alloy Development for Irradiation Performance Task Group is charged with conducting engineering tests on engineering materials using the full range of metallurgical options to develop an acceptable material. The Damage Analysis and Fundamental Studies Task Group is concerned with developing correlations among the several irradiation test environments as well as with conducting fundamental experiments (usually on model materials) directed at uncovering mechanisms of material behavior under high energy neutron irradiation. The Plasma-Materials Interaction Task Group investigates interactions between the first wall surface and the plasma, including both material wastage and plasma contamination processes. The Special Purpose Materials Task Group pursues materials problems in other parts of the reactor system, such as insulators, magnets, coolant and breeding materials and ceramics. Although the task groups are organized around distinct and well identified areas, there is appreciable overlap and interaction, especially between the first two.

---

*The approach is that the very large engineering test matrix is conducted in fission reactors with a limited number of tests in the high energy source to provide the parameters for interpolating to the fusion reactor spectrum. Lower flux and exposure experimentation in the 14 MeV d-t sources such as RTNS will provide complementary data on model materials to help establish the necessary correlations among the various test environments.

Table 2

Task Group Organization of the DMFE Materials and Radiation Effects Program

Alloy Development for Irradiation Performance
Damage Analysis and Fundamental Studies
Plasma-Material Interaction
Special Purpose Materials

Since the fusion reactor environment is outside the range of our experience and since the properties required by reactor design are not yet identified, the Alloy Development for Irradiation Performance Task Group is taking a broad approach in which four distinct classes of materials are investigated in parallel as illustrated below:

PATH A	AUSTENITIC ALLOYS
PATH B	HIGHER STRENGTH Fe-Ni-Cr ALLOYS
PATH C	REACTIVE/REFRACTORY METAL ALLOYS
PATH D	INNOVATIVE CONCEPTS

The Austenitic Alloys are modifications of 300 series stainless steels with composition and microstructure optimized for fusion applications. The principal components are given in Table 3. The

Table 3

Components of Austenitic Alloys

65% Iron
15% Nickel
15% Chromium

Small Additions of

Molybdenum
Silicon
Manganese
Titanium
Carbon

Path B alloys contain significantly larger amounts of nickel as shown in Table 4. Commercial materials in this composition range include the class of so-called Super Alloys. Many of these alloys offer potential for significantly higher strengths via precipitation reactions. These alloys have been developed for service in oxidizing atmospheres, which is not a requirement for first wall applications. By relaxing this requirement many exciting possibilities for alloy development occur. Path C Alloys include both the refractory and reactive metals as indicated in Table 5.

Table 4

Components of Higher Strength Fe-Ni-Cr Alloys

20–75% Nickel
Major Additions of Iron and Chromium
Small Additions of
Aluminum Titanium Niobium Molybdenum Carbon

Table 5

Composition Bases for Reactive/Refractory Metal Alloys

Titanium Zirconium
Vanadium Niobium

Possibilities are even broader in this class since so few commercial alloys based on these materials are available, but the details of the approach are less well defined at this time.

In summary, the Division of Magnetic Fusion Energy has established the planning and organizational basis for the development and testing of alloys for the intense high energy neutron

flux that will be encountered in the first wall of a fusion reactor. Because of the lack of fusion testing environment, most irradiations for obtaining engineering data will have to be carried out in fission reactors. A Key element of the program is the Li (d,n) neutron source which will allow relationships to be established between the fission and fusion environments. Since such a source supplies a broad spectrum of neutrons extending up to about 40 MeV, extensive cross section measurements are required in order for it to be used effectively to develop alloys for fusion reactors. Specific section needs are discussed by D. G. Doran in a separate paper at this conference.

REVIEW OF MAGNETIC FUSION ENERGY NEUTRON CROSS-SECTION NEEDS: NEUTRONICS VIEWPOINT*

Donald J. Dudziak and D. W. Muir
Theoretical Division
University of California
Los Alamos Scientific Laboratory, Los Alamos, New Mexico

INTRODUCTION

Our review is principally from a fusion device neutronics requirement viewpoint. That is, a cross-section user's perspective is taken, in the context of ongoing ERDA Division of Magnetic Fusion Energy (DMFE) projects and systems studies. We include then irradiation facilities as well as fusion reactors. Intense 2.2-pJ (14-MeV) neutron sources (the RTNS at Livermore and the INS at Los Alamos) present few unique cross-section needs beyond those already elicited by reactor studies and designs. However, the neutron emission spectra from high-energy sources such as 6.4-pJ (40-MeV) deuterons on lithium (D-Li) cause additional concerns regarding nuclear data, among neutronics personnel responsible for spectrum, intensity, dosimetry, and shielding calculations. Because of the paucity of hard information on the requirements for neutron cross-section data above 2.2 pJ (14 MeV), we can only point to a few potential problems and speculate on their resolution.

In the overall context of fusion nucleonic analysis most cross-section deficiencies lie in the energy range 2.2 pJ (14 Mev) and below. Perhaps it is appropriate here to sound a note of caution not to allow our concerns with cross sections above 2.2 pJ (14 MeV) to distort unduly the projected national programs in support of fusion reactor requirements. Without in any way denigrating the D-Li source's usefulness in the magnetic fusion energy (MFE) program, we want to bring to your attention the equally important cross-section needs in other MFE programs that compete for limited resources. Prominent if not uppermost in our minds during this Symposium should be an acute awareness of the need to set priorities among needs, all of which probably cannot be satisfied in the time frame of the current construction schedules for reactors (TFTR, TNS, EPR) and irradiation facilities. However, the minimum cross-section requirements for a D-Li facility can be satisfied if a well-planned program is initiated in a timely manner. One conclusion apparent for high-energy data is that we cannot affort to duplicate the measurement/model calculation/evaluation/multigroup processing cycle with the detail and completeness of fission reactor data in the ENDF system. Consequently, much

*Work performed under the auspices of the U. S. Energy Research and Development Administration.

greater dependence will heretofore need to be placed on nuclear model calculations, as opposed to experiments.

Given the primary thrust of this Symposium toward data above 2.2 pJ (14 MeV), perhaps this review serves best as a counterbalance to the centroid of the discussions to follow; i.e., to deal not only with new data requirements generated by current interest in D-Li sources, but also with the needs of conventional nucleonic studies (i.e., 2.2-pJ source calculations). First we will reference the many compilations of requirements, and summarize succinctly the current assessment of high priority needs. Then, following this we give typical methodology and results for quantitative data assessments of the Tokamak Fusion Test Reactor (TFTR) and a fusion Experimental Power Reactor (EPR). Finally, the last section summarizes some probings into data above 2.2 pJ, which have potential applications for D-Li irradiation facilities, D-Be medical therapy sources, and electronuclear fuel production facilities.

REVIEW OF "REQUEST LISTS"

Without attempting to trace the entire history of fusion-related neutron cross-section assessments, it is perhaps useful to describe the genesis of the most recent DMFE request,[1] as presented to the ERDA-NDC.

One of the earliest formal compilations of fusion requirements was a contribution from W. C. Gough, then of the AEC Division of Controlled Thermonuclear Research, to the USNDC Request List in 1971. In 1973 a formal CTR Subcommittee of the USNDC was appointed, and met 11-12 September 1973. From this and subsequent meetings (15 April 1974 and 27 October 1974) evolved a new request list. The basis for this list was, however, still qualitative judgments regarding materials of potential importance in what were yet undefined reactor designs and irradiation facilities. A natural tendency to "cover all bases" resulted in the usual lengthy list with priorities based upon the best consensus judgments possible at that time. Another very useful by-product of this Committee's efforts was a critical review[2] of then extant evaluations relevant to fusion programs.

At about the same time (ca. June 1975) that the USNDC-CTR Subcommittee was being disbanded in a reorganization of the basic USNDC structure, two significant programs were evolving. One was the gestation of conceptual designs for the TFTR and EPR's, which provided specific materials and design parameters upon which data needs could focus. Second was the initiation of quantitative data assessment programs revolving about these designs, and based upon a recently maturing sensitivity and uncertainty analysis methodology rooted in perturbation theory. The latter gave new and greater impetus to faltering efforts aimed at providing covariance data for ENDF evaluations.

After considerable experience with TFTR and EPR nuclear design calculations, it was possible to narrow the scope of near-term

cross-section requirements. The design studies provided firmer information on material selection as well as important nuclear responses (e.g., dpa and nuclear heating in superconducting toroidal field coils). Preliminary sensitivity studies provided quantitative information concerning partial cross sections and energy ranges of greatest importance for the identified materials and responses. Thus, a timely reconsideration of cross-section needs was held at the DMFE Blanket and Shield Workshop[3] in April 1976. At that time a decision on whether to proceed with a D-Li facility was still pending, so the Workshop report could only alert DMFE to potential cross-section needs in support of such a facility. However, in the area of nuclear data measurement needs for reactor design and system studies, the Neutronics Study Session report[3] included a concise list, with three priority categories. Table 1 is a reproduction of this measurement requirements list. In the approximately one year since this list was devised, continuing TFTR, EPR, and TNS (the next step) reactor design efforts have modified it somewhat, but in general it is still considered valid. Table 2 presents the specific modifications proposed by Twining in his 1 April 1977 presentation[1] to the ERDA-NDC. We would comment on Table 2 that if tungsten is in fact selected as the inner shield material for TNS, it will probably become a priority 1 material for evaluation and measurements.

SENSITIVITY AND UNCERTAINTY ANALYSIS

As an illustration of the application of perturbation methods to quantitative data assessment, we review here the results for two fusion reactors. The theory has been well described in the literature,[4-8] so we forego repeating its development.

Past experience in fission programs has amply demonstrated the need to focus nuclear data efforts early on a limited and achievable set of goals. Priorities must follow from needs which are well defined and substantiated in their importance. This implies performing assessments which are as quantitative as possible, prior to undertaking measurement and evaluation programs. Sensitivity and uncertainty analysis is one such method of quantification, especially where there is at least a conceptual definition of reactor designs. Longer range cross section needs, such as for commercial power reactor design studies, are more difficult to quantify. Thus, their definition relies heavily on good engineering judgment regarding materials and responses of importance. Equally vital is a broad insight into the quality of existing evaluated data and measurements. These latter characteristics are reflected in Table 1. Further judgments on fulfilling these cross section needs are pronounced in Ref. 9.

Table 1

ERDA Blanket/Shield Workshop Study Session on Neutronics:
Nuclear Data Measurements Needs

Priority I Recommendations (mainly for EPR (a))

a. neutron emission spectra (>5 angles, E_n' >500 keV)

^{7}Li $_{n,Nem}$ (Θ_n', E_n') Accuracy = 10%, E_n = 11, 14 MeV

^{11}B " " " "

C " " " "

Fe " " " "

b. gas production

$^{7}Li_{\sigma n,n't}(E_n)$ Accuracy = 10%, E_n = thres. - 15 MeV (1-MeV increments)

^{11}B $\sigma_{n,xp}(E_n)$&$\sigma_{n,x\alpha}(E_n)$ Accuracy = 15%, E_n = 14 MeV

^{12}C $\sigma_{n,x\alpha}(E_n)$ " "

^{56}Fe $\sigma_{n,xp}(E_n)$&$\sigma_{n,x\alpha}(E_n)$ " "

Priority II Recommendations (mainly for DEMO)

a. neutron emission spectra (>5 angles, E_n' >500 keV)

^{6}Li $\sigma_{n,Nem}(\theta_n', E_n')$ Accuracy = 10%, E_n = 11, 14 MeV

Al (b) " " "

Mo " " "

Ni " " "

Cr " " "

b. gas production

Al (b) $\sigma_{n,xp}(E_n)$ and $\sigma_{n,x\alpha}(E_n)$ Accuracy = 15%, E_n = 14 MeV

Mo " " " "

Ni " " " "

Cr " " " "

^{6}Li $\sigma_{n,t}(E_n)$ Accuracy = 15%, E_n = 1-15 MeV (a few energies)

Table 1 (cont)

Priority III Recommendations

a. neutron emission spectra for Be, Cu, Ti, V, Nb

b. gas production cross sections for Be, Cu, Ti, V, Nb

c. proton and alpha spectrum measurements (c) at E_n = 14 MeV for Fe, Ni, Cr

d. selected measurements on isotopic data (for nuclear heating and activation calculations) for important elements; e.g., Ni, Cr, and Mo.

(a) Although extensive use of Li is not envisioned for the EPR, it is sufficiently important to the CTR program that ^{7}Li measurements are listed under priority I.

(b) Al could be priority I if a FERF program is pursued.

(c) These measurements for additional materials such as Nb, V, and Mo might become important as DEMO designs evolve.

TABLE 2

New Materials Being Considered by TNS Designers

Material	Priority	Interest
Pb	1	low activation shield
W	2	high efficiency shield
^{10}B	2	shield material
Sn	2	magnet material
O	2	activation in atmosphere or coolant
N	2	activation in atmosphere or coolant

Tokamak Fusion Test Reactor (TFTR)

The first fusion reactor design effort with a potentially significant impact upon the CTR input to the USNDC (subsequently ERDA-NDC) request list was the TFTR. Accordingly, a quantitative data assessment for the TFTR nuclear analysis requirements was undertaken starting in 1974. Personnel dose equivalent (exposure) rate

from activation was identified as the principal response of interest. Material radiation heating or damage were eliminated because of the relatively low neutron source, and thus fluences involved; e.g., the maximum yearly neutron fluence on the first wall is approximately 1.4×10^{19} m^{-2}.

Activation in the TFTR occurs in the steel vessel walls, steel structure, lead-borated-polyethylene shielding, and copper coils. These same materials affect the transport of neutrons in the system, and hence provide sensitivities of activation rates to all the material partial cross sections. A quite detailed sensitivity analysis to total and some partial cross sections of these materials was performed.[5] Covariance matrices were estimated for 23 of these reaction cross sections that appeared potentially important to activation calculations. Using these matrices, an uncertainty analysis was performed. Table 3 (from Ref. 5) shows the total uncertainty in two selected activation rates [R_1 = $^{54}Fe(n,p)^{54}Mn$, and R_{10} = $^{65}Cu(n,p)^{65}Ni$] expected to contribute significantly to dose-equivalent rates. Data in this table were then used for uncertainty analysis of dose equivalent from the induced activity present at various times after assumed operating histories. Additional uncertainties in the activation cross sections themselves were also incorporated. The complete theory and calculational procedures are given in Ref. 5, so suffice it to say here that the resulting dose-equivalent uncertainties must be compared to allowable design uncertainties. A maximum allowable uncertainty (one standard deviation) of 50% was assumed for dose equivalent, E, from all activation sources in the reactor. Table 4 shown the final results*, where all cross-section uncertainties combined give an uncertainty in exposure rate (and hence dose equivalent) of $\simeq$ 41%. Thus, the "bottom line" for the TFTR is that anticipated cross-section errors should not be unacceptable from the viewpoint of exposure rate during required access after reactor shutdown. Such "negative" results may be unsatisfying to cross-section measurers and evaluators, but they warm the hearts of programmatic funding agencies.

Tokamak Experimental Power Reactor (EPR)

Having found no fertile ground at the TFTR for new cross-section measurement requests, attention was then directed to the EPR, a reactor considered for operation in the mid-to-late 1980's. The ANL conceptual design[10] was adopted for the assessment. It is generically similar to the other EPR designs and to subsequent TNS conceptual designs, with many common cross-section requirements. Sensitivity analyses have been performed for the selected EPR, and a multigroup covariance data library has been produced for the pertinent materials. Uncertainty evaluations for EPR materials are

---

*Even these results are conservative in the sense that many of the error estimates in Table 2 are upper limits; cf. column 2 of Table 3.

Table 3

Predicted Uncertainties of Selected Activation Rates [$R_1 = {}^{54}Fe(n,p)^{54}Mn$, and $R_{10} = {}^{65}Cu(n,p)^{65}Ni$] Due to Estimated Errors in Cross Sections

"Perturbed" Transport Cross Sections	Error Estimates: COV[a] or $\left(\frac{\Delta\Sigma}{\Sigma}\right)_{max}$ (%)	Maximum Integral Sensitivity $\hat{S}$ and Predicted Activation Rate Uncertainty $\Delta R/R$ for R_1: $\hat{S}$ (% per %)	for R_1: $\frac{\Delta R}{R}$ or $\left(\frac{\Delta R}{R}\right)_{max}$ (%)	for R_{10}: $\hat{S}$ (% per %)	for R_{10}: $\frac{\Delta R}{R}$ or $\left(\frac{\Delta R}{R}\right)_{max}$ (%)
C	25	0.87	21.8	0.66	16.5
C($n,n'3\alpha$)	COV	---	2.4	---	2.2
Pb	25	1.52	38.0	1.12	28.0
Pb(n, 2n)	COV	---	18.3	---	14.8
O	25	0.47	11.8	0.36	9.0
H	2	1.08	2.2	0.73	1.5
Fe	25	0.70	17.5	0.93	23.3
Fe(n, tot)	COV	---	2.2	---	3.2
Fe(n, abs)	COV	---	0.71	---	1.7
Fe(n,n'cont)	COV	---	4.4	---	7.4
Fe(n, elas)	COV	---	2.5	---	3.7
Fe(n, inel)	COV	---	3.5	---	6.7
Fe(n, 2n)	COV	---	1.2	---	3.6
Cr	25	0.20	5.0	0.25	6.3
Ni	25	0.12	3.0	0.17	4.3
Mn	25	0.021	0.53	0.027	0.68
Al	25	0.45	11.3	0.62	15.5
Cu	25	0.039	0.98	2.05	51.3
Cu(n, elas)	COV	---	0.12	---	5.0
Cu(n, inel)	COV	---	0.13	---	6.8
Cu(n, 2n)	COV	---	0.04	---	9.6
Cu(n, tot)	COV	---	0.12	---	5.1
Cu(n, abs)	COV	---	0.04	---	16.8

[a] COV means Complete Covariance Matrix.

Table 4

Predicted Absolute Uncertainties in Calculated Radiation Exposure Rates Due to All Cross-Section Uncertainties—TFTR Design with Steel Structure

Radionuclide, i	$T_{1/2}$	Production Mechanism	Production Rate, R_i (Atoms per Fusion Neutron)	Exposure Rate $E_i \pm \Delta E_i$ After			
				1 Pulse and 2 h		1 yr and 1 day	
				E_i (rem/h)	ΔE_i (rem/h)	E_i (rem/h)	ΔE_i (rem/h)
^{54}Mn	313 days	^{54}Fe(n, p)	1.35 E-3	7.05 E-4	3.63 E-4	4.38 E-1	2.26 E-1
^{54}Mn	313 days	^{55}Mn$(n, 2n)$	4.80 E-4	2.49 E-4	1.10 E-4	1.72 E-1	7.60 E-2
^{56}Mn	2.6 h	^{56}Fe(n, p)	3.32 E-3	5.11 E+0	2.28 E+0	6.31 E-3	2.82 E-3
^{58}Co	71 days	^{58}Ni(n, p)	2.30 E-3	6.16 E-3	2.92 E-3	1.67 E+0	7.92 E-1
^{62}Cu	9.8 min	^{63}Cu$(n, 2n)$	9.89 E-3	6.94 E-1	4.64 E-2	$<E$-10	$<E$-10
^{60}Co	5.2 yr	^{63}Cu(n, α)	1.03 E-3	2.30 E-4	1.61 E-4	2.19 E-1	1.53 E-1
^{64}Cu	12.7 h	^{65}Cu$(n, 2n)$	9.55 E-3	6.66 E-1	4.29 E-1	4.26 E-1	2.75 E-1
^{65}Ni	2.6 h	^{65}Cu(n, p)	2.69 E-4	1.53 E-1	1.13 E-1	1.91 E-4	1.41 E-4
Total exposure rate (unshielded): $E = \sum_i E_i$, ΔE according to Eq. (35)				6.53 rem/h	3.22 rem/h	2.90 rem/h	1.20 rem/h
Total personnel exposure rate (shielded): $(E^P \pm \Delta E^P) = 3.45 \times 10^{-3}\ (E \pm \Delta E)$				22.5 mrem/h	11.1 mrem/h	10.0 mrem/h	4.14 mrem/h

incomplete, but a brief description of work now in progress is given in Ref. 11. Also, target accuracies for the selected responses are being formulated in order to have a basis of comparison and acceptability for the uncertainties.

Several critical nucleonic responses were selected and the response functions were reduced to multigroup form. Specifically examined were neutron and gamma-ray kerma in the toroidal field (TF) coils and Mylar insulation, displacement and transmutation rates in the copper matrix of the TF coils, and activation of the outboard dewar. In general, these responses must be determined after neutron flux attenuations of approximately 10^6, so potentially large sensitivities to various reaction cross-sections can be immediately anticipated. Although target accuracies have not been completely determined, we do know that a realistic goal is to predice radiation damage and heating in TF coils within at least 10-20%. This contrasts with normal fission reactor shielding problems, where radiation damage is only of concern at moderate attenuation (i.e., higher flux levels than in the TF coils). At deep penetrations in fission reactors the only target accuracies are for personnel exposure rate, where "factor of two" errors are acceptable.

Fusion reactor technology, in particular the EPR and TNS designs, has many implications to the cross-section technology efforts worldwide. First, it has introduced new materials and reactions of importance for nuclear analysis. Secondly, for materials and reactions also of previous interest in fission programs, new neutron energy ranges are now emphasized by the fusion requirements. Not only are new materials (e.g., Cu, W, Pb mortars), reactions, and energy ranges brought to the fore by the EPR, but also the sensitivity-based data assessment must address new high-energy responses and secondary energy/angle distributions.[8]

Application of sensitivity analysis to the EPR is described in detail elsewhere,[6-8] so for our present purpose we illustrate its application in only one sample case. We choose one of the more critical responses, nuclear heating in the inner TF coil, where by "inner" we mean the portion of the torus toward the major axis. This portion has special thinner shielding in order to keep the magnetic field in the plasma as high as possible. Figure 1 shows a one-dimensional traverse along a minor radius through the inner shield.

Transport calculations for forward and adjoint flux determination were performed in S_8-P_3, using ENDF-IV cross sections, by the ONETRAN code.[12] Sensitivities were computed with the SENSIT-1D code,[13] the sensitivity and uncertainty analysis computational module of the LASS system.[6] Sensitivity profiles, P_{Σ_i}, were computed for neutron and gamma-ray interactions, as well as for gamma-ray production.

For our sample case -- the total neutron and gamma-ray heating in the inner TF coil -- Table 5 shows the integral sensitivities,

$$S_\Sigma = \sum_i P_{\Sigma_i},$$

Table 5

Neutron Integral Sensitivity, S_{Σ_T}, of the Inner TFC Nuclear Heating Resonse

To the Total Cross Sections of Stainless Steel Components

Component	Region					Total
	6-8	12	14	16	23	
Cr	-0.601	-0.212	-0.188	-0.150	-0.014	-1.168
Mn	-0.103	-0.034	-0.031	-0.026	-0.005	-0.202
Fe	-2.480	-0.868	-0.767	-0.602	-0.058	-4.775
Ni	-0.526	-0.182	-0.164	-0.140	-0.010	-1.032
Mo	-0.091	-0.033	-0.030	-0.024	-0.008	-0.187
TOTAL	-3.801	-1.330	-1.180	-0.944	-0.097	-7.375

to stainless steel (SS) total cross sections. From this table we find the region(s) in Fig. 1 which contribute most to the sensitivity. From Table 5 it is clear that the SS blanket regions 6-8 are the most important contributors to the integral sensitivity. Also, it can be seen that Fe is the largest contributor to the integral sensitivity, regardless of which region is considered.

Narrowing our example further we show in Table 6 the component sensitivities for Fe in regions 6-8. Here the sensitivity has been divided into the gain and loss terms

$$P_{\chi_i} = P_{\chi^{tot}_{i,loss}} + P_{\chi^{scat}_{i,gain}}$$

Most of the net integral sensitivity is clearly due to scattering. An anomolous appearing result in Table 6 warrants some discussions; viz, the negative loss term for Σ_a. Because of the idiosyncracies of the transport codes, the (n,2n) and (n,3n) reactions appear as a negative component in the absorption and total cross sections, and as a positive component in the scattering matrix. Thus, by using the transport code cross-section sets for scoping sensitivity analyses, one introduces an artifice in the results. This artifice is also seen in the fact that the scattering loss term, computed by summing diagonals of the scattering matrix, is larger than the total loss term. In fusion reactor sensitivity analysis we often observe this effect, in particular when the sensitivity in the top (approximately 2.2 p.f, or 14 MeV) group is manifestly dominant. Such scoping studies do, however, help narrow the field of partial cross

Table 6

Partial and Net Neutron Integral Sensitivities of the Inner TFC Nuclear Heating Response To the Fe Component in Stainless Steel Region 6-8

Neutron Cross Section, Σ_x	Integral Loss Term	Integral Gain Term	Integral Net, S_{Σ_x}
Σ_a	- 0.17	---	0.17
Σ_a	12.98	10.33	-2.65
Σ_a	12.81	10.33	-2.48
Σ_a	---	0.014	0.014

sections required for detailed sensitivity analysis. The latter, in turn, narrow the number of covariance evaluations required for the final uncertainty analysis. A representative sensitivity profile is shown in Fig. 2, where the sensitivity of the TF coil heating to the Fe total scattering cross section was selected.* Notice the high sensitivity in the top two groups, with a subsidary peak below 160 fJ (1 MeV). This general shape is characteristic of all the sensitivity profiles, for all responses and all materials pertaining to this EPR design. It immediately allows us to delete from more than casual concern the cross-section data from approximately 0.5 to 1.9 pJ (3.1 to 12 MeV). Referring again to Table 6, the low sensitivity to the gamma-ray production cross section, $\sigma_{(n,\gamma)}$, is caused by the relatively short mean free path of the gamma rays in SS. However, the sensitivity increases monotonically with proximity to the TF coil.

Turning now to the B_4C component of the shield, Table 7 presents integral sensitivity results for B_4C comparable to those of Table 5 for SS. Here we see that the sensitivity is highest for the outboard regions, where the neutron spectrum is softened somewhat. However, the spatial variation is not nearly as strong as for SS. Also, the ^{10}B component of the B_4C does not overwhelmingly dominate the sensitivity as does, for example, Fe in SS. As would be expected, the net integral sensitivity is in all cases negative, because almost any interaction decreases the probability of a neutron's transmission to the TF coil.

---

*As an aside, it is worth noting that these data also give insight into the sensitivity of the response to design alterations in these regions.

Table 7

Neutron Integral Sensitivity, S_{Σ_T}, of the Inner TFC Nuclear Heating Response to the Total Cross Sections of B_4C Components

Component	Region				Total
	11	13	15	17	
^{10}B	-0.221	-0.268	-0.375	-0.543	-1.409
C	-0.166	-0.190	-0.243	-0.196	-0.796
TOTAL	-0.387	-0.459	-0.618	-0.739	-2.206

Sensitivity profiles for the B and C cross sections show the same general shape as those for Fe, with a peak in the top group and another peak in the 16-160 fJ (100 keV-1 MeV) region. For ^{10}B, however, the sensitivity to the total cross section is of comparable magnitude in the two peaks, and the lower peak is much broader. This high sensitivity at the lower energy peak is due in part to the neutron spectrum, which shows this same peak at all positions in the shield regions 8-10. One can conclude that even though neutrons in the approximately 160 fJ (1 MeV) energy region have lower transmission probabilities to the TF coil, they are so prevalent in the spectrum as to be a major contributor to the flux reaching the TF coil. A more quantitative explanation to this phenomenon can be gleaned from the χ and ψ functionals in Ref. 14.

Table 8 shows the individual cross-section integral loss and gain terms for the ^{10}B in region 17, the region with highest sensitivity. Here the integral loss terms for Σ_a is positive because the $^{10}B(n,2n)$ cross section is very small.

DATA REQUIREMENTS FROM 2.4 TO 6.4 pJ (15 to 40 MeV)

The neutron spectrum to be produced by the proposed D-Li source is bell-shaped, with half of the neutrons being generated above 2.4 pJ (15 MeV). With a few exceptions, such as accelerator shielding and the use of D-Be neutron sources for radiation therapy, up to now there has not been much technological activity that required neutronics data in this high-energy range. This lack of demand, coupled with the lack of widely available monoenergetic neutron sources, has severely restricted the amount of data now available in the 2.4 to 6.4 pJ (15 to 40 MeV) range. Because of resource limitations, it is important that activities intended to remedy this situation be concentrated where the need is greatest.

Table 8

Partial and Net Neutron Integral Sensitivities of the Inner TFC Nuclear Heating Response to Cross Sections of the ^{10}B Component in B_4C Region 17

Cross Section, Σ_x	Integral Loss Term	Integral Gain Term	Integral Net, S_{Σ_x}
Σ_a	0.41	----	-0.41
Σ_s	0.81	0.68	-0.13
Σ_T	1.22	0.68	-0.54
$\Sigma_{(n\to\gamma)}$	----	0.0009	0.0009

With regard to neutron energy, 40% of the output of a 40-MeV D-Li neutron source will be in the 2.4 to 4.0 pJ (15 to 25 MeV) range, with only about 10% above 4.0 pJ (25 MeV).[15] In view of the fact that the important response functions for neutron-induced damage are only weakly energy-dependent in the high-energy region, it seems likely that considerably more damage will be produced by neutrons in the 2.4 to 4.0 pJ (15 to 25 MeV) range than by neutrons in the region above 4.0 pJ (25 MeV).

To discuss the relative importance of particular nuclides and data types, we must first describe the neutronics activities which will probably be conducted in support of a D-Li radiation damage facility.

The first neutronics task that comes to mind is facility design. Since the total source strength will exceed 10^{15} neutrons per second, biological shielding and facility activation will require considerable analysis. Since the D-Li neutron source energy spectrum is somewhat harder than a fusion-reactor spectrum, it will be important also to evaluate the utility of various reflector and moderator materials for spectrum tailoring. By this means one may wish, for example, to reduce the ratio of helium-production to displacement-damage to realistic reactor levels.

On the time scale of actual facility operation, one will want to design particular experiments so that, for example, one experiment does not unduly "shadow" experiments behind it. Also, it may be important to predict the activation induced in samples or apparatus by the intense fluxes of thermal and fast neutrons.

Finally, the analysis of materials irradiation experimental data will require detailed calculations of the neutron flux distributions and energy spectra. Dosimetry foils will no doubt be used to establish absolute flux levels at key locations, but calculations will be required to provide information at intermediate spatial locations and to provide detailed energy spectra.

The data required for these calculations are summarized in Table 9. For the reasons stated above, the most important neutron energies are from 2.4 to 4.0 pJ (15 to 25 MeV). At the present time, it appears to us that most of the needed data can be supplied without the development of major new nuclear model codes and without the construction of new neutron source facilities. Valuable contributions to this data supply effort can be made using existing statistical-preequilibrium nuclear model codes. The results of these calculations should be tested against selected differential measurements using existing monoenergetic neutron sources and integral measurements (in a D-Li type spectrum) of a few important quantities, such as total helium production in candidate structural materials.

Table 9

Neutronics Data Required Above 2.4 pJ (15 Mev)

Material Function	Examples	Cross Sections and Other Data Required
Facility structure	Si, O, Fe, Al	Activation, total
Spectrum tailoring	Be, C, Pb, U	Secondary spectra, angular distributions
Exposure samples	Fe, Ni, Cr, Nb, Mo, V, Be, C	Nonelastic (for damage), He production (for damage), activation, transport
Dosimetry materials	Various thresholds and half-lives	Excitation functions

REFERENCES

1. B. G. Twining, "DMFE Nuclear Data Needs," presented to ERDA-NDC on 1 April 1977.

2. "The Status of Neutron-Induced Nuclear Data for Controlled Thermonuclear Research Applications: *Critical Reviews of Current Evaluations*," U. S. Nuclear Data Committee report USNDC-CTR-1 (1974). (D. Steiner, coordinator).

3. J. R. Powell, J. A. Fillo, B. G. Twining, and J. J. Dorning (eds.), Proc. of the *Magnetic Fusion Energy Blanket and Shield* Workshop - A Technical Assessment, Upton, NY, 29 Mar - 2 Apr 1976, ERDA-76/117/1, CONF-760343.

4. David Leon Prezbindowski, "An Analysis of the Effects of Cross Section Uncertainties on the *Multitable* S_N *Solution of Neutron* Transport Through Air," Doctoral Dissertation, Purdue University (*January* 1968).

5. S. A. W. Gerstl, Donald J. Dudziak, and D. W. Muir, "Cross-Section Sensitivity and Uncertainty Analysis with Application to a Fusion Reactor," Nucl. Sci. Eng. 62, (1), 137 (1977).

6. Donald J. Dudziak, S. A. W. Gerstl, and D. W. Muir, "Application of the Sensitivity and Uncertainty Analysis System LASS to Fusion Reactor Nucleonics," Proc. Specialists' Meeting on Differential and Integral Nuclear Data Requirements for Shielding Calculations, Vienna, Austria, 12-16 October 1976.

7. E. L. Simmons, S. A. W. Gerstl, and Donald J. Dudziak, "Cross-Section Sensitivities of Nucleonic Characteristics in a Fusion Experimental Power Reactor (EPR)," Los Alamos Scientific Laboratory report (to be published).

8. S. A. W. Gerstl, "Sensitivity Profiles for Secondary Energy and Angular Distributions," Proc. Fifth International Conference on Reactor Shielding, Knoxville, TN, USA, 18-23 April 1977.

9. Donald J. Dudziak, "An Assessment of Nucleonic Methods and Data for Fusion Reactors," Proc. Sec. Topical Meeting Technol. of Controlled Nucl. Fusion, Richland, WA, 21-23 September 1976, CONF-760935-P3, p. 819.

10. M. A. Abdou, "Nuclear Design of the Blanket/Shield System for a Tokamak Experimental Power Reactor," Nucl. Technol., 29, 7 (1976).

11. D. W. Muir, "Data Covariance Estimation Methods for Sensitivity-Based Data Assessment," Trans. Am. Nucl. 484, 26 (1977).

12. T. R. Hill, "ONETRAN: A Discrete Ordinates Finite Element Code for the Solution of the One-Dimensional Multigroup Transport Equation," Los Alamos Scientific Laboratory report LA-5990-MS (1975).

13. S. A. W. Gerstl, "SENSIT-1D, A FORTRAN Code to Perform Cross-Section and Design Sensitivity Analyses in One-Dimensional Geometries," Los Alamos Scientific Laboratory report (to be published).

14. S. A. W. Gerstl, "The Application of Perturbation Methods to Shield and Blanket Design Sensitivity Analyses," Argonne National Laboratory report AP/CTR/TM-28 (1974).

15. M. J. Saltmarsh and R. E. Worsham, Editors, "INGRID: A Proposal for an Intense Neutron Generator for Radiation-Induced Damage Studies in the CTR Materials Program," Oak Ridge National Laboratory report ORNL-TM-5233 (January 1976).

Region No.	Region Material	Radius (cm)
		0.0
1	PLASMA	
		210.0
2	VACUUM	
		240.0
3	1st WALL S. S.	
		241.0
4	1st WALL S. S.	
		242.0
5	1st WALL S. S.	
		244.0
6	BLANKET S. S.	
		254.0
7	BLANKET S. S.	
		264.0
8	BLANKET S. S.	
		272.0
9	VACUUM	
		273.0
10	S. S.	
		276.0
11	B_4C	
		281.0
12	S. S.	
		291.0
13	B_4C	
		297.0
14	S. S.	
		307.0
15	B_4C	
		315.0
16	S. S.	
		325.0
17	B_4C	
		333.0
18	S. S.	
		335.0
19	TFC DEWAR S. S.	
		337.0
20	VACUUM, TUBING, ETC.	
		339.8
21	THERMAL SHIELD	
		340.7
22	VACUUM	
		343.2
23	TFC BOBBIN (S. S.)	
		345.7
24	TFC	
		350.7
25	TFC	
		355.7
26	TFC	
		360.7
27	TFC	
		416.2
28	SUPPORT CYLINDER	
		440.0
29	OHC	
		465.0

Fig. 1. One-dimensional model of the EPR inner blanket/shield.

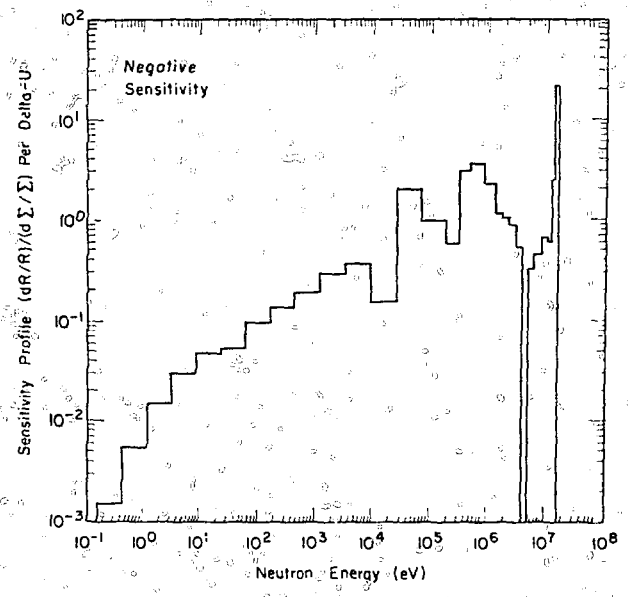

Fig. 2. Sensitivity of the maximum local nuclear heating in the TF coils to all scattering cross-sections of Fe.

SESSION II

INTENSE HIGH ENERGY NEUTRON SOURCES
AND THEIR CHARACTERISTICS

Chairman: G. A. Bartholomew, CRNL, Chalk River

Intense Fast Neutron Source Reactions

M.A. Lone
Atomic Energy of Canada Limited, Chalk River Nuclear Laboratories, Chalk River, Ontario, Canada K0J 1J0

Abstract

A brief review is given of the characteristics and experimental techniques pertaining to charged-particle-induced neutron source reactions for neutron energies ≤ 40 MeV.

INTRODUCTION

The need for intense sources of high-energy neutrons for radiotherapy and materials radiation damage studies has led to a renewed interest in the evaluation of the neutron spectral distributions and yields from charged particle induced reactions. The neutron sources for these applications need not be monoenergetic provided the average neutron energies are high enough (>10 MeV).

Monoenergetic neutron sources are, however, needed for measurements of the associated nuclear data required, e.g., the neutron-induced charged-particle spectra and cross sections, and the differential elastic and inelastic neutron-scattering cross sections.

In this review we compare the characteristics of various charged particle reactions capable of giving the desired neutron intensities with present-day technology.

REQUIREMENTS

Fusion Materials Program - Radiation damage is expected to be more severe in the materials used in the first wall of a fusion reactor than of a fission reactor. In the D-T fusion reaction presently favoured, the energy of the primary neutrons produced is 14.1 MeV, although, because of the backward scattering and moderation of these neutrons, the walls surrounding the plasma will see a neutron spectrum from 14.1 MeV down to thermal range. Production of hydrogen and helium by nuclear reactions can produce swelling, blistering and embrittlement of the wall material. Also, atomic displacements due to recoil, and production of new elements by transmutation, may affect the mechanical properties of the materials.

The neutron fluence requirements for this program have recently been discussed in several reports[1-3]. These range from 10^{16} n•cm^{-2} for surface studies to >10^{22} n•cm^{-2} for studies of mechanical properties. Thus a high-energy neutron-source intensity of ≥10^{14} n•s^{-1} is desired.

Cancer Therapy - Recent clinical trials[4-5] have indicated significant advantages of high energy neutrons over photons in the treatment of tumors but the optimum neutron energy for the treatment of cancer is not yet known. The biological effects of neutrons depend[6] on the absorbed dose, and the radiation quality which determines the relative biological effectiveness (RBE) of the radiation. The dose is defined[7] as the energy imparted by ionizing radiation to the matter in a volume element, divided by the mass in that volume element (the special unit of absorbed dose is the rad and the SI unit is the gray, 1 Gy = 1 $J \cdot kg^{-1}$ = 100 rad). The radiation quality can be related to the neutron energy spectrum or to the linear energy transfer (LET) spectrum.

It is generally accepted[4,6,8,9] that the neutron energies should be high enough to provide 50% of the dose at a depth of 10 cm in human tissue. Also the source should be able to provide a dose of 30-50 rad per minute (0.3 to 0.5 $Gy \cdot min^{-1}$) at a distance of 125 cm from the target. These considerations imply that a source strength of $\gtrsim 1.6 \times 10^{12}$ $n \cdot s^{-1} \cdot sr^{-1}$ is required.

Physics - The materials radiation damage and the radiotherapy programs will require basic neutron nuclear data for the verification of techniques, the calibration of instruments, and computer simulations. These nuclear data, e.g., neutron-induced charged-particle cross sections and spectra, differential elastic and inelastic neutron scattering cross sections, can best be measured with monoenergetic high energy neutrons. Thus it is important to study characteristics of the nuclear reactions which can be used to produce monoenergetic neutrons.

CRITERIA AND EXPERIMENTAL TECHNIQUES

The neutron sources required for the three programs outlined above differ in details, but a source satisfying one need is likely to be useful for others. Table 1 gives a brief summary of the information needed to evaluate the usefulness of a source for a particular program. The most fundamental information needed is a knowledge of the absolute spectral and angular distributions of the neutrons. From these distributions one can calculate other properties.

Neutron Spectral Distributions and Yield

Good Geometry - The time-of-flight (T.O.F.) technique is the best method for measuring neutron spectral distributions. This technique requires a well-defined geometry, a pulsed neutron source and a detector with fast time response. With this technique there is clean separation in time between γ-rays and neutrons reaching the detector from the target; however, if there is an appreciable γ-background from the room, then pulse shape discrimination is essential in order to separate γ-ray and neutron events. This

Table 1

Criteria for Evaluation of Neutron Source Reactions

Use	Quantity of Interest	Environment	Method and Detectors
Materials Radiation Damage	-Neutron fluence -Spectral distributions -Angular distributions -Associated γ-ray yield and spectral distribution	-Poor geometry -High neutron intensities -Long exposure times	-Foil activation
Radiobiology and Cancer Therapy	-Neutron dose -Gamma ray dose -Radiation quality ie. neutron energy spectrum etc. -Angular distributions -Depth dose distributions -Isodose distributions	-In situ eg. in a tissue equivalent phantom -Collimated neutron beam	-Ionization chambers proportional counters or calorimeters
Physics	-Neutron yield -Spectral distributions -Angular distributions -Energy resolution -Associated γ-ray yield and spectral distributions	-Well defined geometry -Controlled operating conditions	-Time-of-flight technique -Scintillators -Proton recoil telescopes -Fission chambers

limits the choice of the detectors to NE213, NE218, NE230 scintillators[10], stilbene crystals, proton recoil detectors[11,12] or fission chambers.

Background due to scattered neutrons and γ-rays can in principle be reduced by using elaborate collimators. However, if the source emits neutrons ranging in energy from the kinematic maximum down to the thermal range, as is usually the case with thick targets, the collimators can perturb the spectral distributions due to in-scattering of the high energy neutrons. The blocking technique which has recently been used by the CRNL[13] and the ORNL[14] groups can, in principle, eliminate such problems and give a reliable measure of the room background.

Figure 1 shows the set-up used by the ORNL[14] group at the ORIC Cyclotron for measuring the thick-target neutron yields from Be and Li targets with 40 MeV deuterons. The room background is measured by blocking the direct neutron beam with a block placed midway in the flight path. This location of the block minimizes its effect on the background events reaching the room walls, the floor and the beam tubes. The CRNL group[13] used a 60 cm long iron-masonite block (50% iron). The block was sufficiently long that the secondary radiation from it was essentially isotropic and of energies below the detector threshold; consequently its effect on the detector was negligible. For the direct measurements the block was moved well away from the flight path in order to eliminate small-angle scattering events reaching the detector.

The time-of-flight spectra[13] shown in fig. 2, from the ^{9}Be+p reaction at 18 MeV, demonstrate the effectiveness of this blocking technique in eliminating the background events from the time-of-flight spectra. Figure 2(a) shows the difference of the T.O.F. spectra of γ-ray events (gated with the γ-ray peak in the time-to-amplitude pulse-height spectra of the pulse-shape-discriminator circuit, figure 2) recorded with block out and block in. The γ-ray events above channel 650 are from (n,n'γ) reactions in materials in the vicinity of the detector. This demonstrates the importance of using pulse-shape discrimination.

The spectrum (d) in figure 2 is the difference between the dead-time-corrected spectrum (b) taken with the block out and spectrum (c) taken with the block in (note the change in scale). The detector threshold was set at 300 keV neutron energy.

The detector response function is needed to convert the neutron time-of-flight spectra to the neutron spectral distributions. Several computer codes are available[15-18] for calculating a scintillator response function. In general the calculated response functions are accurate[16,19] to within ±10% for energies up to 30 MeV.

For better accuracy the response function must be measured. Monoenergetic neutrons from the reactions T(p,n)^{3}He, T(d,n)^{4}He and D(d,n)^{3}He can be used to determine the relative response functions of the detectors. The relative detector efficiency as a function of the neutron energy can be measured by changing the projectile energy or by using the well-known[20-22] angular distributions of the

outgoing neutrons from these reactions. The difficulty in determining the target thickness often creates uncertainties in calculating the absolute efficiencies. This can, in principle, be overcome by calibrating at lower energies with the known cross section[23] of the $^{7}Li(p,n)^{7}Be$ reaction or the $H(n,n)H$ reaction[24].

Scintillation detectors and proton-recoil telescopes can not be used for neutron energies below a few hundred keV. For measurements of these neutrons, particularly in the presence of very high-energy neutrons, new detectors will have to be developed. A promising detector for such applications is a gas-scintillation fission chamber[25] using ^{235}U foils. The fission cross section[26] of ^{235}U is shown in fig. 3. It is known[26] to an accuracy of better than 3% for energies up to 8 MeV. A fission chamber[27] using N_2 gas as scintillator can provide a timing resolution of about 2 ns.

Poor Geometry and DC Sources - If a time-of-flight technique is not practical then the neutron spectral distributions can be determined by unfolding[27-29] the pulse-height spectra recorded with scintillators or by using threshold detectors[14,30-34], a technique which involves foil activation. A list of nuclei and reactions[14,31-34] for foil activation is given in Table 2. The excitation functions for these reactions are known[14,31-34] for neutron energies up to ~20 MeV. For higher energies the excitation functions for some of the reactions have to be calculated.

The foil-activation technique involves calculating the activation produced by assuming the neutron spectral distribution and folding it with the excitation function. Simultaneous activation of foils with different thresholds and excitation functions helps

Table 2

Nuclear Reactions for Foil Activation*

Reaction	Effective Threshold (MeV)	E_γ (MeV)	Branching ratio %	Half-life (days)	References
$^{54}Fe(n,p)^{56}Mn$	1.5	0.835	100	303	31,33
$^{58}Ni(n,p)^{58}Co$	1.0	0.810	99	71.3	14,33
$^{59}Co(n,2n)^{58}Co$	11.0	0.810	99	71.3	14,31,33
$^{89}Y(n,2n)^{88}Y$	11.6	0.898	91	108	31,32
$^{93}Nb(n,2n)^{92m}Nb$	9.5	0.934	99	10.16	14
$^{169}Tm(n,2n)^{168}Tm$	8.1	0.820	88	85	31,32

* *Only reactions with long lived products and large γ-ray branching ratios are listed. For others see references 31, 32 and 33.*

in determining a convergent solution for the spectral distribution. This method is inherently not very accurate (though it is often the only practical one in-situ) for measurements of the spectral distributions. The activation method does give an accurate measure[14] of the neutron fluence provided the spectral distributions are known.

Dose in Tissue - In biological work the dose in tissue is measured[6,35,36] with tissue-equivalent (TE) ionization chambers. These are integral measurements and the relative effects of different parts of the spectral distributions cannot be determined except by introducing absorbers in the beam. Such absorbers affect the spectral distributions which must be measured or determined by Monte Carlo calculations.

SOURCE REACTIONS

Monoenergetic Neutrons

The best known reactions for monoenergetic neutron sources are $T(p,n)^3He$, $T(d,n)^4He$, $D(d,n)^3He$ and $^7Li(p,n)^7Be$. The cross sections and Q values for the first three reactions are shown in fig. 4. With projectile energies up to 16 MeV the neutrons under different reaction angles cover the energy region up to 33.5 MeV. The continuous neutron background, e.g., from break-up processes, is energetically well separated.

Reviews in this field were made more than fourteen years ago by Goldberg[37] and Brolley and Fowler[38].

$T(p,n)^3He$ - A comprehensive evaluation of the data available up to December 1972 for $E_p \leq 10$ MeV is given by Liskien and Paulson[22]. More recent measurements were done by McDaniels et al.[20] and Allas et al.[39], the latter extending to 32.8 MeV proton energy.

For proton energies up to 16 MeV the absolute uncertainties quoted[20] for the zero-degree differential cross sections are ±2.3%. For the angular distributions the relative uncertainties quoted[20] are about ±2.8%.

One difficulty in the use of this reaction is target preparation and handling. Both solid (T implanted in metallic foils) and gas targets are in common use. Solid targets, tritium in Ti or Zr foils, are commercially available. Several papers have described the techniques for preparing metallic[40,41] and gas targets[42].

$T(d,n)^4He$ - This reaction has been thoroughly investigated by McDaniels et al.[21] at deuteron energies ranging from 5 to 15.7 MeV. The uncertainty in the zero-degree cross sections is about ±3.4% and in the relative angular distributions about ±3.8%. Brill et al.[43] have also studied this reaction at deuteron energies between 8 and 17 MeV. Their zero-degree cross-section data agree within errors with the data of McDaniels et al.[21]. A comprehensive

evaluation of the data for deuteron energy up to 10 MeV is given by Liskien and Paulsen[22].

Because of the high Q-value (17.59 MeV) and large cross section at 120 keV this reaction is extensively used to make intense sources of 14 MeV neutrons. The maximum neutron flux attainable[1, 44,48] at present with solid TiT targets is $\lesssim 10^{12}$ $n \cdot s^{-1} \cdot sr^{-1}$. This limitation is due to the target heating which results in thermal dissociation and migration of tritium. Also molecular and triatomic components of the deuteron beam produce[46-48] rapid destruction of the targets due to sputtering and radiation damage. These effects limit the target half-life and the maximum flux attainable. A comprehensive review of the existing and proposed (d,t) neutron generator systems is given in reference 1.

<u>$D(d,n)^3He$</u> - An evaluation of the data for deuteron energy up to 10 MeV is given by Liskien and Paulsen[22]. At higher deuteron energies this reaction has been investigated by Weaver et al.[49] (up to 20 MeV), Drosg and Drake[50] (up to 17 MeV), Hegland et al.[51] (17.5 MeV), Van Oers et al.[52] (25.3 MeV) and Roy et al.[53] (83 MeV).

<u>$^7Li(p,n)^7Be$</u> - This reaction is widely used as a source of monoenergetic neutrons in the keV to MeV neutron energy range. At proton energies above 2.4 MeV the first excited state of ^7Be at 0.43 MeV is excited producing a second group of neutrons. At higher proton energies break-up reactions and the excitation of higher ^7Be states produce lower-energy neutrons (fig. 5)[54].

Gibbons and Newson[55] had given a comprehensive review of the data available up to 1960. More recently Liskien and Paulsen[56] have evaluated the data on differential cross sections and the 0° cross section ratio of the $^7Li(p,n_1)^7Be$ and $^7Li(p,n_0)^7Be$ neutron groups for proton energies up to 7 MeV. Poppe et al.[54] have recently measured these cross sections over the angular range 3.5° to 159° and incident bombarding energies of 4.2 to 26 MeV. Their results are in excellent agreement with the recommended values of Liskien and Paulsen[23]. Table 3 gives the cross sections and the ratio of n_1 to n_0 neutrons measured by Poppe et al.

For applications where the neutron energy resolution is not critical the $^7Li(p,n)^7Be$ reaction can be a very useful source of high-energy neutrons since solid ^7Li targets are relatively easy to make and the forward-angle laboratory cross section approaches ~30 $mb \cdot sr^{-1}$ at $E_p = 29$ MeV.

<u>Low Energy Neutrons from Deuteron Breakup</u> - The ^3He and ^4He nuclei do not have low-lying excited states; therefore, the emitted neutrons are strictly monoenergetic. However, above certain bombarding energies neutrons of lower energies appear (fig. 5) as a result of tertiary and higher processes, e.g., T(p,pn)D, T(d,pn)T, D(d,pn)D and T(p,p2n)H, etc. The neutrons from these break-up reactions are primarily[56] in the direction of motion of the incident particle. Lefevre et al.[56] have studied the spectral and angular distributions of neutrons from deuteron break-up from D, T

Table 3

Laboratory differential cross section at 3.5° for the $^7Li(p,n)^7Be$ (0.0 MeV + 0.43 MeV) reaction and the laboratory ratio of n_1 to n_0 neutrons as a function of bombarding energy [54]

E_p (MeV)	$\sigma_0 + \sigma_1$ (mb/sr)	R
15.1	7.38	0.30
15.9	8.2	0.28
16.9	9.7	0.26
17.9	11.1	0.27
18.9	12.6	0.27
19.9	14.3	0.27
20.9	15.9	0.27
21.9	18.2	0.29
22.9	20.1	0.30
23.9	22.4	0.30
24.9	25.5	0.32
25.9	26.9	0.35

and ^4He targets at deuteron energies near 9 MeV. For application of these sources with non-time-of-flight techniques more data is needed on the cross sections, angular distributions and energy spectra of neutrons from break-up reactions at other deuteron energies.

Protons on D, Be and other Light Elements - Monoenergetic neutron beams with energies above 30 MeV and intrinsic energy spreads of 1 to 2 MeV can be produced by (p,n) reactions on thin D, T, Li or Be targets at proton energies above 32 MeV. Several groups[57-61] have measured the 0° cross sections from these reactions at proton energies ranging from 30 MeV to 64 MeV. Figure 6 shows the 0° cross sections[31] for the high-energy peak ($\sigma_{n_1} + \sigma_{n_0}$) in the $^7Li(p,n)^7Be$ reaction. Figure 7 shows a comparison of the high-energy portion of the neutron spectra observed[58] at 0° from D, T, ^7Li and ^9Be targets bombarded by 30 MeV and 50 MeV protons. At these energies the cleanest spectra are produced with a tritium gas target. At both energies a ^9Be target gives the worst results whereas the ^7Li target gives considerably better results. Batty et al.[58] have discussed the relative merits of various target materials. Jurgerman et al.[60] have also investigated the $^{12}C(p,n)^{13}N$ and $^{27}Al(p,n)^{27}Si$ reactions at 30, 40 and 50 MeV proton energies.

Continuous-Spectrum Neutrons

Intense beams of fast neutrons with a continuous spectrum are produced by bombarding thick targets of light elements in particular Li or Be with protons or deuterons. Under identical conditions the spectra from targets of different elements are similar in shape and change smoothly with change in the projectile energy.

A general feature of the spectra is a decrease in the yield and the mean neutron energy with increase in the charge of the target nucleus and the neutron emission angle[62,63]. Gamma rays are also produced in these reactions. The ratio of the γ-ray yield to the neutron yield increases with the charge of the target nucleus[62]. So far the γ-ray spectral distributions have not been investigated systematically.

Proton Reactions - The Q-values for the $^{9}Be(p,n)^{9}B$, $^{7}Li(p,n)^{7}Be$ and $^{6}Li(p,n)^{6}Be$ reactions are -1.9, -1.7 and -5.1 MeV respectively; however thresholds for several three-body break-up reactions lie below 10 MeV[64]. Thus with thick Be or Li targets these reactions produce a considerable number of low energy neutrons. At proton energies up to about 30 MeV the spectral distributions show[13,65-69] essentially a monotonic decrease with increasing neutron energy. Figure 8 shows the neutron spectral distributions observed[13] at 0° from the $^{9}Be+p$ reaction at 14.8, 18 and 23 MeV. Figure 9 shows similar distributions observed[68] at proton energies of 25 to 55 MeV. At proton energies above 30 MeV there is a broad peak in the spectrum at a neutron energy of about 20 MeV.

Similar behaviour is seen in the neutron spectra from the Li+p reaction. Figure 10 shows the 0° spectral distributions[13] from the $^{7}Li+p$ reaction at 14.8, 18 and 23 MeV. At higher proton energies a broad peak appears in the spectrum at a neutron energy of about 20 MeV, e.g. at $E_p = 65$ MeV the neutron spectral distributions observed at 0° from the Li target look quite similar to those from the Be target[67].

Figure 11 gives the 0° neutron yield from thick Be and Li targets as a function of the proton energy. The data points on the dotted curves give intensities of neutrons with $E_n > 0.3$ MeV, whereas the data points on the solid curves give intensities for neutrons of energies above 5 MeV. The data point for 65 MeV proton energy gives the neutron intensity for $E_n > 9.1$ MeV[67]. These curves show that there are a considerable number of neutrons produced at energies below 5 MeV[13,64,65,66]. At proton energies below 34 MeV the neutron yield from thick Be targets is higher than that from the Li target while above this energy the yields from the two targets are comparable.

As shown in figs. 8 and 9 the Li targets produce larger neutron fluxes towards the kinematic energy limits than do the Be targets. This behaviour is also observed at 35 MeV[67].

The average neutron energy and the total neutron yield from the Be and Li targets decrease with increasing angle. This is seen in fig. 12, which shows the results[68] from the Be+p reaction.

Figure 13 gives the average neutron energy at 0° as a function of the proton energy. The solid curves are for $E_n > 5$ MeV[68] and the dotted curves for $E_n > 0.3$ MeV[13,64].

Deuteron Reactions - The Q-values for the $^9Be(d,n)^{10}B$, $^7Li(d,n)^8Be$ and the $^6Li(d,n)^7Be$ reactions are +4.4, +15.0 and +3.38 MeV. Also the thresholds for several three-body break-up reactions are below 10 MeV deuteron energy[64]. In general these reactions, plus the process that involves the deuteron break-up due to the long range Coulomb field, and the neutron decay to the excited states in the residual nucleus, give rise to a general continuum in the neutron spectra.

Thick-target neutron spectra produced by deuterons are characterized[13,14,63,64] by two components, a broad peak centred at $E_n \approx 0.4\ E_d$, where E_d is the deuteron energy, and an underlying continuum which starts at very low neutron energies and falls off almost exponentially with neutron energy. The intensity of the broad peak decreases rapidly with angle while that of the underlying continuum varies much more slowly. Relatively few measurements[13,14,63,64,65] have been made of the low-energy component of the neutron spectra. The primary difficulty is pulse overlap in time-of-flight measurements carried out with high-frequency accelerators. The broad peak has been studied by several groups[13,14,30,31,36,38,59,62-65,67,70-73].

Figure 14 from Daruga and Matusevich[63] and figure 15 from Meulders et al.[62] show neutron spectra from Be and several higher Z targets bombarded with deuterons. These show that at each deuteron energy the neutron yield decreases with increasing Z. Figure 16 shows the data of Lone et al.[13] from thick Li and Be targets for deuteron energies of 14.8, 18 and 23 MeV and for comparison the results of several other groups in the same energy range. Figure 17 shows the results of Saltmarsh et al.[14] from Be bombarded with 40 MeV deuterons.

Figure 18 shows the angular distribution of the neutron yield from thick Be and Li targets observed at deuteron energies of 14.8, 18 and 23 MeV[13]. At higher deuteron energies the angular distributions are peaked even more in the forward direction[63]. The average energy of the neutron spectra decreases with increasing angle. This decrease is mainly due to the decrease in the intensity of the broad peak at $\sim 0.4\ E_d$.

Figure 19 gives the 0° neutron yield as a function of the deuteron energy for thick Be and Li targets. The scale for the Li curve is on the right hand side. It is evident that the yields for the two targets are similar. The average energies of the spectra from the two targets are comparable, i.e., $\bar{E}_n \approx 0.4\ E_d$ for $E_n > 2$ MeV.

The angular distribution and the energy dependence of this broad peak in the neutron spectra are consistent with deuteron stripping theory[74,75]. Pictorially the stripping process takes place when an incoming deuteron grazes the edge of the nucleus, and one of the two nucleons strikes the nucleus and is stripped off,

while the other misses and continues with almost the velocity of the deuteron. Thus the most probable energy of the outgoing nucleon is 1/2 E_d. The stripping theory as formulated by Serber[76] predicts that for high-energy deuterons the cross section for neutron production varies very slowly with the target mass ($\sigma \approx A^{1/3}$), the full width at half maximum, FWHM, of the neutron energy spread, ΔE, is equal to 2.23 $(E_d\ (MeV))^{1/2}$ and the FWHM of the angular resolution, $\Delta\theta_{1/2}$, is equal to 2.38 $(E_d\ (MeV))^{-1/2}$. August et al.[75] have recently employed this theory to predict the shape of the neutron energy spectra for thick targets.

Another process which predicts strongly forward-peaked neutron emission from deuteron bombardment is deuteron break-up-in-flight due to the Coulomb field near the target nucleus[76]. In this case the deuteron never comes within range of the nucleon force. The cross section is proportional to Z^2 where Z is the target atomic number. For smaller Z the cross section for this process is predicted[76] to be much lower than that for the stripping process[75]. The deuteron break-up gives rise to a broad neutron energy spectrum, but the emission is strongly forward peaked[76].

Gamma-Ray Production - The spectral distributions of the γ-rays have not been measured from thick targets bombarded with protons or deuterons. Meulders et al.[62] have made an estimate of the γ-ray yields from the Be+d reactions by assuming a 10% mean efficiency for a 5.1 cm diameter and 2 cm thick NE111 plastic scintillator. The ratio between the γ-ray and neutron yields was estimated to be 11%, 5% and 2.5% at E_d = 16, 33 and 50 MeV respectively.

DOSE RATES

With Deuterons - Figure 20 shows the values[77] of dose rates 1 m down stream from thick targets of Be, Li and D, per microampere of incident deuterons or protons. The solid line through the Be+d data points corresponds to an $E_d^{2.7}$ relationship suggested by Parnell et al.[78] and the dotted line to an $E_d^{2.99}$ dependence suggested by the NRL group[36,75]. The data points attributed to Lone et al.[13] were calculated by Cross[77] from the observed spectral distributions[13]. Below 25 MeV there is a spread of a factor of about 1.5 among different data points, more recent data tending to give higher values.

For Li-d and D-d reactions only the 0° neutron yields are given on the right-hand side in figure 20. This was necessary because the dose rates at high deuteron energies have not been measured and the necessary data needed to convert the high-energy yields to doses are uncertain. For comparison with the Be+d data the solid line of the Be+d data is also drawn through the Li+d points. This comparison shows that the difference in the outputs of the Be and Li targets is small.

The yield from deuterium gas targets[49], shown by the dashed line on the right hand side of fig. 20, exceeds that from Be, the difference increasing with energy. Up to $E_d = 25$ MeV at least, the differences in dose rates would be somewhat greater than those shown for yields, since D+d neutron have a harder spectrum. Deuterium in the form of D_2O gives only about 55% of the dose rates from Be at 16 MeV[78].

With Protons - For proton reactions fewer thick target data are available. The slope of the dose rate vs. E_p curve for the Li+p reaction (fig. 20) is the same as that for the Be+d reaction; the slope of the dose rate vs. E_p curve for the Be+p reaction is less steep. At proton energies below ~50 MeV the dose rate from Be targets is higher than that from the Li target. Dose rates from protons are 4 to 7 times lower than from deuterons at the same energy.

HALF-DOSE DEPTH

Quam et al.[87] have recently reported the depths for 50% tissue-Kerma-rate measured with neutrons from proton bombardment of thick Li and Be targets and deuteron on Be. These measurements were made using a 0.1 cm^3 (TE) ion chamber filled with air and immersed in a TE fluid composed of 64.9% water, 7.5% urea, 25.8% glycerol and 1.8% ethylene-glycol by weight. The measured density of the fluid was 1.07 g/cm^3.

Table 4 gives the values of half-dose depths measured, by several groups[67,87,88], with neutrons from thick Li and Be targets bombarded with protons and deuterons at various energies. The data for the 10 cm × 10 cm field size are plotted in fig. 21. At energies up to 30 MeV, neutrons from the deuteron reactions are more penetrating (higher half-dose depth) than those from the proton reactions, whereas above 30 MeV neutrons from the p+Li reaction are more penetrating. For proton energies between 30 and 60 MeV, neutrons from the p+Be reaction are less penetrating in tissue than those from the p+Li reaction.

SUMMARY

For calibration of neutron spectrometers in the energy range 10 to 40 MeV data accurate to a few percent are available on monoenergetic neutron sources. However for measurements of the activation cross sections more information is needed on the angular and spectral distributions of the accompanying low-energy neutrons as a function of the charged-particle energy.

As a source of intense neutrons the deuteron reactions on thick Li and Be targets produce higher yields than do the proton reactions. As shown in figures 11 and 19 the yield of neutrons of energies greater than 2 MeV from the deuteron reactions at 0° is

TABLE 4

Half-Dose Depths in Tissue Equivalent Materials

Reaction	E(MeV)	SSD (cm)	Field Size (cm)	Depth of 50% Dose (g·cm⁻²)	Reference
d + Be	16	116	10 × 10	[illegible].8	87,88
d + Be	21.5	150	10 × 10	10.2	88
d + Be	35	125	10 × 10	11.8*	82,88
d + Be	35	351	15 × 15	11.0	67
d + Be	50	140	10 × 10	13.8	88
d + Li	35	351	15 × 15	12.0	67
p + Be	26	125	15 × 15	10.2	82
p + Be**	26	125	15 × 15	11.9	82
p + Be	35	351	15 × 15	10.5	67
p + Be	35	125	10 × 10	13.4	82
p + Be**	35	125	10 × 10	13.3	82
p + Be	45	125	10 × 10	13.1	82
p + Be**	45	125	10 × 10	15.3	82
p + Be	65	351	15 × 15	14.75	67
p + Li	26	125	10 × 10	10.3	82
p + Li	35	125	10 × 10	12.5	82
p + Li	35	351	15 × 15	11.0	67
p + Li	45	125	10 × 10	14.1	82
p + Li	65	351	15 × 15	16.5	67

* *The value given by Smith et al.[88] is 12.8. The value 11.8 is quoted by Quinn et al.[82].*

** *A 6 cm polyethylene filter of density 0.92 g·cm⁻³ was inserted in the beam.*

about a factor of 10 greater than the yield from the proton reactions at the same projectile energy. For each reaction under identical operating conditions the neutron yields from the Li and Be targets are comparable.

More data on the neutron angular distributions are needed in order to estimate the total neutron output from these reactions. At comparable energies neutrons from the proton reactions exhibit

broader angular distributions than those from the deuteron reactions.

The dose rates of neutrons, see Figure 20, from the deuteron reactions on thick Be or Li targets are a factor of about 5 higher than those from the proton reactions at the same projectile energy. However, at $E_p = 25\ MeV$ dose rates from the proton reactions are essentially the same as the dose rates from the deuteron reactions at energy E_p. Under identical conditions the dose rates from Li and Be targets are almost equal.

The depth dose characteristics of the neutrons from the deuteron and the proton reactions are essentially the same at an energy of 25 MeV. Above this energy and, in particular, above 50 MeV the proton reactions produce more penetrating (higher half dose depth) neutrons than those from the deuteron reactions. At $E_p = 2\ E_d$ the protons produce more penetrating neutrons.

At energies below 25 MeV, at least, the proton reactions give relatively more low energy, $E_n < 2\ MeV$, neutrons than do the deuteron reactions (see Figure 19). For energies above 25 MeV the relative yields of the low energy neutrons have not been investigated thus far.

REFERENCES

1. Proceedings of the International Conference on Radiation Test Facilities for the CTR Surface and Materials Program. Report ANL/CTR 75-4 (1975).
2. E.A. Fuzmin, A.A. Sepelbin, N.I. Sidorov, K.I. Latrov and G.B. Yankov. IAEA Symposium on the Use of Nuclear Data in Science and Technology, Paris (1973). Report INDC (CCP) 37/4/ IAEA TP 73 32) (1973).
3. HRPID An Intense Neutron Generator for Radiation Induced Damage Studies in the CTR Materials Program (Ed. M.J. Saltmarsh and P.E. Wareham) ORNL TM 5233.
4. M. Catterall, I. Sutherland and D.F. Bewley, Brit. Medical Journal 2, 651 (1975).
5. M. Catterall, Brit. J. Radiol., 49, 201 (1976).
6. J.J. Broerse in Proceedings of the International Specialists Symposium on Neutron Standards and Applications (1977) p.106.
7. International Commission on Radiation Units and Measurements, Report 19 (1971).
8. J.J. Broerse, G.W. Barendsen, J.F. Cats [illegible] and J. Scherfel. International Symposium on Radiobiological Research Needed for the Improvement of Radiotherapy, Vienna, 1976. Report IAEA SM 212/31.
9. R. G.L. Morgan, Fast Neutron Therapy, Cyclotron 1977, (1977) p.362.
10. Nuclear Enterprises Inc., 935 Terminal Way, San Carlos, California 94070, U.S.A.
11. J. Schooky, J. Cierpka, P. Rocky, D. Grischel and R. Keepers, Nuclear Cross Sections and Technology, NBS 425 V1, 273 (1975).

[illegible] J.R. Stern in Proceedings of the International Specialists Symposium on Neutron Standards and Applications, (1977) p.54.

[illegible] M.A. Lone, A.A. Alexander, C.F. Popham, A.J. Ferguson, J.S. Fraser, A.B. McDonald and W.K. Schneider, Nucl. Instr. & Meth. (1977)

[illegible] M.J. Saltmarsh, C.A. Lindemann, C.F. Popham and L.C. Stokes, Nucl. Instr. & Meth. (1977)

[illegible] E.J. Finn, ORNL-TM-[illegible], Lawrence Radiation Laboratory (1968) and Errata

[illegible] S.T. Thornton and J.F. Smith, Nucl. Instr. & Meth. 96, 551 (1971)

[illegible] H.W. McNaughton, W.S. Flood, J.F. Brady, and J.J. Dillmann, Nucl. Instr. & Meth. 139, 41 (1976)

[illegible] F.J. Toman and V.C. Rogers, ORNL-[illegible] (1968)

[illegible] J.A. Grodzins, M. Hurwitz, C.A. Hilley, J.L. Lerner and F.R. Schwartz, Nuclear Instrumentation and Techniques, NP-[illegible], [illegible] (1975)

70. D.E. McNamara, H. Brugger, J.C. Hopkins and J.D. Sherman, Phys. Rev. [illegible], 1501 (1971)

71. D.E. McNamara, H. Brugger, J.C. Hopkins and J.D. Sherman, Phys. Rev. C7, 1137 (1973)

72. H. Liskien and A. Paulsen, Nucl. Data Tables A11, 569 (1972)

73. H. Liskien and A. Paulsen, Atomic Data and Nucl. Data Tables 15, 57 (1975)

74. C.A. Hilley in Proceedings of the International Specialists Symposium on Neutron Standards and Applications (1977) p.47.

75. D. Ward and F.B. Walter, Atomic Energy of Canada Limited Report, AECL-5504, 30 (1976)

76. See Proceedings of the International Specialists Symposium on Neutron Standards and Applications (1977), p.156.

77. V.V. Verbinski, W.P. Burrus, T.A. Love, W. Zobel, N.W. Hill and R. Textor, Nucl. Instr. & Meth. 65, 8 (1968)

78. Ju. A. Lazarev et al., At. Energ. 40, 113 (1976)

79. Proceedings of a Seminar Workshop on a Review of Evaluation Energy Spectra Unfolding, D.T. Tinkey, Oak Ridge, April, 1977, Report ORNL/RSIC-40

80. F. Schmidt, R. Münzel, Report KFK 1293 (1970)

81. D.F. McChesney, F.A. Van Dongendonck and T.R. Yates, Livermore Laboratory Report, UCRL-5054 (1976)

82. R.P. Baybourd, J.S. Coleman, F.J. Fox-Wood, J.S. Mellitz, R. Lewis, R.R. Kalata and F.A. Hardcastle, Phys. Rev. C13, 451 (1976)

83. R.A. Meyers, ORNL-R-[illegible] Isotopic Data, Brookhaven National Laboratory Report BNL-NCS-50446 (1975)

84. F. Hertse and R.W.W. Avizo, Jr., Physica 39, 555 (1968)

85. H.H. Barschall, in Proceedings of the International Specialists Symposium on Neutron Standards and Applications (1977) p.342.

36. R.B. Theus, R.O. Bondelid, F.H. Attix, L.S. August, P. Shapiro, R.E. Surratt and C.C. Rogers, Cancer 34, 17 (1974).
37. M.D. Goldberg, Progress in Fast Neutron Physics, (G.C. Phillips, J.B. Marion and R.R. Risser Ed.) University of Chicago Press, Chicago (1963) p.3.
38. J.E. Brolley Jr., and J.L. Fowler, Fast Neutron Physics (J.B. Marion and J.L. Fowler Ed.) VI Interscience Publishers Inc., New York (1960) p.73.
39. R.G. Allas, L.A. Beach, R.O. Bondelid, E.M. Diener, E.L. Petersen, J.M. Lambert, P.A. Treado and I. Slaus, Phys. Rev. C9, 787 (1974).
40. R.D. McCormick and J.D. McCormack, Nucl. Inst. & Meth. 13, 147 (1961).
41. J. Pivare, Technische, Universität Dresden 21, H4, 694 (1972).
42. A.B.M.G. Mostafa, Nucl. Instr. & Meth. 125, 493 (1975).
43. O.D. Brill, V.M. Pankratov, V.P. Rudahov and B.V. Rybakov, At. Energ. (USSR) 16, 141 (1964); transl. Soviet J. At. Energy 16, 161 (1964).
44. H.H. Barschall, Nuclear Structure Study with Neutrons, Plenum Press, London (1974) p.289.
45. J.H. Ormrod, Can. J. Phys. 52, 1971 (1974).
46. .. Cranberg, Proceedings of the International Conference on the Interactions of Neutrons with Nuclei, Lowell(1976) p.926.
47. G. Stengl and H. Vonach, Nucl. Instr. & Meth. 126, 235 (1975).
48. R. Booth, UCRL 70138, UCRL 74285; also J.C. Davis, J.E. Osher, R. Booth and C.M. Logan, UCRL-78053 (1976).
49. K.A. Weaver, J.D. Anderson, H.H. Barschall and J.C. Davis, Nucl. Sci. & Eng. 52, 35 (1973); URRL-51310 and Addendum.
50. M. Drosg and D.M. Drake, LA-5732-MS (1974).
51. P.M. Heqland, R.E. Brown, Bull. Am. Phys. Soc. 18, 1381 (1973).
52. W.T.H. Van Oers and K.W. Brockman, Jr., Nucl. Phys. 48, 625 (1963).
53. M. Roy, D. Bachelier, M. Bernas, J.L. Boyard, I. Brissaud, C. Detraz, P. Radvanyi and M. Sowinski, Phys. Letters 29B, 95 (1969).
54. C.H. Poppe, J.D. Anderson, J.C. Davis, S.M. Grimes and C. Wong, Phys. Rev. C14, 438 (1976) and references therein.
55. J.H. Gibbons and H.W. Newson, Fast Neutron Physics (J.B. Marion and J.L. Fowler, Ed.) VI, Interscience Publishers Inc., New York (1960) 133.
56. H.W. Lefevre, R.R. Borchers and C.H. Poppe, Phys. Rev. 128, 1328 (1962).
57. A. Langford, P.H. Bowden, G.C. Cox, P.E. Dolley, R.A.J. Riddle and M.J.M. Saltmarsh, Nucl. Phys. A99, 246 (1967).
58. C.J. Batty, B.E. Bonner, A.I. Kilvington, C. Tschalar, L.E. Williams and A.S. Clough, Nucl. Instr. & Meth. 68, 273 (1969).
59. C.J. Batty, B.E. Bonner, E. Friedman, C. Tschalar and L.E. Williams, Nucl. Phys. A120, 297 (1968).
60. J.A. Jungerman, F.P. Brady, W.J. Knox, J. Montogomery, M.R. McGie, J.L. Romero and Y. Ishizaki, Nucl. Instr. & Meth. 94, 421 (1971) and addendum. See ref. 61.

61. M.W. McNaughton, N.S.P. King, F.P. Brady, J.L. Romero and T.S. Subramanian, Nucl. Instr. & Meth. 130, 555 (1975).
62. J.P. Meulders, P. Leleux, P.C. Macq and C. Pirart, Phys. Med. Biol. 20, 235 (1975).
63. V.K. Daruga, E.S. Matusevich and Kh. Narziev, Atomnaya Energia, 33, 934 (1972).
M.A. Lone, Cross-Sections and Yields for High Energy Neutron Source Reactions, NBS Report p.5 (1977).

65. F.T. Kuchnir, L.S. Skaggs, A.J. Elwyn, F.P. Mooring and N.A. Figorio, Cyclotron-1972, Ed. J.J. Burgerjon and J. Strathdee (Am. Inst. of Phys., New York, 1972) p.638.
66. C.E. Nelson, F.O. Purser, P. Von Behren and H.W. Newson, Cont. PR2/L4. Proceedings of the International Conference on the Interaction of Neutrons with Nuclei, CONF-760715-P1, VII, 1476 (1976).
67. H.I. Amols, J.F. Dicello, M. Awschalom, L. Coulson, S.W. Johnsen and R.B. Theus, Med. Phys. (to be published). Also FERMILAB-Pub-76/102-EXP.
68. S.W. Johnsen, N.F. Peck, G.O. Hendry, J.L. Tom, W.M. Quam and P.H. Heintz, Brit. J. of Radiology, 49, 974 (1976). Also Med. Phys. 4, 2 (1977).
69. M.C. Scott, J. Nucl. Energy 25, 405 (1971).
70. B.L. Cohen and C.E. Falk, Phys. Rev. 84, 173 (1951).
71. C.J. Parnell, Brit. Journ. of Radiology 45, 452 (1972.
72. A.N. Goland, C.L. Snead Jr., D.M. Parkin and R.B. Theus, IEE Trans. on Nucl. Science NS-22, 1776 (1975).
73. E. Tochilin and G.D. Kohler, Health Physics, Pergamon Press 1, 332 (1958).
74. R. Serber, Phys. Rev. 72, 1008 (1947).
75. L.S. August, F.H. Attix, G.H. Berling, P. Shapiro and R.B. Theus, Phys. Med. Biol. 21, 931 (1976).
76. S.M. Dancoff, Phys. Rev. 72, 1017 (1947).
77. W.G. Cross, (CRNL private communication).
78. C.J. Parnell, G.D. Oliver, P.R. Almond and J.B. Smathers, Phys. Med. Biol. 17, 429 (1972).
79. R.R. Almond, J.B. Smathers, G.D. Oliver Jr., E.B. Hranitzky and K. Routt, Rad. Res. 54, 24 (1973).
80. L.J. Goodman, S.A. Marino and J.T. Brennan, Uses of Cyclotrons in Chemistry, Metallurgy and Biology, Ed. C.B. Amplett, London, Butterworth, p.209.
81. G.H. Harrison, Eur. J. Cancer 10, 201 (1974).
82. W.M. Quam, S.W. Johnson, G.E. Hendry, J.L. Tom, P.J. Heinz and R.B. Theus, Phys. Med. Biol. (in press).
83. R.H. Howell and H.H. Barschall, Phys. Med. Biol. 21, 643 (1976).
84. J.P. Meulders, P. Leleux, P.C. Macq, C. Pirart and S. Valenduc, Nucl. Instr. & Meth. 126, 81 (1975).
85. C.J. Parnell, B.C. Page and M.A. Chaudhri, Brit. J. Radiology 44, 63 (1971).
86. A.R. Smith, P.R. Almond, J.B. Smathers and V.A. Otte, Radiology 113, 187 (1974).

87. D.K. Bewley, B. Cullen, S.B. Field, S.H. Hornsey, B.C. Page and R.J. Berry, Brit. J. Radiology 49, 360 (1976).
88. A.R. Smith, P.R. Almond, J.B. Smathers, V.A. Otte, F.H. Attix, R.B. Theus, P. Woolten, H. Bichsel, J. Eenmaa, D. Williams, D.K. Bewley and C.J. Parnell, Med. Phys. 2, 195 (1975).
89. Neutron Cross Sections V II Curves. BNL-325. D.I. Garber and R.R. Kinsey, National Neutron Cross Section Center, BNL (1976).
90. J.C. Hopkins, Nuclear Physics Studies with Fast Neutrons; a survey report LA-DC-11039 (1969).
91. J.L. Romero, F.P. Brady and J.A. Jungerman, Nucl. Inst. & Meth. 134, 537 (1976).

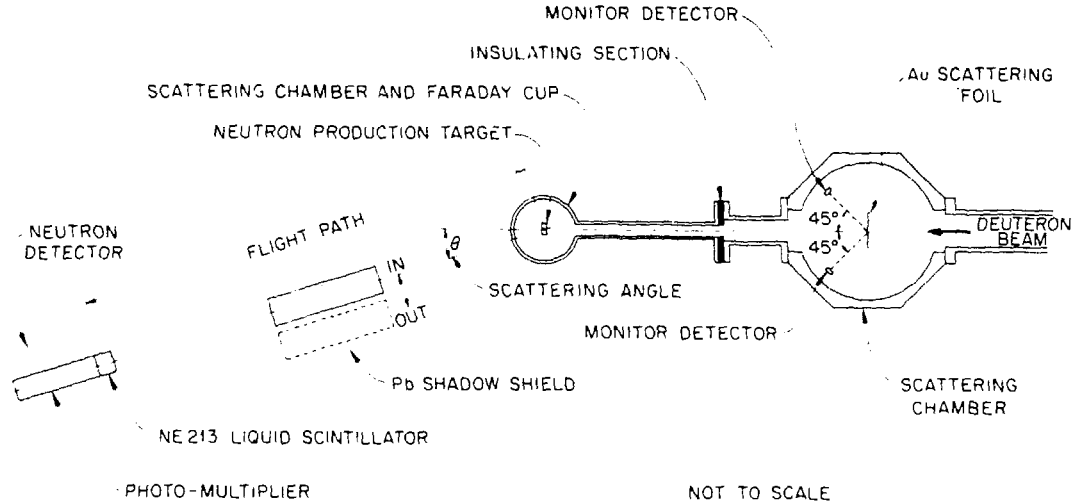

Fig. 1. Layout of the time-of-flight apparatus used by the TRNL group.

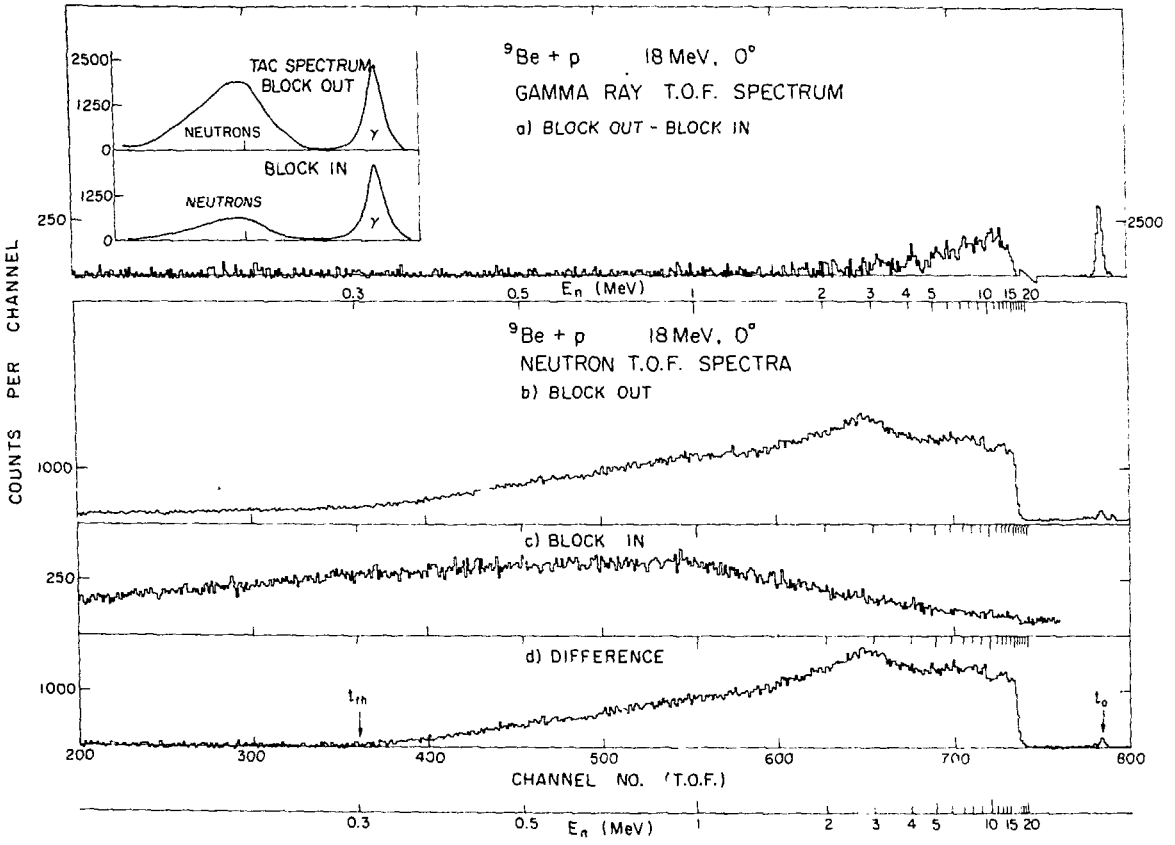

Fig. 2. Time-of-flight spectra; (a) γ-rays; (b) neutrons with no iron-magnetite block in the flight path; (c) with the block in place; and (d) the difference between (b) and (c).

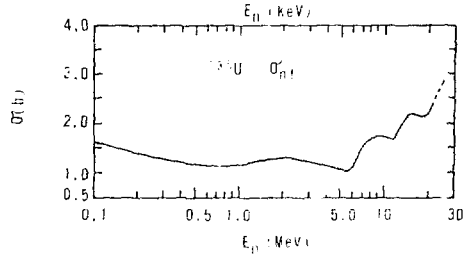

Fig. [illegible] [illegible] cross sections[illegible].

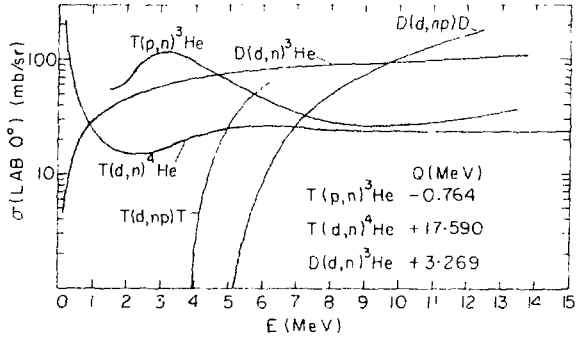

Fig. 4. Cross sections for neutron production [illegible] various reactions[illegible].

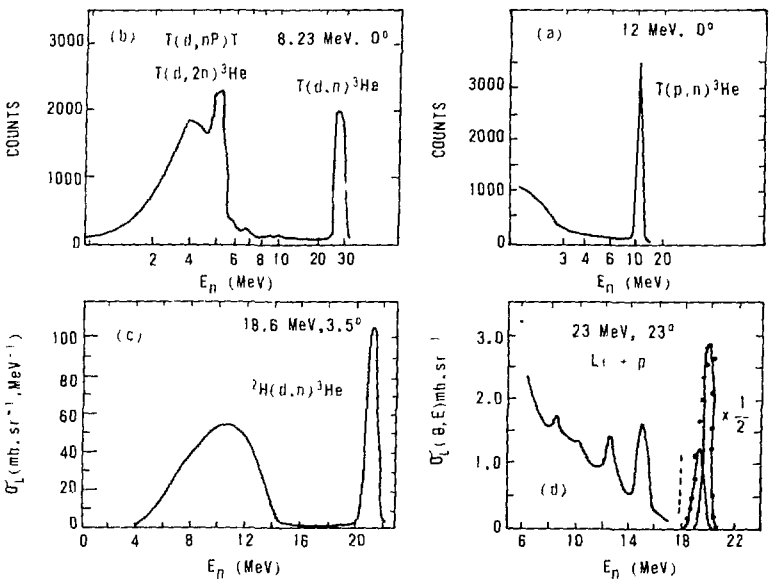

Fig. 5. Neutron spectral distributions from various reactions: (a) ref. 20; (b) ref. 56; (c) ref. 49 and (d) ref. 54.

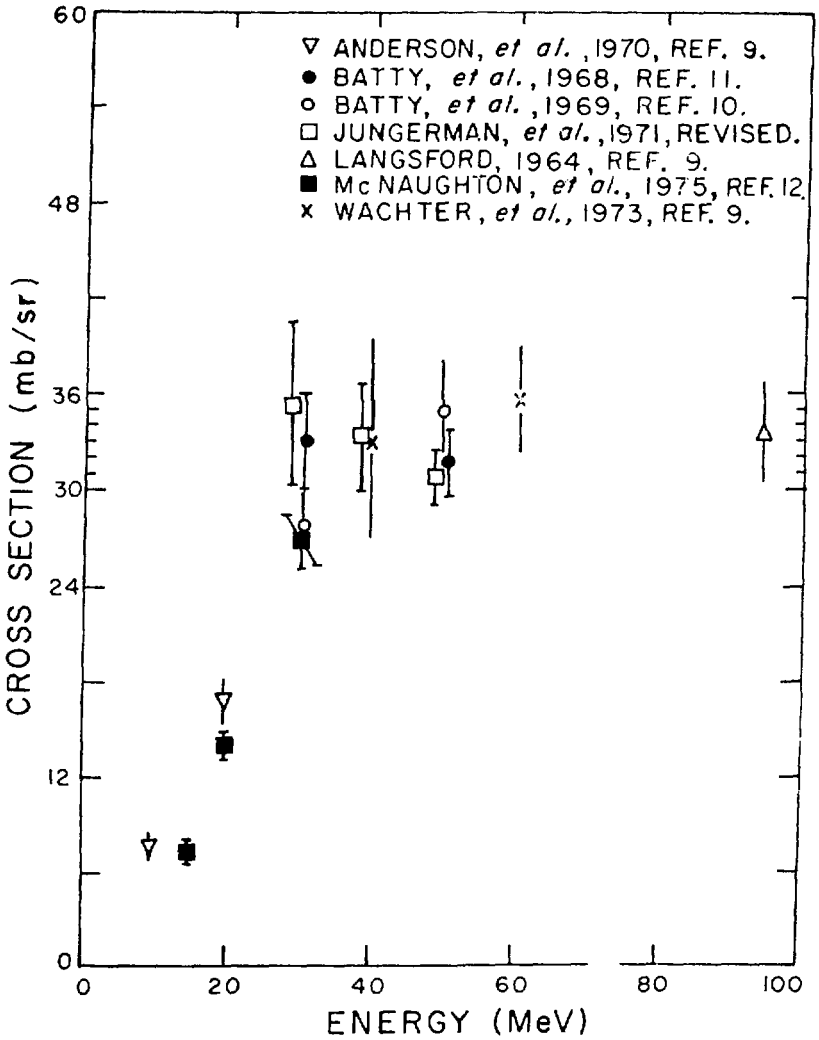

Fig. 6. Zero-degree cross section for the high-energy peak in the $^{7}Li(p,n)$ reaction, as a function of proton energy; ref. 91.

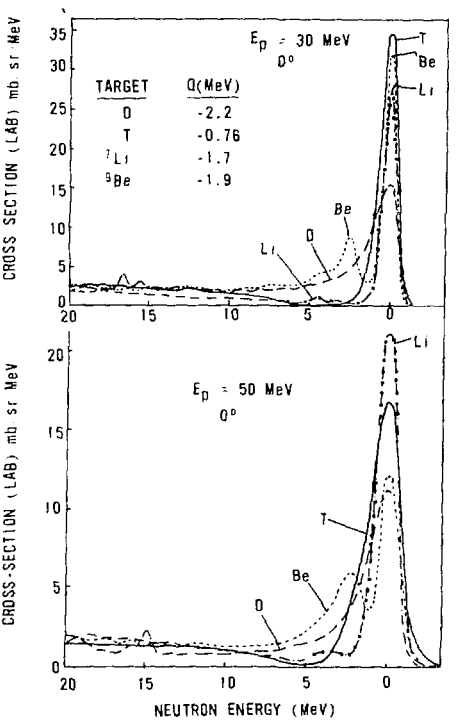

Fig. 7. Neutron spectra observed at 0° from thin D, T, ^{7}Li and ^{9}Be targets bombarded with 30 and 50 MeV protons. The energy scales have been adjusted so that the main peaks coincide and neutron energies are given relative to the peak which is set nominally at 0 MeV; ref. 58.

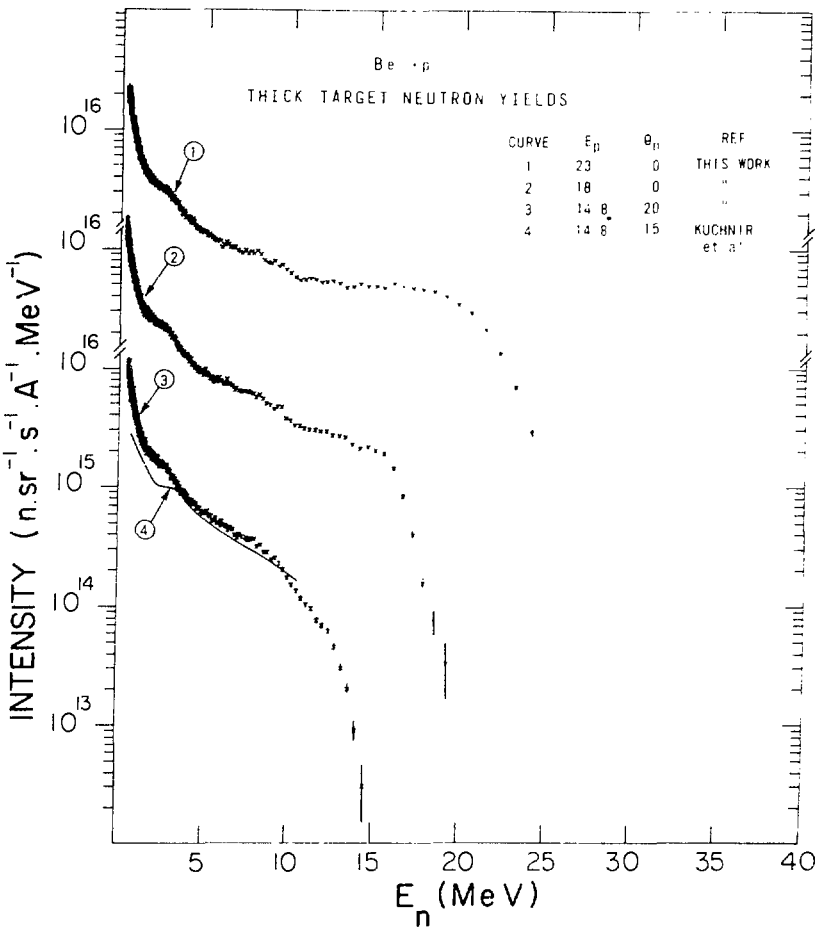

Fig. 8. Neutron spectral distributions from the Be+p reaction; ref. 13.

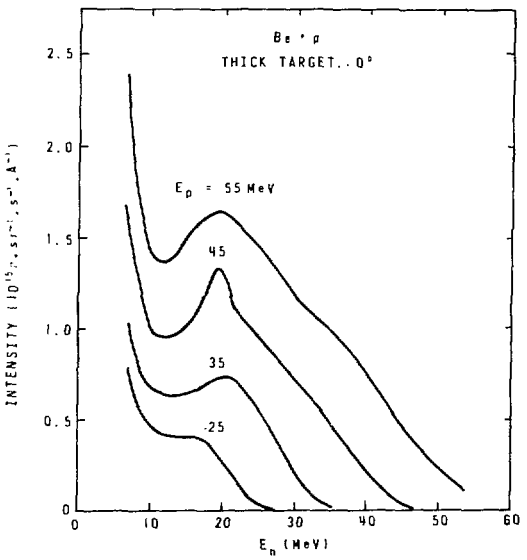

Fig. 9. Neutron spectral distributions from the Be+p reaction; ref. 68.

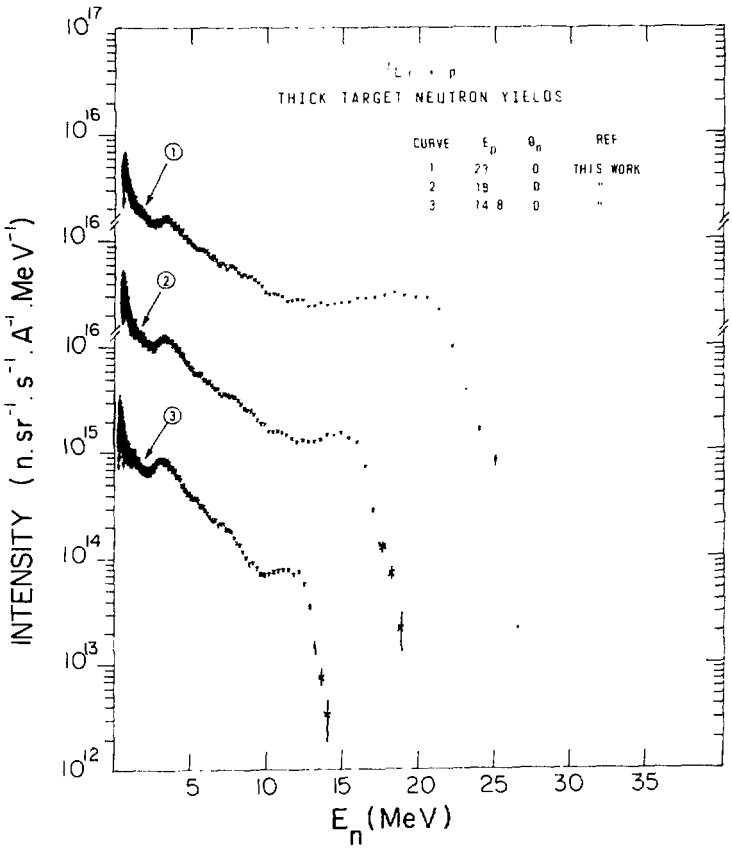

Fig. 10. Neutron spectral distributions from the Li+p reaction: ref. 13.

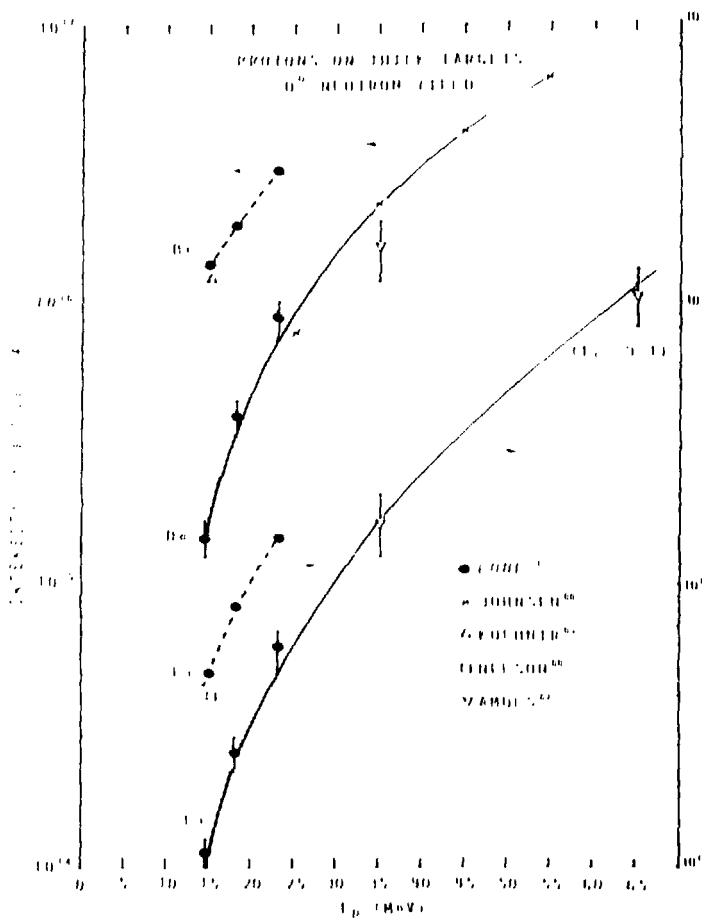

Fig. 11 Zero-degree neutron intensity as a function of the proton energy from thick Be and Li targets. The dashed curves are for T_p = 9.1 MeV and the solid curves are for T_p = 5 MeV.

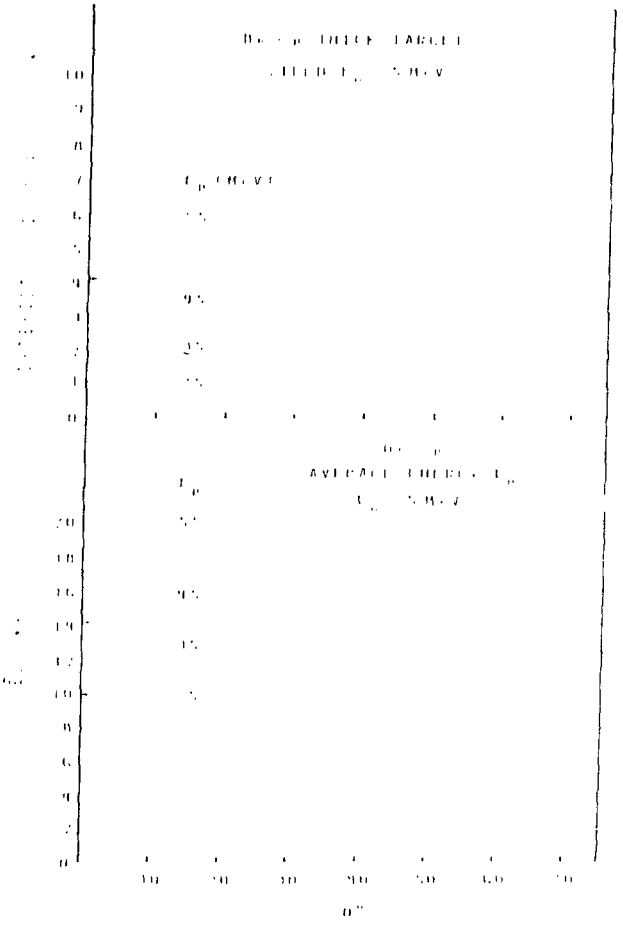

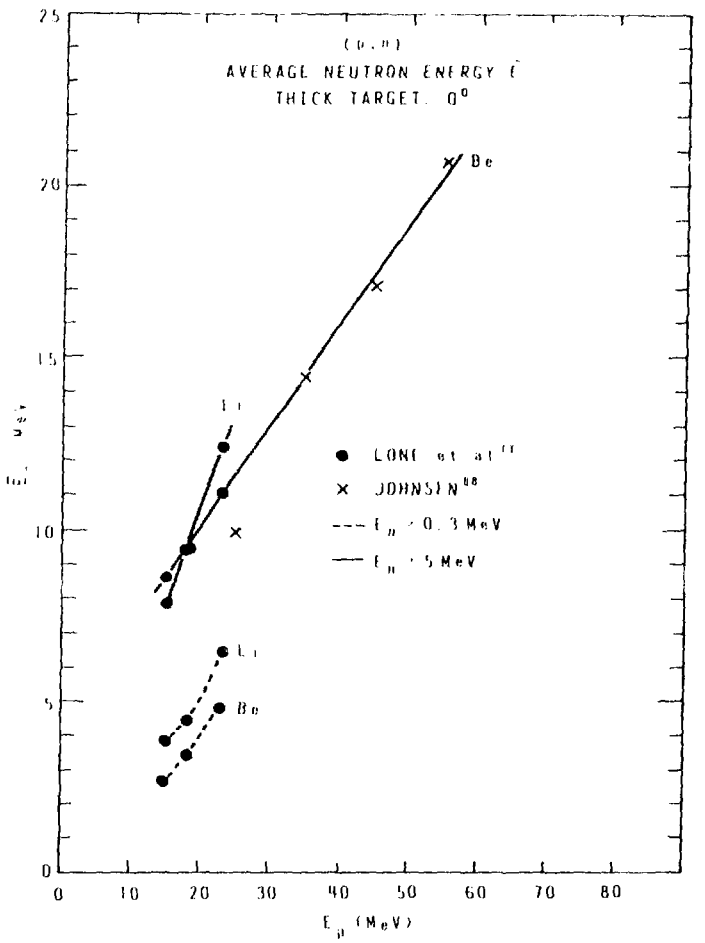

Fig. 14. The average neutron energy as a function of the proton energy for thick Be and Li targets. The solid curve is for E_n = 5 MeV and the dotted curve for E_n = 0.3 MeV.

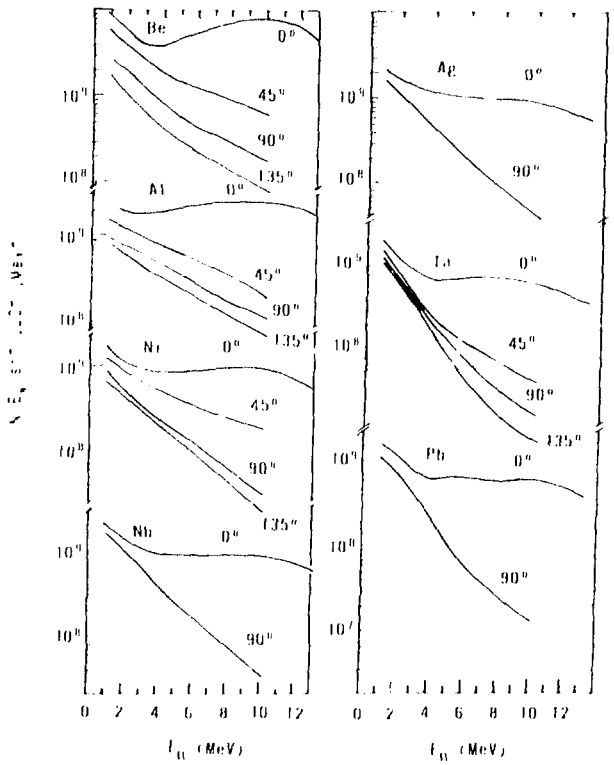

Fig. 14. Neutron spectral distributions from thick targets bombarded with 27.7 MeV deuterons, ref. 61.

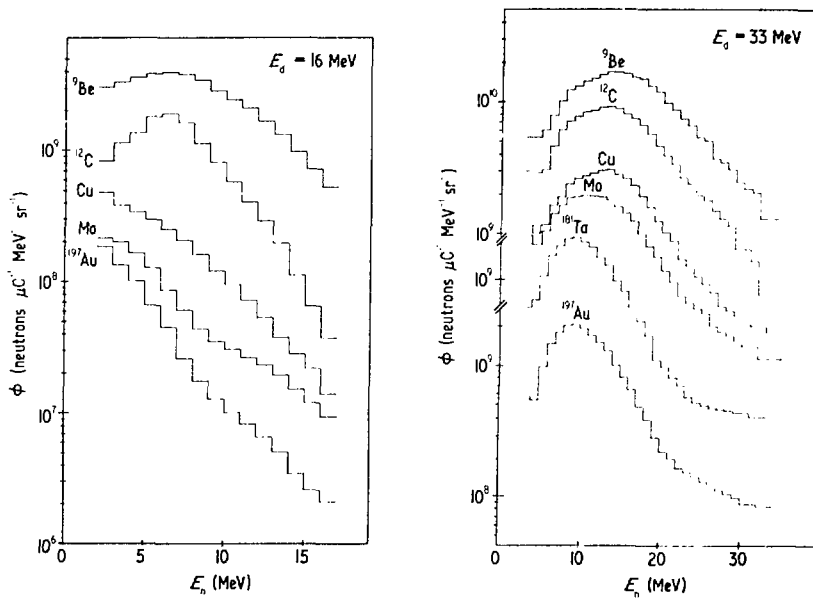

Fig. 15. Neutron spectral distributions at zero degrees from thick targets bombarded with 16 and 23 MeV deuterons; ref. 62.

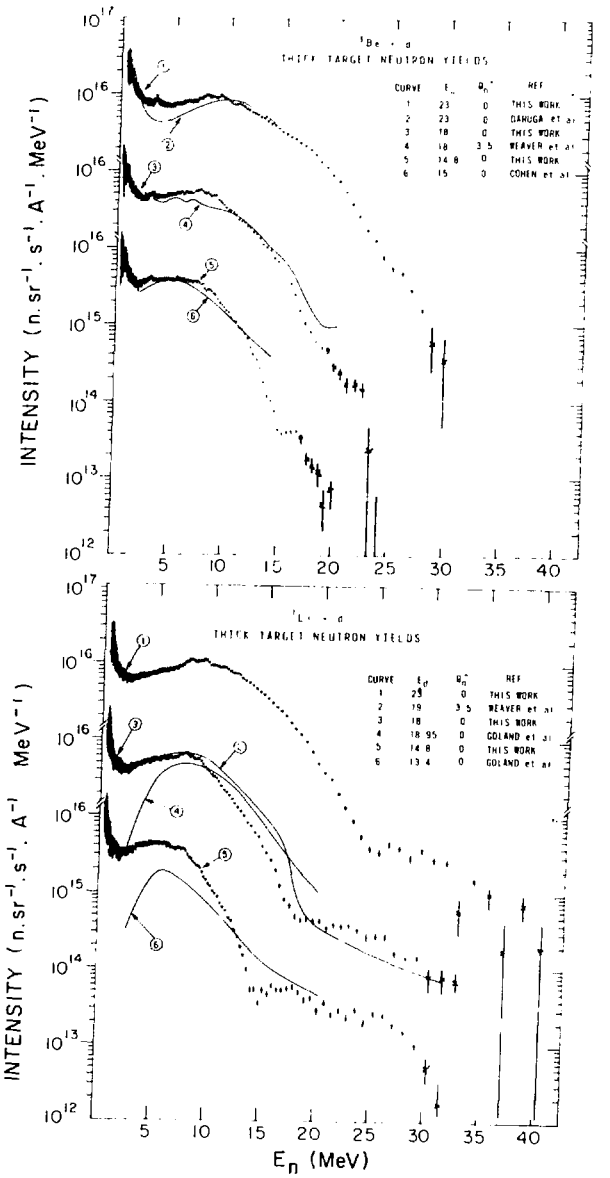

Fig. 16. Neutron spectral distributions from thick Be and Li targets bombarded with deuterons; ref. 13.

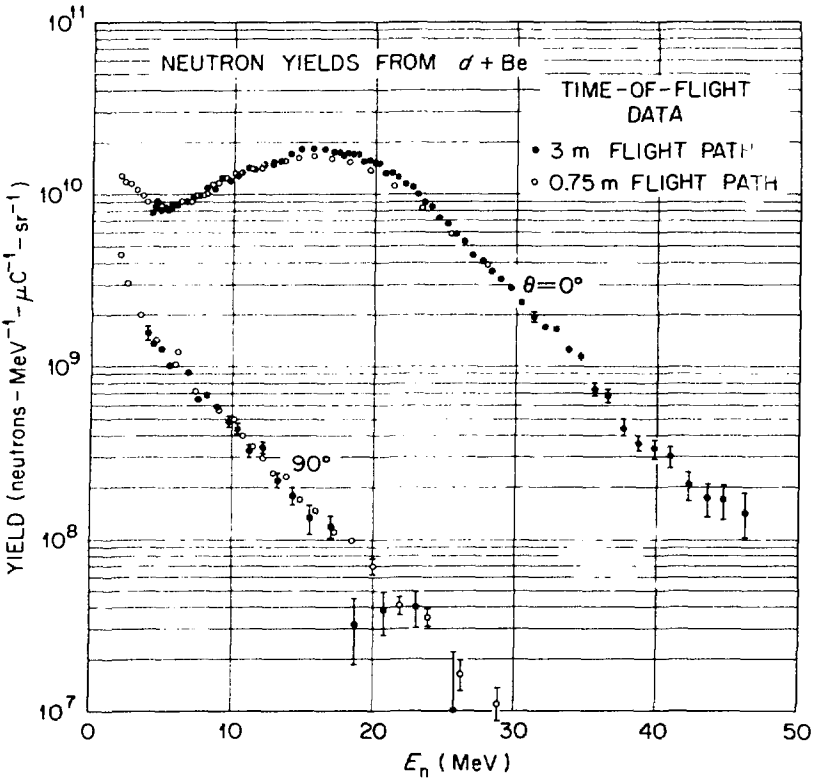

Fig. 17. Neutron spectral distributions from 40 MeV deuterons on a thick Be target; ref. 14.

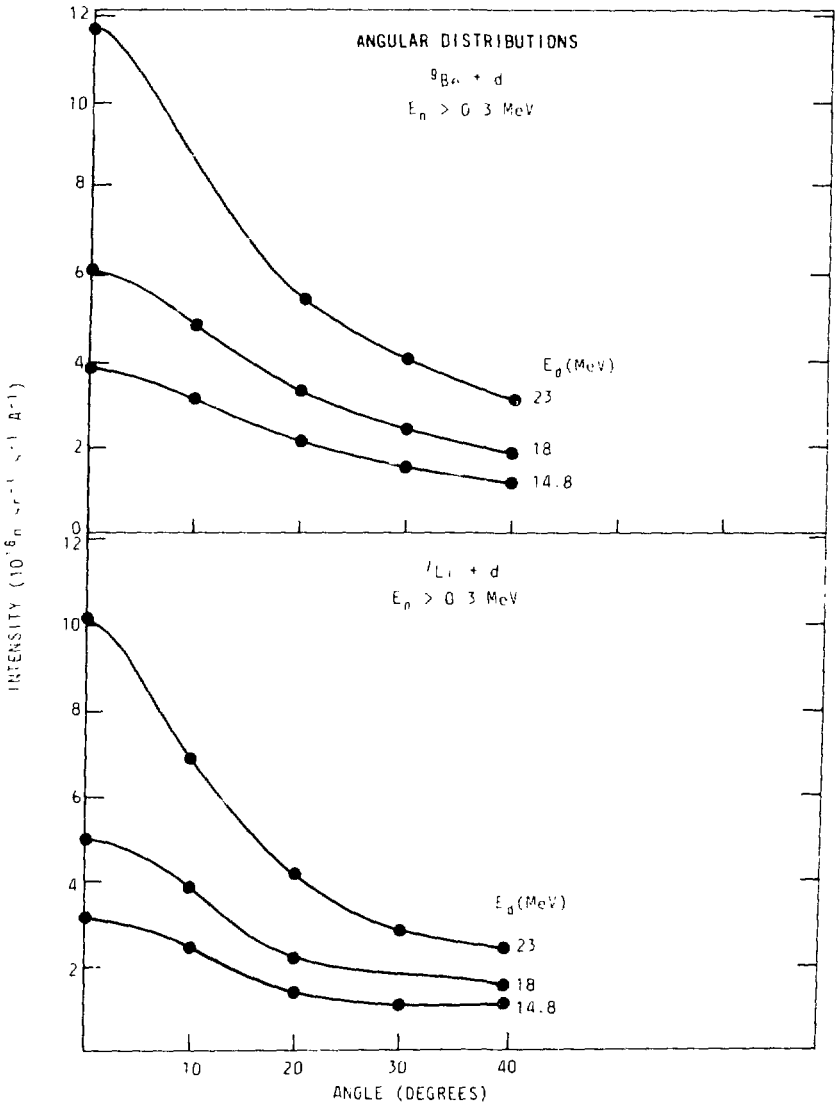

Fig. 18. Angular distribution of the neutron intensity from the Be+d and Li+d reactions; ref. 13.

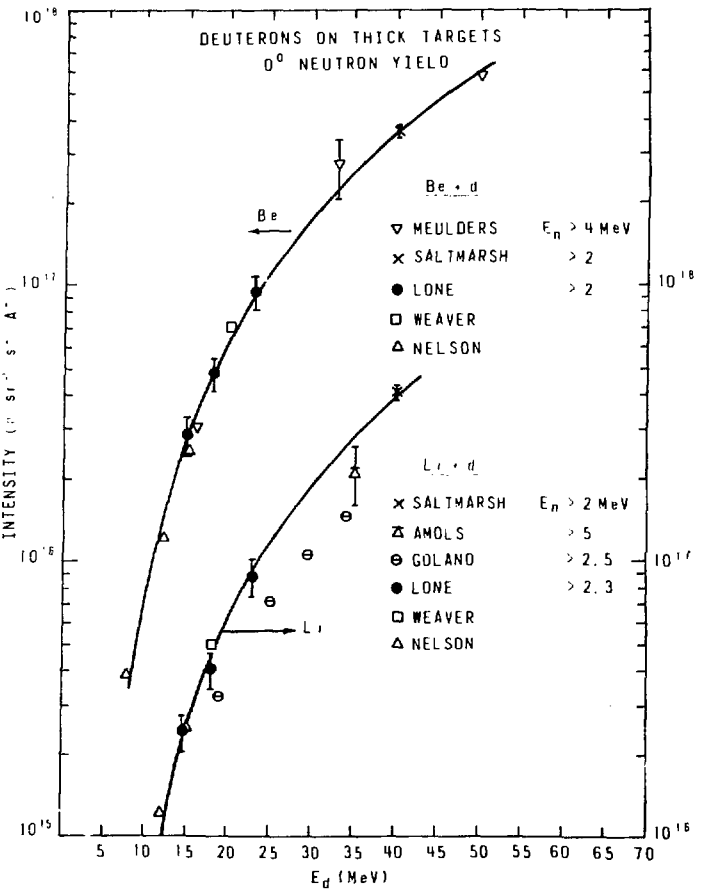

Fig. 19. Zero-degree neutron intensity as a function of the deuteron energy.

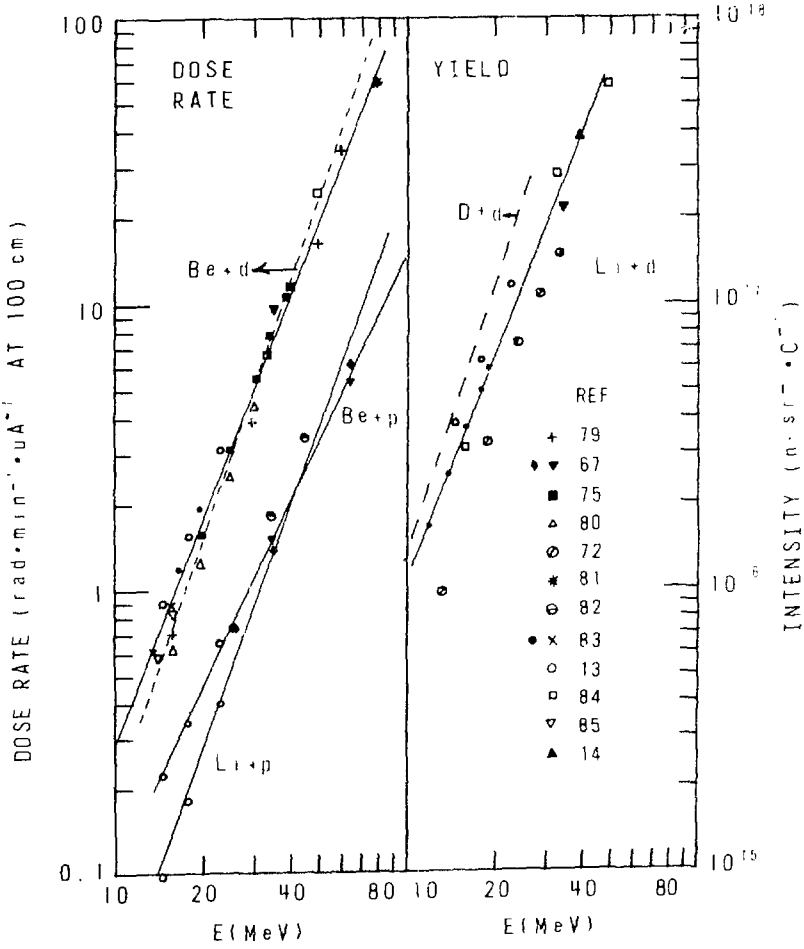

Fig. 20. Dose rate at one meter from thick targets bombarded with protons on Li and Be and deuterons on Be are given on the left side. The solid curve through the Be+d point shows $E^{1.7}$ dependence whereas the dotted curve shows $E^{1.10}$ dependence. Right hand figure gives the neutron yield from Li+d and D+d reactions.

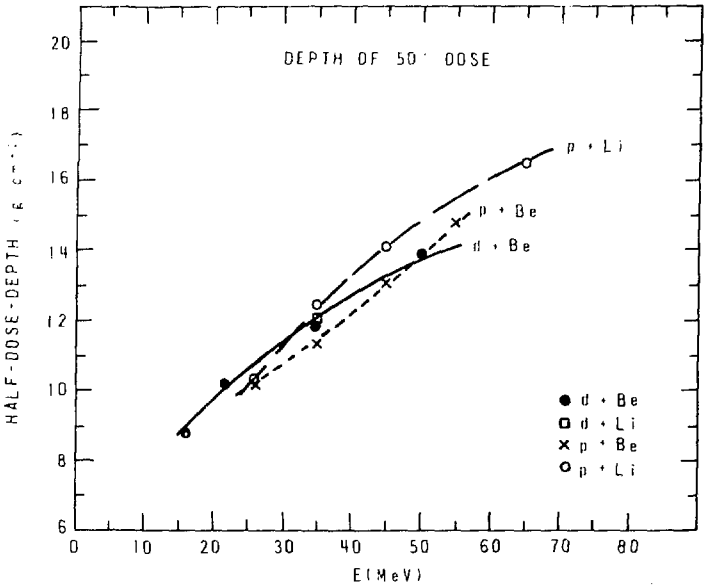

Fig. 21. Variation of the half-dose-depth with the projectile energy for neutrons produced with thick targets for a field size of 16 cm × 16 cm (Table 4).

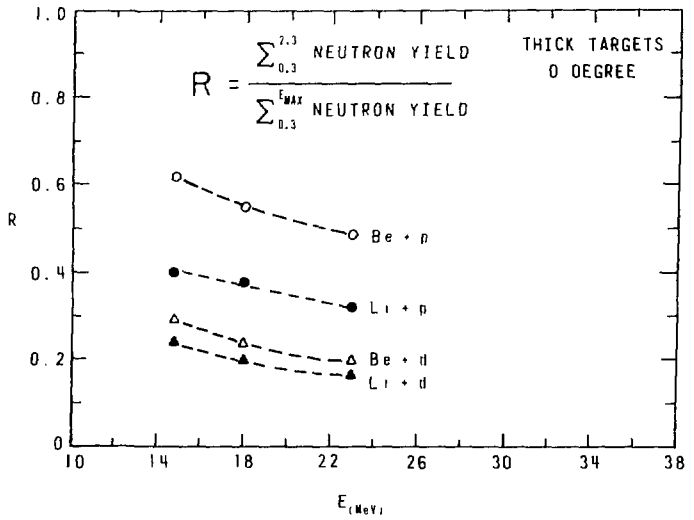

Fig. 22. Relative magnitude of the low-energy, E_n < 2.3 MeV, neutron component as a function of the projectile energy.

Thick Target Neutron Yields From the d-Be Reaction at E_d = 15.6, 29.9 and 49.0 MeV*

R.G. Graves, J.B. Smathers, and N. Hertel,** Texas A&M University, College Station, Texas 77843

and

V.A. Otte, P.R. Almond and W.Grant, The University of Texas Cancer Center, M.D. Anderson Hospital and Tumor Institute, Houston, Texas 77025

INTRODUCTION

The d-Be reaction is used at the Texas A&M Variable Energy Cyclotron (TAMVEC) and other institutions as an intense neutron source for radiobiological and radiotherapeutic studies. To use this reaction properly for these applications, it is essential to know the dosimetric and yield characteristics of the neutrons produced by the reaction. The purpose of this paper is to present the results of the neutron yield measurements; the dosimetric measurements have been presented elsewhere.[1] The present data are compared with previous results and discrepancies are discussed.

EXPERIMENTAL METHOD

The experiment was performed at the TAMVEC 88-inch sector focusing cyclotron (see Fig. 1). Deuteron ions were first accelerated and then transported to the target area in cave 2, the treatment room used for cancer therapy by M.D. Anderson Hospital. Before each run the beam was magnetically deflected for energy analysis by a 135-degree analyzing magnet located near the beginning of beam line 4. The widths of the entrance and exit slits to the analyzing magnet were set at 2.5 mm to reduce the beam divergence and thereby make possible a better determination of the beam energy. The energies of the energy analyzed beams used in this experiment were 15.6, 29.9 and 49.0 MeV. The deuteron beams were "timed tuned" by off-resonance tuning of the accelerator such that the time widths (full width at half-maximum) of the 15.6, 29.9 and 49.0 MeV beams were 2.8, 2.9 and 2.2 nanoseconds, respectively.

---

*Work supported by Public Health Service Grant CA12542 from NCI.

**Present address: University of Illinois, Urbana, Illinois 61801.

The target assembly consisted of a 2.0 cm diameter four-section carbon focus ring followed by a helical wire beam profile monitor, a 2.0 cm diameter combination electron suppresion ring and collimator made of carbon, and 3.18 cm diameter beryllium targets mounted in a copper target wheel. The targets were sufficiently thick to completely stop the incident deuterons: target thicknesses were 1.14, 3.40 and 8.48 mm for the 15.6, 29.9 and 49.0 MeV beams, respectively. Each target was mounted in the bottom of a copper well which served both as a Faraday cup and as a heat sink. A dual aluminum parallel-plate transmission chamber (TC) used to monitor the neutron flux during therapy treatments was mounted approximately 4 cm downstream of the target. The copper well and TC represent an inherent filtration of 4.8 mm Cu + 3.0 mm Al. No attempt was made to eliminate or reduce this filtration because this material is always present during patient treatments and biology experiments. Neutrons from the reaction were collimated at zero degrees by a 70 cm long WEP-B-Fe collimator insert (WEP-B-Fe represents water-extended polyester loaded with 0.3% boron and the equivalent of 18 cm iron). The neutrons were detected 350 cm from the target by a cylindrical NE213 liquid scintillator, 3.81 cm in diameter by 7.62 cm in length. The detector was oriented with its symmetry axis parallel to the direction of the neutron beam.

The data were acquired in spectral form as well as event-by-event by an on-line computer. Three parameters were stored for each event: the pulse height (PH) from the scintillator dynode (amplified and shaped), the neutron time-of-flight (TOF) relative to the cyclotron rf and the pulse shape discrimination (PSD) signal. The PSD signal was derived from a noncommercial PSD circuit.[2] The separation between neutron and gamma ray events was excellent in spectra obtained at all three incident deuteron energies. The contamination of gamma ray events in the neutron spectra was well below 1%. The three parameters were sorted and stored into five different spectra: PH (1x512 channels), TOF (1x512 channels), PSD (1x512 channels), PH vs TOF gated on gamma ray PSD (64x128 channels) and PH vs TOF gated on neutron PSD (64x128 channels). The latter spectrum was used in calculating the neutron yield.

DATA ANALYSIS

The neutron yield, $Y(\bar{E}_i)$, was calculated using the equation

$$Y(\bar{E}_i) = \frac{N(T_i,\bar{E}_i)(1+\tau)}{\varepsilon(T_i,\bar{E}_i)dE_i(\bar{E}_i)d\Omega_n I_0} ,$$

where $\bar{E}_i$ and $d\bar{E}_i$ are the mean neutron energy and energy width for the i-th TOF channel, $N(T_i,\bar{E}_i)$ are the number of counts detected above the PH software threshold T_i for the i-th TOF channel in the PH vs TOF spectra gated on neutron PSD, $d\Omega_n$ is the neutron detector solid angle, I_0 is the total charge collected on target, τ is the dead time and $\epsilon(T_i,\bar{E}_i)$ is the detector efficiency calculated at the neutron energy $\bar{E}_i$ for the PH threshold T_i. Mean neutron energies, $\bar{E}_i$, were calculated using the peak positions of the target gamma rays in the PH vs TOF spectra gated on gamma ray PSD and the time-to-amplitude converter gain as determined in a calibration run with cable delay boxes. I_0 was measured with a calibrated high precision current integrator. Considerable care was taken to minimize, but not make negative, the target leakage current so that it could be subtracted accurately from the measured current. Leakage currents were less than 0.5% of the toal currents. Beam currents on target had to be kept below 0.1 nanoamperes to minimize dead times. Dead times were 6.0, 2.8 and 4.5% for the 15.6, 29.9 and 49.0 MeV data, respectively. No background was subtrated from $N(T_i,\bar{E}_i)$ as measurements with a shadow cone (34 cm of iron placed midway between the target and the detector) showed that room neutron background was negligible.

Detector efficiencies were calculated using an improved version of a method prescribed by Northcliffe et al.[3] Briefly, the method calculates the efficiency for detecting neutrons which scatter only from the hydrogen in the scintillator. Edge effects and plural scattering to first order have been included. The technique eliminates the necessity to know accurately the n-carbon reaction cross sections, which is a common problem in calculating efficiencies, and the elimination of the necessity to correct for frame overlap neutrons, as these events are biased out by the software threshold T_i. Proton response functions which are needed for this method were determined by finding the end points (EP) from the PH vs TOF spectra gated on neutron PSD. The response function then was derived by parameterizing the EP's and their corresponding neutron energies using the equation

$$EP_i = SCL \cdot f(\bar{E}_i) - ZPH$$

where SCL and ZPH are scale factors and $f(\bar{E}_i)$ is Masterson's response function for NE218.[4] Excellent fits to the end point data were obtained using this equation even though NE213 was used. The thresholds, T_i, used in the efficiency calculation and integration of the spectra were generally ($\bar{E}_i$ - 10) MeV if $\bar{E}_i$ was greater than about 15 MeV and were about 2 to 5 MeV if $\bar{E}_i$ was less than 15 MeV. A 10 percent error in calculating the detector efficiency is assumed.

At each incident deuteron energy neutron yields were measured for three different collimator sizes to determine if the

observed neutron yields depend on collimator geometry. The distal end of the collimators measured 4.3 cm by 4.5 cm, 6.2 cm by 6.2 cm and 11.4 cm by 11.4 cm. In all cases the neutron yields showed no systematic dependence on collimator size, a result which is not entirely unexpected since the detector was in good geometry. As a consistency check of our experimental procedure, runs having the same geometry were repeated with a time lapse of several hours between pairs of runs. The neutron yields for these pairs of runs agreed to within ±3% of each other, or approximately twice their statistical error. Final results were obtained by adding all of the runs together.

RESULTS AND DISCUSSION

The neutron yields for 15.6, 29.9 and 49.0 MeV deuterons on thick beryllium are shown in Figs. 2-4. The data have not been corrected for neutron attenuation due to the inherent filtration. Integral yields and the thresholds used in the integration are given in Table 1. The differential and integral yields are subject to a 10% systematic error due to the uncertainty in the detector efficiency. Statistical errors on the differential yields are less than 1% for all data bins except for the few bins near the top of the energy spectra where the errors are somewhat larger. The data of Lone et al.,[5] Meulders et al.,[6] and Amols et al.,[7] are also shown for comparison in Figs. 2-4. All three groups used TOF techniques. Lone detected neutrons with a stilbene crystal using PSD and calculated detector efficiencies with the code DETEFF.[8]

Table 1

Integral Neutron Yields

E_d (MeV)	Target Thickness (mm)	Threshold (MeV)	Neutron Yield (n/sr · nC)
15.6	1.14	3.9	2.37×10^7
29.9	3.40	6.9	13.0×10^7
49.0	8.48	9.5	48.0×10^7

Meulders did not use PSD as they used an NE111 scintillator; detector efficiencies were measured in the 6-14 MeV neutron energy range and were calculated at other energies using the Stanton code.[9] Amols used an NE213 scintillator with PSD and calculated efficiencies with a modified version of the Stanton code.[10]

Considering the differences in incident deuteron energy, the present data agree well with the results of Lone at 14.8 MeV, Amols at 35 MeV and Meulders at 50 MeV. The spectral shape obtained by Meulders at 16 MeV is in good agreement with the present data, but the absolute values do not agree. Also, the results of Meulders at 33 MeV seem to be incorrect as they are in gross disagreement with both the present results and the results of Amols. For neutron energies below about 18 MeV, it is not known why the present data agree well with the results of Meulders at E_d = 50 MeV but disagree with his results at E_d = 33 MeV and 16 MeV.

Future work with the d-Be reaction includes the extension of the present measurements to lower neutron energies using the TAMVEC pulsed deuteron beam. Measurements will be made for both filtered and unfiltered neutron beams.

REFERENCES

1. P.R. Almond, J.B. Smathers, G.D. Oliver, E.B. Hranitzky and K. Routt, Rad. Res. 54, 24 (1973); A.R. Smith, P.R. Almond, V.A. Otte, J.B. Smathers, Radiology 113, 187 (1974).
2. P. Sperr, H. Spieler and M.R. Maier, Nucl. Instr. and Meth. 116, 55 (1974).
3. L.C. Northcliffe, C.W. Lewis and D.P. Saylor, Nucl. Instr. and Meth. 83, 93 (1970).
4. T.G. Masterson, Nucl. Instr. and Meth. 88, 61 (1970).
5. M.A. Lone, C.B. Bigham, J.S. Fraser, H.R. Schneider, T.K. Alexander, A.J. Ferguson and A.B. McDonald, to be published.
6. J.P. Meulders, P. Leleux, P.C. Macq and C. Pirart, Phys. Med. Biol. 20, 235 (1975).
7. H.I. Amols, J.F. Dicello, M. Awschalom, L. Coulson, S.W. Johnsen and R.B. Theus, FERMILAB-Pub-76/102-EXP, 1184.00.
8. R.J. Kurz, LRL Report, UCRL-11339 (1964); S.T. Thornton and J.R. Smith, Nucl. Instr. and Meth. 96, 551 (1971).
9. N.R. Stanton, Ohio State University Report # COO-1545-92 (1971).
10. M.W. McNaughton, N.S.P. King, F.P. Brady and J.L. Ullmann, Nucl. Instr. and Meth. 129, 241 (1975).

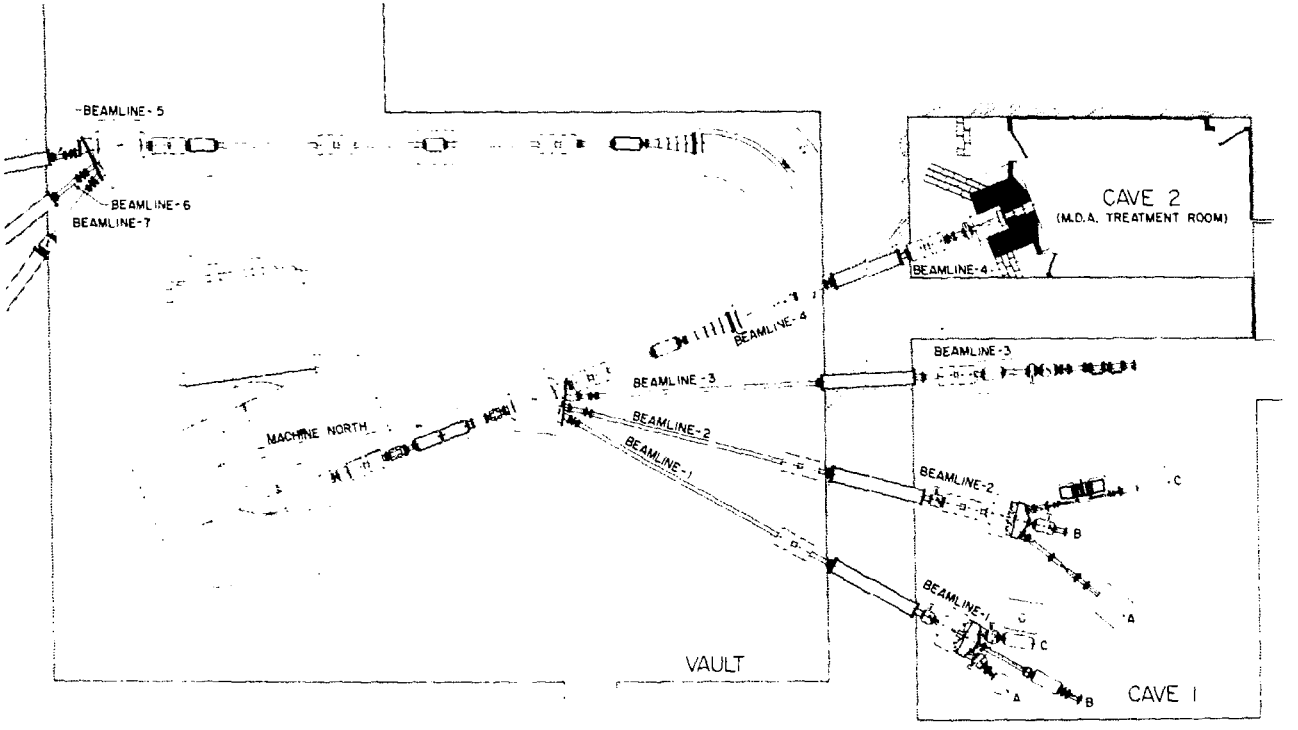

Figure 1. Overall view of Texas A&M Variable Energy Cyclotron, beam lines and two experimental areas.

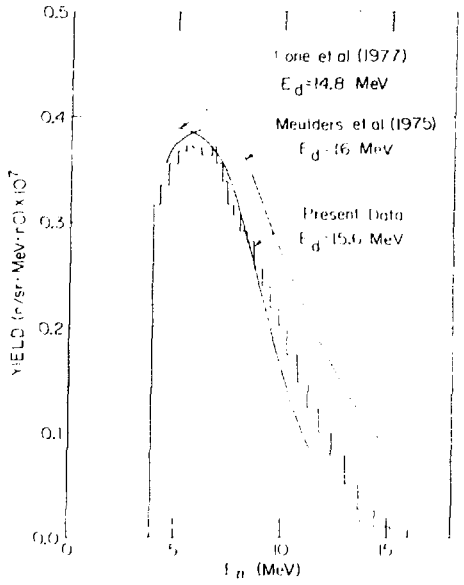

Figure 2. Neutron yield for 15.6 MeV deuterons on thick beryllium. Data of Lone et al.,[5] at 14.8 MeV and Meulders et al.,[6] at 16 MeV are shown for comparison.

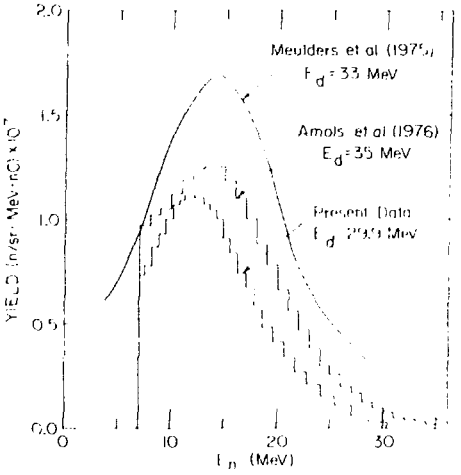

Figure 3. Neutron yield for 29.9 MeV deuterons on thick beryllium. Data of Amols et al.,[7] at 35 MeV and Meulders et al.,[6] at 33 MeV are shown for comparison.

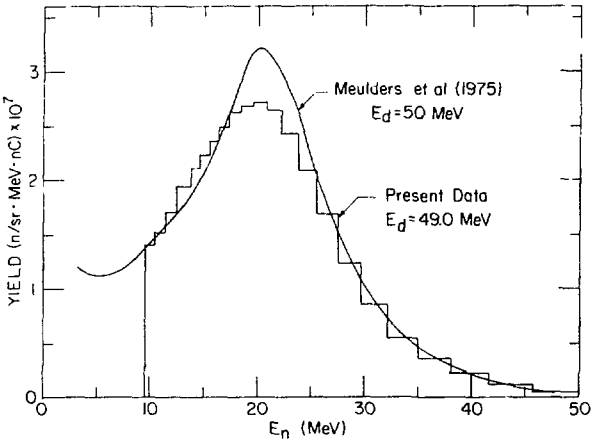

Figure 4. Neutron yield for 49.0 MeV deuterons on thick beryllium. Data of Meulders et al.,[6] at 50 MeV are shown for comparison.

Neutron Spectra From Deuteron and
Proton Bombardment of Thick Lithium Targets

C.E. Nelson*, F.O. Purser, P. Von Behren and H.W. Newson
Triangle Universities Nuclear Laboratory† and Duke University
Durham, North Carolina 27706, U.S.A.

INTRODUCTION

A possible alternative to the D-T generator for a hospital based neutron source is a compact medical cyclotron. Table 1 lists the specifications of some of the cyclotrons presently installed in hospitals in the United States.

Table 1

Medical Cyclotron Specifications*

Cyclotron Model No.	Particle	Energy (MeV)	Extracted Beam (μA)
CS 15	p	15	100
	d	8	100
CS 22	p	22	50
	d	12	50
CS 30	p	26	60
	d	15	100

*Cyclotron Corporation

It is known that at the deuteron energies available to these cyclotrons, a thick beryllium target produces an intense neutron flux, which has an average energy of approximately .4 E_d[2]. The resultant neutron beam is, however, of limited usefulness for radiation therapy because of its poor penetration into tissue. The $^9Be(d,n)$ reaction at E_d=16 MeV, for example, has a central axis depth dose curve which falls to 50% of the surface dose at 9.2 cm for a 10 x 10 cm field at 125 cm TSD[3], whereas Brennan has suggested 10 cm as an acceptable depth for 50% of the surface dose for a 5 x 5 cm field[4].

The large positive Q-value (+15.03 MeV) of the $^7Li(d,n)^8Be$ reaction suggests that bombarding a thick lithium target with

deuterons could result in a substantial increase in the average neutron energy of the resultant neutron yield. Previous measurements of this average neutron energy for these lower energy deuterons are in disagreement, indicating an average neutron energy of .4 E_d to .55 E_d for E_d<15 MeV[2,5,6].

The $^7Li(p,n)^7Be$ reaction is known to be a prolific source of high energy neutrons for thin targets, with over 60% of the neutrons from this reaction going to the ground or first excited state of ^7Be[7]. Thick target spectra have not been measured for proton energies above E_p=4.0 MeV.

The Triangle Universities Nuclear Laboratory neutron time-of-flight facility has been used to determine the average neutron energy and yield of thick lithium (d,n) and (p,n) reactions at deuteron energies of 8, 12 and 15 MeV and a proton energy of 15 MeV.

EXPERIMENTAL

Neutron energy spectra were measured using time-of-flight techniques. A pulsed beam of protons or deuterons from the Triangle Universities Nuclear Laboratory Model FN Tandem Van de Graaff accelerator was used in conjunction with the TUNL neutron time-of-flight facility. Beam currents of 2-5 nA with a time resolution of 1.5 to 2.0 nS were used.

The lithium target was enriched to 99.99% ^7Li and was encapsulated in an aluminum container under a helium atmosphere. The upstream face of the lithium was covered with a 3.5 μm molybdenum foil and the target length was 1.9 cm, sufficient to stop 15 MeV deuterons.

The charged particle beam passed through a 3.2 mm tantalum collimator 15 cm upstream of the lithium target. Collimator currents were kept to less than .1 nA. Beam spot sizes on target were kept to less than 5 mm diameter. Target beam currents, with appropriate electron suppression, were integrated to determine the incident charged particle flux.

The lithium target was mounted at the pivot of the main neutron detector shield at the end of the all metal, wide aperture neutron time-of-flight beam line. The very small collimator currents, combined with the extremely well shielded detector made beam and room associated background measurements unnecessary.

The neutron detector consisted of a 8.89 cm diameter by 5.04 cm thick NE 218 liquid scintillator coupled to a 56 DVP photomultiplier. Pulse shape discrimination was used to discriminate against gamma ray events. This detector was housed in a massive (7300 kg) shield to reduce time uncorrelated background events to a negligible amount[8]. A smaller detector, located at a fixed angle to the charged particle beam, monitored the neutron flux.

Standard time-of-flight electronics, including pulse shape discrimination, were used for all data-taking which was done with

the TUNL DDP 224 computer. Main detector ADC dead times were kept to less than 20%. Spectra were measured at 0°, 10°, 20°, 30° and 45°.

The efficiency of the detector as a function of energy must be known to convert the time-of-flight spectra to energy spectra. The previous measurements of neutron yield have used a detector bias level corresponding to 1.6 to 2.5 MeV neutron energy and have been required to extrapolate the neutron yield to zero neutron energy. In order to minimize errors introduced by such arbitrary extrapolations, the low energy cut-off of the main detector for this work was set at 1/10 the ^{137}Cs compton edge, corresponding to a neutron energy of 200-300 keV. Calculations of detector efficiencies are very unreliable with such low energy thresholds. Thus the relative efficiency of the main detector was measured over the range of .7 MeV to 24 MeV, using two different techniques.

For neutrons between .7 MeV and 5 MeV, the angular distribution of neutrons of 7.5 MeV scattered from hydrogen was measured. A 6 mm diameter by 2.55 cm high polyethylene scattering sample was used and spectra were taken from 35° to 72° in the laboratory system. The data, when corrected for finite geometry effects and normalized to the known H(n,n)H differential cross section, yield a relative efficiency curve. The efficiency from 4.0 MeV to 24 MeV neutron energy was measured by using the well-known $T(p,n)^3He$ and $T(d,n)^4He$ reactions at several charged particle energies[9,10]. The measured yields, normalized to the differential cross sections, give a family of curves spanning different, overlapping neutron energy regions. These curves were overlapped and normalized to the H(n,n)H measurement to yield the relative efficiency data shown in fig. 1. The absolute efficiency of the detector was obtained by normalizing this relative efficiency at E_n=4.0 MeV to a monte carlo calculation of the efficiency of our detector done at Oak Ridge National Laboratory[11]. A least squares fit was then made to this combined data. This fit was used to obtain the calculated efficiency as a function of neutron energy and is shown as the smooth curve in fig. 1.

The time-of-flight spectra, after correction for computer dead time and relativistic effects, were converted to neutron energy spectra using this calculated efficiency curve. The steep slope of the efficiency curve below E_n=1.0 MeV precludes an accurate determination of the neutron yield in this region. All subsequent calculations of neutron yields and average energy therefore, use E_n=1.0 MeV as the low energy cut-off point.

NEUTRON SPECTRA AND YIELDS

The zero degree energy spectra of neutrons obtained with 8, 12 and 15 MeV deuteron bombardment of a thick lithium target are shown in figs. 2, 3, and 4. These spectra are characterized by 1) a broad peak in the energy distribution at approximately .4 E_d,

2) a very small high energy tail and 3) a low energy tail which appears to be increasing rapidly below E_n=1.0 MeV, the low energy cut off point for these measurements.

Fig. 5 shows the zero degree energy spectrum for 15 MeV proton bombardment of a thick lithium target. It is characterized by 1) a peak in the energy distribution at E_n=3.4 MeV and 2) a decrease in yield with neutron energy, varying approximately as $1/E_n$.

The neutron spectra at each angle were integrated to obtain the yield versus laboratory angle data shown in fig. 6. The ^{7}Li(d,n) data indicate a peak in the yield at zero degrees, which becomes more pronounced with increasing deuteron energy, while the ^{7}Li(p,n) data are essentially isotropic.

Table 2 gives the average neutron energies calculated from these neutron yield data and numerical values of the yields.

Table 2

Thick Target Yields and Average Neutron Energies for E_n>1.0 MeV

	E_d=8 MeV		E_d=12 MeV		E_d=15 MeV		E_p=15 MeV	
θ_{lab}	$\bar{E}_n$ (MeV)	Y_n (10^9 $\frac{neut.}{\mu C\text{-}sr}$)	$\bar{E}_n$	Y_n	$\bar{E}_n$	Y_n	$\bar{E}_n$	Y_n
0	4.4	3.8	5.5	12.	6.5	25.	4.7	4.1
10	4.5	3.4	5.7	9.6	6.6	20.	4.6	4.0
20	4.8	2.7	5.9	6.7	6.6	13.	4.5	4.0
30	5.7	2.0	5.7	4.5	5.9	8.2	4.5	3.8
45	6.0	0.85	5.3	3.0	5.4	5.8	4.5	3.4

DISCUSSION

There are several earlier measurements of neutron spectra from thick lithium targets[2,5,6]. Comparisons of the present data with these measurements are shown in fig. 7, where both the yield and average neutron energy are plotted as a function of deuteron energy. The present data are in substantial agreement with the previous measurements of Weaver et al.[2] The discrepancy between the present work and Weaver for the average neutron energy (approximately 10%) is consistent with the different low energy cut off and extrapolation to zero neutron energy used.

The large discrepancies between the present work and that of Jones et al. and Goland are likely the result of similar extrap-

olation or low energy cut off point differences.[5,6] The present work, because it extends to a neutron energy of 1.0 MeV, is less dependent on these differences than the previous measurements.

The present data show that at the deuteron energies available to the smaller cyclotrons, the ^{7}Li(d,n) reaction is not a practical source of neutrons for fast neutron therapy. The neutron yield compares favorably with the neutron yield from thick beryllium targets. However, the average neutron energy is substantially lower than 10 MeV for all deuteron energies, varying with deuteron energy approximately as $\bar{E}_n$=.44 E_d. This is similar to the relationship found for beryllium targets by Weaver, $\bar{E}_n$=.42 E_d. Both the average neutron energy and yield of the ^{7}Li(p,n) reaction indicate that it is not suitable for fast neutron therapy at E_p=15 MeV. The average neutron energy is only 4.7 MeV while the yield is only .4 x 10^{10} n/μC-sr.

To conclude, the present work indicates that neither the deuteron induced or the 15 MeV proton induced reactions on thick lithium produce a suitable fast neutron beam for therapy.

REFERENCES

1. Kelsey, C.A., Medical Physics 2, 185 (1975).
2. Weaver, K.A., Anderson, J.D., Barschall, H.H. and Davis, J.C., Nuclear Science and Engineering 52, 35 (1973).
3. Parnell, C.J., British Journal of Radiology 44, 612 (1971).
4. Brennan, J.T., Radiological Clinics of North America 7, 365 (1969).
5. Jones, D.T.L. and Bartle, C.M., Nuclear Instruments and Methods 118, 525 (1974).
6. Goland, A.M., Snead, C.L. Jr., Parker, D.M. and Theus, R.B., Reported at the Charged Particle Accelerator Conference, Washington, D.C. IEEE, NS521 (1975).
7. Jungerman, J.A., Brady, F.P., Knox, W.J., Montgomery, T., McGie,M.R., Romero, J.L. and Ishizaki, Y, Nuclear Instruments and Methods 94, 421 (1971).
8. Glasgow, D., Purser, F.O., Clement, J.C., Mack, G., Stelzer, K., Boyce, J.R., Epperson, D.H., Hogue, H.H., Bilpuch, E.G., Newson, H.W., and Gould, C.R., NBS Special Publication 425, Proceedings of Nuclear Cross Sections and Technology Conference 1, 99, 1975.
9. Drosg, M., Los Alamos Scientific Laboratory Report LA-5732-MS, (1974).
10. McDaniels, D.K., Drosg, M., Hopkins, J.C. and Seagrave, J.D., Physical Review C, 882 (1973).
11. Morgan, G.L., private communication.

*Supported by National Cancer Institute Research Fellowship #1 F22 CA00332-01

+Supported by U.S. ERDA

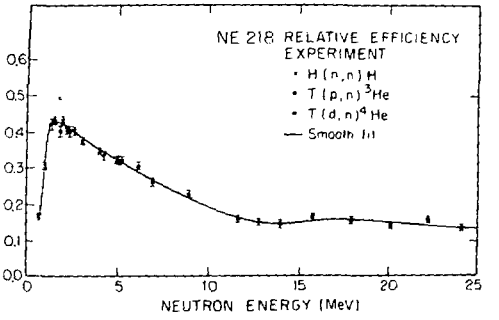

Fig. 1 Efficiency of the main neutron detector.

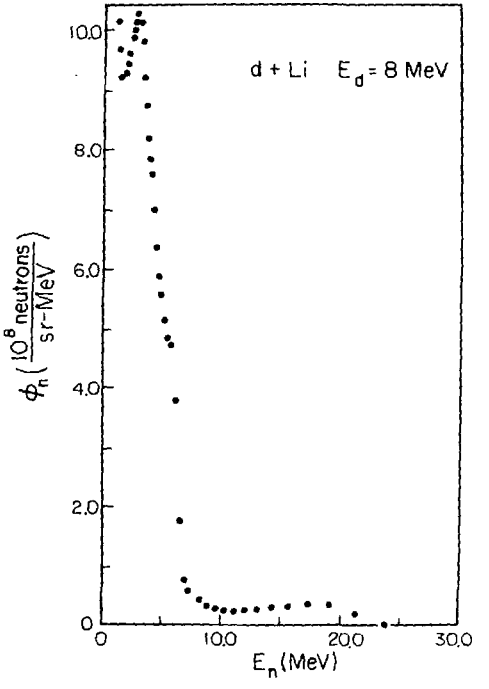

Fig. 2 Neutron energy spectra at zero degrees for 8 MeV deuterons on lithium.

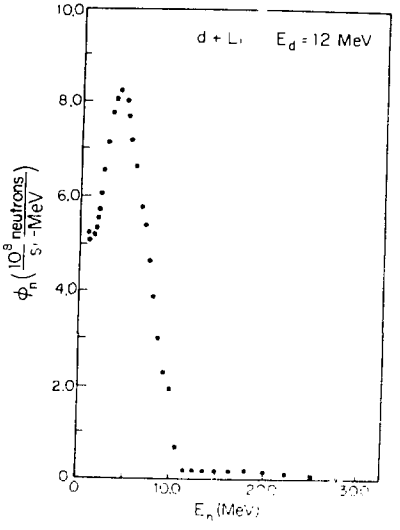

Fig. 3 Neutron energy spectra at zero degrees for 12 MeV deuterons on lithium.

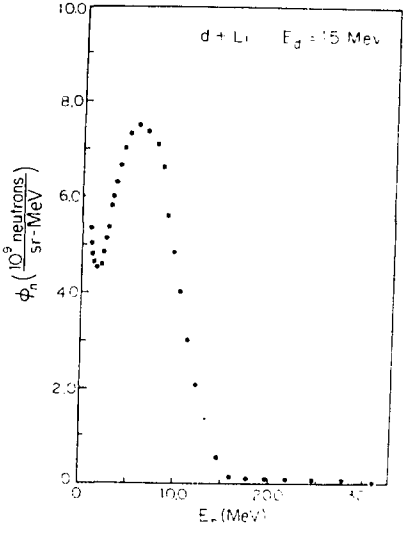

Fig. 4 Neutron energy spectra at zero degrees for 15 MeV deuterons on lithium.

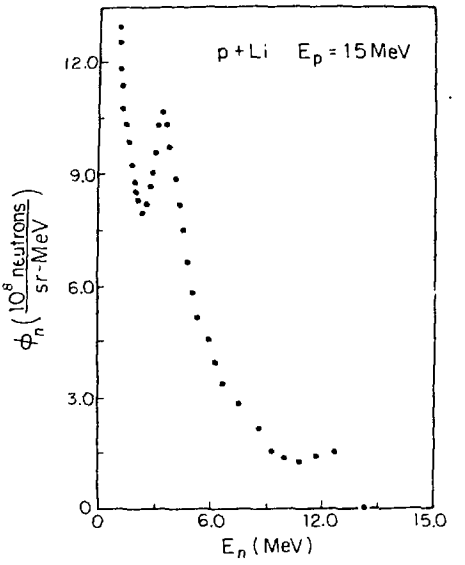

Fig. 5 Neutron energy spectra at zero degrees for 15 MeV protons on lithium.

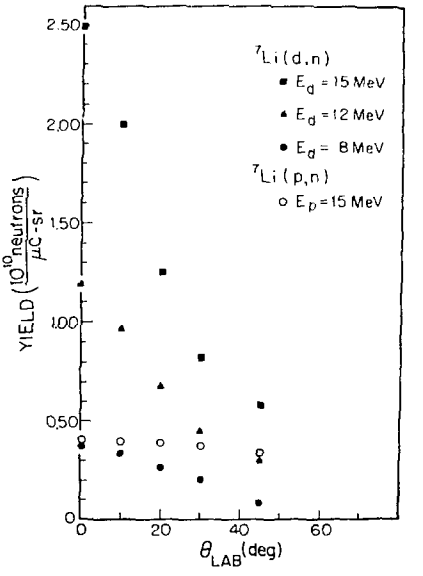

Fig. 6 Neutron yield for E_n>1.0 MeV versus laboratory angle.

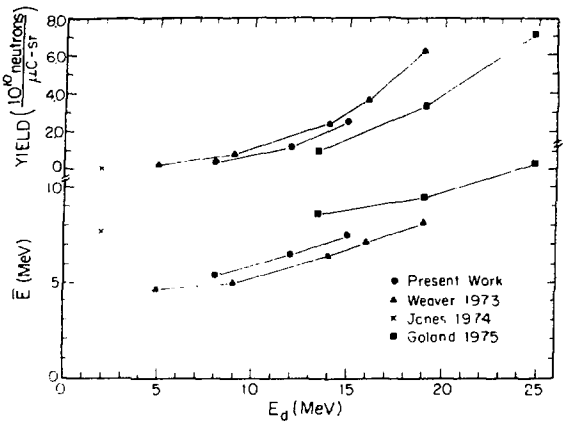

Fig. 7 Average neutron energy and zero degree yield versus deuteron energy.

Neutron Spectra from 30-MeV Deuterons on a Thick Beryllium Target

D. R. Nethaway, R. A. Van Konynenburg, and M. W. Guinan
Lawrence Livermore Laboratory
and
L. R. Greenwood
Argonne National Laboratory

ABSTRACT

We have measured the neutron spectra produced by bombarding a thick beryllium target with 30-MeV deuterons at the University of California, Davis cyclotron. These spectra are of interest in studying the effect of neutrons on materials to be used in future fusion reactors. The spectra were inferred from the activation of two sets of detector foils placed at an angle 0° to the deuteron beam, one immediately behind the beryllium target block, and one 40 mm to the rear. We used the SAND-II program to analyze the foil activation data to obtain the fluence in each of one hundred energy groups. The neutron spectrum (fluence/MeV) close to the target decreases continuously with energy in the range 2-30 MeV, while the spectrum 40 mm back has a minimum at about 8 MeV and a peak at about 14 MeV. The contribution from neutrons of energies less than 10 MeV is much greater than that found in previous spectral measurements made at large distances from the target. We attribute this difference to the neutrons which are emitted at large angles from the deuteron beam. These observations show the importance of evaluating the neutron spectrum near the target if samples of materials are to be irradiated in this location.

INTRODUCTION

The (d,n) reaction on beryllium provides a source of neutrons that may be appropriate for use in studying the effects of intense fast-neutron irradiation on various materials that are to be used in future fusion reactors. The purpose of this experiment was to examine the spectrum and intensity of the neutrons available at the University of California, Davis cyclotron. A beryllium target was bombarded with 30-MeV deuterons, producing a neutron distribution extending up to about 32 MeV. We have used the foil activation technique in which a set of foils of various materials is irradiated with neutrons, and the neutron spectrum is inferred from the relative activation of the various foils. In this preliminary study of near source D-Be neutron spectra, we present the results of analyses on two sets of detector foils placed at 0° to the deuteron beam.

---

* Work performed under the auspices of U.S. ERDA Contract W-7405-Eng-48.

BLANK PAGE

EXPERIMENTAL DETAILS

The irradiation took place at the cyclotron in the Crocker Nuclear Laboratory, University of California at Davis. A beryllium target was bombarded with 30 MeV (±2%) deuterons for 72 min. The beam current varied from 10.2 to 8 μA and averaged 20.8 μA over the run, giving an integrated beam current of 0.0836 C.

The beryllium target[1] was a cylinder 2.5 mm thick and 12.7 mm in diameter, vacuum brazed in a copper plate 1.2 mm thick and 120 mm in diameter. The beryllium was thick enough to completely stop a 30 MeV deuteron. The neutrons born in the target pass on through the rest of the beryllium, an 0.5 mm copper cover, and a 1 mm copper plate containing the cooling water channels. A cross section is shown in Fig. 1.

The deuteron beam was collimated and swept so as to produce a nearly uniform neutron fluence over the detector foils, which measured 1.59 × 6.25 cm. The collimator was a tantalum plate with a slot measuring 5 mm in width and 11 mm in total length. The ends of the slot had a 2.5 mm radius of curvature. The beam was swept back and forth a distance of 6 mm with a trapezoidal current in the bending magnet, such that it paused at each end of the collimator slot for a short time. The ratio of time in transit to time spent at the ends was 4:5.

The arrangement of detector foils is shown in Fig. 2. The front face of the rear assembly was 40 mm behind. The two target assemblies were placed in epoxy fiberglass laminate holders, attached to a mounting rod and covered with thin sheets of mylar. The front target assembly was centered on the deuteron beam. After the irradiation, the alignment was checked by laying the assembly on photographic film and taking an autoradiograph. The alignment of the small central section of the front foil was found to be off center by about 1.5 mm in the length-wise direction and almost exact in the other direction.

The foils in the front packet were dumbbell-shaped, 9.5 mm wide and 22 mm long, with a central rectangular strip 1.59 × 6.25 mm. This shape is identical to that of the ferrite specimens now being routinely irradiated at the Livermore RTNC (ICF) facility. Following the irradiation, the central section was cut away from the larger side strips and used for the radioactivity measurements.

The foils in the rear packet were rectangular strips 12 × 48 mm. These foils were used to check the centering of the target holder and to measure the change in neutron spectrum with increasing angle to the deuteron beam. Following the irradiation, these strips were cut into short segments, 6.4 mm long for individual radioactivity measurements.

The detector foils in the two packets are described in Table 1. Several aluminum foils were included in the packets, so

that corrections could be made for the change in neutron fluence going through the foil stacks.

Table 1

Arrangement of detector foils in the two packets

	Front packet		Rear packet	
	Foil	Thickness (mm)	Foil	Thickness (mm)
1	Al	0.127	Al	0.127
2	Fe	0.127	Fe	0.127
3	Zn	0.127	Zn	0.127
4	Y	0.254	Y	0.254
5	Co	0.254	In_2O_3[a]	0.254
6	Al	0.127	Au	0.127
7	In_2O_3[a]	0.254	Co_2O_3[a]	0.254
8	Au	0.127	Al[b]	0.127
9	Co_2O_3[a]	0.254		
10	Al	0.127		

[a] The In_2O_3 and Co_2O_3 were prepared from thin sheets of the oxide pressed in plastic. Each contained about 70% by weight of the element.

[b] The last Al foil in the rear packet was inadvertently omitted.

DETECTOR REACTIONS AND CROSS SECTIONS

The products from 14 nuclear reactions on the eight target materials were measured. These reactions and their effective threshold energies are listed in Table 2. We attempted to choose reactions whose thresholds and peak cross sections covered all parts of the energy interval up to 32 MeV. However, the number of reactions for which cross section data exist above 20 MeV is very limited, we used the entire inventory at our disposal. It was necessary to extrapolate the cross sections from 33 to 30 MeV. In most cases, this can be done with sufficient accuracy because of the small neutron fluences at the highest energies. For two

reactions, $^{54}Fe(n,\alpha)^{51}Cr$ and $^{59}Co(n,2n)^{58}Co$, the cross-section data[2] are not complete enough and they were included only as a calibration.

Table 2

Nuclear Reactions Used for the Spectrum Determination

Reaction	Effective threshold (MeV)	Reaction	Effective threshold (MeV)
$^{27}Al(n,\alpha)^{24}Na$	5	$^{89}Y(n,2n)^{88}Y$	11.6
$^{45}Sc(n,2n)^{44m}Sc$	11.9	$^{90}Zr(n,2n)^{89}Zr$	12.1
$^{45}Sc(n,\gamma)^{46}Sc$	0	$^{169}Tm(n,3n)^{167}Tm$	15.0
$^{54}Fe(n,\alpha)^{51}Cr$	4	$^{169}Tm(n,2n)^{168}Tm$	8.1
$^{54}Fe(n,p)^{54}Mn$	1.5	$^{169}Tm(n,\gamma)^{170}Tm$	0
$^{56}Fe(n,p)^{56}Mn$	4	$^{197}Au(n,4n)^{194}Au$	23.2
$^{59}Co(n,2n)^{58}Co$	10.6	$^{197}Au(n,3n)^{195}Au$	14.8
$^{59}Co(n,\gamma)^{60}Co$	0	$^{197}Au(n,2n)^{196}Au$	8.1
$^{89}Y(n,3n)^{87}Y$	21.1	$^{197}Au(n,\gamma)^{198}Au$	0

The cross-section for the 18 reactions used in the data analysis were obtained by evaluating the data available in the literature.[2-12] Most of the data are from a recent report by Bayhurst et al.[3] who have made what are probably the most accurate cross-section measurements of this type in the 20- to 30-MeV range and a comprehensive evaluation of the experimental data up to 20 MeV (ENDF/B-IV) by Schett et al.[4] The $^{27}Al(n,\gamma)^{24}Na$ excitation function[5,6] is the best known of the 18.

Since natural elements were used in the detector foils, the production of ^{54}Mn in the iron foils could be due in part to the high energy reactions $^{56}Fe(n,$ "nnp"$)^{54}Mn$ where "nnp" is 2np, nd or t. To correct for this, during a later irradiation of tensile specimens, natural Fe and nearly isotopically pure ^{54}Fe and ^{56}Fe foils were placed at a position corresponding to the front foil packet. The results showed that, at this position, 12.3% of the

^{54}Mn is produced by the high energy (E>12 MeV) reactions with ^{56}Fe. Above 12 MeV the shape of the neutron spectra at both positions are nearly identical. By scaling the results obtained at the front position we estimate that 13.6% of the ^{54}Mn was produced from ^{56}Fe at the position of the rear packet.

RESULTS

Foil Activation Data

The radioactivity in the detector foils was measured with a variety of calibrated Ge(Li) detectors.[13] The Sc_2O_3 and Tm_2O_3 plastic foils were ignited, and pure Sc_2O_3 and Tm_2O_3 samples were weighed and prepared for gamma-ray counting. Corrections were made for decay during the irradiation. The final detector results for the front packet are summarized in Table 3. We used the relative activation in the three aluminum foils to correct for the decrease in fluence in the stack of foils; that is, the data for each of the foils were corrected so that the effective fluence would be the same as that in the front aluminum foil. These corrections are included in Table 3. Assuming the foils are located 3.6 mm from the neutron source, they intercept neutrons at angles up to $\theta = 68°$.

The foils in the rear packet were cut into short segments 6.4 mm long using an autoradiograph as a guide to find the position of maximum radioactivity. The results for three sets of segments are given in Table 4. The set marked A is the central section of the radioactive area. Sets B and C are the next two 6.4 mm sections to one side. The autoradiograph showed that the maximum activation (the center of segment A) was about 4 mm from the expected center. The rod holding the two foil packets was apparently at a small angle to the deuteron beam.

The data in Table 4 have been corrected for the small ($\sim$ 5%) $1/r^2$ decrease in fluence through the foil stack, assuming that the front foil was 43.6 mm from the source of neutrons. The angular position of the foils with respect to the deuteron beam is also given.

Data Analysis

The foil activation data were initially analyzed with SPECTRUM, a computer program that performs a weighted least-squares analysis of the data (atoms/gram and cross sections) to obtain the neutron fluence in seven energy groups. The somewhat unexpected importance of the low energy neutrons revealed by this work[14] led to an attempt to improve resolution at low energies. Experimental results to correct for high energy ^{54}Mn production were obtained, and the (n,γ) data were recovered from the counting results.

Table 3

Final Detector Activation Results for the Front Foil Packet ($\theta = 3 \pm 68°$).

The results are given as atoms of product per gram of detector element.

Product	Atoms/gram	Geometrical correction	Corrected atoms/gram
^{24}Na	1.71×10^{13}	1.00	1.71×10^{13}
^{44m}Sc	6.28×10^{12}	1.49	9.33×10^{12}
^{46}Sc	5.92×10^{11}	1.49	8.82×10^{11}
^{51}Cr	3.86×10^{11}	1.03	3.96×10^{11}
^{54}Mn [a]	3.72×10^{12}	1.03	3.82×10^{12}
^{56}Mn	7.18×10^{12}	1.03	7.38×10^{12}
^{58}Co	3.14×10^{13}	1.17	3.68×10^{13}
^{60}Co	6.66×10^{11}	1.17	7.79×10^{11}
^{87}Y	1.28×10^{12}	1.10	1.41×10^{12}
^{88}Y	3.09×10^{13}	1.10	3.40×10^{13}
^{89}Zr	1.39×10^{13}	1.05	1.47×10^{13}
^{167}Tm	7.23×10^{12}	1.31	9.44×10^{12}
^{168}Tm	3.12×10^{13}	1.31	4.08×10^{13}
^{170}Tm	4.37×10^{12}	1.31	5.72×10^{12}
^{194}Au	2.45×10^{11}	1.39	3.40×10^{11}
^{195}Au	5.67×10^{12}	1.39	7.88×10^{12}
^{196}Au	2.79×10^{13}	1.39	3.87×10^{13}
^{198}Au	1.89×10^{12}	1.39	2.63×10^{12}

[a] The values given here should be reduced by 12.3% to correct for production from ^{56}Fe (see text).

Table 4

Final Detector Activation Results for
Three Sections Cut from the Rear Packet.

The results are given as atoms of product per gram of detector element.

Product	Corrected atoms/gram		
	Set A (θ = 0 - 11°)	Set B (θ = 8 - 11°)	Set C (θ = 16 - 10°
^{24}Na	8.09×10^{11}	6.66×10^{11}	3.44×10^{11}
^{44m}Sc	4.48×10^{11}	4.00×10^{11}	2.30×10^{11}
^{51}Cr	1.96×10^{10}	1.70×10^{10}	9.33×10^{9}
^{54}Mn [a]	1.48×10^{11}	1.29×10^{11}	8.00×10^{10}
^{56}Mn	3.66×10^{11}	3.16×10^{11}	1.70×10^{11}
^{87}Y	5.25×10^{10}	5.24×10^{10}	3.83×10^{10}
^{88}Y	1.87×10^{12}	1.37×10^{12}	7.17×10^{11}
^{89}Zr	7.80×10^{11}	6.68×10^{11}	3.86×10^{11}
^{167}Tm	4.40×10^{11}	4.09×10^{11}	2.62×10^{11}
^{168}Tm	2.04×10^{12}	1.81×10^{12}	9.60×10^{11}
^{170}Tm	2.34×10^{11}	2.35×10^{11}	2.00×10^{11}
^{194}Au	1.05×10^{10}	1.28×10^{10}	1.17×10^{10}
^{195}Au	3.67×10^{11}	3.36×10^{11}	2.24×10^{11}
^{196}Au	1.91×10^{12}	1.64×10^{12}	9.09×10^{11}
^{198}Au	1.04×10^{11}	1.09×10^{11}	1.02×10^{11}

[a] The values given here for Set A should be reduced by 13.6% to correct for production from ^{56}Fe (see text).

Analyses of the foil data for the front foils and Set A of the rear foils have been made using the SAND-II spectral unfolding code. One hundred groups spanned the energy range from 10^{-9} to 30 MeV. The integral neutron flux above a cutoff energy, E, at 20 μA beam current is given in Table 5 for a number of values of E. Note that at both positions half the neutrons have energies less than about 7 MeV.

The differential neutron flux (n/MeV/cm^2 - sec) at 20 μA beam is shown in Fig. 3 for the front foils and in Fig. 4 for the rear foils (Set A). Bar graphs delineating 5% limits on foil response functions are shown superimposed on the differential spectra. The ^{169}Tm (n, γ)^{170}Tm reaction was omitted since it is not yet in the SAND-II library. The ^{54}Fe (n, α)^{51}Cr reaction was rejected by the code and was not used in fitting either spectra. The ^{59}Co(n, 2n)^{58}Co reaction is absent for Set A since Co was not included in the second foil packet.

Only preliminary evaluations for rear sets B and C have been made. Results for Set B are nearly identical to those for Set A. Set C shows a considerable reduction in neutrons above 6 MeV and little change below 6 MeV. This illustrates the large difference in isotropy between high and low energy neutrons.

Error Analysis

Error analysis calculations were performed for the SAND-II spectral unfolding code using the routine SANDANL. This program was written by G. R. Odette (University of California at Santa Barbara) and modified by L. R. Greenwood (ANL) for general usage. A Monte Carlo technique is used to determine the effect on the unfolded spectrum of random changes in foil activities, nuclear cross sections, and the starting trial flux spectrum. Cross section errors were taken from reference 15 and activity errors were estimated from the experimental data. The extent of variations in trial solutions depended on the sensitivity at any particular energy, i.e., the largest variations were at low neutron energies where the foil coverage is least.

The results of the analysis are shown in Fig. 5 for the front foils and in Fig. 6 for Set A. The three curves represent the mean solution plus or minus one standard deviation. The absolute errors are, of course, somewhat arbitrary since precise cross section errors are unavailable. However, relative errors are believed to accurately represent the ability of SAND-II to unfold the spectrum from the available foil coverage. The large errors below 4 MeV are entirely due to variations in the input trial solution since the foil coverage is poor in this energy region.

Table 5

Integrated Neutron Flux (n/cm^2 - sec)
with Energy Greater than E at 20 μA Beam Current.

E (MeV)	Front Foils	Rear Foils (Set A)
1×10^{-9}	4.539×10^{12}	1.970×10^{11}
1×10^{-2}	4.535×10^{12}	1.969×10^{11}
1×10^{-1}	4.494×10^{12}	1.955×10^{11}
5×10^{-1}	4.310×10^{12}	1.885×10^{11}
1	4.090×10^{12}	1.789×10^{11}
3	3.250×10^{12}	1.336×10^{11}
6	2.449×10^{12}	1.040×10^{11}
10	1.684×10^{12}	0.850×10^{11}
14	0.945×10^{12}	0.493×10^{11}
20	0.284×10^{12}	0.125×10^{11}

CONCLUSIONS

Since accurate neutron cross-section data in the 20-30 MeV range have not been available until recently,[3] this experiment probably represents the first attempt to measure the shape of a neutron distribution extending to 32 MeV using the foil-activation technique. Several previous measurements have been made of the 0° neutron spectrum resulting from deuteron bombardment of thick beryllium targets with deuteron energies in the neighborhood of 30 MeV.[16-21] Of these, five were performed by the time-of-flight technique in which the detector is placed in "good" geometry, i.e., well-collimated and at a large distance from the target.[16-20] In the sixth, foil activation was used, but the source-sample distance was not given.[21] In general, these previous measurements have yielded a broad peak with a maximum at about 0.4-0.5 of the deuteron energy, and a full width at half-maximum of about 0.35-0.45 of the deuteron energy. In measurements which extended below 4-5 MeV, the neutron intensity was observed to rise slightly at low energies, showing a minimum at this energy. The present results show a much greater contribution from lower-energy (<10 MeV) neutrons, particularly in the spectrum at a point, just behind the beryllium target, where the peak is not observed at all.

It appears from the present data as well as larger-angle time-of-flight data[22,23] that this difference can be attributed to the fact that foils placed at a distance from the beryllium target which is less than or comparable to the lateral dimensions of the beam spot are able to intercept neutrons emitted at large angles from the direction of the deuteron beam. These neutrons generally have lower energies than the forward-directed component because they arise from compound-nucleus interactions, rather than from stripping. As foils are moved back from the target, the lower energy component drops more rapidly than the forward-directed component because of the geometric effect, and the peaked distribution is revealed.

At the rear foil position 40 mm back, the total yield and differential spectra are in reasonably good agreement with time-of-flight data.[24,25] These observations show the importance of evaluating the neutron spectra near the target if materials are to be irradiated in this location. Because of the importance of the low energy neutrons, further work will require greater foil coverage at low energies.

ACKNOWLEDGEMENTS

We would like to acknowledge the help and support of Professor John Jungerman and the staff of the Crocker Nuclear Laboratory in performing the irradiation, and the assistance of C. M. Logan of LLL who provided the specially designed beryllium target. We would like to thank T. M. Adams, Ruth Anderson, Lila Onstott, and Norman Smith for their help with the counter calibrations and data analysis.

REFERENCES

1. C. M. Logan, R. Booth and R. A. Nickerson, A Compact Beryllium Target for the Production of Fast Neutrons, UCRL 78754 (1976) (submitted to Nucl. Inst. and Methods)
2. M. D. Goldberg et al., Brookhaven National Laboratory, Rept. BNL-325, "Neutron Cross Sections," Vol. IIA, Z=21 to 40, 2ND ED., Supp. No. 2 (1966).
3. B. P. Bayhurst, et al., Phys. Rev. C 12, 451 (1975).
4. B. A. Magurno, ENDF/B-IV Dosimetry File, Brookhaven National Laboratory, Rep. BNL-NCS-50446 (1975).
5. H. Vonach et al., Z. Phyzik 237, 155 (1970).
6. Y. Kanda and R. Nakasima, Proc. Conf. on Neutron Cross Sections and Technology, March 4-7, 1968, Washington, D.C., D. T. Goldman, Ed. (NBS Special Publications 299) Vol. 1, p. 193.
7. R. J. Prestwood and B. P. Bayhurst, Phys. Rev. 121, 1438 (1961).

8. D. R. Nethaway, Nucl. Phys. A 190, 635 (1972).
9. D. R. Nethaway, unpublished results (1975).
10. R. L. Simons and W. N. McElroy, Evaluated Reference Cross Section Library, Battelle Northwest Laboratory, Rept. BNWL-1312 (1970).
11. S. K. Ghorai and W. L. Alford, Bull. Am. Phys. Soc. II, 20, 560 (1975).
12. D G. Gardner, unpublished calculations (1969-1975).
13. R. Gunnink and J. B. Niday, Computerized Quantitative Analysis by Gamma-Ray Spectrometry. Vol 1: Description of the Gamanal Program, Lawrence Livermore Laboratory, Rept. UCRL-51061, Vol. 1 (1972).
14. D. R. Nethaway, R. A. Van Konynenburg and T. M. Adams, Measurement of the Neutron Spectrum from the Reaction of 30-MeV Deuterons on a Thick Beryllium Target, Lawrence Livermore Laboratory, Rept. UCRL-52024 (1976).
15. W. McElroy et al., Nucl. Tech. 25, 211 (1975)
16. J. P. Meulders et al., Phys. Med. Biol. 20, 235 (1975).
17. A. Goland, Brookhaven National Laboratory, personal communication (1976).
18. L. L. Lucas and J. W. Root, J. Appl. Phys. 43, 3886 (1972).
19. R. Theus, Naval Research Laboratory, personal communication (1976).
20. S. Johnsen, University of California at Davis, personal communication (1976).
21. I. Heertje and A. H. W. Aten, Jr., Physica 30, 978 (1964).
22. K. A. Weaver, Neutrons from Deuteron Bombardment of Light Nuclei, Lawrence Livermore Laboratory, Rept. UCRL-51310 (1972) and Addendum (1973).
23. P. J. Persiani, W. Becker, and J. Donahue (paper presented at this symposium).
24. M. A. Lone (paper presented at this symposium).
25. R. G. Graves, J. B. Smathers, N. Hertel, V. A. Otte, P. R. Almond and W. Grant (paper presented at this symposium).

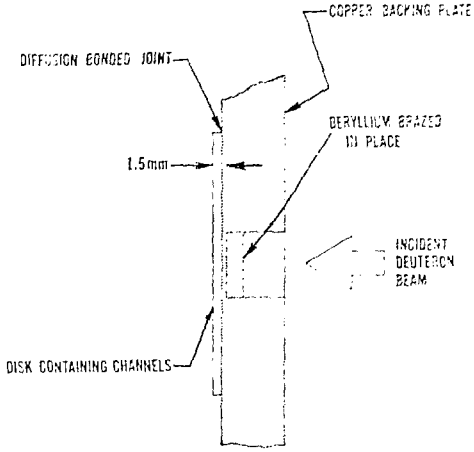

Fig. 1. Cross-section of target system.

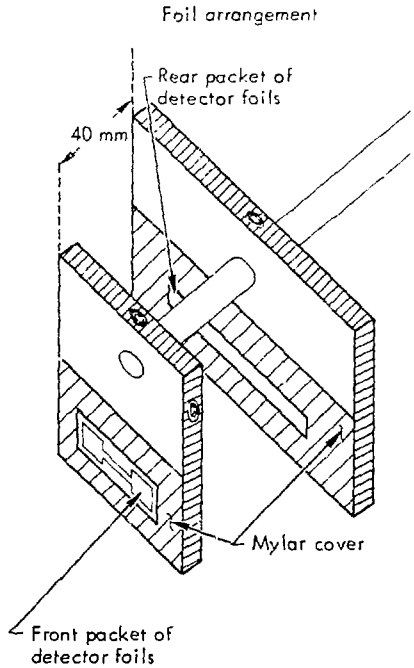

Fig. 2. Diagram showing the arrangement of the front and rear packets of detector foils. The front packet was held against the copper cover plate of the beryllium target assembly.

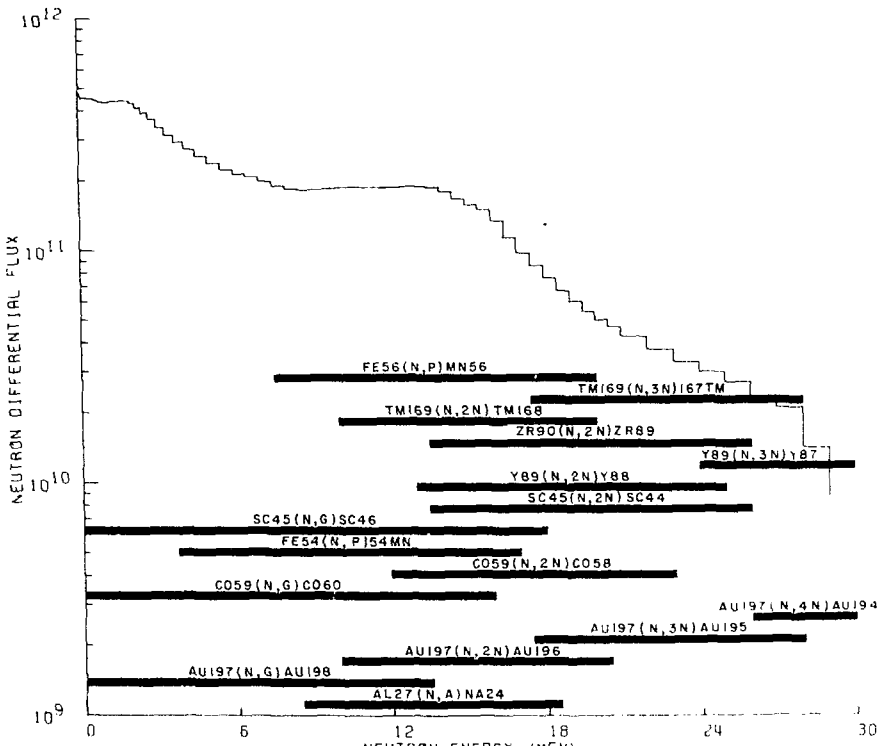

Fig. 3. Differential neutron flux (n/MeV/cm^2-sec) for 30 MeV deuterons on ^{9}Be at 20 μA beam current. Front foils.

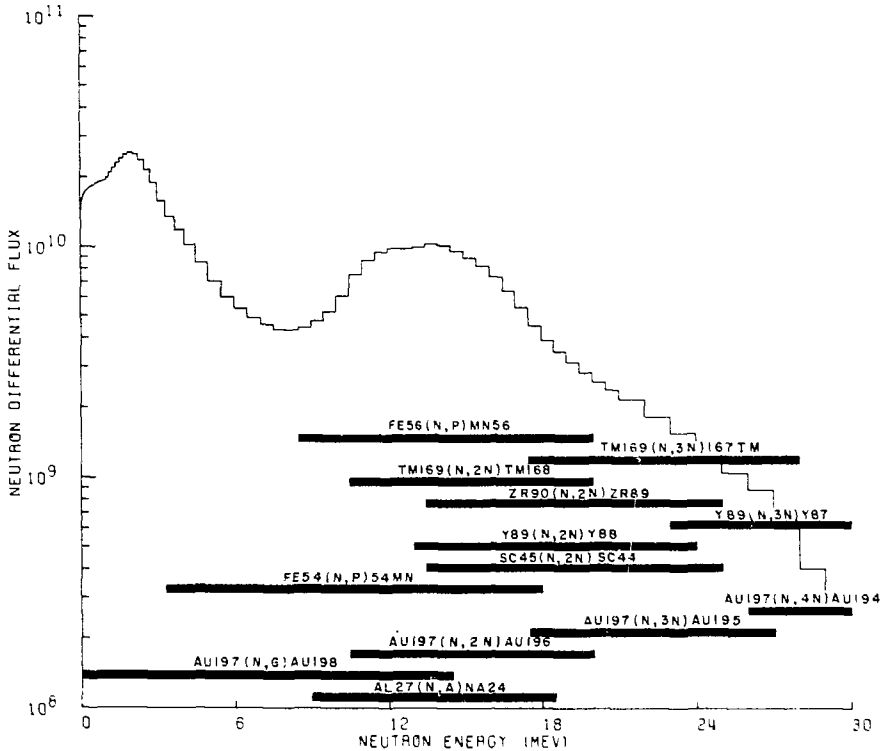

Fig. 4. Differential neutron flux (n/MeV/cm^2-sec) for 30 MeV deuterons on ^{9}Be at 20 μA beam current. Rear foils.

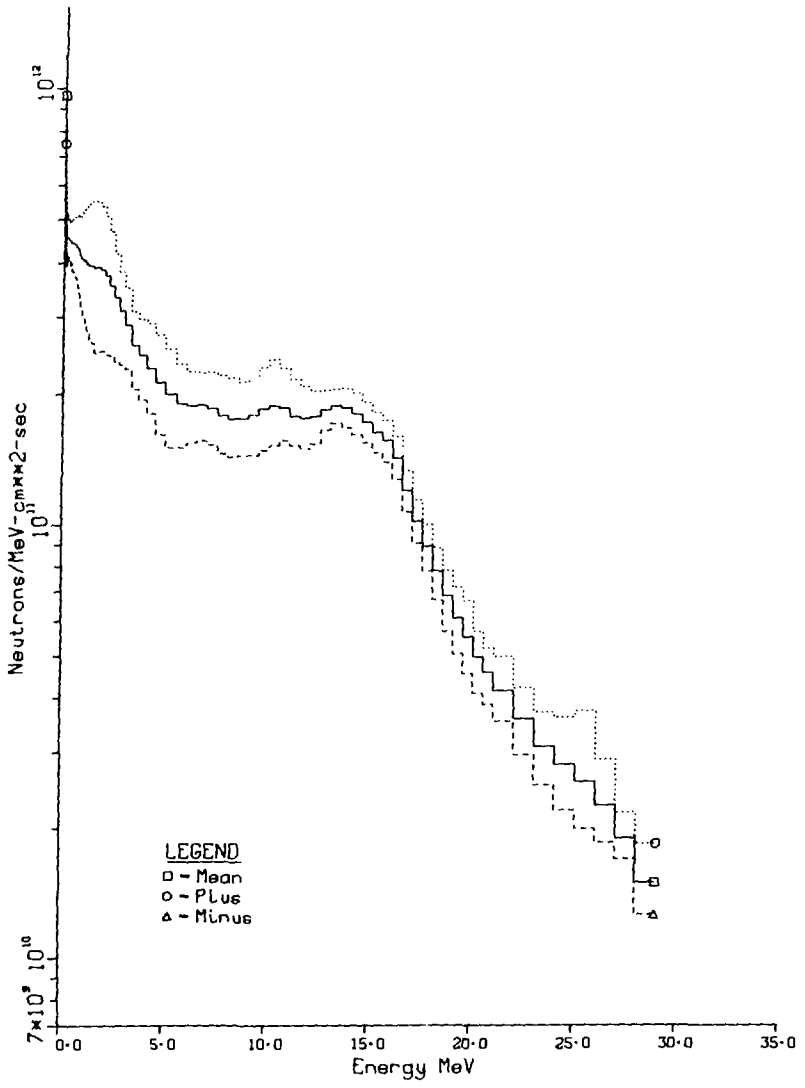

Fig. 5. Error analysis for front foils. The mean spectrum and those corresponding to plus or minus one standard deviation are shown.

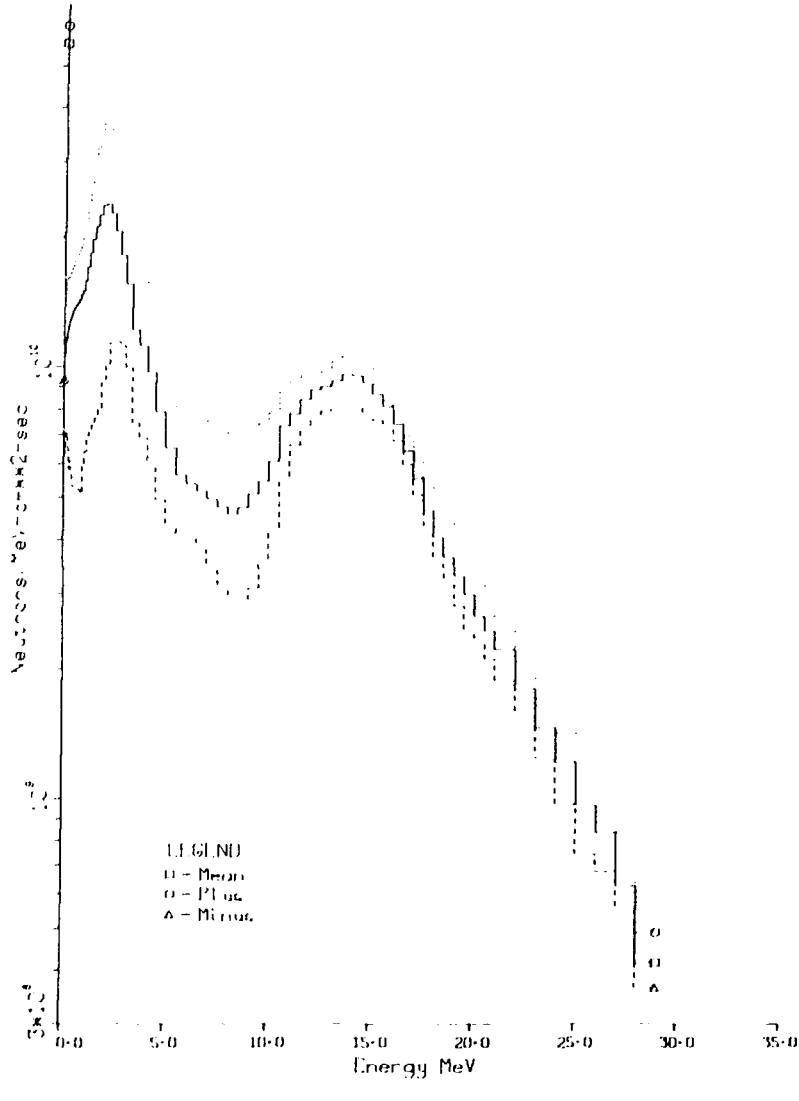

Fig. 6. Error analysis for rear foils (Set A). The mean spectrum and those corresponding to plus or minus one standard deviation are shown.

Conf-770523

Neutron Spectra and Basic Data Requirements for (d,Li) and (d,Be) Target Systems*

P. J. Persiani, W. Becker, and J. Donahue
Argonne National Laboratory, Argonne, Illinois

INTRODUCTION

A primary area of experimental study in the development of the accelerator - (d,Li) target system is the neutronic characteristics of the (d,Li) and/or (d,Be) reactions. Basic differential neutronic data (neutron yield, energy spectra, and angular distribution) are required to effectively understand and interpret the simulated radiation damage effects from this type of testing facility for the purposes relevant to the fusion materials program.

The initial attempt in this direction utilizes the experimental (d,Li) and/or (d,Be) neutronic data which are available but most inadequate at present. However, the attempt does allow articulating the exact basic neutron data needs and the definition of a measurement program.

Target Yields, Angular Dependence and Energy Distribution

The necessary differential neutron data characteristics of a (d,Li) target system is currently inadequate to allow a direct assessment of the neutron radiation environment in the experimental volume of the accelerator - (d,Li) target facility. However, the neutron spectra and intensity available for the material experiments may be initially scoped by utilizing the more extensive (but by no means complete) data available on thick beryllium targets. The lithium target total yields, the angular dependence of the yields, and the varying energy spectra at the different angles, can be assumed as adequately similar to the (d,Be) neutronic characteristics for this preliminary evaluation of the lithium target system. Estimates and extrapolations in generating the necessary detailed differential data for the lithium target are based on interrelating and coalescing the available experimental measurements on beryllium and lithium as reported in the literature.[1-12]

The consistent fitting of data on the total neutron yields[1-7] indicates that the total yields vary approximately as the square of the incident deuteron energy, E_d, over the deuteron energy range of interest for both beryllium and lithium (see Fig. 1). The data point for lithium at the deuteron energy $E_d \approx 22$ MeV, was estimated from integrating the differential data of Daruga and

*Work performed under the auspices of the U. S. Energy Research and Development Administration.

Krasnov,[1] and V. K. Daruga, E. S. Matusevich, and K. Narziev.[2] The direct total yield measurements of Smith and Kruger,[3] and Crandall Millburn, and Schecter[4] utilized the manganese (Mn^{56}) activity in the $MnSO_4$ bath technique. The measurements of Porges, et al.,[5] on beryllium and lithium were obtained from a vanadium solution bath at deuteron energies below 7 MeV. The total yields over a wide range of deuteron energies (15 to 40 MeV) have been measured by Lucas and Root,[7] using the foil distribution method in a paraffin moderator. The reported measurements are approximately 20 to 30% lower than the yields indicated by the curve representing the beryllium data. The energy dependence of the total yields appear to be consistent for the beryllium measurements although the difference will have to be resolved eventually. The two data points for lithium plot approximately with the same energy dependence and with a slightly lower (~25%) total yield in comparison with the beryllium measurements.

The (d,Be) and (d,Li) reactions are comprised of a stripping reaction, with the neutrons emitted in a highly forward bias, and a compound nucleus formation reaction with an isotopic distribution of neutrons. The relative contributions from each of these processes varies for different deuteron energies as can be seen from the composite polar distribution plot in Fig. 2. The data are normalized in the "zero" direction.

The Daruga[2] data for the ~22 MeV incident deuteron extends the neutron energy distribution measurements to 1 MeV and the angular distributions at 0°, 45°, 90°, and 135°. The experimental data are represented as heavy lines in Fig. 3, with the estimated extrapolations represented as normal lines. The extrapolations were based on guidance obtained from Kuchnir's[6] 16 MeV deuteron data and Weaver's[9] 18 MeV deuteron data. As a check on the estimates, the total yield versus neutron energy curves were developed and are presented in Fig. 4. The resulting energy structure curves appear to be consistent with the comparable curves in the Kuchnir and Weaver studies, at least for the 3 MeV cutoff spectrum. The neutron yield per deuteron in the forward direction is presented in Fig. 5 and is found to agree with the Theus et al.,[10] data for the 24.5 MeV deuteron to at least the 3 MeV neutron energy measurement. The solid line represents the experimental yield data as reported by Daruga[2] to the low neutron energy of 1 MeV.

Neutron Spectra and Intensity for Experiments

The Daruga data are more complete in the lower neutron energy region and in the higher angular distributions. At these higher angles, the neutron energy spectrum is softer and as a result contributes significantly to spectra at positions close-in to the target. The Theus et al.,[10] and Saltmarsh et al.,[10,11] data have been obtained at good-geometry positions (i.e., large distances from the source) and this results in a much harder spectrum due to the high forward biased neutrons emitted from the "stripping

reaction" process. It is this spectrum which is usually characterized as the (d,Li) or (d,Be) neutrons to be utilized in simulating radiation damage effects. It is therefore necessary for the materials investigators to determine the spectra existing at irradiation positions close-in to the source (poor-geometry positions).

The preliminary results of a Monte Carlo code developed for the purpose of investigating the neutron spectra to be expected at close-in positions and far-distant positions of material samples, are presented in the set of Figs. 6-12. The 22 MeV deuteron beam current of 100 mA with a Gaussian distribution is assumed to be incident on a cylindrical 10 cm diameter disk source of beryllium. The zones in the figures identify radial zones on a cylindrical target placed at 0.5, 5, and 50 cm from the source. The zones are 1.5 cm annular rings. The first two figures display the spectrum softening variation in placing samples in regions from 3 to 5 cm adjacent to the central zone. This spectrum softening effect is not as marked at a distance 5 cm from source (Figs. 8 and 9). For distances of 50 cm from the source (Figs. 10-12), the spectrum changes are less pronounced, but the flux is decreased by one to two orders of magnitude from the close-in position.

The comparison indicates that to establish a neutron flux mapping and spatial dependence of the neutron spectra in the experimental test region, it is necessary to obtain a more complete angular distribution and energy distribution data for different incident deuteron energies.

To demonstrate the importance that the neutron yields must be measured in the low neutron energy region, the set of Figs. 13 to 19 are included. In this latter set, the Daruga original energy yield data were "cut-off," i.e., flared from the 3 MeV energy to zero. This represents the data usually presented with an absence of information in the energy region below 2 to 3 MeV. A comparison of the previous figures and the 3 MeV cut-off data, clearly demonstrates the significant differences in the energy spectrum that can be expected at all positions from the target.

For higher energy incident deuterons 35 to 40 MeV[10,11,12] where the neutrons result predominently from the stripping reactions with a strong forward bias, and with a more sharply defined energy distribution, the low energy neutrons would not contribute as significantly to the spectra at close-in positions to the source. However, for deuteron energies in the range of 5 to 30 MeV, the spectra at close-in positions will be significantly effected by the yield of low energy neutrons at the higher angular directions.

Differential Data Measurements Program

The experimental data requirements and measurements for (d,Li) and/or (d,Be) neutron characteristics should include:

1. Total neutron yields;

2. Neutron spectra at angles ranging from zero to 150 degrees or higher;
3. Neutron energy spectra should be established over the total neutron energy range;
4. Items (2) and (3) are to be measured at many positions from the source;
5. All of the above measurements are to be completed for the range of deuteron energy between 5 and 40 MeV.

REFERENCES

1. V. K. Daruga and N. N. Krasnov, Atomnaya Energiya, 30, 399 (1971).

2. V. K. Daruga, E. S. Matusevich, and K. Narziev, Atomnaya Energiya, 33, 934 (1974).

3. L. W. Smith and P. G. Kruger, Phys. Rev. 83, 1137 (1951).

4. W. E. Crandall, G. P. Millburn, and L. Schecter, Phys. Rev. 28, 273 (1957).

5. K. Porges, J. L. Snelgrove, R. Gold, A. DeVolpi, R. J. Armani and C. E. Cohn, Thick Target Neutron Yields of Lithium and Beryllium Targets Bombarded with Protons and Deuterons Applied Physics Division Annual Report, 1970 to 1971, ANL-7910.

6. F. T. Kuchnir, L. S. Skaggs, A. J. Elwyn, F. P. Mooring, and N. A. Frigerio, Design of a Neutron Therapy Facility for a 30-Inch Cyclotron," Proc. 6th International Cyclotron Conf., Vancouver, Canada, 18-21 July 1972, p. 638.

7. L. L. Lucas, and J. W. Root, J. Appl. Phys., 43, 3886 (1972).

8. A. J. Allen, J. F. Nechaj, K. H. Sun, and B. Jennings, Phys. Rev. 81, 536 (1951).

9. K. A. Weaver, J. D. Anderson, H. H. Barschall, and J. C. Davis, Nucl. Sci. Eng., 52, 35-45 (1973).

10. R. B. Theus, R. O. Bondelid, F. H. Attix, L. S. August, P. Shapiro, R. E. Surratt, and C. C. Rodgers, Cancer, 34, 17 (1974). See also A. N. Goland, et al., Production and Use of Li(d,n) Neutrons For Simulation of Radiation Effects in Fusion Reactors, Proc. Int. Conf. on Radiation Test Facilities for The CTR Surface and Materials Program, 15-18 July, 1975, Argonne National Laboratory, ANL/CTR-75-4.

11. M. J. Saltmarsh and J. A. Horak, A Large-Volume Intense Neutron Source For CTR Materials Study, Proc. Int. Conf. on

Radiation Test Facilities for the CTR Surface and Materials Program, 15-18 July, 1975, Argonne National Laboratory ANL/CTR-75-4.

12. M. J. Saltmarsh, C. A. Ludemann, C. B. Fulmer, R. C. Styles, Characteristics of an Intense Neutron Source Based on the d+Be Reaction, ORNL/TM-5696 (1976).

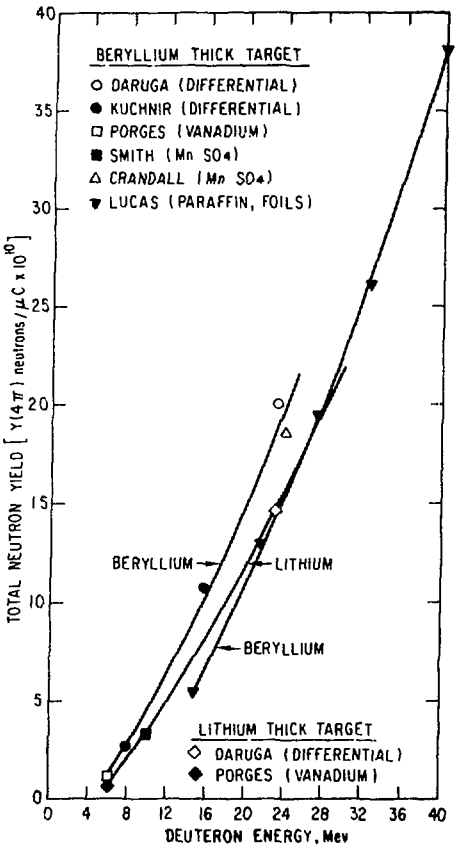

Fig. 1. Total Neutron Yield vs. Deuteron Energy for Thick Beryllium and Lithium Targets.

NEUTRON YIELD AS FUNCTION OF LABORATORY ANGLE
DEUTERONS ON BERYLLIUM & LITHIUM

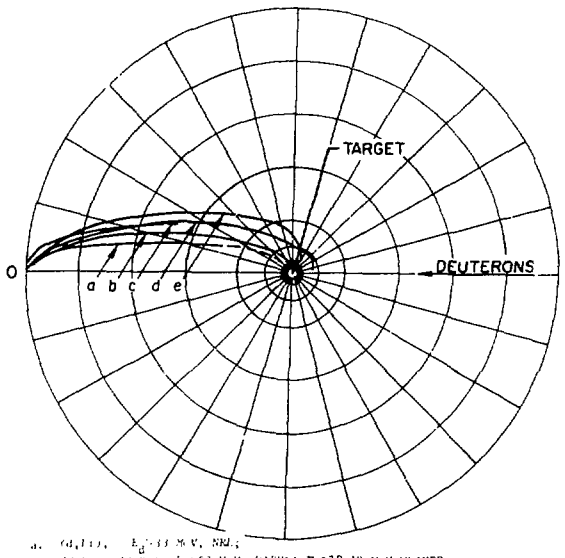

a. (d,Li), E_d~13 MeV, NRL;
b. (d,Li), (d,Be), E_d~22 MeV, DARUGA; E_d~18-19 MeV, WEAVER;
c. (d,Li), E_d~14 MeV, NRL;
d. (d,Be), E_d~15 MeV, ALLEN; E_d~16 MeV, KUCHNIR; E_d~14 MeV, WEAVER;
e. (d,Be), E_d~8 MeV, KUCHNIR; E_d~9 MeV, WEAVER;

Fig. 2. Neutron Yield as Function of Laboratory Angle for Deuterons on Beryllium and Lithium

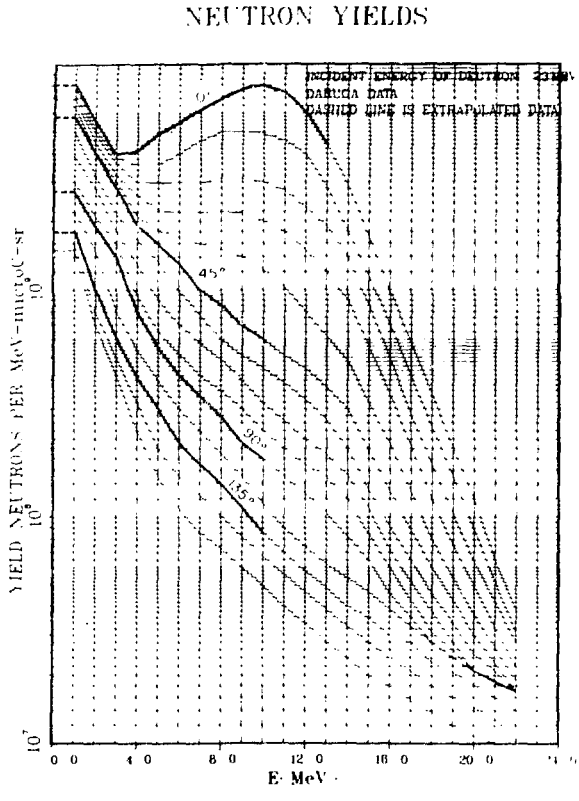

Fig. 4. Neutron Yield vs. Neutron Energy at Various Angles for 23 MeV Deuteron on Thick Beryllium Target.

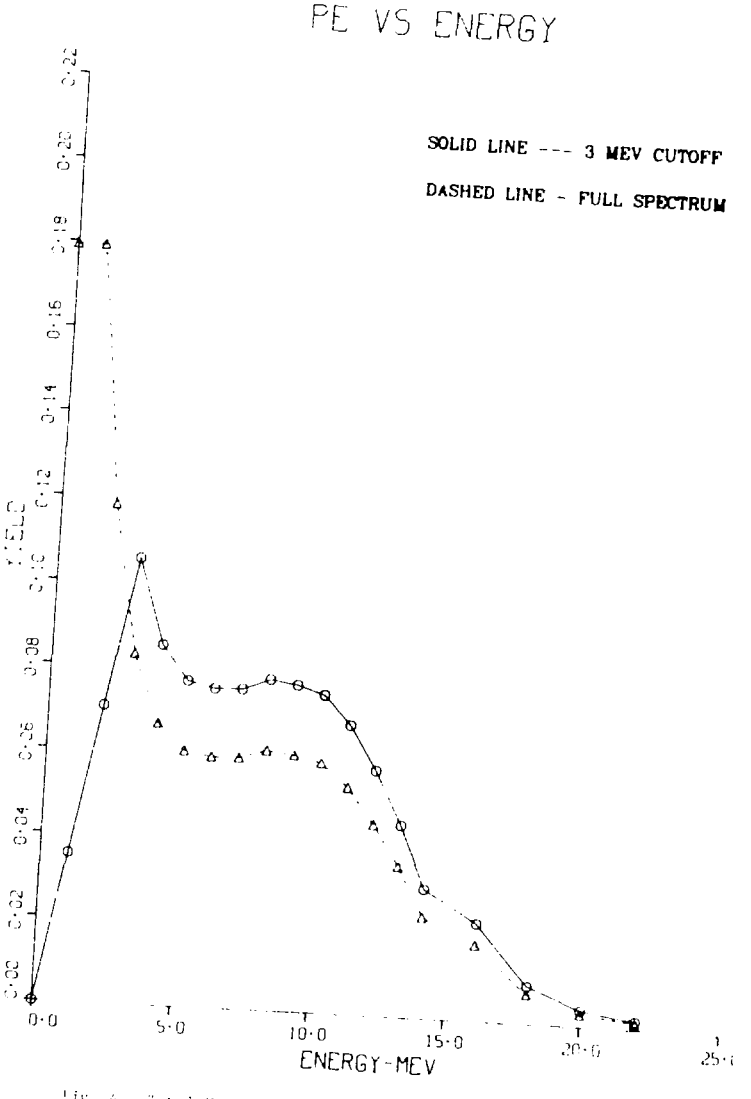

Fig. 4. Total Neutron Yield Distribution vs. Neutron Energy for 22 MeV Deuterons on Thick Beryllium Target.

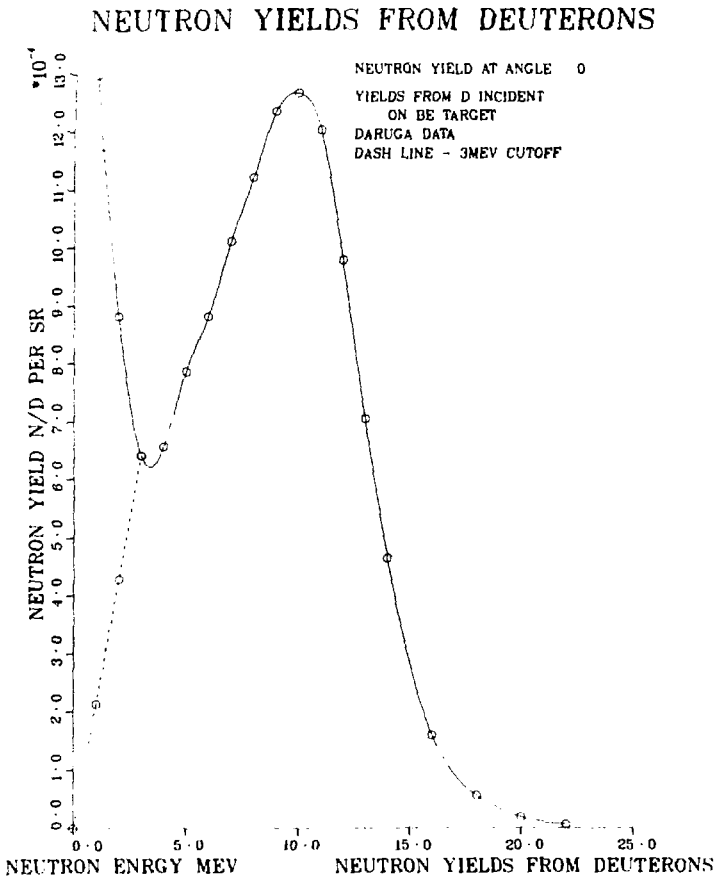

Fig. 5. Neutron Yield in Forward Direction for 23 MeV Deuteron on Thick Beryllium Target.

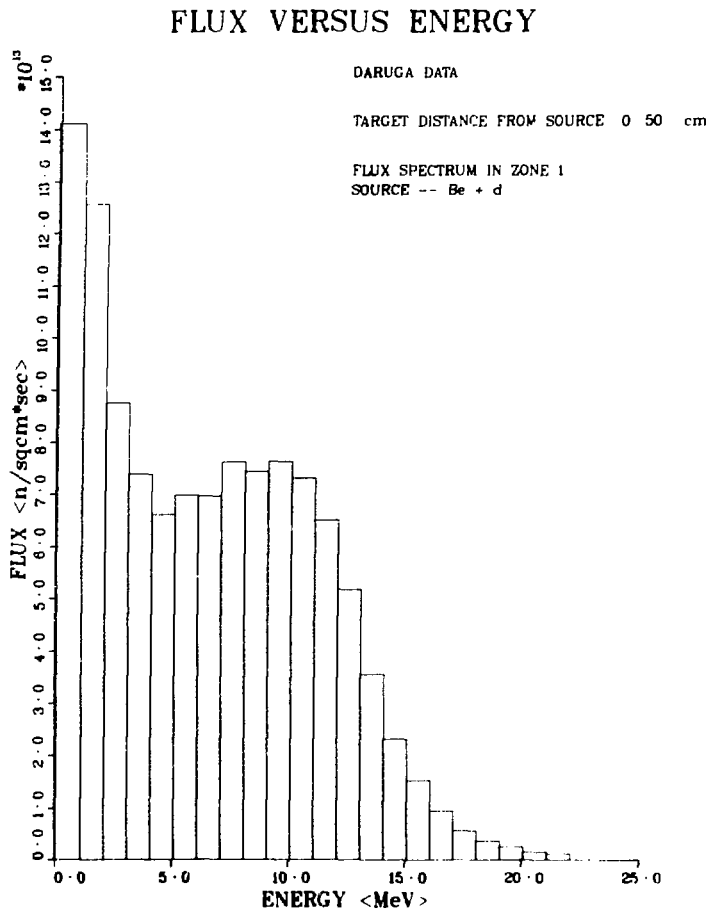

Fig. 6. Neutron Flux Energy Distribution (Be+d) in Zone 1, at 0.5 cm from Target Surface.

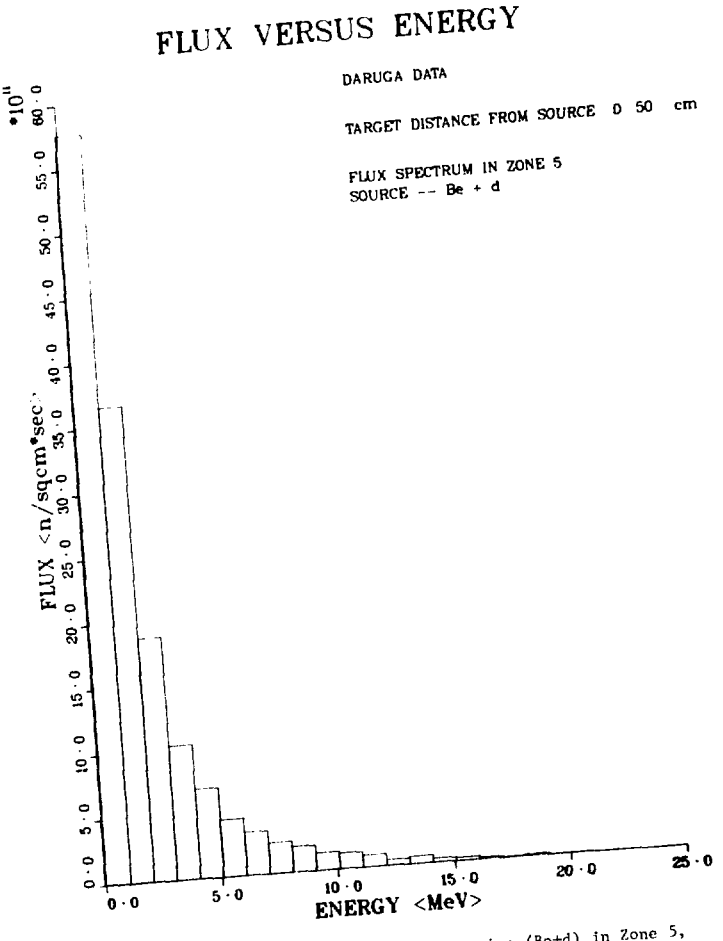

Fig. 7. Neutron Flux Energy Distribution (Be+d) in Zone 5, at 0.5 cm from Target Surface.

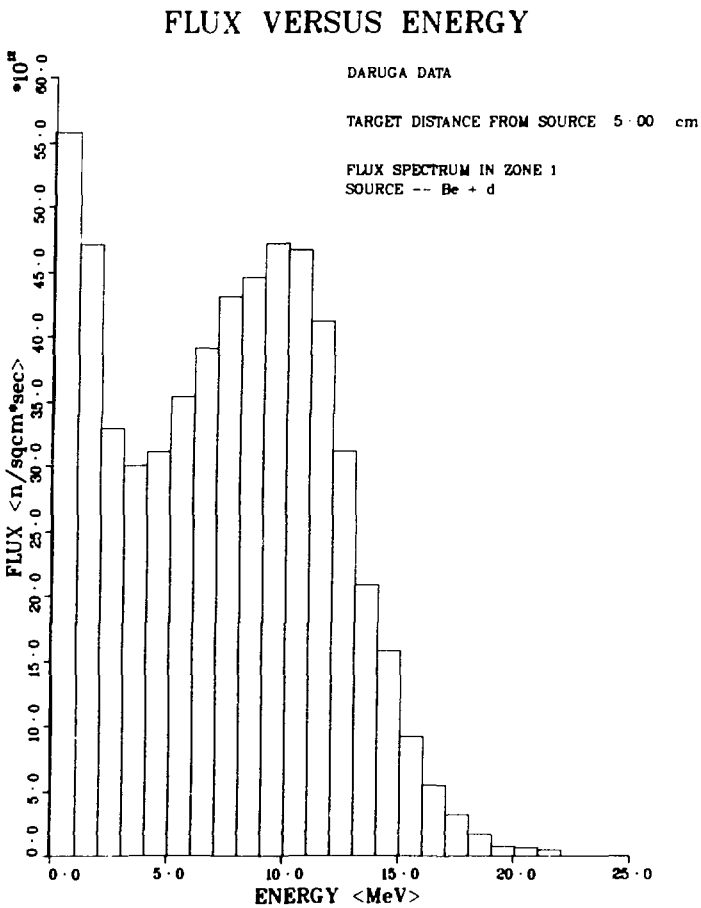

Fig. 8. Neutron Flux Energy Distribution (Be+d) in Zone 1, at 5 cm from Target Surface.

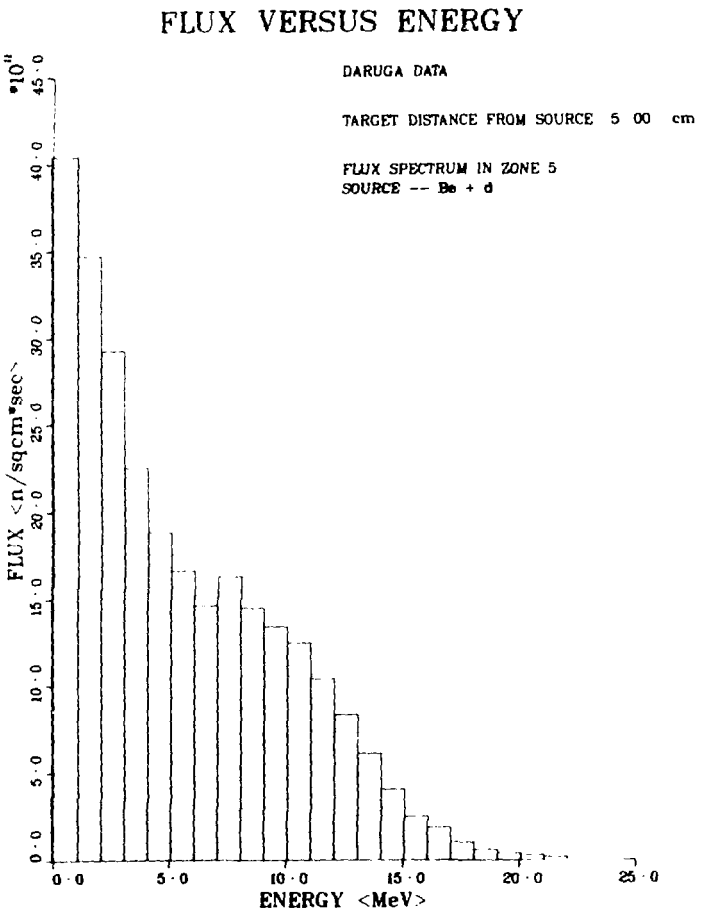

Fig. 9. Neutron Flux Energy Distribution (Be+d) in Zone 5, at 5 cm from Target Surface.

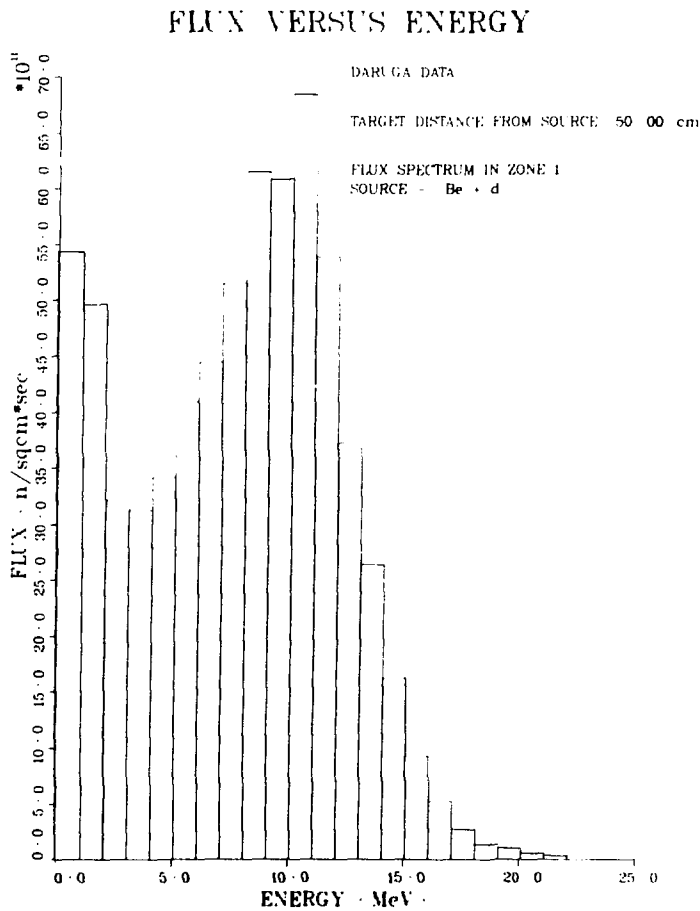

Fig. 10. Neutron Flux Energy Distribution (Be+d) in Zone 1, at 50 cm from Target Surface.

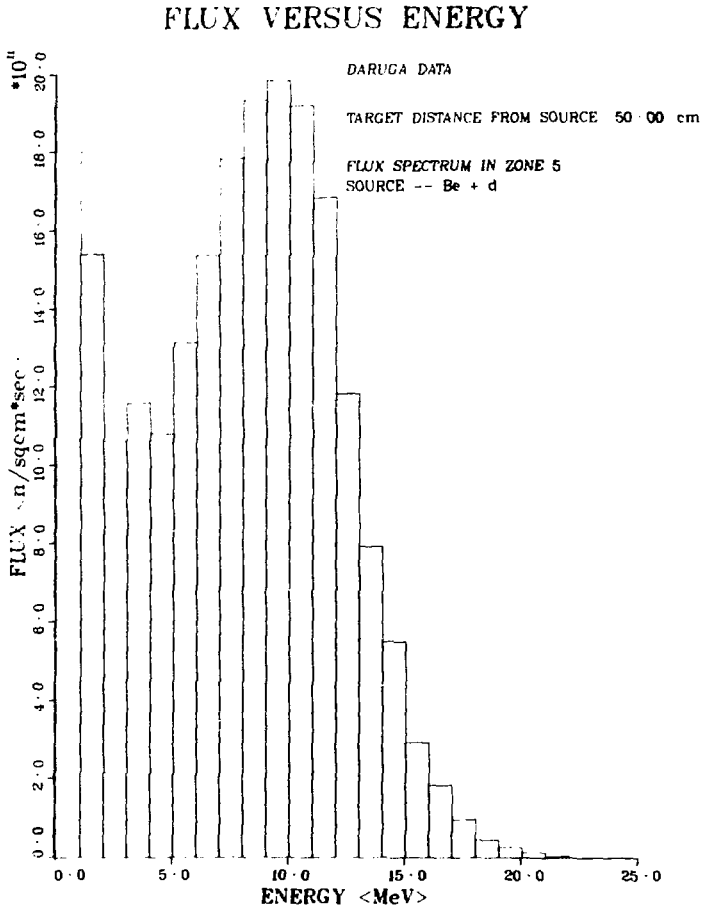

Fig. 11. Neutron Flux Energy Distribution (Be+d) in Zone 5, at 50 cm from Target Surface.

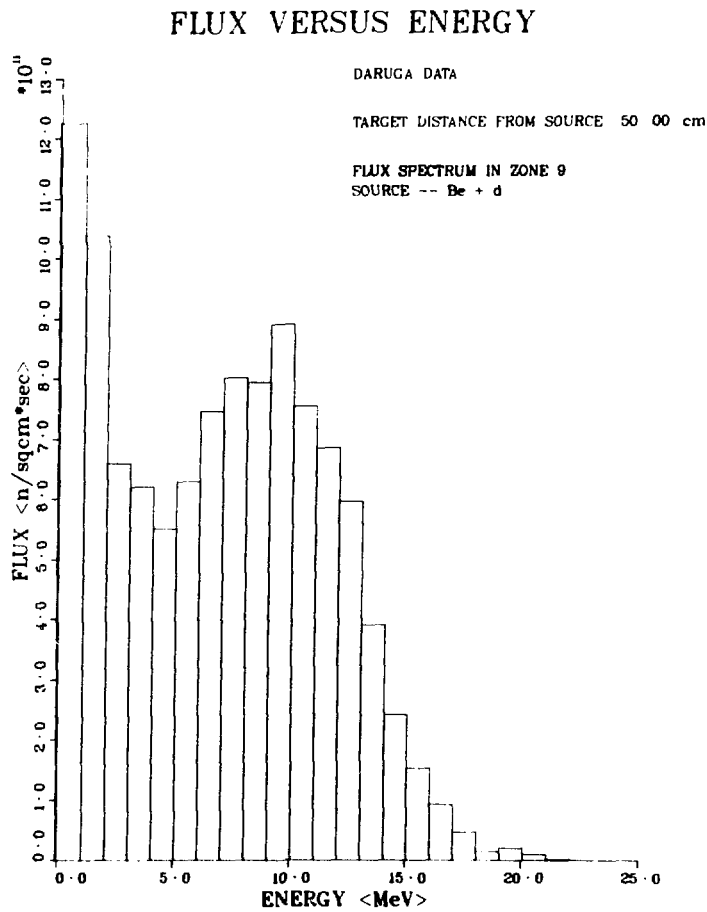

Fig. 12. Neutron Flux Energy Distribution (Be+d) in Zone 9, at 50 cm from Target Surface.

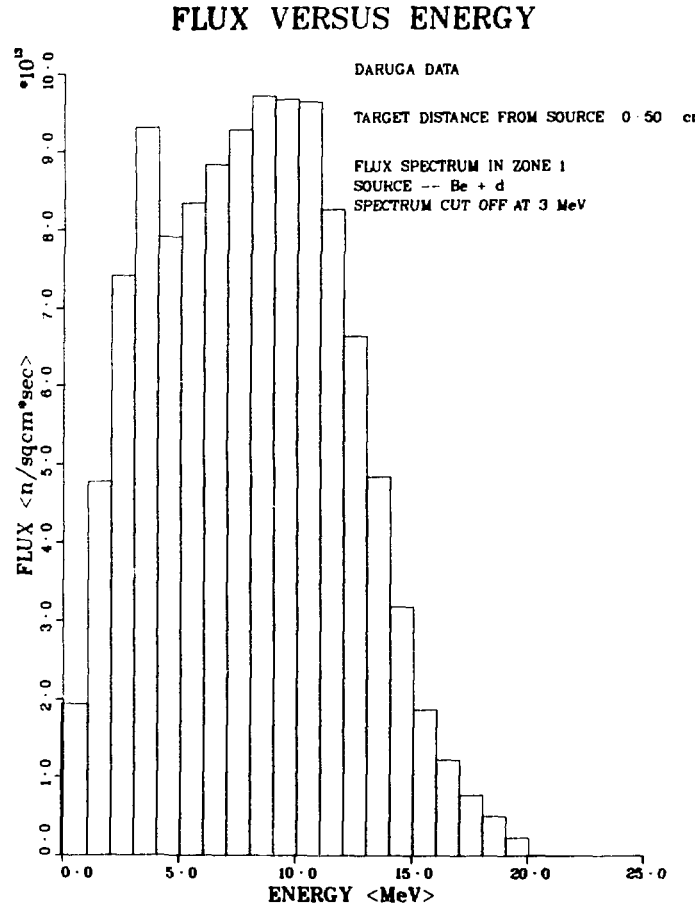

Fig. 13. Neutron Flux Energy Distribution (Be+d) With 3 MeV Cutoff, in Zone 1, at 0.5 cm from Target Surface.

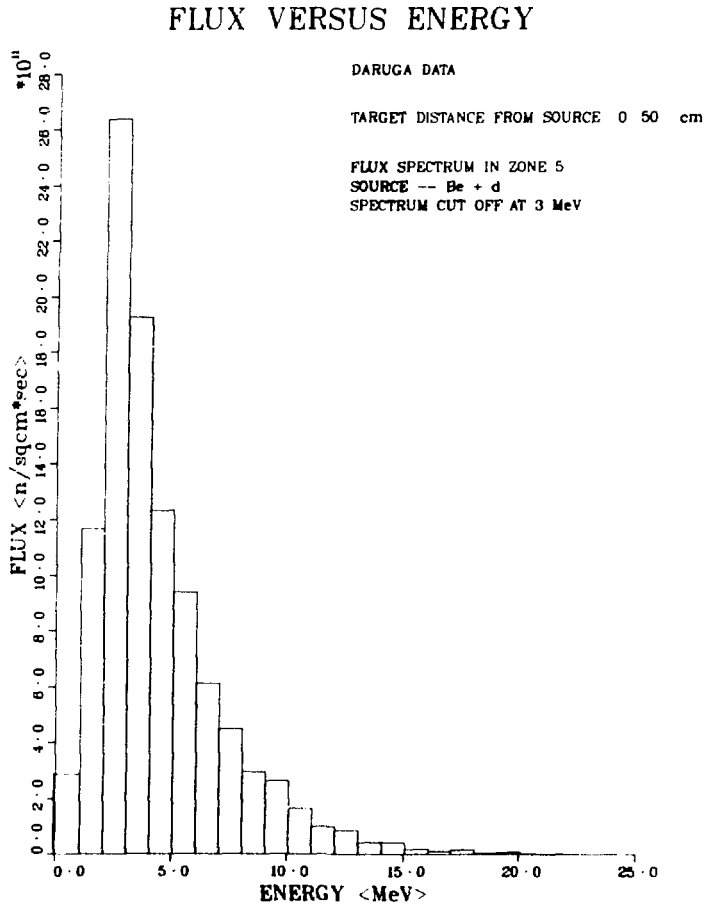

Fig. 14. Neutron Flux Energy Distribution (Be+d) With 3 MeV Cutoff, in Zone 5, at 0.5 cm from Target Surface.

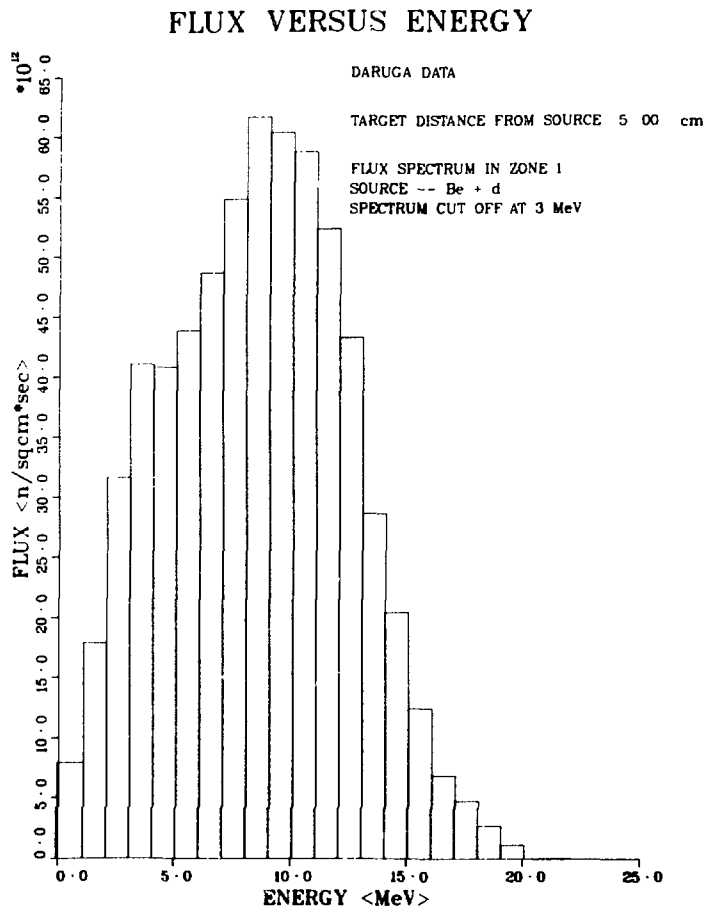

Fig. 15. Neutron Flux Energy Distribution (Be+d) With 3 MeV Cutoff, in Zone 1, at 5 cm from Target Surface.

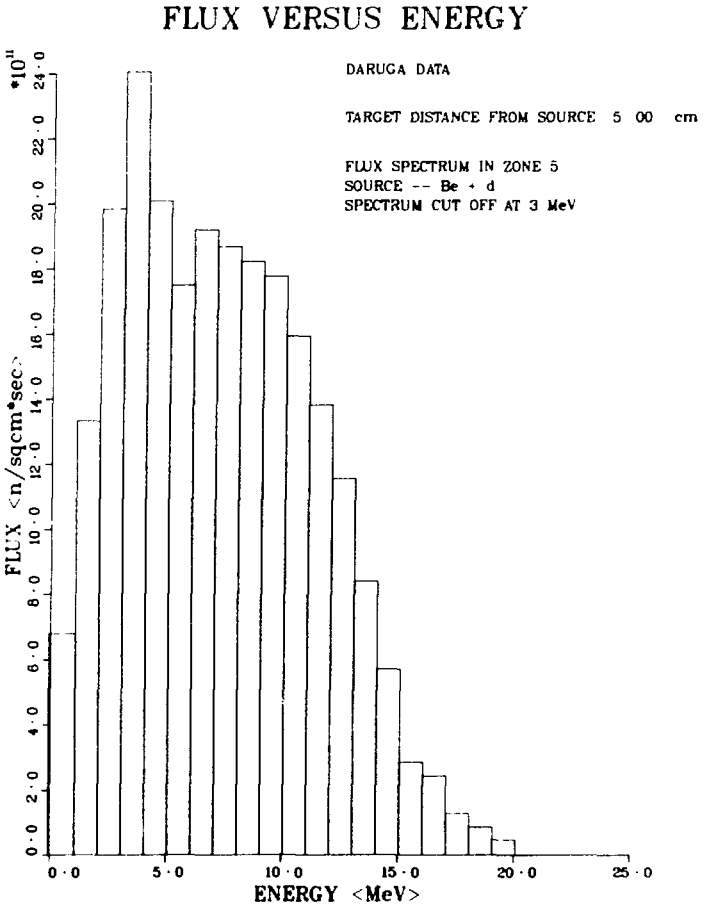

Fig. 16. Neutron Flux Energy Distribution (Be+d) With 3 MeV Cutoff, in Zone 5, at 5 cm from Target Surface.

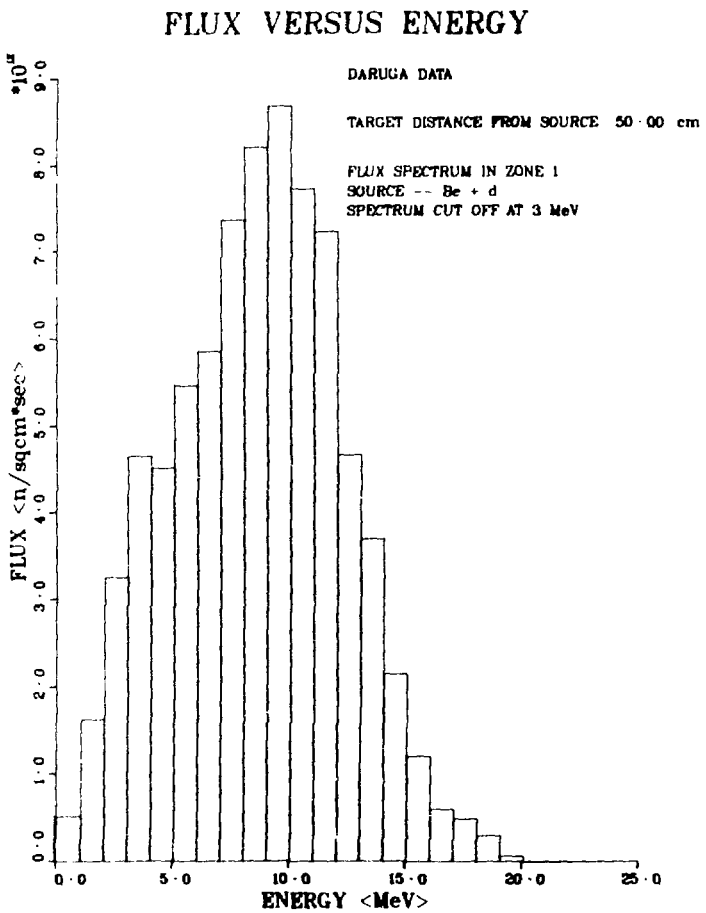

Fig. 17. Neutron Flux Energy Distribution (Be+d) With 3 MeV Cutoff, in Zone 1, at 50 cm from Target Surface.

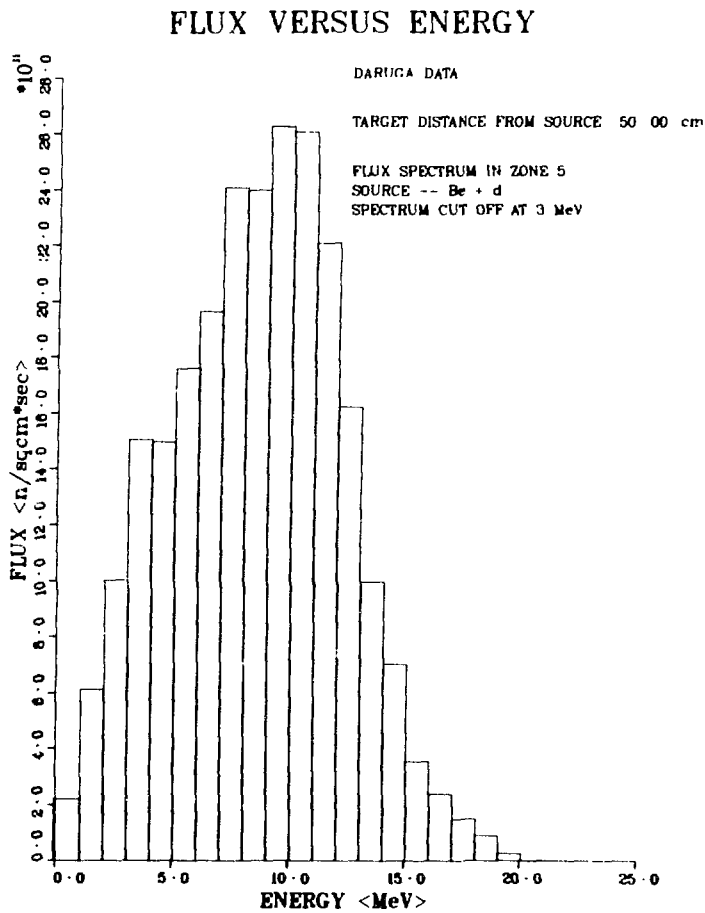

Fig. 18. Neutron Flux Energy Distribution (Be+d) With 3 MeV Cutoff, in Zone 5, at 50 cm from Target Surface.

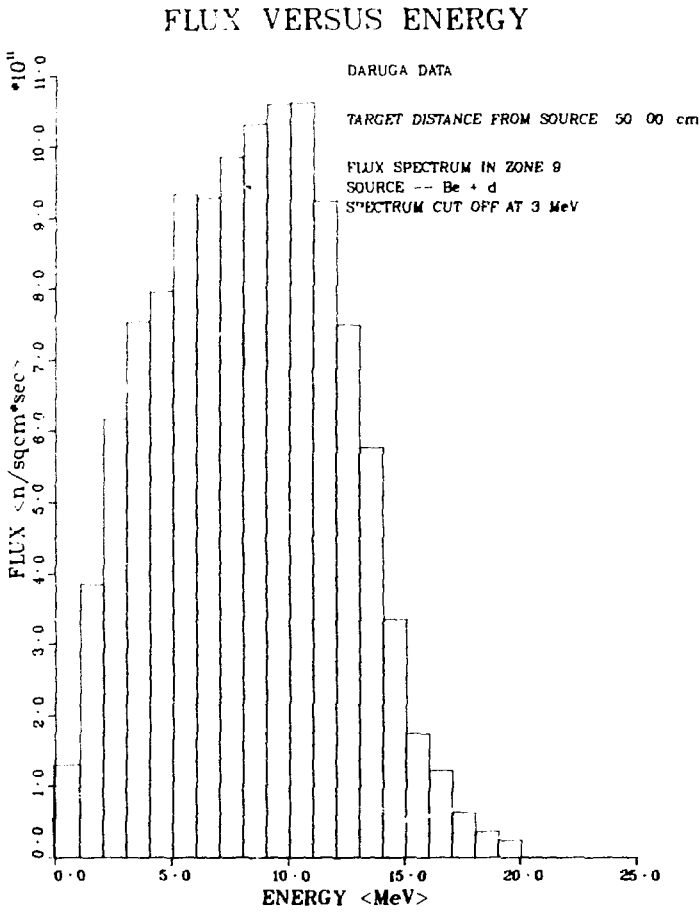

Fig. 19. Neutron Flux Energy Distribution (Be+d) With 3 MeV Cutoff, in Zone 9, at 50 cm from Target Surface.

Fluence Mapping of RTNS-I by Helium Accumulation and Foil Activation Methods

Harry Farrar IV, D. W. Kneff, and R. A. Britten
Atomics International Division, Rockwell International Corporation
Canoga Park, California 91304
and
R. R. Heinrich
Argonne National Laboratory
Argonne, Illinois 60439

INTRODUCTION

The effective use of intense high energy neutron sources for fusion reactor materials studies and other applications requires a detailed knowledge of the neutron energy and fluence distributions in the volume occupied by the irradiated samples. To date, most of the dosimetry information for a given irradiation experiment has come from the integrated neutron fluences received by a few thin but relatively large-diameter radiometric foils irradiated with the target materials. This coarse dosimetry cannot provide detailed neutron energy and fluence information, and is generally insufficient for d-Be and d-Li neutron source irradiations, where the fluence gradients and energy spectrum changes are severe over small dimensions. The problem is further complicated by the need to characterize the neutron environment for each specific irradiation.

The need to know the neutron fluence variation precisely over the volume of an experiment in the d-T neutron environment of the Rotating Target Neutron Source (RTNS-I) at Lawrence Livermore Laboratory (LLL) led to the design of significantly more detailed dosimetry procedures for that experiment. The experiment was conducted as a part of an Atomics International (AI) program to determine helium generation rates and spectrum-integrated (n,α) cross sections of a number of materials. The neutron dosimetry in the AI experiment included the mapping of fluence information both from segmented radiometric foils and from helium accumulation fluence dosimetry materials. The results have provided the most detailed information yet obtained for the innermost fluence variation of the RTNS-I neutron field, and have demonstrated the application of helium accumulation fluence dosimetry to high energy neutron fields as a valuable tool complementary to radiometric foils.

While these results describe only one irradiation, they do provide a check of a more approximate fluence model, and give an estimate of what can be expected in other similar irradiations. The resulting procedures can be used to characterize future d-T irradiations and can be extended to the more complex d-Be and d-Li neutron environments.

DESCRIPTION OF IRRADIATION ASSEMBLY

The geometry of the 1.9-mm thick stainless-steel helium generation assembly irradiated in RINS-I is shown in Fig. 1. It contained two Al wire rings, one Cu wire ring, and many small pure element and alloy specimens, sandwiched between two stacks of three thin Au, Nb, and Ni radiometric dosimetry foils. This sandwich was followed by five thicker Au, Nb, Ni, Fe, and Pt foils and an Fe wire ring.

The assembly was irradiated for 77.55 h, receiving a total neutron fluence of 2.6×10^{7} cm^{-2} at the capsule front center. Following the irradiation, the capsule was disassembled and the dosimetry foils were segmented into a total of 62 pieces for γ ray counting at LLL and Argonne National Laboratory (ANL), and for weighing both at ANL and AI. The wire rings were etched, to remove surface material depleted or enhanced in helium by the effects of α-recoil, and then segmented for weighing and subsequent analysis of their helium content by high sensitivity gas mass spectrometry.

FLUENCE MAP FROM FOIL ACTIVATION DOSIMETRY

The foil counting and weighing results were combined with the irradiation time history to calculate the neutron fluences received by the individual dosimetry foil segments. These fluences and the foil segment geometries were then used to construct a fluence map for the space occupied by the helium generation capsule for this particular irradiation at RINS-I.

The map was constructed by first calculating the offset of the irradiation assembly relative to the 0° neutron source axis. This offset was determined from recording microphotometer scans of autoradiograph negatives made of the assembly after the irradiation, and from quadratic surface fits to the average fluences calculated for the gold foil segments.

This information was then used to calculate radial neutron fluence profiles for the gold foils sandwiching the helium specimens, in the form:

$$\Phi(R) = C_1 + C_2 R + C_3 R^2 + C_4 R \quad , \qquad (1)$$

where R is the radial distance from the 0° neutron source axis. The constants were evaluated by integrating $\Phi(R)$ numerically over the area of each foil segment, and solving several sets of simultaneous equations. The results, corrected for neutron attenuation to represent "free space" profiles, are shown in Fig. 2 as a function of radial distance from the source axis.

The calculations were then extended to find a single three-dimensional expression that reproduced the fluence profiles of all nine Au, Nb, and Ni dosimetry foils:

$$\Phi(R, Z/) = \alpha\left[C_1 + C_2\beta R + C_3(\beta R) + C_4(\beta R)\right]. \qquad (2)$$

Here $Z/$ is the axial distance from the front face of the capsule, β is a correction factor for the changing radial shape of the fluence curve as a function of $Z/$, and α is the normalization of the radial profile as a function of the distance Z from the neutron source.

The dashed line in Fig. 2 is the prediction made by Eq. (2) for the middle gold foil when the constants in Eq. (2) are chosen to match the front gold foil radial profile. The data points shown in Fig. 2 are averages of the measured fluences for each annular foil segment, plotted at average radii.

The axial dependence ($R = 0$) for $\Phi(R, Z/)$ in Eq. (2) is shown in Fig. 3 as the solid line. This figure also includes the axial fluences for all nine foils (data points). These fluences were obtained from Eq. (2), and were normalized by equating the integral of Eq. (2) with the total measured foil fluences. The Z dependence of Eq. (2) was effectively eliminated by the normalization procedure, so the plot of axial fluence versus $Z/$ for the nine foils gave the experimental Z dependence of the fluence. This was found to be linear over the 1.9 mm thickness of the capsule, the linearity being attributable to the finite neutron source spot size.

The axial fluence map also provided a check of the relative cross sections used for the Au, Nb, and Ni foil dosimetry reactions. The data in Fig. 3 show that the cross sections used for the $^{58}Ni(n,p)^{58}Co$ and $^{58}Ni(n,2n)^{57}Ni$ reactions are (7.4 ± 2.3)% high relative to the $^{197}Au(n,2n)^{196}Au$ and $^{93}Nb(n,2n)^{92m}Nb$ cross sections.[7] This information was subsequently used to calculate relative cross sections for these reactions. This required further analysis, however, because the two nickel cross sections are strongly energy dependent over the experimental geometry, and the incident neutron energy at any point in the capsule was an average over a large reaction solid angle.

This analysis showed that the evaluated $^{58}Ni(n,p)^{58}Co$ cross section is (11.9 ± 3.0)% high at 14.8 MeV, while the evaluated $^{58}Ni(n,2n)^{57}Ni$ cross section[7] agrees with the measured value, assuming that the $^{93}Nb(n,2n)^{92m}Nb$ reaction, to which the measured values were normalized, has a cross section of 458 mb at 14.8 MeV.[8] The 14.8 MeV cross sections determined in this work for the three dosimetry reactions, $^{58}Ni(n,p)^{58}Co$, $^{58}Ni(n,2n)^{57}Ni$, and $^{197}Au(n,2n)^{196}Au$ were 294 ± 8, 34.9 ± 1.1, and 2110 ± 40 mb respectively. The quoted uncertainties are relative values, omitting the 5% niobium cross section uncertainty.

The fluence map generated from the present data has been compared with the mathematical model derived at ITI for the PINK I flux distribution.[9] The ITI model was used in the form

$$\Phi(n/cm^2) = \frac{Y}{4\pi a^2} \ln \left[\frac{\sqrt{(w^2+Z^2-R^2)^2 + 4Z^2R^2} + (w^2+Z^2-R^2)}{2Z^2} \right], \quad (3)$$

where Y is the total neutron emission from the source, w is the radius of the target spot (assumed constant), Z is the axial distance from the target spot, and R is the radial distance from the source axis.

Comparisons were made by evaluating the Eq. (3) model at three points on the fluence map, to determine the parameters Y, w, and Z, and comparing the resulting curves with the fluence map profiles generated in this work. While the LLL mathematical model was found to produce fluence profiles that approximately characterize the RTNS-I source, a set of parameters could not be found that accurately reproduced the map. The best match, to within 9% over the space occupied by the capsule, was obtained with an axial source-to-capsule-face distance that was 40% larger than the assumed 3.5-mm experimental distance.

MAP ADJUSTMENTS USING HELIUM ACCUMULATION FLUENCE DOSIMETRY

Helium accumulation fluence dosimetry is based on the post-irradiation measurement of the neutron-induced helium production in segments of a suitable dosimetry material. Detailed fluence profiles can be determined by mapping the relative helium generation in the segments. Total neutron fluences can then be obtained by folding the results with the total helium production cross sections. While this analysis method is generally more time-consuming than activation analysis, it has several advantages. These include the ability to use finer segments, the potential for obtaining neutron energy information by selecting several dosimetry materials that have helium-generation cross sections with different neutron energy sensitivities (also applicable to foil activation), and an absence of the need to know the time-history of the irradiation. The time-history is usually important for interpretation of activation analyses, on the other hand, because corrections must be made for decay during the irradiation, unless the activation product half-life is much longer than the irradiation period. If the half-life is significantly shorter than the irradiation period, the residual activity will be dominated by the neutron flux level during the latter part of the irradiation, and therefore only this flux will be measured.

The helium accumulation dosimetry analysis in this experiment was simplified by the fact that the wire rings were essentially symmetrically placed within the irradiation assembly relative to the neutron source axis. This meant that the incident neutron energy, and hence the helium production cross section, could be assumed constant over the entire extent of each wire ring.

The Cu, inner Al, outer Al, and Fe wires were cut into 25, 9, 14, and 12 segments, respectively, and have been analyzed for helium. Preliminary information from the Cu and Al segments is shown in Fig. 4, as a function of angular orientation about the capsule center (in the plane perpendicular to the 0° neutron source axis). The fluence profiles calculated from the dosimetry foil map [Eq. (2)] for the locations of the wire rings are superimposed on Fig. 4 as solid curves.

Comparison of the fluence profiles with the helium results (normalized in Fig. 4 by dividing the helium results by the average calculated cross sections, which are based on the dosimetry map fluences) leads to two observations. First, the estimated offset of the capsule from the 0° neutron source axis, as determined from the radiometric dosimetry foils, is too small. Increasing the assumed capsule offset in the vertical direction from 0.6 to 1.0 mm in the fluence calculations (dashed curves in Fig. 4) gave a better fit to the helium data. Second, the fluence profile is somewhat asymmetrical, reflecting nonuniformities in the time-averaged deuteron beam profile. Further analysis of the helium dosimetry data indicates that the beam profile was slightly elongated, with some additional structure.

The helium accumulation dosimetry data obtained from the wire rings have not yet been used to adjust the dosimetry foil fluence map to reflect the integrated neutron field nonuniformities. When this is completed, the revised map will be combined with the helium data from the irradiated pure element helium generation specimens, to obtain accurate helium-production cross sections.

IMPLICATIONS FOR FUTURE DOSIMETRY

The present analysis demonstrates the ability to obtain detailed fluence information from foil activation and helium accumulation fluence dosimetry, and it outlines a possible procedure for future fusion program irradiations where accurate fluence information is required. As used here, the foil activation dosimetry has provided an averaged fluence map as a function of position near the target, and the helium accumulation fluence dosimetry has provided a considerable amount of further detail.

Helium accumulation dosimetry could also be used to construct the entire fluence map, with adequate inclusion of dosimetry materials, but the mass spectrometric sample analysis is more time consuming than activation analysis, and the helium generation cross sections are not as well known at present.

The extension of these techniques to the more complex d-Be and d-Li neutron environments can be made by using simultaneously several dosimetry foils and helium accumulation materials with different neutron energy sensitivities. The multiple foil technique has recently been applied to the initial characterization of the d-Be source,[5] where both neutron fluences and energy spectra

were obtained by numerically unfolding the integral yields from the individual dosimetry reactions. A more detailed characterization can be obtained by combining foil activation and helium accumulation mapping procedures with spectrum unfolding techniques to calculate the fluence and energy spectrum at each position of interest. To this end, it is increasingly important to determine accurately the energy dependences of applicable foil activation cross sections. It is also important to determine spectrum-integrated total helium generation cross sections for several candidate helium accumulation dosimetry materials in a number of neutron environments with different energy characteristics.

ACKNOWLEDGEMENTS

The authors gratefully acknowledge the interest and help of R. A. Van Konynenburg (LLL) in the foil analysis and mapping. The help of C. H. Knox and J. F. Johnson (AI) in the preparation of the irradiation package and S. C. MacLean, R. N. Anderson (LLL), and R. Malewicki (ANL) in the radiometric counting is appreciated. R. R. Vandervoort, M. Guinan, R. Booth (LLL), and M. Kaminsky (ANL) made the long irradiation possible, and K. M. Zwilsky, T. C. Reuther, Jr., and L. E. Temple (ERDA) provided continued encouragement and support of this work. The work was performed under contract with the Energy Research and Development Administration's Division of Magnetic Fusion Energy.

REFERENCES

1. H. Farrar IV, W. N. McElroy, and E. P. Lippincott, Nucl. Technol. 25, 305 (1975).
2. D. W. Kneff, H. Farrar IV, R. A. Van Konynenburg, and R. R. Heinrich, Atomics International Report AI-ERDA-13188 (1976).
3. B. A. Magurno, Editor, ENDF/B-IV Dosimetry File, Brookhaven National Laboratory, National Neutron Cross Section Center Report BNL-NCS-50446 (ENDF-216) (1975).
4. S. F. Mughabghab, A. Prince, M. D. Goldberg, M. R. Bhat, and S. Pearlstein, Brookhaven National Laboratory Report BNL 50439 (ENDF-215) (1974).
5. Z. T. Bödy and J. Csikai, Atom. Energy Rev. 11, 153 (1973).
6. D. R. Nethaway, Nucl. Phys. A190, 635 (1972); and private communication with R. A. Van Konynenburg (1975).
7. E. Goldberg, R. Griffith, and C. Logan, Lawrence Livermore Laboratory Report UCRL-51317 (1972); R. A. Van Konynenburg, UCRL-51393, Rev. 1 (1974).
8. D. R. Nethaway, R. A. Van Konynenburg, and T. M. Adams, Lawrence Livermore Laboratory Report UCRL-52024 (1976); L. R. Greenwood, private communication (1977).

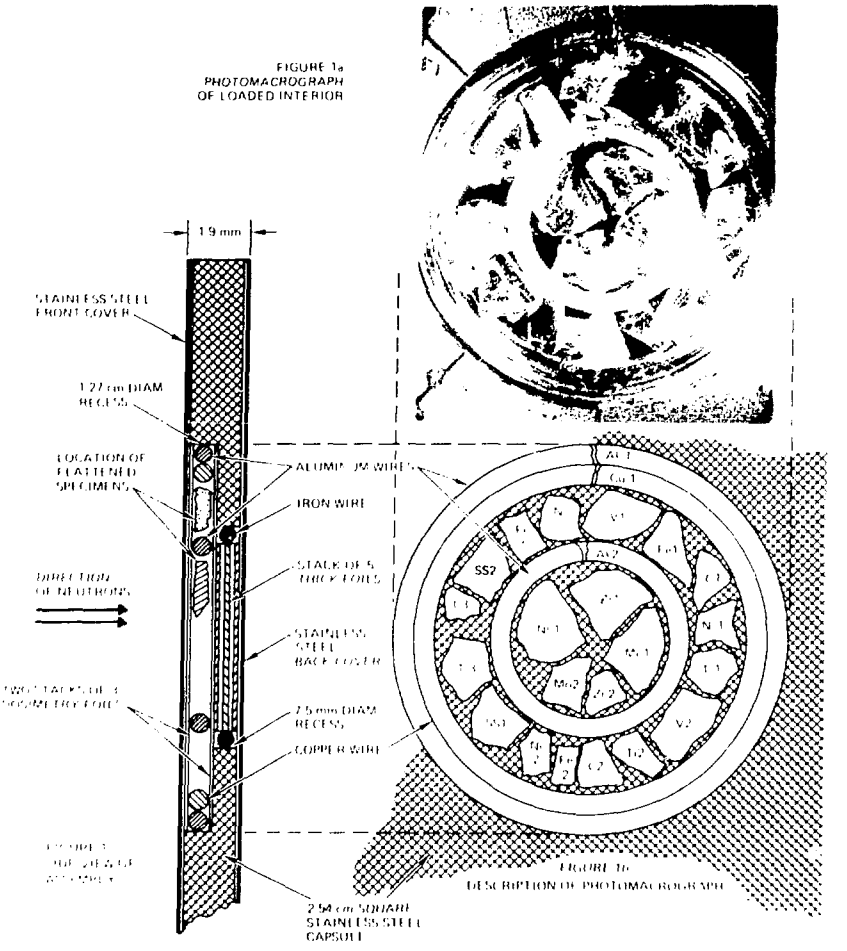

Figure 1. RTNS Irradiation Assembly

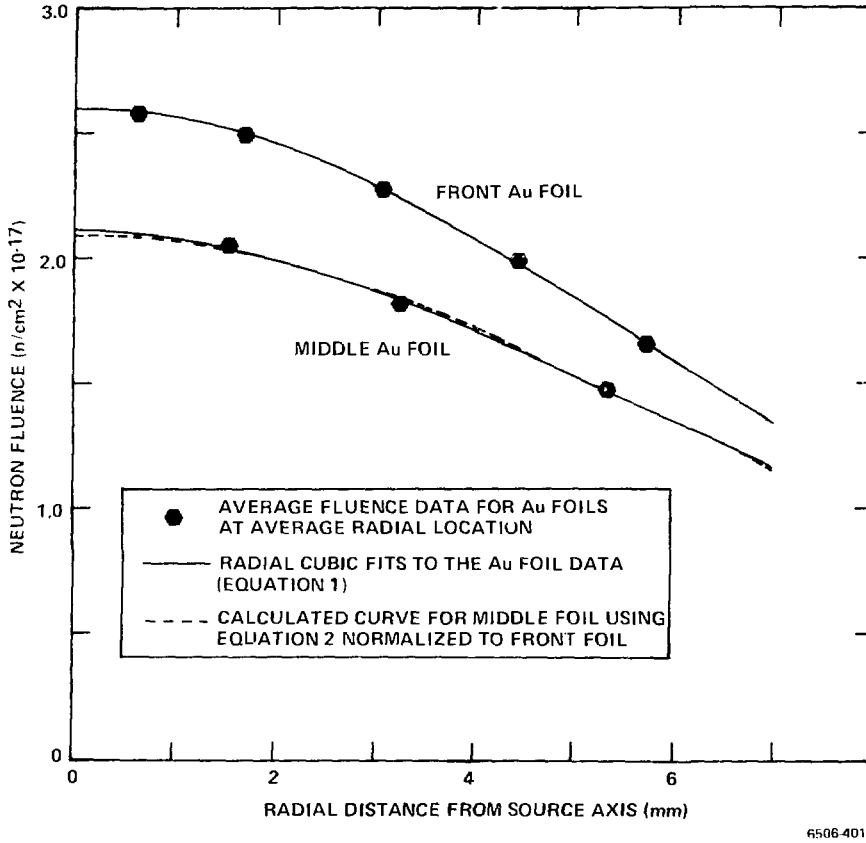

Figure 2. Attenuation-Corrected (Free-Space) Radial Cubic Fits to the Front and Middle Gold Dosimetry Foil Data

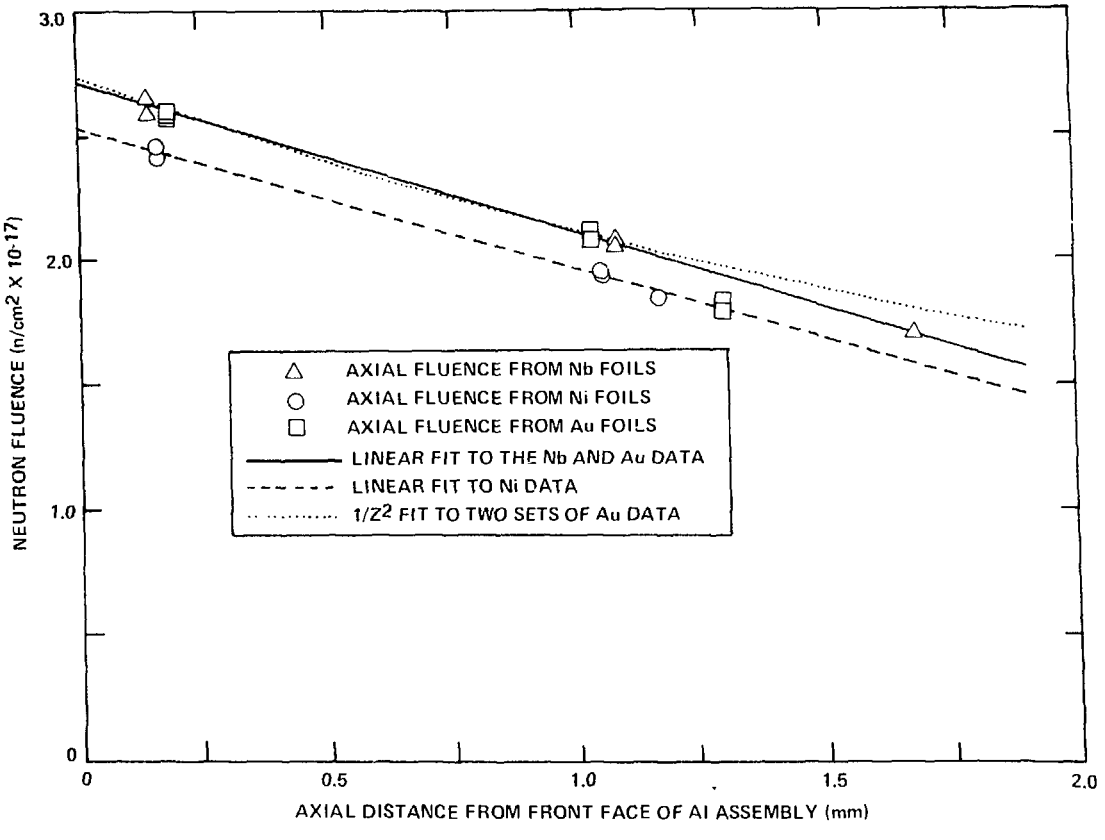

Figure 3. Attenuation-Corrected Axial Neutron Fluence Profile

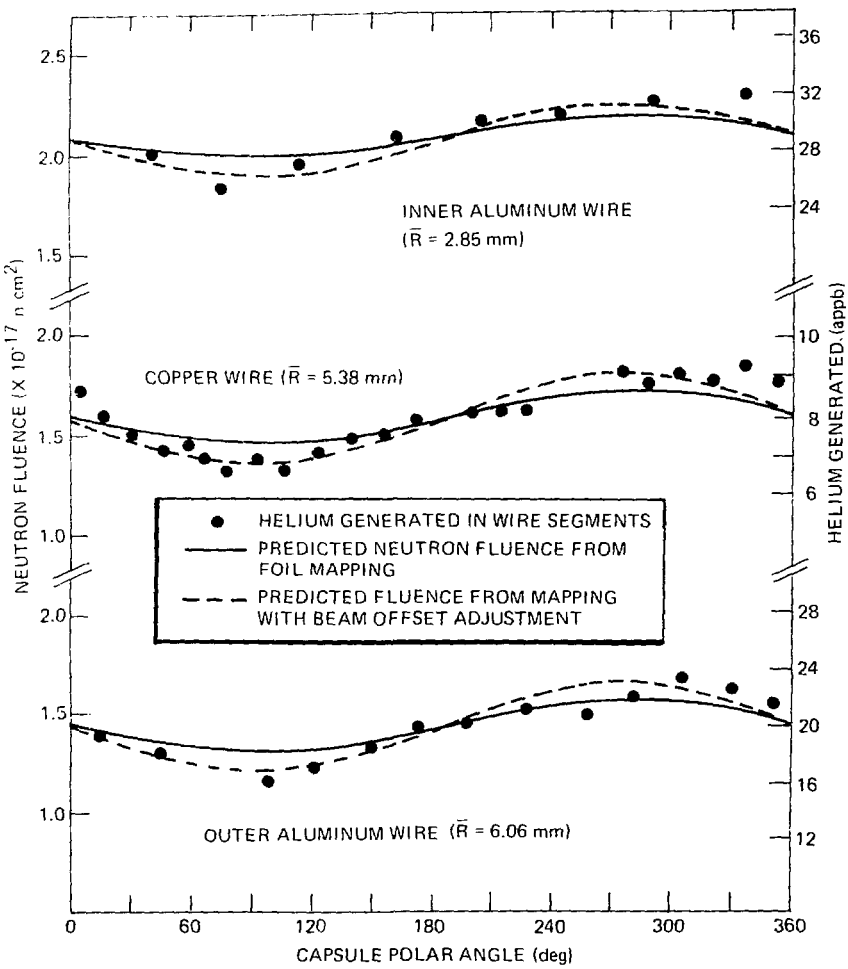

Figure 4. Preliminary Helium Generation Results and Neutron Fluence Calculations for the Cu and Al Wire Rings

Conf-771523--2

Neutron Spectra Characteristics for the Intense Neutron Source, INS

M. Battat, R. Dierckx* and C. R. Emigh
University of California, Los Alamos Scientific Laboratory+
Los Alamos, NM 87545

INTRODUCTION

The Intense Neutron Source, INS, facility is presently under construction at the Los Alamos Scientific Laboratory. Its purpose is to provide a broad base for research work related to the radiation effects produced by 14-MeV neutrons from a D-T burn of a fusion reactor. The INS facility produces a D-T burn-like reaction from the collision of an intense tritium-ion beam with a supersonic jet target of deuterium gas. The reaction produces a typical D-T 14-MeV neutron spectrum. By adding a fission blanket surrounding the D-T "burn", the neutron spectral shape may be tailored to match almost perfectly the anticipated first-wall spectra from presently proposed fusion reactors. With a blanket in place, the total production of neutrons can be as large as 3×10^{16} n/s and experimental volumes of the order of 1000 cm^3 can be available at flux levels greater than 0.6×10^{14} n/cm^2 s.

BASIC REACTION

The INS facility makes use of the basic nuclear reaction

$$T^+ \text{ (300 keV)} + D_2 \rightarrow n\text{(14.1 MeV)} + \alpha^{++}\text{(3.5 MeV)} + D + e^- + Q.$$

This is accomplished by accelerating a 1A-to 3A- tritium-ion beam to 300 keV and allowing it to strike a deuterium gas target. The gas target is a supersonic or transonic stream so as to carry away the 300-900 kW of power, Q, deposited in the target. The INS facility has two separate but identical sources, increasing its diversity to accommodate many different types of experiments.

14-MeV PRIMARY NEUTRON SPECTRUM

The primary spectrum of 14-MeV neutrons is characterized by the kinetics of the colliding tritium beam with the "essentially" stationary deuterium target. In this mode of operation, the neutrons in the forward direction have an energy of ~ 15.7 MeV while those in the backward direction have an energy of ~ 12.8 MeV. The 14-

---

* On assignment to the cooperative research program, IEA/USERDA, construction of LASL's INS facility. On leave from Euratom, CCR, Ispra, Italy.

+ Work performed under the auspices of the U. S. Energy Research and Development Administration.

MeV flux of neutrons is essentially isotropic and falls off as r^{-2} from the approximate point source. The size of the source reaction volume is $\sim 1\ cm^3$ and samples placed next to the source will receive a primary flux of 2-6 x 10^{14} neutrons/cm^2 s. Figure 1 shows the primary spectrum in comparison with other spectra often considered for radiation damage experimental research. The peak values have been normalized to unity for this presentation.

The pure 14-MeV spectrum will be used primarily for doing neutron cross section experiments. The very high intensities will allow determination of neutron activation cross sections of elements which are intensity limited, that is the activation products have very long half-lives, much greater than 100 years. Also the high intensities will allow cross sections to be measured on rare or expensive materials using microgram sample techniques. The specific cross sections for the production of H and He can be accurately measured, along with other transmutation cross sections of interest to the fusion materials program.

Another important area of research needed for developing fusion devices is that of 14-MeV neutron shielding. Very high intensities of fusion neutrons will require massive shielding protection, such as concrete walls greater than 10 ft in thickness. Detailed neutronics is required to thoroughly understand transmission, albedos, and activation of shielding materials.

Surface-physics experiments are important for metals and insulators. Fusion first-wall erosion and resulting plasma contamination are major problems. Plasma contamination in a fusion device could cool the plasma and radically perturb the conditions for optimum thermonuclear burn. Neutron sputtering, radiation blistering, and release of gaseous particles are some of the problems to be considered.*

At distances sufficiently far from the source, the flux pattern can be considered a large homogeneous plane source of $> 10^9$ n/cm^2 s. Benchmark experiments, equipment mock-ups, and blanket concepts can be exposed to this plane source so that measured fluxes and related quantities can be compared with neutron transport and penetration calculations.

TAILORED FIRST WALL SPECTRA

The neutron field present at the first wall of a fusion reactor consists of two components: the directed 14-MeV neutron flux coming from the plasma burn and the backscattered, low-energy ($<$ 14-MeV) neutrons returning from the blanket surrounding the plasma.

At the INS, the same neutron environment can be obtained by surrounding the neutron source with a spherical fission blanket.

---

* M. Kaminsky, "Plasma Contamination and Wall Erosion in Thermonuclear Reactors," IEEE Trans. in Nuclear Sci. V18, 208-217 (1971)

The enclosed spectra can be tailored to match closely the first wall spectra of fusion reactors. The blanket is formed by concentric spheres of lithium, uranium, and beryllium. In very general terms the beryllium outer liner acts both to slow down the 14-MeV primary neutrons and to reflect them back toward the uranium shell. The uranium (93% enriched U^{235}) multiplies the number of neutrons by the fission process and fission neutrons are emitted isotropically. Moderated fission neutrons are filtered by the lithium inner liner to suppress the very low energy neutrons to a desired level, producing in the enclosed space a neutron spectrum that peaks at $\sim 10^{-3}$ MeV. The thickness of the blanket components are determined by calculations made using the computer code, ONETRAN-DA, which is a discrete ordinate transport code.

The tailored spectrum inside the encased volume will consist of a radial outward flux of primary 14-MeV neutrons falling off as r^{-2} and a near-uniform flux of low energy neutrons. peaking at about 10^{-3} MeV. Different sizes of blankets can be used, depending on optimal conditions for a particular series of experiments. A small blanket for experiments desiring high total fluxes, ϕ, at low volumes, V, and a large blanket for experiments desiring high volumes at low total fluxes. The conjugate relationship of the product of $\phi \cdot V^{2/3}$ is conserved for a particular facility and is referred to as the "effective" source strength of the facility. Figure 2 shows the relationship between the irradiation flux versus maximum irradiation volume available, assuming samples of 1 cm^3 in size. In practice, the irradiation samples will be placed at the location within the enclosed volume where the flux matches most nearly that of the first wall spectra ($\phi_{<14}/\phi_{14} \sim 4$).

As an illustration, Fig. 3 shows a typical blanket arrangement surrounding an experimental volume of 33 cm^3. In this case, the required amount of uranium-235 is 7.3 kg and has a multiplication of about 11. The uranium shell has an inner radius of 30 mm and an outer radius of 50 mm. The required Li filter inner shell is 10-mm thick. Using a primary source strength of 10^{15} n/s, the flux levels in the irradiation volume are shown in Figure 4. The primary 14-MeV flux, ϕ_{14}, falls off rapidly with the square of the radius while the low energy component, $\phi_{<14}$, is essentially constant within the volume. Figure 5 shows the total flux, ϕ_T, and the ratio of $\phi_{<14}/\phi_{14}$. The ratios expected in the θ-pinch and Tokamak designs are indicated and determine the optimum location for placement of irradiation samples. At this location, the neutron spectrum is shown in Figs. 6, 7, and 8. In each presentation, the INS spectrum is compared with those calculated first-wall spectra for the θ-pinch and Tokamak reactors. The INS spectrum is a very close match, differing only slightly below the keV region where it is somewhat harder. This is due to the nature of the fission-blanket but the differences are irrelevant for radiation damage and He production effects. A second illustration, shown in Fig. 9, shows a blanket arrangement surrounding an experimental volume of 268 cm^3. The same flux spectra will be generated, but the total flux level in this case is reduced to 0.5×10^{14} n/cm^2s.

RADIATION DAMAGE COMPARISONS

Radiation damage is often characterized by the primary recoil energy spectrum generated by the neutron spectrum environment. The primary recoil energy spectra are calculated for Fe 1192 in the HMS spectra for the fission blanket assembly of Fig. 1 and in the first wall spectra of proposed fusion reactors. Table I summarizes these recoil spectra. The HMS recoil spectrum belongs to the same class as those of the proposed fusion reactors. A pure 14 MeV neutron irradiation gives more high energy primary recoils. In Table II, displacement and He production cross sections are listed together with their ratio. Again, the match is excellent. Deviations of only 20% in the ratio displacement to He production cross section is observed over a 5-cm range.

ACKNOWLEDGEMENT

The authors appreciate the efforts of Don Parkin, LASL, for his contribution in preparing the recoil spectra data and the damage cross sections. The use of a fission blanket around the source to modify the 14-MeV spectra was first suggested by Doug Muir, LASL, in 1974, and his encouragement and advice during these studies is appreciated.

Table I

Recoil Spectra

FE 1191

Recoil Energy keV	L-Mat	DNS Blanket				TOMAK	FUSE	Behal
		1.0 cm	1.5 cm	1.8 cm	2.0 cm			
1-1.1	1.0	3.7	4.0	4.0	4.0	3.7	22.0	3.7
1.1-1.1	1.7	22.1	23.1	23.6	24.3	23.5	22.7	24.8
1.1-5.1	4.4	19.5	22.5	22.5	23.5	20.4	27.	25.2
5.1-10	4.5	22.6	22.3	22.7	23.2	3.4	7.4	22.6
10-50	21.9	27.1	27.4	27.7	28.1	23.4	24.7	24.4
50-100	7.9	6.8	6.7	6.7	6.8	4.1	4.1	4.4
100-200	22.7	6.8	5.5	5.2	4.5	3.3	.7	4.
200-400	24.2	3.2	3.4	4.7	3.3	4.7	4.1	4.4
400-T_{max}	19.1	3.1	3.3	2.7	2.9	2.7	4.4	2.5

Table II

Damage Cross Sections

(IF 1192)

Spectrum	Displacement (10^{-24} cm^2)	(n,γ) (mB)	Dpa/(n,γ) (10^5)
HFR Blanket			
1.2 cm	1.29	15	8.5
1.6 cm	1.08	11	9.8
1.8 cm	0.96	8.9	11
2.1 cm	0.82	6.1	13
First Wall			
OMMAF	1.00	10.9	9.2
PTFP	0.96	9.9	9.7
Bench	1.00	10.7	9.4
"14 MeV"	2.81	43	6.5

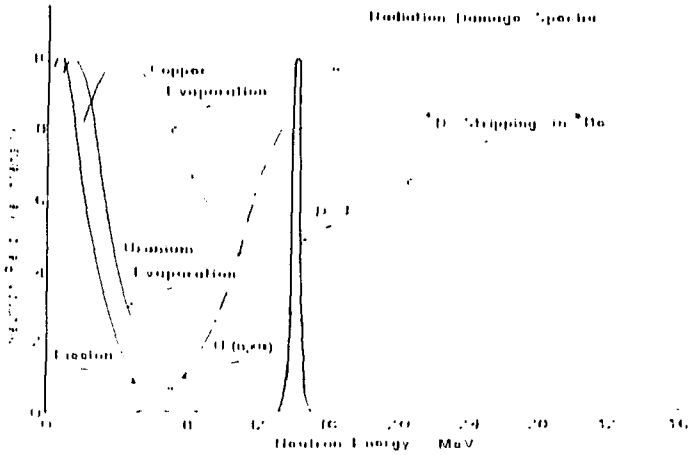

Fig. 1 Primary neutron spectra used for radiation damage research.

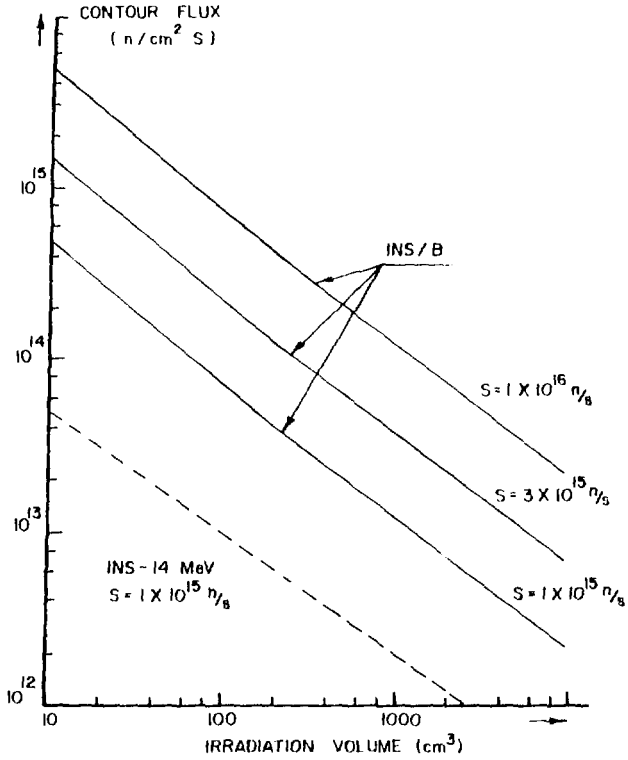

Fig. 2. Flux versus irradiation volume at the INS facility.

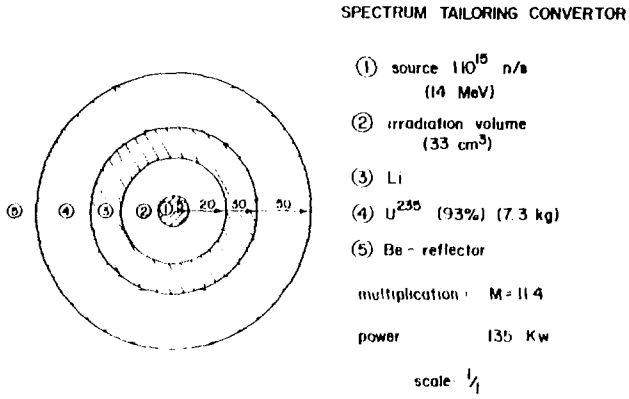

Fig. 3. Blanket arrangement for a high flux, medium irradiation volume facility.

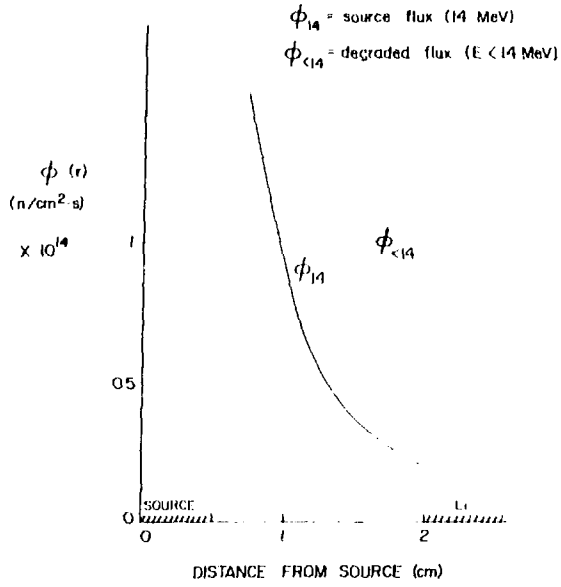

Fig. 4. Spatial flux pattern inside the blanket irradiation volume.

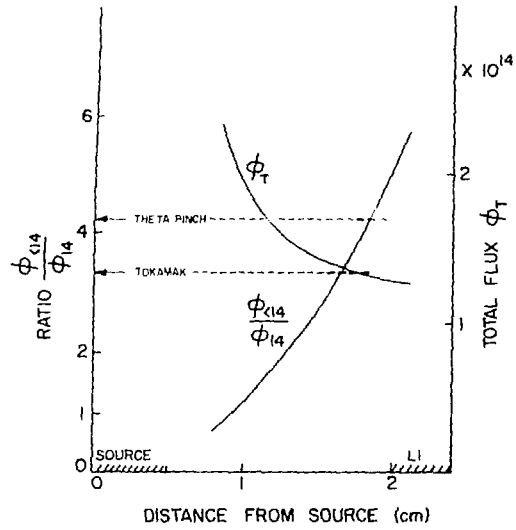

Fig. 5. Total flux and ratio $\phi_{<14}$ to ϕ_{14} inside the blanket irradiation volume.

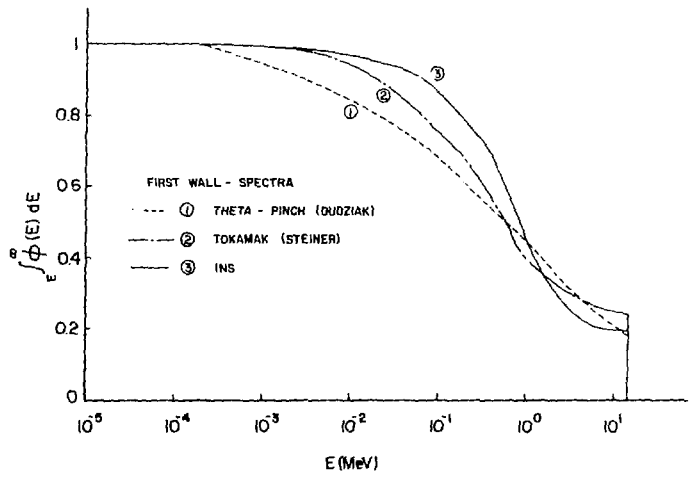

Fig. 6. Integral fluxes, $\int_E^\infty \phi(E)\,dE$, for different first wall spectra

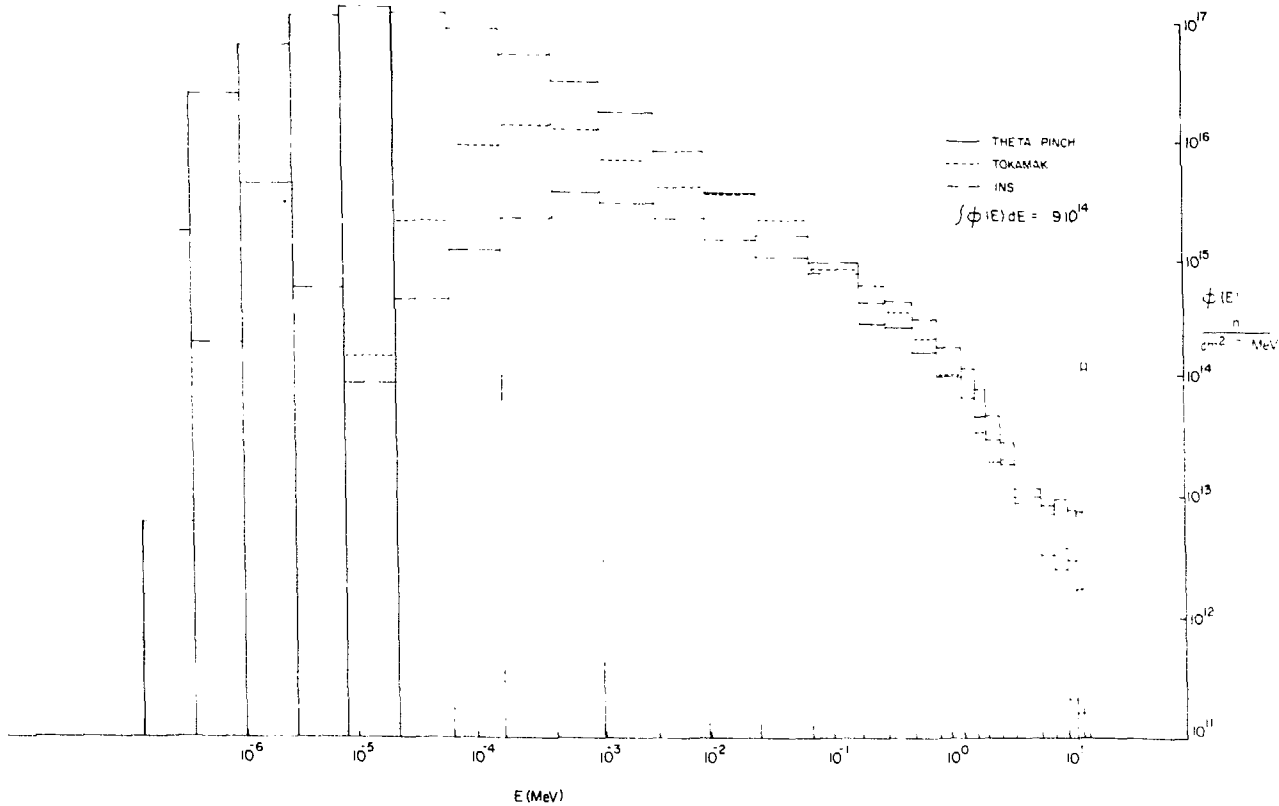

Fig. 7. Differential fluxes for different first wall spectra
l log scale.

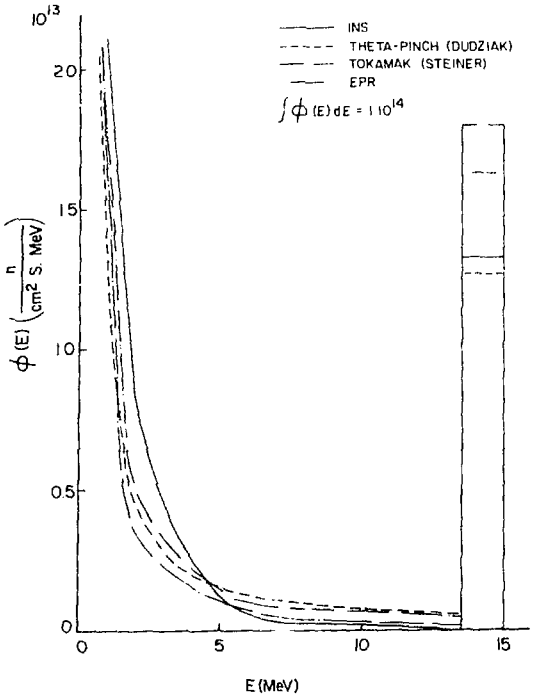

Fig. 8. Differential fluxes for different first wall spectra 1 linear scale.

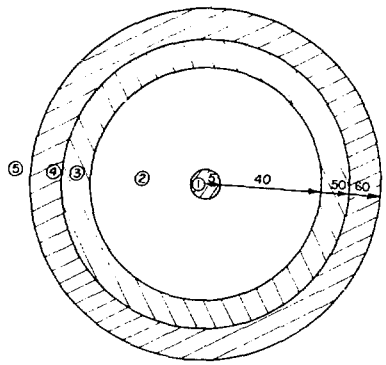

SPECTRUM TAILORING DEVICE

$\phi_T = 5.\ 10^{13}\ n/cm^2\ S$

1 SOURCE : 1 10^{15} n/S (14 MeV)

2 IRRADIATION VOLUME (268 cm^3)

3 Li

4 U^{235} (93%) (~ 7 kg)
M = 4 to 6
power = 40 to 60 kw

5 Be - reflector

at 2.7 cm from source

$\phi_{14} = 1.\ 10^{13}$ $\phi_T = 5\ 10^{13}$

$\phi_{<14} = 4.\ 10^{13}$ $\phi_{<14}/\phi_{14} = 4$

Fig. 9. Blanket arrangement for a low flux high volume facility.

SESSION III

DIFFERENTIAL DATA AND EXPERIMENTAL TECHNIQUES

Chairman: A. B. Smith, ANL

CONF-770523--9

Review of Neutron Data: 10 to 40 MeV.*

Robert C. Haight
Lawrence Livermore Laboratory
Livermore, California

ABSTRACT

Neutron data are reviewed for incident neutron energies between 10 and 40 MeV. A census of the data shows that there are many gaps in this range and that the existing data are primarily for neutron energies around 14 MeV. Aside from total cross sections, there are few data between 10 and 13 MeV and between 15 and 40 MeV. Examples are presented to show the quality of selected data for total, elastic, inelastic, activation, and charged-particle and gamma-ray production cross sections. The spectra of emitted particles are also discussed.

INTRODUCTION

For over three decades, experimentalists have studied nuclear reactions induced by neutrons between 10 and 40 MeV. In recent years the interest in this energy range has intensified because of the need for data for applied purposes. Much of the interest has been stimulated by the fusion reactor community which requires data both in the analysis of the neutronic performance of conceptual reactor designs as well as in the interpretation of radiation damage experiments. Further interest comes from the present use of neutrons in this range for radiation therapy for cancer.

A comprehensive review of the data in this energy range is not intended here. The magnitude of such a task, as indicated in the next section, is prohibitive. Rather the discussion here will treat selected areas of the large body of measurements. The selection is intended to point out agreements as well as discrepancies between the measured quantities. Different experimental techniques that are used to measure the same quantity will be indicated. The examples chosen will, I hope, be of interest for the applied purposes mentioned above.

A CENSUS OF THE DATA

About 83,000 data have been reported for incident neutron energies between 10 and 40 MeV.[1] Although this number is very large, it is small when compared with over 1,600,000 measurements for neutrons of all energies. About 25,000 of the 83,000 data are

*Work performed under the auspices of the U.S. Energy Research and Development Administration, W-7405-Eng-48.

total cross sections and the remainder are spread over the other measurable quantities.

An indication of where the measurements have been made is given in Figs. 1-4. The number of data points is plotted against the atomic number of the target, and no distinction is made in these figures between targets that are isotopically pure and targets that contain a mixture of isotopes. The graphs indicate total cross section data, differential elastic scattering cross sections, neutron emission data, hydrogen-producing and helium-producing reaction cross sections and all other non-elastic cross sections that are energy and angle-integrated (such as (n,γ), (n,n'), (n,2n), (n,3n), (n,f), etc. For the differential elastic scattering, each point of an angular distribution is counted separately; the individual points of a neutron emission spectrum are also considered independent; and reactions that populate different states in the residual nucleus are counted individually if they were measured that way. The data points tallied are those presently compiled in Ref. 1, which is based to a large extent on data transmitted by the National Neutron Cross Section Center and on references in CINDA.[2]

Figures 1 and 3 illustrate data between 10 and 40 MeV whereas in Fig. 2 and 4 only the data between 15 and 40 MeV are tallied. The marked difference between these different energy ranges illustrates that, except for total cross section measurements, there are few measurements above 15 MeV.

The distribution of measurements over the elements fortunately agrees to a remarkably large extent with the relative neutronic importance of the elements for fusion and medical applications. The only connection here, however, is that the important elements are abundant and hence readily accessible for experiments.

STANDARD REFERENCE DATA

In the region 10 to 40 MeV, there is one primary standard, n-p elastic scattering, against which all other cross sections are measured. The accuracy of the angle-integrated elastic cross section is known to better than 1% according to Hopkins and Breit.[3] Usually a flux monitor detects protons recoiling in a certain angular range, so that the angular distribution of n-p scattering must be known. The uncertainty in the center-of-mass angular distribution $(\sigma(180°)-\sigma(90°))/\sigma(90°)$ rises from about 1% at 10 MeV to 2.5% at 30 MeV according to Ref. 3 and is indicative of the errors to be expected in flux monitors from the n-p differential cross section. More recent measurements, summarized by Uttley,[4] have in general confirmed the values of Hopkins and Breit.

Secondary standards include many activation cross sections and fission cross sections, primarily $^{235}U(n,f)$. One of the widely used activation standards is $^{27}Al(n,\alpha)^{24}Na$. The half-life (15 hours) and decay radiation of ^{24}Na make it attractive. On the

other hand the cross section fluctuates fairly rapidly with neutron energy with the amplitude of the fluctuations being about 4 (peak-to-peak).[5] Aside from the fluctuations, the cross section is relatively flat from 12 to 14 MeV and decreases above 14 MeV. The $^{27}Al(n,\alpha)^{24}Na$ monitor reaction should therefore be expected to contribute an error of about 5 near 14 MeV and perhaps more at higher energies unless the energy of the source neutrons is precisely known. The $^{93}Nb(n,2n)^{92}Nb(t_{1/2} = 10$ days) cross section is preferred by some as the standard activation cross section for neutrons near 14 MeV since its excitation function is much flatter there.

The $^{235}U(n,f)$ cross section has been used extensively as a standard fission cross section. Fission cross section ratios are usually measured relative to this standard. The significant discrepancy (10 where the error bars are + 4) in the measurements of this cross section from 14 to 18 MeV have been summarized in the NEANDC/NEARCP Specialists meeting on Fast Fission Cross Sections.[6]

TOTAL CROSS SECTIONS

The extensive development of continuous spectrum or white neutron sources in the past ten years has made possible total cross section measurements of high quality. In the range 10 to 40 MeV, white sources based on cyclotrons (e.g. Ref. 7) have provided much of the new data. Electron linear accelerators have also been used extensively to produce white neutron spectra for total cross section measurements in this range (e.g. Refs. 8-11). The cyclotron produced sources have the advantages of a somewhat shorter initial pulse width, much lower gamma-ray background, and more neutron intensity in the range of 10 to 40 MeV. Nevertheless, total cross section measurements of good quality have been made up to 40 MeV with electron linac sources.

Recently a white source based on a tandem van de Graaff has been developed.[12] The source reaction is $^{9}Be(d,n)$. The characteristics of this source in terms of initial pulse width, low gamma-ray background and neutron spectral shape are similar to the cyclotron sources. The intensity is somewhat lower, however.

For good energy resolution and low background measurements, the use of a monoenergetic neutron source may still be preferred. An example of such a measurement is the shape of the total cross section of ^{207}Pb between 16.3 and 17.1 MeV (Fig. 5). One group had previously reported[13] a bump at 16.8 MeV which was attributed to mixing of the compound states with a isobaric analog resonance. The bump was not confirmed in a more recent measurement.[14] The significance of these measurements for applied purposes is probably not in the particular cross section of ^{207}Pb but rather in the importance or non-importance of analog resonances to total cross sections in general.

The difference between the two measurements of ^{207}Pb, at most about [illegible], is relatively large among total cross section measurements. Agreement of different measurements to [illegible] is more common.

ELASTIC AND DIFFERENTIAL ELASTIC SCATTERING CROSS SECTIONS

Below 15 MeV there are several data for most materials of applied interest (Fig. 1 and 3). The vast majority of these data are for 14 MeV neutrons, because of the availability of inexpensive, low energy d+t (n,α) neutron generators. Data at other energies have been obtained with monoenergetic neutrons produced by electrostatic accelerators or, in isolated cases, with white neutron sources from electron linacs. An example of the data obtainable with monoenergetic sources is the differential elastic scattering cross section of carbon from below 10 MeV to 15 MeV[15,16]. These data are of good statistical precision and the two independent measurements are consistent. The relative errors are quoted to be 2 to 3% from point to point and the normalization is quoted to be accurate to between 2.5% and 5%.

Until very recently, the data on elastic scattering seldom extended to neutron energies above 15 MeV. For example elastic scattering from iron between 15 and 40 MeV was reported in formal publications only at 24 MeV[17]. Recently a group at Ohio University has made extensive measurements of elastic scattering at 11, 20 and 26 MeV over a wide range of targets with Z = 14[18,19]. These measurements have yielded much new information in the energy range above 15 MeV.

For light nuclei there are still very few data above 15 MeV. For example several measurements have been made on carbon between 15 and 25 MeV but there is only one isolated angular distribution between 25 and 40 MeV[20]. The data between 15 and 25 MeV (e.g. Refs. 21,22), although not extensive, appear consistent. Figure 6 gives the angular distributions measured near 19.9 MeV. Most of these data were obtained with monoenergetic neutron sources, but Morgan et al.[23] used a white neutron source. For target nuclei such as[6,7] which have their first excited state at high excitation energy, intense white sources can be powerful tools in the gathering of elastic scattering data in this energy range.

In summary, near 14 MeV there are numerous measurements, as well as some gaps. Those taken with modern techniques are in general agreement. At other energies the field has only recently been attacked and much remains to be done.

TOTAL NON-ELASTIC CROSS SECTIONS

There are many measurements of total non-elastic cross sections near 14 MeV but few at other energies in the range of 10 to 40 MeV. Above 14 MeV, the measurements of Ref. 27 between

.71 and .79 MeV provide much of the non-elastic data. Elements targets from ^{9}Be to ^{209}Bi were studied in that work.

Indicative of the current interest in non-elastic cross sections is the fact that no data between 10 and 40 MeV have been reported since 1970.[1] Because of the importance of non-elastic cross sections for the calculation of displacement radiation damage, perhaps experiments in this field may enjoy a resurgence.

It is possible to calculate non-elastic cross sections with the optical model which is applicable in this energy range. The relevant parameters are known at 14 MeV and at some higher energies, and their dependence on energy is generally smooth for nuclei heavier than carbon. Although it would be useful to have more data to validate the model further, it will give a reasonable guess for non-elastic cross sections in the absence of measurements.

PARTIAL NON-ELASTIC CROSS SECTIONS

Inelastic Scattering (n,n') Cross Sections

The problems with inelastic neutron scattering data between 10 and 40 MeV are similar to, but somewhat more severe than, elastic neutron scattering. The exploration of neutron energy ranges different from the 14 MeV area is just beginning. Of particular note are the measurements with monoenergetic neutrons produced by T(p,n) and D(d,n) reactions. These measurements generally are restricted to a few of the well resolved excited states.

To obtain the total (n,n') cross section, another technique[3,5,7] is applicable to vibrational even-even nuclei and perhaps to other nuclei. The hypothesis is that, following inelastic scattering, the excited state is either the first excited 2_1^+ state or a state which will decay through a gamma ray cascade through the 2_1^+ state. The total inelastic cross section can therefore be determined by measuring the number of $2_1^+ \rightarrow 0^+$ (ground state) transitions by a gamma ray detector. This hypothesis can be checked in two ways. First the gamma ray results can be compared with the difference between the total non-elastic cross section and the sum of the partial non-elastic cross section excluding (n,n'). Table I gives the results for many of these comparisons. Only for ^{110}Cd is there a large disagreement and that is suspicious because of the unreasonably large value for one of the partial non-elastic cross sections. Secondly the probability of the $2_1^+ \rightarrow 0^+$ gamma ray following (p,p') excitation can be compared with the total (p,p') cross section. The result is that for incident nucleons above 10 MeV, only about 4% of the states excited by inelastic nucleon scattering fail to decay through the 2_1^+ state. Thus, rather accurate measurements of the (n,n') cross section can be made at energies where other channels, such as (n,2n), (n,p) etc., are open.

Table I

A Comparison of the $(2_1^+ \to 0^+)$ Gamma Ray Production Cross Section with Reduced (n,n') Cross Sections at 14 MeV (from Ref. 29).

Nuclear	$\sigma(2_1^+ \to 0^+)$ [a]	$\sigma_{non\ el} - \sigma_{1/n,n'}$ [b]
^{56}Fe	720 ± 60	774 ± 95
Nat Fe	720	754 ± 50
^{58}Ni	290 ± 25	830 ± 90
^{60}Ni	700 ± 83	742 ± 50
^{62}Ni	390	945 ± 60
Nat Ni	~420	431 ± 60
^{64}Zn	500 ± 25	597 ± 90
^{66}Zn	820 ± 25	831 ± 60
Nat Zn	640	530 ± 70
^{110}Cd	1370 ± 7	885 ± 120
^{112}Cd	1430 ± 75	1247 ± 60
^{114}Cd	565 ± 83	
^{116}Cd	477 ± 150	257 ± 110

a. Reference 29

b. $\sigma_{non\ el}$ and σ_1 from measured values in ENDF (Ref. 1)

(n,2n), (n,3n), (n,4n) etc. Cross Sections

Many of these cross sections have been measured by activation techniques. Some of the problems of the techniques are indicated in the section on (n,p) reactions below. Another current technique[30,31] is to use a large liquid scintillator to detect neutrons emitted from the target. With suitable electronics, (n,n'), (n,2n), (n,3n) and even (n,f) reactions can be separated. Results reported by the two groups usually are in agreement to the quoted accuracies which are ± 10% or better in general. So

far these measurements have not covered many materials of interest to fusion and medical applications, and they extend only to 24 MeV. Some notable absences in the literature are any measured values for the (n,2n) reaction on ^{16}O above 14 MeV, the (n,2n) reaction on ^{56}Fe above 22 MeV, and the (n,3n) reaction on ^{56}Fe above its threshold of 21 MeV.

(n,p) Cross Sections

The cross sections for (n,p) reactions between 10 and 40 MeV neutron energy are usually measured with activation techniques. At these energies, other channels which emit protons such as (n,n'p) are often open. A measurement of the proton production cross section $\sigma(n,xp)$ therefore would be a sum of $\sigma(n,p)$ + $\sigma(n,n'p)$ + ...

A rather typical state of affairs for activation data is illustrated by the often studied $^{58}Ni(n,p)^{58}Co$ reaction[5,7,41] (Fig. 7). There are no data between 10 and 13 MeV, around 14 MeV the data show some consistency (± 20%) if three sets of measurements (Refs. 37, 35 and 41) are omitted, between 15 and 22 MeV, the measurements diverge; and above 22 MeV the compiled literature[1] contains no data.

Similar discrepancies exist in many other reactions investigated with activation techniques. For (n,p) reactions, some other examples are for targets of ^{27}Al, ^{46}Ti, ^{54}Fe, and ^{56}Fe (around 14 MeV).

(n,α) Cross Sections

The (n,α) data are also obtained usually through activation measurements. These data are about as abundant as the (n,p) data and share many of the same problems.

An interesting (n,α) cross section which cannot be measured by activation is for the $^{12}C(n,\alpha)^{9}Be$ reaction. Because all the excited states of ^{9}Be are unstable with respect to neutron emission, the $^{12}C(n,\alpha)$ cross section is simply the cross section to the ground state of ^{9}Be. (Population of other states in ^{9}Be results in the $^{12}C(n,n'3\alpha)$ reaction.) This means that the inverse reaction $^{9}Be(\alpha,n_0)^{12}C$ can be used to deduce the forward reaction by the principle of detailed balance.

Figure 8 gives the data[42-49] in the literature and in addition, several recently measured points.[50] Because the (n,α) cross section could have fluctuations greater than the total cross section, the points might fall on a rather bumpy curve. Nevertheless, the data of the different groups seem rather inconsistent. One application of this cross section is the calculation of KERMA (Kinetic Energy Released in Materials) for tissue and for so called tissue equivalent dosimeters.

(n,γ) Cross Sections

The (n,γ) reaction is a small fraction of the non-elastic cross section for neutrons between 10 and 40 MeV. Experimentally this cross section is difficult to measure because a small degradation of the neutron spectrum by the sample or other nearby materials produces neutrons of lower energy where the capture cross section is higher, sometimes much higher. This cross section has not been measured above 15 MeV.

One way of checking the capture cross sections on Z N targets would be to measure the (p,γ) cross section (where the degradation of the incident proton energy is insignificant) on Z N targets. Neglecting Coulomb effects and connecting for residual mass differences, the cross sections should be equal. The (n,γ) cross section to the mirror nucleus could be inferred from the (p,γ) result using the direct-semidirect capture model.[51] When $^{40}Ca(n,\gamma_0)$ data are compared with $^{40}Ca(p,\gamma_0)$ data,[49] the only necessary change is to shift the neutron and proton energy scales by the mass difference of the residual nuclei. The agreement is so good up to 13 MeV neutron energy that one is led to suspect that the difference at higher energies could be experimental.

(n,t) and $(n,{}^3He)$ Cross Sections

The cross sections for (n,t) and $(n,{}^3He)$ reactions at 14 MeV have been investigated recently by Qaim and co-workers[53] using activation techniques. At this energy the cross sections are small (~40-100 μb). At higher energies, where they have not been measured in general, the cross sections are likely to be larger, although it is unlikely that they will be a large fraction of the total non-elastic cross section for all but a few, e.g. ^6Li, ^7Li, ^9Be, targets.

In the special case of the $^9Be(n,t_1)^7Li(0.478\ MeV)$ reaction, the cross section between 13 and 15 MeV was measured[54] recently by detecting the 0.478 MeV gamma ray with a Ge(Li) detector. These measurements resolved a discrepancy which was traced to the use, in a previous work, of a poorer resolution NaI(Tl) detector.

(n,f) Cross Sections

Neutron induced fission cross sections have been reviewed at length in the NEANDC/NEACRP Specialists meeting on Fast Fission Cross Sections[6] and, except for the $^{235}U(n,f)$ cross section discussed under Standard Data, will not be discussed further here.

PRODUCTION CROSS SECTIONS AND SPECTRA OF EMITTED RADIATIONS

Charged Particles: (n,xp), (n,xd), (n,xα)

The cross sections for these charged-particle producing reactions can in principle be measured in three distinct ways:

1. For cases where there is only one open channel for production of the charged particle, the residual nucleus, if radioactive, can be measured by radiochemical techniques.
2. The charged particles can be allowed to stop in the material and the resultant hydrogen and helium can be measured by physical or chemical techniques, or
3. The charged particles can be measured directly.

The first approach is the easiest but only applies to certain nuclear reactions. In particular, in the energy range 10 to 40 MeV most (n,xp), (n,xd) and (n,xα) reactions will result in one or more stable residual nuclei where the technique does not apply. The second technique as it applies to (n,xα) reactions is described in this Symposium by H. Farrar.[55] The measurement of hydrogen-producing nuclear reactions appears to be extremely difficult because of inevitable hydrogen contamination of the samples and the mass spectrometer. Neither of these approaches gives the spectra of the emitted charged particles.

The third approach has been advanced in the past two years by the author and his collaborators.[56-58] The new method has been to transport the charged particles from the target by means of a quadrupole doublet or triplet lens onto a detector telescope. The background is reduced between one and two orders of magnitude because the telescope can be moved far (2 to 4 meters) from the neutron source. The signal is not reduced however because of the focusing properties of the lens for charged particles. A typical spectrum obtained with a 3.9 mg/cm^2 Cu target[56] is given in Fig. 9. The quadrupole spectrometer and some recent results are described more fully in a contributed paper in this Symposium.[57]

The data for proton production in ^{27}Al by 15-MeV neutrons are compared in Table 2. The cross section measured with the quadrupole spectrometer is larger than previous results[59-61] because of the large number of protons produced with energies below 2.5 MeV. A combination of background problems and relatively thick targets prevented clean measurements of these lower energy protons.

The data from the quadrupole spectrometer can be checked in some cases against activation measurements. For ^{48}Ti(n,xp) and (n,xd) the measured cross sections[58] are:

^{48}Ti(n,xp)	85 ± 16 mb
^{48}Ti(n,xd)	7 ± 3
Sum	92 ± 16 mb at 15 MeV.

The sum of two activation cross sections[62] should give the same result:

$^{48}Ti(n,p)^{48}Sc$ 65.1 mb

$^{48}Ti(n,np + pn + d)^{47}Sc$ 15.1

Sum 80.2 mb at 15 MeV

which agrees within the quoted experimental error.

Table 2

$^{27}Al(n,xp)$ Cross Section Data

E_n MeV	E_p min MeV	Target Thickness mg/cm^2	$\sigma(n,xp)$ mb	Reference	Method
14.1	2.2	7.5	140	Allan(59)	Emulsion
14.1	2.	6.9	191±25	Alvar(60)	Telescope[a]
14.8	2.	7.1	273±20	Glover(61)	Telescope[a]
15.0	0.7	0.4 to 2.4	405±60	Grimes(58)	Quadrupole Spectrometer[b]

a. Telescope consisted of two proportional Al counters and a CsI(Tl) scintillator.

b. Telescope consisted of two surface-barrier detectors.

(n,xn) Cross Sections

Neutron emission cross sections and spectra have been compared by Hansen et al.[63] for 14-MeV incident neutron energy. The results[64-66] agree generally for iron, where the most extensive comparison can be made. For Al, Ni and Cu the rather complete spectra of Ref. 64 agree with more fragmentary data from other groups. In addition there are extensive data on ^{12}C, Nb, Pb, ^{235}U, ^{238}U and ^{239}Pu.[64] At 10 and 14 MeV measurements on light elements are discussed in this Symposium.[12] An extensive study of the neutron emission from the neutron bombardment of ^{9}Be has been completed in this latter work.

Above 15-MeV incident neutron energy, there are very few measurements as shown in fig. 2. Recently a white source has been used[7] to measure $^{27}Al(n,xn)$ up to 20 MeV. Although the flux of source neutrons above 14 MeV was quite low, a measurement was possible when the data were averaged over a few MeV of incident neutron energy.

$(n,x\gamma)$ Cross Sections

The extensive measurements at ORELA[67-69] and at Gulf Radiation Technology[70] have contributed significantly to the data base of neutron-induced gamma-ray production cross sections and spectra. The incident neutron energy range in these experiments usually extends to 20 MeV. In addition there have been measurements with 14-MeV neutrons, e.g., Refs. 71 and 72.

A comparison of the results for the much studied $^{27}Al(n,x\gamma)$ reaction illustrates some typical discrepancies (Fig. 10). The data have been grouped in 1-MeV bins for ease of comparison, and the white source data have been averaged for a central incident neutron energy of about 14 MeV. First the older work of Tucker et al.[71] differs in the total gamma-ray production section by a factor of two from the other measurements.[67,69,70,72] Secondly there are non-negligible differences in the spectral shapes. It is possible that the difference in incident neutron energy could account for some of these differences, although this possible explanation is probably not sufficient. It is surprising that these discrepancies have not been resolved yet.

CONCLUSIONS

From this review of the existing neutron data between 10 and 40 MeV, we can draw several conclusions. First, there are very few data, aside from total cross sections, for neutron energies above 15 MeV and even fewer for energies above 20 MeV. The region between 10 and 13 MeV is also not well investigated. Of the types of data reviewed, the least measured are those characterizing the emitted particles in non-elastic interactions, i.e., (n,xn), $(n,x\gamma)$, (n,xp), $(n,x\alpha)$ and so forth. Although several groups are investigating these and other reaction properties at many energies between 10 and 40 MeV, much remains to be done before there are enough data to indicate systematic trends.

The second conclusion is that, to provide accurate data, the future experimental techniques must avoid the problems encountered previously near 14 MeV. To this end, the careful experimenter will use state-of-the-art techniques and many cross-checks including comparison of his neutron data with proton-induced reaction data and nuclear models where applicable. The factor-of-two errors appearing in some data clearly can and should be resolved.

Thirdly we can be pleased with much of the present data near 14 MeV, with the elastic scattering cross section data where they have been measured, and with most of the total cross section data throughout the range 10 to 40 MeV.

Finally for fusion, radiation damage, and medical applications, the picture is bright even where the data are sparse because of the present arsenal of experimental techniques. When a well-defined need for a particular type of data arises, it can be satisfied to some reasonable accuracy with a concerted effort

based on present day technology. Many of the techniques and efforts for these applied programs are discussed at this Symposium.

ACKNOWLEDGMENT

The comments of J. D. Anderson, S. M. Grimes, L. F. Hansen, R. J. Howerton and C. Wong on this review are gratefully acknowledged. I also thank L. Veeser for sending data prior to publication.

REFERENCES

1. D. E. Cullen, K. L. Hill, R. J. Howerton and S. T. Perkins "An Integrated System for Production of Neutronics and Photonics Calculational Constants," UCRL-50400, vol. 1, rev. 3: "ECSIL: A System for Storage, Retrieval and Display of Experimental Neutron Data," Lawrence Livermore Laboratory (1976); and ibid. vol. 10, "Tabulated Experimental Data for Neutron-Induced Interactions," (1976). This compilation, based to a large extent on the SCISSORS file, is the primary basis for the statements in this review of what does or does not exist in the literature. Very recent data might not yet have been compiled and therefore could be overlooked in this review.
2. CINDA 76/77, An Index to the Literature on Microscopic Neutron Data, IAEA, Vienna (1976).
3. J. C. Hopkins and G. Breit, Nuclear Data Tables A9, 137 (1971).
4. C. A. Uttley in "Review of Standard Reference Data and Important Cross Section Discrepancies," H. E. Jackson, Chairman, ANL/ND-77-1 Argonne National Laboratory (1976).
5. M. A. Gardner and D. G. Gardner, Nucl. Phys. A265, 77 (1976).
6. W. P. Poenitz and P. T. Guenther, "Proceedings of the NEANDC/NEARCRP Specialists Meeting on Fast Neutron Fission Cross Sections of U-233, U-235, U-238 and Pu-239. Supplement Material Presented for Consideration by the Working Groups" Supplement to ANL-76-90, Argonne National Laboratory (1976).
7. S. Cierjacks, P. Forti, D. Kopsch, L. Kropp, J. Nebe and H. Unseld, "High Resolution Total Neutron Cross Sections for Si, Cr and Ni between 0.5 and 30 MeV," KFK-1000, Suppl. 1, Karlsruhe (1968).
8. R. B. Schwartz, R. A. Schrack and H. T. Heaton III, "MeV Total Neutron Cross Sections," NBS Monograph 138, National Bureau of Standards (1974).
9. F. G. Perey, T. A. Love, and W. E. Kinney, "A Test of Neutron Total Cross-Section Evaluations from 0.2 to 20 MeV for C, O, Al, Si, Ca, Fe and SiO_2," ORNL-4823, Oak Ridge National Laboratory (1972).
10. P. F. Yergin et al., Conf. on Neutron Cross Sections and Technology, p. 690, Washington D.C. (1966).

11. T. Phillips, B. L. Berman, W. A. Barletta, and J. D. Seagrave, Bull. Am. Phys. Soc. 21, 534 (1976).
12. D. M. Drake, L. Veeser, D. Barr and G. Auchampaugh, "Differential Data Measurements at LASL in the Energy Range 1-30 MeV," this Symposium.
13. B. A. Benetzky, V. V. Nefedov, I. M. Frank, and I. V. Shtranikh, Sov. J. Nucl. Phys. 17, 10 (1973).
14. J. D. Anderson, H. H. Barschall, and J. C. Davis, Sov. J. Nucl. Phys. 19, 483 (1974).
15. D. W. Glasgow, F. O. Purser, H. Hogue, J. C. Clement, K. Stelzer, G. Mack, J. R. Boyce, D. H. Epperson, S. G. Buccino, P. W. Lisowski, S. G. Glendinning, E. G. Bilpuch, and H. W. Newson, Nucl. Sci. Eng. 61, 521 (1976).
16. G. Haouat, J. Lachkar, J. Sigaud, Y. Patin, and F. Cocu, "Sections Efficaces Differentielles de Diffusion Elastique et Inelastique des Neutrons par le Carbone dans la Gamme l'Energie Comprise Entre 8.8 et 14.5 MeV," CEA-R-6414, Commissariat a l'Energie Atomique, Centre d'Etudes Nucleaires, Saclay (1975); also Proc. Conf. Nuclear Cross Sections and Technology, National Bureau of Standards Special Publication 425, p. 889 (1975).
17. T. P. Stuart, J. D. Anderson, and C. Wong, Phys. Rev. 125, 276 (1962)).
18. J. C. Ferrer, J. D. Carlson, and J. Rapaport, Nucl. Phys. A275, 325 (1977).
19. J. Rapaport, J. D. Carlson, D. Bainum, T. Cheema, and R. W. Finlay, Proc. Int. Conf. on the Interaction of Neutrons with Nuclei, ed. E. Sheldon, vol. II, p. 1320, Lowell, Massachusetts (1976).
20. J. D. Carlson, J. Rapaport, T. Cheema, D. Bainum, and J. Ferrer, ibid. p. 1305.
21. J. Rapaport, R. W. Finlay, D. E. Bainum, J. D. Carlson, and T. Cheema, "Neutron Scattering Measurements at Ohio University in the Energy Range 7-26 MeV," this Symposium.
22. A. Ashmore, D. S. Mather and S. K. Sen, Proc. Phys. Soc. (London) 71, 552 (1958).
23. G. Deconnink and J. P. Meulders, Phys. Rev. C1, 1326, (1970).
24. M. V. Harlow, Jr., R. L. Robinson, and B. B. Kinsey, Nucl. Phys. 67, 249 (1965).
25. F. Boreli, B. B. Kinsey, and P. N. Shrivastava, Phys. Rev. 174, 1147 (1968).
26. G. L. Morgan, T. A. Love, and F. G. Perey, Nucl. Inst. and Meth. 128, 125 (1975).
27. M. H. MacGregor, W. P. Ball, and R. Booth, Phys. Rev. 111, 1155 (1958).
28. F. S. Dietrich and R. P. Koopman, private communication.
29. R. P. Koopman, thesis, University of California at Davis (1977).
30. L. R. Veeser and E. D. Arthur, Proc. Int. Conf. on the Interaction of Neutrons with Nuclei, ed. E. Sheldon, vol. II, p. 1351 Lowell, Massachusetts (1976).

31. J. Fréhaut and G. Mosinski, Nuclear Cross Sections and Technology, NBS Special Publication 425, 2, 855, National Bureau of Standards (1975).
32. R. S. Storey, W. Jack, and A. Ward, Proc. Phys. Soc.(London) 75, 526 (1960
33. M. Bormann, F. Dreyer, H. Neuert, I. Riehle and U. Zielinski, Nuclear Data for Reactors, vol. 1, 225, IAEA, Vienna (1967).
34. J. K. Temperley, Nucl. Sci. and Eng. 32, 195 (1968).
35. P. Decowski et al., Nucl. Phys. A112, 513 (1968).
36. A. M. Bresesti, M. Bresesti, A. Rota, R. A. Rydin and L. Lesca, Nucl. Sci. and Eng. 40, 531 (1970).
37. A. Paulsen and R. Widera, Proc. Conf. on Chem. Nucl. Data - Measurements and Applications, M. Wurrell, ed., Institute of Civil Eng., London (1971).
38. D. Smith, "Cross Sections for (n,p) Reactions on ^{27}Al, ^{46,47,48}Ti, ^{54,56}Fe, ^{58}Ni, ^{59}Co and ^{64}Zn from Near Threshold to 10 MeV," ANL/NDM-10, Argonne National Laboratory (1975).
39. R. W. Fink and W-D. Lu, Bull. Am. Phys. Soc. 15, 1372 (1970).
40. W. G. Cross and R. L. Clarke, "Progress Report," AECL-1542, Chalk River Ontario (1962).
41. J. M. F. Jeronymo, G. S. Mani, J. Olkowski, A. Sadeghi, and C. F. Williamson, Nucl. Phys. 47, 157 (1963).
42. M. Brendle, M. Morike, G. Staudt, and G. Steidle, Z. Naturforsch 23A, 1229 (1968).
43. D. Kopsch and S. Cierjacks, Nucl. Inst. and Meth. 54, 277 (1967).
44. H. Kitazawa and N. Yamamuro, J. Phys. Soc. Japan 26, 600 (1969).
45. E. R. Graves and R. W. Davis, Phys. Rev. 97, 1205 (1955).
46. M. L. Chatterjee and B. Sen, Nucl. Phys. 51, 583 (1964).
47. A. W. Obst, T. B. Grandy, and J. L. Weil, Phys. Rev. C5, 738 (1972).
48. V. V. Verbinski, F. G. Perey, J. K. Dickens, and W. R. Burrus, Phys. Rev. 170, 916 (1968).
49. J. Kjellman and A. Nilsson, Arkiv för Fysik 22, nr17, 277 (1962).
50. R. C. Haight, S. M. Grimes. B. Pohl, C. H. Poppe, and C. Wong, unpublished (1977).
51. F. S. Dietrich, D. W. Heikkinen, K. A. Snover, and K. Ebisawa Phys. Rev. Lett. 38, 156 (1977).
52. F. S. Dietrich, private communication (1977).
53. S. M. Qaim and R. Wolfle, Proc. Int. Conf. on the Interactions of Neutrons with Nuclei, ed. E. Sheldon, vol. II, p. 1339, Lowell, Massachusetts (1976).
54. F. S. Dietrich, L. F. Hansen and R. P. Koopman, Nucl. Sci. Eng. 61, 267 (1970).
55. H. Farrar, IV, D. W. Kneff, R. A. Butten and R. R. Heinrich, "Fluence Mapping of RTNS by He Accumulation and Foil Activation Methods," this Symposium.
56. S. M. Grimes, R. C. Haight, J. D. Anderson, K. R. Alvar and R. R. Borchers, Bull. Am. Phys. Soc. 22, 631 (1977).

57. S. M. Grimes, R. C. Haight, J. D. Anderson, K. R. Alvar and R. R. Borchers, "Development of a Spectrometer for the Measurement of (n,xp), (n,xd) and (n,xα) Cross Sections, Angular Distributions and Spectra at E_n = 15 MeV," this Symposium.
58. S. M. Grimes, R. C. Haight and J. D. Anderson, Nucl. Sci. Eng. 62, 187 (1977).
59. D. L. Allan, Proc. Phys. Soc. (London) A70, 195 (1957).
60. K. R. Alvar, Nucl. Phys. A195, 289 (1972).
61. R. N. Glover and E. Weigold, Nucl. Phys. 24, 630 (1961).
62. B. A. Magurno, ed., ENDF/B-IV Dosimetry File, BNL-NCS-50446, Brookhaven National Laboratory (1975).
63. L. F. Hansen, S. M. Grimes, R. J. Howerton and J. D. Anderson, Nucl. Sci. Eng. 61, 201 (1976).
64. J. L. Kammerdiener, "Neutron Spectra Emitted by ^{239}Pu, ^{238}U, ^{235}U, Pb, Nb, Ni, Fe, Al and C Irradiated by 14-MeV Neutrons," UCRL-51232 (thesis), Lawrence Livermore Laboratory (1972).
65. S. C. Mathur, P. S. Buchanan, and I. L. Morgan, Phys. Rev. 186, 1030 (1969).
66. G. Clayeaux and J. Voignier, "Diffusion Non-Elastic de Neutrons de 14-MeV Sur Mg, Al, Si, S, Ca, Sc, Fe, Ni, Cu, Au, Pb et Bi," CEA-R-4279, Centre d'Etudes de Limiel (1972).
67. G. L. Morgan and F. G. Perey, "Cross Sections for the Al(n,xn) and Al(n,xγ) Reaction Between 1 and 20 MeV," ORNL-TM-5241, Oak Ridge National Laboratory (1976)
68. J. K. Dickens, G. L. Morgan, G. T. Chapman, T. A. Love, E. Newman, and F. G. Perey, Nucl. Sci. Eng. 62, 515 (1977).
69. J. K. Dickens, T. A. Love, and G. L. Morgan," Gamma-Ray
70. V. J. Orphan, C. G. Hoot and J. John, "Gamma-Ray Production Cross Sections for Iron and Aluminum," Gulf-RT-A10/43, DNA2736F, Gulf Radiation Technology (1971).
71. W. E. Tucker et al., "Anual Progress Report," ORO-2791-30, Texas Nuclear Division, Nuclear-Chicago Corp. (1969).
72. D. M. Drake, E. D. Arthur, and M. G. Silbert, "Fourteen-MeV, Neutron-Induced Gamma-Ray Production Cross Sections," LA-5662-MS, Los Alamos Scientific Laboratory (1974).

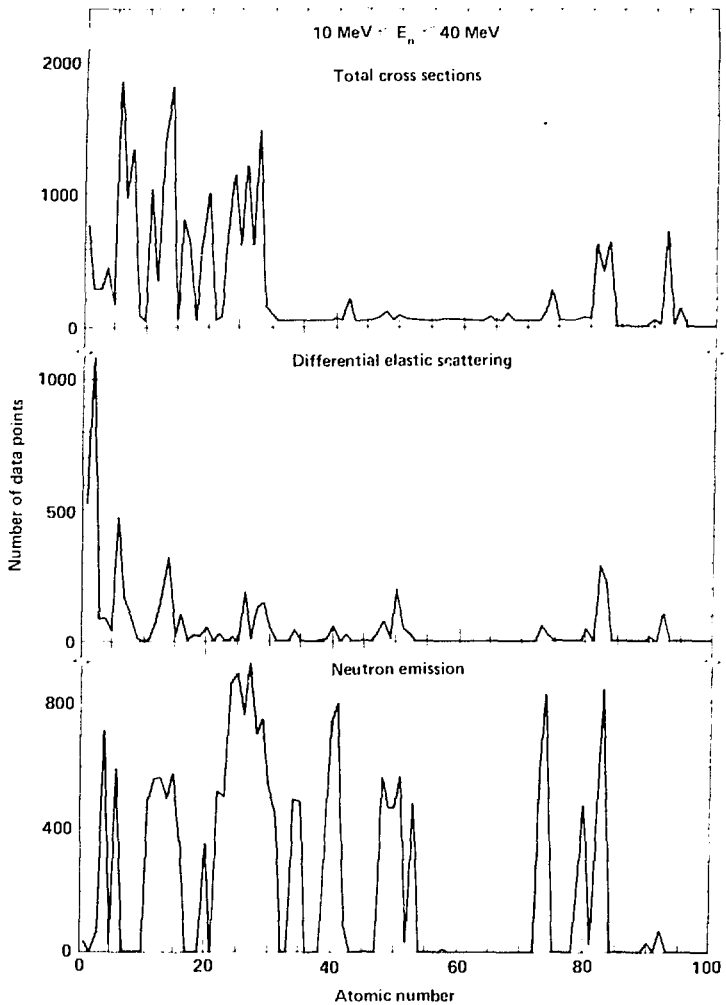

Figure 1. Number of data points versus atomic number for (top) total, (middle) differential elastic and (bottom) neutron emission data for incident neutrons between 10 and 40 MeV.

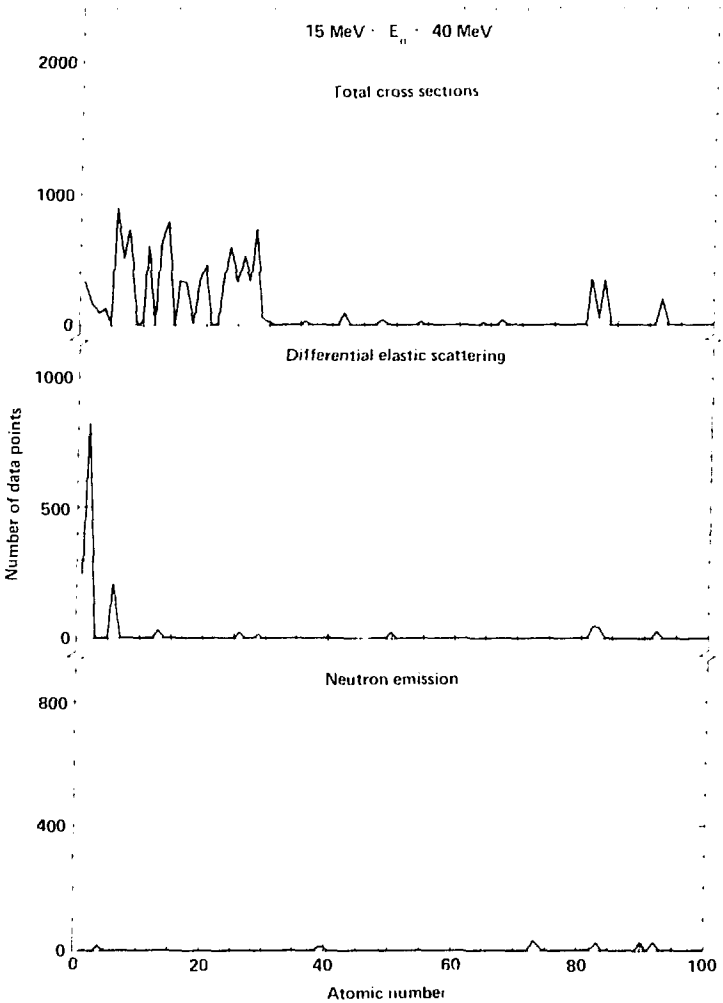

Figure 2. Number of data points versus atomic number for (top) total, (middle) differential elastic and (bottom) neutron emission data for incident neutrons between 15 and 40 MeV.

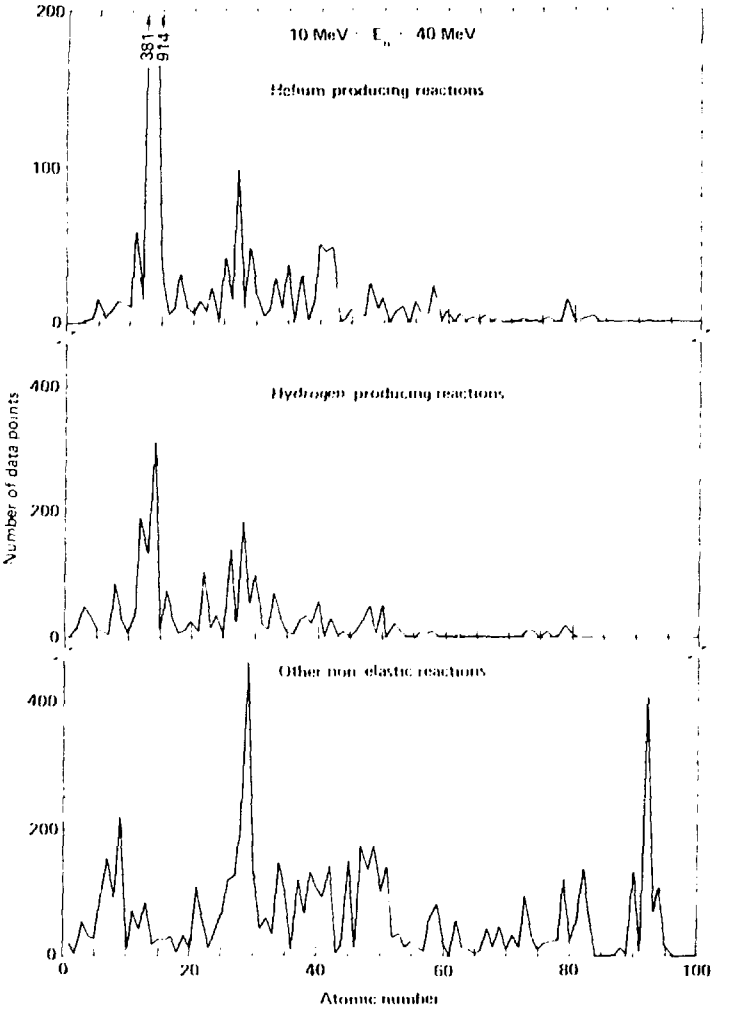

Figure 3. Number of cross section measurements versus atomic number for (*top*) helium producing reactions, (middle) hydrogen producing reactions, and (*bottom*) all other partial non-elastic reactions. The incident neutron range is 10 to 40 MeV.

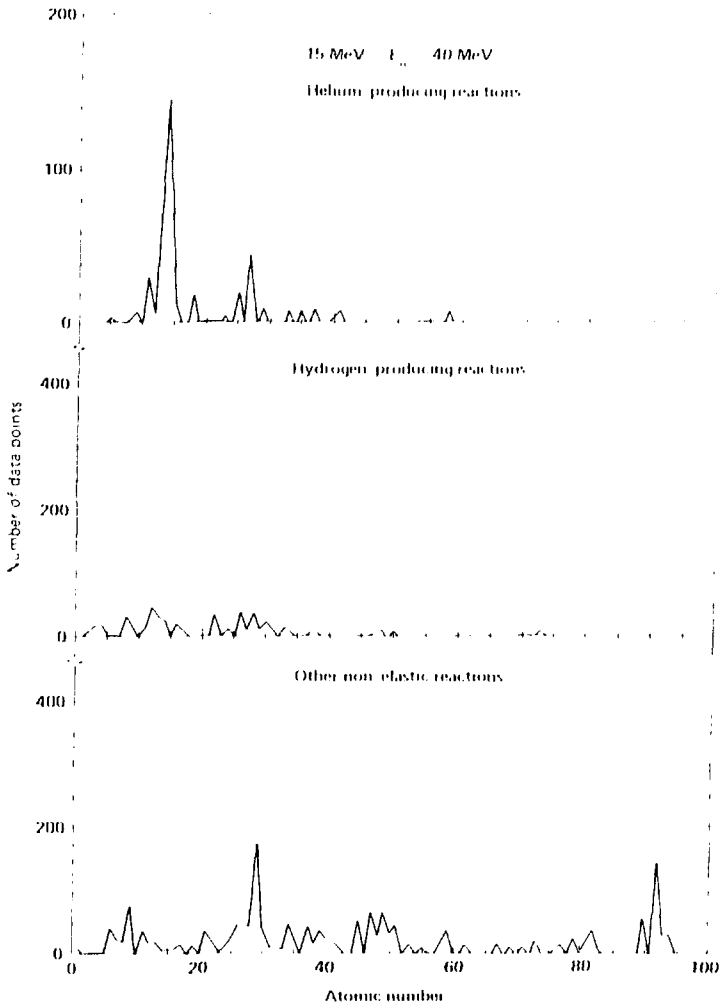

Figure 4 Number of cross section measurements versus atomic number for (top) helium producing reactions, (middle) hydrogen producing reactions, and (bottom) all other partial non elastic reactions. The incident neutron range is 15 to 40 MeV.

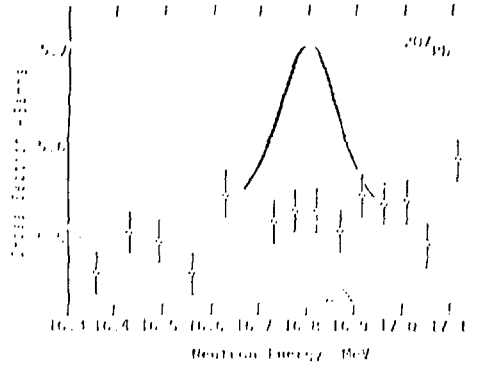

Figure 5. ^{207}Pb total cross section. The data points are from Ref. 14 and the solid curve represents the earlier data of Ref. 13.

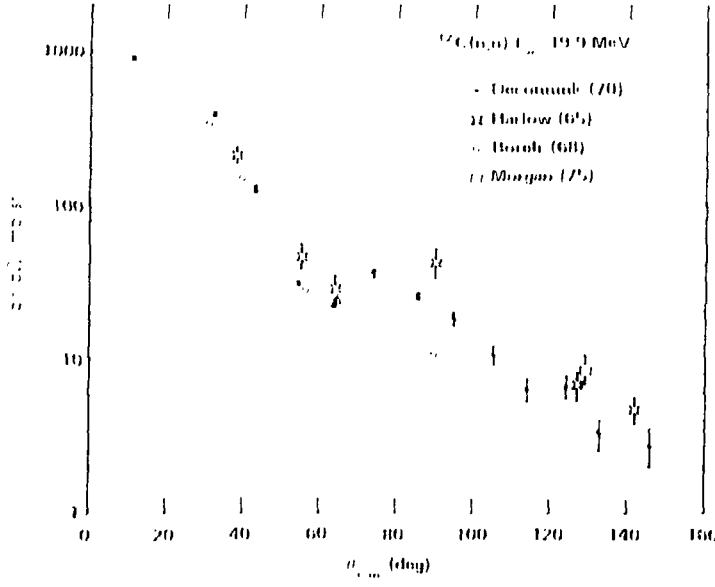

Figure 6. Differential elastic scattering data at 19.9 MeV from Ref. 23 (dots), 24 (crosses), 25 (diamonds) and 26 (squares).

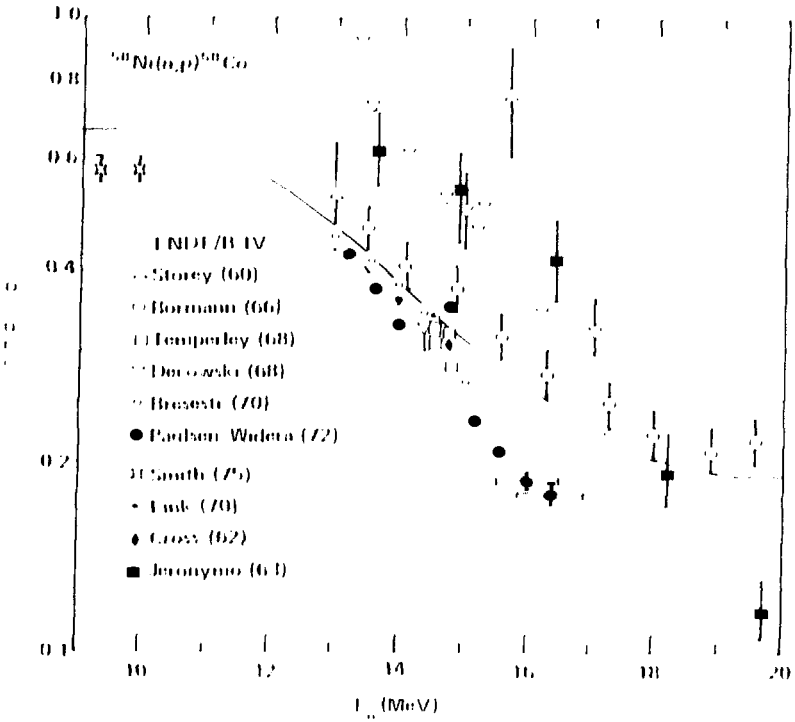

Figure [illegible] data for the ^{58}Ni(n,p)^{58}Co reaction as determined by activation. The references are labeled by [illegible] Bormann [illegible] Temperley [illegible] Dorozwski [illegible] Bresesti [illegible] Paulsen Wadera [illegible] Smith [illegible] Fink [illegible] Cross [illegible] and Jeronymo [illegible]

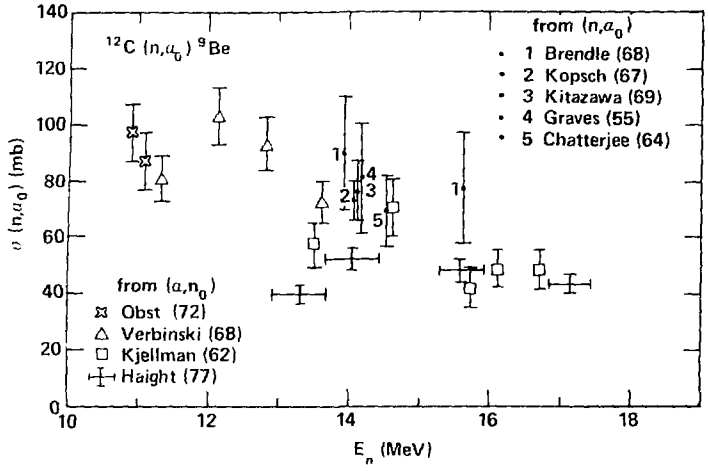

Figure 8. Data for the $^{12}C(n,\alpha)^9Be$ reaction. The references are to Brendle,[42] Kopsch,[43] Kitazawa,[44] Graves,[45] and Chatterjee[46] for experiments with neutrons incident. For data deduced from the inverse reaction, the points are from Obst,[47] Verbinski,[48] Kjellman,[49] and Haight.[50]

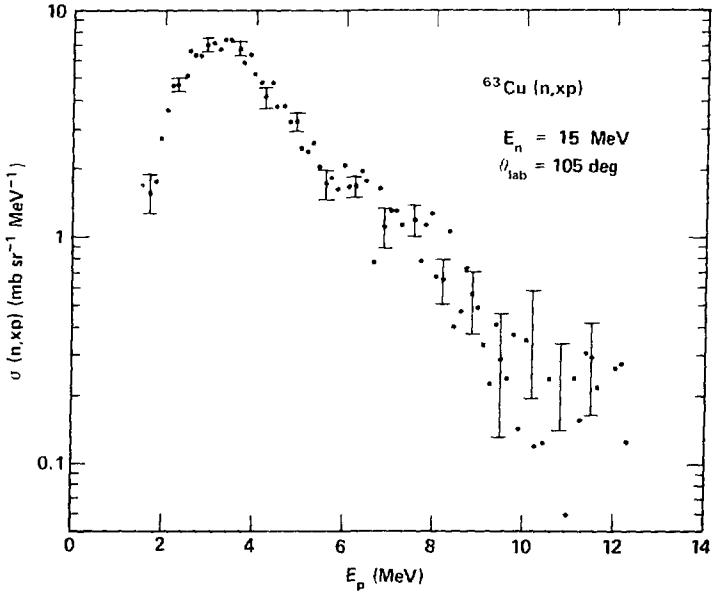

Figure 9. Proton spectrum at 105° from ^{63}Cu under bombardment by 15-MeV neutrons from Ref. 56.

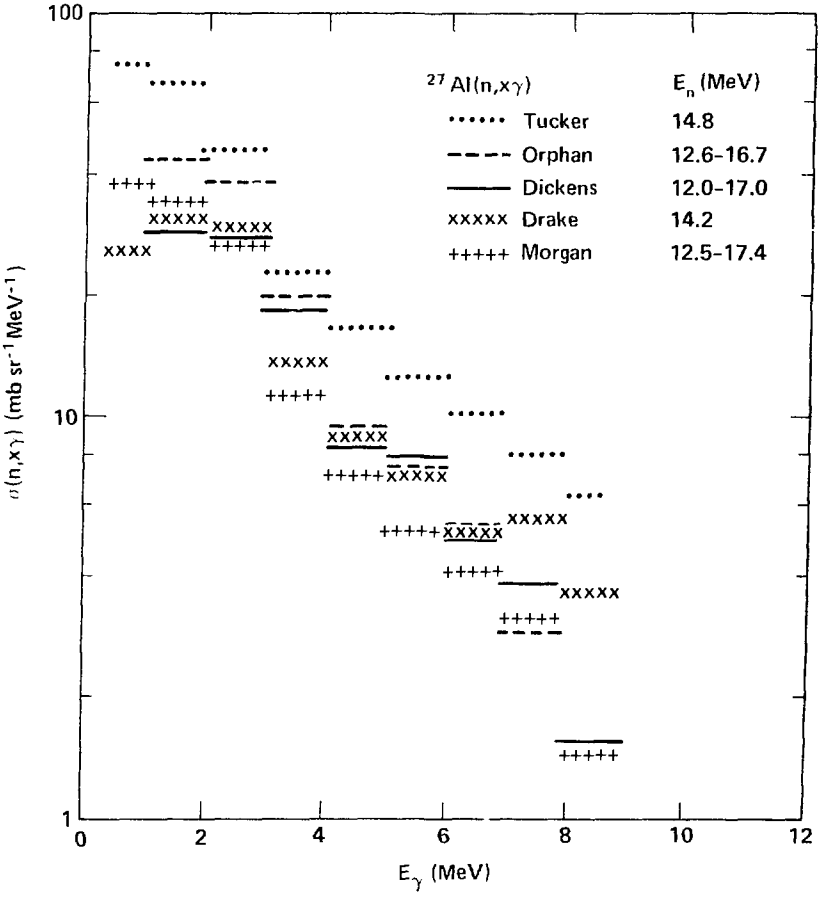

Figure 10. Data from $^{27}Al(n,x\gamma)$ measurements near 14 MeV. The references are to Tucker,[71] Orphan,[70] Dickens,[69] Drake,[72] and Morgan.[67]

Differential and Integral Neutron Standards for High Energy Neutrons

Oren A. Wasson
National Bureau of Standards, Washington, D. C.

INTRODUCTION

There is a need for standard neutron fields near 14 MeV neutron energy for applications in fusion power dosimetry and at higher energies for medical dosimetry. There is a large uncertainty in the cross section for the ^{58}Ni(n,p) ^{58}Co reaction[1] used for reactor dosimetry near 14 MeV while there still remains a 10% uncertainty in the ^{235}U(n,f) cross section[2] which is the standard for all fission reaction measurements. The accuracy in the neutron spectrum shape measurements from the deuteron and proton induced reactions on lithium and beryllium useful for medical treatment is limited by the efficiency of the neutron detectors. The availability of a standard neutron spectrum for calibration of various neutron flux monitors should provide a useful contribution to the standardization of neutron measurements in these fields. This paper is devoted to an investigation of the standard 14 MeV neutron fields which can be provided at the 3MV Van de Graaff facility at the National Bureau of Standards.

THE ^{3}H(^{2}H,n) ^{4}He REACTION

The nuclear reaction used with a 3 MV Van de Graaff accelerator is the well known ^{3}H(^{2}H,n) ^{4}He process using a deuteron beam incident on a tritiated titanium target. This two body reaction has a large Q Value of 17.58 MeV which at threshold produces a 14.1 MeV neutron and a 3.5 MeV alpha particle. The cross section peaks at approximately 5 barns for an incident deuteron energy of 110 keV and decreases by a factor of 7 at 500 keV. The neutron angular distribution is fairly isotropic for deuteron energies less than 3 MeV. As the deuteron energy increases, the neutron energy varies greatly with angle. At 100 keV deuteron energy the neutron energy changes by 1.3 MeV between 0° and 180° in the lab. At 500 keV this variation increases to 3 MeV.

The neutron energies that can be produced with the Van de Graaff for various neutron angles are shown in Fig. 1. These extend from 12 to 19.5 MeV. It is necessary to work at several angles in order to investigate the entire neutron energy region available with this reaction. At the higher neutron energies, one works in the forward direction where the minimum neutron energy is controlled by the lowest deuteron energy available at the Van de Graaff, which is expected to be approximately 500 keV without the use of energy degrading foils in the beam. Near 90° in the

laboratory system, the neutron energy variation about 14.1 MeV is a minimum. Lower neutron energies require backward angles.

The neutron flux produced in this reaction can be measured by means of the associated particle technique. Since the reaction is a two-body process, the energy and angle of the emitted neutron is uniquely related to the energy and angle of the associated alpha particle. The collimated alpha particles can be detected with a solid state counter since the backgrounds produced by neutron interactions in silicon appear to be manageable. Experience using Ti-T solid targets[3] indicates that scattering of the incident deuteron beam and migration of the tritium in the target produce a minimum spread in the neutron cone of approximately 5°, FWHM. This angular spread is quite acceptable for cross section measurements and detector calibrations.

MEASUREMENTS USING ASSOCIATED PARTICLE TECHNIQUE

Calibration of Proton Recoil Telescope

Since two of the more common neutron flux monitors for 14 MeV neutrons are the associated particle technique and the proton recoil telescope, it would be useful to compare the two techniques directly. A diagram for this comparison is shown in Fig. 2. The alpha particles from the d,t reaction are collimated onto a solid state detector. The corresponding neutron cone is incident upon the radiator of the telescope. It is essential that the area of the radiator exceed the dimensions of the neutron beam. The telescope functions by detecting the recoil proton from n-p scattering in a thin polyethylene foil. The energy of the proton, E_p, is given by

$$E_p = E_n \cos^2 \psi$$

where E_n is the incident neutron energy and ψ is the proton angle in the laboratory system. A practical film thickness for 14 MeV protons is 20 mg/cm^2 which produces a 1 MeV proton energy loss.[4] Since less than 1% of the incident neutrons interact in the foil, and less than 10% of the recoil protons hit the detector, the neutron flux incident on the proton detector is more than 1000 times the proton flux. In order to reduce the neutron induced background, several transmission detectors are operated in coincidence with the proton detector.[5,6]

The uncertainty in the efficiency of the telescope monitor depends on the uncertainty in the hydrogen concentration in the radiator and the angular distribution of the n-p reaction. Since both of these quantitites are thought to be known to better than 1% uncertainty, a test of the telescope response by means of the associated particle technique should help tie together a larger group of results.

Neutron Flux Monitor Calibration

The associated particle technique will also permit the calibration of the efficiency of larger plastic scintillation detectors for use in different geometries as neutron flux monitors. The experience of Meier at NBS at lower energies[5] and the work of Cookson and co-workers[6] near 15 MeV indicate that detector efficiencies can be measured with an uncertainty of a few percent near 14 MeV. The efficiency measured with the diverging neutron beam in the associated particle technique can be corrected by computer calculation for use in a parallel neutron beam as well as by probing the neutron beam across the face of the detector. A typical detector is a 5 cm diameter by 5 cm thick plastic or liquid scintillator.

Standard Neutron Induced Fission Cross Section

Measurements of the standard ^{235}U, ^{238}U, and ^{237}Np neutron induced fission cross sections in the neutron energy range from 12 to 16 MeV are planned using the associated particle technique. The ^{235}U sample is deposited onto a thin backing and placed inside an ionization chamber which detects the fission fragments. Backgrounds are reduced by means of pulsed beam and time-of-flight measurements. The deduced fission cross section is independent of the size of the alpha particle and neutron cones as long as the fission deposit is larger than the associated neutron cone. The accuracy of the cross section measurement is limited by the variations in the sample thickness. Recent measurements by Gance and Gronier list errors in the ^{235}U cross section at 14.6 MeV of between 1.5 and 2.5% due to this source. On the other hand Adamov and co-workers claim an error of only 0.5% due to the ^{235}U thickness. However the two measurements, taken at slightly different energies, differ by approximately 6% (3 standard deviations).

The expected fission counting rates for single fission deposits of 100 μg/cm^2 thickness are approximately 300 events per hour for 500 keV deuterons incident on a Ti-T target with a 40 keV thickness to deuterons and a 1 μA pulsed beam. These rates are low but do allow accurate measurements of standard fission cross sections.

LARGE GEOMETRY NEUTRON BEAM

For the production of large size neutron beams a different arrangement and neutron flux monitor are required. An arrangement which we at NBS have found successful at 1 MeV neutron energies[1] is shown in Fig. 3. The neutron source is surrounded by a large neutron shield which provides a collimated neutron beam with 4.5° half angle. The neutron flux at the sample position near 1.5 m is determined by a secondary flux monitor located 5 m downstream in a shield with a precision collimator. The

purpose of the shield around the source is to reduce the room background at both the sample and monitor positions. The flux monitor with an efficiency of over 90% at 1 MeV was both calibrated with the associated particle technique and calculated by Monte-Carlo programs.

We propose to modify this set up for use at 14 MeV by redesigning the source shield to obtain additional neutron beams at 90° and several back angles. The system is flexible to provide for different beam sizes and flux monitors. If this geometry is unsuccessful at 14 MeV we have the option of using open beam geometry and measuring backgrounds by means of shadow bars.

SUMMARY

A standardized flexible 14 MeV neutron field will be available at NBS for calibration of various neutron flux monitors. The availability of a common neutron source should be of value in inter-laboratory flux rate measurements. This facility will also be used for measurements of the standard neutron induced fission cross sections as will those reactions used for reactor dosimetry.

REFERENCES

1. L. Stewart, Contribution to this conference.
2. W.P. Poenitz and P.T. Guenther, in Proceedings of the Specialists Meeting on Fast Neutron Fission Cross Section of U-233, U-235, U-238, and Pu-239, W.P. Poenitz and A.B. Smith, Editors, Supplement, p. 39, Argonne National Laboratory Report ANL-76-90, (1976).
3. M.M. Meier, in International Specialists Symposium on Neutron Standards and Applications, C.D. Bowman and A.D. Carlson, Editors, To be published, (1977).
4. C.H. Johnson, in Fast Neutron Physics, J.B. Marion and J.L. Fowler, Editors, p. 247-295, Interscience Publishers Ltd., London, (1960).
5. T.W. Burrows, Phys. Rev. C7, 1306 (1973).
6. C.A. Uttley, in International Specialists Symposium on Neutron Standards and Applications, C.D. Bowman and A.D. Carlson, Editors, To be published (1977).
7. J.A. Cookson, M. Hussian, C.A. Uttley, J.L. Fowler, and R.B. Schwartz, in Nuclear Cross Sections and Technology, R.A. Schrack and C.D. Bowman, Editors, U.S. Govt. Printing Office, Washington, D.C., pp. 66-68, (1975).
8. M. Cance and G. Grenier, Ibid, pp. 237-244.
9. V.M. Adamov, et al., in International Specialists Symposium on Neutron Standards and Applications, C.D. Bowman and A.D. Carlson, Editors, To be published, (1977).
10. O.A. Wasson, Ibid.

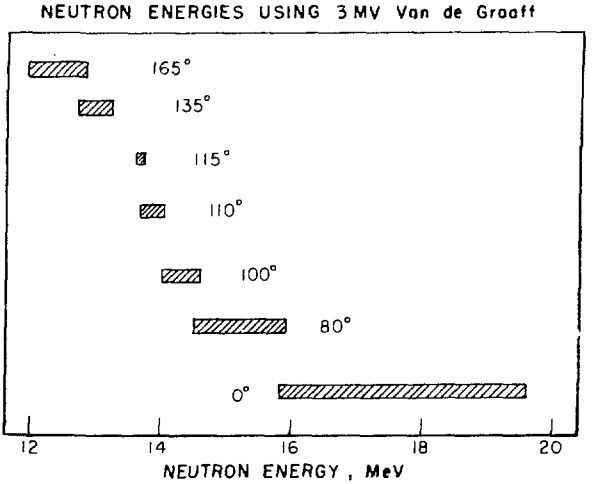

Fig. 1. Neutron energies from (d,t) reaction using 3 MV Van de Graaff

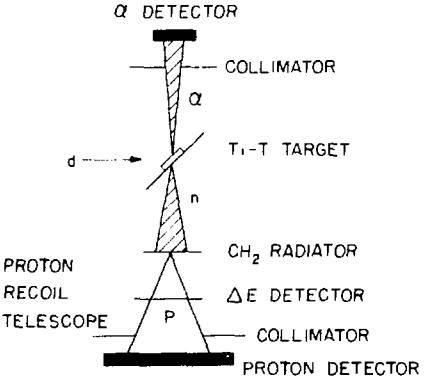

Fig. 2. Associated particle technique and proton recoil telescope

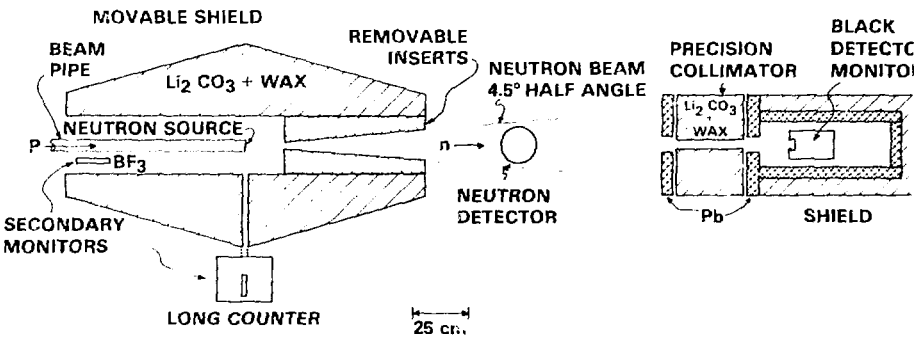

Fig. 3. Standard neutron beam line used for 1 MeV neutrons

CONF-770523-8

Neutron Cross Section Programs in the Energy Region from 1 to 24 MeV at the LASL Van de Graaff Facilities*

G. F. Auchampaugh, D. M. Drake, and L. R. Veeser
University of California, Los Alamos Scientific Laboratory
Los Alamos, New Mexico 87545

Neutron measurements relevant to the Los Alamos Scientific Laboratory's (LASL) programmatic efforts and to the U. S. fission and fusion energy programs can be divided into four categories: secondary neutron emission cross sections on light elements,[1] gamma-ray production cross sections,[2] total cross sections on light isotopes,[3] and (n,2n) and (n,3n) cross sections.[4] Many of these measurements have been performed using the unusual capabilities of the LASL's Van de Graaffs. This is especially true for the high-energy ($\geqslant$ 20 MeV) measurements on (n,2n) and (n,3n) cross sections. The purpose of this paper is to describe briefly the four types of measurements, to illustrate each measurement with some examples, and to present any new data that are not as yet available in the literature. We will also indicate in which programs new measurements are planned for the next year.

SECONDARY NEUTRON EMISSION CROSS SECTION PROGRAM

Differential elastic and inelastic cross sections and double-differential continuum cross sections have been measured for 5.9-, 10.1-, and 14.2-MeV incident neutrons on beryllium using the LASL tandem and single-ended Van de Graaff facilities. Inelastic here refers collectively to the states at 1.6-, 2.43-, 2.8-, and 3.06-MeV in ^{9}Be. Data were taken at scattering angles between 25° and 145°.

The H(t,n) reaction was used for the 5.9- and 10.1-MeV measurements instead of the customary inverse reaction because, in principle, all sources of neutron background can be investigated (the breakup neutron threshold lies above the energy region of interest at about 24 MeV) and because the H(t,n) reaction produces about a factor of 20 more neutrons in the forward direction than the inverse reaction. The H(t,n) reaction, however, does produce a sizeable, but measureable, neutron background in the continuum region from triton reactions in the entrance and beam stop materials. The hollow samples were placed about 164 mm from the center of the target cell and the scattering angle changed by rotating the detector about the axis of the sample.

The ^{2}H(t,n) reaction was used for the 14.2-MeV measurements. The triton beam was stopped in the deuterium gas of the target. The samples were placed in the plane perpendicular to the beam direction about 100 mm from the target. The scattering angle was

*Work performed under the auspices of the United States Energy Research and Development Administration.

changed by rotating the sample in this plane about the target. In this geometry the energy of the incident neutron beam does not change with scattering angle.

The neutron detector was a NE-213 scintillator 100 mm in diameter by about 76-mm thick, which was directly coupled to the photocathode surface of an RCA-8854 photomultiplier. The bias on the detector was set to correspond to a neutron energy of approximately 300 keV. Pulse-shape discrimination using the zero-crossover technique[5] was used to reduce the gamma-ray background. The detector was located about 2.7 m from the sample inside of a massive neutron shield that consisted of paraffin impregnated with lithium hydride.

The multiple scattering correction was calculated using the LASL Monte Carlo code MCN.[6] The neutrons were tallied by emission-energy and -angle according to the type of reaction that created them: elastic, inelastic, elastic-elastic, elastic-inelastic, and inelastic-inelastic. Calculations were made on normal density and on 0.01 normal density samples at each incident neutron energy. The multiple scattering correction as a function of emission-energy and-angle was obtained by taking a ratio of the results from the different sample runs. The beryllium cross section data in the ENDF/B-IV files were used in these calculations. The corrections were nominally less than 10%.

The beryllium data were converted to cross section by normalizing the data to the hydrogen scattering data obtained from samples of polyethylene and using the Hopkins and Breit n,p scattering cross section.[7] At high energies and small scattering angles the hydrogen elastic peak was not completely resolved from the carbon elastic peak and therefore it was necessary to take data on a carbon sample to correct the polyethylene sample data for the carbon contaminant.

Since the cross section was obtained from a ratio of the beryllium data to the hydrogen data it was only necessary to measure the relative efficiency of the neutron detector. The relative efficiency of the detector was measured from 0.3 MeV to 20 MeV using the $^{2}H(d,n)$, $^{2}H(p,a)$, and $^{3}H(d,n)$ reactions and by elastically scattering neutrons off of hydrogen and using the n,p scattering cross section.[7]

As a self-consistency check on the elastic data, data were taken with the $^{3}H(p,n)$ reaction at 5.9 and 10.1 MeV. The agreement between the sets of data was better than 4%. Since the statistics in the continuum region were poor and the background very large, a meaningful comparison could not be made with the H(t,n) data. At this time we did not have the benefit of the source reaction studies[8] made at LASL that showed that the gold beam stop, which we were using, created several orders of magnitude more background than either a ^{28}Si or ^{58}Ni beam stop.

To check the multiple scattering correction we made several measurements on samples of beryllium with different dimensions. The elastic and inelastic cross sections obtained agreed to within 3% and the continuum cross sections to better than 10%.

[illegible] beryllium for [illegible] MeV incident neutrons is shown in Fig. 1. The [illegible] at the [illegible] peak [illegible] 1.4% is due to [illegible] of the [illegible] neutrons [illegible] to the 1.4% [illegible] [illegible] excitation [illegible] 1.4% [illegible] [illegible] [illegible] level.

It is instructive to compare [illegible] of production from the ENDF/B-IV [illegible] file to compare with our measured distributions. An example of such a comparison [illegible] shown in Fig. 2 for [illegible] MeV neutrons. The data are plotted as a solid line and the calculation as a short- and long-dashed line. This comparison, which is typical, clearly shows the overemphasis on the low-lying states in ^{9}Be in the ENDF/B-IV beryllium cross section file. We have also plotted (dash-dot line) the result of a statistical phase space calculation of the energy distribution for the three-body final state configuration consisting of two neutrons and the ^{9}Be nucleus. Clearly the phase-space calculation oversimplifies the neutron production mechanism in beryllium by failing to account for the maxima in the cross section that correspond to transitions to states in ^{9}Be.

During the next year we plan to measure the secondary neutron emission cross sections for 6-, 10-, and 14-MeV incident neutrons on ^{9}Be. For these measurements we will use the ^{3}H(p,n) reaction. A recent study at LASL[7] has shown that with the proper choice of beam stop and entrance materials neutron background in the continuum region from proton reactions in these materials can be several orders of magnitude less than from triton reactions in similar materials. This study also showed that the breakup process is not a serious problem for neutron energies below 10 MeV. In fact, the background from this process is comparable to that from the beam stop and entrance foil materials.

NEUTRON GAMMA-RAY PRODUCTION CROSS SECTION PROGRAM

Neutron gamma-ray production cross sections at selected angles and for 14.2-MeV neutrons have been measured for a wide range of nuclei including beryllium, carbon, niobium, magnesium, aluminum, titanium, vanadium, chromium, iron, nickel, and copper.

The data were taken at the LASL Van de Graaff using a nanosecond pulsed beam of tritons and the neutron producing reaction ^{3}H(t,n). The geometry was the same as that used for the beryllium secondary neutron emission measurements at 14 MeV. The samples were elemental disks of dimensions 6-mm thick by 44-mm diam and were located in the plane perpendicular to the beam direction about 100 mm from the target.

The gamma-ray detector was a 15.2-cm-diam by 25.4-cm-long NaI (Tl) crystal with an annular anti-Compton NaI (Tl) scintillator surrounding the main crystal. The distance between the detector and the samples was about 1 m. The time-of-flight technique (with

(~ns timing resolution) was used to sort out the desired gamma rays from neutron induced and other background events in the crystal.

Response functions were measured with monoenergetic gamma ray sources from 0.28 MeV to 4.4 MeV. Due to the size of the center crystal of the detector and the anti-Compton shield, the response function could be represented by a single gaussian with a nearly flat tail extending to zero energy at a level of approximation 1/30 of the gaussian peak height. Gamma-ray attenuation in the sample required a correction to the measured response functions, which was determined experimentally by placing monoenergetic gamma ray sources behind standard absorbers (for example, iron) at the sample position and varying the thickness of the absorbers.

The neutron flux was calculated from the geometry of the system, triton beam current, deuteron gas pressure and the appropriate $^{2}H(t,n)$ cross section[7] and confirmed by direct measurements of the flux using a proton recoil telescope and the Hopkins and Breit n,p cross section.[7] The measurements agreed to 4.5% with the neutron-flux calculation.

Differential gamma ray production cross sections were measured from 0.2-MeV to 9.0 MeV gamma ray energy for the elements listed in Table I at the angles indicated by an x. Differential gamma ray cross sections for prominent gamma rays produced in the neutron reaction were measured for the elements listed in Table II. Beryllium is a special case because all of its known excited states are particle unstable and the $^{9}Be(n,n'\gamma)$ reaction is improbable. The only gamma ray observed in the beryllium measurement was that for the 480-keV first excited state in ^{7}Li that is formed by the $^{9}Be(n,t)^{7}Li^{*}$ reaction.

TABLE I

List of differential gamma ray production cross sections that have been measured at LASL for neutrons of 14.2 MeV. The x indicates the measurement angle.

ELEMENT	ANGLE			
	90°	110°	120°	130°
Magnesium	x	x		x
Aluminum	x	x		x
Titanium	x	x		x
Vanadium	x	x		x
Chromium	x	x		x
Iron	x	x		x
Nickel			x	
Copper		x		
Niobium	x	x		x

TABLE II

List of differential gamma ray cross sections for prominent gamma rays that have been measured at LANL for neutrons of 14.2 MeV. The x indicates the measurement angle.

ELEMENT	GAMMA RAY ENERGY (MeV)	ANGLE 45°	67°	90°	110°	120°	125°	130°
Beryllium	0.48			x				
Carbon	4.44	x	x	x	x			x
Magnesium	1.37			x	x			x
Aluminum	0.844-1.01			x	x		x	
	1.7-1.8			x	x		x	x
	2.2			x	x		x	x
	3.0			x	x		x	x
Chromium	1.434-1.44			x	x	x		x
Iron	0.85			x	x		x	x
	1.24			x	x		x	x

An example of the type of data available is given in Table III for Iron. The data are tabulated in 0.1 MeV energy bins from 0.2 MeV to 4.0 MeV and in 0.5 MeV bins from 4.0 MeV to 9.0 MeV. The cross sections are averaged over these energy bins. The uncertainty on each datum point represents a quadrature of the statistical uncertainty and the systematic uncertainty. The various sources of systematic errors and the uncertainties used in calculating the total uncertainty are listed in Table IV. The gamma ray production cross sections on iron at 90° (o) and at 120° (x) are plotted in Fig. 4. The solid curve is a calculation of the gamma ray production cross section based upon the ENDF/B IV cross sections assuming that the gamma rays are emitted isotropically.

There are no plans to measure additional gamma ray production cross sections at 14 MeV.

TABLE III

Iron Gamma Ray Production Cross Sections as a Function of Gamma Ray Energy

Energy Interval (MeV)		90° σ ± Δσ (mb/sr)		Energy Interval (MeV)		90° σ ± Δσ (mb/sr)	
0.2	0.3	10.4	4.5	3.0	3.1	2.4	.3
0.3	0.4	11.7	4.7	3.1	3.2	2.0	.2
0.4	0.5	10.2	2.7	3.2	3.3	2.3	.2
0.5	0.6	6.3	.7	3.3	3.4	1.9	.2
0.6	0.7	4.3	.5	3.4	3.5	2.0	.2
0.7	0.8	15.3	1.5	3.5	3.6	2.2	.3
0.8	0.9	38.6	3.7	3.6	3.7	2.0	.2
0.9	1.0	14.9	1.5	3.7	3.8	1.7	.2
1.0	1.1	7.4	.7	3.8	3.9	1.6	.2
1.1	1.2	9.8	1.0	3.9	4.0	1.14	.15
1.2	1.3	19.8	2.0	4.0	4.5	1.28	.17
1.3	1.4	13.3	1.3	4.5	5.0	1.07	.15
1.4	1.5	5.8	.6	5.0	5.5	.92	.14
1.5	1.6	3.4	.4	5.5	6.0	.95	.15
1.6	1.7	3.9	.4	6.0	6.5	1.03	.17
1.7	1.8	5.0	.5	6.5	7.0	.90	.15
1.8	1.9	4.9	.5	7.0	7.5	.61	.12
1.9	2.0	3.9	.4	7.5	8.0	.63	.12
2.0	2.1	3.2	.3	8.0	8.5	.40	.09
2.1	2.2	3.2	.3	8.5	9.0		
2.2	2.3	2.8	.3				
2.3	2.4	2.8	.3				
2.4	2.5	2.7	.3				
2.5	2.6	3.4	.4				
2.6	2.7	3.5	.4				
2.7	2.8	2.6	.3				
2.8	2.9	2.1	.2				
2.9	3.0	2.2	.2				

TABLE IV

Systematic Uncertainties in the Differential
Gamma Ray Production Cross Sections.

Type	Uncertainty (Percent)	
Gamma ray efficiency	± 3	0.2 to 3 MeV
	±12	at 9 MeV
Unfolding	± 5	
Neutron multiple scattering	± 2.5	
Flux	± 7	
Sample position	± 2	
TOTAL	± 9.7	0.2 to 3 MeV
	±15.1	at 9 MeV

LIGHT ELEMENT TOTAL CROSS SECTION PROGRAM

High resolution and high accuracy total cross sections of ^{9}Be, ^{10,11}B and ^{12,13}C have been measured from 1.0 to 14 MeV. The LASL tandem accelerator was used to produce a "white" source of neutrons by stopping a pulsed beam of 15 MeV deuterons in a thick beryllium target. The deuteron pulses occurred every 1.2 μs and produced an average current on target of between 100 and 400 nanps.

Two NE 110 plastic scintillator detectors were used for the measurements. Both pieces of plastic were machined to fit the curvature of the photocathode surface of an RCA 8575 photomultiplier tube. The carbon and beryllium data were taken with a scintillator 15.5 cm in diameter with a center thickness of 2.2 cm. The boron data were taken with a scintillator 10 cm in diameter with a center thickness of 1.2 cm. The electronics of this detector was designed to take advantage of the less than 1 ns deuteron pulse width available from the accelerator. However, the deuteron beam could not be bunched to less than about 1.8 ns for these measurements and therefore the boron data have poorer resolution than the other data.

The open beam counting rate for the thicker detector at 400 nanps was approximately 20000 per second. The multiple pulse probability at this rate is less than 4%.

The overall resolution of the detector system as measured by the width of the gamma ray peak that occurred at zero time and by the widths of narrow resonances in ^{16}O and ^{18}O was 1.8 ± 0.1 ns (2.0 ± 0.1 ns) for the thicker (thinner) detector. This timing uncertainty is equal to an energy uncertainty in keV of $1.3\,(1.4)\,E^{3/2}$ with E measured in MeV for our flight path of 48.9 m.

Since the resolution of the system was less than 2 ns the data were recorded in channel widths of 0.5 ns.

The accuracy of the neutron energy scale is given by $\pm$ 0.070 E $\sqrt{1.79E+0.75}$ with E measured in MeV. This means, for example, that the energy of the narrow resonance in ^{12}C at 2.077 MeV has an uncertainty of less than $\pm$ 260 eV.

The data were corrected for backgrounds that varied from 3% of the open beam spectrum at 1.5 MeV, 0.5% at 4 MeV, to 1% at 14 MeV.

The systematic uncertainty in the transmission is estimated to be $\pm$ 1.7%. This uncertainty is determined from a quadruture of the following estimates of the various sources of errors: sample thickness $\pm$ 0.7%, background $\pm$ 1%, normalization $\pm$ 1%, and dead-time $\pm$ 0.5%. Since the fractional uncertainty in the cross section is equal to the fractional uncertainty in the transmission multiplied by $1/n\sigma$, the systematic uncertainty in the cross section is somewhat larger because, for our samples, $n\sigma$ was generally less than one.

As an example of the data obtained with the Be(d,n) reaction we present the total cross section of ^{11}B from 1.0 to 14 MeV in Figs. 4-6. The cross section has been corrected for the ^{10}B isotopic impurity present in the sample. The data from 1.0 to 1.5 MeV in Fig. 4 and 4.0 to 14 MeV in Fig. 6 have been averaged over five channels. Note the suppresssed zero origin on the vertical scale in Fig. 6. This was done to reveal the fine structure present in the data that could only be seen with high statistical accuracy data. The statistical uncertainty in the cross section varies from a few percent at 1.5 MeV to about 0.5 percent at 9 MeV to about 1 percent at 14 MeV. These data required about six hours of machine time.

There are no plans to continue the light element total cross section program at the Van de Graaff because a time-of-flight facility is being built at the Los Alamos Meson Facility that will have a potential for much higher energy resolution than the Van de Graaff facility.

(n,2n) AND (n,3n) CROSS SECTION PROGRAM

(n,2n) and (n,3n) cross sections for $^{6,7}Li$, Be, Ti, V, Cr, Mn, Fe, Co, Ni, Cu, and Nb have been measured from 14.7 to 24 MeV using the LASL Van de Graaff and a large gadolinium-loaded liquid scintillator tank to detect the neutrons.

The neutrons were produced by the $^{3}H(d,n)$ reaction. The deuteron beam was chopped into pulses 1-μs wide at a repetition rate of 25 kHz. The current was adjusted to keep the average number of (n,xn) reactions per burst much less than one, thus minimizing the correction for multiple events in any single burst.

The detector was a 75-cm-diam tank filled with 200 ℓ of NE 323 that was loaded with 0.5% by weight gadolinium. The tank was located 2.6 m from the source in a well-shielded room. It was viewed by eight photomultiplier tubes (type RCA 4522) divided into two banks of four tubes each. A coincidence was required between

the two banks to reduce events from tube noise. Since the capture half life of neutrons in the tank was much longer than the response time of the electronics, individual neutron events could be resolved. A fast scaler gated on for 21 μs after the beam pulse counted the number of tank pulses per beam pulse and a computer sorted them out according to the number detected.

The neutron flux was measured by a 5.1-cm-long by 5.1-cm-diam cylinder of NE-213 liquid scintillator mounted on an RCA-8575 photomultiplier and located 4.7 m behind the sample. The pulse height was recorded during each run and the neutron flux was found by relating the height and end point of the plateau from the recoil protons to the absolute differential efficiency measurements of Verbinski.[10]

The neutron efficiency of the tank was measured by a ^{252}Cf source on a solid state detector placed at the center of the tank. Corrections were applied to the measured efficiency for differences between the Cf fission neutron spectrum shape and the (n,2n) and (n,3n) spectra shapes. The (n,xn) shapes were calculated using a statistical model that included preequilibrium neutron emission.[4]

The data were corrected for backgrounds and for losses of tank pulses that occurred during the deadtime associated with each pulse. Since the probability for two single events occurring during a gate was not negligible compared with the number of true (n,2n) events, a multiple-event correction was applied to each sample run. A similar correction to the (n,3n) data was negligible. The final correction, which varied with the incident neutron energy and with the multiplicity of the (n,xn) reaction, removed the effects of detector efficiency to give the multiplicities of neutrons emitted from the target.

Preliminary results on the (n,2n) cross sections of Be, Ti, V, Cr, Mn, Fe, Ni, and Cu are listed in Table V. The measured (n,3n) cross sections are essentially zero up to 21 MeV. The uncertainty given for each cross section represents a quadrature of the statistical uncertainty and a systematic uncertainty that varied from 3 to 6%. The ^{6,7}Li(n,2n) cross sections are both about 100 mb and roughly constant between 14.7 and 21 MeV except that ^{7}Li drops off to about 80 mb at 14.7 and 16 MeV. When the final results become available, the 21-MeV cross sections in the table will probably go up by about 5 to 10%, the 18-MeV ones should remain unchanged, and the 14.7-MeV ones may go down 3 to 5%. The Be data have already been roughly corrected.

The data on Nb and Co are tabulated in ref. 4. The (n,2n) and (n,3n) cross sections for Nb are plotted in Fig. 7. The data of Frehaut et al.[11] are represented by the closed circles and our data by the open circles (n,2n) and open triangles (n,3n). The solid line represents a calculation of the (n,xn) cross sections using a statistical model that includes preequilibrium neutron emission.

Since we have measured (n,xn) cross sections for most available materials, no additional measurements are planned for the next year.

TABLE V

Preliminary (n,2n) Cross Sections

E (MeV)	Be	Ti	V	Cr	Mn	Fe
6.0	0.545±0.042					
14.7	0.472±0.026	0.51±0.03	.66±.04	.47±.03	.85±.05	.50±.04
16	0.475±0.041	0.58±0.04	.70±.06	.53±.04	.89±.06	.56±.05
17	0.431±0.038	0.63±0.03	.77±.05	.65±.03	.85±.04	.59±.03
18	0.422±0.035	0.67±0.04	.82±.06	.68±.04	.85±.04	.68±.04
19	0.365±0.033	0.65±0.03	.79±.05	.65±.03	.81±.04	.64±.04
20	0.389±0.033	0.65±0.03	.74±.04	.64±.03	.80±.04	.64±.04
21	0.378±0.035	0.65±0.03	.78±.04	.63±.03	.75±.04	.60±.04

E (MeV)	Ni	Cu
14.7	.20±.02	.74±.04
16	.23±.02	.87±.05
17	.26±.03	.79±.04
18	.26±.02	.86±.05
19	.25±.02	.79±.04
20	.27±.02	.82±.04
21	.27±.02	.76±.04

REFERENCES

1. D. M. Drake, G. F. Auchampaugh, E. D. Arthur, C. E. Ragan, and P. G. Young, Los Alamos Scientific Laboratory Report, LA-6257, 1976. Accepted for publication in Nucl. Sci. and Eng.
2. D. M. Drake, E. D. Arthur, and M. G. Silbert, accepted for publication in Nucl. Sci. and Eng., 1977.
3. G. F. Auchampaugh, C. E. Ragan, S. Plattard, and N. W. Hill, Los Alamos Scientific Laboratory Report, LA-6761, 1977.
4. L. R. Veeser, E. D. Arthur, and P. G. Young, to be published, 1977.
5. T. K. Alexander and F. S. Goulding, Nucl. Instrum. Methods 13, 244 (1961).
6. E. D. Cashwell, J. R. Neegaard, W. M. Taylor, and G. D. Turner, Los Alamos Scientific Laboratory Report, LA-4751, 1972.

7. J. C. Hopkins and G. Breit, Nucl. Data Tables A9, 137 (1971).
8. M. Drosg, G. F. Auchampaugh, and F. Gurule, Nucl. Instrum. Method 140, 515 (1977).
9. J. E. Brolley, Jr., and J. L. Fowler, Fast Neutron Physics, Part I, p. 94, Interscience Publishers Inc., New York, 1960.
10. V. V. Verbinski, W. R. Burrus, T. A. Love, W. Zobel, and N. W. Hill, Nucl. Instrum. Method 65, 8 (1968).
11. J. Frèhaut and G. Mosinski, Nuclear Cross Sections and Technology, NBS Spec. Publ. 425, Vol. II, 1975.

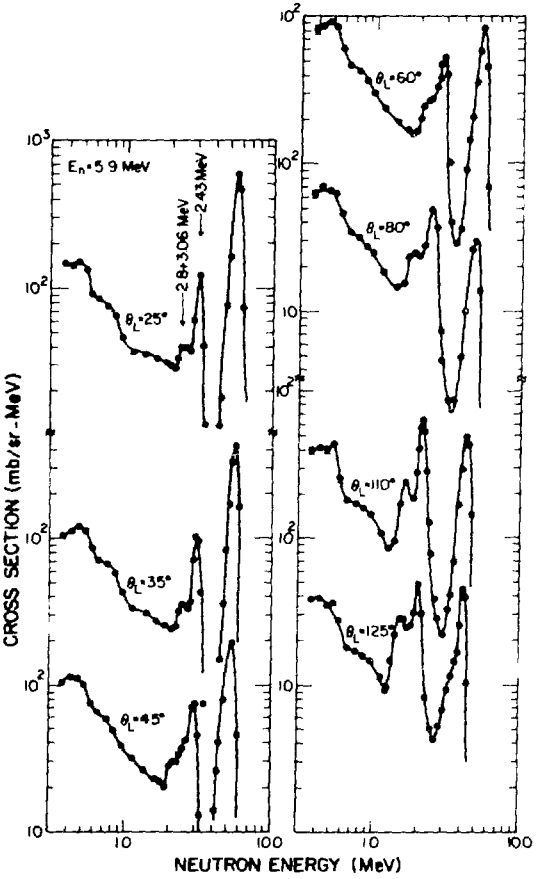

Fig. 1. Double-differential cross sections for 5.9-MeV incident neutrons on beryllium. The cross sections are given in the laboratory system. The arrows indicate the positions of the low-lying states in ^{9}Be, which may contribute to the observed maxima in the cross sections at the indicated energies. The low-energy shoulder on the elastic peak θ_L = 125° is due to poor bunching of the charged particle beam.

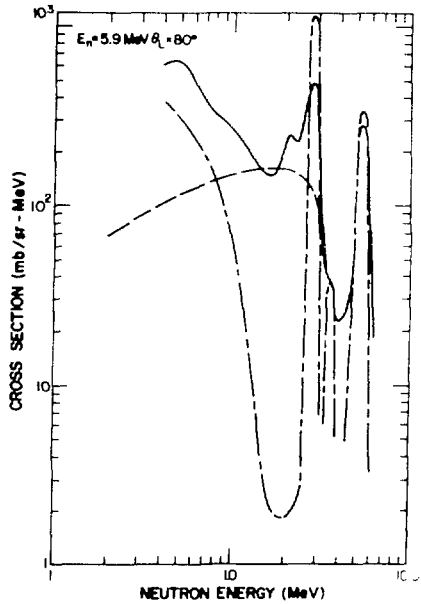

Fig. 2. Comparison of beryllium double-differential cross sections for a laboratory angle of 80°, and an incident neutron energy of 5.9 MeV. Our data are plotted as a solid line, the ENDF/B data as a short and long dash line, and the unnormalized three-body phase-space calculation as a dashed line.

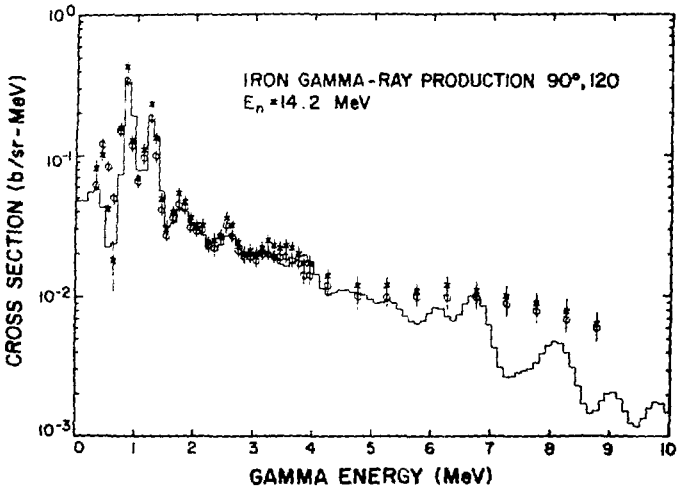

Fig. 3. Spectrum of gamma rays observed from iron, circles and crosses representing angles of 90° and 120° respectively, compared to the ENDF/B-IV file (histogram).

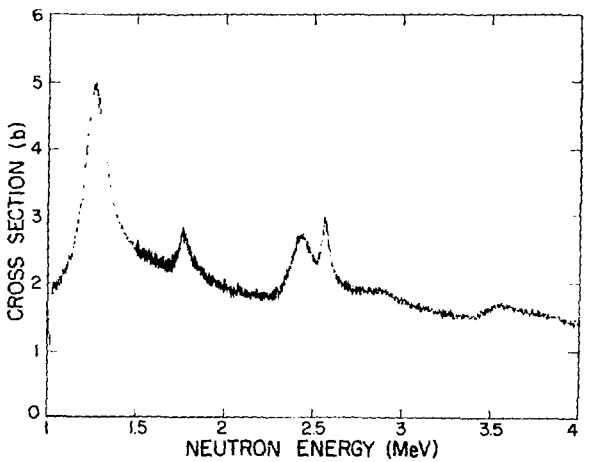

Fig. 4. Total cross section of ^{11}B from 1.0 MeV to 4 MeV. The data below 1.5 MeV have been averaged over five channels.

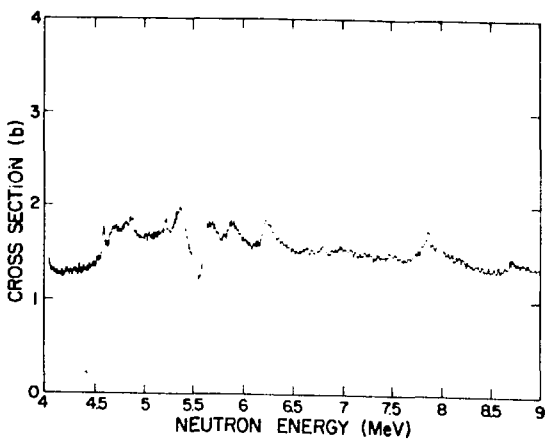

Fig. 5. Total cross section of ^{11}B from 4.0 MeV to 9.0 MeV.

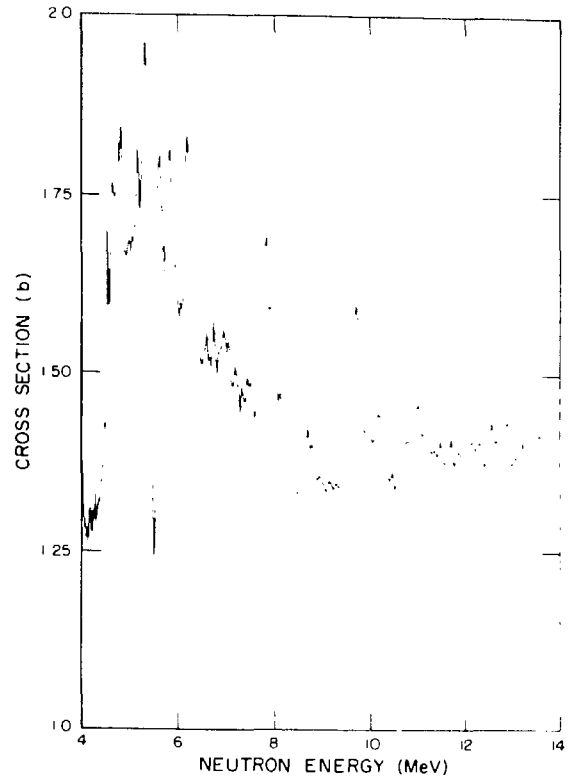

Fig. 6. Total cross section of ^{11}B from 4 MeV to 13.9 MeV. Note the suppressed zero origin on the vertical scale. The data have been averaged over five channels.

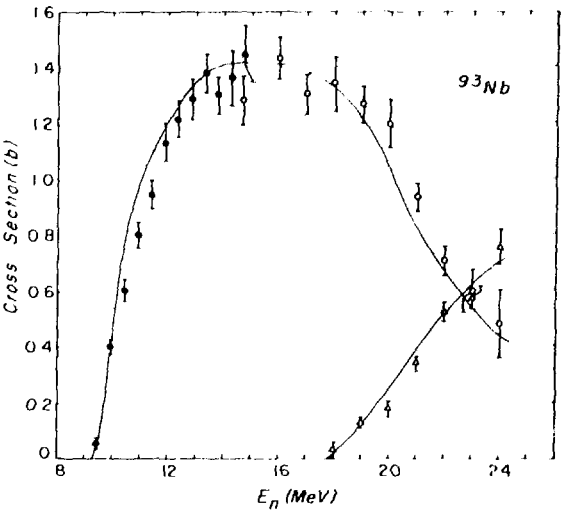

Fig. 7. Cross sections for ^{93}Nb (n,xn). The closed circles are from Ref. 11, the open circles are our (n,2n) results, the open triangles are our (n,3n) results, and the solid line is a statistical model calculation of the (n,xn) cross sections.

A Facility for Neutron-Induced Charged Particle Reactions in the Energy Range E_n 20-60 MeV*

J.L. Romero, T.S. Subramanian, F.P. Brady,
N.S.P. King# and J.F. Harrison
University of California, Davis, CA 95616

Variable energy, nearly monoenergetic, neutron beams are produced via proton beams from the sector focusing isochronous cyclotron at Crocker Nuclear Laboratory. The simultaneous measurement of the continuum spectra of charge 1 and 2 particles is accomplished by using three-element telescopes incorporating fast timing in each detector. Energy and time parameters from the detectors and fast logic are interfaced to a PDP 15/40 computer via CAMAC. On-line and off-line data processing is performed on each type of particle. As illustration, results are presented for the 4-30 MeV alpha spectrum produced by 40 MeV neutrons on carbon.

I. INTRODUCTION

The unpolarized neutron facility at the Crocker Nuclear Laboratory was originally designed for few nucleon experiments.[1] Several years ago modifications were made, including the incorporation of a scattering chamber, to allow neutron induced charged particle reactions involving hydrogen and high energy helium nuclei to be measured using a ΔE-E detection system.[2] The most recent development has been the installation of a system which allows the measurement down to a few MeV of the complete range of hydrogen and helium particles which are produced by neutron beams in the range ~20-60 MeV. Of particular interest to us is to measure (n,xp), (n,xd), (n,xt) and (n,xα) reactions on tissue-resident elements in human body in order to allow kerma calculations to better predict dosimetric quantities for neutron cancer therapy. However, the data obtained have proved and will be of interest in understanding nuclear reaction mechanisms and studies of giant resonances.[3] In addition, applications such as calculations of neutron detector efficiencies require this type of data.[4]

The range of energies and types of particles involved imply difficulties such as: 1) the detection of low energy (~3 MeV) helium particles which requires very thin targets, typically about

---

*Supported in part by Grant #PHS CA 16261 from the National Cancer Institute, DHEW and by PHY 71-03400 from the National Science Foundation.

#Present address: P-11, Los Alamos Scientific Laboratory, Los Alamos, New Mexico.

2 mg/cm , with a decrease in counting rate; 2) the achievement of the simultaneous measurement of several particles with a wide range of energies (continuum) which requires the use of a combination of detectors, with considerable complexity in the electronics; 3) the fact that our neutron beam contains a tail of low energy neutrons makes it necessary to derive timing signals (of good resolution) from all the detectors. The ability to achieve this depends strongly on the type of detector used; 4) because of the low counting rate involved, the system must consist of several telescopes, set at different (simultaneous) angles, and a sophisticated data capture system and computer interface is necessary for optimum utilization of each telescope.

The neutron beam is discussed briefly in the next section, followed by a description of the three element telescope detecting system designed to handle above mentioned problems. A telescope system with some of the characteristics of ours has been discussed by Bertrand et al.[5] The final section presents some results.

2. NEUTRON BEAM

Fig. 1 shows the unpolarized neutron beam facility.[4] Protons in 1 ns beam bunches from the 76" isochronous cyclotron at the Crocker Nuclear Laboratory of variable energies between about 10 to 40 MeV hit a ^{7}Li target. Neutrons from the reaction ^{7}Li(p,n)^{7}Be (Q = 1.64 MeV), 60% of which are contained in the high energy neutron peak, are collimated at 0° by a 1.75 m steel collimator to a beam size of 12 x 24 mm. There is a provision for inserts to give other rectangular sizes. For a 10μA, 40 MeV proton beam, the high energy neutron peak intensity is about 5 x 10^{5} neutrons per cm^{2} sec per MeV of ^{7}Li target thickness. A neutron time of flight technique allows rapid measurement of the neutron energy to within 100 keV. Further details on the neutron producing aspect of the facility are given in refs. 1 and 2.

The collimated beam passes into a recently built scattering chamber which houses up to 4 sets of telescope detectors on each of the two independently rotating arms. The distance from the ^{7}Li target to the target position in the scattering chamber is 4 meters, and the neutron bursts of peak energy with 1 ns FWHM arrive approximately every 50 ns at the target on the chamber.

3. CHARGED PARTICLE DETECTOR SYSTEM

The problem of measuring the continuum spectra of different charged particles down to a few MeV which are produced by a neutron beam that contains a low energy neutron tail has been approached by us by the use of a triple detector telescope. Each telescope consists of two Δ1 detectors, a 50μm, 300 mm surface barrier (detector A) placed 20 cm from the target, followed by a 300 or 400μm, 450 mm surface barrier (detector B) and a

detector capable of stopping 60 MeV protons. The latter is either a CsI scintillator coupled to an EMI 9813 B photomultiplier or a high purity germanium detector.[illegible]

For those events that stop in detectors 1 or 2, particle identification is achieved by a conventional ΔE - E or E vs E display (see Fig. 6a). Charged particles produced by the low energy neutrons in the target are largely eliminated by time of flight (TOF) with respect to a beam pick off (BPO) placed upstream from the Li target (Fig. 1). Corrections can be made for the small number of events due to low energy (< 10 MeV) neutrons from a previous beam burst which arrive at the same time as the beam pulse. Both particles that stop in detectors 3 are identified by TOF vs. a display (see Fig. 6b). Table 1 illustrates, for the detector thicknesses indicated above, the energies and mass of detection for different particles.

TABLE 1

[illegible]

Detector Particle Stopping	Particle Identification Equation	Energy Thresholds for Each Particle (MeV)				
		p	d	t	^{3}He	α
1	TOF vs. ΔE	TOF vs. ΔE				[illegible]
2	ΔE vs. E	TOF vs. E	[illegible]	[illegible]	[illegible]	[illegible]
3	E vs. 3	TOF vs. 3	[illegible]	[illegible]	[illegible]	[illegible]

[illegible]

In order to get the best timing for each pair of detectors and to have also the minimum spread in the total energy position, a double time shift technique for each detector is used. This is done by splitting the fast signal from the preamplifier and integrating one of these to produce a better signal for timing, thus affecting the setting of a best time shift [illegible] from the timing signal.

Fig. 2 shows schematic diagrams of the [illegible] at the different events. For detector 1, [illegible] signals, [illegible] the first (timing) and the later [illegible] respectively. A particle stopping in detector [illegible] in part 1 (condition A) being set, [illegible] coincidence (A*E'1). Time information, [illegible] is denoted by t_1 (i.e., [illegible]). These pulses are indicated by underlined symbols [illegible].

Except for particles stopping in detector 3, all [illegible] associated to them a TOF signal derived from the [illegible] pair of detectors, so allowing to optimize the [illegible] energy and type of particle. [illegible] for are shown as indicated in Fig. 7, most of the [illegible]

electronics for digitizing pulse height and time-of-flight parameters being shared. The bottom of Fig. 2 indicates the CAMAC interface to an on line PDP15/40 computer for transferring and recording on magnetic tape event by event data, each event being characterized by a route and condition signal and by energies from detectors A, B or E and corresponding TOF parameters.

In addition to the event by event storage in magnetic tape of all data, the CSL data acquisition system allows a continuous, updated, display of the data during the run in a variety of formats, including prerestriction cuts in two parameter spectra,[7] selecting particle type and/or events due solely to the beam peak.

Fast timing for the ~600 pf capacitance detectors A is achieved through the use of ORTEC's 140 preamplifiers, a modified version of the voltage sensitive amplifier designed by Sherman et al.[7] Ortec 142B preamplifiers are used for the ~400 pf capacitance detectors B. Conventional constant fraction timing is used for all detectors and the beam pick off. The overall time resolution due to the time structure of the proton beam burst and the detector time resolution varies from 1.5 to 2.5 ns depending on the detector capacity and the energy deposited.

4. EXAMPLE OF RESULTS

Fig. 3 displays data corresponding to 49 MeV neutrons (ΔE_n = 1 MeV) incident on a 1.3 mg/cm^2 CH target, the angle being 20°. In what follows, we will describe a data analysis done on the alpha spectrum at all energies. Of course, simultaneously protons, deuterons, and tritons were detected and could be analyzed as described in ref. 2.

Fig. 3a displays pulse height in detector A vs pulse height in detector B for those events stopping in the latter (Condition B). Fig. 3b displays TOF obtained from detector B vs pulse height in B, for events stopping in B and subject to the particle cut indicated in Fig. 3a ("alpha particles"). Events that fall below the lower curve in Fig. 3b are alphas produced by the neutron tail. Events in the lower left corner of Fig. 3a are protons, deuterons and tritons of up to ~40 MeV (see Table 1). They are easily separated by plotting Fig. 3a with a larger display gain. Fig. 3c displays TOF vs pulse height for particles stopped in detector A. The vertical line of events around 3 MeV corresponds to up to 3 MeV n p scattering protons produced by the neutron tail.

Fig. 4 was obtained from the corresponding projections of Fig. 3c (E > 8 MeV) and Figs. 3a and 3b (E > 8 MeV). For E > 8 MeV, the alpha spectrum could contain also helium-3 particles, as indicated in Table 1. This contribution is however probably small, as it is for E > 8 MeV (see Fig. 3a). Absolute normalization to the n p cross section was achieved automatically in this case, since a CH target was used. Binstock's n p parametrization was used.[8] Otherwise, a separate run with a hydrogen target and normalization through the neutron monitor or Faraday

cup (Fig. 1) is performed. As shown in Fig. 3 (i.e. the [illegible] cup, [illegible] spectrum is measured by Bertrand et al.[illegible] One does not expect complete agreement, *but it is* reasonable that allowing for [illegible] differences, etc., the spectra are quite similar.

We wish to acknowledge P. Fahim [illegible] and [illegible] Goodart for building the new scattering chamber, [illegible] Cline for assistance with the electronics and [illegible] Ellmann for help at the computer end.

Journal References:

1. [illegible] Emersam and [illegible] Brady, Nucl. Instr. and Meth. 39, [illegible] (1966).
2. [illegible] Brady, [illegible] King, [illegible] McLaughlin, [illegible] Harrison and [illegible] Bonner, Conf. on Nucl. Cross-Sect. and Tech., [illegible] D.C., Mar. 3-7, 1975, NBS Spec. Publ. 425, Vol. 1.
3. [illegible] Brady, [illegible] King, [illegible] McLaughlin, and [illegible] Stachler, Phys. Rev. Lett. 36, [illegible] (1976).
4. [illegible] McLaughlin, [illegible] King, [illegible] Brady, and [illegible] Gilmore, Nucl. Instr. and Meth. 129, 251 (1975).
5. [illegible] Bertrand, [illegible] Burrus, [illegible] Hill, [illegible] Love and [illegible] Poelle, Nucl. Instr. and Meth. 101, 475 (1972).
6. [illegible] King and [illegible] Subramanian, Bull. Am. Phys. Soc., [illegible], 656 (1976).
7. [illegible] Jackson, [illegible] Fuchler and [illegible] Metz, Trans. in Syst. Science, 15, 300 (1963).
8. [illegible] Binstock, Phys. Rev. C10, [illegible] (1974).
9. [illegible] Bertrand and [illegible] Poelle, ORNL [illegible], 1973 (unpublished).

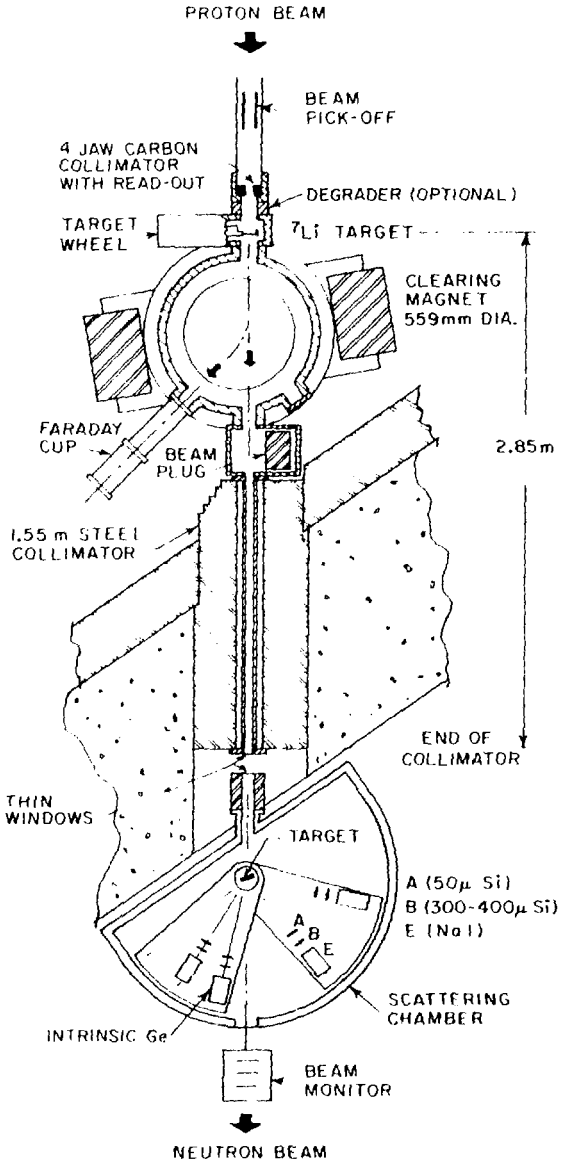

Fig. 1 Schematic of the neutron beam line and scattering chamber. The incident beam of protons is focused onto a ^{7}Li target. The protons are then deflected into a Faraday cup and a neutron beam is formed by a 1.55 meter collimator. Neutron-induced charged particle reactions are studied in the scattering chamber.

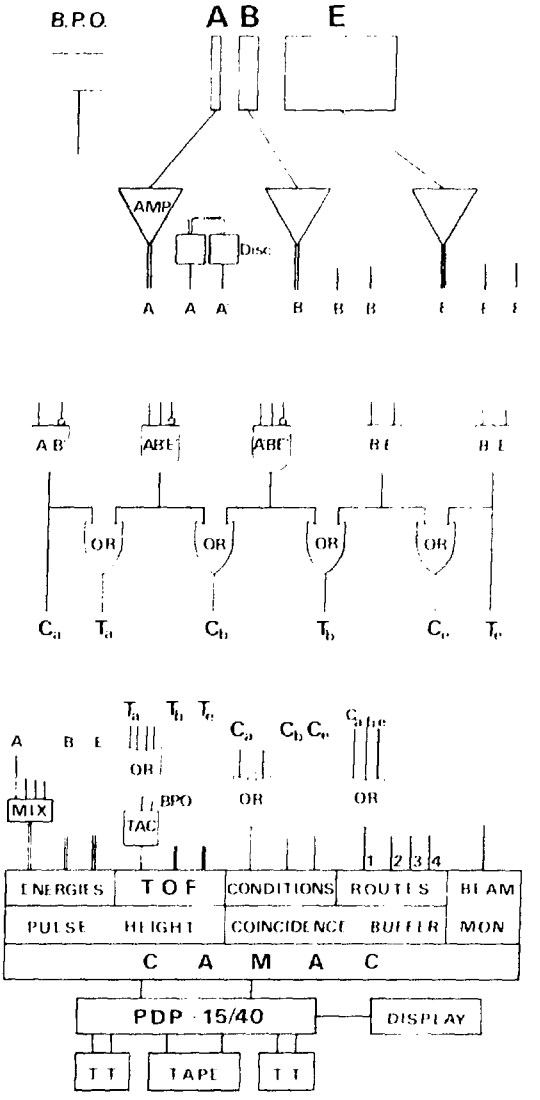

Fig. 2 Logic diagram and computer interface for the detection system.

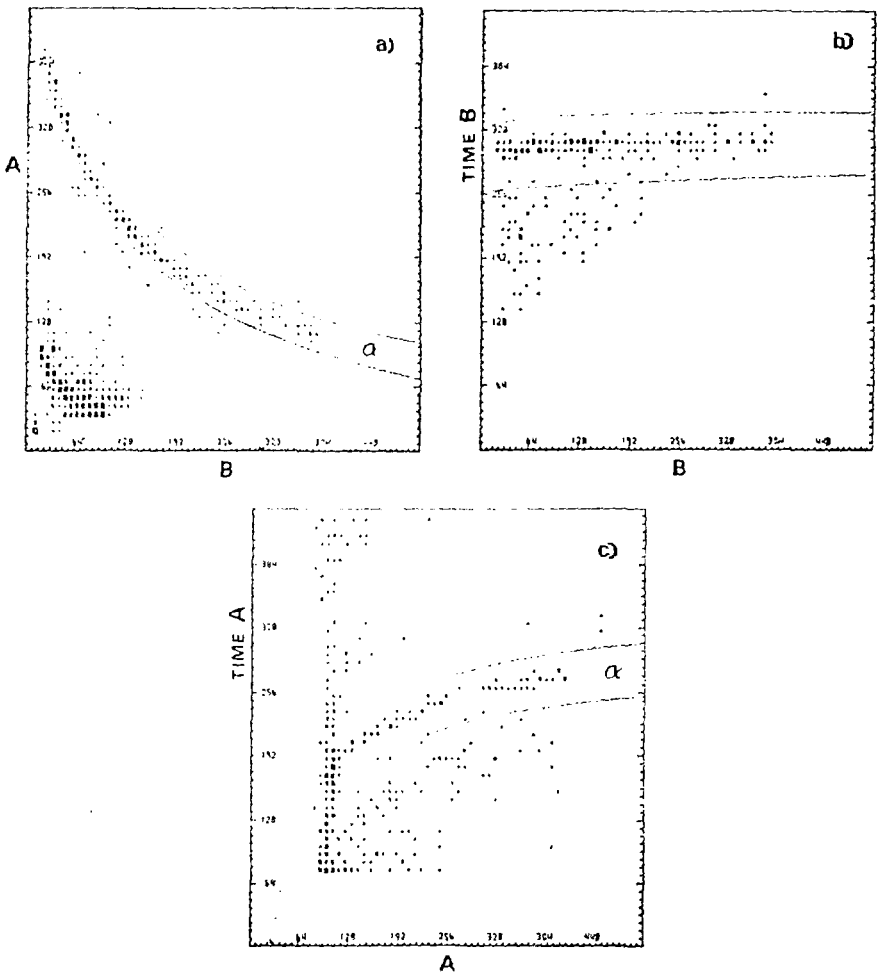

Fig. 3 Spectra for 39 MeV neutrons on a 1.8 mg/cm² CH target at 20° lab. a) Energy in detector A vs energy in detector B, for particles stopping in the latter. Indicated cuts correspond to alpha particles. b) TOF from detector B vs energy in B, for events subject to the particle cut in a). c) TOF from A vs energy in A for particles stopping in A. Indicated cut correspond to helium particles. Scales are arbitrary.

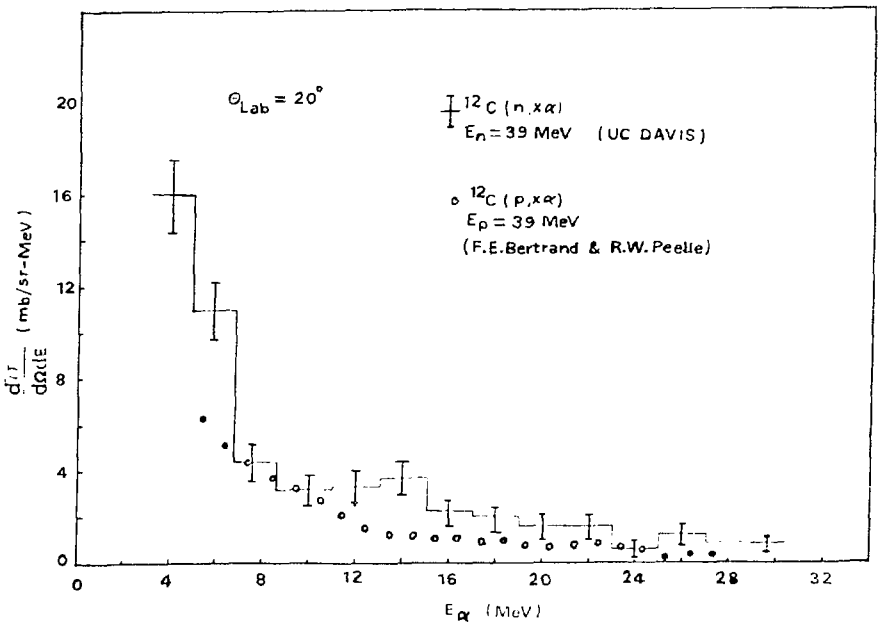

Fig. 4 Energy spectrum for alpha particles produced by 39 MeV neutrons on C at 20° lab, as obtained from Fig. 3. Also shown is the corresponding data for a proton beam.

Neutron Scattering Measurements at Ohio University in the Energy Range 7 - 26 MeV *

J. Rapaport, R.W. Finlay, D.E. Bainum, J.D. Carlson,
and T.S. Cheema[++]
Ohio University, Athens, Ohio 45701

INTRODUCTION

The understanding and the evaluation of the nucleon optical model potential (OMP) are of extreme interest since it is assumed that the OMP describes the interaction between an incident nucleon and a target nucleus. Such an interaction, we know, is an exceedingly complicated process. Thus it is quite remarkable that high quality fits are obtained with nucleon OMP which vary smoothly with incident energy and target isospin. This indicates that these OMP are physically meaningful and contain, from a physical point of view, relevant information.

The main bulk of the studies about the OMP has been obtained empirically and mainly through the analysis of proton data, elastic scattering and polarization measurements. Empirical global potentials have been reported by Perey[1] and by Becchetti and Greenlees[2] among others. The input of neutron data to the above analyses has been very limited because of the relatively low accuracy of the up-to-then available neutron elastic scattering data. This work tries to remedy this situation by providing accurate neutron elastic and inelastic scattering data in the energy region between 7 and 26 MeV, for a large number of nuclei including several enriched isotope samples.

The understanding of the OMP from a theoretical point of view and its relation to the phenomenologically determined OMP has been the subject of recent studies. Manweiler[3] has reported on a successful unified treatment of unbound and bound states relating the unbound state effective interaction to the standard OMP, using Hartree-Fock theory. The real and imaginary part of the equivalent local potentials are calculated and their energy dependence is given. Jeukenne, Lejeune and Mahaux[4] have done microscopic calculations of the OMP using a Brueckner-Hartree-Fock approach with realistic nucleon-nucleon interactions, and calculated several components of the OMP.

In this talk we will present a brief description of the experimental facilities at Ohio University used to obtain the data, and our understanding of the phenomenological OMP.

---

*Supported in part by NSF.
†Now at Lord Corporation, Erie, Pennsylvania.
++Now at Panjab University, Chandigarh, India.

EXPERIMENTAL FACILITIES AND RESULTS

During the last 3 years we have been involved at Ohio University in a high energy neutron scattering program.

The Ohio University 11 MeV Tandem is a unique T-shape high current accelerator. Proton beam currents up to 100 μamp DC on target may be achieved. A floor layout is shown in figure 1. A diode source produces by direct extraction either protons or deuterons up to 80 keV of energy, which are injected through a 30° inflection magnet to the low energy extension of the beam transport system. In this section the beam may be chopped and bunched at a repetition rate of 5 MHz or lower. After acceleration, the beam may again be chopped, if desired, to clip the tails of the beam pulse to a total width of less than 2 nsec. For neutron work the pulsed beam is focused on a gas cell in the center of a large room that allows a flight path up to 7 [m] between 0° and 160° or to another location where a flight path up to 14 [m] may be achieved in the forward angles.

The accelerator provides pulsed protons and deuterons that are used in the production of monoenergetic neutrons. Pulses of about 700 psec FWHM with a 5 MHz rep rate may be obtained, with currents up to 5 μamp on target. The different reactions used to produce neutrons and their energy are shown in figure 2.

The 0° yield of the monoenergetic neutrons per sr per μamp per sec per 10 keV energy loss in the gas cell is presented versus incident energy. A minimum of 2 MeV and a maximum of 11 MeV have been assumed for the incident particles.

The gas cell system has been described elsewhere.[5]

A summary of the experimental setup is presented in table 1.

Elastic scattering data has been taken for over 100 cases with monoenergetic neutrons at 7, 9, 11, 20, and 26 MeV. Data has been obtained between 15° and 155° in steps of $\Delta\theta = 5°$ for up to 29 points per angular distribution. The average data-taking time was about 1.5 hr for each experimental point which represents well over 4000 hr of data acquisition.

A list of the scattering samples and the energies at which both elastic and inelastic data were taken is shown in table 2. The atomic mass is included in those cases where either enriched samples (about 1/3 - 1/2 mole) were used or the element is naturally monoisotopic. A large number of cases were done at 11 MeV while the Mo and Pb isotopes were studied at several energies.

Data were accumulated for enough time so as to have yield statistics better than 3%. In the back angles, however, this restriction had to be lifted, but yield statistics less than 10% were achieved. In those cases where inelastic scattering was measured, the counting statistics for the elastic scattering were generally much better than 3%. The sample out background which was obtained in each case was subtracted after monitor normalization from the sample in spectra. The obtained elastic yields were corrected for the following factors: dead time, source anisotropy, relative detector efficiency, finite geometry, neutron flux attenuation,

Table 1

Experimental Setup

Neutron Source Reaction		$T(p,n)^3He$	7 MeV Neutrons
		$D(d,n)^3He$	9,11 MeV Neutrons
		$T(d,n)^4He$	20,26 MeV Neutrons
Sample	Cylindrical	Diameter	1.99 cm
		Height	1.88 cm
Source-Sample Distance		12 cm	
Detector		Liquid Scintillator	NE 224
		Size (cm)	5 x 18.5
		Very Long Detector	VLD
		Size (cm)	30 x 18.5
Photomultiplier		RCA 4522	
Detector Threshold (MeV)		1/2 Neutron Energy	
Flight Path (m)		5.5 - 10	
Beam Time Spread (FWHM)		.7 - .9 ns	
Overall Time Resolution (FWHM)		1.3 - 2.0 ns	
Energy Resolution (FWHM)		550 keV at 26 MeV	
		180 keV at 11 MeV	
Average Beam (Pulsed)		2 - 4 μamps	

Table 2

Ohio University Neutron Scattering Data

Sample	Neutron energy (MeV) 7.0	9.0	11.0	20.0	26.0	other
Mg			X			
^{27}Al			X		X	
Si			X	X In*	X In	
S			X	X In	X In	
Ca			X In	X In	X In	
^{51}V			X			
^{55}Mn			X			
Fe			X	X	X	
^{59}Co			X			
Ni			X			
^{90,92}Zr			X In			
^{93}Nb			X			
^{92,96,98,100}Mo	X	X	X In	X	X	
In			X			
^{118,120,122,124}Sn			X In			^{120}Sn: 9.4; 22.8
^{165}Ho			X			
^{181}Ta			X			
^{206,208}Pb	X	X	X In	X	X In	
Pb			X			
^{209}Bi			X			

*In = Inelastic measurements

multiple scattering, compound nucleus contributions, and contaminants. Source anisotropy and relative detector efficiencies were both measured and calculated obtaining good agreement. Finite geometry, neutron flux attenuation and multiple scattering within the sample were done using a Monte Carlo code developed by W.E. Kinney[6]. Compound nuclear contributions were evaluated using the code Helene[7] which performs a Hauser-Feshbach calculation with a Porter-Thomas width fluctuation correction. This contribution was found to be significant for neutron energies less than 11 MeV and for the light nuclei. In some cases (Mg) the correction reaches up to 15% at the back angles. Corrections for contaminants were important, especially in the Mo isotope enriched samples which are known[8] to have a few percent (in number of atoms) of oxygen. The O(n,n) cross section was measured at the forward angles to correct the data properly. The estimated overall relative uncertainty is between 5 - 10%. The uncertainty in the normalization is estimated to be less than 5%.

Absolute cross sections were obtained by measuring the scattered neutron flux and the incident 0° flux (with the sample removed) using the same detector.

In the next few figures the obtained angular distribution is presented with OMP fits obtained with individual searches. Figure 3 has the 11 MeV neutron elastic angular distribution for Mg through Mo. Relative errors are indicated by the error bars. Figure 4 has the rest of the 11 MeV data Mo through Bi. It covers, as in the previous case, the angular range between 15° - 155°. Figures 5, 6, and 7 present the neutron angular distribution between 7 and 26 MeV obtained for ^{92,96}Mo, ^{97,100}Mo and ^{208}Pb, respectively.

ANALYSIS OF THE DATA

The data were analyzed using the OMP search code Genoa[9] that allows individual as well as global fit to a set of data with prescribed constraints on the parameters.

Before we present the results of such analyses, let us discuss briefly the parameterization of the OMP.

We use the general notation

$$U(r,E) = V(r,E) + i\,W(r,E)$$

where U is the generalized OMP with a real term V(r,E) and an imaginary term W(r,E). The phenomenological OMP is usually written as a sum of the following terms:

$$-U(r,E) = V(E)f(x_R) - V_C(r) - V_{so}(\vec{\sigma}\cdot\vec{\ell})\left(\frac{\hbar}{M_\pi c}\right)^2 \frac{1}{r}\frac{d}{dr} f(x_{so})$$

$$+ i\left[W_V f(x_V) - 4W_D \frac{d}{dx_d} f(x_D)\right]$$

$V_C(r)$ represents the Coulomb potential due to a uniformly charged sphere of total charge Ze and radius R_C.

The radial dependence is generally taken to be a Woods-Saxon

$$f(x_i) = (1 + e^{x_i})^{-1} \quad \text{where } X_i = (r - r_i A^{1/3})/a_i$$

which is a shape obtained from electron scattering experiments.

The spin-orbit term is taken to be of the Thomas form.

The imaginary part usually consists of a surface term W_D and a volume term W_V.

The isospin dependence of the OMP is generally written as suggested by A. Lane[11] as

$$U(\vec{r},E) = U_o(\vec{r},E) + \frac{4}{A}\, \vec{t} \cdot \vec{T}\, U_1(\vec{r},E)$$

where $\vec{t}$ and $\vec{T}$ are the isospin of the incident nucleon and target, respectively. U_o is referred to as the isoscalar and U_1 as the isovector part of the OP. This splits the radial part of the potential in two diagonal terms, one for n, another for p, and a non-diagonal term which is responsible for the (p,n) quasi elastic scattering. This last is given by

$$U_{pn}(\vec{r},E) = 2\sqrt{\frac{\epsilon}{A}}\, U_1(\vec{r},E).$$

Thus it has been assumed that the knowledge of the proton OMP and the fit to the (p,n) quasi elastic scattering suffice to determine the neutron OMP. This has been tried by several authors[12,13] with some success. However, several questions still remain unsolved and we believe that a thorough knowledge of both (n,n) and (p,p) data are needed to determine the isovector term $U_1(\vec{r},E)$.

The central and imaginary potential depths of eq. 1 may be written explicitly as:

$$\begin{aligned} V(E)\, F(X_R) &= V_o(E) f(X_R) \pm \epsilon V_1(E)\, f_1(X_R) + \Delta V_c(r) \\ W(E)\, G(X_I) &= W_o(E) g(X_I) \pm \epsilon W_1(E)\, g_1(X_I) + \Delta W_c(r) \end{aligned} \qquad (2)$$

where the upper sign (+) is valid for protons while the (-) sign is for neutrons and $\epsilon = (N-Z)/A$ represents the nuclear asymmetry.

The last term in both above equations corresponds to the so-called Coulomb correction term. This term arises because the local optical potential is energy-dependent and charged particles lose energy penetrating the Coulomb barrier, thus having smaller KE inside the nucleus than an uncharged particle. It is the average kinetic energy of the nucleon inside the nucleus that determines the strength of the average potential. Thus

$$\Delta U_c(r) = \Delta V_c(r) + i\, \Delta W_c(r).$$

The real part $\Delta V_c(r)$ is generally parameterized as having the same radial form factor as the isoscalar part, $f(X_R)$, and its

strength estimated to be $\Delta Z/A^{1/3}$, with Δ = 0.4. The imaginary term $\Delta W_c(r)$ is usually neglected and set equal to zero. It is apparent from this equation that a knowledge of both terms, ΔV_c and ΔW_c, is important in the evaluation of the isovector part of the potential from the analysis of proton data alone.

In the remainder of this presentation we shall report on our efforts to evaluate the following components of the nucleon-nucleus OMP and our results on inelastic neutron scattering:

1) The Coulomb correction term $\Delta U_c(r)$
2) The isospin dependence of the OMP $U_1(r)$
3) A global fit: energy dependence
4) Inelastic neutron scattering: the $W_D a_I$ ambiguity.

The Coulomb Correction Term

The Coulomb correction term may be determined empirically by comparing protons and neutrons OMP analyses on T = 0 nuclei. A rather complete OMP analysis of p + ^{40}Ca elastic scattering from 10 - 180 MeV has been reported by van Oers.[14] An average geometry reported for E_p = 75 MeV was used in the neutron analyses of Ca + n at 11, 20, and 26 MeV. From the comparison of the real strength a value of 2.7 ± 0.4 MeV was obtained for the Coulomb correction term which may be parameterized as (0.46 ± 0.07) $Z/A^{1/3}$. This empirical value obtained for the first time is about 15% larger than the commonly used 0.4 $Z/A^{1/3}$ as evaluated in ref.[1]. Recently Jeukenne et al.[11] have performed microscopic OMP calculations in the case of ^{208}Pb at 25 MeV. A value for ΔV_c about 25% larger than the phenomenological value was obtained, which agrees well with the present increased empirical value.

The present data were also examined in an effort to determine an imaginary part to the Coulomb correction term. No positive indication was found.

The Isospin Dependence $U_1(r)$

Simultaneous analyses of proton and neutron elastic scattering were used to determine the real and imaginary strengths of U_1. This was done at the same nucleon bombarding energy, 11 MeV, and also at energies such that $E_p = E_n + \Delta V_c$. The results are shown in figures 8 and 9. The obtained average values are V_1 = 22 ± 1 MeV (assumes a volume form factor) and W_1 = 13 ± 1.7 MeV (assuming a surface derivative Woods-Saxon form factor).

A Global Fit: Energy Dependence

A subset of the total neutron scattering data was selected to do a global fit and search for the energy dependence of the real, imaginary, and isospin terms of the OMP. The neutron elastic scattering on Ca at 11, 20, and 26 MeV and the 7, 9, 11, 20, and 26 MeV neutron scattering on the ^{92,94,96,98,100}Mo and ^{208}Pb were used, representing a total of 28 angular distributions. A fixed geometry

was imposed. This geometry was obtained by averaging the individual best fit for all cases. The results are shown in Table 3.

Table 3

Results of Global Fits

$r_R = 1.19$ $\quad R_I = 1.26$

$a_R = 0.68$ $\quad a_I = 0.56$

$V = 54.7 - 0.32E - (22.2 - 0.18E)\,\varepsilon$

$W_v = 0$ $\quad E < 15$ MeV

$W_D = 5.7 + 0.5E - 14\,\varepsilon$

$W_v = 0.4E - 7$ $\quad E > 15$ MeV

$W_D = 21.2 - 0.54E - 12.3\,\varepsilon$

The following facts should be emphasized: a) For energies less than 15 MeV the imaginary part of the potential W_D increases with energy. This contradicts the results of Becchetti and Greenlees[2] where a decrease of W_D with energy is indicated. b) An energy dependence of V_I is incorporated. c) The energy dependences of the other potential depths are similar to other global fits.[1,2]

Inelastic Scattering

The extension of the nucleon-nucleus OMP to inelastic scattering is most easily understood in terms of the collective model according to which low-lying collective states can be populated by allowing the OMP to deform. In the usual DWBA analysis of differential cross section measurements, both the real and imaginary parts of the potential are described by a common deformation parameter β_L. Description of polarization data may also require deformation of the spin-orbit potential. If the Lane term of the OMP is also subject to deformation, isospin dependent effects should be observed in inelastic nucleon scattering. Madsen, Brown, and Anderson[16] have recently studied the isospin dependence of core-polarization effects in inelastic scattering to the first 2^+ states in single-closed-shell nuclei. They show that the usual

deformation parameter, β_L, for these states is a function of the external field which produces the transition. Specifically, they predict that $\beta nn'$ should be larger than $\beta pp'$ for closed-neutron-shell nuclei, and vice versa for closed proton shell nuclei.

We have studied inelastic neutron scattering on several isotopes of Zr and Mo and the relevant results for N = 50 nuclei (^{90}Zr and ^{92}Mo) are shown in Fig. 10. Quadrupole deformation parameters of $0.085 \pm^{0.010}_{0.005}$ for ^{90}Zr and 0.099 ± 0.005 for ^{92}Mo were extracted from the data by means of a DWBA analysis. These numbers are 10-20% larger than the values of $\beta 2$ obtained from (p,p') experiments in agreement with theoretical expectations. A similar study is being performed for the closed-proton-shell nuclei ^{118,120,122,124}Sn.

Analysis of inelastic scattering by means of the collective model is troubled by both ambiguities and insensitivities of the optical model analysis. Not surprisingly, the inelastic scattering cross section is more sensitive to small changes in the imaginary part of the optical model than is the shape of the elastic scattering cross section from which these parameters are derived. Furthermore, the product of the strength and diffuseness $W_D a_I$ of the (surface) imaginary term is correlated with the nuclear deformation parameter. A more careful analysis on inelastic and reaction cross sections may be required before the imaginary part of the OMP is understood with the same confidence as is the real potential.

REFERENCES

1. F.G. Perey, Phys. Rev. 131, 745 (1963).
2. F.D. Becchetti and G.W. Greenlees, Phys. Rev. 182, 1190 (1969)
3. R.W. Manweiler, Nucl. Phys. A240, 373 (1975).
4. J-P. Jeukenne, A. Leujene, and C. Mahaux, Phys. Rev. 10C, 1391 (1974).
   J-P. Jeukenne, A. Leujene and C. Mahaux, in Proceedings of the International Conference on the Interaction of Neutrons with Nuclei, Lowell, Mass., 1976.
5. J.D. Carlson, Nucl. Inst. and Methods 113, 541 (1973).
6. W.E. Kinney, Nucl. Inst. and Methods 83, 15 (1970), and private communication.
7. S.K. Penny, ORNL-TM-2590, Oak Ridge National Lab., 1969 (unpublished).
8. P. Lambropoulos, P. Guenther, A. Smith, and J. Whalen, Nucl. Phys. A201, 1 (1973).
9. F.G. Perey, private communication, 1975.
10. L.R.B. Elton in Nuclear Radii, H. Schopper, Editor, p. 5, Springer-Verlag, Berlin, 1967.
11. A.M. Lane, Phys. Rev. Lett. 8, 171 (1962); Nucl. Phys. 35, 676 (1962).
12. J.D. Carlson, C.D. Zafiratos, and D.A. Lind, Nucl. Phys. A249, 29 (1975).
13. D.M. Patterson, R.R. Doering, and A. Galonsky, Nucl. Phys. A263, 261 (1976).
14. W.T.H. van Oers, Phys. Rev. C3, 1550 (1971).
15. J-P. Jeukenne, A. Leujene and C. Mahaux, Phys. Lett. 62B, 256 (1976), and J-P. Jeukenne, A. Leujene and C. Mahaux, to be published.
16. V.R. Brown and V.A. Anderson, Phys. Rev. C11, 1298 (1975); V.A. Madsen, V.R. Brown, and J.D. Anderson, Phys. Rev. Lett. 34, 1398 (1975); and V.A. Madsen, V.R. Brown, and J.C. Anderson, Phys. Rev. C12, 1205 (1975).

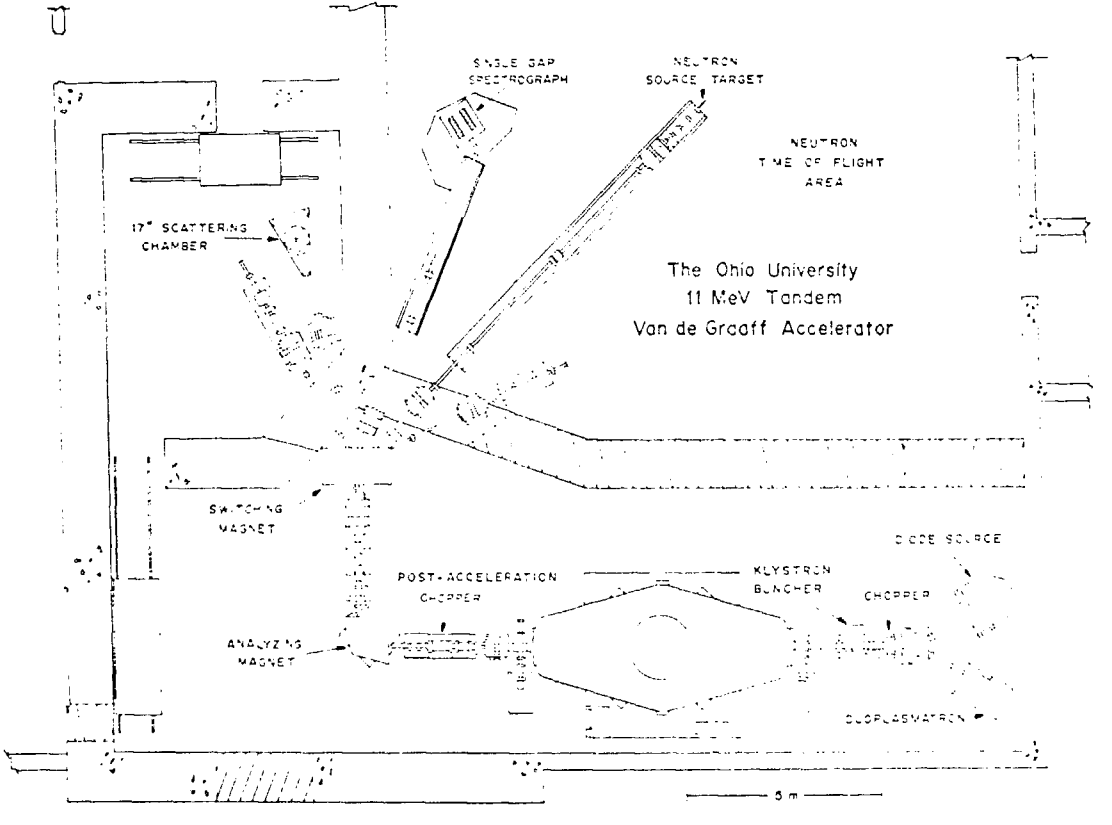
SINGLE GAP SPECTROGRAPH
NEUTRON SOURCE TARGET
NEUTRON TIME OF FLIGHT AREA
17" SCATTERING CHAMBER
The Ohio University
11 MeV Tandem
Van de Graaff Accelerator
SWITCHING MAGNET
POST-ACCELERATION CHOPPER
KLYSTRON BUNCHER
CHOPPER
ANALYZING MAGNET
5 m

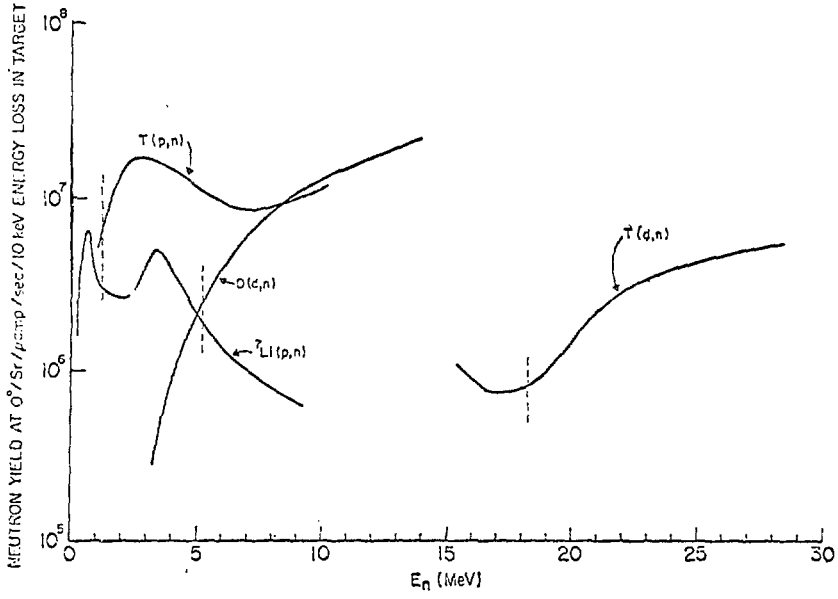

Fig. 2. Neutron yield at 0° for the indicated neutron sources.

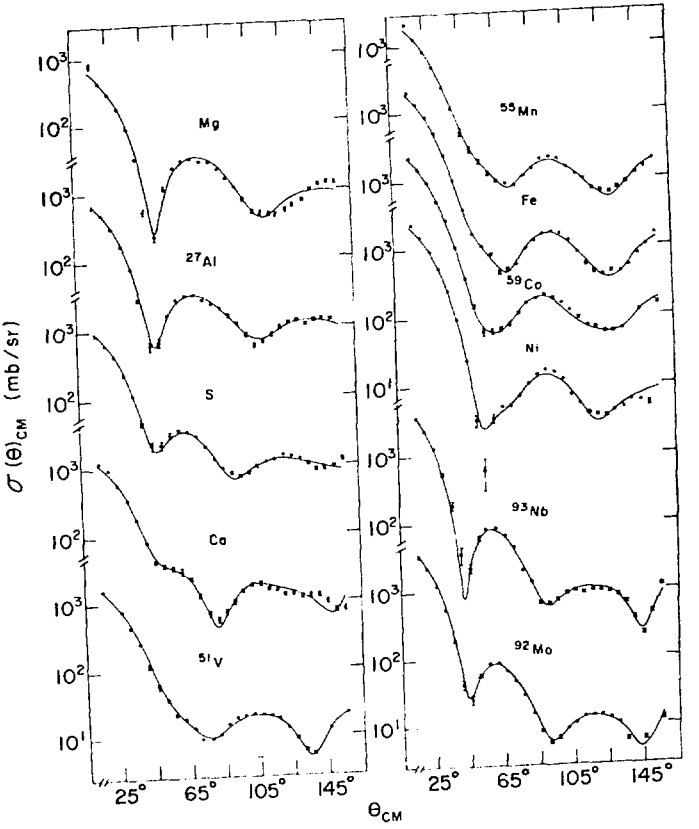

Fig. 3. 11 MeV neutron elastic scattering, Mg through [illegible]Mo.

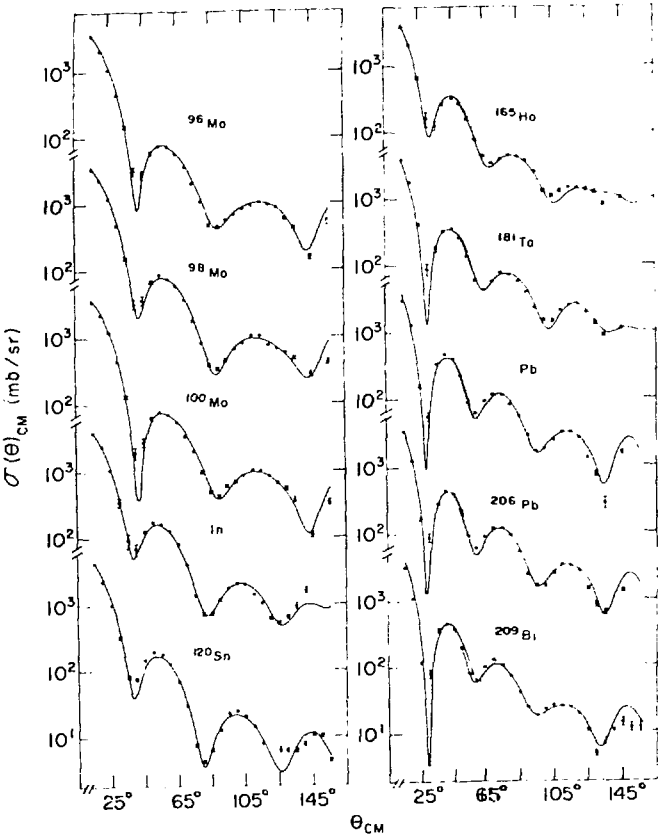

Fig. 4. 11 MeV neutron elastic scattering, ^{96}Mo through ^{209}Bi.

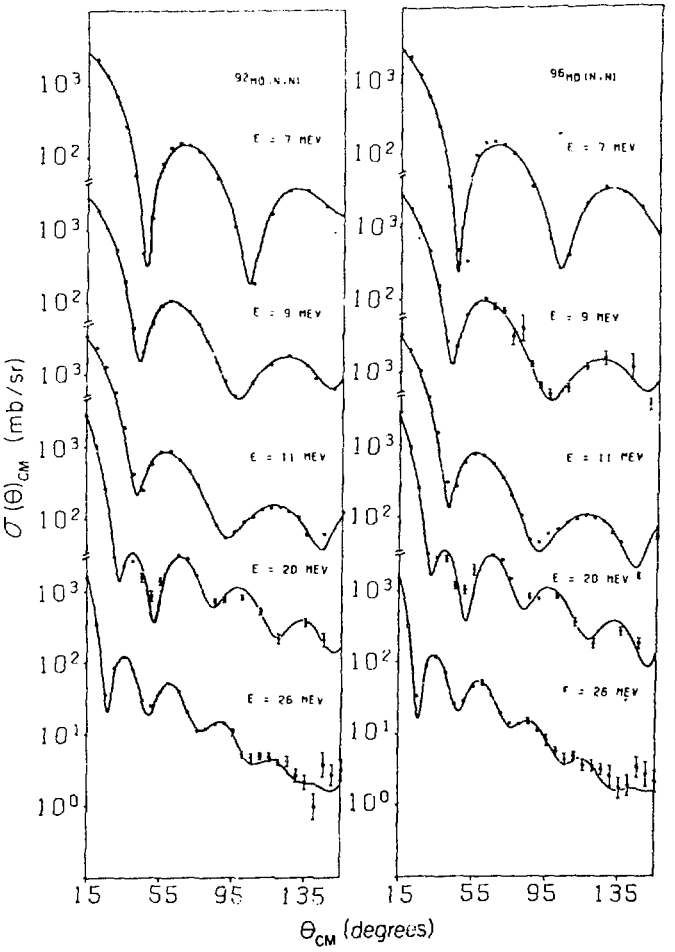

Fig. 5. [illegible] Mo (n,n) at 7, 9, 11, 20, and 26 MeV

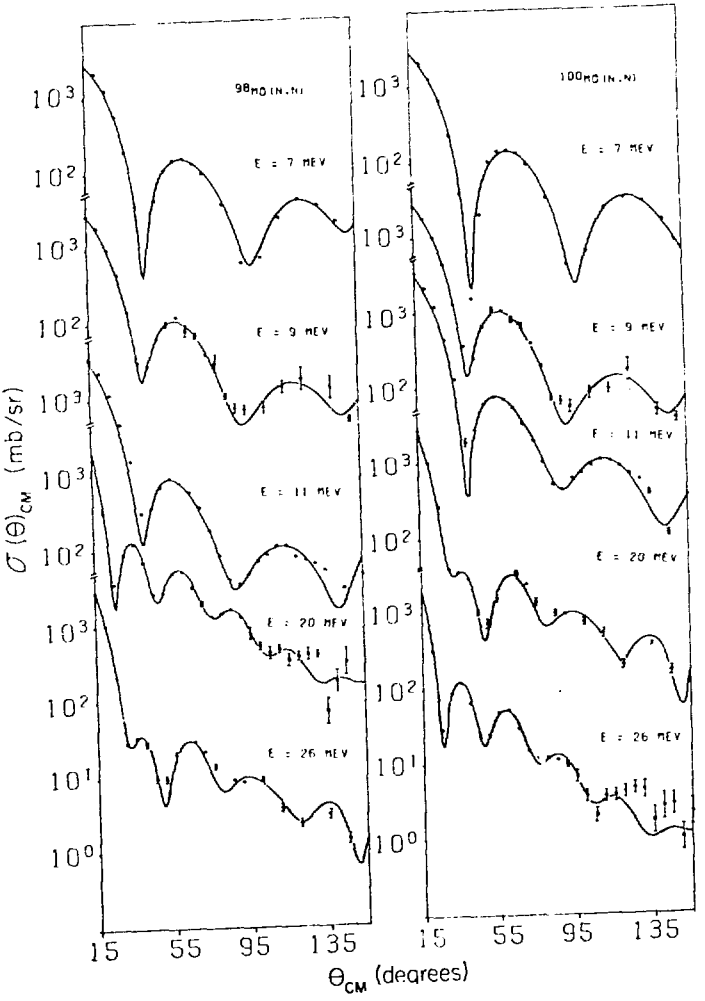

Fig. 6. ^{98,100}Mo (n,n) at 7, 9, 11, 20, and 26 MeV

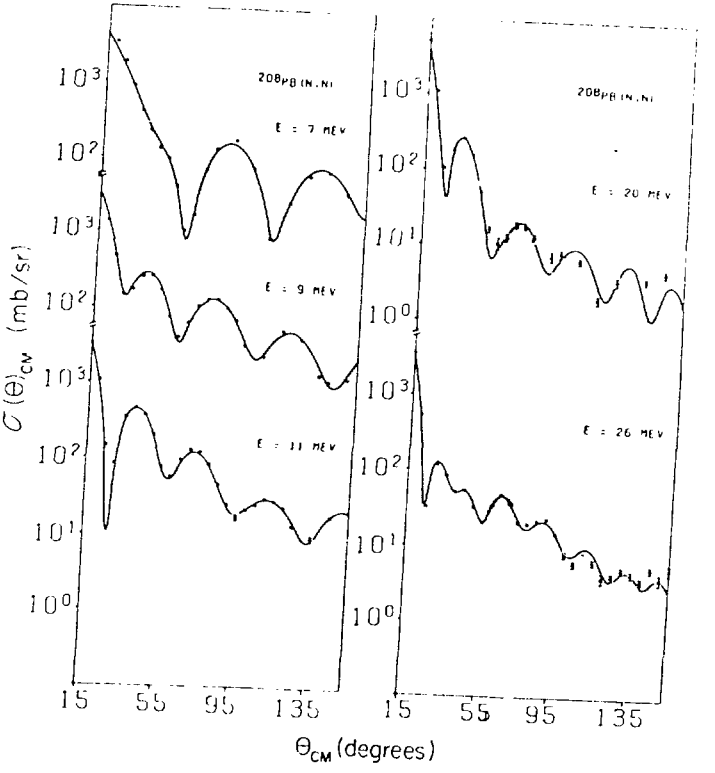

Fig. 7. ^{208}Pb (n,n) at 7, 9, 11, 20, and 26 MeV.

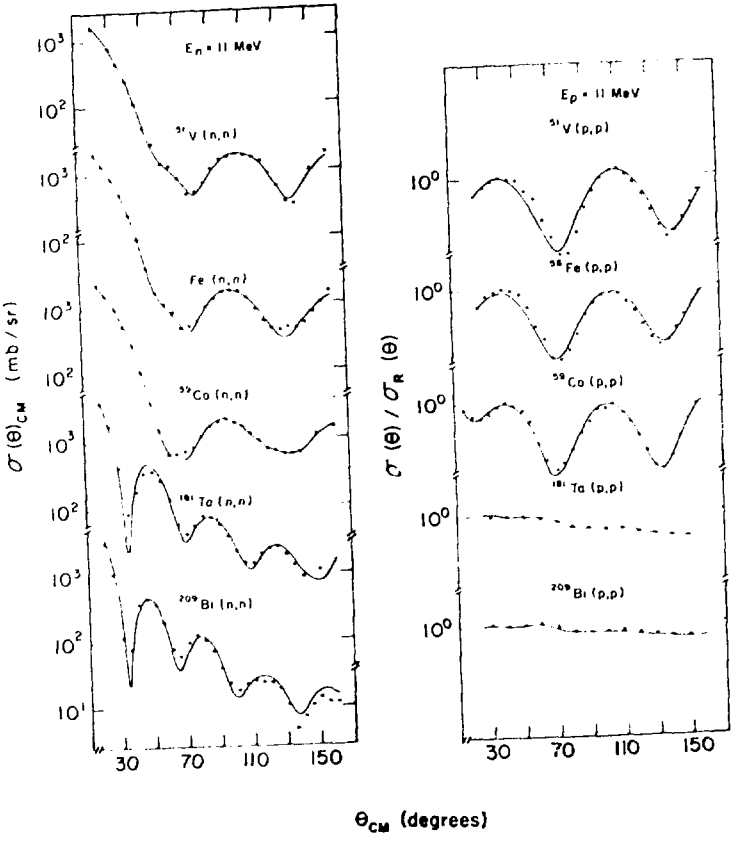

Fig. 8. Simultaneous p and n elastic scattering at 11 MeV.

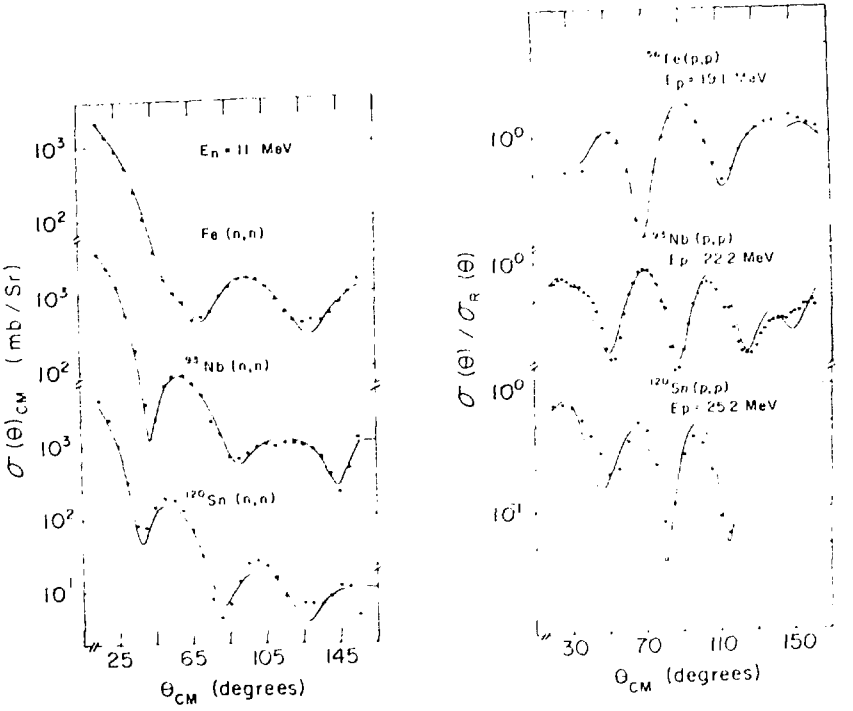

Fig. 9 Simultaneous analysis for n and p elastic scattering such that $E_p = 11 + 2E_n$

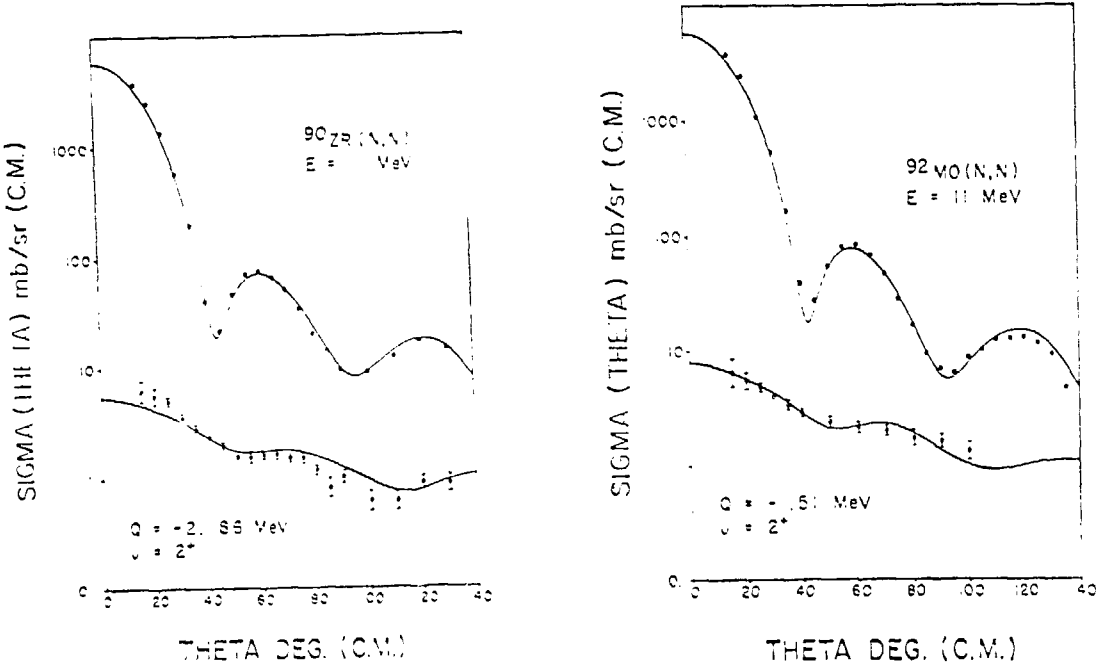

Fig. 1: Differential cross sections for 1 MeV neutrons scattered elastically and inelastically from Zr and Mo. Solid lines through the inelastic data are the results of DWBA calculations using collective model form factors.

AN EVALUATION OF THE NEUTRON INDUCED REACTION CROSS SECTIONS ON CARBON FROM 10 TO 20 MeV

G. Haouat, J. Lachkar, J. P. Delaroche, Y. Patin, J. Sigaud
Service de Physique Nucléaire. Centre d'Etudes de
Bruyères-le-Châtel B.P. n. 561 - 92542 Montrouge cedex, France

Available data on the neutron induced reactions on carbon are reviewed for the energy range from 10 to 20 MeV. Evaluated cross sections obtained at Bruyères-le-Châtel are discussed. Comparisons with coupled-channel calculations are presented for the total, elastic, and inelastic (to the 2^+ level) cross sections of ^{12}C.

Introduction

Cross section data for neutron induced reactions on carbon are important in a number of areas of applied interest. Detailed knowledge of differential cross sections for fast neutrons scattered by carbon is required for calculations of neutron transport in shielding material of fusion and fission reactors. In scattering experiments, the data are generally normalized to n-p scattering, the sample being replaced by a polyethylene scatterer. In addition, emitted neutrons are detected usually by using organic scintillators. Thus, carbon data are needed either for estimation of the sample size effects or for calculation of the detector efficiency. Recently, it has been suggested that the present need for high-energy neutron standards could be satisfied by carbon data.[1]

Here we review the carbon data between 10 and 20 MeV, with primary emphasis on the recent measurements. An evaluation[2] has been carried out and is discussed. We also present a coupled channel optical model analysis of the data on the total cross section and scattering cross sections for the ground state and first excited (2^+) state of ^{12}C.

Neutron Induced Reactions On Carbon

Natural carbon consists of 98.8927 ^{12}C and 1.1087 ^{13}C. Considering the accuracy of the data discussed below, natural carbon can be treated as ^{12}C. For neutron energies above 10 MeV, the resonances reached in the ^{12}C+n compound system are broad and generally overlapping so that the cross section variations with neutron energy are rather smooth.

Total Cross Section. The total cross section has been measured over a wide energy range.[3] Between 10 and 15 MeV the data from KFK,[4] NBS,[5] ORNL,[6] BNW,[7] and the University of Wisconsin[8] are consistent with each other within 8% of the average cross section. The recommended values, based on these data, are very close to the results from ORNL.[6] The evaluated curve from 15 to 20 MeV was obtained from the measurements of KFK[4] and ORNL[6] which

agree remarkably well; these data are consistent with the total cross sections previously reported by Bowen et al.[9] and Harlow et al.[10] The evaluated total cross section is shown in Fig. 1 for the energy range 8.5-20 MeV; data are given with an accuracy of 4% below and 6% above 15 MeV.

Radiative Capture (Q = 4.947 MeV). The radiative capture cross section, between 0.2 and 20 MeV, was deduced from the $^{12}C(\gamma,n)$ measurement of Cook[11] by using the reciprocity theorem. The radiative capture cross section from thermal energy up to 20 MeV is very low and does not exceed 0.07% of the total cross section.

Elastic Scattering. Below 15 MeV the proposed values for elastic scattering cross sections were mainly based upon the measurements from BRC[12,13] between 8 and 14.5 MeV; these data are generally in good agreement with the results from TUNL[14] between 9 and 15 MeV. Several data from 14 to 15 MeV were also taken into account (see ref. 2). Above 15 MeV we considered the differential cross sections of Deconnink et al.[15] at 17.27-18.25 and 19.88 MeV and the integrated cross sections measured by Boreli et al.[16] over the energy range 14-25 MeV. The evaluated elastic scattering data are displayed in Fig. 1; they are given with an accuracy of 7% below and 10% above 15 MeV.

Inelastic Scattering From The First Excited 2^+ State in ^{12}C (Q = -4.439 MeV). We consider here only the inelastic scattering from the first excited state in ^{12}C (2^+, 4.439 MeV) since most, if not all, of the higher excited states decay preferentially by emission of α-particles and contribute to the $^{12}C(n,n'3\alpha)$ cross section which will be examined below. As a consequence, the 4.439-MeV γ-ray production is a direct measure of the yield of the first excited state by inelastic scattering. Below 15 MeV, the inelastic scattering data from BRC[12,13] and TUNL[14] were taken into account as well as other data between 14 and 15 MeV. The measurements from BRC[12,13] were found to be very consistent, within the uncertainties, with the $(n,n'\gamma)$ cross sections of Morgan et al.[17] at 125°, when multiplied by 4π. We may then conclude that the fourth order coefficient in the Legendre polynomial expansion of the 4.439-MeV γ-ray angular distribution is very small between 10 and 15 MeV. Between 15 and 20 MeV a few data have been reported.[15-17] The inelastic (2^+) curve was mainly based upon the $(n,n'\gamma)$ data of Morgan et al.[17] at 125°, assuming that the fourth order coefficient is still negligible. The evaluated curve is shown in Fig. 2.

$^{12}C(n,\alpha_0)^9Be$ Cross Section (Q = -5.702 MeV). Only the (n,α_0) reaction leaving ^9Be in its ground state is considered as an absorption reaction. The (n,α) reactions leading to the ^9Be excited states contribute to the $^{12}C(n,n'3\alpha)$ process. The (n,α_0) cross section was measured between 13.9 and 18.8 MeV. Other information was obtained from measurements of the $^9Be(\alpha,n_0)^{12}C$ reaction by using the reciprocity theorem (see ref. 2). Thus, data for the (n,α_0) cross section are proposed from threshold up to 20 MeV with an accuracy of 12% to 20%.

$^{12}C(n,n'3\alpha)$ Cross Section ($Q = -7.276$ MeV). The $^{12}C(n,n'3\alpha)$ reaction cross section becomes significant above 10 MeV. The secondary neutrons cover a wide energy range. The cross sections were measured by Green et al.[19] between 10.6 and 14.6 MeV, Frye et al.[15] from 12.85 to 18.8 MeV and Vasil'ev et al.[20] from threshold to 19 MeV; however the experimental uncertainties vary between 30% and 50%. The recommended values for the $^{12}C(n,n'3\alpha)$ cross section were mainly obtained by subtracting from the total cross section the sum of the cross sections for the other reactions. The estimated errors vary from 20% to 25%.

$^{12}C(n,p)^{12}B$ Cross Section ($Q = -12.586$ MeV). The cross section for the $^{12}C(n,p)^{12}B$ reaction was measured by Rimmer et al.[21] and Kreger and Kern[22] by counting the β-particles emitted from the decaying ^{12}B nucleus. The data of Rimmer et al.[21] were adopted for the present evaluation; the given accuracy is 15%.

$^{12}C(n,d)$ Cross Section ($Q = -13.733$ MeV). The evaluated data for the $^{12}C(n,d_0)^{11}B$ reaction were derived from the $^{11}B(d,n_0)$ measurements of Ames et al.[23] and Class et al.[24] by means of the reciprocity theorem; the values are given with 15% uncertainty. The cross sections for the (n,d) reaction to the excited states in ^{11}B and for the (n,np) reaction were estimated to be very small; they were ignored in this work.

Neutron and γ-ray Differential Cross Sections. Evaluated Legendre coefficients of the neutron elastic scattering and inelastic (2^+) scattering angular distributions were deduced from the available data.[7] Energy and angular distributions for secondary neutrons from the $^{12}C(n,n'3\alpha)$ reaction were also obtained. Only the 4.439-MeV γ-ray differential cross sections were estimated since the photon production from the other reactions is comparatively negligible.

Analysis of the Data

The excitation functions for neutrons scattered from ^{12}C show smooth variations with energy above 8.5 MeV. Thus, nuclear structure effects may be assumed to be sufficiently averaged out for the reactions to be described within the framework of the optical model. Because ^{12}C is a strongly deformed (oblate) nucleus,[25] an analysis of the data, using the coupled-channel optical model,[26] was attempted.

Coupled-channel calculations were performed with the ground state (0^+) and the first excited 2^+ state coupled together; complex coupling was assumed. An extensive set of data was used to fix the potential parameters and their energy dependence. Differential cross sections for the inelastic (2^+) and elastic scattering from 8.5 to 20 MeV[12-15] were analyzed in approximately 1-MeV steps; calculated angular distributions and experimental data are shown in Fig. 3 for 14.5 and 19.9-MeV neutron energies. In addition, the geometric parameters and potential depths were adjusted to fit the energy dependence of the total cross section. The potential parameters deduced from this analysis are given in

Table 1

Potential parameters used in the coupled-channel calculations above 8.5 MeV. V_R, W_D, V_{SO}, and E (neutron energy) are given in MeV. R and a are given in fm.

Ref.	Real part			Imaginary part			Spin orbit part			Deformation paramater
	R_R	a_R	V_R	R_D	a_D	W_D	R_{SO}	a_{SO}	V_{SO}	β_2
This work	1.25	0.40	51.50-0.3E	1.25	0.30	0.74+0.38(E-8.5)	1.05	0.40	5.0	-0.60
27	1.25	0.35	58-0.9E	1.25	0.20	0.28E	1.25	0.35	5.0	-0.64

Table I and compared to those obtained at Duke University[27] for neutron energies below 15 MeV. The present parameters are similar to those found to describe the nucleon scattering from heavier nuclei with one exception: the small diffuseness parameters. Such small values were also obtained in other studies of nucleon scattering from ^{12}C.[25,27,28] The calculations reproduce the average behavior of the recommended total and elastic values (Fig. 1) as well as the inelastic (2^+) cross section and the sum of the remaining cross sections (Fig. 2).

Preliminary calculations have been extended over the neutron energy range from 20 to 40 MeV. For the absorptive potential W_D, the energy dependence given in Table I was taken up to 30 MeV; between 30 and 40 MeV, W_D was kept constant. No volume absorption term was needed. For the real part of the potential, the energy dependence of Table I had to be changed to the following form: $V = V_0 - \alpha E - \beta E^2$, with $\alpha = 0.27$ and $\beta = 0.0018$.

The calculations of the total cross section and the non-elastic (or reaction) cross section have been compared to data compiled by Del Guerra.[3] The agreement for the total cross section is quite good (Fig. 4). For the reaction cross section, the data are scarce and not consistent but the agreement is still good (Fig. 4).

Summary

Recommended values based upon experimental data are proposed for the neutron-induced reactions on carbon between 10 and 20 MeV. An analysis of the data shows that the coupled-channel optical model can give a good description of the main features of the total, elastic, and inelastic (2^+ level excitation) cross sections for ^{12}C at intermediate energies. The fits to the data could be improved by adding Breit-Wigner resonance amplitudes to the optical model scattering amplitudes.[29]

REFERENCES

1. J. C. Lachkar, Intern. Spec. Symp. on Neutron Standards and Applications, N.B.S. Gaithersburg, March 28-31 (1977).
2. J. C. Lachkar, F. Coçu, G. Haouat, P. LeFloch, Y. Patin, and J. Sigaud, Report NEANDC (E) 168 "L" - INDC (FR)-7/L (1975).
3. A. Del Guerra, Nucl. Inst. Meth. 135, 337 (1976).
4. S. Cierjacks, P. Forti, D. Kopsch, L. Kropp, J. Nebe, and H. Unseld, Report NEANDC (E) 111 "U" - KFK 1000 (1968).
5. H. T. Beaton, II, J. L. Menke, R. A. Schrack, and R. B. Schwartz, Nucl. Sci. and Eng. 56, 27 (1975).
6. F. G. Perey, T. A. Love, and W. E. Kinney, Report ORNL 4823-(ENDF) 178) (1972).
7. I. Foster and D. W. Glasgow, Phys. Rev. C3, 576 (1971).
8. D. B. Fossan, R. L. Walter, W. E. Wilson and N. B. Barschall, Phys. Rev. 123, 209 (1961).

9. P. H. Bowen, J. P. Scanlon, G. H. Stafford, J. J. Treshet, and P. E. Hodgson, Nucl. Phys. 22, 640 (1961).
10. M. V. Harlow, Jr., R. L. Robinson, and B. B. Kinsey, Nucl. Phys. 67, 249 (1965).
11. B. C. Cook, Phys. Rev. 106, 300 (1957).
12. G. Haouat and F. Coçu, Neitronaya Fisika Vol. 3, 233 (1974) (Kiev conf.)
13. G. Haouat, J. Lachkar, J. Sigaud, Y. Patin, and F. Coçu, Report CEA R4641 (1975).
14. D. W. Glasgow et al., Nucl. Sci. and Eng. 61, 521 (1976).
15. G. Deconninck and J. P. Meulders, Phys. Rev. C1, 1326 (1970).
16. F. Boreli, B. B. Kinsey, and P. N. Shrivastava, Phys. Rev. 174, 1147 (1968).
17. G. L. Morgan, T. A. Love, J. K. Dickens and F. G. Perey, Report ORNL TM 3702 (1972).
18. L. L. Green and W. Gebson, Proc. Phys. Soc. A62, 296 (1949).
19. G. M. Frye, L. Rosen, and L. Stewart, Phys. Rev. 99, 1375 (1955).
20. S. S. Vasil'ev, V. V. Komarov, and A. H. Popova, J.E.T.P. 6., 1016 (1958).
21. E. H. Rimmer and P. S. Fisher, Nucl. Phys. A108, 567 (1968).
22. W. E. Kreger and B. D. Kern, Phys. Rev. 113, 890 (1959).
23. O. Ames, G. E. Owen, and C. D. Swartz, Phys. Rev. 106, 775 (1957).
24. C. M. Class, J. E. Price, and J. R. Risser, Nucl. Phys. 71, 433 (1965).
25. G. A. Grin, C. Joseph, C. Y. Wong, and T. Tamura, Phys. Lett. 25B, 387 (1967).
26. T. Tamura, Rev. Mod. Phys. 37, 679 (1965).
27. F. O. Purser, et al. Report BNL-NCS-21501, 274 (1976).
28. J. S. Nodvik, C. B. Duke, and M. A. Melkanoff, Phys. Rev. 125, 975 (1962).
29. T. Tamura and T. Terasawa, Phys. Lett. 8, 41 (1964).

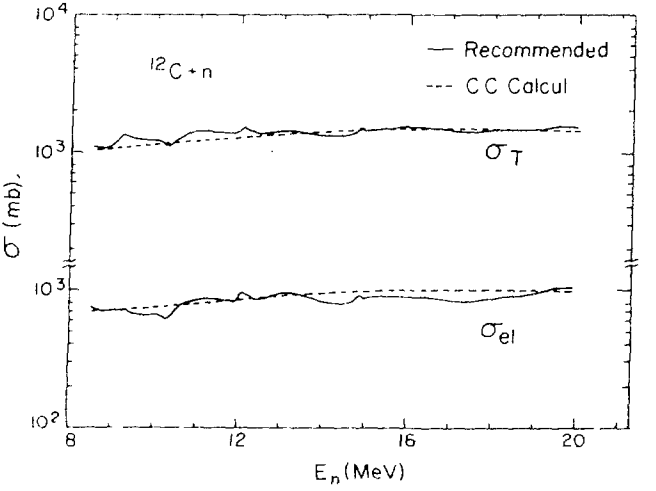

Fig. 1. Neutron total (σ_T) and elastic scattering (σ_{el}) cross sections for carbon between 8.5 and 20 MeV. Full curves are the recommended values,[2] dashed curves are coupled-channel calculations as described in the text.

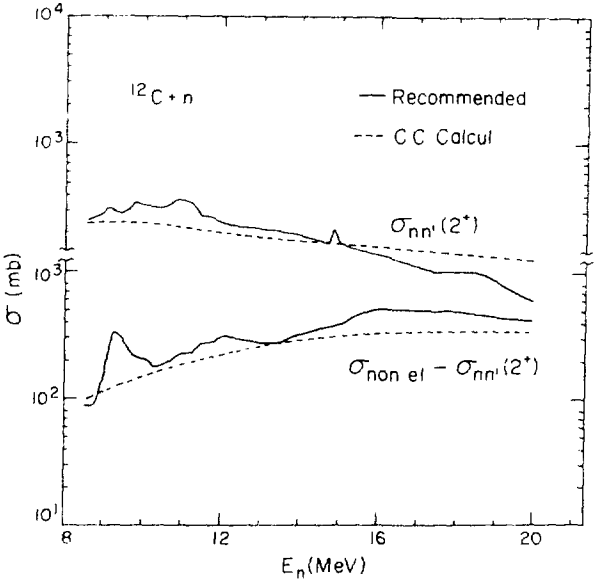

Fig. 2. Recommended data[2] (full curves) and coupled-channel calculations (dashed curves) between 8.5 and 20 MeV for the inelastic (2^+) scattering cross section [$\sigma_{n,n'}(2^+)$] and the sum of the other partial nonelastic cross sections [$\sigma_{nonel} - \sigma_{n,n'}(2^+)$] of ^{12}C.

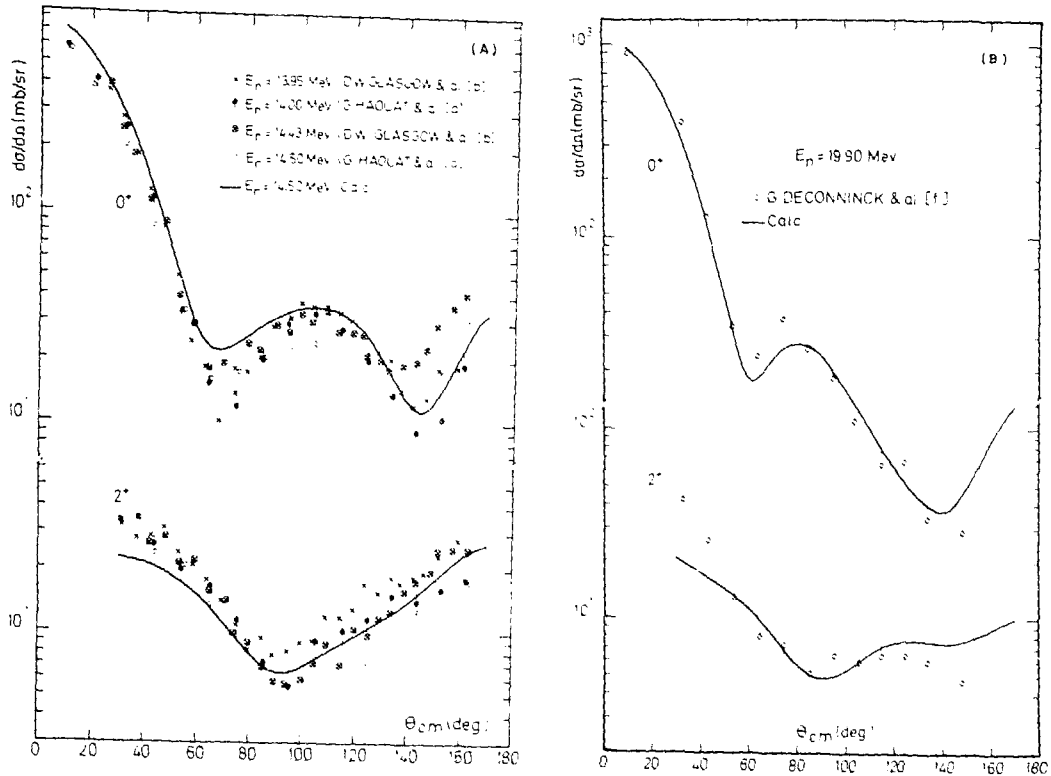

Fig. 3. Comparison of measurements of the elastic (0^+) and inelastic (2^+) scattering differential cross sections of ^{12}C with angular distributions calculated for 14.5 MeV (Fig. 3a) and 19.9 MeV (Fig. 3b) neutron energies.

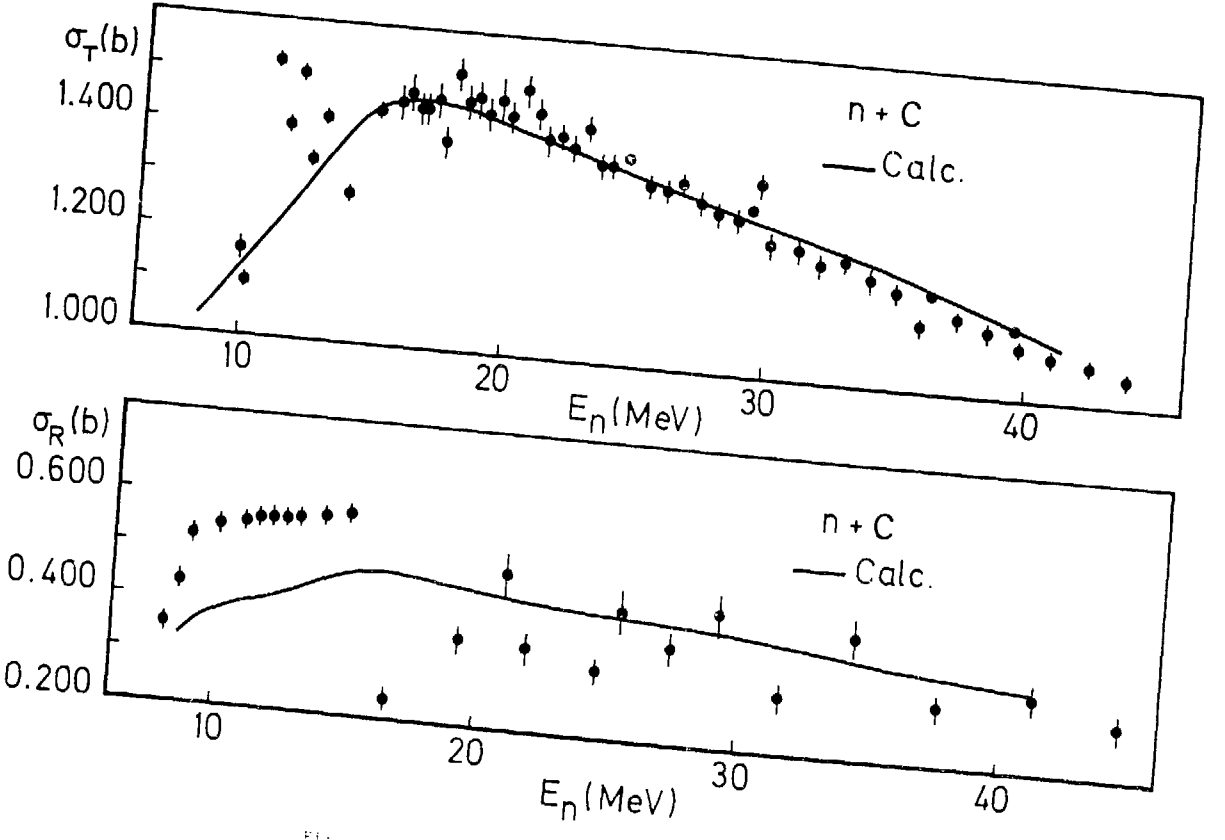

Fig. 4. Carbon total (above) and reaction (below) cross sections between 10 and 40 MeV. Measurements are taken from ref. 3. Full curves are coupled-channel calculations.

Nuclear Emulsion Techniques and Data Needs[1] for Fast Neutron Angular Spectrometry

James H. Roberts* and Raymond Gold
Westinghouse Hanford Company, Richland, WA 99352

ABSTRACT

The significance of angular neutron flux observations in reactor environments is discussed. Special emphasis is placed on effects arising in scalar neutron spectrometry which stem from the existence of angular neutron spectra. The applicability of nuclear emulsion techniques for observing angular neutron spectra is stressed. Cross section requirements are reviewed for nuclear emulsion passive neutron spectrometry above 10 MeV.

INTRODUCTION

In the characterization of neutron fields, be they reactor or accelerator based, very little attention has been directed toward the measurement of neutron angular distribution. Yet, the quantity invariably used for the analytical description of the neutron field is the angular rather than the scalar neutron flux. The angular neutron flux ψ can be defined in the classical Boltzmann sense as

$$\psi = \psi(\mathbf{r}, \mathbf{v}, t), \tag{1}$$

where ψ is the neutron density in phase space and $\mathbf{r}$, $\mathbf{v}$, and t are the phase space variables of position, velocity, and time, respectively. Transforming the phase space variables

$$(\mathbf{r}, \mathbf{v}, t) \rightarrow (\mathbf{r}, E, \Omega, t), \tag{2}$$

where E is the neutron energy and Ω is the solid angle direction of the velocity vector $\mathbf{v}$, provides an equally conventional representation of the angular flux, namely $\psi(\mathbf{r}, E, \Omega, t)$.

Under conditions of high symmetry, ψ is expected to be independent of Ω, i.e., the angular flux will be isotropic. Such conditions may be valid near core center in many reactors, provided local operating conditions do not perturb in core symmetry. However, even at core center, perturbations often exist that can violate symmetry conditions such as the proximity of control or safety rods, adjacent subassemblies of substantially different loadings, changing fuel and/or moderator densities or isotopic composition, differences between axial and radial loadings, etc. Furthermore, the angular flux is not

[1]Work performed under auspices of U.S. DOE.

*On leave from Macalester College, St. Paul, Minnesota 55105.

likely to be isotropic at most other reactor locations, such as close to core-blanket or core-reflector interfaces or outside the core proper, i.e., inside or outside reactor shields.

The assumption of neutron isotropy often produces profound benefits for both theory and experiment. Many calculations and measurements would often be totally precluded were it not for fruitful simplifications which follow directly from such an assumption. However, no matter how desirable from an experimental or theoretical viewpoint, one cannot arbitrarily postulate neutron isotropy. Indeed, it is an assumption which should be tested, preferably by both theory and experiment. Such assessments would hopefully quantify the degree to which this assumption is satisfied and thereby provide a basis for estimating errors entailed by any deviation from neutron isotropy.

The present work stresses the utility of nuclear emulsions in furnishing data to characterize fast neutron angular distributions. Beyond assessing assumptions of possible isotropy introduced in theoretical models, angular distribution data provide independent tests of the validity of calculations. Comparisons of theory and experiment to date have almost exclusively relied upon predictions and observations of the energy-dependent scalar neutron flux at a specified location or upon the spatial variations of neutron induced reaction rates. Angular distribution data can provide significant independent tests of calculational capability, especially considering that an energy-angle $(E,\bar{\Omega})$ matrix of only modest resolution can possess a very large number of elements. Actually the dimensions of the energy-angle matrix should be chosen to match experimental conditions, of which the energy and angular resolving power of the nuclear emulsions are no doubt the most important considerations.

Comparisons of fast neutron reactor spectrometry methods have been carried out for some time now. These comparisons have been extremely fruitful in eliminating systematic biases, which would otherwise be extremely difficult to uncover. However, even in the most rigorous of these comparative efforts,[1] agreement of no better than 5% has been attained over the dominant intensity domain of the spectrum. Moreover, the observed agreement often deteriorates markedly in the low and high energy wings of the spectrum, where the results of different spectrometry methods can differ by as much as 20-25%. Very recent discrepancies underscore such difficulties.[2]

Placement of a neutron spectrometer in a neutron field will not actually provide a measurement of $\bar{\phi}$, but rather a observation of $\bar{\phi}$ averaged over the dimensions of the detector. This space and solid-angle averaging, $\langle\langle\phi\rangle_{\bar{r}}\rangle_{\bar{\Omega}}$, has already been stressed in a recent review[3] and perhaps bears further elaboration. This averaging process obviously depends on both the size of the given neutron detector and the specific method of neutron spectrometry utilized. Each detector size-spectrometry method will provide a unique spatial and angular average of

$\bar{\phi}$ and thereby give rise to a correspondingly unique scalar neutron flux, namely that scalar neutron energy distribution observed with the given detector size-spectrometry method.

Unfortunately spectrometry intercomparisons tacitly assume the existence of a unique in-core scalar neutron spectrum and that all valid spectrometry methods should ideally produce this unique energy distribution. However, it has already been stressed that the observed scalar spectrum $\bar{\phi}(\vec{r})$ depends upon the detector size-spectrometry method utilized. Hence, different detector size-spectrometry systems will not produce identical scalar neutron energy spectra. Observed differences which arise in these spectrometry comparisons can therefore be attributed to the specific interaction between the given detector size-spectrometry method and the in-core radiation environment. Data quantifying the spatial and angular variations of the in-core neutron flux may well play a key role in understanding these observed effects.

A direct approach to resolve such difficulties lies in the construction of spherically symmetric detectors, perhaps the most useful of which have been spherical proportional counters.[4] Apart from the question of whether such detectors truly possess a spherically symmetric response, one can not assume that such detectors automatically resolve this uniqueness problem, i.e., it is not alone sufficient to assume even truly spherically symmetric detectors provide unique measurements of the scalar neutron flux. Since any active spectrometer must possess finite sensitive volume, one must also assume that the angular flux is independent of $\vec{r}$. If this is not the case, employing detectors of different size with the same given spectrometry method can still produce different results.

Consider the simple case of spectral observations in an infinite homogeneous medium. In order to conduct measurements, a void must be created not only for the detector, but the pre-amplifier, cables and other accessories. The very existence of the spectrometry system in this void can produce a deviation from what would otherwise be a uniform isotropic angular flux. In contrast with active spectrometry methods, emulsions afford a passive detection technique which in principle introduces minimal voids in the medium of interest. Consequently, emulsions provide the critical advantage of considerably less (and in most instances, negligible) spectral perturbation.

Inherent differences exist between active spectrometry methods and passive nuclear emulsion techniques which are perhaps even more profound. Measurements with active detectors produce electronic signals, which after suitable amplification are subsequently processed on-line with sophisticated pulse analyzing instrumentation. Consequently, the space and solid-angle averaging of $\bar{\phi}$ is an intrinsic aspect of active spectrometry methods, wherein all information related to neutron direction (or neutron angular distribution) is lost. In contrast,

nuclear emulsions can thus provide an important complement to active spectrometry methods. Although of poorer energy resolution, emulsions afford an angular and spatial sensitivity that would be difficult, if not impossible, to duplicate by active spectrometry techniques.

Although the relevance of emulsions for spatial and angular observations has been emphasized for reactor dosimetry, applications for accelerator-based neutron dosimetry appear to be emerging. Recent interest in the development of intense accelerator neutron sources[5,6] for simulation of fusion radiation damage augurs for similar applications of nuclear emulsions. Indeed, angular flux distributions produced by these higher energy accelerator sources exhibit greater spatial variation than customarily found in in-core reactor environments. As a consequence, there is an equivalent need for spatial and angular neutron dosimetry data in order to interpret fusion-simulated radiation damage experiments.

ANGULAR DISTRIBUTION MEASUREMENTS

A number of different neutron reactions, which produce charged particle reaction products, can be employed in emulsion observations of neutron angular distributions. Three specific reactions are advanced as probable candidates for such emulsion observations and these reactions are listed in Table I along with the associated energy region that probably can be covered by each reaction. The following three sub-sections provide separate descriptions of how each of these reactions can be applied.

Table I

Neutron Reactions Selected for Emulsion Observations

Reaction	Q-Value[a]	Energy Coverage[a]
$^{6}Li(n,\alpha)^{3}H$	+ 4.8	0.1 ≤ E ≤ 10.0
$^{3}H(n,n')^{3}H$	0	2.0 ≤ E ≤ 20
$^{10}B(n,t)2\text{-}^{4}He$	- 0.29	4 ≤ E ≤ 20

[a]MeV energy units.

The $^{6}Li(n,\alpha)^{3}H$ Reaction

The $^{6}Li(n,\alpha)^{3}H$ reaction has already been exploited in nuclear emulsion techniques for fast neutron spectroscopy by

loading emulsions with specks of glass containing ^6Li. It is therefore feasible to use this very same method to obtain information about the neutron angular distribution. This reaction has a large exoergic Q, 4.8 MeV, giving rise to measurable charged particle reaction tracks. In this reaction, both the alpha and the triton possess sufficient range in the emulsion to accurately determine their respective directions. Moreover, by measuring the range of each particle, the kinetic energies of the alpha particle and triton, E_α and E_t, can also be deduced. Since $E_t = |p_t|^2/2m_t$, where p_t is the linear momentum of the triton and m_t the triton rest mass, p_t can be determined. The momentum of the α particle, p_α, can be similarly deduced. *The neutron momentum p_n is obtained from conservation* of linear momentum in the laboratory system,

$$p_n = p_\alpha + p_t. \qquad (3)$$

This vector equation not only provides neutron direction, but makes it possible to estimate neutron energy E_n from the equation $E_n = p_n^2/2m_n$, where m_n is the rest mass of the neutron.

It has been shown,[7] however, that the best neutron energy resolution is obtained when the angle θ between p_t and p_n is small. Thus, for track pairs meeting this condition, i.e., $\theta < 10°$, *data on the angular distribution as a function of* E_n in the region 0.1 MeV $< E_n < 2$ MeV can be determined. Good statistics are readily determined in the vicinity of the broad resonance at 240 keV for spectra rich in neutrons at this energy. The practical value of the upper energy limit depends on the shape of the neutron spectrum, but for sufficiently hard spectra this reaction might be used up to 10 MeV or possibly higher. For the region above 2 MeV where the $^6Li(n,\alpha)$ cross section starts dropping more rapidly, the restriction on small θ can be somewhat relaxed without sacrificing the relative energy resolution. By accepting a larger fraction of the triton-alpha pairs at higher energies this reaction should be useful in giving data on angular anisotropy up to at least 10 MeV for fusion type spectra.

Introducing lithium into the emulsion in the form of glass specks containing ^6Li serves three purposes: (a) the glass can be placed in the median plane of the emulsion to reduce the escape probability of both the triton and alpha particle, (b) only the plane containing the glass specks need be scanned, thus increasing scanning speed; and (c) the glass speck tags the point of disintegration of the reaction and strongly discriminates against proton recoil tracks that might be confused with the triton-alpha pairs.

Neutron-Proton Scattering

Two crucial advantages of proton-recoil emulsions for angular neutron flux measurements lie in the ability to measure the recoil angular proton flux and the accurate knowledge of the scattering kernel. It is therefore not surprising that proton-recoil emulsions have been applied for angular neutron flux measurements some time ago.[9]

In nuclear emulsions, the direction of proton recoil tracks can be determined with good precision for $E_p \gtrsim 2$ MeV. For shorter proton tracks, as E_p decreases below 2 MeV, the direction of the proton becomes less certain due to grain density fluctuations and small angle scattering considerations. Consequently for $E_p \gtrsim 2$ MeV, one can measure the angular proton recoil flux $R(E_p, \bar{\Omega})$ arising in an exposed nuclear emulsion. Here $R(E_p, \bar{\Omega})$ is just the observed number of recoil protons possessing energies between E_p and E_p+dE_p that are traveling in the solid angle direction between $\bar{\Omega}$ and $\bar{\Omega}+d\bar{\Omega}$.

The angular proton flux $R(E_p,\bar{\Omega})$ is related to the angular flux $\phi(E_n,\bar{\Omega}')$ by the integral equation

$$R(E_p, \bar{\Omega}) = \int_{E_n} \int_{\bar{\Omega}'} \chi_s (E_n \to E_p, \bar{\Omega}' \to \bar{\Omega}) \times \phi (E_n, \bar{\Omega}') \, d\bar{\Omega}' \, dE_n, \tag{4}$$

where $\chi_s (E_n \to E_p, \bar{\Omega}' \to \bar{\Omega})$ is the (n,p) scattering kernel for protons in the emulsion, i.e., the probability that neutrons of energy E_n traveling in direction $\bar{\Omega}'$ give rise to protons of energy E_p traveling in direction $\bar{\Omega}$.

This scattering kernel is particularly simple for $E_n \lesssim 10$ MeV, where (n,p) scattering is isotropic in the center of mass system. Morever, for $m_n \cong m_p$, one has the kinematic constraint

$$E_n = E_p \cos^2 \theta, \tag{5a}$$

where

$$\cos \theta = \bar{\Omega} \cdot \bar{\Omega}' \tag{5b}$$

is the scattering angle in the laboratory system. Consequently, one can write for $E_n \lesssim 10$ MeV

$$\chi_s (E_n \to E_p, \bar{\Omega}' \to \bar{\Omega}) = \frac{N \sigma_H(E_n)}{2\pi E_n} \delta (\bar{\Omega} \cdot \bar{\Omega}' - \sqrt{E_p/E_n}), \tag{6}$$

where N is the hydrogen atom density of the emulsion, $\sigma_H(E_n)$ is the total hydrogen scattering cross section at neutron energy E_n, and δ is the customary notation for the Dirac delta function.

This approach is clearly not as straightforward as that provided by the $^6Li(n,\alpha)^3H$ reaction and careful unfolding calculations will be entailed to provide comparable quantitative data. The properties of Equations (4) and (6) are currently under study in an effort to define an efficient unfolding procedure to extract (E_n, Ω). In addition, deviation from pure S-wave scattering should be taken into account above 10 MeV.

The $^{10}B+n \rightarrow {}^4He + {}^7Li + {}^3H$ Reaction

Nuclear emulsions can be loaded with ^{10}B for observation of the $^{10}B + n \rightarrow {}^4He + {}^7Li + {}^3H$ reaction, having a Q of -0.29 MeV. For $E_n \geq 4$ MeV, all three charged particle reaction products have sufficient range that their respective vector momentum and kinetic energy can be measured with good accuracy. Both E_n and $\vec{p}_n$ can be deduced from these measurements. Emulsions can be loaded in the median plane with specks of glass containing ^{10}B. As in the $^6Li(n,\alpha)$ reaction, scanning is simplified and the probability of a triton or alpha particle leaving the emulsion surface is reduced.

For 4 MeV $\leq E_n \leq$ 10 MeV the reaction does offer a method of measuring the neutron angular flux in a medium. For $E_n \geq$ 10 MeV the situation is complicated by competition with $^{10}B(n,n'd2\alpha)$, and this problem needs to be carefully evaluated.

DATA NEEDS FOR MEASURING ANGULAR NEUTRON FLUX WITH NUCLEAR EMULSIONS FOR NEUTRONS $\leq$ 10 MeV

Fortunately, the n-p scattering cross section is well known in the full energy range of neutrons for fusion-type reactors, but at the higher energies there are competing reactions with other nuclides in the emulsion that produce tracks of charged particles that can be confused with recoil protons. The principal isotopes together with their atomic densities in the emulsion are given in Table II. This table also gives approximate Q values of (n,p) and (n,α) reactions for these nuclides together with some approximate values of the macroscopic cross sections for these reactions in the emulsion for $\leq$ 14 MeV neutrons. The last column gives the ratio of the macroscopic cross section for n,p scattering in hydrogen to the (n,p) or (n,α) reactions. A ratio of 100 signifies that there would be a background contribution of 1 %. Table II indicates that the reaction which would be most troublesome is $^{16}O(n,\alpha)$. If the α track were confused with a track of a recoil proton, it would be at a proton energy four times lower (α particles and protons with the same velocity have the same range). Knowledge of the differential cross section for this reaction as a

Table II
Atomic Density of Principal Nuclides in Nuclear Emulsions;
Q-Valves, and Macroscopic Cross Sections of Some Neutron Induced Reactions at ∿14 MeV

		n,p Reactions		n,α Reactions		
Nuclide	Atoms*/cm³	Q(MeV)[Δ]	Σ(cm⁻¹)[+]	Q(MeV)[Δ]	Σ(cm⁻¹)[+]	Σ n,p in ^{1}H / Σ n,x in nuclide
^{107}Ag	5.3×10^{21}	+0.75		+4.6		
^{109}Ag	4.8×10^{21}	-0.33	$\sim7.2\times10^{-5}$			∿290
				+3.6	$\sim1.8\times10^{-4}$	∿120
^{79}Br	5.15×10^{21}	-0.62				
				+1.8	$\sim6.7\times10^{-5}$	∿310
^{81}Br	4.9×10^{21}	-0.65				
				+0.63	$\sim5\times10^{-4}$	∿ 40
^{12}C	1.4×10^{22}	-12.6	$\sim2.8\times10^{-5}$			∿750
				-5.7		
^{1}H	3.2×10^{22}	(Elastic Scattering)	2.1×10^{-2}			1
^{16}O	9.3×10^{21}	-9.6	$\sim4.7\times10^{-4}$			∿ 45
				-2.2	$\sim2.8\times10^{-3}$	∿ 8
^{14}N	3.2×10^{21}	0.63	$\sim2.5\times10^{-4}$			∿ 85
			[$\sim1.5\times10^{-4}$ for (n,np)]			∿140
				-0.16	$\sim3.2\times10^{-4}$	∿ 66

* W. H. Barkas, Nuclear Research Emulsions, Vol. 1, p. 70, Academic Press (1963).
Δ V. J. Ashby and H. C. Catron, "Tables of Nuclear Reaction Q-Valves," UCRL-5419 (1959).
\+ D. I. Garber and R. R. Kinsey, "Neutron Cross Sections," Vol. 2, BNL-325 (1976).

function of neutron energy in the region of 14 MeV and higher is needed.

Table II is intended as a guide to the problem of using n,p scattering in emulsions to evaluate the neutron angular flux up to ∿ 20 MeV or even higher. Very little data for any of these reactions at the required accuracy is available to properly assess emulsion background problems in the energy region from 10 to 40 MeV.

As stated in Paragraph 3 above, the $^{10}B(n,t2\alpha)$ and the $^{10}B(n,n'd2\alpha)$ reactions need to be much better understood before the feasibility of using the $^{10}B(n,t2\alpha)$ reaction to give knowledge of the neutron angular flux above 10 MeV can be evaulated.

CONCLUSIONS

If radiation damage to fusion reactor components is to be properly understood, materials must be tested in environments where neutron fluences in the energy region above 10 MeV can be measured. Due to scattering in the materials making up the environment, in-situ methods of measuring neutron angular flux are needed. Nuclear emulsions offer a promising approach for neutrons up to ∿ 20 MeV or higher, but various neutron induced reactions occuring in the emulsion need to be more accurately known so that background corrections can be properly applied.

REFERENCES

1. A. Fabry, G. DeLeeuw, and S. DeLeeuw, "The Secondary Intermediate-Energy Standard Neutron Field at the MOL-ΣΣ Facility," Nucl. Technol. 25, 340 (1975).
2. J. W. Rogers, Y. D. Harker, and D. A. Millsap, "The Coupled Fast Reactivity Measurement Facility (CFRMF)", Proceeding of the IAEA Consultants' Meeting on Integral Cross Section Measurements in Standard Neutron Fields, INDC(NDS)-81/L+DOS, IAEA, Vienna (1976).
3. R. Gold, "Neutron Spectrometry for Reactor Applications: Status, Limitations and Future Directions", 1st ASTM-EURATOM Symposium on Reactor Dosimetry, Petten, Netherlands (1975).
4. P. W. Benjamin, C. D. Kemshall, and J. Redfearn, "The Use of a Gas-Filled Spherical Proportional Counter for Neutron Spectrum Measurements in a Zero Power Fast Reactor", AWRE Report No. NR2/64 (1964).
5. R. Booth and H. H. Barshall, "Tritium Target for Intense Neutron Source", Nucl. Inst. and Meth. 99, 1 (1972).
6. A. N. Goland, C. L. Snead, D. M. Parkin, and R. B. Theus, "Use of Li(d,n) Neutrons for Simulation of Radiation Effects in Fusion Reactors", IEEE Trans. Nucl. Sci. NS-22, 1776 (1975).

7. J. H. Roberts and F. E. Kinney, "Measurement of Fast Neutron Energies by Observation of ^{6}Li Glass Specks", Review of Sci. Instr. 28, 610 (1957).
8. G. R. Keepin and J. H. Roberts, "Measurement of Fast Neutron Energies by Observation of $^{6}Li(n,\alpha)^{3}H$ in Photographic Emulsions", Rev. Sci. Instru. 21, 163 (1950).
9. T. Iijima and S. Nomoto, "Measurement of Anisotropic Fast-Neutron Spectrum with Nuclear Emulsion", Nucl. Sci. Engng. 22, 102 (1965).
10. G. M. Frye and J. H. Gammel, "$^{10}B(n,t2\alpha)$ and $^{10}B(n,dn'2\alpha)$ Reactions for 6-20 MeV Neutrons", Phys. Rev. 103, 328 (1956).

CONF-770523-3

Development of a Spectrometer for the Measurement of (n,xp), (n,xd), and (n,xα) Cross Sections, Angular Distributions and Spectra at E_n = 15 MeV*

S. M. Grimes, R. C. Haight and J. D. Anderson
Lawrence Livermore Laboratory, Livermore, California

and

K. R. Alvar and R. R. Borchers
University of Wisconsin, Madison, Wisconsin

ABSTRACT

A spectrometer to measure neutron-induced charged-particle producing reactions has been developed and yields data with greatly improved signal-to-background ratios. It consists of a magnetic quadrupole lens which focusses the charged particles onto a silicon surface barrier detector or a two-detector telescope which is more than 2 meters from the sample being irradiated. The efficiency of the spectrometer is calibrated experimentally and depends only on values for the (n,p) elastic cross section and the stopping power of polyethylene. Further development is underway to replace the surface-barrier ΔE counter with a proportional counter of larger area. This detector, conbined with a larger E counter (surface barrier) could increase the effective solid angle by a factor of five.

The results for (n,xp), (n,xd) and (n,xα) cross sections are summarized for the eight target materials studied so far. Measurements of the charged particle spectra have established that cross sections for production of protons below 2.5 MeV are significant for some targets; in fact protons as low as 800 keV have been detected from aluminum. These low energy protons would be quite difficult to measure with conventional counter telescope spectrometers.

INTRODUCTION

Cross sections and spectra for neutron-induced charged-particle producing reactions are important in estimating materials damage effects from neutron bombardments. Two aspects of this damage, nuclear transmutation and hydrogen and helium production, are direct functions of the cross sections for (n,xp), (n,xd) and (n,xα) reactions. An additional factor in damage estimates, the energy distribution of primary recoil atoms from the lattice, is related to the spectra and angular distributions of particles emitted in neutron-induced reactions. In this context, alpha-

*Work performed under the auspices of the U.S. Energy Research and Development Administration, W-7405-Eng-48.

particle angular distributions and spectra are important because the large alpha particle mass causes more energetic recoil atoms than neutron or proton emissions.

Radiochemical measurements can supply angle- and emission-energy integrated cross sections for many of these reactions. Because not all of the nuclei reached by charged particle emission are unstable, however, some cross sections must be measured using another technique. In addition, the radiochemical measurements are less useful in determining cross section systematics for neighboring nuclei, since without data differential in angle or energy, it is more difficult to determine the reaction mechanism involved.

Farrar and co-workers[1] have developed a technique to measure the helium produced in (n,xα) reactions. After a period of irradiation, the samples are analyzed for helium content by a mass spectrometer. This method appears not feasible for measuring hydrogen production, however.

Direct measurement of the charged particles produced is an alternative procedure. If such measurements are to extend to low emission energies, however, thin targets are required. Backgrounds caused by the interaction of neutrons or gamma rays with the detector or reaction chamber may then overwhelm the signal produced by the target of interest. Moving the detector farther from the neutron source permits additional shielding to be placed between detector and neutron source, but the solid angle is reduced at the same time.

EXPERIMENTAL TECHNIQUES

To reduce the background we move the solid state detectors 2 to 4 meters away from the target and the source. Then to increase the solid angle for detecting charged particles, we interpose a magnetic quadrupole lens between the target and the detectors. Considerable shielding can be placed between the neutron source and the detector in this arrangement. An additional advantage of the quadrupole lens is its directionality; that is, when it is adjusted to bring particles produced in the target to a focus on the detector, particles of the same energy produced in the reaction chamber are focussed away from the detector.

The original version of this spectrometer[2] utilized a quadrupole doublet, but this lens has now been replaced by a quadrupole triplet,[3] which has better transport properties and a higher field gradient.

Neutrons were produced by the Lawrence Livermore Laboratory rotating target neutron source. Beam currents of between 15 and 20 mA of 400 keV deuterons impinged on a rotating tritiated-titanium disc to produce 15-MeV neutrons with the T(d,n) reaction. Because of the thin targets used in these measurements, a high source strength was required. Typical intensities were about 3×10^{12} neutrons/sec into 4π steradians.

Figure 1 is a diagram of the spectrometer and neutron source. The large mass of the quadrupole and associated shielding made it convenient to change reaction angles by sliding the entire assembly on a track rather than rotating it about the source; thus, the central axis of the spectrometer is located 5 cm from the position of the neutron source, denoted by the circled numbers on the figure, and is oriented perpendicular to the beam direction. Changes in reaction angle are made by sliding the assembly relative to the neutron source so that the radiator foil is at various angles between 0° and 78° to the deuteron beam, which correspond to reaction angles 90 ± ∞ for the (n, charged particle) reaction.

For neutrons produced from the T(d,n) reaction induced by 400 keV deuterons, such changes result in a change in average neutron energy between 15.1 and 14.6 MeV as the reaction angle is changed.

The quadrupole transports particles of a given momentum from a specific point on the target to a specific point on the detector. Integrating over both these areas gives an efficiency function with a finite energy width. For the targets and detectors used in the present measurements, the peak had a width ΔE/E of about 35 , full-width at half-maximum.

Absolute values for the efficiency function at each gradient setting were determined by measuring the proton spectrum from a stopping target of polyethylene. This spectrum may be calculated from the incident neutron flux, the n-p elastic scattering cross section and the stopping power of polyethylene. Comparison of the observed spectrum with the calculated one yields the efficiency of the spectrometer.

In principle, the efficiency for other particles could be deduced from that for protons, since the trajectories in the magnetic fields will be functions of Z^2/ME, where Z is the charge and M and E the mass and energy of the particle. Thus, the efficiency for deuterons should peak at an energy half as large as that for protons and that for alpha particles at the same energy as that for protons. To check this, efficiency measurements were carried out with a CD_2 target as well as a CH_2 target. Over most of the energy range, the two measurements yielded consistent results. For high energy protons, the small pulse height in the ΔE counter caused some loss of coincidence efficiency (~20) in the counter telescope. For this reason, the deuteron efficiency measurement was shifted in energy and used in analyzing alpha particle data, while proton and deuteron data were reduced using the measured proton or deuteron efficiency, respectively.

To cover the charged-particle energy range 1 to 14 MeV, measurements at nine field gradient settings are usually required. Figure 2 shows the result of one such measurement for the $^{27}Al(n,xp)$ reaction. The open circles denote the results of the measurement with the aluminum target in place; the x's show the results of a background measurement. Each of these two measurements was made in about forty minutes. The solid line marked "acceptance" gives the measured efficiency (= product of counter efficiency and the effective solid angle of the quadrupole). Note

the favorable signal to background ratio even at a proton energy as low as 1.5 MeV.

RESULTS AND DISCUSSION

Data have been obtained for (n,xp), (n,d) and (n,xα) reactions on ^{27}Al, ^{46}Ti, and ^{48}Ti;[4] on ^{51}V and ^{93}Nb;[5] on ^{63}Cu and ^{65}Cu;[6] and on stainless steel 304 and 316.[7] Angle integrated proton and deuteron spectra are shown for ^{63}Cu and ^{93}Nb targets in Figs. 3 and 4.

An impressive feature of the cross section data is that the proton spectra for some of the targets extend far below the Coulomb barrier (Al, ^{46}Ti and ^{63}Cu) while for other targets (^{48}Ti and ^{93}Nb) the spectrum below the Coulomb barrier falls rapidly. This difference is related to the importance of the (n,n'p) reaction for targets for which a sub Coulomb barrier peak is observed. In these targets, the neutron binding energy is larger in magnitude than the corresponding proton binding energy, thus, excited levels of the target nucleus within a given energy range have no neutron decay width but can emit a sub Coulomb barrier proton. This width is expected to be small, but since the only other available channel is gamma decay, proton decay will occur in many cases. A similar sub Coulomb barrier decay is possible in the alpha particle channel, if the alpha particle binding energy is less than that for protons and neutrons. Some indication that second stage alpha decay at present is found in the spectra for ^{46}Ti, ^{63}Cu and ^{93}Nb. Apparently, the small difference between B_α and B_p in these nuclei is not in general sufficient to compensate for the larger Coulomb barrier for alpha particles. Evidence that these sub barrier particles are not due to some unknown spectrometer background is found in the absence of the low energy peak for ^{48}Ti[4] and for the ^{51}V(n,xα)[5] reaction, where the binding energies are such that the (n,n'p) reaction on ^{48}Ti and (n,n'α) reaction on ^{48}Ti and ^{51}V should have small cross sections.

Integrated cross sections for the reactions studied are listed in table 1. For these nuclei, large charged particle cross sections appear to be correlated with large compound nuclear contributions. Deuteron production cross sections are small for all the nuclei studied to date, and proton and alpha particle cross sections are small for nuclei with small neutron binding energies (i.e., those which are neutron-rich). Large variations (a factor of three or more) occur between proton and alpha production cross sections for various isotopes of the same element.

The development of this spectrometer has enabled charged particle spectra produced by neutron-induced reactions at E_n 15 MeV to be measured over the range 1 to 15 MeV in emission energy. The signal-to-background ratio is increased significantly through use of the quadrupole lens between target and detector, with the result that charged particles with energies as low as 1 MeV could be detected. Data obtained to date indicate that for

Table I

Summary of Proton, Deuteron and Alpha Particle Cross Sections Measured with the Magnetic Quadrupole Spectrometer at 15 MeV Incident Neutron Energy. The errors on the proton, deuterons and alpha production cross sections are typically ± 12 %, ± 40 %, and 16 % respectively.

Target	σ(n,xp)(mb)	σ(n,d)(mb)	σ(n,xα)(mb)
^{27}Al	405	19	121
^{46}Ti	669	9	98
^{48}Ti	336	7	33
^{51}V	94	7	17
^{55}Mn	257	8	48
^{63}Cu	273	9	56
^{65}Cu	44	9.8	13.5
^{93}Nb	51 [illegible]	8.5	14

many targets the total charged particle cross section will be significantly underestimated unless the measurements extend to energies below the Coulomb barrier.

Nuclei in the region already investigated have cross sections sufficiently large that the present spectrometer yields acceptable count rates. To extend these measurements to isotopes with smaller cross sections, an increased efficiency would be desirable. Efforts are presently underway to develop a detector telescope of larger area than presently used. A proportional counter would serve as the ΔE detector and a larger area surface barrier detector would be the E detector. These modifications would increase the counting rate by about a factor of five and would allow cross sections as small as a few millibarns to be measured with good signal to background ratios.

REFERENCES

1. H. Farrar IV, D. W. Engel, R. A. Britten and F. R. Hermach, "Fluence Mapping of RINS by He Accumulation and Foil Activation Methods," this Symposium.

2. R. C. Haight, S. M. Grimes, B. J. Tuckey, and J. D. Anderson, UCRL 77151 (Lawrence Livermore Laboratory report, unpublished) 1975.
3. K. R. Alvar, H. H. Barschall, R. R. Borchers, S. M. Grimes, and R. C. Haight, Bull. Am. Phys. Soc. 22, 646 (1977).
4. S. M. Grimes, R. C. Haight and J. D. Anderson, Nucl. Sci. and Eng. 62, 187 (1977).
5. R. C. Haight, S. M. Grimes, and J. D. Anderson, Bull. Am. Phys. Soc. 21, 987 (1976); and to be published.
6. S. M. Grimes, R. C. Haight, J. D. Anderson, K. R. Alvar, and R. R. Borchers, Bull. Am. Phys. Soc. 22, 631 (1977); and to be published.
7. R. C. Haight, S. M. Grimes and J. D. Anderson, Nucl. Sci. and Eng. (in press).

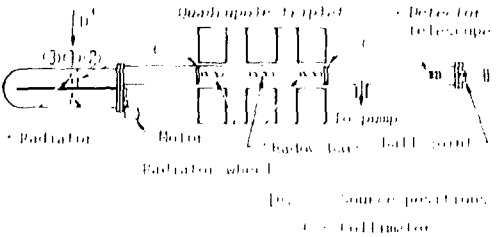

Figure 1 Schematic drawing of the magnetic quadrupole charged particle spectrometer for neutron induced reactions.

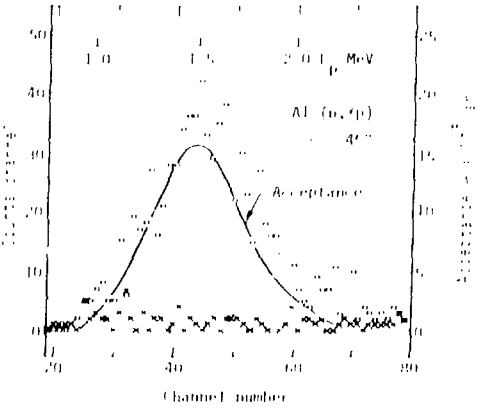

Figure 2 Raw data at one magnet setting for the proton spectrum at 45° from 17 MeV neutron bombardment of Al. The proton production angle was 45° with respect to the incident neutron. The circles denote data with a 2.4 mg/cm² alumina foil in and the ×'s denote background with the foil out. The solid line is the measured acceptance function of the spectrometer.

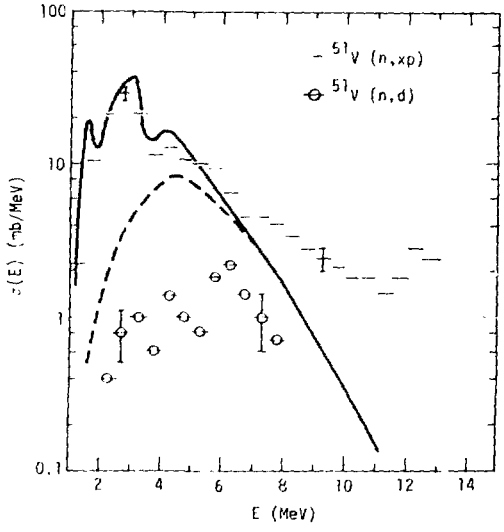

Figure 3. Proton and deuteron spectra from 15-MeV neutron bombardment of ^{51}V. The data are integrated over the angular distribution of emitted particle. The curves are statistical model calculations described in Ref. 5.

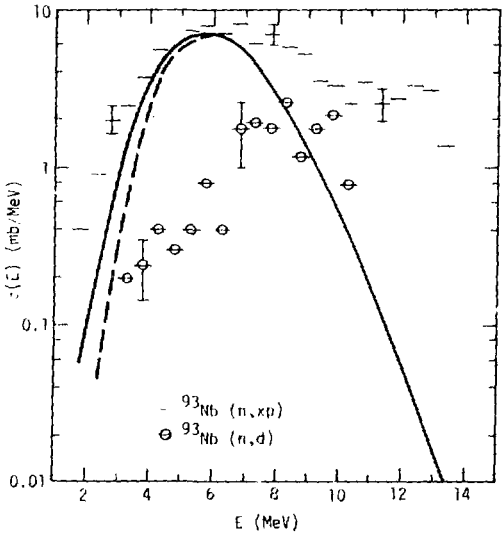

Figure 4. Proton and deuteron spectra from 15-MeV neutron bombardment of ^{93}Nb. The data are integrated over the angular distribution of the emitted particle. The curves are statistical model calculations described in Ref. 5.

Cross Sections for the Nb(n,xn) and Nb(n,x_1) Reactions Between 1 and 20 MeV*

G. L. Morgan and F. G. Perey
Oak Ridge National Laboratory, Oak Ridge, Tennessee 37830

INTRODUCTION

In recent years considerable interest has been shown in using niobium as a structural material in practical fusion reactors. Most conceptual design studies (see, for example, Ref. 1) use the evaluated nuclear data files (e.g., ENDF/B) as the source of basic microscopic cross section data.

The accuracy of the prediction of design criteria such as tritium breeding ratios, radiation damage, and neutron-induced heating is dependent on the accuracy of the evaluated data for energies up to the primary energy of 14 MeV.

The existing experimental data on niobium cross sections have been assembled, evaluated, and supplemented with model calculations by Smith, Guenther, and Whalen[2] to form the most recent data file for this nuclide (ENDF/B-IV, MAT 1189). The purpose of the measurements reported here was to provide data to test some aspects of this evaluated cross-section file in the MeV region. The technique used here has the global testing power of an integral experiment, yet retains a sufficiently differential character to allow localization of discrepancies. Differential cross sections are presented for the Nb(n,xn) and Nb(n,x_1) reactions as a function of the incident neutron energy at an average scattering angle of 129 deg. (lab). The data cover the incident neutron energy range from 1 to 20 MeV. Comparisons are presented with cross sections obtained from the evaluation.

EXPERIMENTAL PROCEDURE

The experimental procedure used in this work has been described in detail elsewhere[3] and is only briefly outlined here. The Oak Ridge Electron Linear Accelerator (ORELA) was used as a white neutron source. The scattering sample was located 47.8 m from the neutron source and consisted of 2678 g of niobium. Details of the sample-detector geometry are shown in Fig. 1. Secondary radiation from the sample was detected by an NE-213 scintillation counter located on the axis of the ring at a position corresponding to an average scattering angle of 129 deg. A shadow bar shielded the detector from the direct neutron beam.

*Research sponsored by the U.S. Energy Research and Development Administration under contract with Union Carbide Corporation.

The energy of the incident neutron was determined by the time after the electron pulse at which the neutron-induced radiation from the sample was detected. Each event in the detector was identified as either a neutron or gamma ray by pulse-shape discrimination techniques. The event was then recorded in a two-parameter array of pulse height versus time-of-flight (one each for secondary neutrons and secondary gamma rays). Backgrounds were determined by measurement with the sample removed. The neutron flux incident on the sample was measured relative to a monitor counter with the NE-213 detector using one-parameter time-of-flight techniques.

DATA REDUCTION

Two methods of data reduction were employed, each intended to make use of the available counting statistics to provide a maximum of information about a particular aspect of the cross section. In the first, the neutron or gamma-ray pulse-height spectra were integrated over intervals of neutron time-of-flight to form pulse-height spectra for specific incident neutron energy ranges. These intervals ranged in width from ΔE_{inc} = 0.25 MeV at E_{inc} = 1 MeV to ΔE_{inc} = 2.5 MeV at E_{inc} = 20 MeV. The pulse-height spectra so formed were then converted to neutron or gamma-ray energy distributions by unfolding with the FERD code[5] using the measured neutron or gamma-ray response functions of the NE-213 detector. These distributions were then normalized to cross sections using the measured neutron flux, average sample-to-detector distance, and sample thickness.

The neutron data were corrected for finite sample effects (multiple scattering and attenuation). The gamma-ray data were corrected for self-absorption in the sample and for attenuation of the incident neutron beam.

The unfolded data described above provide detailed information about the secondary neutron and gamma-ray spectra, but because the unfolding technique requires good statistical accuracy, the data must be binned over rather large incident energy intervals. Therefore, a second type of data reduction, pulse-height weighting,[7] was also used. This technique provided only integral information about the secondary spectra (i.e., total yield and average energy), but because the demands on statistical accuracy are less severe, it allowed better resolution in the incident neutron energy. The finite sample effects described above were also applied to these data.

DISCUSSION

The work reported here provides data to test the evaluated secondary cross sections over a wide range of energies. The experimental resolution in the incident energy is limited only

by the bin width necessary for adequate statistical accuracy. Energy resolution for the secondary spectra is due to the NE-213 detector's pulse height resolution and is rather poor. Because of this inability to completely resolve different contributions to the secondary spectra, results have been obtained only as laboratory cross sections.

The incident neutron energy spread, the secondary energy resolution, and the angular spread are much broader in this measurement than in the more standard types of differential cross-section measurements. This has the advantage of allowing a comprehensive check of the cross sections in a mode that is compatible with the averaging generally used to produce group cross sections for practical applications. However, it complicates and sometimes makes impossible the comparison of the present results with previous measurements. To correctly average over the experimental spreads, one needs a complete prescription for cross sections as a function of incident energy, scattering angle, Q value, etc. The evaluated file provides the information and reflects previous measurements to the extent that the evaluators base their results on existing data.

Secondary neutron and gamma-ray spectra were generated from the evaluation by suitably weighted averages over the incident energy interval and angular spread. The resulting secondary spectra were then smeared by a Gaussian function corresponding to the resolution of the detector.

Several cautions are in order before proceeding to a detailed comparison of evaluation and measurement. The gamma ray emission specified in the evaluation is isotropic. For a medium weight nuclide such as niobium this is undoubtedly very close to the real angular dependence. Thus a comparison of the evaluation with differential measurements taken at 129 deg. checks the gamma ray production data of the evaluation rather well. In the case of the neutron emission spectra, the test may not be as rigorous, especially with respect to the elastic scattering cross sections. Because of the strong anisotropy of the elastic angular distribution with its energy dependent diffraction pattern, a single differential measurement covering a large angular range (the angular resolution function is approximately triangular with a base 28 deg. in width) provides little or no check on the validity of the elastic scattering cross section in the evaluation. However, for neutron emission through processes other than elastic scattering, the situation is much better since most such emissions are only weakly anisotropic, particularly when averaged over the broad incident neutron energies of this experiment.

Figures 2 and 3 show the pulse-height weighting results for the total yield and average energy of gamma rays above E_γ = 0.7 MeV. Figures 4 and 5 show examples of detailed secondary gamma-ray spectra for the wider intervals in incident neutron energy. Figure 2 indicates that the evaluated total yield is generally low, particularly for E_n > 10 MeV. Figure 3 shows the average energy from the evaluation to be 20-30% high over the whole range studied. Reference to Figs. 4 and 5 indicates that the measured and evaluated

spectra generally agree except at the low gamma-ray energies where the differences are pronounced. These comparisons pretty well explain the variation between the total yields (Figs. 2 and 3) as due to discrete gamma-ray transitions at about 0.95 and 1.5 MeV. Reference to the evaluation[1] indicates that for $E_n > 100$ keV the gamma-ray production is based on calculations using the formalism of Howerton and Plechaty[7] as modified by Perkins, Haight and Howerton.[8] This is an empirical formalism based on systematics for $A > 20$. As such, it appears to do a rather good job of estimating the continuum components of the gamma-ray spectra in Figs. 4 and 5. However, the inclusion of discrete gamma-ray transitions would improve the evaluation.

Examples of comparisons between the measured and evaluated neutron emission data are shown in Figs. 6-9. In general, the evaluated neutron emission spectra are in fairly good agreement with the measurements. The worst disagreements are above E_{inc} = 6 MeV (see Figs. 8 and 9) and occur in the region of low secondary energies where the evaluated spectra are systematically low and decrease with energy more rapidly than the measured spectra.

Since the evaluation was prepared several new sets of data[9-11] on emission spectra have been reported. Figs. 10 and 11 show comparisons between the present results, ENDF/B-IV, and curves taken from Refs. 9, 10 and 11. Note that our data and the evaluated curve are averages over broad incident energy ranges while the data of Refs. 9, 10 and 11 have small spreads on the incident energies. In spite of these differences, the comparisons are informative. The measured data sets are generally consistent and show slopes for the non-elastic emission spectra which are distinctly different from the evaluation.

CONCLUSIONS

The evaluation for niobium in ENDF/B-IV has been found to give generally satisfactory agreement with the measurement. Some improvements are suggested by the present work. The gamma-ray production cross sections could be improved by the inclusion of discrete lines. At the higher neutron energies a less pronounced slope and larger magnitude on the non-elastic emission spectra would better represent existing measurements. For the reasons listed previously, the present data do not provide a valid test of the elastic scattering.

Numerical values of the differential cross sections measured in this work are given in the tables of Ref. 12.

ACKNOWLEDGEMENTS

The authors wish to thank J. W. McConnell and J. G. Craven for their assistance with electronics and data acquisition computers and H. A. Todd and the ORELA staff for operation of the accelerator.

Special thanks are due Dr. W. E. Kinney for his help with the multiple scattering corrections.

REFERENCES

1. D.E. Bartine, R.G. Alsmiller, Jr., E.M. Oblow, and F.R. Mynatt, Nucl. Sci. Eng. 53, 304 (1974).
2. A.B. Smith, P.T. Guenther, and J.F. Whalen, Z. Physik 264, 379 (1973).
3. R. Howerton, A. Smith, P. Guenther, and J. Whalen, "Evaluated Neutronic Cross Section File for Niobium," ANL/NDM-6, Argonne National Laboratory (1974).
4. G.L. Morgan and F.G. Perey, Nucl. Sci. Eng. 61, 337 (1976).
5. G.L. Morgan, T.A. Love, and F.G. Perey, Nucl. Instrum. Methods 128, 125 (1975).
6. W.R. Burrus and V.V. Verbinski, Nucl. Instrum. Methods 67, 181 (1969).
7. R. Howerton and E. Plechaty, Nucl. Sci. Eng 32, 178 (1968).
8. S. Perkins, R. Haight, and R. Howerton, Nucl. Sci. Eng. 57, 1 (1975).
9. N.S. Birykov, B.V. Zhuralev, N.V. Kornilov, V.I. Plyaskin, A.P. Rudenko, O.A. Sal'nikov, and V.I. Trykova, Yad. Fiz. 19, 1190 (1974).
10. A.A. Luk'yanov, O.A. Sal'nikov, and E.M. Saprykin, Yad. Fiz. 21, 67 (1975).
11. D. Hermsdorf, S. Sassonoff, D. Seeliger, and K. Seidel, J. Nucl. Energy 27, 747 (1973).
12. G.L. Morgan and F.G. Perey, "Cross Sections for the Nb(n,xn) and Nb(n,x_γ) Reactions Between 1 and 20 MeV," ORNL-TM-5829, Oak Ridge National Laboratory (1977).

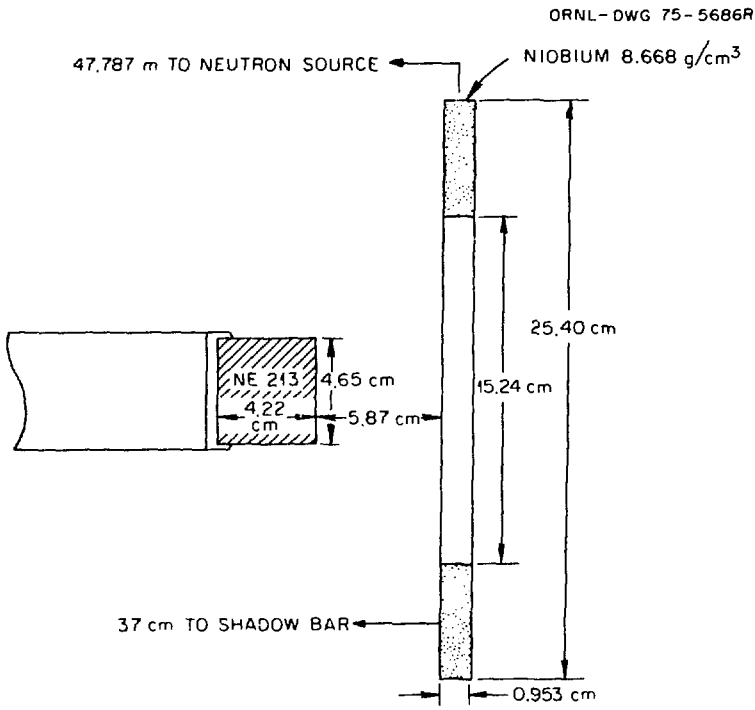

Fig. 1. Schematic diagram showing details of the sample-detector geometry.

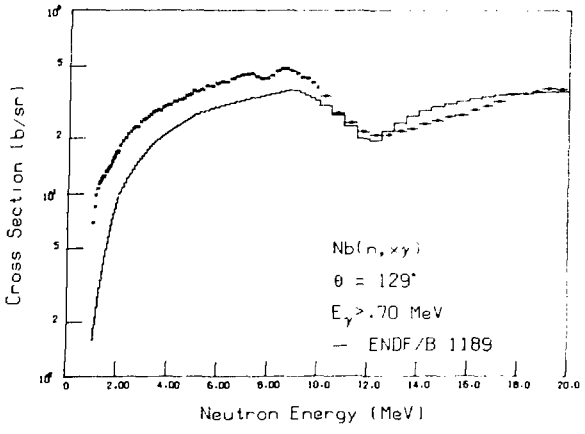

Fig. 2. Total yield for the Nb(n,x·) reaction for $E_{\gamma} > 0.7$ MeV as a function of the incident neutron energy. Error bars shown in this and succeeding figures do not include a 10% uncertainty in absolute normalization.

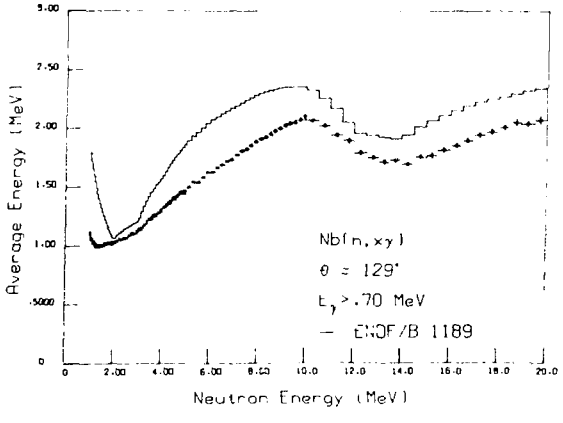

Fig. 3. Average secondary gamma-ray energy as a function of incident neutron energy.

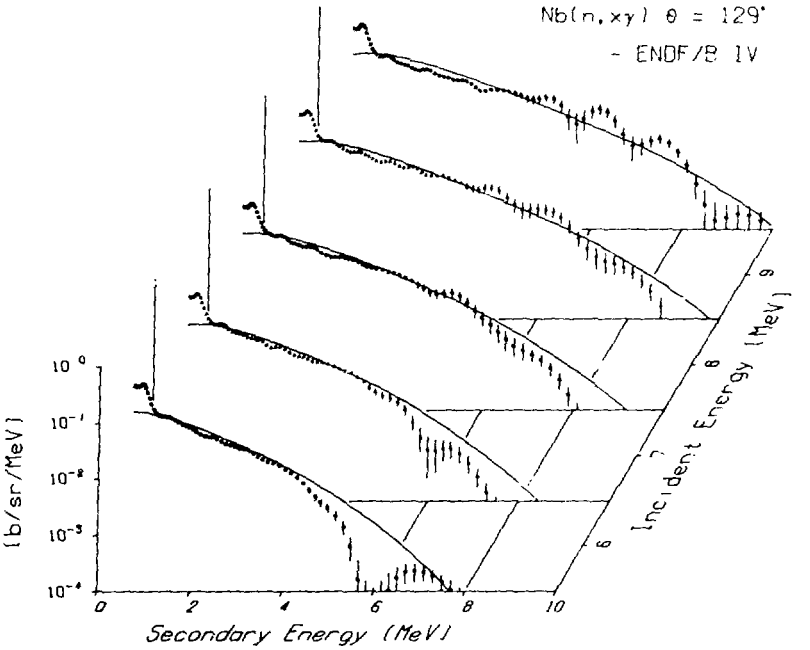

Fig. 4. Secondary gamma-ray spectra for incident neutron energies between 5 and 10 MeV.

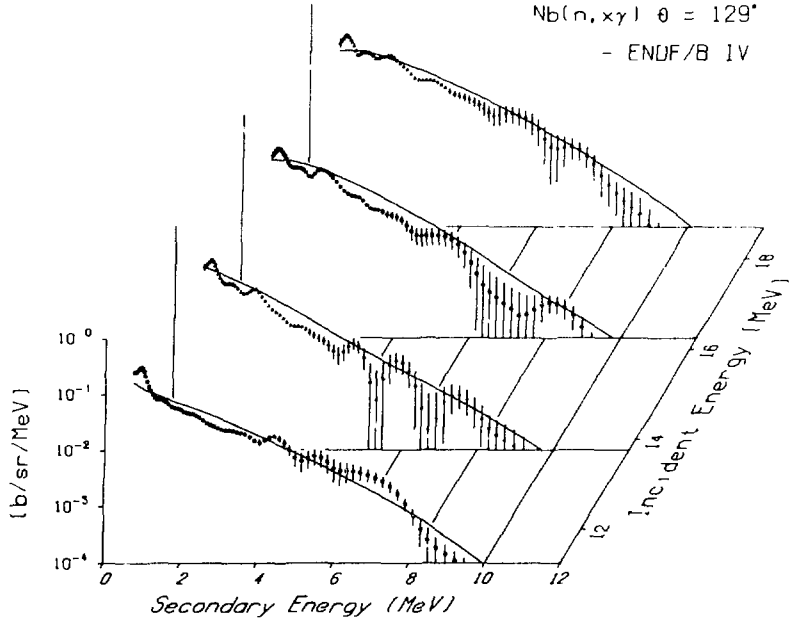

Fig. 5. Secondary gamma-ray spectra for incident neutron energies between 10 and 20 MeV.

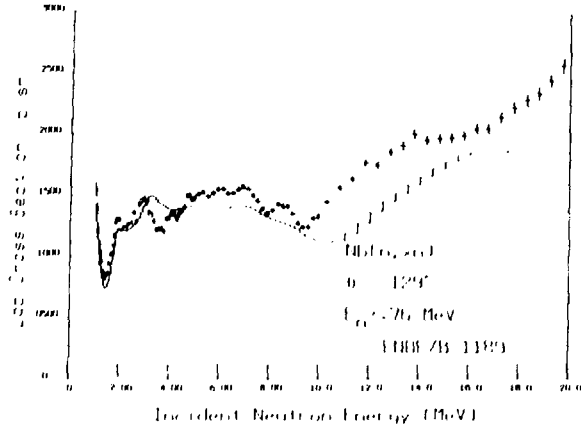

Fig. 6. Total yield at 120° for the Nb(n,xn) reaction as a function of incident neutron energy for secondary neutron energies of 0.76 MeV and above

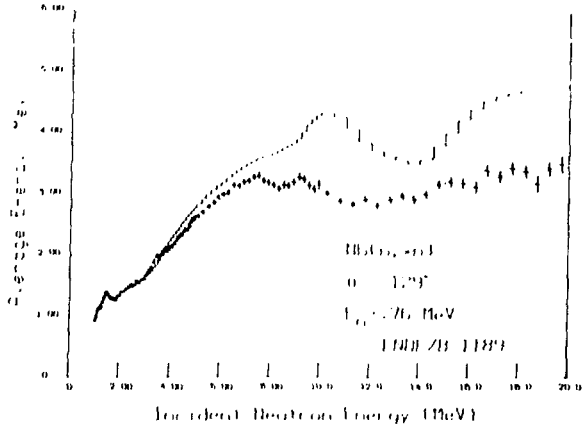

Fig. 7. Average secondary neutron energy as a function of the incident neutron energy.

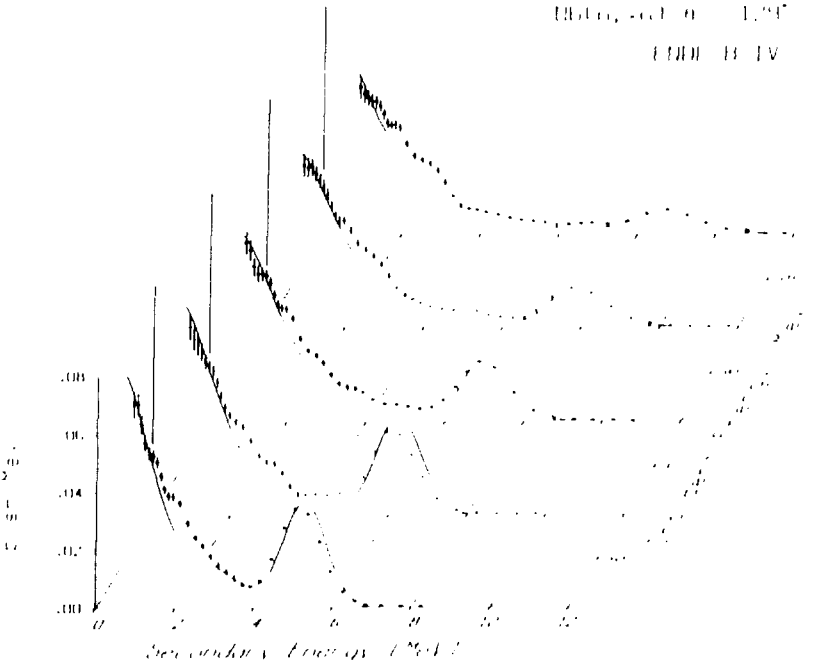

Fig. 8. Secondary neutron spectra for incident neutron energies between 5 and 10 MeV

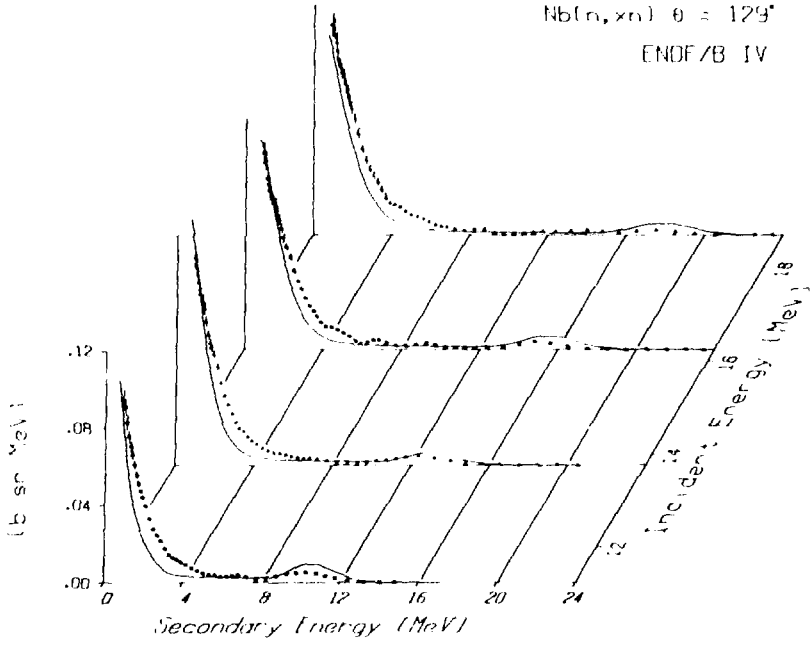

Fig. 9. Secondary neutron spectra for incident neutron energies between 10 and 20 MeV.

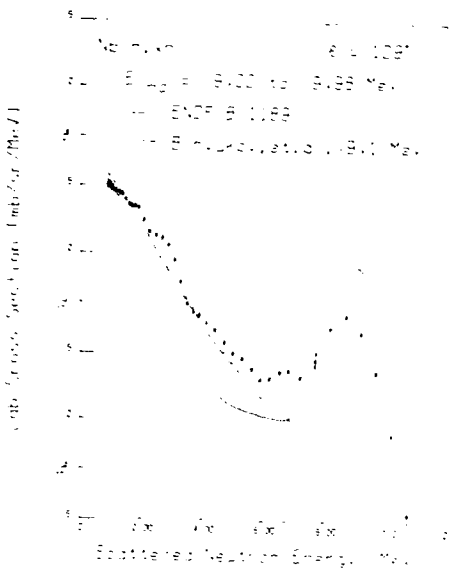

Fig. 10. Secondary neutron spectrum from this work, E_{inc} = [illegible] Me., data from Ref. [illegible] E_{inc} = [illegible] Me., and from ENDF/B-[illegible], E_{inc} = [illegible] Me.. The curve from Ref. [illegible] is their values of the total cross section divided by 4π.

Fig. 11. Secondary neutron spectrum from this work, E_{inc} = 12.5-15 Me., data from Ref. [illegible] E_{inc} = 14.6 Me., Ref. [illegible] E_{inc} = [illegible] Me., and from ENDF/B-[illegible], E_{inc} = 12.5-15 MeV. The curves from Refs. [illegible] and [illegible] are their values divided by 4π.

SESSION IV

MATERIALS DAMAGE STUDIES

Chairman: T. C. Reuther, Jr., DMFE, ERDA

MFE Damage Analysis Program Nuclear Data Needs*

D. G. Doran
Hanford Engineering Development Laboratory

R. R. Heinrich, and L. R. Greenwood
Argonne National Laboratory

H. Farrar IV
Atomics International

ABSTRACT

Nuclear data needs for the ERDA-DMFE Damage Analysis and Fundamental Studies program fall into three categories: 1) reaction cross sections for dosimetry. 2) cross sections for transmutation reactions, especially those producing helium and hydrogen, and 3) differential scattering cross sections and emitted particle angular and energy distributions for calculating primary recoil spectra. The ENDF/B Dosimetry File must be expanded and extended to 30-40 MeV (specific reactions are given); integral testing of cross sections in high energy fields is especially needed. Gas production files must also be extended to 30-40 MeV although high accuracy is not generally needed. Direct measurements of accumulated helium can be made. Cross sections must be adequate in the 15-40 MeV range to estimate solid transmutant concentrations as well. Sensitivity studies are desirable to assess needed accuracies of cross sections and emission spectra for damage calculations. For this application, it may be that theoretical calculations, supplemented by a limited experimental program, will suffice.

* Work supported by United States Energy Research and Development Administration.

MFE Damage Analysis Program Nuclear Data Needs

D. G. Doran
Hanford Engineering Development Laboratory

R. R. Heinrich, and L. R. Greenwood
Argonne National Laboratry

H. Farrar IV
Atomics International

INTRODUCTION

The ERDA Division of Magnetic Fusion Energy (DMFE) damage analysis program is to be coordinated by a recently established Task Group on Damage Analysis and Fundamental Studies (DAFS). The scope of this program includes:

a) development of procedures for characterizing neutron environments of test facilities and fusion reactors,
b) theoretical and experimental investigations of the influence of irradiation environment on damage production, damage microstructure evolution, and mechanical and physical property changes,
c) identification and, where appropriate, development of essential nuclear and materials data,
d) development of a methodology based on damage mechanisms for correlating the mechanical behavior of materials exposed to diverse test environments and projecting this behavior to MFR environments.

This task group, formed in October 1976, is currently developing a long range program plan, one segment of which recognizes that a responsible definition of nuclear data needs must rest on reasonable sensitivity analyses. Such analyses have not yet been performed, generally speaking, hence this paper must necessarily lack specificity.

A word about the task group is in order. It comprises four subtask groups in the areas of environmental characterization, damage production, damage microstructure evolution, and mechanical behavior. Task group members and subtask group chairmen are presented in Table 1. The task group has just completed a first draft of the aforementioned program plan, which is now under review by the Fusion Materials Coordinating Committee.

This paper is focused on nuclear data needs in the damage analysis program. The scope of the program includes charged particle as well as neutron irradiation test facilities and some data needs relative to the former will be discussed.

A sometimes convenient dichotomy exists between neutron data below and above ∿15 MeV. Only data below 15 MeV are needed for currently projected fusion reactors. If a suitable materials test facility were available now or would be available in the near

Table 1

DMFE Task Group on Damage Analysis and Fundamental Studies

Task Group Members

D. G. Doran, HEDL, Chairman
H. Farrar, IV, AI
A. N. Goland, BNL
R. R. Heinrich, ANL
F. V. Nolfi, ANL
G. R. Odette, UC Santa Barbara
D. M. Parkin, LASL
T. C. Reuther, Jr., ERDA-DMFE
M. T. Robinson, ORNL
F. A. Smidt, Jr., NRL
R. R. Vandervoort, LLL
P. Wilkes, Univ. Wisconsin

Subtask Groups

A. Environmental Characterization, R. R. Heinrich, Chairman
B. Damage Production, M. T. Robinson, Chairman
C. Damage Microstructure Evolution, G. R. Odette, Chairman
D. Mechanical Behavior, R. R. Vandervoort, Chairman

Joint subtask group -- links Damage Analysis and Fundamental Studies task group with Alloy Development and Irradiation Performance task groups; F. V. Nolfi, Chairman

future, higher energy data would not be needed. A "suitable" facility utilizing the D-T reaction would have a flux above 10 MeV exceeding 10^{14}n/cm^2 sec over a volume of at least several liters. In the absence of such a facility it is considered imperative to make use of existing high energy sources. Highest fluxes are currently obtainable from 30-40 MeV deuteron beams incident on Be targets. Furthermore, the major proposed materials irradiation test facility, featuring a relatively high flux of high energy neutrons in a relatively large test volume, will utilize a 35 MeV deuteron beam incident on a flowing lithium target. These so-called stripping sources produce a broad neutron spectrum which peaks in the neighborhood of 40% of the deuteron energy but extends to about the deuteron energy. Hence certain nuclear data are needed by the MFE program in the 15-30 MeV range but only, strictly speaking, on an interim basis until a fusion materials test reactor is built.

ENVIRONMENTAL CHARACTERIZATION

The subtask on environmental characterization includes in its scope both theoretical and experimental determinations of neutron fields. Data needs for neutronics calculations were reviewed earlier by Dudziak,[1] so only the latter will be

emphasized here.

The objective of neutron dosimetry development in the DMFE program is to provide the capability of characterizing a variety of test and fusion reactor neutron environments in terms of flux, fluence, and the neutron energy distribution averaged over the duration of the irradiation. This capability is required for 1) the analysis of radiation effects data, and 2) the evaluation of neutron irradiation facilities for DMFE applications. The initial emphasis is on characterizing those test environments currently being used for bulk and surface radiation effects studies. Neutron fluences in the former range from $10^{[illegible]}$ to 10^{22} n/cm^2, while in the latter they may be as low as $10^{[illegible]}$.

Multiple foil fluence-spectrum unfolding techniques[1] are expected to provide the bulk of the dosimetry data for near-term MFE applications. The term "multiple foil analysis" (MFA) will be used generically for the procedure in which a number of identifiable reaction products are detected; the products may be radioactive or stable and may be detected by gamma counting, mass spectrometry, track recording, etc. From the unique energy dependence of each reaction cross section, the fluence and energy spectrum can be unfolded. The fluence results are the most accurate because they are derived from spectrum-averaged cross sections. Spectrum definition, on the other hand, depends upon the accuracy of the energy dependent cross sections, the number and sensitivity spread of the reactions used, and the appropriateness of the initial estimate of the spectrum to be measured. The advantages of MFA are 1) it is adaptable to fluxes ranging from 10^9 to 10^{14} n/cm^{2}s and to fluences from 10^{14} to $10^{[illegible]}$ n/cm^2, 2) geometry constraints are minimal, and 3) it can be made compatible with hostile chemical and thermal environments.

The energy resolution of MFA is not great, hence instrumental dosimetry techniques such as time-of-flight (T-O-F) and ^{6}Li spectrometry are also used, where applicable, to aid in characterizing neutron fields. The T-O-F method requires accurate scattering and reaction cross sections of carbon in order to calculate detector efficiencies above 15 MeV; however, accurate calibrations can be obtained from the well known hydrogen scattering cross section. The ^{6}Li coincidence spectrometry technique requires accurate knowledge of the ^{6}Li(n,α)T reaction. This cross section is also well known in the energy range over which the technique is applicable.

Current MFA procedures emphasize radiometric analysis of activated foils. Most of the reactions of current interest for DMFE application are given in Table 2. As indicated, data are available for some of the reactions up to 30 MeV, but the accuracy is insufficient in many cases. However, almost no data exist above 30 MeV. Reactions currently included in the ENDF/B-IV Dosimetry Cross Section file[3] are included here for convenience in Table 3. It is important to recognize that this file was evaluated primarily for fission reactor applications for which the emphasis is below 10 MeV (although limited data testing has

Table 2

Status of Cross Sections Used for MFE Dosimetry

Reaction	Estimated Energy Response (MeV)	Half-Life of Reaction Product	Desired Accuracy/ Energy Range (5-8%) 0-14 MeV	(10-20%) 14-30 MeV
^{232}Th(n,f)FP	6 50	T	A*	A
^{235}U(n,f)FP	0-50	T	A*	A
^{237}Np(n,f)FP	0.5-50	T	A*	A
^{238}U(n,f)FP	1.5-50	T	A*	A
^{45}Sc(n,γ)^{46}Sc	0-10	83.8 d	A*	-
^{58}Fe(n,γ)^{59}Fe	0-10	44.6 d	A*	-
^{59}Co(n,γ)^{60}Co	0-10	5.27 y	A*	-
^{197}Au(n,γ)^{198}Au	0-10	64.8 h	A*	-
^{238}U(n,γ)^{239}Np	0-6	2.35 d	A*	-
^{46}Ti(n,p)^{46}Sc	4-25	83.8 d	A*	X
^{54}Fe(n,p)^{54}Mn	3-23	312 d	A*	X
^{56}Fe(n,p)^{56}Mn	4-20	2.58 h	A*	X
^{59}Co(n,p)^{59}Fe	5-20	44.6 d	A	X
^{58}Ni(n,p)^{58}Co	2-20	71 d	A*	X
^{60}Ni(n,p)^{60}Co	3-25	5.27 y	A*	X
^{27}Al(n,α)^{24}Na	8-20	15.0 h	A*	X
^{54}Fe(n,α)^{51}Cr	1-20	27.7 d	A	X
^{59}Co(n,α)^{56}Mn	5-25	2.58 h	A*	X
^{63}Cu(n,α)^{60}Co	6-25	5.27 y	A*	X
^{45}Sc(n,2n)^{44m}Sc	12-30	2.44 d	A	A
^{58}Ni(n,2n)^{57}Ni	12-35	36 h	A*	X
(n,3n)^{56}Ni	22-50	6.1 d	-	X
^{59}Co(n,2n)^{58}Co	10-30	71 d	A*	X
(n,3n)^{57}Co	20-40	272 d	-	X
(n,4n)^{56}Co	30-50	77.3 d	-	-
^{89}Y(n,2n)^{88}Y	12-30	106.6 d	A	A
(n,3n)^{87}Y	22-40	80 h	-	A
^{90}Zr(n,2n)^{89}Zr	12-30	78.4 h	A	X
(n,3n)^{88}Zr	22-40	82.6 d	-	X
^{93}Nb(n,2n)^{92m}Nb	9-20	10.13 d	A	X
^{107}Ag(n,2n)^{106m}Ag	10-30	8.3 d	A	A
(n,3n)^{105}Ag	18-40	40.8 d	-	A
^{169}Tm(n,2n)^{168}Tm	8-30	93 d	A	A
(n,3n)^{167}Tm	15-35	9.3 d	-	A
(n,4n)^{166}Tm	26-50	7.9 h	-	A
^{191}Ir(n,2n)^{190}Ir	8-30	11.8 d	A	A
(n,3n)^{189}Ir	14-40	13.1 d	-	A
(n,4n)^{188}Ir	24-50	41.5 h	-	A
^{193}Ir(n,2n)^{192}Ir	8-30	74.2 d	A	A

Table 2 (Continued)

Reaction	Estimated Energy Response (MeV)	Half-Life of Reaction Product	Desired Accuracy/ Energy Range (5-8%) 0-14 MeV	(10-20%) 14-30 MeV
$^{197}Au(n,2n)^{196}Au$	8-30	6.2 d	A	A
$(n,3n)^{195}Au$	15-35	183 d	-	A
$(n,4n)^{194}Au$	23-45	39 h	-	A
$(n,5n)^{193}Au$	35-50	18 h	-	-
$^{203}Tl(n,2n)^{202}Tl$	8.5-30	12.5 d	A	A
$(n,3n)^{201}Tl$	16-40	3.0 d	-	A
$(n,4n)^{200}Tl$	23-50	26.1 h	-	A
$^{238}U(n,2n)^{237}U$	6.5-25	6.75 d	X	X

T) ^{140}Ba(12.8 d), ^{95}Zr(65 d), ^{137}Cs(30.0 y) are typical monitors.
A) Denotes data available; asterisk indicates reaction currently included in ENDF/B Dosimetry File.
X) Denotes data not available.

Table 3

Contents of ENDF/B-IV Dosimetry File

Isotope/Reaction	MAT	Isotope/Reaction	MAT
$^{6}Li(n,total\ He)$	6271	$^{59}Co(n,\alpha)$	6199
$^{10}B(n,total\ He)$	6273	$^{58}Ni(n,2n)$	6419
$^{23}Na(n,\gamma)$	6156	$^{58}Ni(n,p)$	6419
$^{27}Al(n,p)$	6193	$^{60}Ni(n,p)$	6420
$^{27}Al(n,\alpha)$	6193	$^{63}Cu(n,\gamma)$	6411
$^{32}S(n,p)$	6407	$^{63}Cu(n,\alpha)$	6411
$^{45}Sc(n,\gamma)$	6415	$^{65}Cu(n,2n)$	6412
$^{46}Ti(n,p)$	6421	$^{115}In(n,n')$	6406
$^{47}Ti(n,np)$	6422	$^{115}In(n,\gamma)$	6416
$^{47}Ti(n,p)$	6422	$^{127}I(n,2n)$	6414
$^{48}Ti(n,np)$	6423	$^{197}Au(n,\gamma)$	6283
$^{48}Ti(n,p)$	6423	$^{232}Th(n,f)$	6296
$^{55}Mn(n,2n)$	6197	$^{232}Th(n,\gamma)$	6296
$^{54}Fe(n,p)$	6417	$^{235}U(n,f)$	6261
$^{56}Fe(n,p)$	6410	$^{238}U(n,f)$	6262
$^{58}Fe(n,\gamma)$	6418	$^{238}U(n,\gamma)$	6262
$^{59}Co(n,\gamma)$	6199	$^{237}Np(n,f)$	6263
$^{59}Co(n,2n)$	6199	$^{239}Pu(n,f)$	6264

been performed above 10 MeV[4,5]). In Table 4 are listed the reactions proposed recently by the Cross Section Evaluation Working Group (CSEWG) Dosimetry Task Group for addition to the ENDF/B Dosimetry Cross Section file. They are divided into immediate and long-range needs; some are intended only for high energy fusion applications while others are for application to fission reactor spectra.

MFA is a well developed technique for breeder reactor spectra, with present emphasis on decreasing uncertainties. Uncertainties are currently 10-30% in broad group energy spectra for the energy regions of greatest interest, and 5-15% in flux and fluence for in- and near-core locations. The uncertainty is greater in softer out-of-core spectra because of the lack of reaction sensitivity in the 0.01-0.5 MeV range. The primary problem in MFA is to achieve a reasonable reaction sensitivity over the energy range of interest. For high energy applications, many more reactions become possible but care must be taken to evaluate competing reactions leading to the same product. Such considerations, along with criteria such as appropriate half-life, adequate specific activity, availability of material in desired purity, etc., result in a large inventory of reactions in order to optimize the MFA procedure in a variety of spectra.

An important point must be made concerning data needs associated with the reactions to be used in MFA. For differential cross sections $\sigma(E)$ to be useful for spectrum unfolding, they must be consistent with integral cross sections. Integral data testing, in which a reaction rate is measured in a known neutron field $\phi(E)$ for comparison with $\int \phi(E)\, \sigma(E)\, dE$, is considered to be a primary data requirement for dosimetry applications. Differential data that are not consistent with integral measurements should be reevaluated to seek a rational basis for adjustment. The status of integral data testing of the ENDF/B-IV dosimetry cross section files in selected benchmark fields was the subject of a recent IAEA Consultants meeting.[4]

So far we have stressed radiometric MFA. Other possibilities exist -- indeed it is likely that high energy neutron fields, because of their directional properties and steep gradients, will provide fertile ground for the development of new and improved dosimetry techniques. MFA using stable reaction products is currently under development in the breeder program. In particular, helium accumulation fluence monitors (HAFMs) are being used; the total helium content is measured by high sensitivity gas mass spectrometry. The application of the technique to fusion neutron dosimetry is described in another symposium paper[6]; included is a list of materials on which measurements have been made at 14 MeV.

Another possible MFA technique for low power applications would be to use appropriate nuclear emulsions or solid state track recorders as reaction product detectors. Materials are now available to permit absolute measurements of helium and hydrogen production. It is likely that emulsions and track recorders will be useful for direct low power neutron field measurements.

TABLE 4A

Reactions Proposed for Dosimetry File - Immediate Needs

Reaction	Principal Application	Current Status
$^{19}F(n,2n)^{18}F$	c	
$^{27}Al(n,total\ He)$	b	1,2
$S(n,total\ He)$	a	
$^{37}A(n,\gamma)^{38}A$	d	
$^{45}Sc(n,2n)^{44m}Sc$	b	
$^{52}Cr(n,\gamma)^{51}Cr$	a	
$^{56}Fe(n,\alpha)^{53}Cr$	b	
$Fe(n,total\ He)$	a,b	2
$^{59}Co(n,p)^{59}Fe$	b	1
$Ni(n,total\ He)$	a,b	2
$^{63}Cu(n,2n)^{62}Cu$	c	
$Cu(n,total\ He)$	b	1,2
$^{90}Zr(n,2n)^{89}Zr$	b	
$^{93}Nb(n,2n)^{92m}Nb$	b,c	1
$^{93}Nb(n,n')^{93m}Nb$	b,c	1
$^{103}Rh(n,n')^{103m}Rh$	c	
$^{109}Ag(n,\gamma)^{110m}Ag$	a,c	
$^{181}Ta(n,\gamma)^{182}Ta$	a	1
$^{197}Au(n,2n)^{196}Au$	b	1
$^{197}Au(n,3n)^{194}Au$	b	1

TABLE 4B

Reactions Proposed for Dosimetry File - Future Needs

Reaction	Principal Application	Current Status
$^{13}C(n,\gamma)^{14}C$	a	
$^{14}N(n,p)^{14}C$	a	1
$^{23}Na(n,2n)^{22}Na$	a	1
$^{26}Mg(n,p)^{26}Na$	a	
$^{31}P(n,p)^{31}Si$	a	
$^{55}Mn(n,\gamma)^{56}Mn$	a	1
$^{56}Fe(n,\gamma)^{57}Fe$	a	
$^{56}Fe(n,x)^{54}Mn$	b	
$^{64}Zn(n,p)^{64}Cu$	a	
$^{164}Dy(n,\gamma)^{165}Dy$	c	

TABLE 4B (Continued)

$^{197}Au(n,\gamma)^{198}Au$	c
$^{197}Au(n,4n)^{193}Au$	b
$^{197}Au(n,total\ He)$	b
$^{199}Hg(n,n')^{199m}Hg$	c
$^{241}Am(n,f)$	c

Application: a) Fission Reactor Dosimetry (U.S.)
b) Fusion Reactor Dosimetry (U.S.)
c) European Applications
d) Other

Status: 1) Presently on Gas Production file
2) To be included in Gas Production file.

The use of nuclear emulsions to measure angular variations in flux-spectra is discussed in another paper in this symposium.[7] Solid state track recorders, featuring negligible gamma sensitivity, can also be used.

Next let us consider briefly some dosimetry needs at specific types of facilities. Currently the most utilized facility for DMFI irradiations is the Rotating Target Neutron Source (RTNS I) at the Lawrence Livermore Laboratory (LLL), which produces a nearly monoenergetic beam of 14.8 MeV neutrons. Minimum fluence dosimetry can be accomplished using the $^{93}Nb(n,2n)^{92m}Nb$ reaction.[8] This reaction was chosen because of its convenient half life, large and relatively constant cross section around 15 MeV, easily counted gammas, and lack of competing isotopes or interfering reactions. Absolute accuracy is reported to be ±2.5%, including a 5% uncertainty in reaction cross section relative to the $^{27}Al(n,\alpha)^{24}Na$ cross section.[9] The variation of dose over the lateral dimension of even a small sample, however, can exceed 7.5%.

The addition of nickel and gold dosimeters provides spectral indices as well as a desirable redundancy in the fluence measurement. The spectral indices are the reaction rate ratios $^{58}Ni(n,p)/^{58}Ni(n,2n)$ and $^{197}Au(n,\gamma)/^{197}Au(n,2n)$. The former provides high sensitivity in the 14.8 MeV peak region; the primary purpose of the latter is to monitor possible low energy neutrons scattered from adjacent apparatus, etc. These reactions are currently among those on the ENDF/B dosimetry file that have been recommended for reevaluation, or, in the case of Nb, for addition to the file. It is anticipated that accuracies of 5% or better will be desired eventually for the threshold reactions in the 14-15 MeV region, but less stringent requirements will apply at lower energies.

The RTNS-I is essentially a point source so that neutron flux varies rapidly with position. A high resolution fluence map[10] was recently obtained using both conventional radiometric dosimetry foils and helium accumulation fluence monitor wires.

Nine nickel, niobium, and gold dosimetry foils spaced within a small irradiation assembly close to the rotating titanium tritium target were segmented for individual radiometric counting following an 80 hour irradiation. Precise determinations of the helium produced at numerous locations in aluminum, iron, and copper wire rings surrounding the irradiation assembly provided fluence distribution detail not obtainable from the radiometric foils. There was good correlation between the helium production and the radiometric data.

Neutron facilities in which cyclotron accelerated deuterons strike a thick beryllium (or lithium) target are becoming of increasing interest to MFE experimenters. The on axis neutron spectra peak at 40 of the deuteron energy with typical energy spreads (FWHM) of 50-100 . A significant low energy component is usually associated with these spectra. The peaked spectrum transforms gradually into an approximately exponentially decreasing spectrum as the off axis angle is increased. A much larger number of monitor reactions are required in general to perform adequate dosimetry for such sources than for the RINS. Flux levels are 10^{8} to 10^{11} n/cm^{2} s, hence relatively short half lives are required for radioactive monitor reactions in order to achieve adequate specific activity. All the reactions in Table 2 with thresholds (roughly the lower value for the energy response in column 2) below 12 MeV and with half lives less than 200-300 days are useful in characterizing these sources. Good dosimetry would require cross section accuracies of 5-8% in the energy region of primary response.

On the other hand, a different approach has been taken for some materials irradiations performed at the Oak Ridge Isochronous Cyclotron using 40 MeV deuterons on a thick Be target.[9] The neutron yield was determined by averaging four measurements: one was I-O-I and the others were foil activations using the ^{58}Ni(n,p)^{58}Co, ^{59}Co(n,2n)^{58}Co, and ^{93}Nb(n,2n)^{92m}Nb reactions. The extrapolations of ENDF/B-IV cross sections above 20 MeV, as shown in Figure 1, were based on the work of Pearlstein.[10] The estimated overall uncertainties in calculated spectrum averaged cross sections were 10% for Co and Nb and 15% for Ni. The neutron spectrum (above 2 MeV) was deduced from the I-O-I data. The best estimate of neutron yield was then combined with good geometry (i.e., far from the Be target) measurements of the σ(Co)/σ(Ni) ratio to determine the angular dependence of the ratio and to infer improved values for σ(Co) and σ(Ni) as a function of angle. The procedure for characterizing the close in neutron field consisted of measuring the σ(Co)/σ(Ni) ratio, inferring from it an effective angle, and then inferring from the angle the appropriate value of σ(Ni) [or σ(Co)]. Lastly, σ and the measured activity were combined to determine the fluence. A lateral mapping at 10 mm from the center of the Be target is shown in Figure 2. Clearly spatial resolution of the order of 1 mm is needed. The overall uncertainty in the neutron fluence is estimated to be ±10%, due primarily to an estimated 7% uncertainty in neutron

yield. This procedure may be adequate for irradiations under fully repeatable conditions where there are no effective sources of neutrons other than the Be target. Potential shortcomings, however, are 1) inadequate sensitivity to the lowest and highest energy neutrons that may be present, 2) lack of desirable redundancy in foil coverage, and 3) inability to account for effects of the finite size of the source and the slowing down of the deuterons in the Be target. An experiment to more fully map the neutron field has been performed using many more reactions, but data analysis is not yet complete.

Some materials irradiations have also been performed with 30 MeV deuterons on Be using the Crocker Nuclear Laboratory cyclotron at UC-Davis. Spectrum measurements are discussed in another paper in this symposium,[11] so only a few comments are made here. In order to irradiate tensile specimens uniformly, the beam was swept over a collimator 5 mm wide by 11 mm long. Multiple foil activation (14 reactions) was employed at 4 and 44 mm from the midrange of the deuterons. Reaction cross section data requiring only minor extrapolation from 28 to 32 MeV were used. The spectra were found to differ substantially at the two positions, suggesting the inadequacy of time of flight data for close-in irradiations (see Fig. 3). It should be noted that the in close foil detectors perform not only an angular averaging of the spectra emitted from different points of the finite source but also a temporal averaging that depends on the schedule used for beam rastering.

A fluence mapping experiment using helium accumulation monitors is in the planning stage. Using the helium generation data and the fluence mapping results obtained from the first RINS I irradiation, two similar but larger irradiation packages have been designed and will be exposed at both UC Davis and at the RINS I (see Transmutation Reactions in next section)

DAMAGE PRODUCTION

There are two principal sources of radiation damage in metals: displacement of atoms from their normal lattice sites and the introduction of foreign atoms through transmutation reactions.

Displacement Damage by Neutrons

Displacement damage in metals is described by damage energy cross sections. Their calculation[12,13] requires two steps: 1) determination of the primary knockon atom (PKA) spectrum, and 2) determination of how the dissipation of the PKA energy (1) is partitioned between kinetic energy given to atoms (the "damage energy") and energy given to electrons (assumed to cause no lattice damage in metals). In the context of this symposium our concern is with the PKA spectrum.

To calculate the PKA spectrum $\phi(A,E)$ in a material of atomic weight A corresponding to a given neutron energy E requires a knowledge of the cross sections $\sigma(E)$ for all nuclear reactions in which the target atom (the PKA) receives a kinetic energy $\geq E_d$, where E_d is an effective displacement threshold energy of the order of 15-90 eV. The only reactions excluded are elastic scattering for $E \leq [(1+A)^2/4A]\, E_d$, in which case the maximum energy transfer is less than E_d, and (n,γ) reactions at low energies in certain materials for which the total recoil energy from the incident neutron and from gamma emission is less than E_d.

The cross section data must be sufficient to calculate the recoil energy spectrum; that is, differential angular cross sections for elastic and inelastic scattering and the energy distribution of emitted particles in nonelastic events are needed. For application to fission reactors, the reactions of interest are elastic and inelastic scattering and there is no particular problem with ENDF/B IV data and format, other than the question of the accuracy of the data. For applications to fusion reactors, however, calculations must extend to 14 MeV and contributions from other nonelastic reactions become significant. This is illustrated in Figures 4-9. Figs. 4-6 are PKA spectra calculated using ENDF/B IV data supplemented by some kinematical approximations.[18] Representative spectra are shown for a range of atomic weights at several neutron energies (such spectra have been calculated for sets of neutron energies so that any neutron spectrum can be transformed to a PKA spectrum.[19]) By folding a function describing the number of atomic displacements produced by a PKA of energy E with the PKA spectrum corresponding to a neutron of energy E, a displacement cross section is calculated as shown in Figs. 7-9. These figures illustrate the relative contributions of the various reaction types. There are some inadequacies in the data to 14 MeV — appreciated better no doubt by the nuclear physics community than by some of the materials oriented physicists making damage energy calculations. For example, the treatment of $(n,2n)$ reactions does not provide for a unique treatment of the kinematics, hence detracts from efforts to standardize damage energy calculations. There is a paucity of data on emitted particle angular and energy distributions for charged particle out reactions, although great accuracy is generally not needed even at 14 MeV as can be seen in Figures 7-9.

Odette[20] has considered the effects of some refinements in the calculations. For example, he has determined $(n,2n)$ recoil spectra using a sequential emission evaporation model in a Monte Carlo approach. Where comparisons have been made with single particle emission calculations, the agreement is usually within 10%. A similar conclusion was reached by Gabriel et al[21]. Odette also compared damage energy calculations for (n,α) reactions at 14 MeV using measured angular distributions of alpha emission with calculations using the usual assumption of isotropic emission (see Fig. 10). For ^{63}Cu the effect was negligible, but for ^{93}Nb the isotropic emission model overpredicted by 50%.

Clearly some further investigation of the effect of nuclear models on calculations at yet higher energies is warranted.

As has already been made clear, damage energy calculations must be extended to the neighborhood of 40 MeV for potential fusion reactor structural materials. Current calculations have been carried to 20 MeV because they are based on ENDF/B-IV. However the materials community has been warned repeatedly not to trust the files above 15 MeV, so we assume some revising in the 15-20 MeV range can be anticipated. At higher energies the multiplicity of energetically possible reactions complicates the calculations. Accuracy needs will drop however because the spectra of interest fall off above 15 MeV.

One materials experiment utilizing a broad energy spectrum peaking near 16 MeV [Be(40 MeV d,n)] has been analyzed using theoretical cross sections.[15] Nuclear reactions were divided into four groups: elastic scattering and nonelastic interactions in which the first particle emitted was a neutron, proton, or alpha particle. Particle emission was assumed to be isotropic in the center-of-mass system. Subsequent particle emission was ignored. Damage energy calculations for copper are illustrated in Figure 11. The increased importance of nonelastic reactions is clear. No estimates of calculational accuracy were made. Such calculations, combined with a few corroborative experiments, may be adequate for the region above 20 MeV.

Displacement Damage by Charged Particles

Although this is a neutron cross section symposium, a word should be said here about charged particle reactions. There is increasing use of light charged particles for studying irradiation effects in bulk specimens. This means that the total energy loss should be small over specimen thicknesses of ~100μm or larger, e.g., proton energies of ~16 MeV and α energies of 60 MeV have been used. Increasing the particle energy carries a penalty of a decreased ratio of displacement rate to total energy dissipation rate (unless one goes to energies of hundreds of MeV); the maximum useable displacement rate is generally limited by heat transfer requirements. Although the energy loss is dominated by electronic interactions, our interest is in nuclear reactions that can cause atomic displacements. Elastic scattering data seem to be relatively well known and they can be supplemented by optical model calculations. Nonelastic processes are also important at the energies being used but they have not yet received adequate treatment. Logan et al[11] estimated the nonelastic contribution for 16 MeV protons incident on niobium by lumping together reactions producing a single proton or neutron (and ignoring the rest). A small (10%) contribution from preequilibrium emission was included. This approach may be the only practical one. Attempting to determine all the partial reaction cross sections, as has been done generally for neutron calculations, can be frustrating in the absence of a convenient charged

particle analog to the ENDF/B files. (Certain partial cross sections are of intrinsic interest, however, as discussed in the following Section.) The authors are unaware of any published damage calculations for deuterons or alphas which include non-elastic interactions. There is a clear need for work in this area.

Transmutation Reactions

Transmutation reactions are of intrinsic interest beyond the fact that they result in atomic displacements. This is because the product nuclei may strongly influence the development of the damage microstructure that leads to property changes. The production of helium, in particular, is currently one of the major damage mechanisms expected in fusion reactors. Hence there is a strong need to determine total helium production cross sections. A helium production file -- one of the special applications files under the Cross Section Evaluation Working Group (CSEWG) -- was begun to meet breeder reactor program needs (see Table 5); it must be extended to 30-40 MeV. Accuracies of 20-50 are sufficient for characterizing helium production in structural materials irradiated in high energy fields. Higher accuracies are needed in the development of HAEMs for dosimetry.

TABLE 5

Gas Production Cross Sections*

Element**	Element**	Element**	Element**
Li	Cr	^{10}B	Co
Be	Fe	C	Cu
^{10}B	Ni	F	Nb
N	Zr	Si	W
Al	Mo	V	
Ti	Ta	Mn	

* From minutes of Special Meeting of CSEWG Standards Subcommittee on Neutron-Induced Gas Production, Activation, and Dosimetry Cross Sections, LASL August 1976.

** Includes all important isotopes.

The experimental approach has been highly developed at Atomics International where absolute total helium measurements are made with high sensitivity gas mass spectrometry. Multiple specimens of twelve pure elements (C, Al, Ti, V, Fe, Ni, Cu, Zr, Nb, Mo, Au, and Pt) and Type 316 stainless steel have been irradiated in the PTNS-I and have been subsequently analyzed. An irradiation planned for later this year using the UC-Davis

Be(d,n) source will include, in addition to the pure elements listed above, the elements Li, B, Si, Cr, and Cu, four alloys of interest to the fusion program, and 21 separated isotopes of the elements Li, B, Fe, Ni, Cu, and Mo. Future Be(d,n) irradiations will be conducted with different neutron energy distributions obtained by using several target to irradiation assembly distances and angles. Possibly other irradiations will be performed using different deuteron energies to provide neutron spectra peaked at different energies. These experiments will provide ideal helium generation data for integral testing of differential helium production cross sections.

While helium has the center stage, other transmutation products are also of concern. Scoping of the potential problem of hydrogen embrittlement requires estimating equilibrium hydrogen concentrations which requires, in turn, knowledge of total hydrogen production cross sections.

The presence of certain impurities in minor concentrations in stainless steels, as well as small changes in the major constituents, are known to have a strong influence on the swelling experienced under irradiation. Furthermore, small concentrations of certain elements are known to cause embrittlement in certain unirradiated alloys. The major body of irradiation effects data on structural materials will continue to come from fission reactors because they provide the only high flux test environments with sufficient test volumes. It will be important to determine the validity of these data for fusion reactor applications through limited irradiations with the proposed high flux, high energy Li(d,n) source. High helium contents in nickel bearing alloys can be produced in mixed spectrum fission reactors through the two stage reaction $^{58}Ni(n,\gamma)^{59}Ni(n,\alpha)^{56}Fe$. However, all other transmutation products will be produced at much lower rates in fission reactors than in a Li(d,n) spectrum. Hence estimates of total production rates in the latter environment of certain impurities, or classes of impurities, are needed for scoping studies to determine the extent of the problem.

SUMMARY

Nuclear data needs in the 10-40 MeV neutron energy range of the DMEE damage analysis program fall into several categories. High energy neutron fields needed for materials studies must be well characterized. The primary dosimetry tool is expected to be multiple foil analysis for which data are seriously lacking.

Calculations of damage production must be extended to 30-40 MeV. For displacement calculations, differential scattering cross sections and emitted particle energy and angular distributions are needed to calculate PKA spectra. It is possible that this need can be met primarily through theory, validated by a limited experimental program.

Total cross sections for the production of certain transmutation products, especially helium and hydrogen, in structural

materials are needed for damage calculations.

Better definition of data needs should soon be forthcoming from studies coordinated by the DMII task group on Damage Analysis and Fundamental Studies. It appears that existing CSEWG committees and the data files and formats proposed for ENDF/B-V constitute an adequate structure to deal with these data needs.

ACKNOWLEDGMENTS

The authors wish to acknowledge the continuing participation in defining nuclear data needs of other members of the DAFS task group (see Table 1), as well as fruitful discussions with T. A. Gabriel, R. Gold, L. P. Lippincott, W. N. McElroy, L. G. Perey, and J. H. Roberts.

REFERENCES

1. D. J. Dudziak and D. W. Muir, "Review of MFE Neutron Cross Section Needs: Neutronics Viewpoint," this symposium.
2. W. N. McElroy and L. S. Kellogg, "Fuels and Materials Fast Reactor Dosimetry Data Development and Testing," Nucl. Tech. 25, 189-277 (1975).
3. B. A. Magurno, ed., "ENDF/B-IV Dosimetry File," BNL-NCS-50446, April 1975.
4. M. F. Vlasov, ed., "IAEA Consultants Meeting on Integral Cross Section Measurements in Standard Neutron Fields," Vienna, Nov. 15-19, 1976, INDC(NDS)-81/LIM, March 1977.
5. L. R. Greenwood and R. F. Heinrich, "Integral Testing of Neutron Activation Cross Sections Using the ^{9}Be(d,n) Reaction at 14-16 MeV," this symposium.
6. H. Farrar IV, D. W. Knell, R. A. Britten, and R. R. Heinrich, "Fluence Mapping of RTNS by He Accumulation and Foil Activation Methods," this symposium.
7. J. H. Roberts and R. Gold, "Nuclear Emulsion Techniques and Data Needs for Fast Neutron Angular Spectrometry," this symposium.
8. P. A. Van Konynenburg, "Neutron Dosimetry (14 MeV) for Foil Samples Irradiated with the Lawrence Livermore Laboratory Rotating Target Neutron Source," UCRL-51393, Rev. 1, May 24, 1974.
9. M. J. Saltmarsh, C. A. Ludemann, C. B. Fulmer, and R. L. Styles, "Characteristics of an Intense Neutron Source Based on the d+Be Reaction," ORNL/TM-5696, Nov. 1976.
10. S. Pearlstein, "Neutron Induced Reactions in Medium Mass Nuclei," J. Nucl. Energy 27, 81-99 (1973).
11. D. Nethaway, P. Van Konynenburg, M. Guinan, and L. R. Greenwood, "Neutron Spectra from 40 MeV Deuterons on a Thick Be Target," this symposium.
12. G. R. Odette and D. R. Doiron, "Neutron Energy Dependent Defect Production Cross Sections for Fission and Fusion Applications," Nucl. Tech. 29, 346-368 (1976).

13. T. A. Gabriel, J. D. Amburgey, and N. M. Greene, "Radiation-Damage Calculations: Primary Recoil Spectra, Displacement Rates, and Gas-Production Rates," Nucl. Sci. Eng. 61, 21-32 (1976).
14. D. G. Doran and N. J. Graves, "Displacement Cross Sections and PKA Spectra: Tables and Applications," HEDL-TME 76-70, Dec. 1976.
15. J. B. Roberto and M. T. Robinson, "The Energy Dependence of Neutron Damage in Cu and Nb," J. Nucl. Mat. 61, 149-152 (1976).
16. C. M. Logan, J. D. Andersen, and A. K. Mukherjee, "Proton Simulation of Displacement Effects Induced in Metals by 14 MeV Neutrons," J. Nucl. Mat. 48, 223-232 (1973).
17. H. Farrar IV and D. W. Kneff, "Helium Generation in Fusion Reactor Materials," Tech. Prog. Rept. A.I.-ERDA-13201, May 1977.

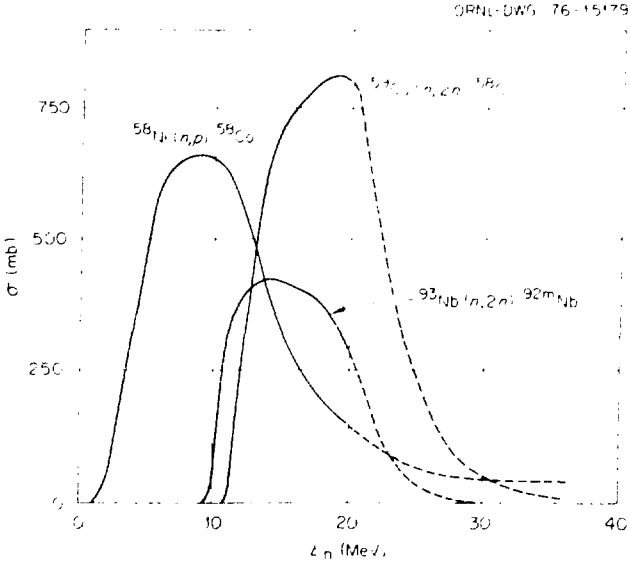

Figure 1. Excitation functions used to calculate spectrum averaged cross sections. The solid lines represent the energy regions for which data were available; the dotted portions were extrapolations (see Ref. 9).

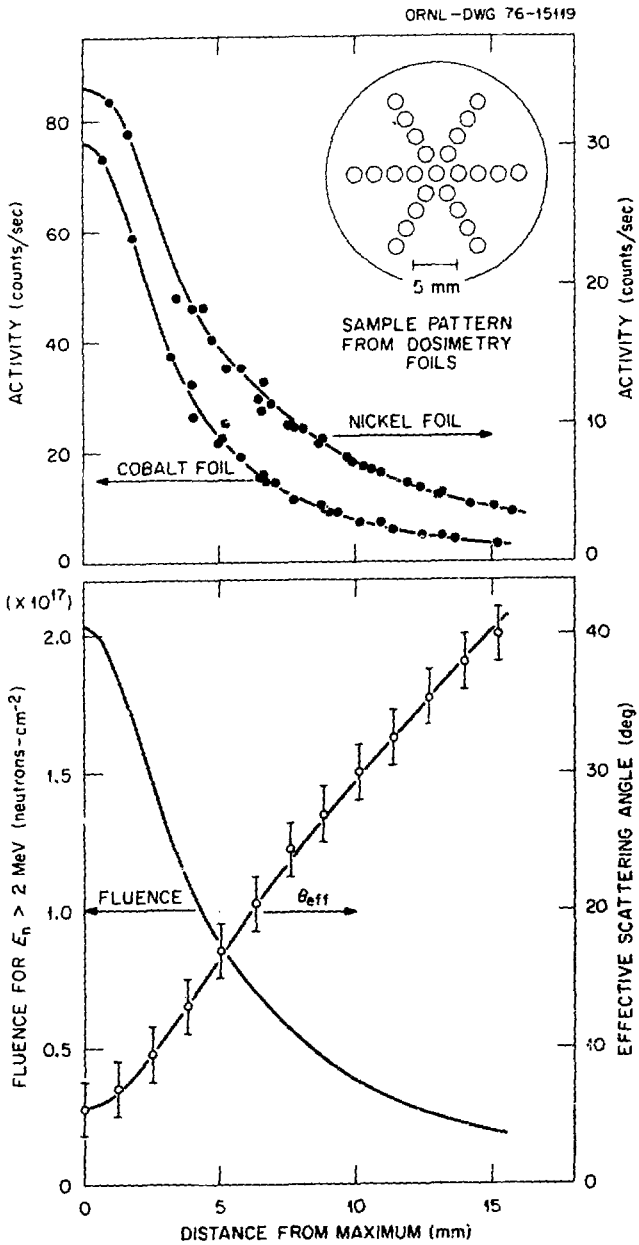

Figure 2. Dosimetry method used for d + Be neutron source. The upper graphs show the distribution of ^{58}Co activity for the cobalt and nickel dosimetry foils. The lower plots show the spatial dependence of θ_{eff} and neutron yield inferred from these measurements (see Ref. 9).

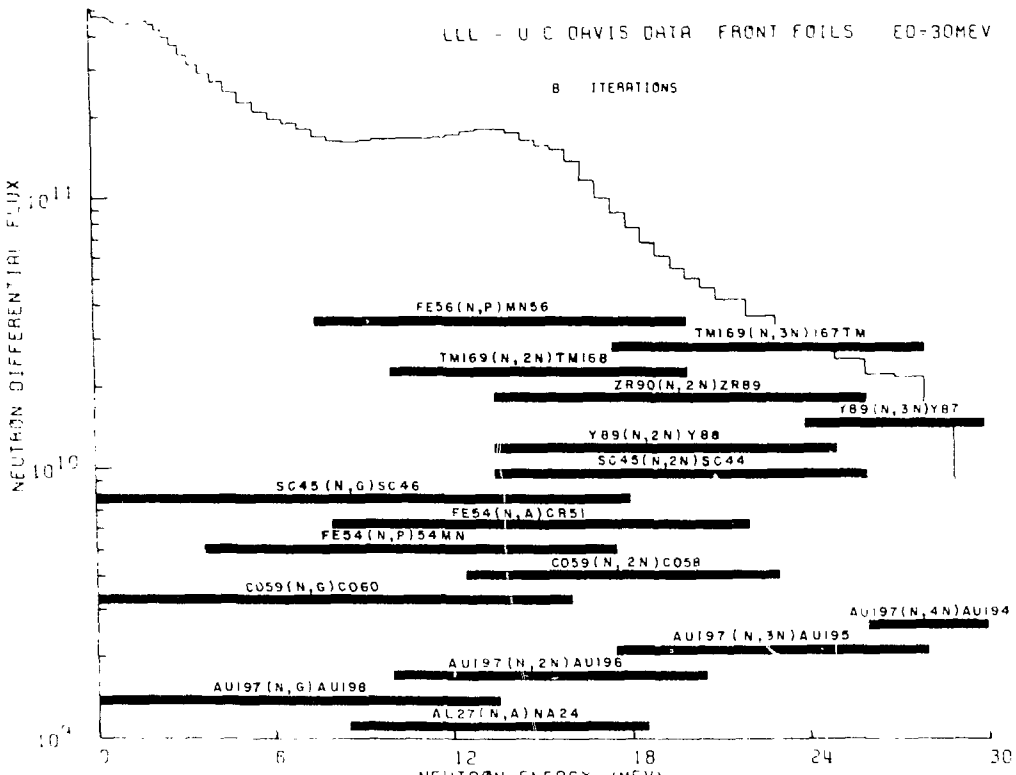

Figure 3A. Unfolded spectrum (neutron/cm^2-sec-MeV) at 4 mm from midrange of 30 MeV deuterons in Be target. The horizontal bars indicate the 95 sensitivity range for the reactions used in the unfolding (see text).

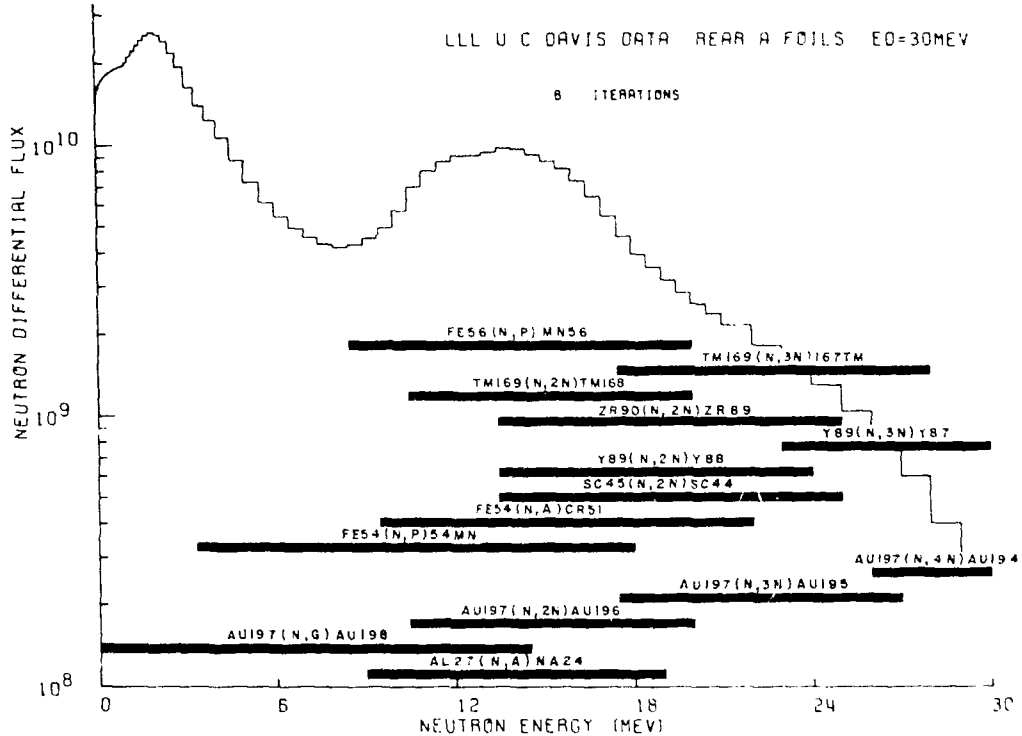

Figure 3B. Unfolded spectrum (neutron/cm²-sec-MeV) at 44 mm from midrange of 30 MeV deuterons in Be target. The horizontal bars indicate the 95 sensitivity range for the reactions used in the unfolding (see text).

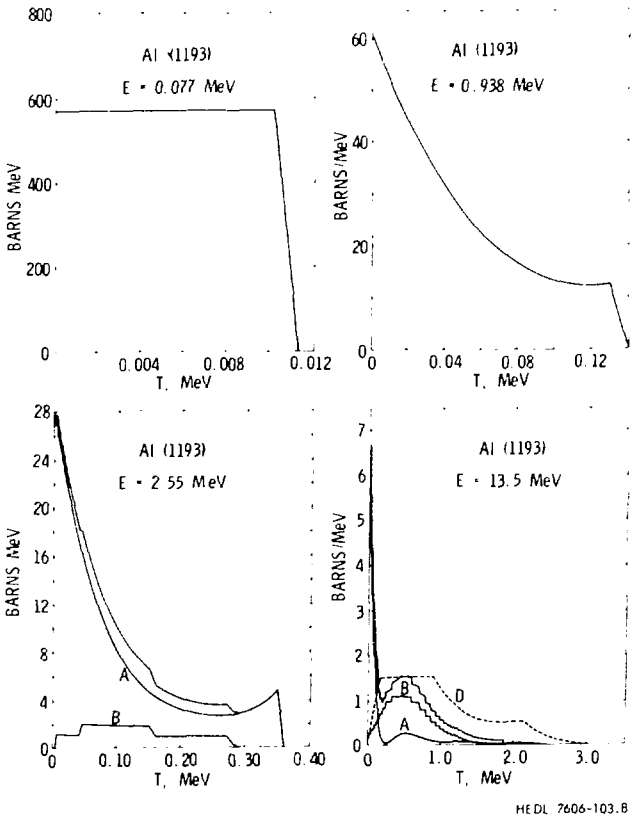

Figure 4. PKA spectra $\nu(T,E)$ for aluminum at several neutron energies. The various contributions are indicated by A (n,n), B (n,n'), C (n,2n), and D (n,c), where c is a charged particle. The (n,c) contribution has been increased tenfold for clarity.

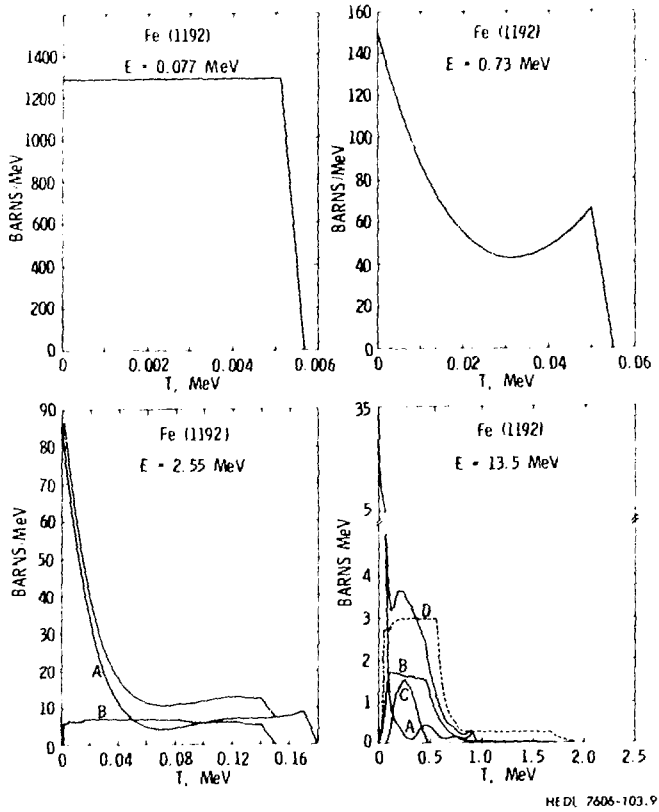

Figure 5. PKA spectra for iron. See caption for figure 4.

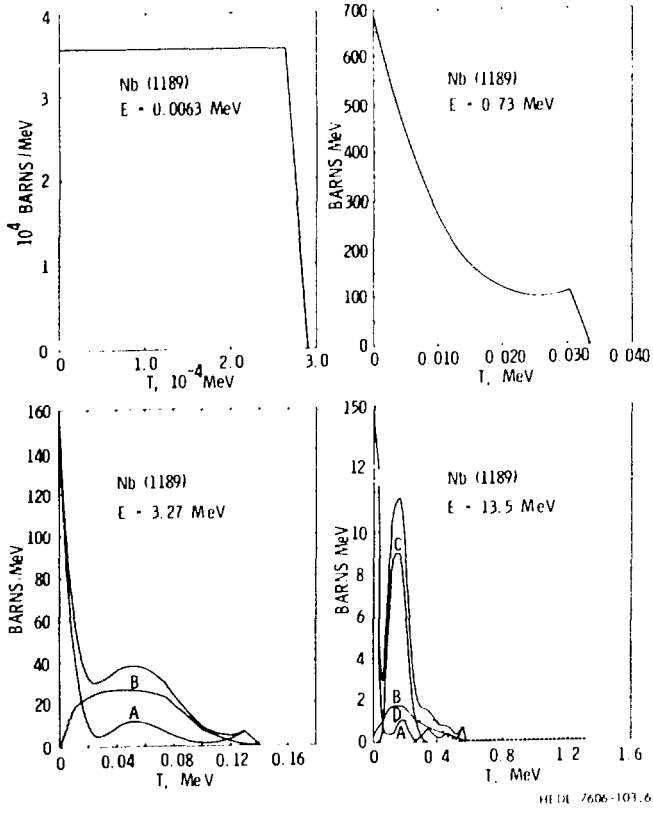

Figure 6. PKA spectra for Niobium. See caption for Figure 4.

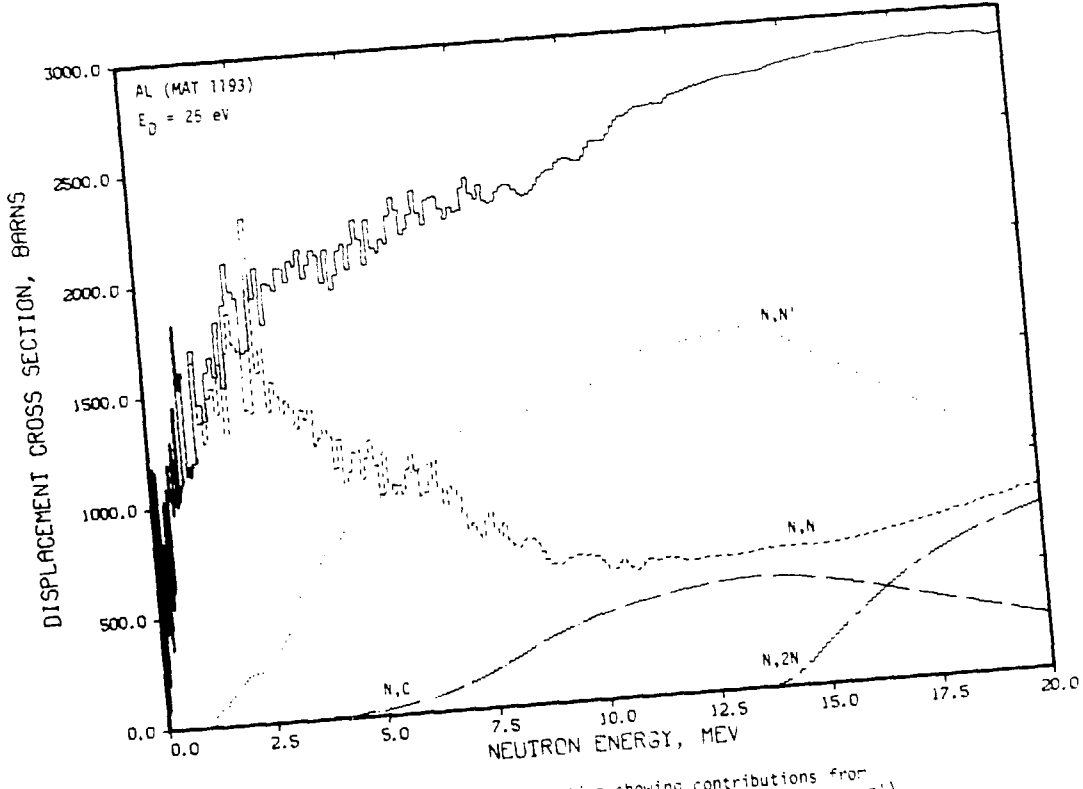

Figure 7. Displacement cross section showing contributions from various reactions, e.g., elastic (n,n), inelastic (n,n') and charged-particle-out (n,c). Aluminum.

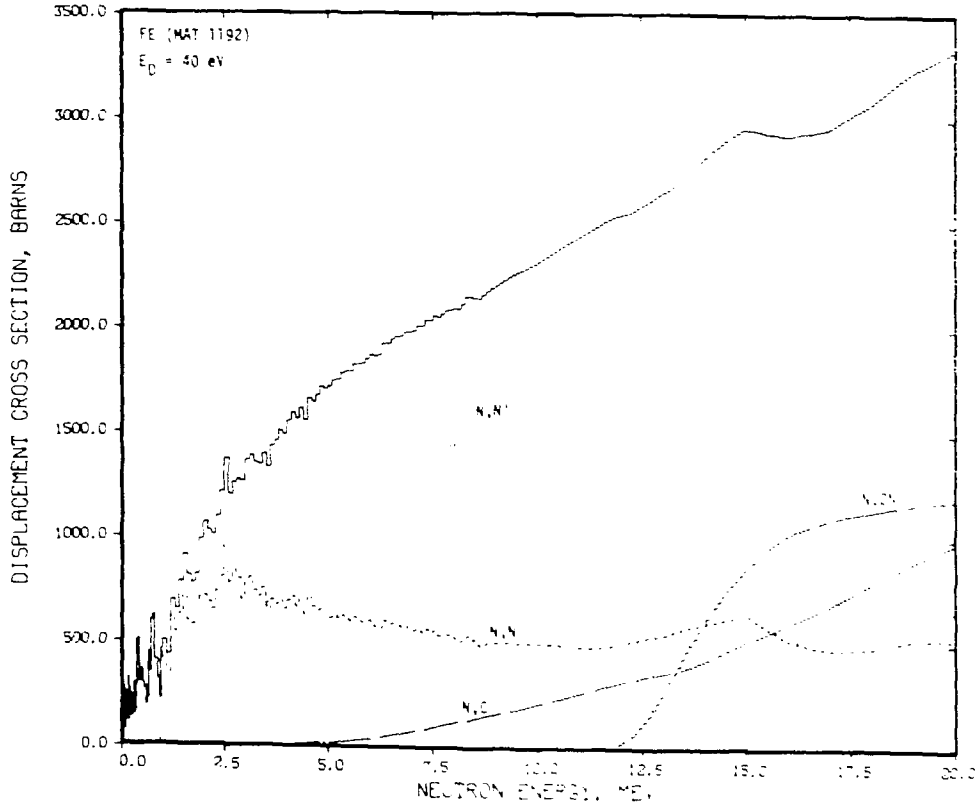

Figure 6 Iron See caption for Figure 7

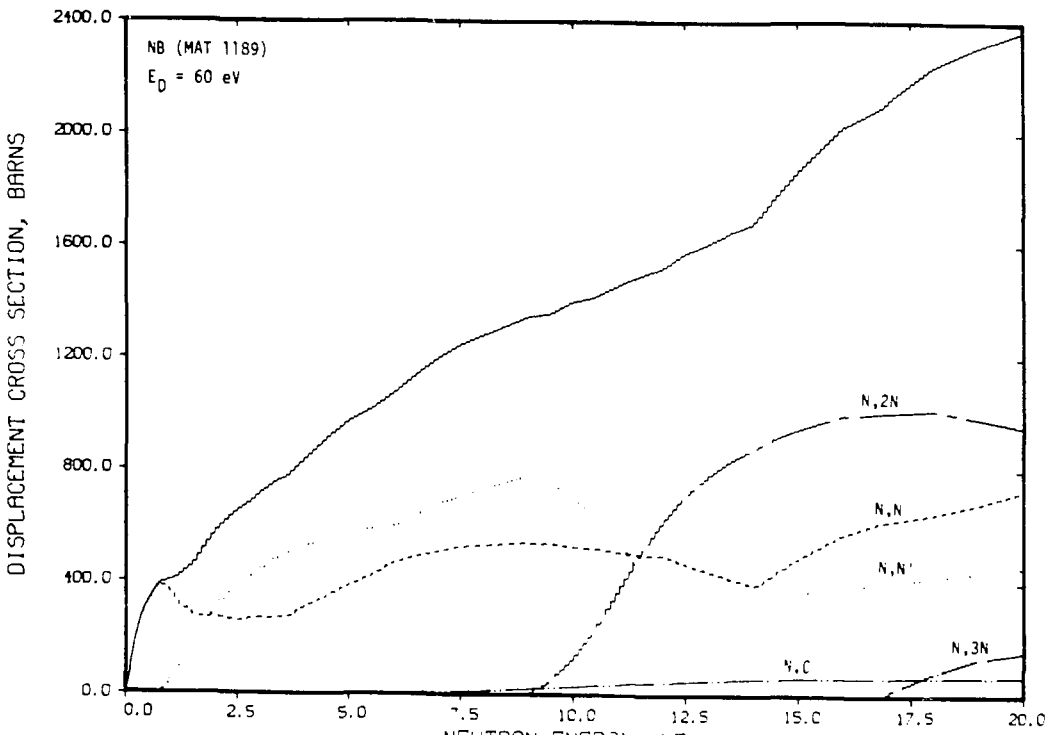

Figure 9. Niobium. See caption for Figure 1.

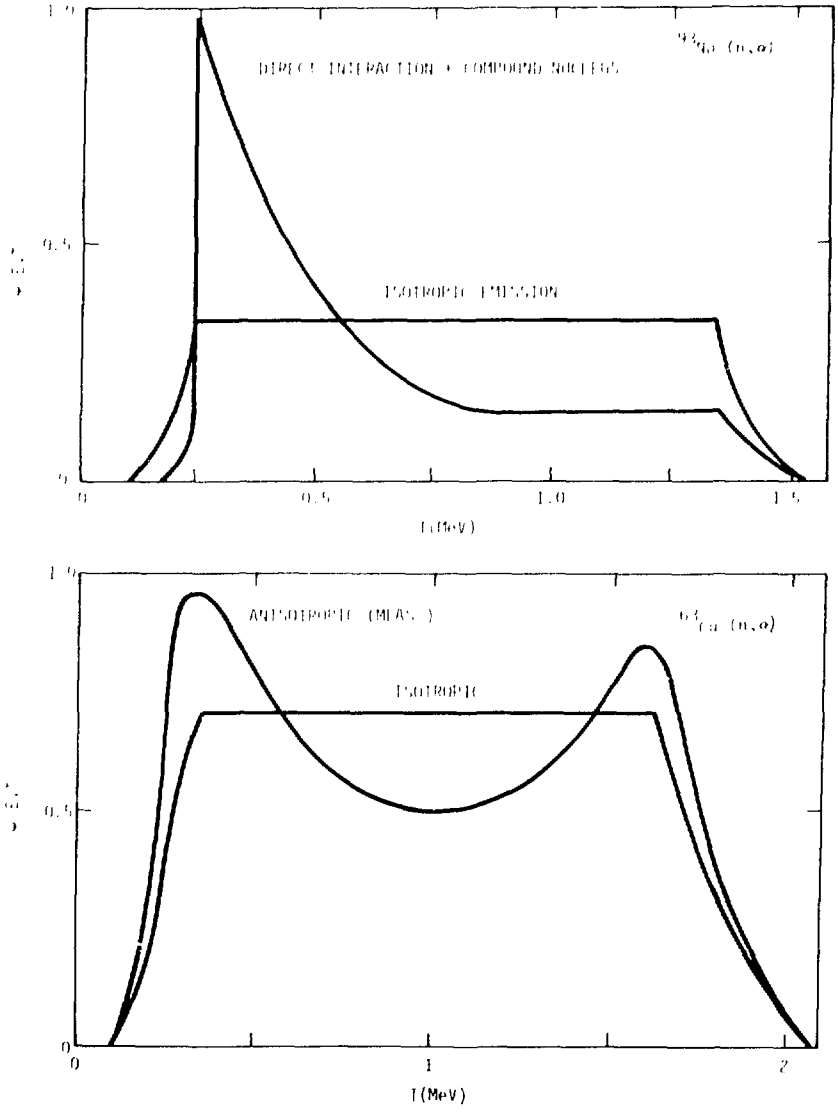

Figure 10. PKA spectra from (n,α) reactions using different emission models.

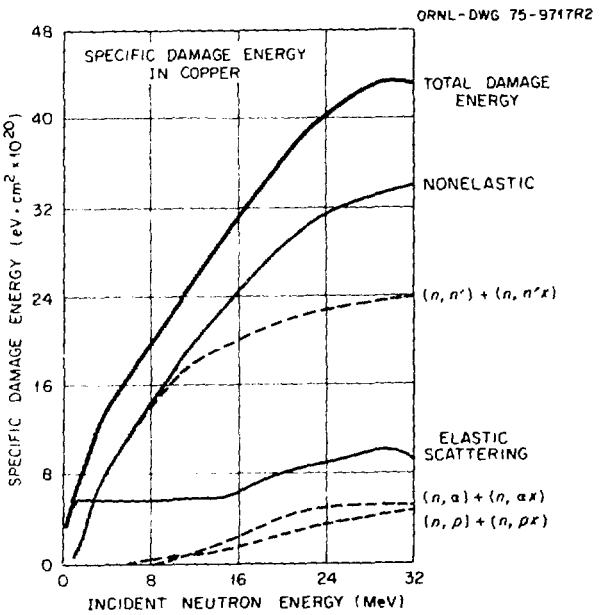

Figure 11. Theoretical damage energy in copper (after Roberto and Robinson[1]).

CONF-770523--6

Neutron Dosimetry at the Intense Neutron Source (INS)

Ronald Dierckx*

University of California, Los Alamos Scientific Laboratory+
Los Alamos, New Mexico 87545

INTRODUCTION

Radiation damage occurs whenever a material is irradiated in a neutron field for a certain time. Different neutron fields can be used to study the effect of neutron irradiation on the material's properties. Whatever the neutron field is, a correlation must be established between a property change and its primary cause.

The radiation effects depend fundamentally on the primary atom recoil energy spectrum. The recoil energy spectrum is defined by the energy of the neutron which hits the atom. Thus the neutron spectrum determines unequivocally the recoil energy spectrum and with the neutron fluence the resultant radiation effects. Therefore an accurate determination of the neutron spectrum as well as the fluence is required for each radiation damage experiment.

Even if today's knowledge of radiation damage cross-sections is rather poor, an accurate measurement of the neutronic environment is useful. It will permit one to reevaluate the results of today's experiments in the future, when more accurate knowledge of radiation damage cross-sections is available. Radiation damage experiments will always be done in a few typical neutron spectra. Data obtained in these few spectra will have to be interpreted in order to calculate the irradiation effects in the neutronic environment of future power plants.

MFE NEUTRONIC ENVIRONMENT

Up to now most radiation damage experiments are done in fission reactor spectra. At low fluence levels, irradiations are also performed in 14-MeV neutron spectra at the RTNS-I facility of LLL (Lawrence Livermore Laboratory). The neutron spectra encountered in the Magnetic Fusion Energy field (MFE) are different from the fission reactor spectra. In these spectra, the high energy neutrons above 10 MeV, notably those in the 14 MeV neutron peak, are missing.

---

*On assignment to the cooperative research program, IEA/USERDA, construction of LASL's INS facility. On leave from Euratom, CCR, Ispra, Italy.

+Work performed under the auspices of the U.S. Energy and Research Administration.

In the MFE program for radiation damage, two types of neutron sources may be used, based on either the D-T reaction (14 $\pm$ 0.6 MeV neutrons) or the D-Li stripping reaction (14 $\pm$ 11 MeV neutrons). The D-T source target can be surrounded by composite lithium-uranium 235-beryllium blankets giving rise to tailored neutron spectra in the irradiation volume similar to fusion reactor spectra at the first wall.[1]

Because of the nature of the sources and their typical spectra, fission reactor dosimetry can not be applied as such. Fortunately, dosimetry needs at these sources are recognized, and the design and construction may be implemented for these dosimetry requirements.

NEUTRON MONITORING

The neutron monitoring consists of two parts: the spectral characterization and the fluence determination. The experimental measurements are combined with theoretical calculations.

Spectral Characterization

Several methods are proposed for measuring the neutron spectrum. Simultaneous use of these methods produces a reliable picture of the neutron spectrum. A computer code "RADAK" developed at Winfrith-UKAEA permits a simultaneous analysis of the measured data coming from different spectrometers.[2]

The following methods are proposed for determining the spectra: a telescope (np) spectrometer, a telescope $Li^6(n\alpha)T$ spectrometer, spectrometers needing unfolding, time-of-flight technique, and multiple foil technique.

Telescope (np) spectrometer. With a telescope counter consisting of a radiator foil, two proportional chambers, and a scintillation or solid state detector,* the neutron spectrum may be measured using triple coincidence techniques. It is characterized by good resolution, low background but low efficiency. The telescope counter will be placed so that only protons emitted at a certain angle θ will be counted. Figure 1 gives a schematic view of the counter and its setup.

Such a spectrometer may result in a resolution of $\Delta E/E \approx 5\%$, an efficiency of $\varepsilon = 6 \times 10^{-8}$ counts/n cm^{-2} at 14-MeV, and it may be used down to about 5 MeV. By using a combination of radiator foil thicknesses, high efficiency response for both high energy as well as low energy neutrons can be obtained. Thinner radiator foils will permit the spectrometer performance to extend to lower energies ($\approx$ 1 MeV). Thicker radiator foils will increase the efficiency for the 14-MeV neutrons, at the cost of resolution.

---

*The use of solid state detectors may be limited due to their short life caused by radiation damage.

Telescope $Li^6(n\alpha)T$ spectrometer. The use of the $Li^6(n\alpha)T$ reaction is proposed for measuring the lower energy part of the spectrum. The triton (T) and alpha (α) particles are detected with a solid state detector or CsI crystal. The Li^6 radiator will be placed inside the neutron beam and the charged particle detectors shielded outside the beam, in an arrangement similar to the (np) counter.

With solid state detectors, the lowest energy neutron detectable with a good resolution is ~ 10 keV; with a CsI crystal, this lowest energy will increase at least by an order of magnitude.

In principle there is no upper energy limit, 14-MeV neutron spectrometry is possible with this system. However, the cross section and angular distribution of the charged particles are not well known, especially at higher energies. Therefore, its solitary use is not recommended.

General Spectrometry. Other spectrometers which measured data unfolded to obtain the neutron spectrum can be utilized inside the source cell. They will measure the flux at special positions. With some of these spectrometers, special measurement runs at INS will be needed, some of them at low power. Some of the direct spectrometers available are the following: gas proton-recoil counters with different gas pressures, He^3 sandwich spectrometer, Li^6 sandwich spectrometer, and scintillation-proton recoil counters.

Measuring with several of these spectrometers, the energy range can extend from 10 keV to 14 MeV.

Time-of-Flight Technique (T-O-F). The telescope counter and spectrometers can not be used to measure the lower energy range of a tailored spectrum; therefore a T-O-F technique is necessary to measure the lower energy tail of the spectrum accurately. With T-O-F it is also possible to measure the fast neutron spectrum, which provides a check of the telescope counter results and gives more confidence in the measured spectrum and its absolute value.

INS is a continuous source; so a mechanical device, or fast chopper[3] must be used to create a pulse with a 600-ns width at a frequency of 400 p/s. The fast chopper may be used at full power of the source or at a reduced power level of about 10%, with the INS source pulsed at 20-30 μs pulses. The latter operation results in a lower background. Convenient locations for the measuring stations are at 200 m, 50 m, and 25 m.

Multiple Foil Method. Both the telescope and T-O-F techniques measure a directional spectrum which can deviate from the flux spectrum at the location of sample irradiation. Foils placed in the beam and at the irradiation position will monitor the difference between the beam and the irradiation spectrum, then comparisons may be made by calculations.

With the use of unfolding codes, the multiple foil activities may be analyzed. A mean spectrum without much detail will be

obtained. Evidence for resonance structure has to be obtained out of the telescope and T-O-F results.

In order to make multiple foil techniques a potent instrument, use of the reference or standard spectra is necessary as a comparison for all measurements.[4] These standard spectra may be calculated and measured by refined method. Two standard spectra are necessary: (1) The pure 14-MeV spectrum, from the INS source, (2) A degraded, first-wall fusion-like spectrum.

Foil and detection chains are calibrated by means of the standard spectra. Further, only relative measurements versus these standard spectra need to be used. Figure 2 demonstrates the effect of intercalibration in standard spectra on the errors in the measured neutron spectra. Peak errors of up to 60% are reduced to ± 5% using the intercalibration technique.

Fluence Determination

Each sample irradiated by the INS source has to be monitored for the neutron spectrum in which it has been irradiated and for the time-integrated neutron flux or neutron fluence.

The fluence may be determined by two means: by the telescope counters, and by multiple foil method with a limited set of foils.

Telescope Counters. The telescope counters will function continuously and register as a function of time the source strength and mean neutron spectrum. Connected to the process computer, an exact picture of the neutron output and its characterization could always be available.

Multiple Foil Method. In the multiple foil method, a limited set of foils will accompany the samples to be irradiated, experiencing the same conditions (time, neutron spectrum, and temperature).

The foils will occupy a minimum space in small tube assemblies (2 mm of diameter, 20 mm of length), which will contain up to 12 foil materials all having a long half-life. This is a technique developed by McElroy.[5] In this way, the neutron fluence may be determined as a function of irradiation position for all samples irradiated.

Calculations

Extended two- or three-dimensional Sn and Monte-Carlo calculations will be necessary. Comparison of the theoretical results with the experimental measurements will give a high degree of confidence in the neutron fluence and mean neutron spectrum.

NEW PROBLEMS WITH THE MULTIPLE FOIL TECHNIQUE

Multiple foil technique is the only way to monitor the neutron spectrum and the fluence at the irradiation position in the presence of the samples. They permit a spectrum and fluence mapping of the entire irradiation volume.

The neutron spectrum below 11 MeV can be determined quite easily. Possibilities and limitations in this energy range need not be emphasized here.

New problems arise in the energy range of 10- to 15-MeV for the D-T source spectra which we have at INS. The presence of a high 14-MeV peak is our additional source of difficulties.

A good coverage with detectors, specially around 14-MeV, is needed to obtain a separation of the 14-MeV peak and the degraded spectrum in the range of 10- to 15-MeV. Table 1[6, 7] gives a preliminary list of possible reactions to be used. A sensitivity study is necessary to define the possibilities and limitations of the multiple foil technique in fusion reactor first-wall spectra in view of radiation damage dosimetry.

Table 1

Possible Reactions in the 10- to 15-MeV Range

Reaction	Threshold (MeV)	Half-life
$^{238}U(n,2n)^{237}U$	6.17	6.75 d
$^{nat}Lu(n,xn)^{174}Lu^{*}$	7.70	142 d (m) 1204 d (g)
$^{169}Tm(n,2n)^{168}Tm$	8.11	93 d
$^{197}Au(n,2n)^{196}Au$	8.12	6.18 d
$^{107}Ag(n,2n)^{106}Ag^{m}$	9.64	8.27 d
$^{89}Y(n,2n)^{88}Y$	11.6	106.6 d
$^{90}Zr(n,2n)^{89}Zr$	12.12	78.4 h
$^{58}Ni(n,2n)^{57}Ni$	12.41	36.0 h
$^{23}Na(n,2n)^{22}Na^{*}$	12.60	2.601 y
$^{46}Ti(n,2n)^{45}Ti$	13.2	3.08 h
$^{197}Au(n,3n)^{195}Au$	14.82	183 d

*Possible use as fluence monitors.

PRACTICAL SOLUTION FOR INS

For each neutron source, three permanent set-ups are possible for telescope counter placements and one permanent set-up for later installation of a T-O-F channel.

Three beams, M-1, M-2, and M-3 could be equipped for neutron source monitoring with telescope counter set-ups, so that at least two will always be functioning. (See Figs. 3 and 4). Figure 5 shows a typical set-up for a telescope counter.

Channel M-1 is located at the west side of the source cell. (See Figs. 3 and 4). It is a horizontal channel looking through the ion-beam tube directly into the source.

With the detector located at M-1, the pure 14-MeV source may be monitored independently from any experiment in the source cell.

Channel M-2 may be located in the southeast corner of the source cell, looking towards the source and spectrum modifier. The channel will be at an angle of about 30° above the horizontal so that the detector may be placed near the ceiling leaving the space below free. The detector will measure the 14-MeV source and the backscattered spectrum from a spectrum modifier.

Channel M-3 may be located at the north side of the source cell, and is identical to channel M-2. In Figs. 3 and 4, the T-O-F set-up is shown at channel NM-1.

ACKNOWLEDGEMENTS

My appreciation to C. R. Emigh for the general discussions, to Don Barr and J. S. Gilmore for their help.

REFERENCES

1. M. Battat, R. Dierckx, C. R. Emigh: "Neutron Spectra Characteristics for the Intense Neutron Source, INS," presented at this conference.
2. A. K. McCracken and M. J. Grinstone, "The Experimental Data Processing Program RADAK," Symposium on Reactor Dosimetry, Petten, The Netherlands, 1975.
3. R. Dierckx "Neutron Monitoring and Neutron Measurements: Experimental Possibilities at the INS Source," Los Alamos Scientific Laboratory LA-6742-MS, May 1977.
4. R. Dierckx, "Uncertainties on the Neutron Spectra Measurement by Activation Techniques," to be published in a monograph on "Reactor Neutron Metrology," in the USSR.
5. W. McElroy, Hanford Engineering Development Laboratory, private communication.
6. Don Barr, James S. Gilmore, LASL, private communications.
7. B. P. Bayhurst, et al., "Cross-sections for (n,xn) Reactions Between 7.5 and 28 MeV" Phys. Rev. C., Vol. 12 No. 2, pp. 451-467, August 1975.

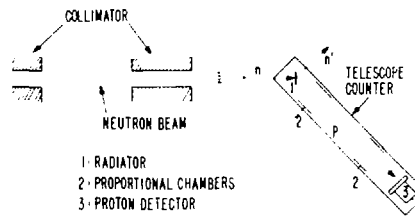

Fig. 1. Telescope counter for neutron monitoring at INS source.

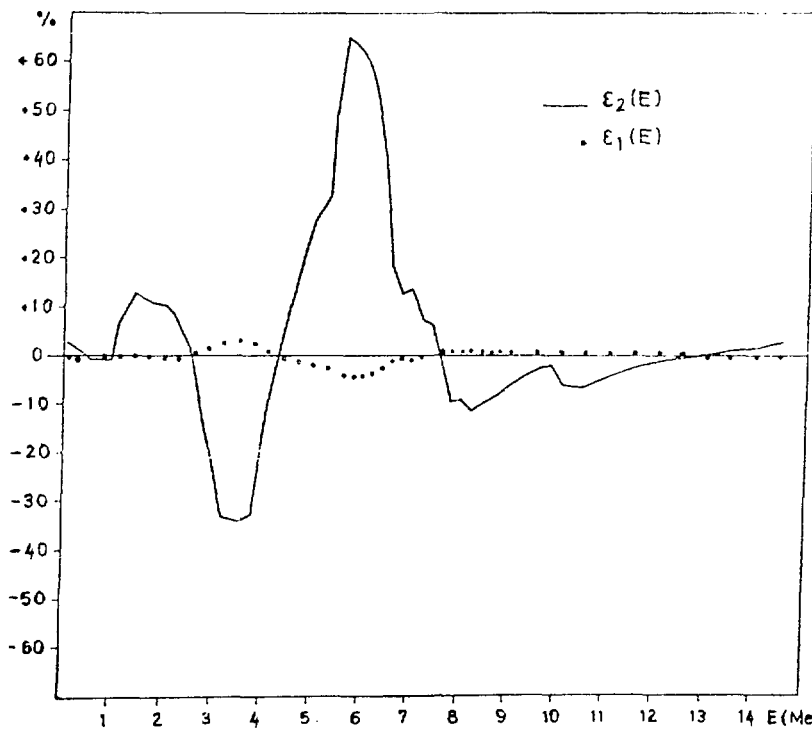

Fig. 2. Errors due to inaccuracy of cross-section data
$\varepsilon_1(E)$ with intercalibration
$\varepsilon_2(E)$ without intercalibration

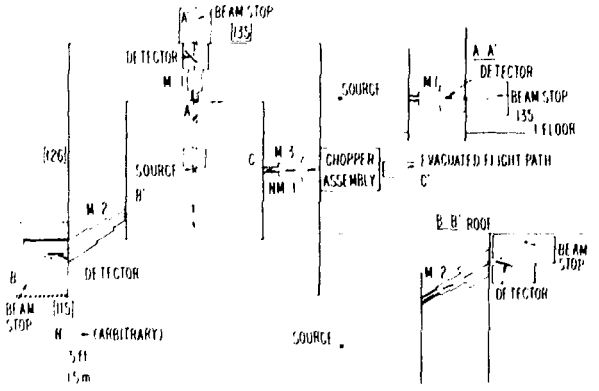

Fig. 3. Plan view of the monitoring instrumentation and sections A-A' and B-B'.

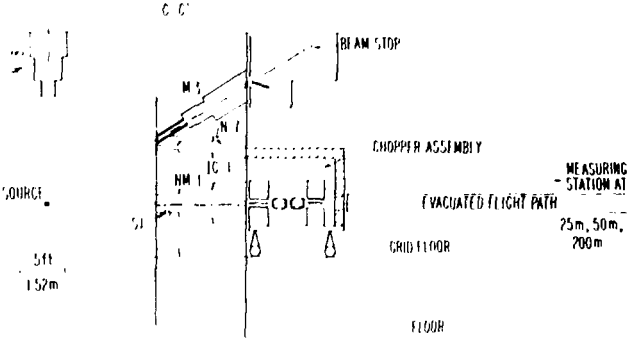

Fig. 4. Layout of monitoring instrumentation along C-C' axis. (See Fig. 3).

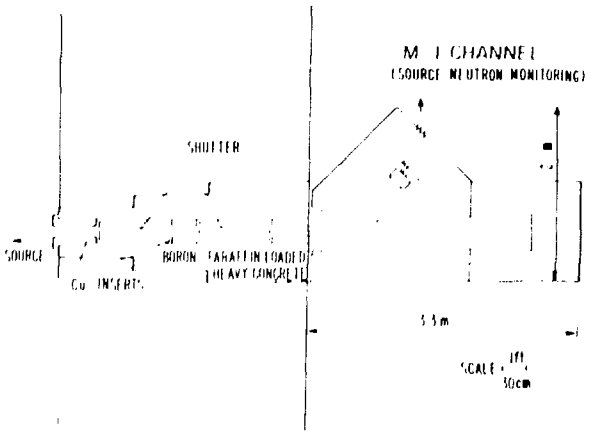

Fig. 5. Neutron detection setup.

Initial Damage Rates in Nb, V, and Mo from 30 MeV D-Be Neutrons

M. W. Guinan and C. E. Violet
Lawrence Livermore Laboratory

ABSTRACT

Changes in electrical resistivity at liquid helium temperature have been used to monitor the production of damage in dilute alloys of Nb, V, and Mo irradiated with high energy neutrons. The neutrons were produced at the University of California, Davis cyclotron by the reaction of 30 MeV deuterons on a thick beryllium target. Damage rates are compared to those produced at the Livermore rotating target neutron source. The relative damage production rates are in agreement with predictions based on damage energy calculations.

INTRODUCTION

The measurement of damage rates at low temperatures using resistivity or other techniques can provide a basis for comparison of total defect production in a variety of irradiation sources. Experiments covering a wide range of materials in diverse but well-characterized sources will produce a firm data base against which models of the displacement process can be compared.

This work is part of an interlaboratory program to study low-temperature damage rates in dilute alloys of niobium, vanadium, and molybdenum with electrons, protons, fission neutrons and high energy neutrons. The samples were prepared by R. E. Reed of Oak Ridge National Laboratory. A list of participants and a detailed description of alloy preparation are given elsewhere.[1]

Dilute alloys rather than high purity materials were chosen for two reasons: first, to supress transient variations in the damage rates observed at low dose in high purity bcc materials; second, to suppress the strong texturing that develops on annealing high purity foils. This is necessary due to the strong anisotropy of displacement rates in bcc metals.[2] All three alloys contained 300 appm Zr. Jung and Lucki[3] have previously published the results of fast electron irradiation of identical alloys.

EXPERIMENTAL DETAILS

Samples were received from ORNL in the form of foils 28-35 microns in thickness, 100 mm in length and 10 mm wide. Ribbon specimens 100 mm x 150 μm were cut from the foils using a precision shear. Three ribbons, one of each alloy, were wound onto a sample holder to form a helix 3.3 mm in diameter by 6 mm long. Potential

and current leads were spot welded to the samples and the assembly secured by varnish. A set of samples mounted on a sample holder is shown in Fig. 1(a).

To supress the superconductivity of vanadium and niobium at 4.2K the sample holder was inserted in a superconducting solenoid with a critical current of 12.35 amperes at about 10 kOe. During irradiations the assembly was immersed in liquid helium. Fields of 2.3 kOe and 9.2 kOe respectively were applied to the vanadium and niobium during measurement. A photograph of the superconducting solenoid with the sample holder partially inserted is shown in Fig. 1(b). The sample holder and solenoid were placed in a conventional upright cryostat with a specially designed 1" diameter irradiation thimble. The small scale of the entire experiment was required to allow the samples to be positioned close enough to the neutron sources to intercept reasonable fluxes. To ensure uniformity of flux, the samples and solenoid were continuously oscillated 360° about their axis during irradiation.

Conventional DC potentiometric techniques were employed with a sensitivity of ·10 nV. The measuring current was 100 ma. Noise levels were typically 30-50 nV. at both neutron sources. Typical sample resistances at 4.2K were Nb(45mΩ), V(35mΩ), and Mo(20mΩ) respectively. Resistivities, ., and room temperature resistivity ratios for a typical set of samples are given in Table 1. All sets were within 2 of these values.

Table 1

Initial Sample Resistivities

Sample	Nb(Zr)[a]	V(Zr)[b]	Mo(Zr)
$\rho_{4.}$ (n -cm)	217.31	186.46	71.70
$\rho_{296K}/\rho_{4.2K}$	68	111	78

[a]9.2 kOe transverse field [b]2.3 kOe transverse field

IRRADIATIONS

Irradiations were performed at both the Livermore rotating target neutron source (RTNS)[4] and at the University of California, Davis cyclotron using 30 MeV deuterons on a thick beryllium target.[5]

At the RTNS the cryostat was positioned as close as possible to the neutron source, which located the sample axis 16 mm away. At this position the neutron flux is of the order of 4-6 x 10^{10} n/cm^2-sec with an average energy of 14.8 MeV. An initial run of 11 hours was made to check operation in which only the vanadium

and molybdenum were measured. In a later run of 55 hours all three samples were measured. The relative fluence received by the samples during the runs was monitored by the use of a proton recoil counter. Absolute fluences were determined from the activation of the niobium samples thru the $Nb^{93}(n,2n)Nb^{92m}$ reaction for which a cross-section of 458 mb was used[6]. Corrections were made for decay during the runs.

At the Davis cyclotron the cryostat was positioned so the sample axis was located 40 mm behind the beryllium target where the neutron spectrum had been previously determined[7]. This spectrum was corrected for attenuation thru the cryostat and a room temperature experiment located closer to the target by using the total cross-sections given in ENDL[8]. The resulting spectrum is shown in Fig. 2. by the solid lines. For comparison the differential spectrum at RTNS is given by the dashed lines. One run of 18.5 hours was made at a deuteron energy of 30 MeV. The average beam current was 26 .a. At the sample position the neutron flux (E .1 MeV) was 1.8 x 10^{11} n/cm²-sec. The relative fluence during the run was monitored by the integrated beam current. The absolute fluence was estimated to be 1.25 x 10^{16} n/cm² from the spectrum given in Fig. 2 and the integrated beam current of 1.809 C. This is about 6 less than that determined from the activity of the Nb sample using a spectrum averaged cross-section for $Nb^{93}(n,2n)Nb^{92m}$ of 169 mb[9]. A summary of all three experiments is given below in Table 2.

Table 2

Summary of Irradiations

Source	Flux(10^{11} n/cm²-s)	Fluence(10^{16} n/cm²)	σ(mb)[a]
RTNS(run 1)	5.9	2.34	458
RTNS(run 2)	4.4	8.63	458
D-Be(30 MeV)	17.8	13.13	169

[a] $Nb^{93}(n,2n)Nb^{92m}$

RESULTS

The results of the three experiments are summarized in Table 3. For each experiment, the total observed change in resistivity, Δρ, and the damage production rate, dρ/dφ, are given for each alloy. The damage production rates are least squares fits to all the data taken in the run. The data for vanadium and molybdenum exhibit a small but definate decrease in rate in the two longer

irradiations. In both cases however, the change is less than 3% over the total range of $\Delta\rho$ covered. Niobium exhibits no measurable change in slope in either experiment. The data for Mo-.03%Zr, shown in Fig. 3, is typical of all three alloys.

Table 3

Experimental Damage Production Results[a]

Source	Nb(zr) $\Delta\rho$	Nb(zr) $d\rho/d\phi$	V(zr) $\Delta\rho$	V(zr) $d\rho/d\phi$	Mo(zr) $\Delta\rho$	Mo(zr) $d\rho/d\phi$
RTNS(1)	----	-----	4.63	1.974	2.35	1.007
RTNS(2)	9.69	1.126	16.45	1.906	8.65	0.998
D-Be	9.49	0.726	19.91	1.516	3.53	0.651

[a] $\Delta\rho(10^{-9}\ \Omega\text{-cm})$, $d\rho/d\phi(10^{-24}\ \Omega\text{-cm}^3/n)$

Relative uncertainties in $d\rho/d\phi$ are Nb(6%), V(3%), and Mo(1%) respectively. The absolute uncertainty in all cases is dominated by the fluence determination, 7.5% for RTNS and 15% for D-Be.

DISCUSSION

We will first compare the relative damage production from the two high energy neutron sources to that predicted from damage energy calculations. We will then consider the question of absolute defect production rates.

The experimental damage rates $d\rho/d\phi$ can be expressed as

$$d\rho/d\phi = \rho f \sigma_d \qquad (1)$$

where ρf is the resistivity increment per atomic fraction of Frenkel pairs and σ_d is the displacement cross-section. If we assume that the number of defects produced in energetic cascades is proportional to the damage energy, i.e., the energy of the primary recoil less the energy lost from all generations of recoils to electron excitation, then the ratio of two experimental damage rates should be equal to the ratio of the corresponding damage energy cross-sections, σ_{DE}.

For niobium and molybdenum the theory predicts ratios about 10% higher than experiment, while for vanadium, theory predicts a value 8% lower. In all cases, the comparison is within the uncertainty in either experiment or theory.

Roberto et al[11] have irradiated Cu, Nb and Pt with 40 MeV D-Be neutrons and compared experimental damage production with pure fission neutron damage. Again the measured damage ratios are within ~10% of those predicted by theory. It appears that within uncertainties damage production scales with damage energy at least over the recoil energy range of from below 10 KeV to above 200 KeV.

Damage Production Efficiency

To convert damage energy cross-sections to the displacement cross-sections needed to evaluate Eq. 1, we must specify the constant of proportionality. Following Robinson[19] we can write

$$\sigma_d = K \sigma_{DE}/2 T_d \qquad (2)$$

where K is the displacement efficiency and T_d is an effective displacement energy which accounts for the anisotropy of the displacement threshold. If K = 1 and $T_d = T_0$, the measured threshold displacement energy, we have the Kinchin and Pease model[7]. Lucasson[22] has reviewed both experimental and computer data on the anisotropy of displacement thresholds in fcc, bcc, and hcp metals and for bcc metals finds $T_d = 2.2\ T_0$. Values of T_0 for these alloys have been measured by Jung and Lucki[5]. Once ρf is specified, the displacement efficiency can be obtained for a given experiment by substituting Eq. 2 in Eq. 1 and solving for K, i.e.

$$K = (d\sigma/dE)*2\ T_d/\sigma_{DE}\rho f \qquad (3)$$

For Nb, V and Mo we have used values of ρf from Benedek[3] based on melting point resistivities. We note that this brings the molybdenum alloy displacement function[3] more in line with that for other bcc materials. We also note that for niobium and molybdenum, Benedek's values are in agreement with those recommended by Lucasson.[22]

In Table 7, we list values for T_0, T_d and ρf for each of the three materials. Values for the displacement efficiency, K, in each source are calculated from these values, the experimental $d\sigma/dE$ in Table 3 and the damage energy cross-sections of Gabriel et al in Tables 4 and 5.

Damage Energy Cross-Sections

Damage energy cross-sections at or near 14 MeV (RTNS) have been reported for a number of years[9-17]. In Table 4 we have tabulated four recent values for each alloy, both the ENDF/B-IV and the 1976 ENDL evaluated neutron cross-section files have been used. All used the LSS model for electronic stopping.

Table 4

Damage Energy Cross-Sections[a] at RTNS

Reference	Nb	V	Mo
Gabriel et al (15)	294	274	284
Doran and Graves (17)	274	265	263
Logan and Russell (16)	263[b]	247[b]	246[b]
Parkin (18)	285[b]	260	332[b]

[a]Damage energy cross-sections in b-KeV

[b]Values using 1976 ENDL, others used ENDF/B-IV.

Both Gabriel et al and Doran and Graves have tabulated damage cross-sections as a function of neutron energy up to 20 MeV. Their values were extrapolated to 30 MeV and damage cross-sections obtained for the D-Be spectra of Fig. 2. For this spectra, less than 15% of the damage results from neutrons above 20 MeV so that the total cross-sections are not sensitive to the extrapolation. By comparison, neutrons below 5 MeV contribute 20-25% of the damage. The results are given in Table 5, again in units of b-KeV.

Table 5

Damage Energy Cross-Sections for D-Be (30 MeV)

Reference	Nb	V	Mo
Gabriel et al (15)	205	204	205
Doran and Graves (17)	190	196	183

Doran and Graves estimate that errors in damage energy cross-sections will be of the order of ± 20% in the energy ranges considered here. For all the materials, and particularly vanadium, the values will be systematically high by up to 10% due to the use of LSS electronic stopping as discussed by Robinson[19]. However, when ratios are taken the uncertainty will probably be of the order of 10% or less.

Damage Ratios

The experimental ratios of damage from 30 MeV D-Be neutrons to that from 14.8 MeV D-T neutrons (Table 3) are given in Table 6. They are compared to the ratios of damage energy cross-sections from tables 4 and 5. Only one theoretical damage ratio is given, since ratios obtained from Gabriel et al and Doran and Graves were within 1%.

Table 6

Damage Ratios (D-Be(30 Mev)/RTNS)

Material	Experiment	Theory
Nb(zr)	.65 ± .12	.69 ± .07
V(zr)	.80 ± .14	.74 ± .07
Mo(zr)	.65 ± .11	.71 ± .07

Table 7

Damage Efficiency

Sample	T_0(eV)	T_d(eV)	$\rho f(10^{-4}\Omega\text{-cm})$	K(RTNS)	K(D-Be)
Nb(zr)	28	62	16.1	.29	.27
V(zr)	25	55	18.0	.43	.45
Mo(zr)	34	75	14.2	.37	.34

The damage efficiencies vary from 27% to 45% and are comparable to those calculated for fission neutrons.[22] From both binary computer simulations[24] and analytic cascade calculations[25], efficiencies of about 80% are expected. The values here and those for fission neutrons are a factor of two to three lower. Merkle et al[26] have recently reported efficiencies in silver of 80% for recoils below 3 KeV and values of 15 - 25% for recoils in the 10-200 KeV range. Robinson's observation[19] that thermal neutrons are 1.7 ± 0.8 times as effective as fission neutrons would also support the conclusion that damage efficiencies decrease rapidly in the low KeV range and change much slower as the recoil energy increases.

CONCLUSIONS

Resistivity damage rates from neutrons produced by 30 MeV deuterons on a thick Be target in dilute alloys of Nb, V, and Mo are about 2/3 those produced by 14.8 MeV neutrons. This ratio is in agreement with predictions based on damage energy calculations. On an absolute basis, high energy neutrons are a factor of two to three less effective than one would expect on a modified Kinchin-Pease model.

ACKNOWLEDGMENTS

We would like to thank R. A. Van Konynenburg for his contributions to the design of the irradiation cryostat, C. Rowe for support through all phases of the experiments, J. Kinney and L. Allison for experimental help and S. MacLean for neutron dosimetry.

REFERENCES

1. R. Reed, C. E. Klabunde, J. K. Redman, and R. R. Coltman, Jr., ORNL-4952, Solid State Division Annual Progress Report (1973).
2. P. Jung and W. Schilling, Phys. Rev. B 5, 2046 (1972).
3. P. Jung and G. Lucki, Rad. Effects 26, 99 (1975).
4. R. Booth and H. H. Barschall, Nucl. Inst. Meth. 99, 1 (1972).
5. C. M. Logan, R. Booth and R. A. Nickerson, UCRL-78754 (to be published) Nucl. Inst. Meth. (1977).
6. D. Nethaway (private communication) (1977).
7. D. Nethaway, R. A. Van Konybenburg, M. W. Guinan and L. R. Greenwood (This symposium) (1977).
8. R. J. Howerton, R. J. Doyas, T. C. Michels and S. T. Perkins, Livermore Evaluated Neutron Cross-Section Library, Lawrence Livermore Laboratory Rept. UCRL-50400 (1976).
9. M. T. Robinson in "Nuclear Fusion Reactors," British Nuclear Soc., London (1970), p. 364.
0. D. M. Parkin, A. N. Goland, and H. C. Berry in "Proc. First Topical Mtg. Tech. Controlled Nuc. Fusion", San Diego (1974). Vol. 1, p. 339.
1. D. G. Doran and H. H. Yoshikawa, Eds., CTR Quarterly Report, Hanford Engineering Development Laboratory Rept. HEDL-TME-75-90 (1975), p. 20.
2. D. M. Parkin and A. N. Goland, Rad. Eff. 28, 31 (1976).
3. J. B. Roberto, M. T. Robinson and C. Y. Fu in "Proc. Intnl. Conf. Surface Effects Controlled Fusion Devices, San Francisco (1976).
4. A. M. Omar, J. E. Robinson and D. A. Thompson, J. Nucl. Mat. (1976).
5. T. A. Gabriel, J. D. Amburgey, and N. M. Greene, Nucl. Sci. Eng. 61, 21 (1976).
6. C. M. Logan and E. W. Russell, "Radiation Damage at the RTNS Facility at Lawrence Livermore Laboratory," Lawrence Livermore Laboratory Rept. UCRL-52093 (1976).
7. D. G. Doran and N. J. Graves, "Displacement Cross-Sections and PKA Spectra", Hanford Engineering Development Laboratory Rept. HEDL-TME-76-20 (1976).
8. D. M. Parkin (private communication)(1977).
9. M. T. Robinson in Fundamental Aspects of Radiation Damage in Metals, USERDA, NSF, ORNL CONF-751006 (175), Vol. I, p. 1.
0. G. H. Kinchin and R. S. Pease, Rep. Prog. Phys 18, 1 (1955).
1. J. Roberto, C. E. Klabunde, J. M. Williams, R. R. Coltman, Jr., M. J. Saltmarsh and C. B. Fulmer, Appl. Phys. Lett. 30, 509 (1977).
2. P. Lucasson in Fundamental Aspects of Radiation Damage in Metals, USERDA, NSF, ORNL CONF-751006 (1975), Vol. I, p. 42.
3. R. Benedek (in press) J. Appl. Phys. (1977).
4. M. T. Robinson and I. M. Torrens, Phys. Rev. B 9, 5008 (1974).
5. P. Sigmund, Rad. Effects 1, 15 (1969).
6. K. L. Merkle, R. S. Averback, and R. Benedek, Phys. Rev. Lett. 38, 424 (1977).

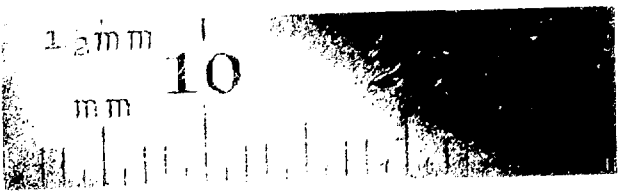

A)

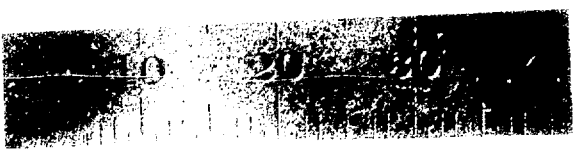

B)

NEUTRON ENERGY (MeV)

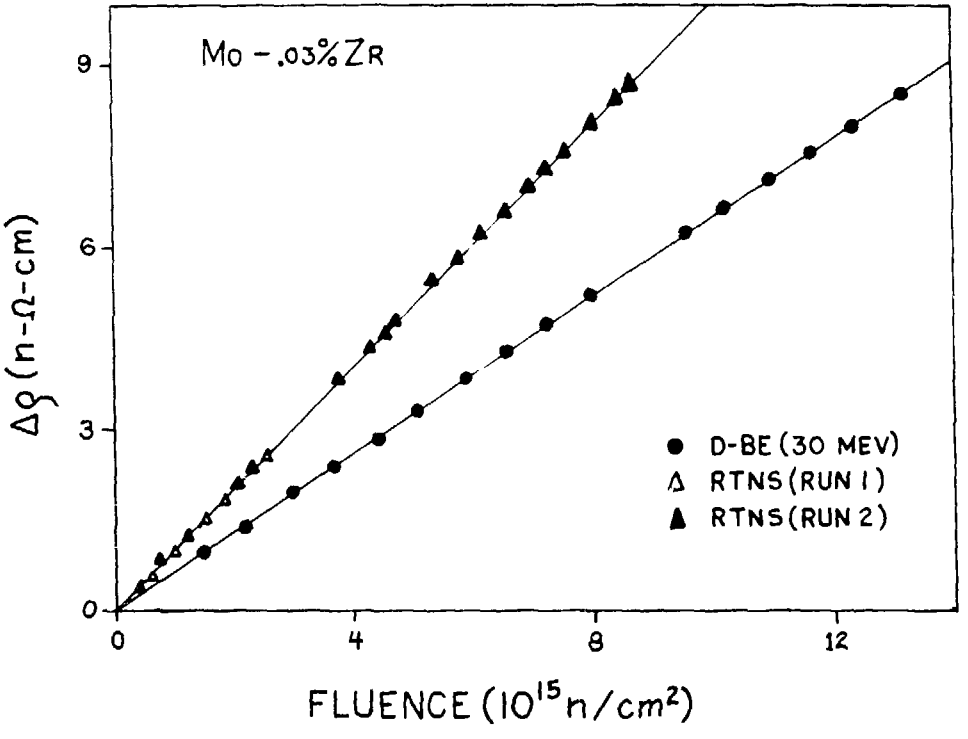

Fig. 3. Resistivity increment as a function of neutron fluence for the molybdenum alloy.

SESSION V

INTEGRAL EXPERIMENTS AND DATA TESTING

Chairman: R. J. Howerton, LLL

Integral Experiments for CTR Nuclear Data

Professor Charles W. Maynard
Nuclear Engineering Department, University of Wisconsin

Integral experiments have played an important role in the development of data and calculational models for fission reactors. It is reasonable to expect them to play an important role for fusion, although the analogy cannot be carried too far as there is nothing comparable to the criticality problem in fusion. The data situation while by no means perfect is probably much better than in the earlier cases of LWR's and LMFBR's. Calculational models are also far superior to those available in the early phase of fission. In addition, there is a formalism available for guiding the experimental program before most of the experiments have been run.

The key results of the combined theory of data adjustment and integral experiments are reviewed and discussed from the point of view of their relevance to CTR work. Integral experiments available to date are then reviewed.

The key quantities in discussing data uncertainties and their consequences are the sensitivity coefficients and the dispersion or covariance matrices. A reactor performance index or a measurement on a system have the common feature of being an integral property for the system, i.e. an integral or sometimes a ratio of integrals of the fluxes, adjoint fluxes and weight functions over phase space. However, the fluxes and ajoint fluxes are determined by the dimensions, compositions, and nuclear data and thus the calculated value of property I can be designated by

$$C_I = C_I(\underline{x}, \underline{\sigma}) \tag{1}$$

The vector $\underline{x}$ has components which are the variables of the system over which the designer or experimenter has control, hence the x_i are control variables. The components σ_i of $\underline{\sigma}$ are physical parameters with fixed but unknown values.

Our interest here is in the σ_i and the vector $\underline{x}$ will be suppressed and I treated as an index representing the experiment and reactor response of interest. However, in the design of experiments, the sensitivity and uncertainty due to a particular choice of the value of $\underline{x}$ should be studied.

The development will be simplified by linearizing the quantity C_I about the reference value $\underline{\sigma}_o$ of $\underline{\sigma}$, i.e.

$$C_I = C_I(\underline{\sigma}_o) + \sum_i \left.\frac{\partial C_I}{\partial \sigma_i}\right|_{\sigma_i = \sigma_{io}} (\sigma_i - \sigma_{io})$$

$$= C_{I_o} (1 + S_I^T f) \tag{2}$$

where $C_{I_o} = C_I(\sigma_o)$, and f has elements

$$f_i = \frac{\sigma_i - \sigma_{io}}{\sigma_{io}}$$

the relative variation of σ_i about the reference value, and the components of S_I are

$$S_{I,i} = \frac{\sigma_{io}}{C_{I_o}} \frac{\partial C_I}{\partial \sigma_i}\bigg|_{\sigma_i = \sigma_{io}}$$

This is the sensitivity coefficient of property I to the parameter σ_i.

The variance (second moment about the mean) of C_I is related to the covariance of f through

$$\epsilon_I^2 = S_I^T r S_I ,$$

where the relative covariance matrix r is

$$r = \overline{ff^T} - \overline{f}\,\overline{f}^T .$$

This is a standard result of elementary statistical regression analysis. The elements r_{ij} must be obtained from analysis of the data σ_i. If the data is distributed symmetrically σ_o is the average value and $\overline{f} = 0$.

If integral experiments are available, the f_i may be adjusted to give a least squares discrepancy relative to experimental uncertainty for all data, differential and integral. This results after N_o integral experiments in the adjusted values of f given by

$$f = rY ,$$

where

$$Y_i = \sum_{I=1}^{N_o} \frac{D_I}{\epsilon_I^2} S_{I,i} .$$

In this result ϵ_I^2 is the dispersion of the experimental result for the Ith integral experiment, and

$$D_I = \frac{E_I - C_{I_o}}{C_{I_o}}$$

is the difference of the experimental result E_I and the reference

calculated value C_{I_o} relative to C_{I_o}. The matrix $D(N_o)$ is the dispersion or relative covariance matrix after N_o integral experiments have been included. If the data are independent, it is the inverse of the information matrix M with elements

$$M_{ij}(N_o) = \sum_{I=1}^{N_o} S_{I,i} S_{I,j} w_I + \frac{\delta_{ij}}{g_i^2}$$

where w_I has been used for $(\sigma_I^2)^{-1}$ and g_i^2 is the dispersion of f_i. A recursion solution for D is

$$D(N_o + 1) = \begin{bmatrix} 1 & \dfrac{w_{N_o+1} D(N_o) G G^T}{1 + w_{N_o+1} G^T D(N_o) G} D(N_o) \end{bmatrix}$$

Here the elements of G are $S_{N_o+1,i}$. The dispersion in a response R using this data is

$$\Delta R^2_{N_o} = S_R^T D(N_o) S_R$$

where S_R is the sensitivity vector for response R in a particular reactor. The improvement in S_R due to the last $(N_o + 1)$ integral experiment is

$$\Delta R^2_{N_o} - \Delta R^2_{N_o+1} = \frac{w_{N_o+1} (S_R^T D(N_o) G)^2}{1 + w_{N_o+1} G^T D(N_o) G}$$

w_{N_o+1} is a measure of the accuracy with which the experiment is performed. A very accurate experiment corresponds to a large value of w and a limiting value for the improvement in the dispersion is

$$\text{I.C.} = \frac{(S_R^T D(N_o) G)^2}{G^T D(N_o) G}$$

This is called the information content of the experiment. This is the maximum information which can ever be extracted from this experiment for the response R with the current knowledge of the data as incorporated in $D(N_o)$. Half of the potential is realized for $w_{N_o+1} = G^T D(N_o) G$, but there is no sharp break in this function.

The theory outlined can tell us the improvement in a response for a particular reactor and a particular experiment for a given

status of the data including all experiments good or bad which may have been carried out. It allows for some comparison of experiments. It does not as it stands tell us how much an improvement in data is worth, what it will cost, or what to do if you don't know what reactor to plan for. Further, it is a formalism which is difficult to apply for lack of input data and calculational costs may be a burden, especially if the theory must be modified to account for correlations. It will tell us to choose w very large (e^2 small) and G equal to S_R, i.e. the best experiment is to build the reactor itself and measure the required response which in the absence of economic information is the correct answer.

A more direct comparison of different experiments requires a basis for comparison which in turn requires an economic analysis of the benefits resulting from an error reduction. A simple approach is to recognize that the cost of electricity from a plant or of thermal power from a reactor is a function of many variables, but in particular of the nuclear responses R_α calculated during design. For a set of changes δR_α, the cost ξ changes by

$$\delta \xi = \sum_\alpha \frac{\partial \xi}{\partial R_\alpha} \delta R_\alpha$$

Now if specified performance is $R_\alpha \pm R_{\alpha_0}$ and there is an uncertainty presumably one must design to $R_{\alpha_0} \pm \delta R_\alpha$ and an uncertainty reduction allows a reduction

$$\sqrt{\delta R_{\alpha 1}^2 - \delta R_{\alpha 2}^2}$$

in the design basis. The benefit of the reduction due to the $(N_0 + 1)^{\underline{st}}$ experiment is then

$$\sum_\alpha \frac{\partial \xi}{\partial R_\alpha} \sqrt{\delta R_{\alpha N_0}^2 - \delta R_{\alpha N_0 + 1}^2} \quad ,$$

or

$$\sum_\alpha \frac{\partial \xi}{\partial R_\alpha} \sqrt{\frac{w_{N_0+1} \left(S_{R_\alpha}^T D(N_0)\, G\right)^2}{1 + w_{N_0+1}\, G^T D(N_0)\, G}} \quad .$$

On setting

$$\sum_\alpha \frac{\partial \xi}{\partial R_\alpha} \quad S_{R_\alpha}^T = H^T ,$$

This becomes

$$\sqrt{\frac{w_{N_o+1}\,(H^T D(N_o)\,G)^2}{1 + w_{N_o+1}\,G^T D(N_o)\,G}}$$

If the cost of the experiment is K_{N_o+1}, the benefit to cost ratio B is

$$B = \frac{1}{K_{N_o+1}}\sqrt{\frac{w_{N_o+1}\,(H^T D(N_o)\,G)^2}{1 + w_{N_o+1}\,G^T D(N_o)\,G}}$$

If two experiments are proposed, presumably one finds the one with the larger value of this ratio. The influence of the experiment appears through w_{N_o+1} and G, while the reactor for which information is obtained influences the result through the benefit sensitivity vector H.

One might envision meeting potential data needs by considering a set of reactors which represent a best current estimate of the reactors one may build. A set of sensitivity vectors H could be obtained and the choice of experiments made to maximize the average benefit to cost ratio.

The experimental costs depend on the accuracy as reflected in the quantity "w" and on the control variables x which influence the vector G and optimize B or choose a set of values x sequentially to obtain an overall optimal improvement in B. One could in principle even present value results to tell when to carry out the experiment.

While the complete implementation and execution of data improvement based on the above theory is a major program which would involve many people and may never be completed, it provides a rather complete framework for discussing integral experiments for CFF nuclear data. The most immediate needs are the D(o), (denoted by "r" earlier) and the economic studies. Some covariance data is available, but far more is needed to carry out complete studies. The S_I, S_R, and G can be calculated fairly well and fairly cheaply now. A word of caution is perhaps in order here; for the number of sensitivity coefficients can become very large and most will contribute little to the response uncertainty. Careful planning and thought can reduce the labor enormously without greatly affecting the results. To the extent that the data ignored is statistically independent of the data considered, contributions not included are additive and can readily be added later if it turns out the neglected data is more important than was originally thought.

It should also be noted that the theory is developed for a true integral experiment. If the data generated consists of the neutron flux spectrum at a point so that the data gives the flux in ΔE and ΔV, a sensitivity vector for this can be calculated. However if data are obtained at many energy and space points, new sensitivity vectors are required at each and the calculational cost may well become prohibitive as a new adjoint flux is necessary in each case followed by the generalized perturbation theory calculations.

The experiment is categorized in the benefit by w and G. The cost is determined essentially by w and x. G only influences the cost through the x required. The reactor environment for which data are needed appears only through the sensitivities H or the S_R. As the economic approach has not been employed to date, emphasis has been on data chosen to determine a specific responce. This leads to one class of common integral experiments, the "mock up" in which one chooses the experiment so G closely approximates an S_R. The second class of common experiment focuses on some part of the data which has large dispersion and at least reasonably large components S_R and chooses the experiment to be sensitive and account for that data, i.e. chooses large values of the G_i for the appropriate choices of the index "i". A third class of common experiment allows a spectrum and materials choice leading to G which is moderately close to that of a reactor, but with fewer materials and very simple geometry in order to minimize problems with the calculational model.

The case of a hybrid reactor on first inspection appears to be a special case involving as it does fission, important resonance behavior and fertile materials. However, it is possible to separate the problem into a source problem without fission and a multiplying medium driven by the first generation fission source. The data for the second part has already been subjected to very close study and the data problem for the first is very similar to the pure fusion data assessment problems. The difference being more in the choice of materials. This can be made explicit by taking the angular distribution as a superposition of two parts ϕ_1 and ϕ_2. The transport operator is separated into the sum of the transport operator without fission H and a fission source operator F. Thus

$$\phi_1 = H\phi_1 + S, \qquad \phi_2 = (H + F)\phi_2 + F\phi_1,$$

$$\phi = \phi_1 + \phi_2, \qquad \phi = (H + F)\phi + S.$$

The advantage of this division is that ϕ_1 and ϕ_2 can be solved using different calculational models and different data sets if this seems appropriate. For example, the Soviet calculational model employed in their hybrid studies uses Monte Carlo

calculations and a variety of data sets in determining ϕ_1, ϕ_2, on the other hand results from diffusion theory calculations using a well tested data set from their fast reactor program. This calculational procedure allows the treatment of three dimensional problems rather easily but is not as easily adapted to sensitivity studies.

The formalism described here allows direct treatment of errors and can be coupled with other statistical procedures to assess the consistancy of the data adjustments. This will aid the analyst in deciding when hidden or overlooked errors are present. However, the calculations traditionally performed must still be carried out in order to obtain the sensitivity coefficients. They will still be needed in order to find the source of the discrepancy unless one is willing to do pointwise sensitivities.

The responses of interest in pure fusion are all linear functionals of the flux. In the case of hybrid systems bilinear and ratios of linear functions may be important. The nuclear responses fall into five categories. These are fuel production, energy production, radiation damage, shielding, and radioactivity generation. In the fuel category is tritium production, and in the case of hybrids fissile isotope production. Energy production responses include neutron and gamma energy deposition and the "Q" value weighted sum over all reactions including fission in the case of hybrids. The radiation damage responses are the displacement production, the charged particle production, and the transmutation rates. Of course there are uncertainties in the displacement rate due to other sources than nuclear data, but these will be independent and therefore additive. The shielding responses are weighted sums over the leakage spectrum which summarize the energy leakage and dose. Finally, the radioactivity responses include decay heat, biological hazard potential, activity, and dose after shutdown. Integral experiments may be chosen to determine one of these responses directly if it is desired to eliminate uncertainties in interpretation of instrumentation responses.

A search for integral experiments in this field located ten of them dating from 1951 to 1976.* These are listed and numbered chronologically with the laboratory and the numbers of the references in Table I. Table II describes briefly the experimental facility and the quantities measured. Table III contains information about analysis methods and accuracies.

The neutron sources are all D T sources employing an accelerator for the deuterons to a tritiated metal target. The source intensities are often not mentioned. Four are metallic Lithium assemblies, either spheres or cylinders, one is a Li D sphere. Three employ graphite as the medium, an iron sphere and

---

*An additional experiment referred to in reference 12 was discovered too late for inclusion.

a metallic Uranium pile round out the group. They all make serious attempts at keeping the geometry simple. For example five of the experiments employed spherical geometry.

None of these experiments is intended to be a mock up of a reactor blanket, although the large metallic Lithium assembly with the graphite reflector should produce a spectrum moderately close to that of a graphite reflected Lithium cooled blanket. Most measured quantities are rather unlike the reactor responses except for the tritium production. Thus the experiments tend to fall in the category of benchmark experiments which are reasonably easy to calculate and test data in a general way. The pulsed sphere experiments are an exception in that they focus attention on some of the high energy data where uncertainties may be large. This will result in a large sensitivity for energy leakage and helium production which are sensitive to this data.

A wide variety of detectors are employed. The NE 213 Proton Recoil System is used in experiment numbers 6,8,9, and 10. These are all recent experiments and this was the only detector in several cases. Experiments 3 and 5 use a wide variety of foils. These are capable of extracting a great deal of information. Particularly when they detect reactions expected in a fusion reactor. Experiments 2 and 7 use fission and breeding reactions and should yield information of value in hybrids. Spectral measurements with track detectors produce large amounts of data. However, this is not directed to a specific response and this requires some care and effort in determining its quantitative relevance to our needs.

Regarding the use of a flux measurement, if the theory outlined earlier is to be used, the experiments sensitivity to the data must be calculated. This is normally done with perturbation theory and an adjoint for the perturbation calculation must be determined. If the flux in a narrow energy range at a point is measured, the adjoint source is a delta function in both position and energy. The term $w(G_R^T D G)^2$ in the error improvement depends on G having a large scalar product with

$$N^T \quad G_R^T D$$

where one might call N the "need" vector as it incorporates the response sensitivity and the uncertainty in the data. Choice of appropriate flux measurements to make G and w large where N is large is difficult. Due to the expense of analysis at each point, it is probably appropriate to combine experimental data into a new partly experimental and partly numerical integral result suited to the user's needs.

Most of he references report experimental accuracies, and then test data by calculating the measured quantities and comparing calculated and experimental results. This is often done with more than one data set. The data difference between sets and the relative agreements with experiment are then used to gain insight into the data adjustments likely to give better agreement.

This may lead to data adjustment and guide future experiments. In an earlier era, it was almost impossible to discuss results between different institutions as they used different data bases and calculational procedures. An inspection of the references here shows that the situation has almost reached the opposite extreme. For example, two reports gave no analyses, five used 1D calculations implemented with the ANISN computer code for the calculations. One employed DTF IV and one DTF which are hardly independent codes. Two experiments were analyzed with the TAPI program (an analogue Monte Carlo) which represents an independent calculational method. The two dimensional discrete ordinates programs DOT and TWOTRAN were also used occasionally as was the MORSE Monte Carlo program. The data sets also tended to be the same. Generally only ENDF/B III and ENDF/B IV were used. The only exception being the LLL analyses which employed ENDL as well as ENDF/B. The limited independence in this respect leads to some concern that all will miss important errors together.

The final points of importance to be discussed are the errors in the experiments and the discrepancies between the calculated and experimental results. The experimental results are mostly accurate to 5 to 10%. Volume integrated results are at the lower end of this range. Pointwise results are at the upper end of the range and in some cases somewhat worse. This is significantly better than the comparison between calculated and experimental results. These disagree by amounts ranging from around 5 to 30% with a few worse cases. However, discrepancies are not a factor of two or more if the most recent data are used. The discrepancies imply the errors in the differential data result in large enough response errors (C_F DTO) C_p) that sequential adjustment of the data using these integral results should result in significant improvement in the calculation of reactor performance.

The use of the theory presented, as was pointe , has not been employed in the analyses of the data in most instances. One exception is noted. In the analyses of experiment I given by Bemple and Muir[1] a covariance matrix has been constructed for the tritium production in ^{6}Li and this was used in evaluating the data adjustment implied and its consistency with experimental errors.

The experiments discussed above are primarily related t blanket design or to testing some specific data. They do not directly address specific design quantities except for tritium production. If tritium production can easily exceed unity by an amount necessary to make up losses, an error in its determination may have little economic consequences. This other response should be given increased attention.

The DCTT program plan in the shielding area calls for a major program of integral experiments to address the neutron and gamma ray problems aimed particularly at the needs of TFR. This program is to be carried out at ORNL and began in October, 1976. The five year program will involve four phases. The first will study an unpenetrated design approximately one meter thick. It is

expected to be a laminated structure of steel and borated polyethylene. A heavy metal laminate to stop gamma photons at the back will be considered. The first results are expected in 0 to 6 ... later phases will address penetrations, and unpenetrated and penetrated mock ups of the actual TNS design.

Integral experiments will be important in testing data and calculational models in fusion power development. A theory is available for quantifying the value of proposed experiments and of adjusting data using results from available experiments. At the present time, this can only be used to give perspective on the choice of experiments. There is a need for covariance data to allow application of the theory. There is also a need for economic studies to allow a better value judgement on errors.

There are a number of competently chosen and executed experiments already available. They have aided in data assessment and should contribute to data adjustment which will significantly reduce expected response errors when covariance data becomes available.

The author would like to acknowledge assistance and helpful discussions with a number of people. These include in particular P. F. Haight, D. W. Muir, W. G. Vogelsang and Tang Wu.

This research is supported by the U.S. Energy Research and Development Administration under Contract No. EX-76-C-02-2272.

REFERENCES

1. Federov, V. V., Theory of Optical Experiments, Academic Press, New York, 1972.
2. Bracchev, L. N. and Bobkov, Yu. G., Mathematical Theory of Experiments and Generalized Perturbation Theory — An Effective Approach to Reactor Physics Investigations, IAEA (CEP) 53/L, IAEA, Vienna, 1974.
3. Fotov, V., and Shatalov, G.I., Gas Cooled Blankets for a Hybrid Thermonuclear Reactor with Solid Li Containing Materials, Proceedings of the IPPJ-IAEA Symposium on Fusion Fission Reactors, CONF-760744 pp. 179, July 1976, LLL.
4. Muir, D. W., and Wyman, M. L., Neutronic Analysis of a Tri Fusion Production Integral Experiment, Tech. of Controlled Nuclear Fusion Experiments and the Engr. Aspects of Fusion Reactors, CONF-771111, 1978.
5. Pemple, W. A. and Muir, D. W., Neutronic Data Consistency Analysis for Lithium Blanket and Shield Design, Tech. of Controlled Nuclear Fusion, CONF-760935, p. 3, p. 861, 1976.
6. Weale, J. W., Goodfellow, H., McTaggart, M. H. and Mullendyr, M. L., Reactor Science and Tech., 18, 91, 1964.
7. Haight, P. G., Lee, J. D., and Manrescalo, J. A., Nuclear Sci. and Eng., 61, 57, 1976.

5. Benjamin, P. W., Goodfellow, H., Gray, J., Wertle, F. W., Measurements of Neutron Reaction Rate Produced by a 14 MeV Neutron Source at the Center of a Cylindrical Lithium Pile, AWRE Report No. SP 164, Aldermaston, Berk., 1964.

9. Cloth, P., Filges, D., Gruber, H., Herrmann, F., Stockhausen, G. F., and Wolle, F., Studies of the Space Dependent Tritium Production and the Fast Flux Distribution in a Lithium Blanket Experiment, Proc. 5th Symposium on Fusion Technology, The Netherlands, 1-5 June 1964.

10. Hall, P. F., Measurement of 14 MeV Neutron Slowing Down in Graphite, RNL Annual Report for 1965 on Controlled Thermonuclear Reaction Technology, RNL 1965, Richland, Washington, 1965.

11. Kappler, F., Resch, H., Wertle, H., and Wick, H. W., Determination of Neutron Spectra in a Lithium Sphere, 5th Symposium on Fusion Technology, The Netherlands, 1964.

12. Nakasima, H., Sekiguchi, T., Hirayama, H., and Morimoto, H., Nuclear Sci. and Eng., 1, 1, 1965.

13. Johnson, P. H., Dorning, J. J., and Wehring, B. W., Integral Tests of Neutron Cross Sections for Iron above 1 Mev, Trans. American Nuclear Soc., 17, 1973, 1-2.

14. Smith, W. F., Jr., and Draper, Jim, Jr., Measured and Calculated Fast Neutron Spectra in a Graphite Medium, Trans. American Nuclear Soc., 17, 502, 1973.

15. Hansen, E. F., Wong, C., Komoto, T., and Anderson, J. P., Nuclear Sci. and Eng., 60, 1, 1976.

16. Hansen, E. F., Wong, C., Komoto, T., Anderson, J. P., Dean, P. N., and Henderson, P. N., Nuclear Sci. and Eng., 54, 1, 1974.

Table I

Experiment Number	Year Reported	Laboratory	Key References
1	1964	Los Alamos Scientific Laboratory	3,4
2	1971	Atomic Weapons Research Establishment	5,6
3	1974	Atomic Weapons Research Establishment	7
4	1974	Institut fur Reaktorentwicklung, Julich	8
5	1974	Battelle Pacific Northwest Laboratories	9
6	1974	Institut fur Neutronenphysik and Reactortechnik, Karlsruhe	10
7	1975	Japan Atomic Energy Research Institute	11
8	1975	University of Illinois	12
9	1975	University of Texas	13
10	1975	Lawrence Livermore Laboratory	14,15

Table II

Experiment Number	Experimental Facility	Measurements
1	30 cm sphere of natural Li D	Reaction rates for Li 7(n,t) and natural Li(n,t) as a function of detector position
2	Natural Uranium metal pile 106.6 cm high and up to 99 cm in diameter	Reaction rates as a function of position for Cu 63(n,2n), U 235 (n,f), U 238(n,f), U 238(n,γ), Pu 239(n,f)
3	Metallic natural Lithium cylinder 101.6 cm high and 99 cm in diameter	Li 7(n,t), Li 6(n,t), Au(n,γ) Au(n,2n), Pu 239(n,f), U 235 (n,f), U 238(n,γ), Np 237(n,f), Th 232 (n,f), U 236 (n,f), P 31 (n,p), Al 27 (n,p), Al 27(n,α), Ag 107 (n,2n), Cu 63(n,2n), and flux spectra and neturon leakage
4	Metallic natural Lithium cylinder 120 cm high, 120 cm outer diameter, 20 cm void at the axis	As a function of position, Li (n,t) reactions by radiochemical methods and by solid state track recorders, fast flux by thorium fission fragment track recorders
5	Large graphite stack	As a function of position, reaction rates for Au 197(n,γ), Au 197(n,2n), Mn 55(n,γ), Cu 63 (n,γ) Cu 63(n,2n), Ni 58(n,p), Cr 53(n,2n), Al 27(n,p), Al 27 (n,α), Mg 27(n,p), Ti 48(n,p)
6	100 cm Lithium metal sphere with 6 cm stainless steel shell	Flux spectra at 10 and 32 cm by time of flight, 10 m flight path, Li 6 glass detector 10 KeV to 1 Mw, NE 213 detector, 250 KeV to 14 meV.
7	Pseudo spherical metallic Li with and without graphite reflector. Inner cavity 10 cm, lithium to 34.1 cm, graphite to 55.4 cm	As a function of position, fission rates in U 235, Np 237, U 238, Th 232.

Table II (cont.)

Experiment Number	Experimental Facility	Measurements
8	76 cm diameter iron sphere	NE 213 neutron spectrometry
9	244 cm cube of graphite	NE 213 proton-recoil spectrometry
10	Spheres of carbon, oxygen, aluminum, titanium, and iron. 1-5 mean free paths in radius.	Time of flight NE 213 detector measurement of leakage spectra at two angles. Flight paths of 766 and 975 cm.

Table III

Experiment Number	Data and Calculational Basis	Appropriate Experimental Error and Experiment-Calculation Discrepancies
1	ENDF/B-III, IV; NJOY; DTF-IV; ALVIN	Experimental 5% volume integrated results ≲ 12% spatial Discrepancies from Figure 3 · 20% of the reference case.
2	ENDF/B-IV, ENDL, CLYDE, TART	Experimental 3-6% except for U-238 (n,3n) reaction rate. Discrepancies 5-40%.
3		Experimental: total tritium production < 5%. Spatial scatter in excess of 10%.
4	ENDF/B-I, III; SUPERTOG; ANISN, DOT-II, MORSE	Not given quantitatively but figures indicate large experimental errors and discrepancies with calculations
5	ENDF/B-III, ETOG, ANISN, TWOTRAN	
6	ENDF/B-III, DTK(SN)	10% mean error, spectral error, 5-10%. Discrepancies around 30%.
7	ENDF/B-III, SUPERTOG, ANISN	Experimental Ratio 6-7% Discrepancies 10-50%.
8	ENDF/B-III, IV; DNA; DLC-2D, 27C, ANISN	
9	ENDF/B-IV, SUPERTOG-III, DLC-2D, ANISN	Discrepancies as large as 73%.
10	ENDF/B-III, IV; ENDL, CLYDE, TART	Experimental errors ± 7%. Discrepancies generally 10-20% but as high as 5 [illegible]

Integral Testing of Neutron Activation Cross Sections Using the $^{9}Be(d,n)$ Reaction at 14-16 MeV*

L. R. Greenwood and R. R. Heinrich
Argonne National Laboratory, Argonne, Illinois

ABSTRACT

Integral measurements have been made for 22 neutron activation cross sections using the $^{9}Be(d,n)$ source at 14-16 MeV at the Argonne Tandem Accelerator. The differential neutron flux and spectra were measured in the angular range from 0-25° by the time-of-flight technique. Comparison of the integral and differential results allows an evaluation of accuracy and consistency of differential neutron cross section data.

DIFFERENTIAL MEASUREMENTS

The 14 and 16 MeV deuteron beams from the Argonne Tandem Accelerator were stopped in a thick (6.4 mm) beryllium target backed by 1.6 mm of brass. Beam currents up to 2 μA produced neutron fluxes as high as 3×10^{10} neutrons/cm^2-sec immediately behind the beam stop. The flux at 5-10 cm distances from the source was in the range of 10^8-10^9 neutrons/cm^2-sec which is quite adequate for testing dosimetry data in the 1-20 MeV energy range with irradiation times of 6-12 hr.

Time-of-flight measurements were made with a pulsed beam from the accelerator with a time resolution of about 4 ns at flight paths of 2.0 and 3.7 meters. Neutrons were detected by a cylindrical NE213 liquid scintillator measuring 4.7 cm in diameter by 4.6 cm in length. Pulse shape discrimination was used to suppress the gamma background which was less than 1% of the neutron flux. The detector efficiencies were computed with a Monte Carlo code[1] and were checked by measuring the spectra from a ^{252}Cf source (5.9 ng) using the time-of-flight technique. The measurements and calculations were found to agree within 10% in the energy range 1-10 MeV.

Figure 1 shows the measured differential neutron spectra at 16 MeV at angles from 0-25° and illustrates how rapidly the spectral shape changes with angle. The integrated flux, shown with various lower energy limits in Fig. 2, drops rapidly with increasing angle, decreasing by a factor of two from 0° to 20°. Note that the low energy flux steadily declines with angle, whereas the flux above 14 MeV actually increases out to an angle of 15° and then declines at larger angles. Obviously, these rapid

*Work performed under the auspices of the U.S. Energy Research and Development Administration.

changes in the flux and spectra with angle, coupled with the decline in flux with distance from the source, necessitated that geometric corrections be made for samples placed close to the source.

INTEGRAL MEASUREMENTS

Thirteen foil materials[2] were irradiated under three different conditions, as listed in Table I. Gold and aluminum foils were placed at several positions in the package in order to provide a check on the geometry and absorption corrections. The circular foils measured 0.953 cm in diameter, which corresponded to an average angle of about 5° at a distance of 5 cm from the source. Weights were chosen to obtain adequate activities for Ge(Li) gamma counting for an irradiation of approximately 12 hr duration.

Table I

Irradiation Parameters and Foil Specifications

Run Label:	A	B	C
Deuteron Energy (MeV):	16	14	16
Distance from Source (cm):	4.88	4.88	2.01
Average Beam Current (μA):	0.61	0.96	1.02
Length of Irradiation (hr):	12.42	11.42	6.52

Foil Material	Thickness (mm)
Au	0.051
Al	0.127
Ni	1.524
^{235}U	0.224
Ti	1.016
^{238}U	0.457
Sc	0.508
Au	0.051
Al	0.127
Fe	0.127
Zr	0.762
Cu	0.635
Co	0.762
In	0.127
Nb	0.508
Au	0.051
Al	0.127
Total	7.183

The 13 different foils provided twenty-two separate reactions for testing as listed in Table 2. The 95% sensitivity limits of the various reactions are shown graphically in Fig. 3. At least 18 additional reactions were also seen, however, no cross section data is generally known for these reactions [e.g., $^{63}Cu(n,p)^{63}Ni$, $^{58}Ni(n,np)^{57}Co$, $^{40}Ca(n,\alpha)^{37}K$, $^{90}Zr(n,p)^{90m}Y$, and $^{238}U(n,2n)^{237}U$]. The $^{63}Cu(n,\gamma)$ and $^{63}Cu(n,2n)$ reactions both lead to ^{62}Cu and hence cannot be resolved. This problem also occurs in zirconium and indium.

Table 2 also lists the half-lives, gamma-ray energies, and branching ratios which we used in this study. All foils were counted on one of three Ge(Li) gamma detectors at least three times in order to establish good counting precision and to check the accuracy of half-lives. The calibration of our detectors has been checked against other laboratories in the ILRR program and found to be in agreement within 1.5%.

The saturated foil activities were calculated from the activity rate at the end of irradiation ($\dot{N}_0$) from the relationship:

$$\bar{\Phi} = \frac{\dot{N}_0}{m\,B\,A\,F\,S}$$

where m = number of target atoms
A = isotopic abundance
F = fission yield for fission foils
S = gamma self-absorption in foil
B = correction for decay during irradiation

For a steady state flux, $B = 1 - e^{-\lambda t}$, where t is the total length of the irradiation. For our irradiations, an accurate record of the beam current was recorded versus time, and B was computed by integrating over each time segment.

The calculated saturated activities were then corrected to the common geometry of the front foil position. This was done by fitting the time-of-flight fluxes to simple polynomials as a function of neutron energy and angle and integrating over the specific foil geometry for each of the 22 reactions. Absorption corrections were also made by calculating the average absorption due to each foil and these corrections were checked experimentally by the gold and aluminum reactions at three locations in the foil stack. An NBS-type[1] fission chamber was also used to check both corrections by first moving the chamber along the beam axis and then measuring with and without foil packets in front of the chamber.

COMPARISON OF INTEGRAL AND DIFFERENTIAL RESULTS

The final saturated activities which we have measured should be directly calculable by integrating the measured time-of-flight

Table 2

Activation Reactions and Nuclear Data

Reaction	$t_{1/2}$ [a]	E_γ, keV	Branch, %	Data Source [b]
$^{27}Al(n,\alpha)^{24}Na$	15.00 H	1368.599	99.993	A
		2753.965	99.873	
$^{45}Sc(n,2n)^{44}Sc$	2.44 D	270.9	98.6	B
$^{46}Ti(n,p)$ / $^{45}Sc(n,\gamma)$ ^{46}Sc	83.9 D	889.253	99.984	A
		1120.521	99.987	
$^{47}Ti(n,p)^{47}Sc$	3.40 D	159.381	69.0	A
$^{48}Ti(n,p)^{48}Sc$	1.83 D	983.4	99.987	A
		1037.4	97.5	
		1311.8	99.992	
$^{54}Fe(n,\alpha)^{51}Cr$	27.7 D	320.076	9.83	A
$^{54}Fe(n,p)^{54}Mn$	312.5 D	834.827	99.97	A
$^{56}Fe(n,p)$ / $^{59}Co(n,\alpha)$ ^{56}Mn	2.58 H	846.6	99.0	B
$^{59}Co(n,p)^{59}Fe$	44.6 D	1099.228	56.1	A
		1291.568	43.6	
$^{59}Co(n,2n)^{58}Co$ / $^{58}Ni(n,p)^{58}Co$	70.85 D	810.75[illegible]	99.44	A
$^{58}Ni(n,2n)^{57}Ni$	36.0 H	1377.6	84.9	B
		1919.6	14.9	
$^{90}Zr(n,2n)^{89}Zr$	78.5 H	909.2	100.0	B
$U(n,f)^{95}Zr$	64.1 D	724.179	44.1	A
		756.710	54.6	
$^{93}Nb(n,2n)^{92m}Nb$	10.13 D	934.46	99.15	B
$U(n,f)^{103}Ru$	39.43 D	497.08	89.0	A
$^{115}In(n,n')^{115m}In$	4.486 H	336.23	45.9	A
$U(n,f)^{140}Ba$ [c]	12.789 D	537.35	24.4	A
$U(n,f)^{140}La$ [c]	40.26 H	1596.18	95.4	A
$^{197}Au(n,2n)^{196}Au$	6.1 D	355.73	87.7	A
$^{197}Au(n,\gamma)^{198}Au$	2.6956 D	411.794	95.52	A
$^{238}U(n,\gamma)^{239}Np$ [d]	2.355 D	277.60	14.3	A

[a] H = hour, D = day

[b] A = R. G. Helmer and R. C. Greenwood, Nucl. Technol. 25, 258 (1975), as updated to the ILRR Program in February 1977.
B = Nuclear Data Tables 13, 2-3 (1974).

[c] ^{140}Ba decays to ^{140}La - products are counted in equilibrium.
[d] ^{239}U decays to ^{239}Np with a half-life of 23.5 minutes.

neutron spectra times the differential reaction cross sections over neutron energy. Due to the finite angular size of the foils, the time-of-flight spectra as a function of angle must be averaged over the area of the foils. The resulting averaged spectra were close to the spectra obtained at 5°.

All neutron cross sections were taken either from the ENDF/B-IV[7] library or from the results of Bayhurst [illegible] at Los Alamos. The latter include the $^{27}Al(n,\alpha)$, $^{45}Sc(n,2n)$, $^{58}Ni(n,2n)$, $^{90}Zr(n,2n)$, and $^{197}Au(n,2n)$ reactions. The $^{59}Co(n,p)$ and $^{93}Nb(n,2n)$ reactions were taken from the general ENDF/B-IV files. The $^{56}Fe(n,\alpha)$ cross sections were taken from BNL-325.[8] The THRESH[9] code was used to extrapolate several cross sections into energy regions where data were not available.

The integral and differential measurements are compared in Table 3 which lists the ratio of the measured-to-calculated saturated activities. As can be seen, the ratios obtained for the three independent experiments agree quite well. Absolute values of the ratio are estimated to be accurate within ±10% except for the (n,γ) and $^{235}U(n,f)$ reactions. These reactions are more uncertain since our time-of-flight measurements did not extend below 1 MeV.

CONCLUSIONS CONCERNING NUCLEAR DATA

The activity ratios shown in Table 3 are grouped according to reaction type for easy comparison. Several reactions show large discrepancies, notably the $^{59}Co(n,p)$, $^{46}Ti(n,p)$, $^{45}Sc(n,2n)$, $^{58}Ni(n,2n)$, and $^{197}Au(n,2n)$. The ratios for reactions sensitive below 1 MeV are hard to evaluate since we do not know the spectra in this region and (n,γ) data is generally unreliable for high energy neutrons. For example, the $^{197}Au(n,\gamma)$ cross section will apparently be lowered about a factor of five above 6 MeV in ENDF/B-V.[7]

The errors in the ratios due to uncertainties in the neutron spectra are believed to be small. In order to test the reliability of the differential spectral data, we have used the SAND-II[10] spectral unfolding code to see if changes in the spectra noticeably improve the overall fit to the integral data. We found that only minor improvements could be made and that the $^{59}Co(n,p)$, $^{46}Ti(n,p)$, and $^{45}Sc(n,2n)$ reactions were consistently rejected as being outside of the normal standard deviation limits. This result is easily understood by examining the ratios for reactions with similar energy dependence listed in Table 3. That is, if two (n,p) or (n,2n) reactions with similar thresholds badly disagree, then no change in the spectra will improve the situation since both will be changed by about the same amount.

We thus conclude that the reaction cross sections which show the largest discrepancies in the ratio must be in error. In several discrepant cases, recently obtained cross-section data agrees much better with our observations. Data from D. L. Smith

Table 3

Tandem Activities

Ratio of Measured $\sigma\bar{\phi}/\sigma_{(ENDF)} \cdot \phi_{(TOF)}$

E_d, MeV Distance	16A 4.88 cm	16C 2.01 cm	14B 4.88 cm
AU197G	0.93	0.90	0.83
SC45G	0.88	0.86	0.81
U238G	0.86	0.94	0.81
U235F	0.92	0.93	0.79
U238F	0.98	0.98	0.82
IN115N	1.05	0.98	0.84
CO59P[a]	0.64	0.61	0.58
FE54P	0.96	0.94	0.86
NI58P	1.02	1.01	0.87
TI46P	1.10	1.11	0.99
TI47P	0.89	0.90	0.78
TI48P	1.45	1.34	1.55
FE56P	1.11	1.07	1.02
AL27A[b]	1.07	1.05	1.05
CO59A	1.13	1.12	1.08
FE54A[a]	0.89	0.82	0.97
AU197[b]	1.21	1.16	1.32
CO59[b]	1.12	1.12	1.30
NI58[b]	0.74	0.77	0.91
SC45[b]	1.24	1.27	1.55
ZR90[b]	0.99	0.97	1.15
NB93[a]	1.05	1.00	1.15
Std. Dev. %	18.7	16.2	25.9

[a]Data from general ENDF/B-IV[6] or BNL-325.[7]

[b]Data from B. P. Bayhurst *et al.*, Phys. Rev. C12, 451 (1975).

of [7,11] for the ^{59}Co(n,p), ^{46}Ti(n,p), and ^{115}In(n,n') reactions were used to recalculate the saturated activities and these results are shown in Table 4.

Table 4

Ratio of Measured-to-Calculated Activities Using Data from Ref. 11

Reaction	Data	E_d (MeV) 16A	16C	14B
^{59}Co(n,p)	ENDF/B-IV	0.64	0.61	0.58
	Smith	1.21	1.17	1.05
^{46}Ti(n,p)	ENDF/B-IV	1.45	1.36	1.55
	Smith	1.17	1.17	1.15
^{115}In(n,n')	ENDF/B-IV	1.05	0.98	0.84
	Smith	0.99	0.99	0.87

We should note that for the ^{59}Co(n,p) reaction, the data of D. Smith stops at 10 MeV and extrapolations were required from 10 to 20 MeV. For the (n,2n) cross sections from LASL, some extrapolation was also required in the threshold energy region where we have most of the neutron flux. The ^{58}Ni(n,2n) values from LASL disagree by at least 40% from those in ENDF/B-IV, however, the ENDF values were found to be in worse disagreement with our results, but in the opposite direction. The correct cross section values would thus appear to lie in between the ENDF and LASL values.

In conclusion, the techniques which we have used in this work will be quite valuable for testing the integral consistency of differential neutron cross sections. We have now performed similar measurements at incident deuteron energies of 30 and 40 MeV. At these higher neutron energies, cross section data is virtually nonexistent and must be either calculated or extrapolated from lower energy data. However, by comparing data obtained at a variety of neutron energies, it should be possible to evaluate the differential cross sections accurately enough to arrive at an integrally consistent set of reaction. for use in obtaining the neutron flux and spectra in close geometry at existing or planned (d,n) facilities.

REFERENCES

1. Neutron efficiencies were computed by a version of the GSS code of R. F. Hester and R. Y. Verbinski, ORNL 4160 (1968), modified by W. P. Poenitz, ANL 7915 (1972), and further modified by us.
2. Most of the Mark grade foils were obtained from Material Research Corp., Orangeburg, N.Y.
3. Nucl. Technol. 25 (1975).
4. J. A. Grundl, D. M. Gilliam, S. D. Dudey, and R. L. Popek, Nucl. Technol. 25, 247 (1975).
5. ENDF/B IV Dosimetry File, BNL 20-5 50446 (1975).
6. R. P. Haybron, J. S. Gilmore, R. J. Prestwood, J. H. Wilhelmy, N. Lurie, R. H. Erkkila, and F. A. Hondebrod, Phys. Rev. C12, 451 (1975).
7. BNL 325, Vol. 3, Third Edition (1976).
8. S. Pearlstein, BNL 16271 (1972) and ENDF/B-V revision (1975).
9. Preliminary data presented by A. Paulsen (CBNM Geel, Belgium) at the International Symposium on Neutron Standards and Applications, NBS (March 29-31, 1977).
10. Neutron Flux Spectra Determination by Multiple Foil Activation, ASTM STP 682 (1979).
11. D. L. Smith and J. W. Meadows, ANL/NDM-13 (1975); D. L. Smith, ANL/NDM-26 (1976), D. L. Smith and J. W. Meadows, Nucl. Sci. Eng. 55, 415 (1975), and Nucl. Sci. Eng. 60, 197 (1976).

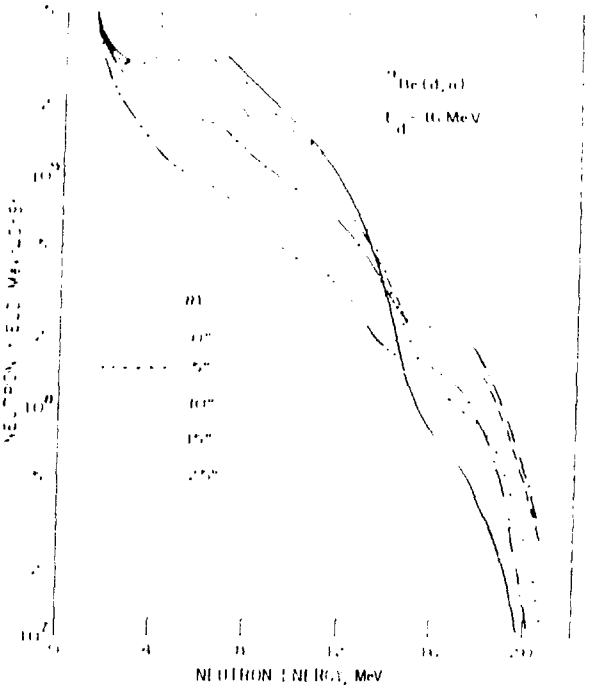

Fig. 1. [illegible]

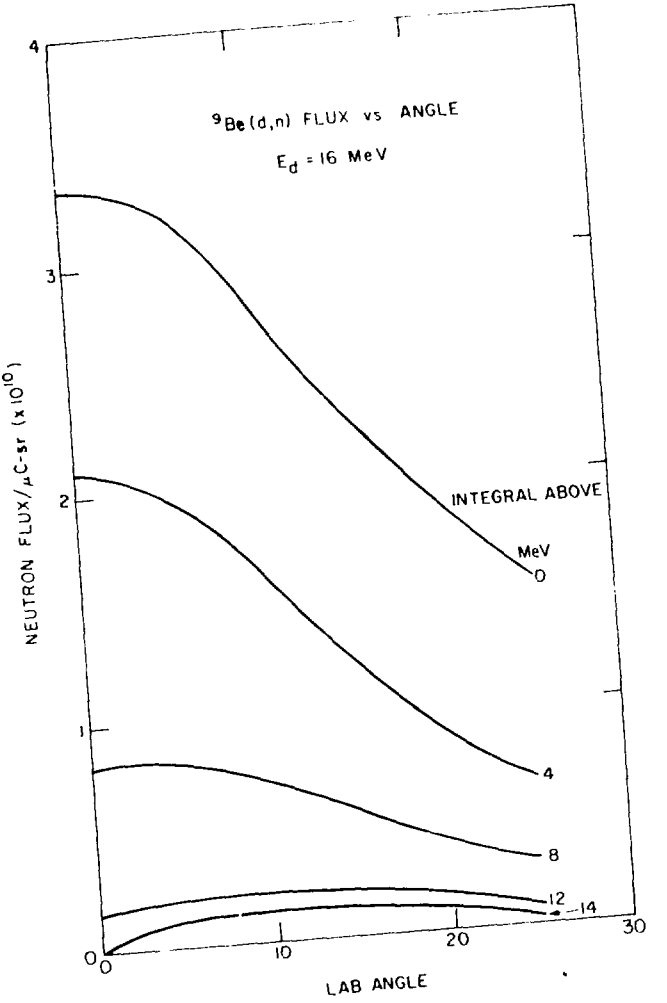

Fig. 2. The integral neutron flux is shown versus angle for ^{9}Be(d,n) at 16 MeV. The top curve is the total flux whereas the lower curves represent the flux above the neutron energy indicated.

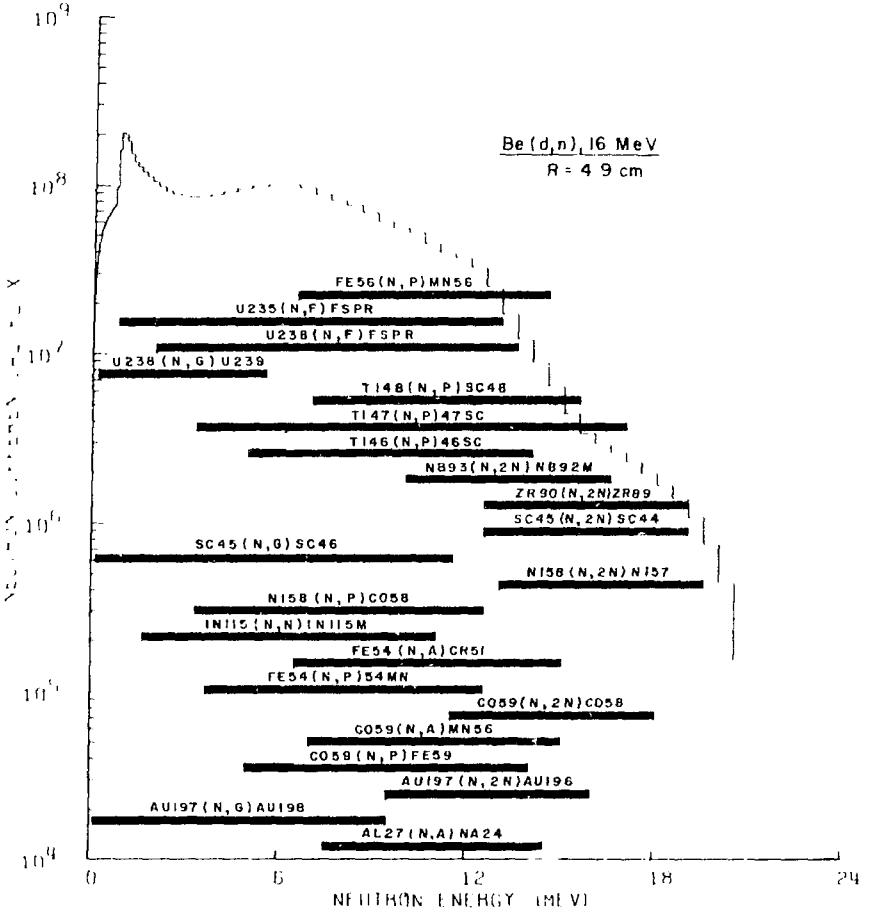

Fig. 3. The 95% sensitivity limits are indicated for the 22 reactions we have studied. The curve is the calculated average flux for 16 MeV at 4.88 cm from the source.

Conf-770523 -1

Differential Integral Experiments for Testing Cross Section Evaluations for Fusion Reactors*

L. F. Hansen, J. D. Anderson, C. Wong and T. Komoto
Lawrence Livermore Laboratory, Livermore, California

ABSTRACT

The conceptual design of fusion reactors and fusion-fission hybrid reactors brings into focus a large number of problems dealing with the interaction of 14-MeV neutrons with materials to be used in the design of the different components of the reactor. These components include the first wall, the blanket, the magnets and the shielding system. The accuracy of the design calculations can be assured providing the transport codes correctly describe the interaction of 14-MeV neutrons with these materials. As part of the Pulsed Sphere Program at Livermore, measurements of the neutron and gamma emission spectra from a large number of materials ranging from Li to Pu have been carried out using the sphere transmission and time-of-flight techniques. The comparison of these measurements with calculations has provided a powerful tool to test the accuracy of the cross sections used in the calculations, the mathematical assumptions and approximations introduced in solving the transport equations and to check for possible errors in the coding stage of the calculations. Some specific cases will be discussed to illustrate the value of the measurements.

INTRODUCTION

A large number of feasibility studies and optimum design studies of fusion and fusion-fission hybrid reactors have been carried out in the last couple of years.[1] These studies have employed neutron and photon libraries such as the ENDF/B-III (Ref. 2), the ENDF/B-IV (Ref. 3), and the ENDL (Ref. 4), and Monte Carlo and/or discrete ordinate transport codes, available at different laboratories. Questions related to the radiation damage of the first wall, neutron economy, energy deposition in the blanket, shielding of the superconducting magnets, penetration shields and biological shields can only be resolved if the transport of neutrons and photons in the materials being used in these reactors can be correctly calculated. The accuracy of these calculations can be estimated by finding out how well the neutron-photon libraries and transport codes can reproduce integral measurements of the neutron and photon spectra from the interaction of 14-MeV neutrons with these materials. Pulsed Sphere Measurements carried out with good resolution for a simple geometry and composition provide a stringent test of input cross sections and transport codes.

*Work performed under the auspices of the U.S. ERDA.

EXPERIMENTAL METHOD

The nominal 14-MeV neutrons are produced by the Livermore insulated-core-transformer (ICT) accelerator. The neutron and gamma spectra are measured using the sphere transmission and time-of-flight techniques. Flight paths between 7 and 10 m are used in these measurements. Measurements of the emitted neutron spectra are carried out for two different energy regions: a) neutrons between 15 and 2-MeV, (high energy spectra) and b) neutrons between 1-MeV and a few keV (low energy spectra). The gamma spectra are measured between 250-keV and 10-MeV. The high energy neutron spectra and the gamma spectra are detected using NE213 liquid scintillators (5.08 cm diam., 5.08 cm long). The swept and bunched deuteron beam (2.5 or 0.5 MHz and $\sim$1 ns width) is used for the high energy neutron measurements. The low energy measurements employ just a swept beam (1 or 10 KHz and $\sim$100 ns to 10 μs width). The deuteron beam impinges upon a tritium-titanium target mounted at the end of a low mass assembly and centered at the spherical targets. The 2.06 cm diameter titanium layer is evaporated on a tungsten backing 0.051 cm thick. The neutron production is monitored by counting the recoil alpha particles with a thin ($\lesssim$ 50 μ) lithium-drifted silicon solid state detector set at 174° with respect to the deuteron beam line. A schematic drawing of the experimental set-up is shown in Fig. 1. The targets, solid spheres of the materials to be studied, have a truncated cone opening into which the low mass tritium assembly is inserted.

CALCULATIONAL METHOD

The neutron time-of-flight (TOF) spectra and the electron recoil spectra are calculated using a coupled neutron-photon Monte Carlo Transport Code, TARTNP. The variation in energy and intensity of the neutrons from the T(d,n)α reaction with angle is taken into account in the calculations. The low mass target assembly, the neutron detector collimator, and the air between the spheres and the detector have been programmed into the Monte Carlo calculations.

The neutron TOF spectra are converted to energy spectra to facilitate the comparison with energy spectra calculated by the time-independent transport method. The transformation is done relativistically assuming a flight path equal to the distance between the detector and tritium target. Since the flight path is much larger than the sphere radii, this approximation is justified, except for near critical systems.

The gamma measurements are presented as recoil electron spectra in the NE213 scintillators. The unfolding of the electron recoil spectra to obtain gamma spectra has not been attempted primarily because it is easier to fold in the detector response to obtain recoil electron spectra for comparison with measurements.

COMPARISON BETWEEN MEASUREMENTS AND CALCULATIONS

The Pulsed Sphere integral measurements have been called Differential-Integral measurements in this paper in order to call attention to the fact that for light elements where several MeV separation exists between the first excited level and the ground state, the measurements are sensitive to differential elastic and inelastic angular distributions. Typical cases are carbon and oxygen. Fig. 2 shows the TOF and energy spectra from 1.3 mfp carbon (10 cm) measured at 120° and the calculations with the ENDF/B-IV library. The energy spectrum shows structure dependent upon the differential elastic and 4.4-MeV inelastic angular distributions. This is possible since there is a good separation between inelastic neutrons from the 4.43-MeV level, elastic neutrons, and transmitted 14-MeV neutrons. In Fig. 2 the elastic neutrons contribute mainly between 15 and 10-MeV while the 4.43-MeV level inelastic neutrons extend mainly from 10 to 6-MeV. It is an integral experiment in the sense that the neutron spectrum is integrated over the 4π geometry. The disagreement in the energy spectra in the region of the transmitted peak in Fig. 2 results from the absence of the appropriate resolution function in the calculations.

Carbon, nitrogen and oxygen were the first materials measured and compared with calculations.[5] In 1971 a detailed description of the experimental method, together with the measurements for a large number of materials from Li to Pu was presented[6] in UCRL-51144, Rev. I. Different laboratories used these measurements to test their codes and input cross sections.[7,8] As a result of these comparisons, the following important revisions were carried out in the Monte Carlo transport Code: 1) A new code TART was written at this laboratory to replace the old SORS code. SORS used a temperature model for the secondary neutrons, while TART uses directly the evaluated secondary neutron distributions. 2) Angular distributions and cross sections were revised in the ENDL library, and 3) The number of energy groups was increased from 60 to 176 in order to better represent the energy dependence of the cross sections.

Calculations[9] with the ENDF/B-III existing at that time showed discrepancies of as much as a factor of 2. In 1974 this library was superseded by the ENDF/B-IV. Table I shows a comparison between the measured and calculated integrals for 1.3 and 2.9 mfp of carbon; for three neutron energy intervals: 15 to 10, 10 to 5 and 5 to 2-MeV. The disagreement in the energy spectra observed in the region of the transmitted peak in Fig. 2 does not affect the magnitude of the high energy integral since the integral from 10 to 15-MeV is sufficiently broad to be insensitive to the omission of the pertinent resolution functions.

It is surprising that the agreement found is so poor for the region between 2-10-MeV since carbon presumably is a material where a large number of cross section measurements are available.

The high energy integrals from 10-15-MeV are in good agreement which suggests that ENDF/B-IV has the correct total non-elastic cross section.

Table 1

Measured and calculated integrals using ENDF/B-IV for 1.3 and 2.9 mfp of carbon. The integrals are given as emitted neutrons/source neutron.

Thickness (mfp)	Energy Interval (MeV)	Experiment + 7%	TART ENDF/B-IV	Ratio %
1.3	15-10	4.473-02	4.444-02	1
	10-5	0.808-02	0.939-02	10
	5-2	0.829-02	0.520-02	59
	Total	6.110-02	5.903-02	4
2.9	15-10	2.394-02	2.254-02	6
	10-5	0.994-02	1.092-02	10
	5-2	1.148-02	0.710-02	62
	Total	4.536-02	4.056-02	12

From similar comparisons[10] for oxygen, aluminum, titanium, and iron it was concluded that ENDF/B-IV was a clear improvement over version III. The total integrals calculated with the version IV are consistently larger than those obtained with III, and in good agreement with the experimental values for all the 1 mfp spheres. However the discrepancies become larger than the 7% error quoted for the measurements as the number of mean free paths increases. For 2.6 mfp aluminum (24.8 cm), 3.5 mfp titanium (24.8 cm) and 4.8 mfp iron (21.7 cm) the calculated values with the ENDF/B-IV library are respectively 16, 9 and 20% lower than the measured values for the total integrals between 15 to 2-MeV. The discrepancy is even larger in the interval 5 to 2-MeV. Although superior to ENDF/B-III, ENDF/B-IV still is not adequate to completely describe the measurement, particularly that for the larger spheres.

The comparison[11,12] for the measured electron recoil spectra with calculations has been carried out only for a few materials of interest to air transport and to shielding applications. These especially relevant materials include nitrogen, water, concrete and iron. These studies are for low Z materials since the gamma contribution to the dose becomes dominant at large mfp. Calculations carried out by Battat and Dudziak[13] have shown that for 3.5 m of concrete (∿50 mfp) the gamma contribution to the total dose is 90%. The calculations carried out with the ENDL and ENDF/B-IV give similar results for nitrogen with discrepancies

between measurements and calculations[11] no larger than 10%. Table II gives the measured and calculated integrals for water, concrete and iron for two electron recoil intervals: 10-5 and 5-1 MeV. ENDF/B-IV gives excellent agreement in the total integrals for water and concrete. For iron discrepancies increasing from ∿ 5% at 0.9 mfp up to 60% at 4.8 mfp are encountered. Fig. 3 shows graphically this disagreement as a function of mfp for Fe.

Recently neutron measurements have been repeated for Be, ^{6}Li, ^{7}Li and teflon with better time resolution. Preliminary measurements for other materials of interest to magnetic confinement fusion reactors, such as Nb, Cu and Sn have also been done. The comparison of these data with calculations has proceeded slowly since no support exists for this effort. Fig. 4 shows the comparison between the measurements for 1.1 mfp ^{6}Li and ^{7}Li and the calculations carried out with the ENDF/B-IV. Overall, the agreement is good. However, the calculations do not reproduce too well the neutrons emitted between 11 and 7 MeV and underestimate the low energy neutrons, 6-2 MeV. It would be very interesting to extend the comparisons to larger numbers of mfp. Gamma emission spectra studies are also relevant for shielding and radiation damage studies in fusion reactors.

CONCLUSIONS

The different measurements presented in this paper were selected to illustrate the following points:

(1) Pulsed Sphere integrals experiments are sensitive to differential neutron elastic and inelastic scattering angular distributions. The 14-MeV component of the spectrum is directly affected by the non-elastic cross section.

(2) Comparisons between measurements and calculations have resulted in improvements in existing neutron transport codes and have provided checks on the input cross sections.

(3) Measurements of neutron and gamma spectra on materials of interest to the MFE community are very relevant since they provide a check on the codes and cross sections used in the design of conceptual fusion reactors. Agreement in the above comparisons would give us added confidence in the more complex fusion reactor calculations. The experiments are deliberately simple in design to allow close examination and criticism so that broad community attention is encouraged. By such means, discrepancies among calculations from different institutions may be more rapidly resolved.

Table II

Material	Energy Interval (MeV)	Experiment ± 7%	TART ENDF/B-IV	Ratio %
Water (ρ=1 g/cm^3)				
1.1 mfp	10-5	.192-08*	.298-08	55
	5-1	2.618-08	2.504-08	5
	Total	2.810-08	2.802-08	.3
1.9 mfp	10-5	.220-08	.355-08	61
	5-1	2.793-08	2.931-08	5
	Total	3.013-08	3.286-08	9
Concrete (ρ=2.35 g/cm^3)				
2.0 mfp	10-5	.254-08	.405-08	59
	5-1	5.001-08	4.910-08	2
	Total	5.255-08	5.315-08	1
3.8 mfp	10-5	.174-08	.280-08	61
	5-1	3.465-08	3.606-08	4
	Total	3.639-08	3.886-08	7
Iron (ρ=7.85 g/cm^3)				
0.9 mfp	10-5	.157-08	.209-08	33
	5-1	4.729-08	4.822 08	2
	Total	4.886-08	5.031-08	3
2.9 mfp	10-5	.089-08	.126-08	42
	5-1	2.920-08	3.872-08	33
	Total	3.009-08	3.998-08	33
4.8 mfp	10-5	.031-08	.041-08	32
	5-1	1.073-08	1.728-08	61
	Total	1.104-08	1.769-08	60

*08 same as 10^{-8}

Measured and calculated integrals using the ENDF/B-IV for 0.9 29 and 4.8 mfp of Iron. The integrals are given in electron pulses/ source neutron.

REFERENCES

1. First and Second Topical Meetings on The Technology of Controlled Nuclear Fusion. First: Conf. 740402-P1, April 16-18, 1974, San Diego, Ca. Second: Conf. 760935-P1, Sept. 21-23, 1976, Richland, Wa.
2. S. K. Penny, W. E. Kinney and F. G. Perey, ENDF/B Material 1180, Brookhaven National Laboratory.
3. ENDF-B Summary Documentation for ENDF/B-IV, Data File ENDF-201 to be published by Brookhaven National Laboratory, Neutron Cross Section Center.
4. R. J. Howerton, R. J. Doyas, T. C. Michels and S. T. Perkins, "Evaluated Nuclear Cross Section Library", Vol. 4, UCRL-50400, Lawrence Livermore Laboratory (1971).
5. L. F. Hansen, J. D. Anderson, E. Goldberg, E. F. Plechaty, M. L. Stelts and C. Wong, Time Spectra from Spheres Pulsed with 14 MeV Neutrons, Nucl. Sci. Eng. 35, 227 (1969).
6. C. Wong, J. D. Anderson, P. Brown, L. F. Hansen, J. L. Kammerdiener, C. Logan and B. A. Pohl, "Livermore Pulsed Sphere Program, UCRL-51144 Rev.", Lawrence Livermore Laboratory (1971).
7. E. D. Cashwel and G. D. Turner, "Pulsed Sphere Calculations at LASO CSEWG Shielding Subcommittee Meeting, May, 1973.
8. W. W. Rousin, E. A. Straker, G. W. Morrison, Calculation of Nitrogen and Iron LLL Pulsed Sphere Experiments, Oak Ridge National Laboratory, Amer. Nuc. Soc. 1971 Winter Meeting, 14, 925 (1971).
9. L. F. Hansen, J. D. Anderson, P. S. Brown, R. J. Howerton, J. L. Kammerdiener, C. M. Logan, E. F. Plechaty and C. Wong, "Measurements and Calculations of the Neutron Spectra from Iron Bombarded with 14-MeV Neutrons", Nucl. Sci. Eng. 51, 278 (1973).
10. L. F. Hansen, C. Wong, T. Komoto and J. D. Anderson, "Measurements of the Neutron Spectra from Materials Used in Fusion Reactors and Calculations Using the ENDF/B-III and IV Neutron Libraries", Nucl. Sci. Eng. 60, 27 (1976).
11. L. F. Hansen, T. Komoto, E. F. Plechaty, B. Pohl, G. S. Sedhu and C. Wong, "Measurements and Calculations of the Electron Recoil Spectra from Gamma Rays Emitted by Nitrogen for a 14-MeV Neutron Source", Nuc. Sci. Eng. 62, 550 (1977).
12. L. F. Hansen, T. Komoto and C. Wong, "Radiation Doses as a Function of the Thickness and Shielding Material Surrounding a 14-MeV Neutron Source", Fifth International Conference on Reactor Shielding, Knoxville, Tennessee, April 18-22, 1977.
13. M. E. Battat and D. J. Dudziak, "Shield Analysis for Intense 2.2-pj (14 MeV) Neutron Sources, Fifth International Conference on Reactor Shielding, Knoxville, Tennessee, April 18-22, 1977.

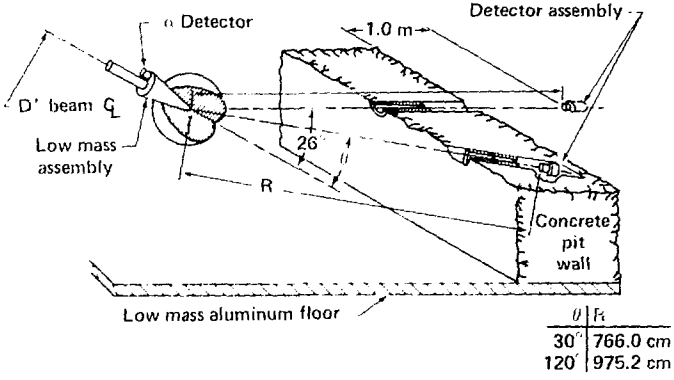

Figure 1. Schematic drawing of the experimental set-up.

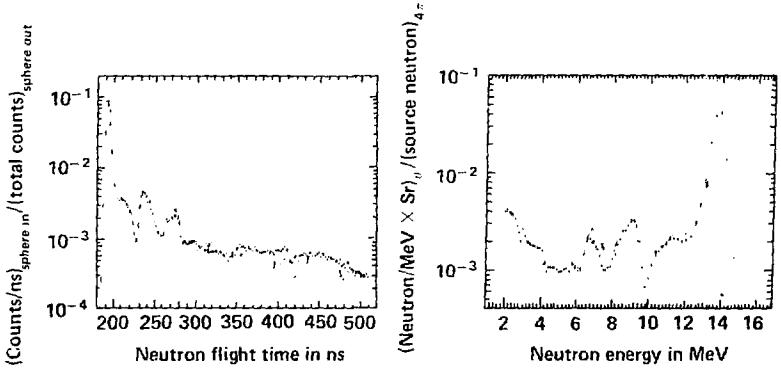

Figure 2. Measured and calculated neutron time-of-flight and energy spectra for 1.3 mfp of carbon. The calculations employed ENDF/B-IV cross sections.

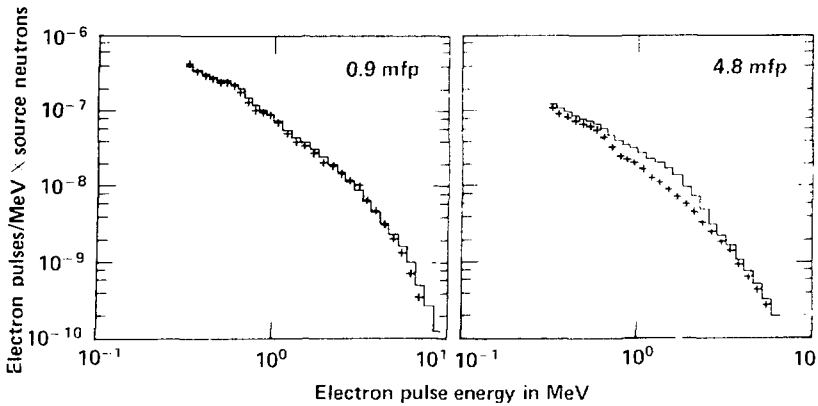

Figure 3. Measured and calculated recoil electron energy spectra using ENDF/B-IV for 0.9 and 4.8 mfp of iron.

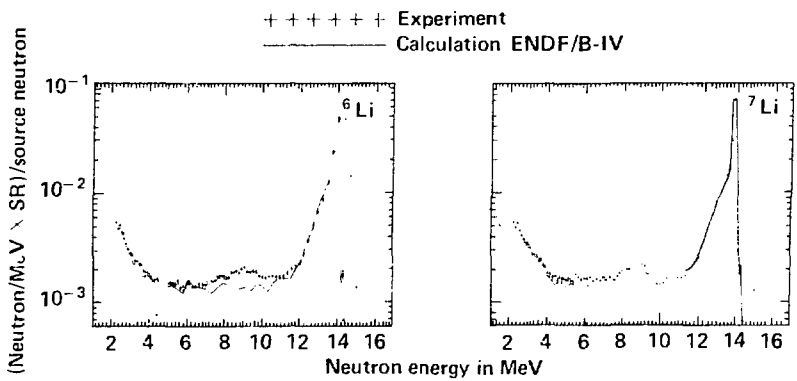

Figure 4. Measured and calculated neutron energy spectra using ENDF/B-IV for 1 mfp ^{6}Li and ^{7}Li.

An Integral Measurement to Test Evaluated Neutron Cross Sections for Carbon*

G. L. Morgan
Oak Ridge National Laboratory, Oak Ridge, Tennessee 37830

INTRODUCTION

Measurements have been made of the spectra of scattered neutrons from a thick carbon sample for incident neutron energies from 1 to 20 MeV. This experiment was performed as part of a program[1-10] at ORNL to provide data suitable for testing the evaluated neutron data files for those elements which are important in the analysis of radiation transport problems for thermonuclear neutron sources.

The experimental technique is capable of sufficient resolution in the energy and angle of both incident and secondary neutrons to provide data with localized sensitivity. Thus, although it is necessary to compare the evaluated cross-section file to the experiment by means of a calculation to include the finite-sample effects, there is still an essentially direct differential relation between the calculated secondary spectra and the cross-section data.

This technique offers the additional advantage of testing the cross-section sets in the same context as they are used in applied transport problems. That is, the process by which microscopic evaluated cross sections are converted to tailored group constants is also checked.

Results of measurement and calculation based on the current evaluation, ENDF/B-IV MAT 1274,[11] are presented in graphical form.

EXPERIMENTAL PROCEDURE

The experimental procedure used in this work has been described in detail elsewhere[12] and will be only briefly outlined here. The Oak Ridge Electron Linear Accelerator was used as the neutron source. An electron beam pulse width of 5 ns at a repetition rate of 800 sec^{-1} was employed.

The scattering sample was located 47.8 m from the neutron source and consisted of 8498 grams of reactor grade graphite formed in an annular cylinder. The cylinder was 25.40 cm in outer diameter, 15.24 cm in inner diameter, with a length of 15.30 cm (see Fig. 1 for details of the sample-detector geometry).

Secondary neutrons from the sample were detected by an NE-213 scintillation counter located on the axis of the ring at a position corresponding to scattering angles between about 25° and 75°. A shadow bar shielded the detector from the direct neutron beam.

*Research sponsored by the U.S. Energy Research and Development Administration under contract with Union Carbide Corporation.

The energy of the incident neutron was determined by the time after the electron pulse at which the secondary neutron from the sample was detected. Each event in the detector was identified as either a neutron or gamma ray by pulse-shape discrimination techniques. Neutron events were then recorded in a two-parameter array of pulse-height versus time-of-flight.

Backgrounds were due to air scattering in the region near the detector and were determined by measurement with the sample removed. Overall background was less than 10%.

The neutron flux incident on the sample was determined using the same detector employed for the secondary radiation. This measurement was made with the sample and shadow bar removed and utilized one-parameter time-of-flight techniques. The incident flux is shown in Fig. 2.

The spectra of secondary neutrons were obtained by unfolding the background-corrected pulse-height distributions resulting from integration of the two-parameter data over ranges of time-of-flight. The extent of these time-of-flight intervals was determined by the need to get adequate statistical accuracy in the pulse-height spectra. The widths of the corresponding incident energy intervals range from $\Delta E = 1$ MeV for $E_{inc} = 10$ MeV to $\Delta E = 2.5$ MeV at $E_{inc} = 20$ MeV. Thus while these data provide detailed information about the energy distribution of the secondary radiation, they represent averages over rather wide intervals of the incident energy.

The resulting secondary neutron spectra still retain the effects of the finite pulse-height resolution of the detector. The resolution of the detector is a gaussian function whose width is a function of energy and follows the relation

$$R = \sqrt{250 + 670/E}$$

where R = FWHM in percent and E is neutron energy.

Units for the secondary spectra are neutrons/cm²/MeV averaged over the detector. These results have been normalized to unit incident neutron using the integral of the measured incident flux over the same incident energy range from which the pulse-height distribution was formed. The results have been tabulated in Ref. 14 and are shown in Figs. 3-14. The uncertainties shown in the figures do not include a 10% uncertainty in overall normalization.

CALCULATIONS

As a test of the current evaluation for carbon (ENDF/B 1274) the experimentally determined secondary spectra were compared to the results of a simple Monte Carlo calculation using the evaluated data. This calculation used group cross sections generated with the AMPX code[13] system. The group structure was as follows:

Energy Range	Group Width
0.1-4.0 MeV	0.100 MeV
4.0-6.0	0.125
6.0-10.0	0.200
10.0-20.0	0.625

A P_{15} expansion of the angular dependence was used.

For a given incident energy range, the neutrons were started randomly from the energy groups covering that range, each group being assigned a relative weight determined by the measured incident flux in that group (see Fig. 2).

In tracking through a given history, if the neutron spent sufficient time in the sample that its time-of-arrival at the detector would cause it to be assigned to a lower incident energy, it was flagged to be included in the calculation for the next lower incident energy bin rather than the bin in which it originated. Simple estimates based on the 48-m flight path show that the probability of remaining in the sample long enough to be assigned to any but the next lowest incident energy bin was negligible. This type of time slewing was largest at the high incident energies where it was about 10%.

After completion of the calculation for a given incident energy range, the resulting secondary spectra were smeared by the energy resolution of the detector. In each case sufficient histories were run that the statistical standard deviation (as calculated by the batch method) was less than 10% for any neutron group. Smoothing by the instrumental resolution further reduces statistical variations. Because of the difficulty in propagating the statistical error through the resolution smearing, no uncertainties are indicated for the final result of the calculation; however, the uncertainty should be less than 10% for the smoothed curves shown in Figs. 3-14. Results are not shown for the 17.5-20.0 MeV group since the evaluated data do not go beyond 20 MeV and the effects of time slewing cannot be calculated correctly for this incident energy bin.

RESULTS

The comparison between calculation and experiment is shown in Figs. 3-14. Several aspects of the interaction of neutrons with carbon are relevant: below 5 MeV only elastic scattering can occur. Above 5 MeV inelastic scattering to the 4.43-MeV level becomes possible and above about 8 MeV there is inelastic scattering to various levels which decay by alpha particle breakup.

Insight into the extent to which the experiment can be considered to have a differential nature can be gained from the calculation. For instance, in Fig. 3 (E_{inc} = 1-2 MeV) the peak in the secondary spectrum (≈ 1 MeV) is about 50% first collided events, the rest multiple scattering. At E_{inc} = 4-5 MeV (Fig. 6) the elastic

peak (≈ 4.2 MeV) is about 70% first collided; however, the secondary peak at 2.4 MeV is all multiple scattering. For E_{inc} = 8-9 MeV (Fig. 10) the elastic peak (≈ 8.1 MeV) is 75% single scattering, the inelastic peak (≈ 3.7 MeV) is 65% first collided while the small peak at 2 MeV is 100% multiple scattering. In Fig. 13, E_{inc} = 12.5-15.0 MeV, the percentage of first collided events varies from 25% near 1 MeV to about 75% for the elastic peak.

The comparisons indicate the evaluated data for elastic scattering are very good up to incident energies of about 8 MeV. Above 8 MeV there are discrepancies of the order of 20-40%. For the angular range of this measurement, the evaluated inelastic scattering to the 4.43-MeV level appears to be 10-20% too low for E_{inc} < 10 MeV, but rather good above E_{inc} = 10 MeV. This conclusion agrees with a comparison presented in Ref. 12 for backangle scattering from a thin carbon ring.

Figure 12, E_{inc} = 10-12.5 MeV, indicates the evaluated data for the (n,n'3α) reaction may be somewhat too low, but agreement is reasonably good for higher incident energies.

SUMMARY

The results reported here indicate that the current evaluation for carbon is generally good, with small improvements possible in the higher energy region. The conclusions reached in this work are generally in agreement with the results of a similar experiment given in Ref. 7. The major difference is that in Ref. 7, the evaluated inelastic scattering was found to be high rather than low. However, this work covers a somewhat different angular range which may explain this difference.

ACKNOWLEDGEMENTS

The author wishes to thank T. A. Love for help in fabrication of the sample, J. W. McConnell and J. G. Craven for help with the electronics and data acquisition system, and H. A. Todd and the ORELA staff for operation of the linac. W. E. Ford helped greatly in preparation of the group cross sections. Special thanks are due Dr. W. E. Kinney for many helpful discussions concerning the Monte Carlo calculations.

REFERENCES

1. G.L. Morgan, T.A. Love, and F.G. Perey, Integral Neutron Scattering Measurements on Carbon from 1 to 20 MeV, ORNL-TM-4157 (April 1973).
2. G.L. Morgan, T.A. Love, and F.G. Perey, Integral Neutron Scattering Measurements on Iron from 1 to 20 MeV, ORNL-TM-4193 (June 1973).

3. G.L. Morgan, Measurement of Secondary Neutrons and Gamma Rays Produced by Neutron Bombardment of Water over the Incident Energy Range 1 to 20 MeV, ORNL-TM-5018 (August 1975).
4. G.L. Morgan, Measurement of Secondary Neutrons and Gamma Rays Produced by Neutron Interactions with Nitrogen and Oxygen over the Incident Energy Range 1 to 20 MeV, ORNL-TM-5023 (August 1975).
5. G.L. Morgan, Measurement of Secondary Neutrons and Gamma Rays Produced by Neutron Interactions in Silicon Dioxide over the Incident Energy Range 1 to 20 MeV, ORNL-TM-5024 (August 1975).
6. G.L. Morgan, Measurement of Secondary Neutrons and Gamma Rays Produced by Neutron Interactions in Aluminum over the Incident Energy Range 1 to 20 MeV, ORNL-TM-5072 (November 1975).
7. S.N. Cramer and E.M. Oblow, Nucl. Sci. Eng. 58, 33 (1975). (See also S.N. Cramer and E.M. Oblow, Analyses of Neutron Scattering and Gamma-Ray Production Integral Experiments on Carbon for Neutron Energies from 1 to 15 MeV, ORNL-TM-4494 (September 1974).
8. S.N. Cramer and E.M. Oblow, Analysis of Neutron Scattering and Gamma-Ray Production Integral Experiments on Nitrogen for Neutron Energies from 1 to 15 MeV, ORNL-TM-5220 (March 1976).
9. S.N. Cramer and E.M. Oblow, Analysis of a Neutron Scattering and Gamma-Ray Production Integral Experiment on Oxygen for Neutron Energies from 1 to 15 MeV, ORNL-TM-5535 (September 1976).
10. S.N. Cramer and E.M. Oblow, Analysis of a Neutron Scattering Integral Experiment on Iron for Neutron Energies from 1 to 15 MeV, ORNL-TM-5548 (November 1976).
11. F.G. Perey, Evaluation of Carbon Cross Sections for ENDF/B-IV Carbon MAT 1274, Oak Ridge National Laboratory, unpublished (1975).
12. G.L. Morgan, T.A. Love, and F.G. Perey, Nucl. Instrum. Methods 128, 125 (1975).
13. N.M. Greene et al., AMPX: A Modular Code System for Generating Coupled Neutron-Gamma Libraries from ENDF/B, ORNL-TM-3706 (1974).
14. G.L. Morgan, Secondary Neutron Spectra from Neutron Interactions in a Thick Carbon Sample, ORNL-TM-5814 (1977).

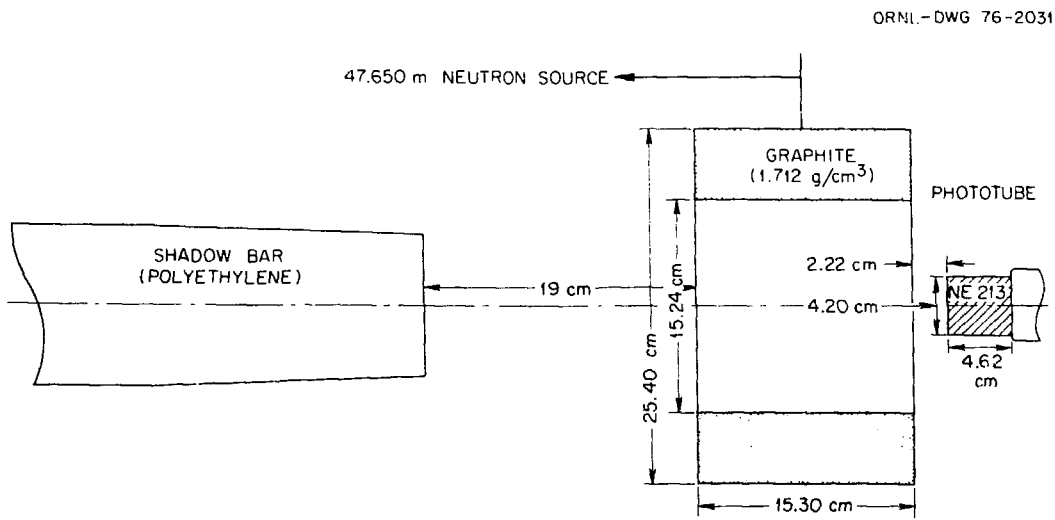

Fig. 1. Details of the geometry for scattering sample and detector.

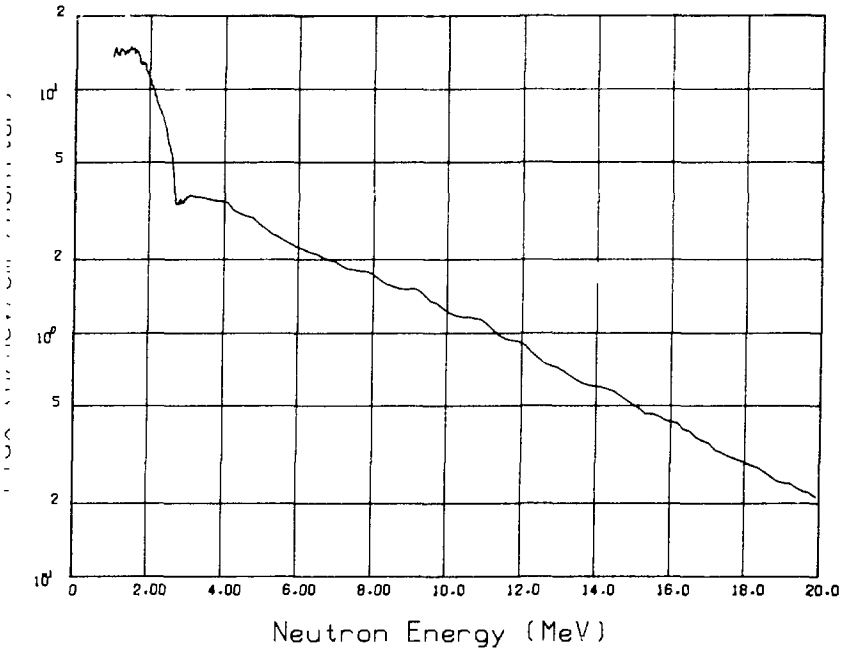

Fig. 2. Energy dependence of the neutron flux incident on the scattering sample.

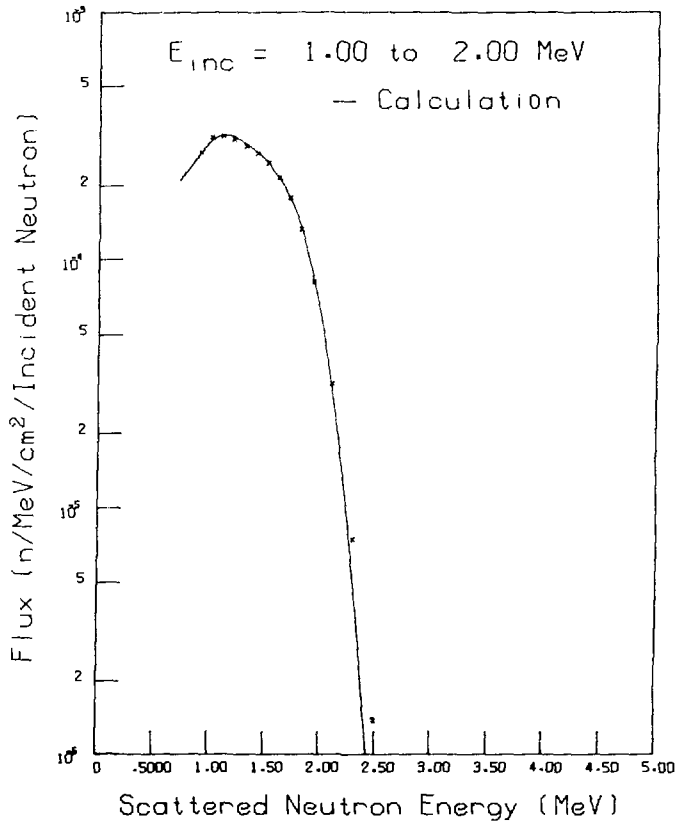

Fig. 3. Measured and calculated secondary neutron spectrum for incident neutron energies from 1 to 2 MeV.

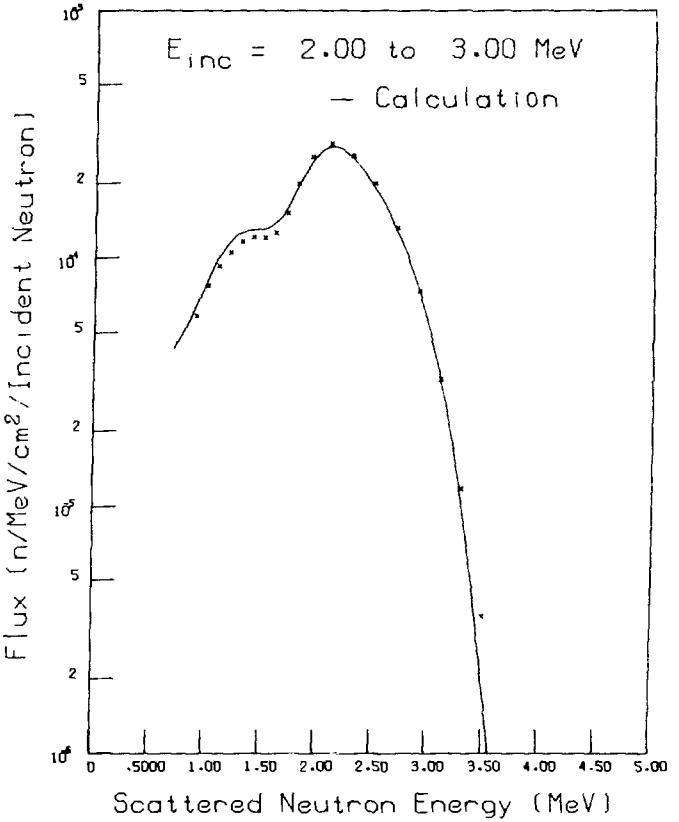

Fig. 4. Measured and calculated secondary neutron spectrum for incident neutron energies from 2 to 3 MeV.

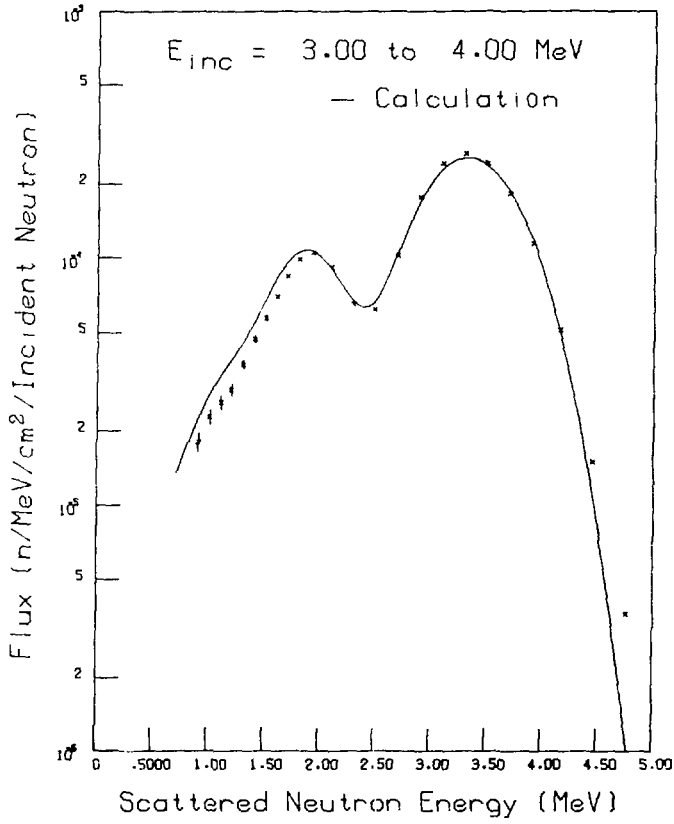

Fig. 5. Measured and calculated secondary neutron spectrum for incident neutron energies from 3 to 4 MeV.

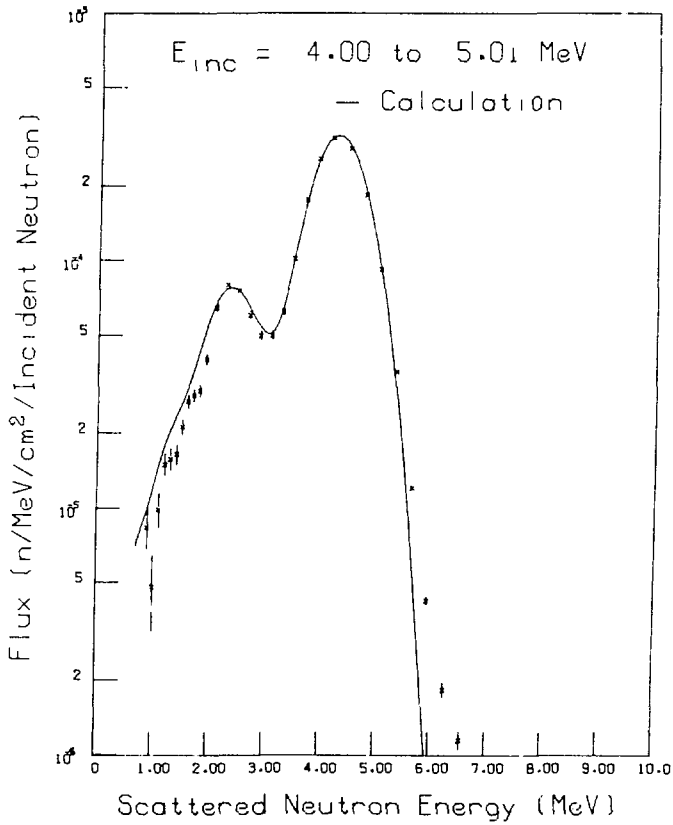

Fig. 6. Measured and calculated secondary neutron spectrum for incident neutron energies from 4 to 5 MeV.

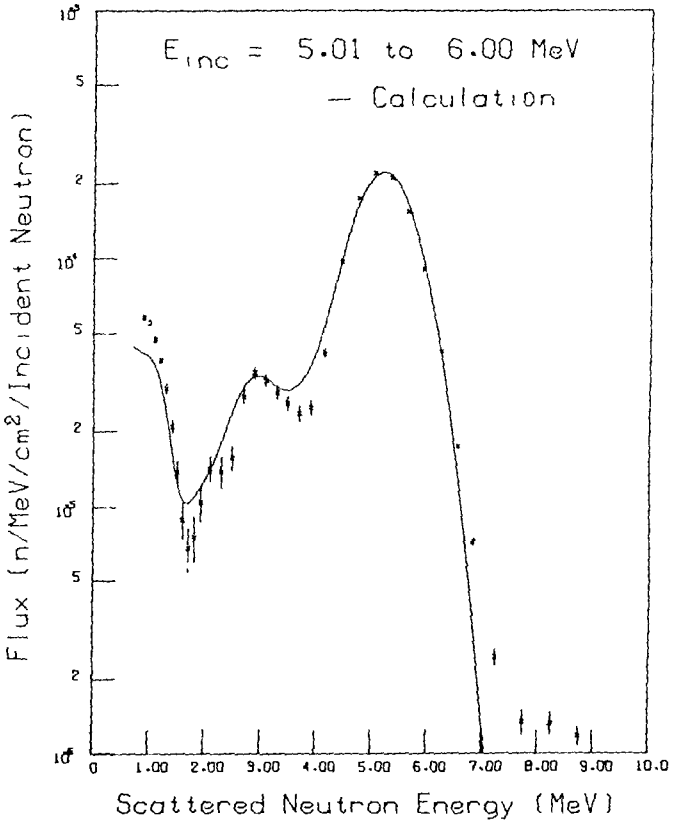

Fig. 7. Measured and Calculated secondary neutron spectrum for incident neutron energies from 5 to 6 MeV.

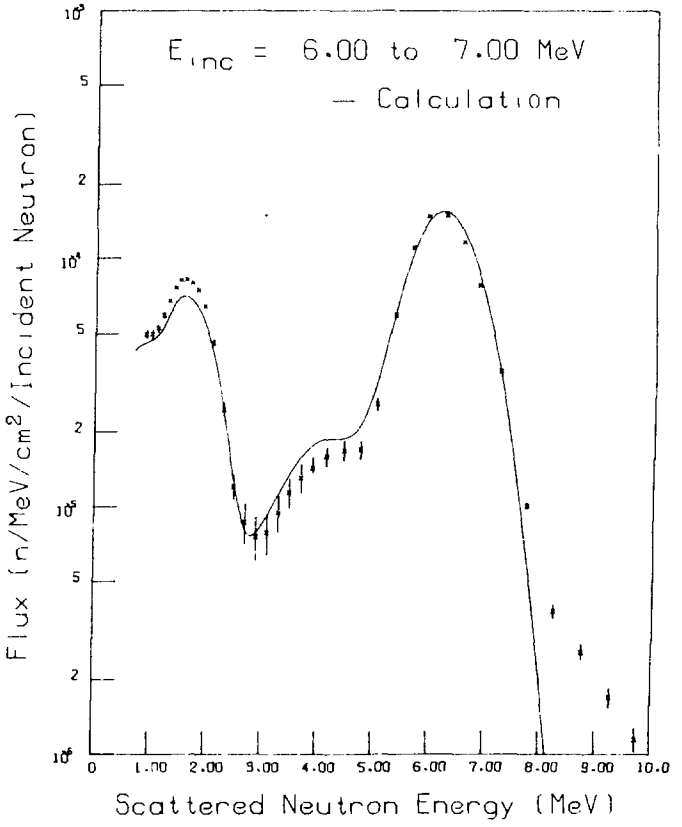

Fig. 8. Measured and calculated secondary neutron spectrum for incident neutron energies from 6 to 7 MeV.

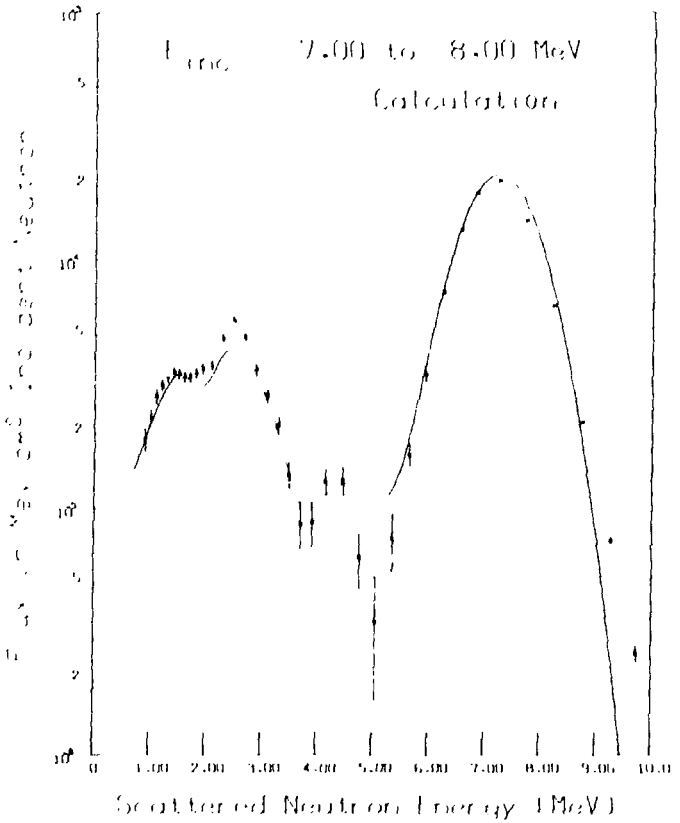

Fig. 9. Measured and calculated secondary neutron spectrum for incident neutron energies from 7 to 8 MeV.

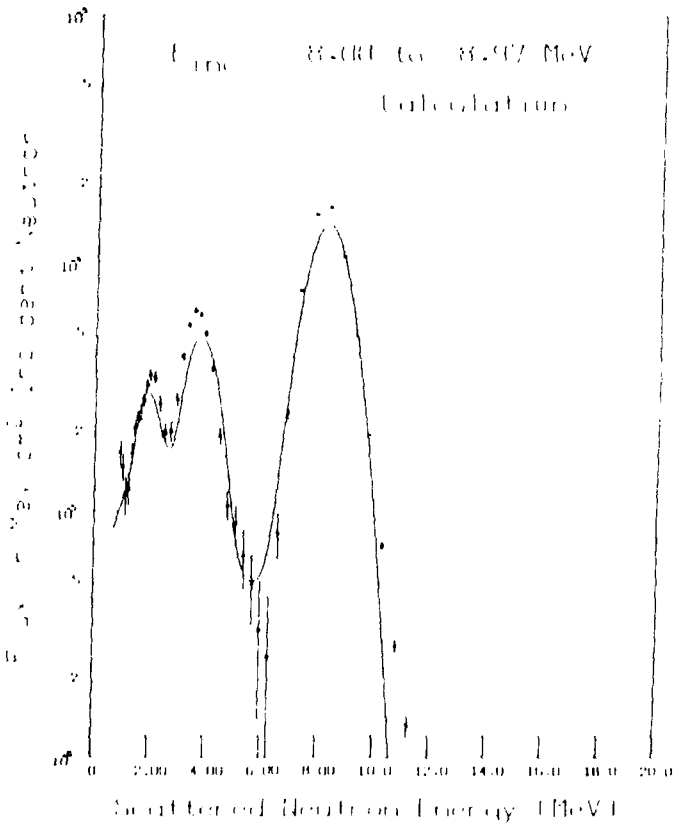

Fig. 10. Measured and calculated secondary neutron spectrum for incident neutron energies from 8 to 9 MeV

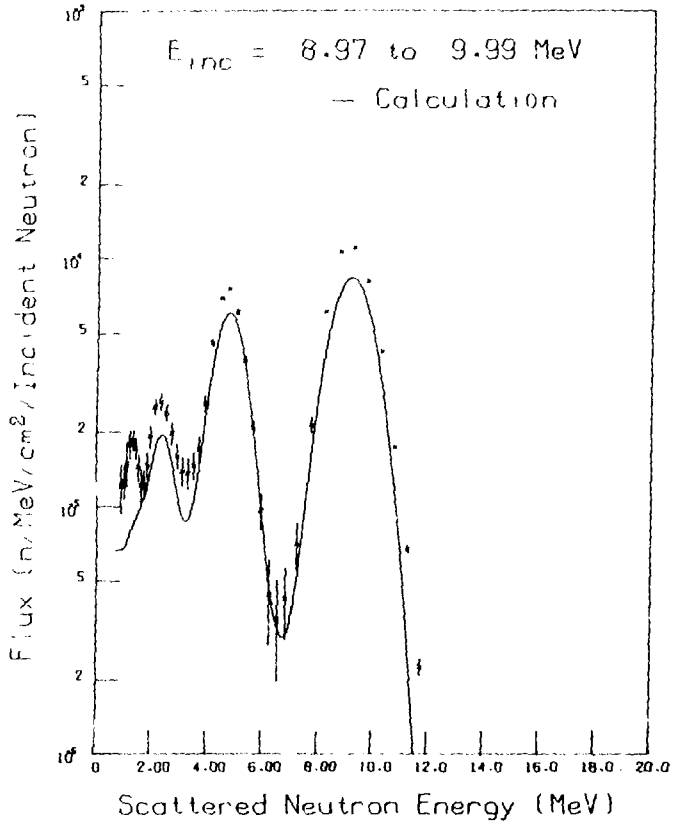

Fig. 11. Measured and calculated secondary neutron spectrum for incident neutron energies from 9 to 10 MeV.

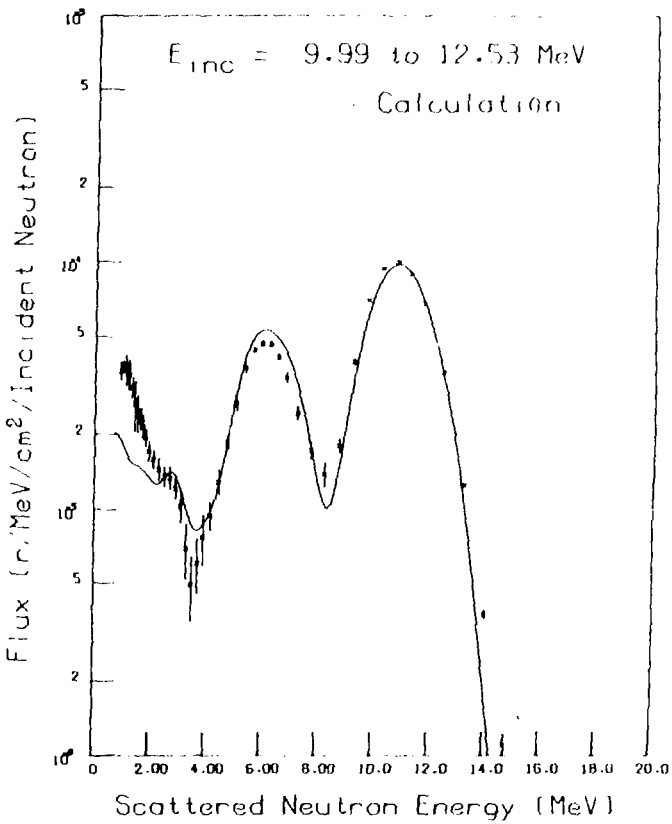

Fig. 12. Measured and calculated secondary neutron spectrum for incident neutron energies from 10 to 12.5 MeV.

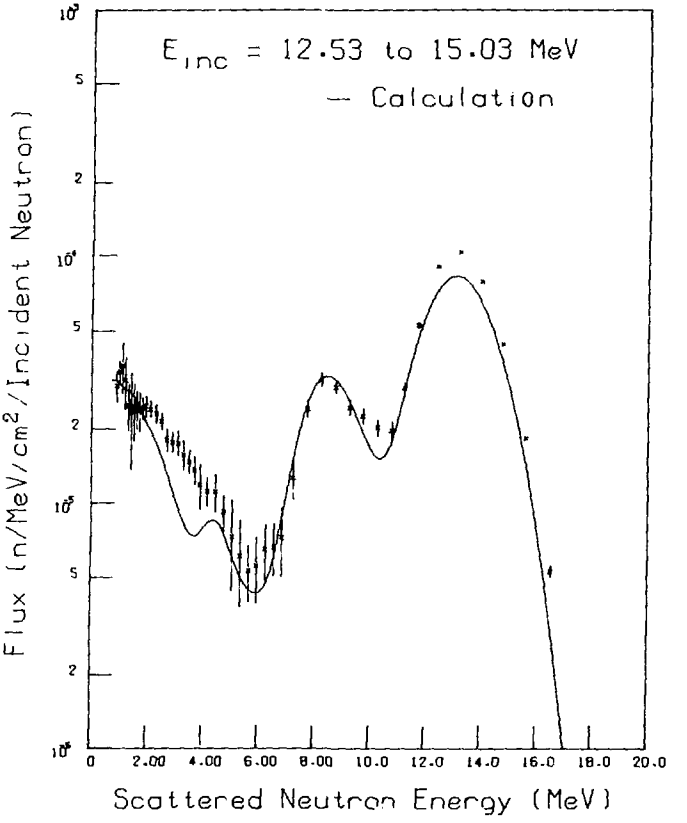

Fig. 13. Measured and calculated secondary neutron spectrum for incident neutron energies from 12.5 to 15.0 MeV.

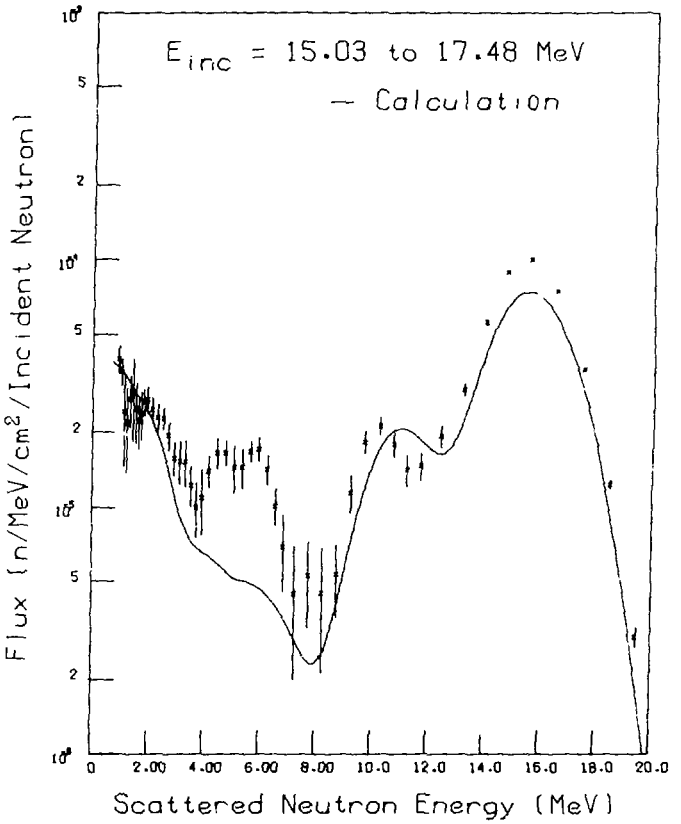

Fig. 14. Measured and calculated secondary neutron spectrum for incident neutron energies from 15.0 to 17.5 MeV.

SESSION VI

DATA EVALUATION AND NUCLEAR MODEL CODES

Chairman: A. Prince, BNL

Neutron Evaluation at High Energies -- Problems and Prospects*

Leona Stewart and Edward D. Arthur
Los Alamos Scientific Laboratory, University of California
Theoretical Division
Los Alamos, New Mexico 87545

INTRODUCTION

Although the near-term fusion reactor is designed to operate on the T(d,n) reaction, which has a maximum neutron energy slightly above 14 MeV, the d-Li reaction has excellent potential for bulk radiation damage experiments and analyses. For high-energy deuterons stopped in a thick-lithium target, the maximum neutron energy for a significantly high flux compares closely to the injected-deuteron energy. The first-wall spectrum[1] for a fusion reactor is compared with the d-Li spectrum for 40-MeV incident deuterons in Fig. 1. The 14-MeV peak will be reduced and the number of low-energy neutrons increased as the neutrons traverse various blanket and structural materials. In addition, the multiplication effects due to (n,2n) and (n,3n) reactions will contribute to the build up of the spectrum at low energies. It is obvious, therefore, that the operating fusion reactor will be considered a degraded 14-MeV neutron source. The nuclear data needs for an operating fusion reactor, listed in Table 1, have been described in detail by various authors[2] in the past.

Table 1

Nuclear Data Needs for an Operating
Fusion Reactor Energy Range up to 14 MeV

1. The Fuel Cycle
2. Tritium Breeding
3. Nuclear Heating
4. Radiation Damage Effects
5. Induced Activity
6. Radiation Shielding
7. Hybrid Concepts
8. Neutron Dosimetry

For the d-Li source, however, which is designed primarily for radiation damage studies, more than half the neutrons may have energies above 14 MeV, depending upon the incident deuteron energy

*Work performed under the auspices of the United States Energy Research and Development Administration.

and any special "tailoring" of the output spectrum. With the extension of nuclear data requirements to high-neutron energies, the need to understand the specific evaluation requests becomes crucial due to the fact that the complexity of the reaction mechanisms increases with increasing neutron bombarding energy. Some of the problems which beset the evaluator in this high-energy region and some "probable" solutions for a near-term data base are briefly described.

PROBLEM AREAS

Experimental

Since the evaluator serves as liaison for the experimentalist and user, both experimental and user problems reflect directly upon the evaluation programs. Table 2 outlines a few basic experimental problems, which when combined with lead-times and cost, may place extensive measurement programs outside the realm of possibility. The experimental programs have been addressed elsewhere in this Symposium; therefore, only one point need be made here. The experimentalist should measure the cross sections which are important to the user programs. Since the evaluator must provide the data for the user, he may be able to provide input into the measurement programs. Where measurements are undertaken, they should be directed toward improving the reliability of the user-oriented input data, which are, in turn, generated by the evaluator.

Evaluation

The evaluator's life is one of decision making; on the one hand, experimental data may exist that show large discrepancies and, on the other hand, the measurements provided are not exactly those requested by the user. One of the worst offenders with respect to discrepant measurements is shown in Fig. 2. While the ^{58}Ni(n,p) reaction near 14 MeV is not a typical case, it is an important one chosen for the ENDF/B special purpose dosimetry file. More importantly, perhaps, the points on the figure come from several experimental groups, cover an important energy region, and date from the early 1960's to 1973; therefore, discarding them on the basis of age and innocence is not necessarily justified. The energy region near 14 MeV was chosen since absolute fluxes, and therefore absolute cross sections, can be obtained using the associated particle technique. Other general problems are outlined in Table 3.

At high-neutron energies, multiplication effects become important in neutron transport in addition to the increasing number and complexity of the reaction channels themselves. Therefore, it becomes correspondingly more important for the evaluator to correctly interpret the user needs and also the available experimental information. Figure 3 shows typical reaction mechanisms

TABLE 2

Experimental Problems Pertinent to the Evaluation Effort for Incident Neutron Energies 10-13 and 15-40 MeV

1. Few differential experiments have been undertaken on the structural materials of interest.

2. Clean monoenergetic neutron sources are difficult to develop from 8-13 MeV. They are essentially non-existent above 20 MeV.

3. Available neutron sources have low fluxes at high energies and resolution must often be sacrificed.

4. White neutron sources cannot generally be used for many important differential measurements such as:

   Elastic Scattering
   Gas Production
   Activation
   Local Heat Deposition
   Angular Dependence, $\sigma(\theta_{n'})$

   Non-elastic Processes
   Dosimetry
   Transmutation
   Multiple Particle Processes
   Energy dependence $\sigma(E_{n'})$

5. Even with available sources many experiments are difficult, if not impossible, to implement with reasonable accuracy such as 3- and 4-body studies $[\sigma(\theta_{n'}, E_{n'})]$.

---

expected for (n,2n), (n,3n), and (n,4n) reactions on ^{56}Fe. Using the (n,2n) as an example, the total (n,2n) would be needed for transport while the (n,2np) contributes to the hydrogen production and the (n,2nα) is part of the helium production cross section. Each, individually, may be required for the study of radiation efects and/or dosimetry applications. The various components that make up the hydrogen and helium production cross sections for ^{56}Fe at high energies are shown in Table 4. Isotope-versus-elemental evaluations further complicate the problems. Sometimes all are needed, at least on the important isotopes.

Niobium has been chosen to show some of the different breakup cross sections for neutrons above 10 MeV. Even though Nb has a high Coulomb barrier for charged-particle emission, note that the total proton production cross section (Fig. 4) and total alpha particle production cross section (Fig. 5) continue to rise for

the highest energy shown here (24 MeV). The curves are calculated with the preequilibrium statistical code GNASH[3] but they agree rather well with available experimental measurements, especially for the alpha production. It is obvious from both figures that the most important components of these cross sections at the higher energies are due to the 3-body reactions.

The transmutation products resulting from (n,2n), (n,3n), and (n,4n) reactions on ^{93}Nb are outlined in Fig. 6, while cross sections for the respective reactions are shown in Fig. 7. The solid lines are again the GNASH calculations, and the dashed lines are estimates of the cross sections -- used as trends. The experimental data shown are for the total (n,2n) and (n,3n) cross sections measured by Frehaut et al.[4] and Veeser et al.[5] with large liquid scintillators using coincidence techniques. Note that the value of the (n,2n) cross section leading to the 10.15-day isomeric state in ^{92}Nb is less than half of the total (n,2n) cross section. While the cross section for the production of the metastable state would be required for dosimetry and/or residual activity determinations, the total (n,2n) cross section is required for all neutron transport calculations.

The cross sections in Fig. 7 are large and so is the multiplication factor above 11 MeV; therefore, a calculation was performed to point out another problem area -- that of determining the complex spectra of individual neutrons resulting from each of these reactions. For 24-Mev incident neutrons, the emitted neutron spectra were calculated using GNASH as shown in Fig. 8. Nonelastic events have been shown[6] to be very important in damage analyses; therefore it might be most informative to determine whether spectral information is a sensitive parameter in the radiation effects program. Certainly these nonelastic neutrons are emitted with significant cross sections and with very high energies, contrary to the usual ENDF/B evaluations, which give practically all the nonelastic neutrons very low energies. If neutron transport is to be carried out, as it must be at energies below 14 MeV, then a wealth of information is required in each evaluation to improve the the files above 8-10 MeV. It would also be useful to compare calculations among different laboratory programs to ensure that the predicted spectra are the most reasonable estimates available.

Finally, it must be appreciated that for activation and dosimetry data, elemental evaluations have no meaning. Also, if activation cross sections are needed, then the decay information is also necessary. If this type of information is required up to the 40-MeV range, it would be a tremendous undertaking.

PROSPECTS

The general needs for radiation damage analyses have usually emphasized helium production and heavy-particle recoil spectra.[7]

Table 3

General Problems for the Evaluator

1. Experiments exist but they are significantly discrepant.

2. Experiments exist but the measurements may or may not provide the specific data required by the user.

3. Experiments do not exist; how can the relevant data be obtained?

4. Experiments exist on the elemental target but isotopic evaluations are required.

5. A few reactions have been measured for one isotope but an elemental evaluation is required.

6. Difficulty in satisfying individual users; everyone seems to need something different, with a lead time of the week before last.

7. To understand and be able to provide the specific details required.

Table 4

Major Hydrogen and Helium Production Reactions Induced by Neutrons on ^{56}Fe

$_1H^1$ Production

$$n + {}^{56}_{26}Fe \qquad n,p + n,n'p + n,pn' + n,npn' + n,2np + n,p\alpha + n,2p + \ldots$$

α Production

$$n + {}^{56}_{26}Fe \qquad n,\alpha + n,n'\alpha + n,\alpha n' + n,n\alpha n' + n,p\alpha + n,2n\alpha + n,2\alpha + \ldots$$

If this is so, then the model code calculational programs, described in the following papers in this Symposium, will probably suffice. An attempt has been made in this paper, however, to indicate that high-energy neutron transport through the bulk media may be required to ensure, at least for a few important elements or isotopes, that the simulation of low-energy damage functions from high-energy sources is reasonably correct. With this idea in mind, some suggestions are offered for a possible evaluation program and prospects, perhaps, for providing some of the necessary data.

The general evaluation needs for the fusion programs are outlined in Table 5. The term "SUPPORT OPERATING MFE SYSTEMS" covers a large area of nuclear data that has been the subject of many excellent review papers. It should be pointed out that Steiner,[7] Doran,[6] Parkin,[8] Abdou,[9] and others agree that many of the ENDF/B files require significant extensions and improvements above 8-10 MeV before they can be reliably employed in the majority of MFE applications.

Table 5

General Evaluation Needs for Fusion

1. Cross Sections: $\sigma(E_{n'})$ and $\sigma(\theta_{n'})$
   a. $E_n < 15$ MeV; <u>support operating MFE systems</u>
   b. $E_n > 15$ MeV; only for materials testing activities
   c. For charged particles (>8 MeV/amu)
2. Transmutation cross sections for selected products for neutrons and energetic charged particles.
3. Atomic data.

An evaluation effort is suggested in Table 6 that may provide some insight for setting up guidelines and priorities for fusion evaluation programs. In many cases, special purpose files should be generated rather than the complete ENDF general purpose evaluations. This suggestion may be particularly important for activation and dosimetry, where the evaluations are required isotope-by-isotope.

Table 6

Suggested Evaluation Effort
(Near Term)

1. Improve ENDF/B in the 10-20 MeV range, where important.

2. Add special purpose ENDF/B files for important reactions on specific isotopes up to 20 MeV. For example:

   a. Hydrogen Production
   b. Helium Production
   c. Activation Cross Sections
   d. Dosimetry (needs to be determined)
   e. Heavy Particle Recoil Data (methods and formats to be determined)

3. Set up a specific but small request list of user needs for the near term and a dialogue with users on long term needs.

4. Extend the data to 40 MeV (methods and formats to be determined).

Finally, Table 7 gives a limited prospectus. Although model calculations are expected to carry the heaviest burden in providing most of the data at high energies, it would be very useful to have total cross-section measurements on a few of the most important isotopes and/or elements. Such experiments are the least expensive in time and money, and they can be performed with presently available white sources by implementing time of flight. In addition, certain activation, (n,2n), (n,3n) and gas production cross section measurements might be undertaken at a few selected energies. Activation and gas production may also be determined in an integral sense although differential data must be generated for simulation. Admittedly, the total cross section is not the important cross section for radiation damage, but the nonelastic cross section is important. If we are to accept the model predictions for the elastic, it would be useful to know whether that same model predicts correctly the total and the nonelastic. In addition, broad structure has been observed in several total cross sections for structural materials in the region above 10-15 MeV. The elastic would be expected to have similar structure, hopefully reproduced by the model.

Table 7

Prospects

1. Near term will depend on model calculations.

2. Differential experiments (limit to most important isotopes).

3. Interpretation of integral results to help determine reliability of differential data.

4. Above 20 MeV, DMFE is the only customer except for medical applications on H, C, N, and O. Therefore the data will not be available from other sources.

In evaluating neutron data, it is sometimes possible to obtain relevant information from proton-induced reaction measurements already available. For example, (p,p') is often very similar to (n,n'), especially where the energy is high enough to reduce the effect of the Coulomb barrier. Similarly, many breakup cross sections might be simulated from experimental and theoretical data already available on proton scattering experiments. Such data should be used in future evaluation programs where applicable and available.

Finally, the need for close cooperation between the user, experimental, and the evaluation communities is an important aspect in obtaining maximum input for evaluation programs combined with a minimum of lead time and costs. This aspect is very important in the high-energy range where data needs are complex and may often vary from isotope to isotope.

REFERENCES

1. M. J. Saltmarsh and R. E. Worsham, ORNL-TM-5223 (1976).
2. See, for example, D. Steiner, Nuclear Cross Sections and Technology, NBS Special Publication 425, Vol. II, p. 646 (1975), and references contained therein.
3. E. D. Arthur and P. G. Young, Trans. Am. Nucl. Soc. 23, 500 (1976).
4. J. Frehaut and G. Mosinski, Nuclear Cross Sections and Technology, NBS Special Publication 425, Vol. II, p. 855 (1975).
5. L. R. Veeser, E. D. Arthur, and P. G. Young, to be published.
6. D. G. Doran, Proceedings of this Symposium.
7. P. J. Persiani, Conf. on Radiation Test Facilities for CTR Surface and Materials Programs, July, 1975, Argonne National Laboratory, ANL/CTR-75-4.

8. D. Parkin, presented at the Special Meeting of the CSEWG Standards Subcommittee, Los Alamos, New Mexico (August 1976).
9. M. A. Abdou and C. W. Maynard, Nucl. Sci. Eng. 56, 360 and 381 (1975).

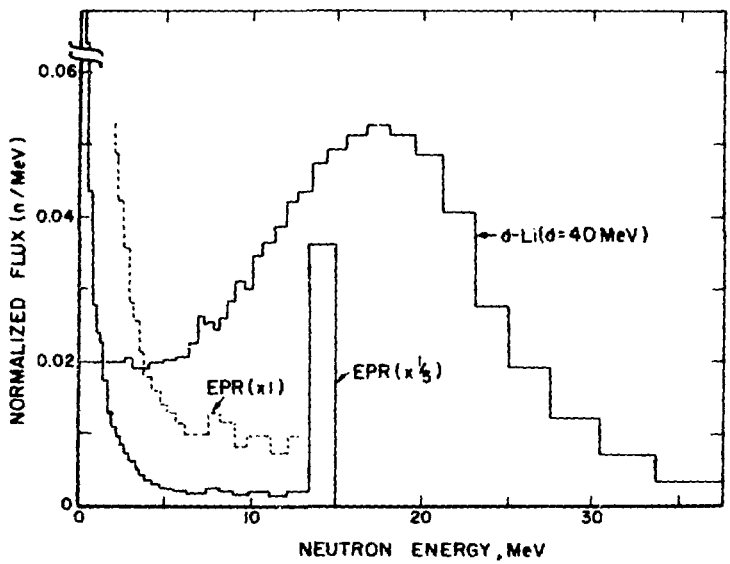

Fig. 1. A comparison of the first wall spectra for a fusion reactor with that from d-Li source employing 40-MeV incident deuterons.

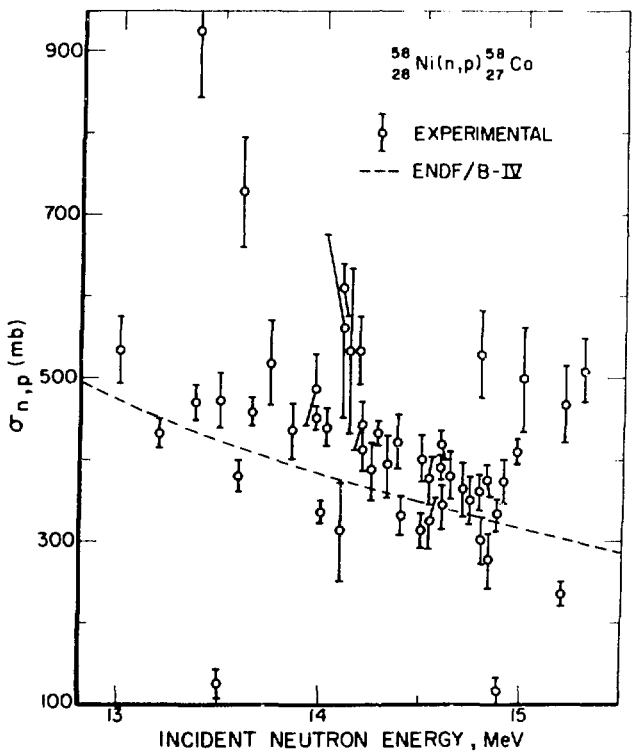

Fig. 2. Experimental values for the $^{58}Ni(n,p)$ cross section in the energy range from 13 to 15 MeV.

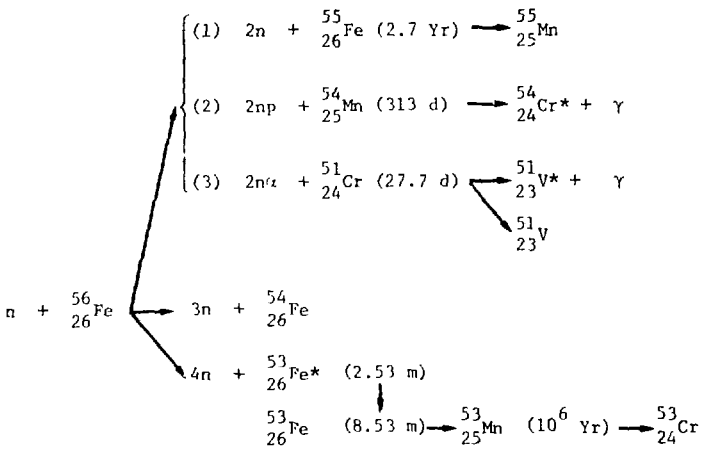

Fig. 3. Reaction mechanisms for (n,2n), (n,3n), and (n,4n) reactions on ^{56}Fe.

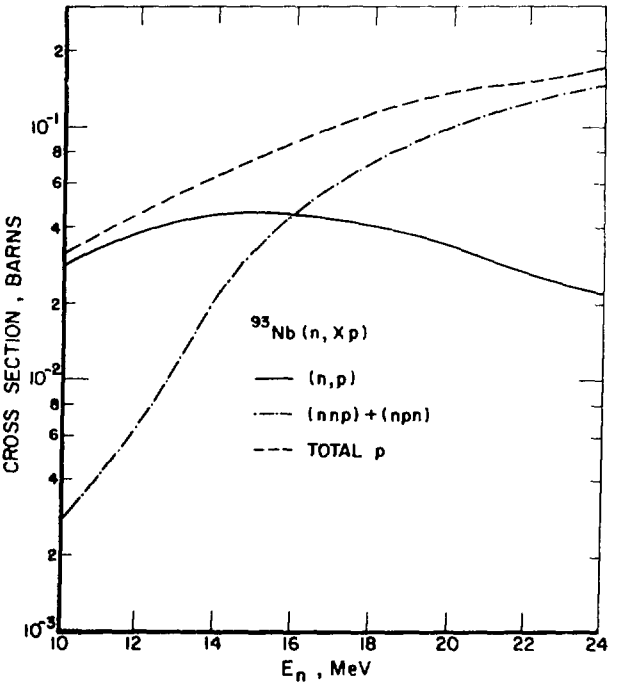

Fig. 4. Calculated total and partial hydrogen production cross sections resulting from neutron bombardment of Nb.

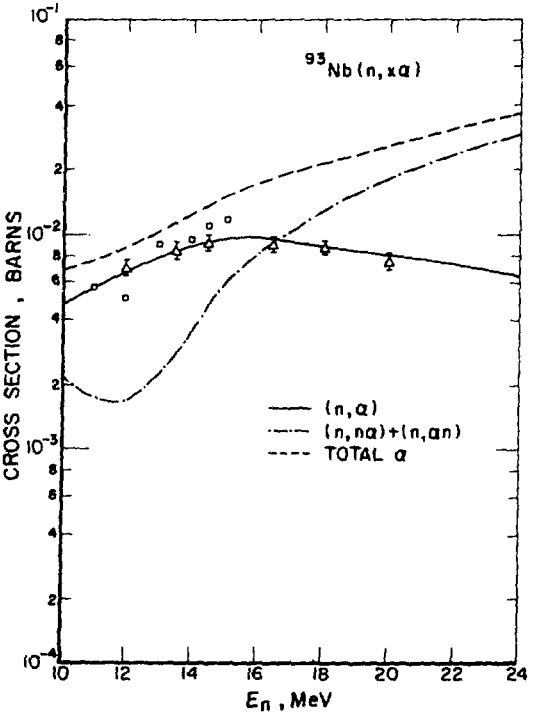

Fig. 5. Calculated alpha production cross sections induced by neutrons on Nb.

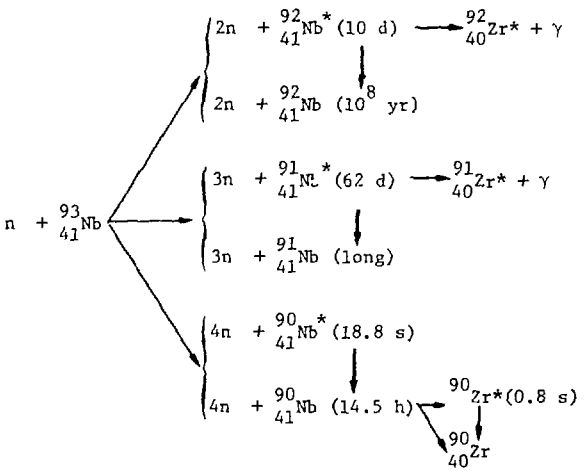

Fig. 6. Transmutation products resulting from (n,2n), (n,3n), and (n,4n) reactions on Nb.

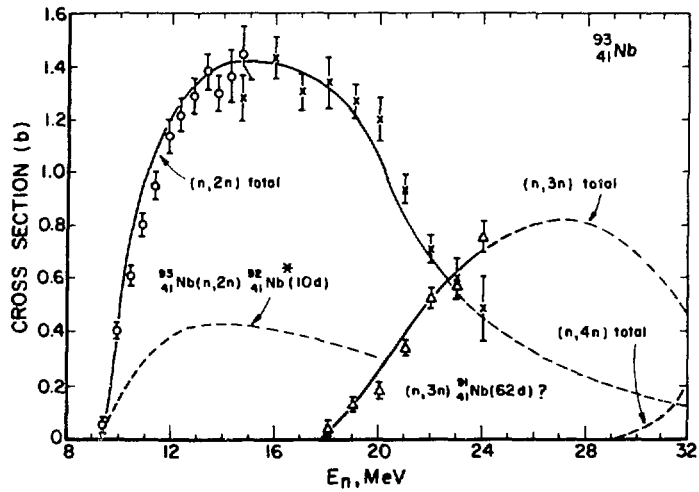

Fig. 7. Calculated (solid curves) and estimated (dashed curves) (n,2n), (n,3n), and (n,4n) reaction cross sections for Nb.

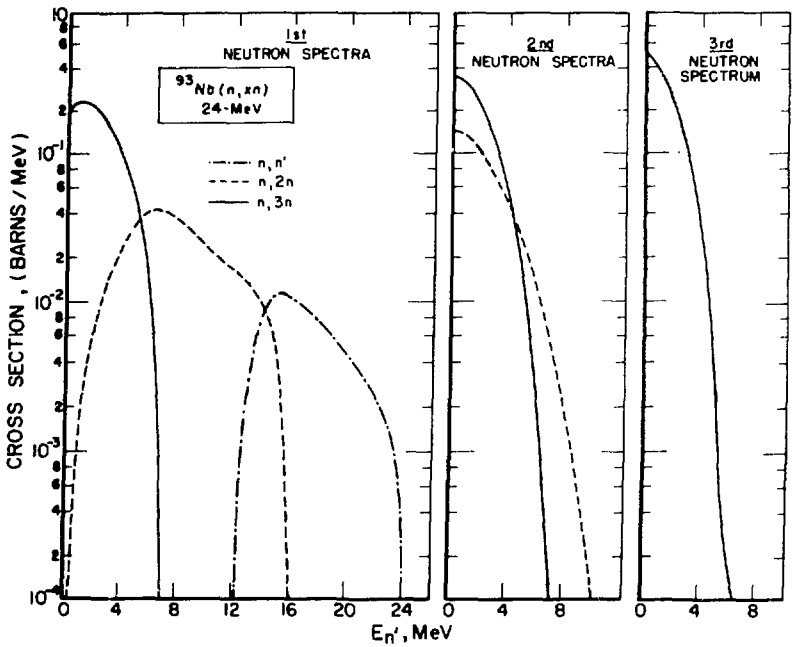

Fig. 8. Calculated complex spectra of neutrons resulting from (n,n'), (n,2n), and (n,3n) processes on Nb for 24-Mev incident neutrons.

Multi-Step Hauser-Feshbach Codes with Pre-Compound Effects: A Brief Review of Current and Required Developments and Applications up to 40 MeV*

C. Y. Fu
Oak Ridge National Laboratory, Oak Ridge, Tennessee 37830

Mainly for applications to fusion energy research, several multi-step Hauser-Feshbach codes with pre-compound effects were developed.[1-4] An effort to intercompare these codes by their authors is in progress.[5] Because extensive reviews on the relevant theories have recently become available,[6-7] we will discuss only a few points of interest with respect to the developments and applications of these codes.

DEVELOPMENTS

Multi-Step Hauser-Feshbach Model

Table 1 lists a segment of calculated 14-MeV ^{63}Cu(n,nα) and 2-MeV ^{62}Cu(n,α) level-excitation cross sections. The average

Table 1

Calculated ^{63}Cu(n,nα) and ^{62}Cu(n,α) Cross-Section Variations with Residual-Level Spins

^{59}Co Levels		14 MeV ^{63}Cu(n,nα)	2 MeV ^{62}Cu(n,α)
E_{ex}(MeV)	J^{π}	σ(mb)	σ(mb)
1.48	$5/2^-$	0.56	1.09
1.46	$9/2^-$	1.21	0.63
1.43	$1/2^-$	0.16	0.71

alpha-particle energies are nearly the same in both cases and the three residual levels shown are close, thus the variations in the excitation cross sections are mainly due to differences in level

*Research sponsored by the U.S. Energy Research and Development Administration under contract with Union Carbide Corporation.

spins. The variations in the excitation cross sections in the (n,nα) case are much larger than in the (n,α) case. The most favored spin is 9/2 for (n,nα), but 5/2 for (n,α). While this result is expected, we emphasize with this example that explicit inclusion of the residual-level spins in the second step is even more important than in the first step.

An indication as to how well the two-step Hauser-Feshbach model works was given before,[8] from where we reproduce in Fig. 1 the 18.5-MeV ^{40}Ca(n,xγ) data and calculation. In ^{40}Ca(n,np) reaction, the 7/2$^-$ level in ^{39}K is much more strongly excited than its neighboring levels with smaller spins, and there is good agreement with the available data.[9]

From the above we know that spin distributions in excited states in intermediate nuclides must be calculated carefully. This is not trivial if pre-compound effects are included, as explained below.

Pre-Compound Model

Near 14 MeV the pre-compound component is small and may be treated as a correction to the spectum calculated by the Hauser-Feshbach model. The various components of the neutron-production cross sections of ^{56}Fe near 14 MeV, taken from Ref. 3, are shown in Fig. 2. The pre-compound fraction was adjusted to fit the data[10] for outgoing neutron energies from 5 to 9 MeV, thus bridging the gap between the compound-nucleus and direct components. The direct component was based on DWBA calculations for 16 of the 26 discrete levels.

As the incident neutron energy increases, the pre-compound component may become dominant. Pre-compound fractions for Cu and Nb up to 40 MeV, calculated with the code PRECOA,[11] are shown in Fig. 3. Because the pre-compound calculation does not explicitly include spin and parity effects, these larger pre-compound components can no longer be treated as corrections to the Hauser-Feshbach calculations. To see this point somewhat quantitatively we did a "synthetic" Hauser-Feshbach calculation for 14.5-MeV ^{56}Fe(n,n') reaction in which densities of 1p-1h states[12] were used for the residual nuclides. The resulting spin distribution for 13-MeV excited states in ^{56}Fe is compared in Fig. 4 with that of the compound-nucleus calculation. The true spin distribution is of course somewhere in between the two extremes. The difference between the true spin distribution and that of the compound-nucleus will increase with increasing incident neutron energy, and using the latter may cause significant errors in second-step and third-step calculations.

Brute-force solution of the pre-compound decays in the Hauser-Feshbach model is straightforward and is similar to what we did for the 1p-1h case, but the computer time required will be excessive.

We propose a simple method, described below, for combining the pre-compound and Hauser-Feshbach calculations with approximate conservation of angular momentum.

Defining

$\Omega(I,p,h,E_x)$ = the density for levels having spin I, particle number p, hole number h, and excitation energy E_x,

$f(p,h,E)$ = the pre-compound fraction of a given reaction for exciting residual levels having p particles and h holes, and for incident neutron energy E, and

$\rho(I,E_x)$ = the conventional level density,

then after a pre-compound calculation that determines $f(p,h,E)$, we use in the Hauser-Feshbach calculation the following effective level density:

$$\rho_{eff}(I,E,E_x) = [1-f(E)]\,\rho(I,E_x) + \sum_p f(p,h,E)\,\Omega(I,p,h,E_x) \quad ,$$

where $f(E) = \sum_p f(p,h,E)$.

This method is being executed in the code TNG[3] by adopting the pre-compound code PRECOA[11] as a subroutine. Discrete levels in the Hauser-Feshbach calculation will carry the weight $\rho_{eff}(I,E,E_d)/\rho(I,E_d)$ where I is now the spin of a given discrete level and E_d its excitation energy.

APPLICATIONS

Sputtering and Displacement

Elastic scattering and reaction cross sections, along with the first outgoing particle spectra, are required for calculating the primary recoil distributions and specific damage energies.[13,14] Above 15 MeV, where experimental data are generally unavailable, the required cross sections may be generated from theories. Figures 5 and 6 display calculated cross sections and first outgoing particle spectra for Cu.[13] The specific damage energies for Cu, Nb, and Au up to 32 MeV calculated from the theoretical cross sections are shown in Fig. 7.[15] The damage energy is that part of the recoil energy that is ultimately available for producing atomic displacements, and is also useful for the description of sputtering. Retained damage and projected ranges for sputtered particles calculated from the theoretical specific damage energies agree reasonably well with the available measurements.[14,15] This seems to indicate that calculated neutron cross sections in the

above form are adequate for analyzing forward sputtering and bulk effects. However, neutron cross-section requirements for studying backward sputtering may be much more stringent and angular distributions as well as second- and third-particle spectra may be needed.

Gas Production and Transmutation

Reactions such as (n,p) and (n,nα) in potential structural materials for fusion reactors are also important for radiation damage studies because these reactions produce both gases and transmutations. Below 20 MeV, the helium production cross section is mainly composed of (n,αx) and (n,nα) reactions. An example for ^{63}Cu is shown in Fig. 8.[15] Above 20 MeV, (n,2nα) reaction may become important. However, inclusion of the pre-compound component "correctly" in the Hauser-Feshbach calculation to conserve angular momentum is necessary before (n,2nα) cross sections can be calculated adequately.

High-Energy Neutron Dosimetry

^{59}Co has been chosen by the authors of several codes and their users[1-6] as a target for intercomparison. The ^{59}Co(n,2n) reaction is widely used in fission reactor dosimetry works. We show in Fig. 9 our calculated ^{59}Co(n,2n) and (n,3n) cross sections up to 30 MeV, along with ENDF/B-IV[16] and more recent data[17,18] taken with the scintillation-tank method. It is seen from both the data and the calculation that this (n,2n) cross section does not drop very fast above the (n,3n) threshold. Thus for high-energy neutron dosimetry applications, such as involved in deuteron-breakup neutron sources with deuteron energies of 35 MeV or higher, the upper energy limit of the dosimetry cross sections should be extended to at least 30 MeV. For the evaluation of (n,nx) and (n,2nx) cross sections, which are good candidates for high-energy dosimetry applications, the multi-step Hauser-Feshbach codes with pre-compound effects will be very useful.

CONCLUSION

We have illustrated the usefulness of the multi-step Hauser-Feshbach codes for a few important applications to fusion energy research below 40 MeV. A method is proposed to combine the pre-compound and Hauser-Feshbach calculations with approximate conservation of angular momentum, thus permitting reliable calculations for complex reaction cross sections above 20 MeV. The model will not give correct angular distributions for high-energy outgoing particles, for which multi-step direct or intranuclear cascade models can do a better job.

REFERENCES

1. D. G. Gardner, in Nuclear Cross Sections and Technology, Vol. II, p. 651, National Bureau of Standards Special Publication SP-425, Washington, D.C., 1975.
2. F. M. Mann and Z. E. Switkowski, in Nuclear Cross Sections and Technology, Vol. I, p. 354, National Bureau of Standards Special Publication SP-425, Washington, D.C., 1975, and private communication (1976).
3. C. Y. Fu, in Nuclear Cross Sections and Technology, Vol. I, p. 328, National Bureau of Standards Special Publication SP-425, Washington, D.C., 1975.
4. E. D. Arthur and P. G. Young, Trans. Am. Nucl. Soc. 23, 500 (1976), and private communication (1976).
5. A. Prince, in Nuclear Theory in Neutron Nuclear Data Evaluation, IAEA-190, Vol. I, pp. 31-158 (1976), and private communication (1976).
6. P. A. Moldauer, in Nuclear Theory in Neutron Nuclear Data Evaluation, IAEA-190, Vol. I, pp. 167-90 (1976).
7. D. Seeliger, in Nuclear Theory in Neutron Nuclear Data Evaluation, IAEA-190, Vol. I, pp. 313-25 (1976).
8. C. Y. Fu, Atom. Data and Nucl. Data Tables 17, pp. 127-56 (1976).
9. J. K. Dickens, et al., Nucl. Sci. Eng. 53, 277 (1974).
10. J. L. Kammerdiener, "Neutron Spectra Emitted by ^{239}Pu, ^{238}U, ^{235}U, Pb, Nb, Ni, Fe, Al, and C Irradiated by 14-MeV Neutrons," Lawrence Livermore Laboratory UCRL-51232 (1972); R. M. Schectman and J. D. Anderson, Nucl. Phys. 77, 241 (1965); G. C. Bonazzola et al., Nucl. Phys. 51, 353 (1965); S. C. Mathur, P. S. Buchanan, and I. L. Morgan, Phys. Rev. 186, 1038 (1969); G. Clayeux et al., Centre d'Etudes de Limeil CEA-R-4279 (1972).
11. C. Kalbach, "PRECOA: Programme for Calculating Pre-Equilibrium Particle Energy Spectra," DPh-N/BE/74/3, Centre d"Etudes Nucléaire de Saclay, May 1974.
12. H. Feshbach, private communication (1975).
13. C. Y. Fu and F. G. Perey, J. Nucl. Materials 61, pp. 153-57 (1976).
14. J. B. Roberto and M. T. Robinson, J. Nucl. Materials 61, 149 (1976).
15. J. B. Roberto, M. T. Robinson and C. Y. Fu, J. Nucl. Materials 63, pp. 460-65 (1976).
16. A. B. Smith and D. L. Smith, in ENDF/B-IV Dosimetry File, B. A. Magurno, Editor, Brookhaven National Laboratory Report BNL-NCS-50446 (ENDF-216), Upton, New York (1975).
17. L. R. Veeser and E. D. Arthur, "Measurement of (n,2n) and (n,3n) Cross Sections above 14 MeV," to be published.
18. J. Fréhaut and G. Mosinski, in Nuclear Cross Sections and Technology, R. A. Schrack and C. D. Bowman, Editors, Vol. II, p. 855, National Bureau of Standards Special Publication SP-425, Washington, D.C., 1975.

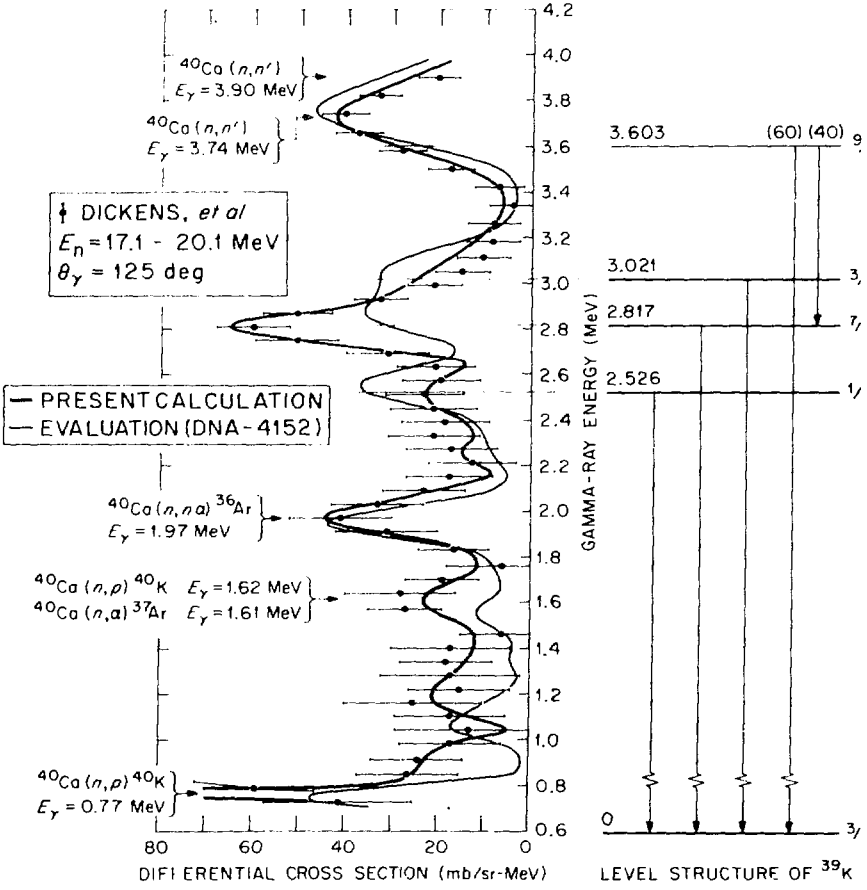

Fig. 1. Gamma-ray production cross sections in ^{40}Ca, calculated and experimental, for incident neutron energies from 17 to 20 MeV. In ^{40}Ca(n,np) reaction, the 2.817-MeV 7/2$^-$ level in ^{39}K, which decays to the ground state, is much more strongly excited than its neighboring levels with smaller spins (reproduced from Ref. 8).

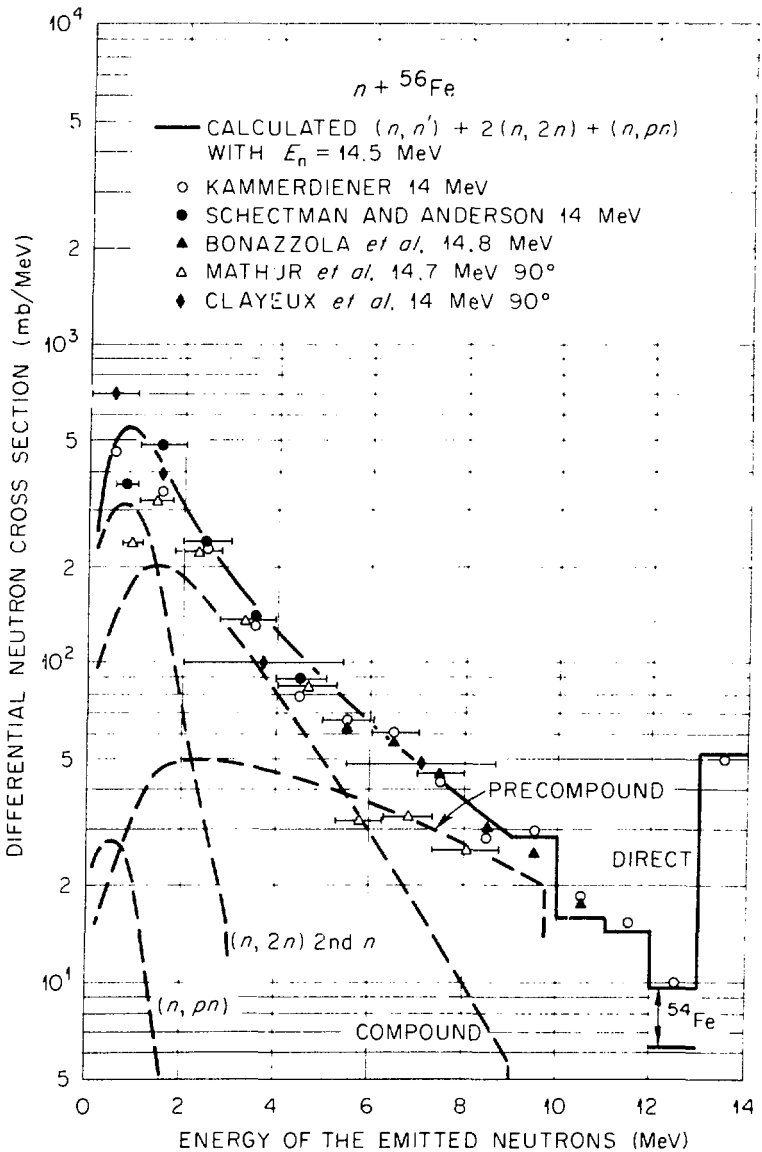

Fig. 2. Near 14 MeV, the pre-compound component is small and may be treated as a correction to the neutron spectrum calculated with the Hauser-Feshbach model (reproduced from Ref. 3).

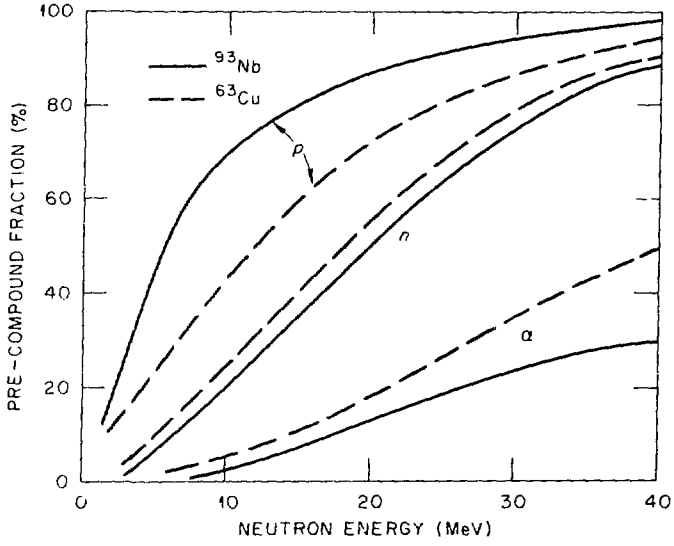

Fig. 3. Above 20 MeV, the pre-compound fractions become large and and can no longer be treated as a correction to the Hauser-Feshbach calculation.

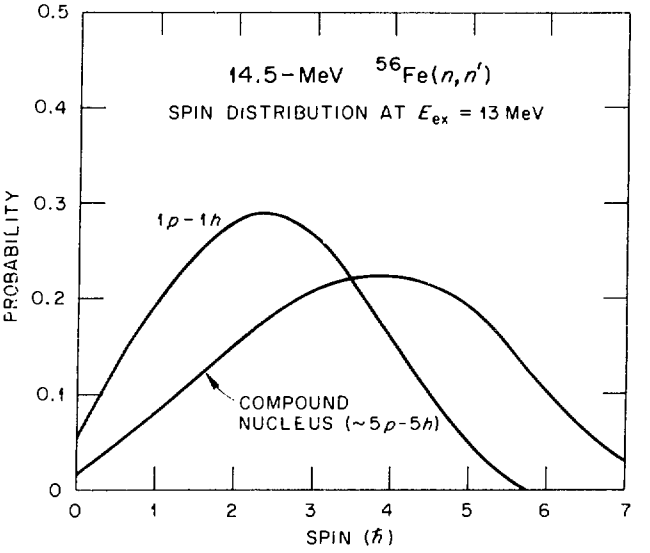

Fig. 4. Spin distributions in states excited by the first stage of pre-compound decay (1p-1h) and by compound-nucleus decay are quite different. The true distribution, somewhere in between the two extremes, should be estimated carefully for use in second-step and third-step Hauser-Feshbach calculations.

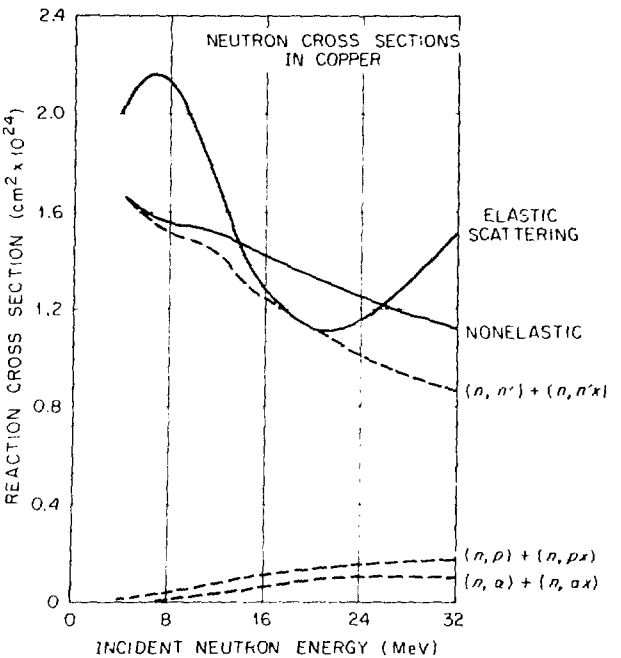

Fig. 5. Calculated cross sections for Cu as used in the calculation of specific damage energies shown in Fig. 7 (reproduced from Ref. 13).

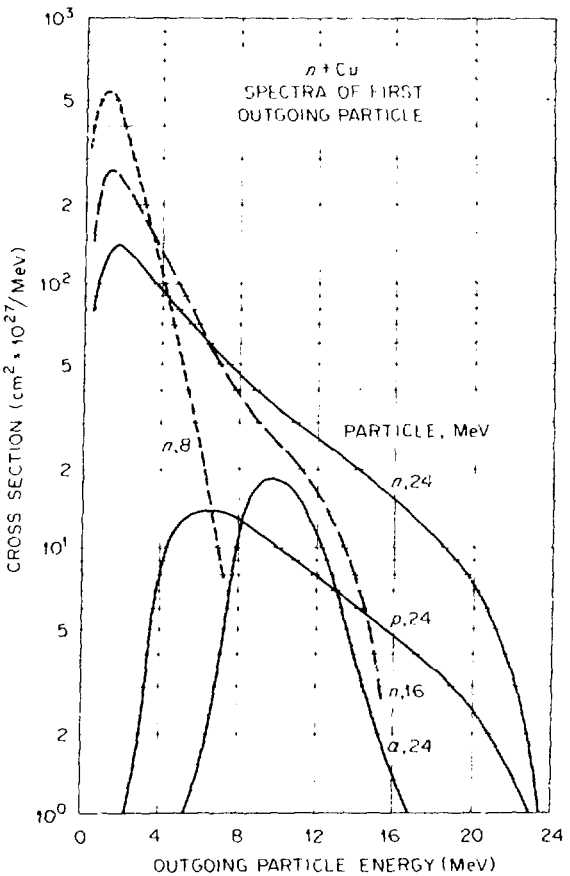

Fig. 6. Calculated first outgoing particle spectra for Cu as used in the calculation of specific damage energies shown in Fig. 7. Curves are labelled by (particle, MeV), indicating outgoing-particle type and incident neutron energy (reproduced from Ref. 13).

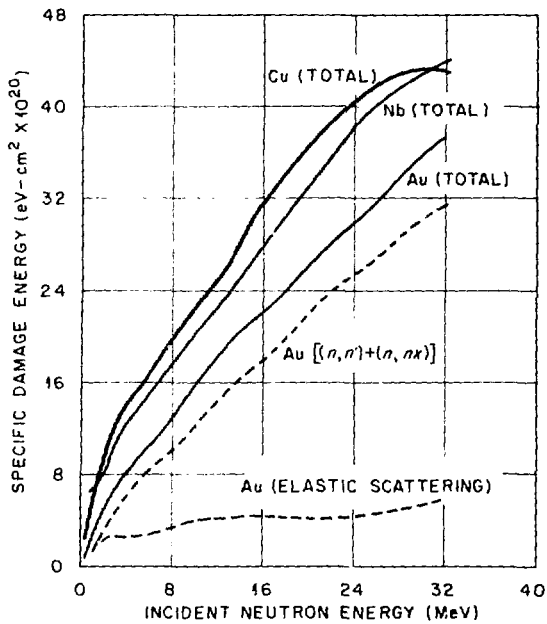

Fig. 7. Specific damage energies for Cu, Nb, and Au calculated from theoretical cross sections. For Au, the components due to elastic and inelastic scatterings are shown (reproduced from Ref. 15).

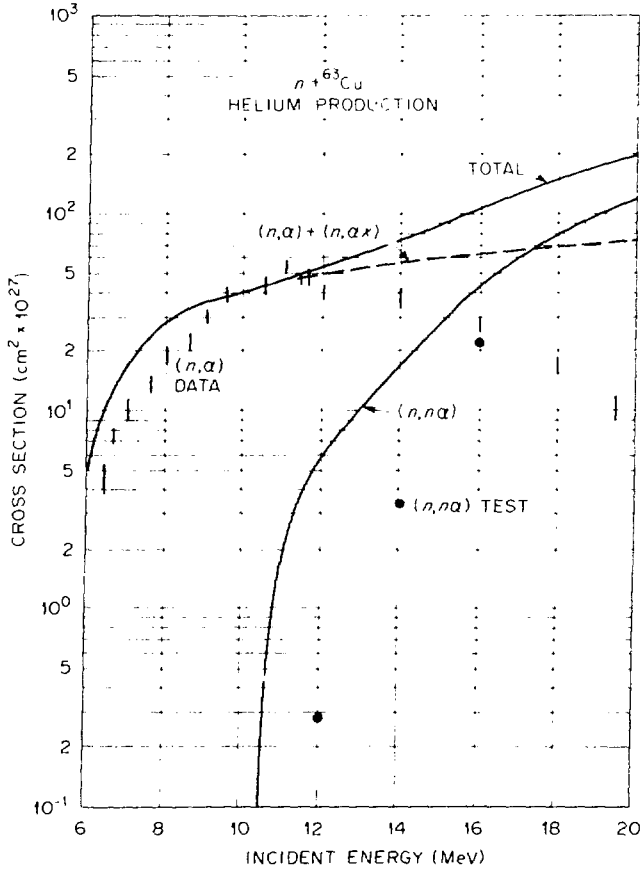

Fig. 8. Calculated helium-production cross sections for ' Cu. Depending on residual-level densities and spins, the (n,n_1) component may be rather large near 20 MeV, suggesting the possible importance of $(n,2n_1)$ cross sections above 20 MeV. The dots represent "synthetic" calculations for (n,n_1) in which spins of the lowest 8 residual levels are set equal to 1/2 instead of their correct values of 7/2, 3/2, 5/2, 3/2, 1/2, 9/2, 5/2, and 7/2 (reproduced from Ref. 13).

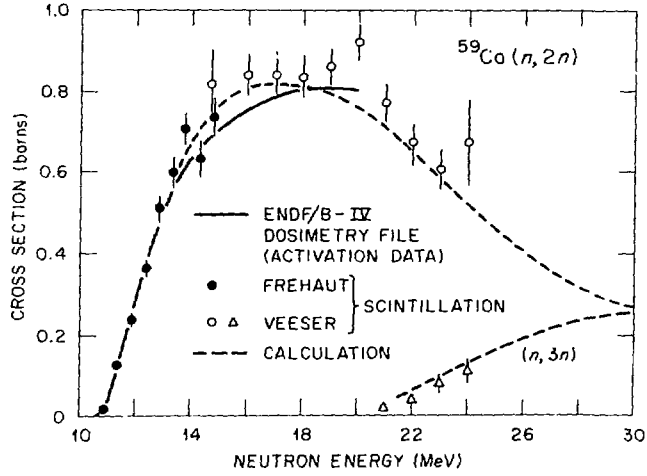

Fig. 9. Calculated and experimental $^{59}Co(n,2n)$ and $(n,3n)$ cross sections. Application of the $^{59}Co(n,2n)$ cross sections to high-energy dosimetry, such as involved in deuteron-breakup sources with deuteron energies greater than 35 MeV, requires extending the upper energy limit of ENDF/B dosimetry file to at least 30 MeV.

CONF-770523-5

Cross Sections in the Energy Range from 10 to 40 MeV Calculated with the GNASH Code*

E. D. Arthur and P. G. Young
Los Alamos Scientific Laboratory, University of California
Theoretical Division
Los Alamos, New Mexico 87545

ABSTRACT

A brief description of the preequilibrium-statistical model code GNASH is given. Features which make the code applicable to the calculation of cross sections induced by nucleons of energy 40 MeV or less are described. Finally, examples of calculations of neutron- and proton-induced reaction cross sections, activation cross sections, and secondary spectra made with global input parameters are given.

Nuclear model calculations will be important in helping meet neutron cross sections and data needs up to 40 MeV prompted by radiation damage facilities using 35-40 MeV deuteron beams on light production targets. We describe in this paper calculations of cross sections in the energy range from 10 to 40 MeV made with the preequilibrium-statistical nuclear model code GNASH developed at Los Alamos Scientific Laboratory.

The statistical portion of the code includes angular momentum and parity effects explicitly and follows closely the formalism described by Uhl.[1] Preequilibrium corrections to cross sections, level populations, and spectra are made with a simplified preequilibrium form similar to that of Braga-Marcazzan.[2] Previous reports[3] and papers[4,5] have described in detail the theoretical basis and workings of the GNASH code so no detailed description will be presented here. Instead, the general characteristics of the code, the quantities calculated by the code, and special features which lend the code to calculations of higher energy particle-induced cross sections and spectra will be briefly presented. Table 1 lists some general characteristics of the GNASH code, while Fig. 1 illustrates input features (as they exist at Los Alamos) and ouput capabilities. Features which aid in problem calculations are a level data file containing energies, spins, parities, and transition probabilities for approximately 200 nuclei and a mass table based on the Wapstra and Gove results[6] which provides automatic computation of masses and separation energies as well as

*Work performed under the auspices of the United States Energy Research and Development Administration.

ground state spin and parity values for most nuclei in the periodic table. Transmission coefficient data files are generated using external optical model routines, while card input provides information to the code concerning reaction chains, target and projectile type, gamma-ray strengths, etc. As output, one receives reaction and activation cross sections, isomer ratios, spectra (particle and gamma-ray) from individual reactions, and composite spectra obtained from all reactions. Decay chains involving up to ten compound nuclei, each of which can emit up to six types of radiation (gamma-rays, neutrons, protons, alphas, etc.), can be handled in one computation. This feature provides considerable flexibility in the calculation of complicated reactions induced by higher energy particles. Figure 2 shows a decay chain for the n + ^{59}Co reaction which was used in a 30-MeV gas-production calculation.

With this brief introduction complete, we will describe calculations aimed at verification of the applicability of the code to providing cross sections at higher energies. We have been attempting to determine how well calculations with global input parameters reproduce available experimental results since reliance upon values determined from systematics will be important for cases where little experimental data exist.

Recently measurements have been made at Lawrence Livermore Laboratory of charged particle spectra resulting from 15-MeV neutron bombardment of various materials of CTR interest.[7] These measurements were generally made with low detector thresholds so that reasonably accurate integrated cross sections for proton, deuteron, and alpha production could be determined. We have made several calculations in which "global" sets of optical model parameters were used to generate neutron, proton, and alpha particle transmission coefficients. Generally these consisted of Wilmore-Hodgson[8] parameters for neutrons, the values of Perey[9] for protons, and the alpha parameters of McFadden-Satchler[10] or those appearing in Ref. 11 for the particular nucleus of interest. Level densities using the Gilbert-Cameron formalism[12] were computed with

Table 1

GNASH Characteristics

(A) Conservation of angular momentum and parity
(B) Handles deexcitation of up to 10 nuclei.
(C) Allows emission of up to 6 types of radiation from each nucleus.
(D) Up to 50 discrete levels can be included for each nucleus
(E) Preequilibrium particle emission effects included
(F) Complex reaction chains can be handled easily in one computation

global shell and pairing corrections.[17] Also a global preequilibrium normalization determined from fits to various experimental data was used in these calculations. Figure 3 shows the calculated and experimental proton spectra resulting from 15-MeV neutrons on ^{47}Ti and ^{48}Ti. A large (n,np) contribution results for ^{47}Ti, whereas for ^{48}Ti this contribution is substantially reduced. With the global parameters described above and with no adjustments, satisfactory agreement to the measured results was obtained.

Spectral proton and alpha-particle measurements have also been made for stainless steel 316.[18] To compare with these data we calculated charged particle spectra induced by 15-MeV neutrons on ^{52,53}Cr, ^{54,56}Fe, and ^{58,60}Ni and combined them appropriately to obtain values for stainless steel 316. The same global parameter sets as those described above were used for these calculations. Figure 4 compares the calculated curves for proton and alpha spectra to the experimental results. Again the agreement for the proton spectra is satisfactory except at low proton energies where the dotted portion of the calculated curve indicates a low energy proton contribution resulting from (n,np) reactions on ^{53}Cr and ^{56}Fe. Experimentally protons having this low an energy may have been difficult to detect because of target thickness and the fact that Si detectors were used. The agreement of the alpha particle spectrum is not striking but is probably reasonable considering uncertainties in the determination of good parameter sets for alpha transmission coefficients.

In Table 2 integrated experimental and calculated proton and alpha production cross sections are compared for ^{27}Al, ^{46,48}Ti, and stainless steel 316. The agreement is within 20-30% and illustrates our experience that global parameter sets can provide reasonable integrated cross sections in this energy region.

Table 2

Charged Particle Production Cross Sections
for 15 MeV Neutrons

Target	Emitted Particle	Calculated (mb)	Experimental (mb)
^{27}Al	proton	349	305 ± 69
	alpha	113	121 ± 25
^{46}Ti	proton	711	669 ± 70
	alpha	100	98 ± 18
^{48}Ti	proton	114	85 ± 16
	alpha	20	28 ± 6
SS316	proton	316*	252 ± 38
	alpha	45	48 ± 7

*(E_p > 1.5 MeV)

A second area in which considerable effort has been made using the GNASH code has been in the calculation of (n,xn) cross sections from threshold to 24 MeV. Calculations have been compared to measurements made with large liquid scintillator tanks[15,16] as well as activation measurements.[17] In particular, for the higher energy measurements of Vonach et al.[18] (E_n = 14.7 MeV), GNASH calculations of the spectra of first and second neutrons from (n,2n) events and first, second, and third neutrons from (n,3n) events were used to correct the experimental data measured with a scintillator tank for efficiency effects related to the spectrum of the emitted neutrons. Examples of such calculated spectra appear in Fig. 5 for 24 MeV neutrons on ^{197}Au. To generate such spectra, population information computed by the code was written onto disk and then was used by a second code which handled bookkeeping for the various decay reactions to produce the results shown here. This procedure also provides a calculational method by which DDX/B spectra from (n,xn) processes can be obtained in a reliable manner.

The next two figures provide examples of the agreement obtained from calculations of (n,xn) cross sections with global parameters similar to those described in previous paragraphs. Figure 6 shows a comparison of the calculations to the ^{59}Co(n,xn) data, while in Fig. 7 the effects of various preequilibrium approximations upon the calculated ^{209}Bi(n,xn) cross sections are shown. The preequilibrium cross section computed using the exciton model of Griffin[19] and Blann[11] depends inversely upon the value of the absolute square of the average matrix element of residual two body interactions, $\langle M^2 \rangle$. In Fig. 7 the short dashed curve was made with $\langle M^2 \rangle = A^{-3}$ while the solid curve (as well as the one in Fig. 6) was made with $\langle M^2 \rangle = A^{-1}$ as determined by Feshbach-Kerman-Koonin.[20] The long dashed curve shows the effect when no preequilibrium component is included. From calculations of the (n,xn) cross section, the necessity to include preequilibrium effects at higher energies is apparent.

At energies up to 40 MeV, GNASH calculations have been made for two general problem sets. The first concerns investigation of the n + ^{59}Co reaction suggested by the Cross Section Evaluation Working Group (CSEWG) Model Codes Subcommittee. This problem was chosen to test model code results because ^{59}Co is monoisotopic and because various amounts of cross section data exist for energies less than or equal to 14 MeV, as well as total cross section data beyond 30 MeV. Except for (n,2n) and (n,3n) data (see Fig. 6), there is a lack of reaction data above 30 MeV.

Of particular interest in these calculations was (a) determination of the energy dependence of gas production (proton and alpha), (b) a check of the sensitivity of the calculated results to reaction types included, and (c) an estimation of the cost of computer calculations for incident energies around 40 MeV. Figure 8 shows the calculated proton and alpha particle production cross sections. The shoulder in the total proton production cross section results from the (n,np) reaction. The enhancement occurs because in the ^{59}Co compound nucleus, the proton separation energy lies about 4 MeV below

that for neutrons. Since only a small competition results from gamma ray emission, the (n,np) reaction proceeds exponentially until the neutron threshold opens. At higher incident energies, the (n,2n) reaction begins to dominate, resulting in a decrease in the (n,np) cross section.

In these calculations of total production cross sections, only the neutron decay chains (middle chains in Fig. 7) were followed. From each compound nucleus, gamma rays, neutrons, protons, and alpha particles were emitted. At 30 MeV, a check was made to see the effect upon the calculated values when the upper proton and alpha decay chains shown in Fig. 7 were also followed. The total production cross section calculated with the complicated and simpler decay chains agreed to within 1 %. Of course, in other calculations, for example, gamma ray production it may be necessary to include all major chains.

The amount of computer time needed for model calculations at higher energies is an important quantity. Figure 9 shows the central processor time needed on a Control Data 7600 Computer for the n + ^{90}Zr calculation for incident neutron energies between 20 and 30 MeV. For these calculations the neutron decay chain described above was used along with an integration bin size of 1 MeV.

Since relatively little neutron data exist for neutron energies above 15-20 MeV, data from proton induced reactions (spectral and integrated cross sections) can be used to test assumptions regarding, for example, preequilibrium models and level densities inherent in statistical model codes. We have calculated reaction cross sections on ^{89}Y and ^{115}In induced by protons up to 40 MeV and compared them with available experimental data. Again, we used global level density and preequilibrium parameters and employed Gilmore-Hodgson neutron parameters, while the Reinetti-Greenlees[21] (^{89}Y) and Perey parameters[22] (^{115}In) were used for protons. Figure 10 compares the calculated and experimental cross section values for ^{89}Y(p,n) reactions. It should be noted that the measured (p,2n), (p,3n), (p,pn), and (p,p2n) cross sections of Saha[23] have been shifted downward in energy by 2 MeV. This energy shift brings their (p,n) data into agreement with that of Bhattari et al.[24] where proton beam energies were known quite accurately. In Fig. 11 the calculated and experimental ^{89}Y(p,pxn) values are shown while Fig. 12 compares calculated ^{115}In(p,xn) cross sections to the data of Bhattari et al.[24] Again satisfactory agreement is obtained from the use of global parameters for these types of calculations.

A final area in which calculations have been made concerns activation cross sections and gamma ray production cross sections and spectra. The GNASH code handles gamma ray cascades in detail, allowing E1, E2, E3, M1, M2, and M3 transitions in the cascades. This capability permits calculation of activation cross sections for specific states of residual nuclei, as well as the accompanying spectra of emitted gamma rays. Figure 13 compares experimental and calculated activation cross sections for neutron induced reactions on various Pb isotopes. Similarly, calculated energy spectra of emitted γ-rays from 14-MeV neutron bombardment of ^{56}Fe and ^{93}Nb are

compared in Fig. 14 to the measurements of Drake et al.[25] The same global parameter sets described above[8] were used for the calculations in both figures, together with a giant dipole resonance form for the γ ray strength function. Again, reasonable agreement with experiment was obtained with these parameters.

In conclusion, we have attempted to determine how well existing model parameters based on studies of systematics reproduce available data. Since much of the data required for higher energy neutrons will be based on calculations made where little or no data exist, an investigation of the applicability of such parameters is important in order to obtain confidence in calculated results. Based on calculations described here (as well as others made with the GNASH code), generally we feel that accuracies on the order of 25-40% can be obtained for integrated cross sections and average spectral energies using global parameters. The details of calculated spectra are somewhat less accurate although improvements can be made by optimizing parameters for specific nuclei. Although angular distributions have not been addressed in this paper (or in our statistical preequilibrium calculations to date), such effects are important for reactions induced by higher energy neutrons. We presently compute direct reaction cross sections and angular distributions with separate coupled channel codes. In the future we plan to incorporate in the GNASH code preequilibrium models which will provide angular distribution information.

REFERENCES

1. H. Ehl, Acta Phys. Austria 31, 245 (1970)
2. G. M. Braga Marcazzan, L. Cadilli Lina, L. Milazzo Colli, and P. G. Sona, Phys. Rev. C6, 1398 (1972).
3. E. D. Arthur, presented at the Special Meeting of the CINDA Standard Committee, Los Alamos, N.M. (August 1976).
4. E. D. Arthur and P. G. Young, Trans. Am. Nucl. Soc. 23, 500 (1976).
5. E. D. Arthur and P. G. Young, International Conference on the Interactions of Neutrons with Nuclei, Lowell, Mass., 1452 (1976).
6. A. H. Wapstra and N. B. Gove, Nucl. Data Tables 9, 265 (1971).
7. S. M. Grimes, R. C. Haight, and J. D. Anderson, Nucl. Sci. Eng. 62, 187 (1977).
8. D. Wilmore and P. E. Hodgson, Nucl. Phys. 55, 673 (1964).
9. F. G. Perey, Phys. Rev. 131, 745 (1963).
10. Lynne McFadden and G. R. Satchler, Nucl. Phys. 84, 177 (1966).
11. C. M. Perey and F. G. Perey, Atomic Data and Nuclear Data Tables 13, 293 (1974).
12. A. Gilbert and A. G. W. Cameron, Can. J. Phys. 43, 1446 (1965).
13. J. L. Cook, H. Ferguson, and A. R. de L. Musgrove, Aust. J. Phys. 20, 477 (1967).
14. R. C. Haight, S. M. Grimes, and J. D. Anderson, Hydrogen and Helium Production Cross Sections for 14 MeV Neutrons on Stainless Steels 316 and 304, Lawrence Livermore Laboratory preprint 78785 (1976).

15. J. Frehaut and G. Mosinski, Nuclear Cross Sections and Technology, NBS Spec. Publ. 425, Vol. II, 555 (1975).
16. L. P. Geesey, J. D. Arthur, and P. G. Young, to be published.
17. R. P. Reynolds, J. S. Gilmore, P. J. Prestwood, J. R. Wilhelmy, H. Lamme, R. H. Erkkila, and F. A. Hardekopf, Phys. Rev. C12, 451 (1975).
18. J. J. Griffin, Phys. Rev. Lett. 17, 478 (1966).
19. H. Blann, Phys. Rev. Lett. 21, 1357 (1968).
20. G. Fulbach Cline, Nucl. Phys. A210, 390 (1973).
21. F. D. Becchetti, Jr., and G. W. Greenlees, Phys. Rev. 182, 1190 (1969).
22. G. B. Saha, S. T. Porile, and L. Yaffe, Phys. Rev. 144, 962 (1966).
23. G. Rinaldi, I. Gadioli, E. Gadioli Erba, A. M. Grassi Strini, G. Strini, and G. Tagliaferri, Nucl. Phys. A201, 529 (1973).
24. G. Rinaldi, I. Gadioli, A. M. Grassi Strini, G. Tagliaferri, and L. Zetta, Nucl. Phys. A166, 25 (1971).
25. D. M. Drake, J. D. Arthur, and M. G. Silbert, "Cross Sections for Gamma Ray Production by 14 MeV Neutrons," accepted for publication in Nucl. Sci. and Eng. (1977).

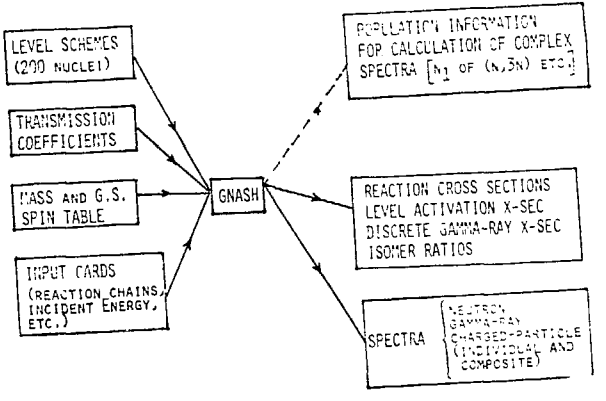

Fig. 1. GNASH input and output features implemented at Los Alamos.

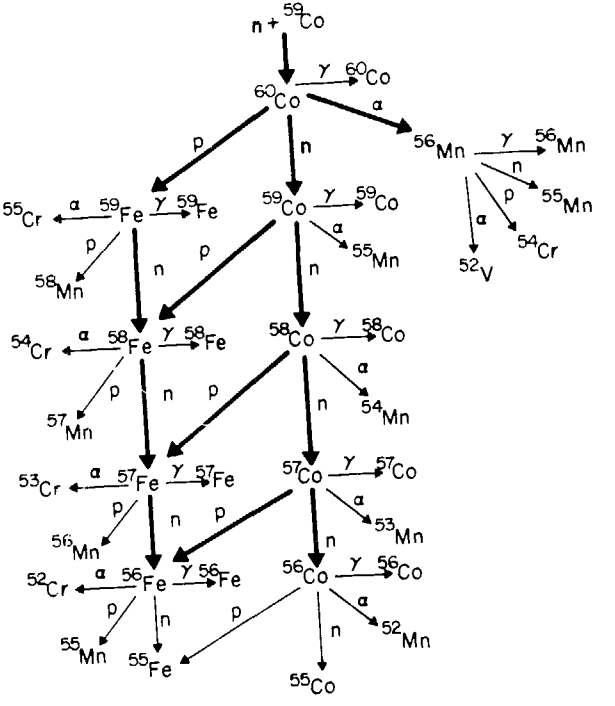

Fig. 2. Sample decay chain used in 30 MeV n + ^{59}Co calculations.

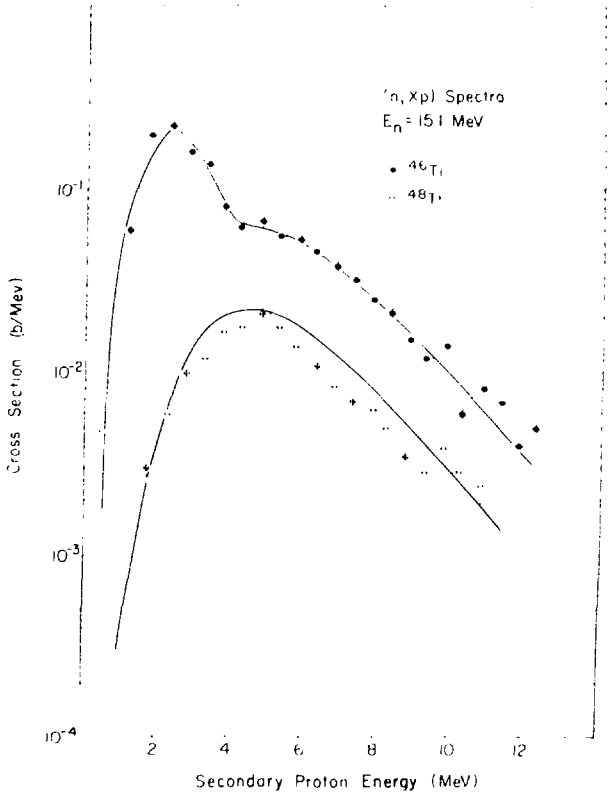

Fig. 4. Calculated and experimental values for the proton spectra resulting from 15-MeV neutron bombardment of ^{46}Ti and ^{48}Ti.

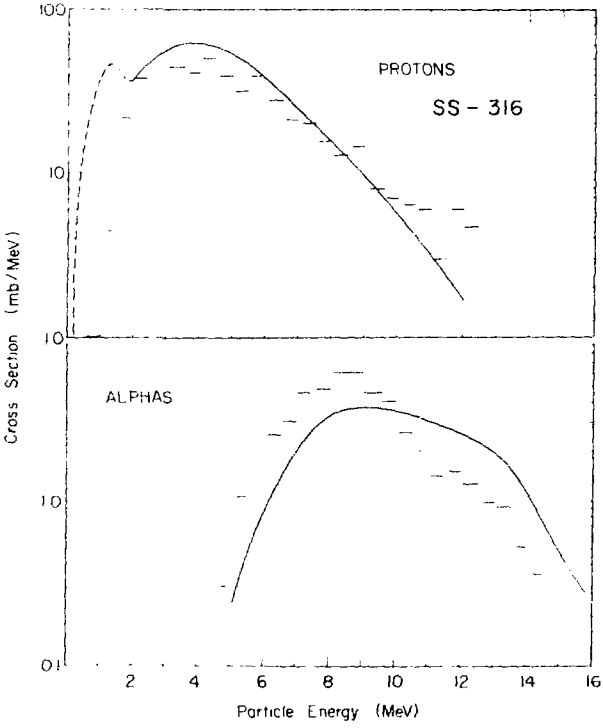

Fig. 4. Calculated curves versus experimental values for protons and alpha spectra produced by 15-MeV neutrons on stainless steel 316. The dotted portion of the calculated curve for protons is described in the text.

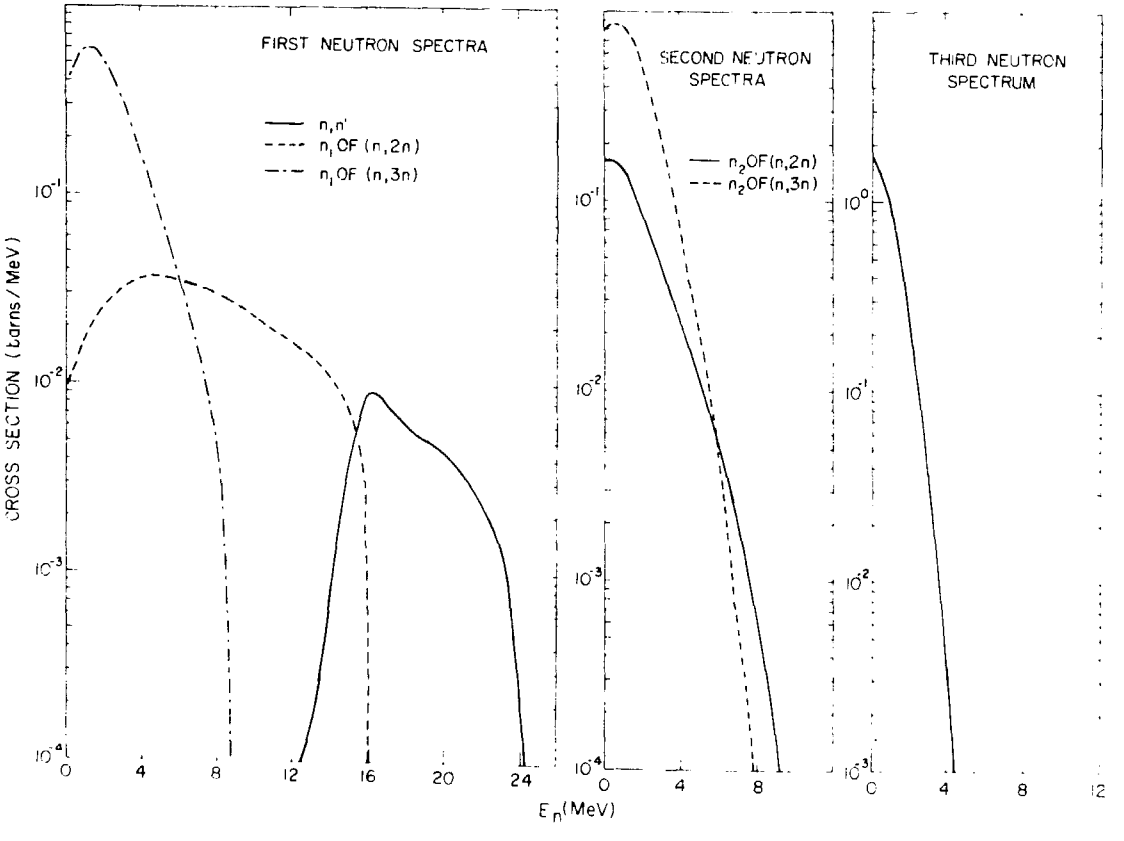

Fig. 5. Calculated complex neutron spectra resulting from $^{197}Au(n,xn)$ reactions induced by 24-MeV neutrons.

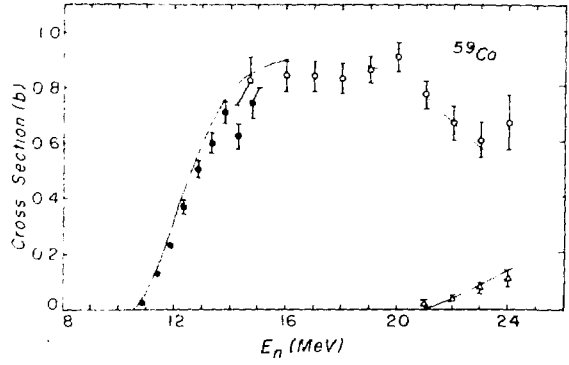

Fig. 6. Comparison of calculated and experimental values for ^{59}Co(n,xn) reactions.

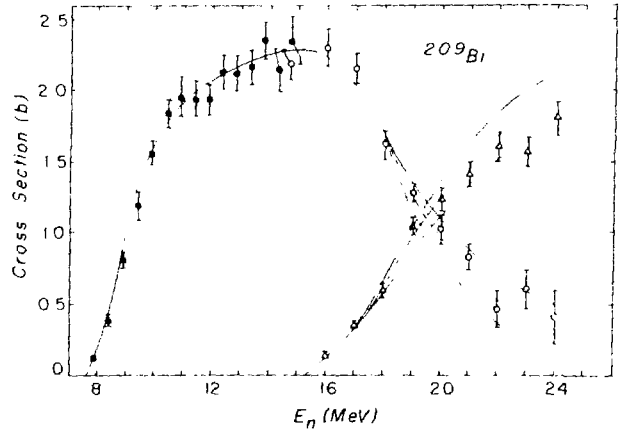

Fig. 7. Calculated and experimental values for ^{209}Bi(n,xn) reactions. At higher energies the solid curve was calculated using a preequilibrium component normalized to mass and energy. The short dashed curve included a preequilibrium component whose normalization depended only on mass, while the long dashed curve was made with no preequilibrium component.

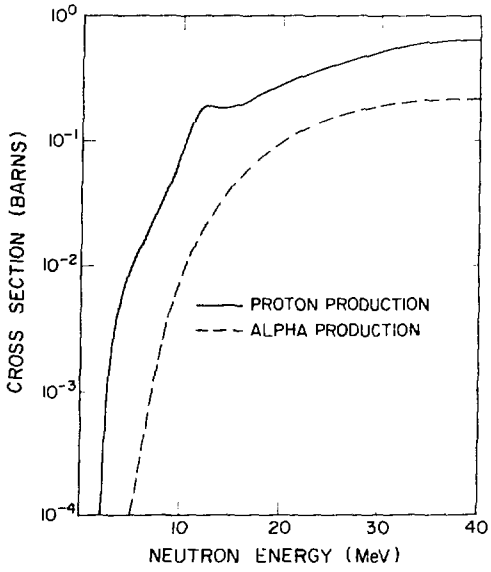

Fig. 8. Total calculated proton and alpha production cross sections for n + ^{59}Co.

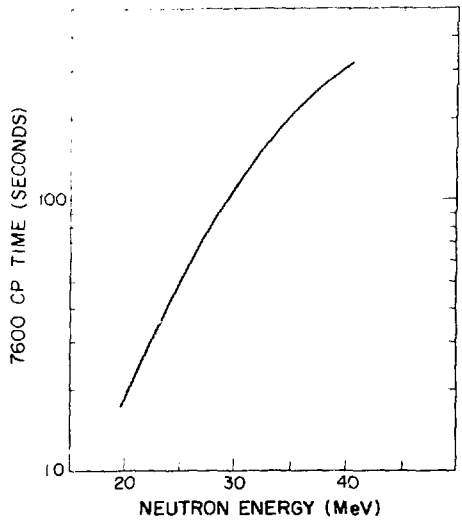

Fig. 9. CDC 7600 computer cental processor time (in seconds) required for GNASH calculations from 20 to 40 MeV for n + ^{59}Co.

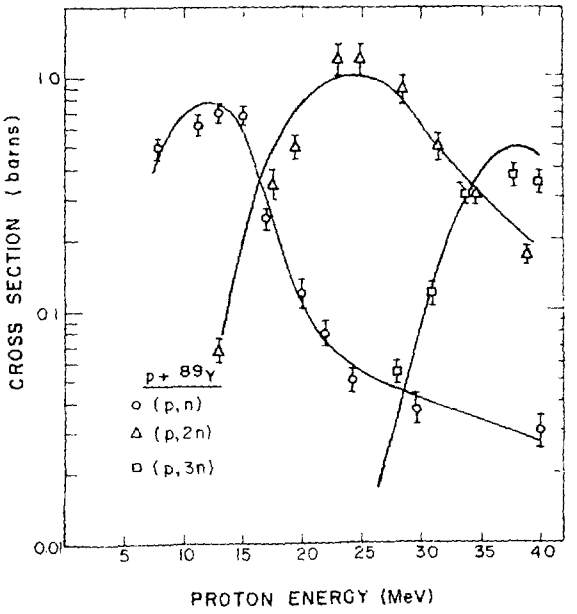

Fig. 10. Experimental and calculated $^{89}Y(p,xn)$ values.

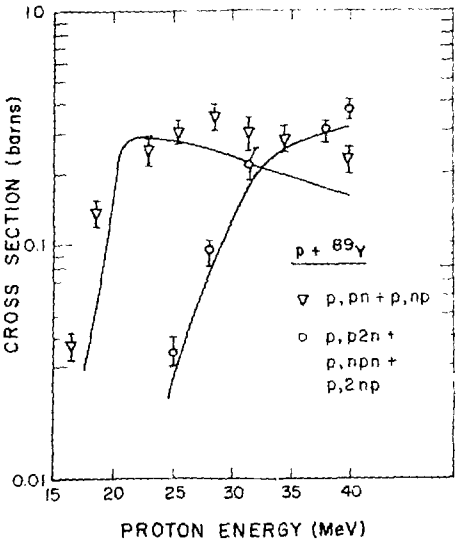

Fig. 11. $^{89}Y(p,pxn)$ experimental and calculated results.

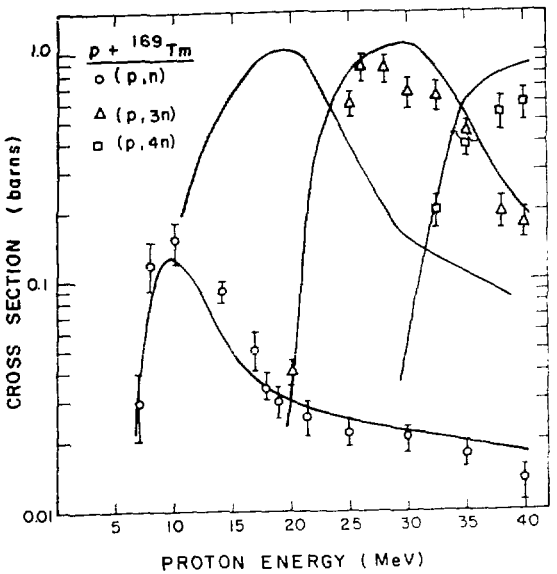

Fig. 12. Comparison of calculated $^{169}Tm(p,xn)$ cross sections to experimental data.

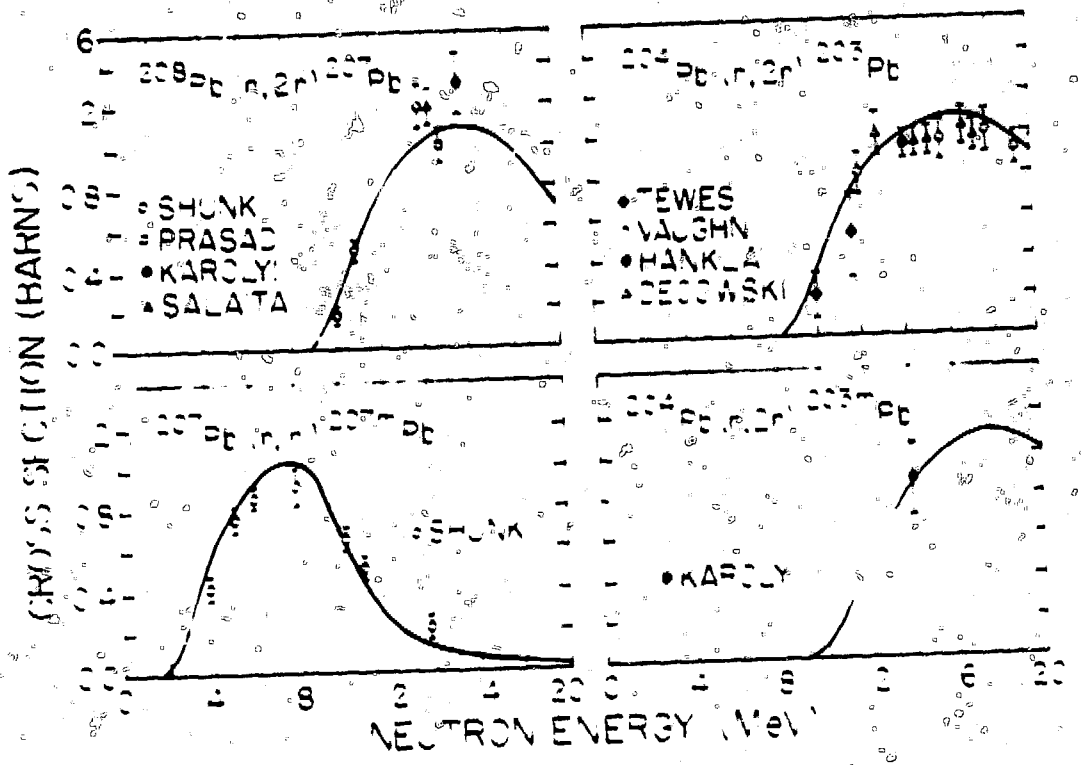
CROSS SECTION (BARNS)
NEUTRON ENERGY (MeV)
SHONK
PRASAD
KAROLY
SALATA
EWES
VAUGHN
HANKLA
DECOWSKI
SHONK
KAROLY

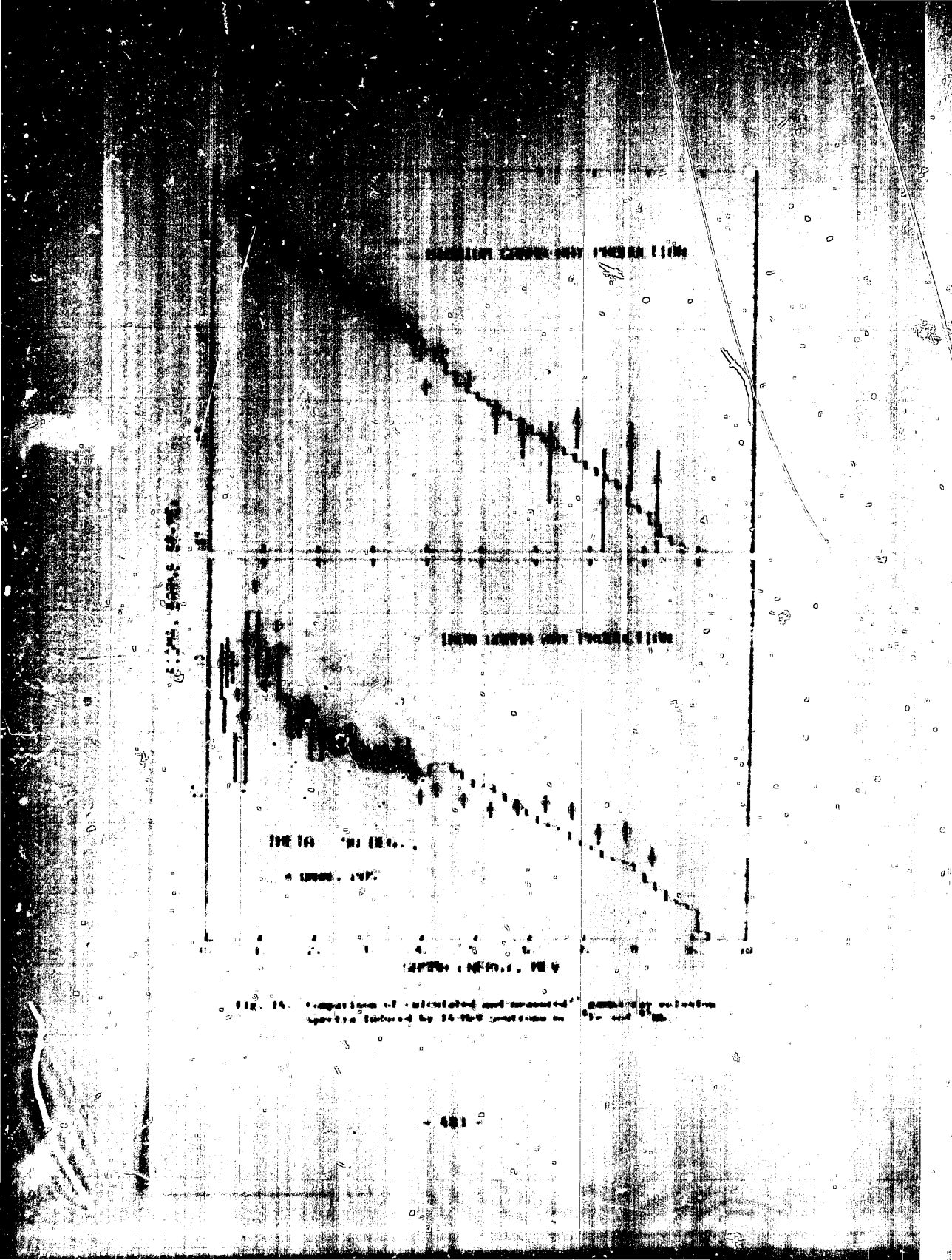

FIG. 14. Comparison of calculated and measured gamma-ray excitation spectra induced by 14-MeV neutrons on [illegible]

[illegible] Calculations

[illegible]
[illegible]
[illegible] Engineering Development Laboratory.

[illegible]

Unfortunately, it is difficult to experimentally measure helium production at [illegible] the alpha particle [illegible] difficult to measure at the beam [illegible] It would be [illegible] International, [illegible] [illegible] [illegible]

[illegible]

[illegible]

1. [illegible]

2. [illegible]

3. [illegible]

4. [illegible]

5. [illegible]

6. [illegible]

7. [illegible]

8. [illegible]

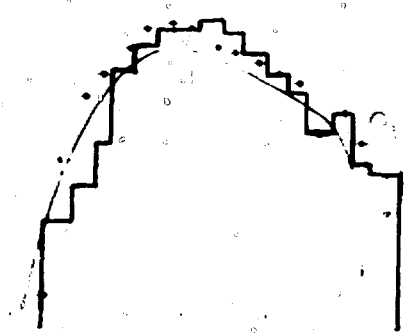

1. [illegible]

fireball size
HEDL calculations

NEUTRON, PROTON AND DEUTERON INDUCED REACTION PRODUCTS IN THE 10-40 MEV RANGE.

M. Divadeenam*

Brookhaven National Laboratory

ABSTRACT

Neutron, proton and deuteron induced excitation functions for several target nuclei (^{51}V, ^{56}Fe, ^{58}Ni, ^{65}Cu, ^{90}Zr, ^{93}Nb, and ^{181}Ta) were calculated employing the GDH pre-equilibrium model of Blann and the Weisskopf-Ewing evaporation model in the 10-40 MeV range. In some instances calculations were extended beyond 40 MeV. Agreement between theory and experiment is fair to good in most of the cases investigated in spite of the simple nature of the theoretical model employed. Limitations of the nuclear model and possible improvements are discussed.

INTRODUCTION

Interest in the energy range of 10-40 MeV has intensified because of the need for cross sections in fusion reactor design and radiation damage experiments. In addition, the fabrication of intense neutron source, a topic of current interest, requires the knowledge of neutron, proton and deuteron induced cross sections in the high energy region. In the absence of the desired experimental data one can meet these requirements by estimating cross sections based on a theoretical model. Some level of confidence could be expected in applying the theoretical model discussed below, if good agreement is found between theory and experiment for most of the excitation functions investigated.

NUCLEAR MODEL ASSUMPTIONS

Several nuclear model codes are available for the estimation of reaction cross sections. Most of the codes are limited to low energy projectile energy and can handle only few residual nuclei in a reaction sequence. In addition, some sophisticated codes take enormous computer time even on large computers. For the purpose at hand Blann's code ALICE[1] running on the NNDC PDP-10 computer was used. Details of the model and the code description are given below.

*Supported by the U.S. Energy and Research Development Agency.

[illegible]

[illegible] other words, [illegible] in the entire calculation [illegible]. For example if [illegible] is the target, the final residual nucleus is [illegible].

7. Equi-distant fermi-gas level density parameter [illegible] levels/MeV [illegible] where [illegible] is the target mass.
8. At each incident projectile energy the emission spectra of neutrons, protons, alphas and deuterons are calculated as a function of the emitted particle energy. Integrals of these spectra are listed in the output.
9. For the pre-compound decay [illegible], the initial exciton number [illegible] and deuterons. Values of [illegible] are considered for deuteron in one case.

Limitations of the model employed and possible future improvements are discussed at the end of the paper.

Usually the experimentalists employ the activation technique to measure the production cross sections of residual nuclei. Few examples of excitation functions with possible cross-section components are listed below.

(p,pn) = (p,[illegible]) + (p,np) + [illegible]
(p,p2n) = (p,[illegible]) + (p,2n[illegible]) + [illegible]
(p,2pn) = (p,[illegible]) + (p,pd) + [illegible]
(p,2p2n) = (p,[illegible]) + (p,2p2n) + (p,3pn[illegible]) + (p,3np) + ...

[illegible]	[illegible] MeV	Error	Ref[a]
[illegible]	[illegible]	[illegible]	[illegible]
[illegible]	[illegible]	[illegible]	[illegible]
[illegible]	[illegible]	[illegible]	[illegible]
[illegible]	[illegible]	[illegible]	[illegible]
[illegible]	[illegible]	[illegible]	[illegible]
[illegible]	[illegible]	[illegible]	[illegible]
[illegible]	[illegible]	[illegible]	[illegible]
[illegible]	[illegible]	[illegible]	[illegible]
[illegible]	[illegible]	[illegible]	[illegible]
[illegible]	[illegible]	[illegible]	[illegible]
[illegible]	[illegible]	[illegible]	14
[illegible]	[illegible]		[illegible]
[illegible]	[illegible]	[illegible]	[illegible]
[illegible]	[illegible]	[illegible]	[illegible]
[illegible]			
[illegible]	[illegible]	[illegible]	18

a) Most of these references were [illegible] in ref. 7.
b) [illegible] quoted (used as a monitoring standard).

[illegible] residual nuclei at [illegible] MeV neutron [illegible] similar. Note that a particular value [illegible] (n,xn) cross-section curves [illegible] tional models. The proton irradiation [illegible] neutron curve toward the neutron deficient [illegible] neutron. The calculations predict the peak [illegible] indicated by the experimental results [illegible], etc., [illegible] in the insert. The ratio $\frac{\sigma(n,2pxn)}{\sigma(n,xn)}$ [illegible] and [illegible] in Fig. 4. The solid points refer to the [illegible] calculations. Straight lines are drawn [illegible] experimental data [illegible] and insert [illegible] for the ratio as a function of x, the number of [illegible].

[illegible]. Proton Induced Reactions

Extensive experimental data exists for the proton induced reaction excitation functions, [illegible] shown [illegible], [illegible], [illegible] and [illegible] in the present investigation.

The theoretical excitation functions are compared with the corresponding experimental data in Figs. [illegible] to [illegible]. Unless otherwise noted the calculated curves in these figures correspond to a situation when pairing correction to the [illegible] energy calculation is included. In a few instances, results for both pairing and shell correction are shown. The expected [illegible] multipole excitations are [illegible] excitation functions. [illegible] excitations [illegible] excitations [illegible] the agreement between experiment and theory.

[illegible]

The calculated (p,n), (p,2n), (p,pn), (p,3n) and (p,2pn) excitation functions are compared with the corresponding experimental data [illegible] in Fig. 5.

(p,n): The agreement between experiment and theory is good up to 30 MeV. Calculations with pairing plus shell correction is better than those with pairing only. Beyond 30 MeV, calculations agree with Holzman's data but not with Cadilla's. Giant quadrupole excitation is expected to contribute significantly to the (p,n) cross section at and 15 MeV proton energy.

(p,3n): Theory reproduces the shape and magnitude of the experimental excitation function.

(p,2pn): Predicted excitation function is lower than the experimental data, however, the general shape is reproduced.

(p,3pn), (p,3p2n): Theory predicts the order of magnitude in each of these cases, however the experimental data has some

[illegible]

[illegible]

[illegible]

[illegible]

[illegible]

[illegible]

σ(p,5n) and σ(p,6n): both of these excitation functions are fairly reproduced by the model calculations.

σ(p,pn), σ(p,p2n), σ(p,p3n), σ(p,p4n): The predicted shapes for all of these excitation functions are similar to the corresponding experimental data. However, theory under-predicts in each case. The reason for under-prediction has been pointed out before-absence of direct interaction component.

^{58}Ni Gas Production

^{58}Ni gas production cross sections for neutron and proton projectiles are displayed in Fig. 12. There is no experimental data beyond 20 MeV to make any comparison with the predictions. Note that proton and α-production cross sections are numerically larger than deuteron, triton and helion production cross sections. Triton and ^{3}He production cross sections do not include the actual ^{3}H and ^{3}He emission (cf Fig. 12 caption).

III. Deuteron Induced Reaction:

Deuteron induced reaction excitation functions measured by Bisplinghoff, et.al., of ^{181}Ta up to 80 MeV are considered for comparison with the model calculated cross sections (cf Figs. 13 & 14)

As noted earlier the initial excitation number for nucleon is 3. However, for deuteron it is not a well studied quantity. Calculations were performed for three different values of n_0 =2,3 and 4 sensitivity of the calculated results for different values of n_0 is shown in Fig. 13. For the rest of the cases, theoretical results for n_0=3 are compared with experiment.

In all of the calculations the resulting excitation functions start at somewhat lower energies than what is suggested by the experimental data, an exception being the (d,p4n) cross section. However, theory in the (d,p4n) case deviates from the experimental trend beyond 60 MeV. To what extent the lowered threshold behaviour is attributable to the mass-binding prescription or to the optical model parameters is not clear. This aspect will be investigated in the near future.

DISCUSSION AND CONCLUSIONS

In summary, ALICE code does predict cross sections up to and beyond 40 MeV incident energy for neutron, proton and deuteron induced reactions. Even though the model used is a simple one, about 75% of the 50 (not all discussed) calculated excitation functions agree with the corresponding data fairly well. In some cases when direct interaction component is expected to be significant agreement with experiment is not good. No parameter variation was entertained to improve the fits.

For a given target nucleus if the neutron induced excitation functions are not available, it should be possible to correct the corresponding proton induced excitation functions to obtain neutron induced cross sections. Both coulomb and nuclear effects have to be considered. Such "synthetic" neutron excitation functions could be used to test the applicability of the nuclear reaction theory. Some general comments regarding the limitations of the model are in order:

The (p,n) excitation functions have a bump at the low energy end and the width of this bump becomes narrower as the number increases. Giant Dipole Resonance is expected to play an important role in the vicinity of the broad peak. Discrepancy between experiment and theory cannot be improved without introducing Giant Multipole Resonance components. It seems, one of the reasons for poor agreement beyond about [illegible] between theory and experiment may be due to over-simplifying the compound nucleus process. Furthermore, more feedback treatment particularly for the primary reaction product is preferred over the evaporation theory.

In most cases considered, the calculated (p,pn) and (p,2n) excitations are smaller than the corresponding experimental [illegible]. As has been pointed out earlier, this is due to the absence of direct interaction components, for example, pick-up, knock-on [illegible] processes. Supplementing the presently calculated [illegible] cross sections based on the "GDR model" is expected to improve the fits. The (p,2pxn) excitation functions, [illegible] two humps; the first one corresponds to the [illegible] channel and the second to the [illegible] channel. Pre-compound [illegible] part, should improve the fits in the valley region between the two humps. The initial exciton number for [illegible] treated as a parameter to fit the experimental data well.

The pre-compound multiple emission processes considered in the present investigations might improve the fit at high projectile energy. This might also improve the agreement between theory and experiment in the case of deuteron induced excitation functions.

Finally, improved level density descriptions, suitable especially for nuclei around magic number, further sensitivity of the predictions to the choice of the optical model parameters and details of the energy dependence of the potential remains to be investigated.

Some of the improvements suggested above will be taken up later in the next stage of our investigation of reaction cross sections in the high energy region.

ACKNOWLEDGEMENT

The author thanks Marshall Blann for useful discussions.

REFERENCES

1. M. Blann, OVERLAID ALICE, University of Rochester Report COO-3494-29.
2. M. Blann, Ann. Rev. of Nucl. Science, 25, 123 (1975) Phys., Rev. Lett. 27, 337 (1971); 28, 757 (1972).
3. F.E. Bertrand, ORNL-50-4000, Vol. 9.
4. E.P. Bayhurst, J.S. Gilmore, R.J. Prestwood, J.B. Wilhelmy, N. Jarmie, B.H. Erkkila and R.A. Hardekopf, Phys. Rev. C12, 451 (1975).
5. Katcoff, J.B. Cumming, J. Gedel, V.J. Buchanan, H. Susskind and C.J. Hsu, Nucl. Inst. and Methods 129, 473 (1975).
6. J.C. Hill, D.G. Shirk, K.F. Petry and K.H. Wang, Phys. Rev., C12, 1978 (1975).
7. T.W. Burrows and J.S. Burt, BNL-NCS-50640 (1977), and private communication.
8. E. Gadioli, A.M. Grassi Strini, C. La Bianco, Il Nuovo Cimento, 22, 567 (1974).
9. S. Bhattacharya and L. Yaffe, Can. J. of Chem. 41, 2194 (1963).
10. J. Wing and J.R. Huizenga, Phys. Rev. 128, 280 (1962).
11. J.L. Jenkins and A.C. Wahl, J. Inorg. Nucl. Chem. 32, 1419 (1969).
12. D.A. Newton, S. Sarkar, L. Yaffe and R.B. Moore, J. of Inorg., Nucl. Chem. 35, 361 (1972).
13. C.B. Saha and V.T. Porile and L. Yaffe, Phys. Rev. 144, 962 (1966).
14. B.L. Cohen, I. Newman, F.A. Charpie and T.H. Handley, Phys. Rev. 96, 620 (1954).
15. N.V. Kantele and J.J. Hogan, Phys. Rev. C14, 64 (1976).
16. C.L. Rao and L. Yaffe, Can. J. of Chem. 41, 2516 (1963).
17. C. Pirat Ari, E. Gadioli, A.M. G. Strini, and G. Tagliaferri, Il Nuovo Cimento, 7, 101 (1973).
18. J. Bisplinghoff, J. Ernst, A. Mayer-Kuckuk, P. Jahn and C. Mayer-Böricke, Nucl. Phys. A228, 18 (1974).
19. T. Tamura and T. Udagawa, "Multi-step Direct Reaction Analysis of Continuous Spectra in Nuclear Reactions", these proceedings; and T. Tamura, T. Udagawa, D.H. Feng and K.-K., Kan, Phys. Lett. 66B, 109 (1977).
20. H.R. Weller, et.al. Phys. Rev. C13, 1055 (1976).

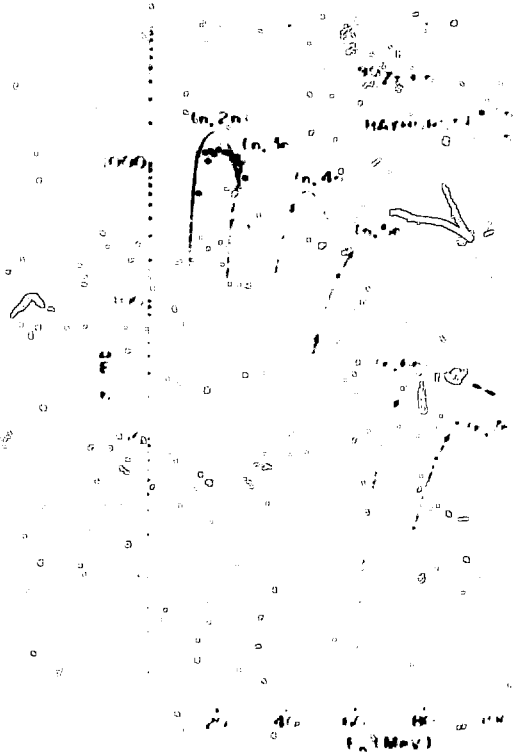
(n, 2n)
(n, γ)
(n, 4n)
(n, n)
E
E_n (MeV)

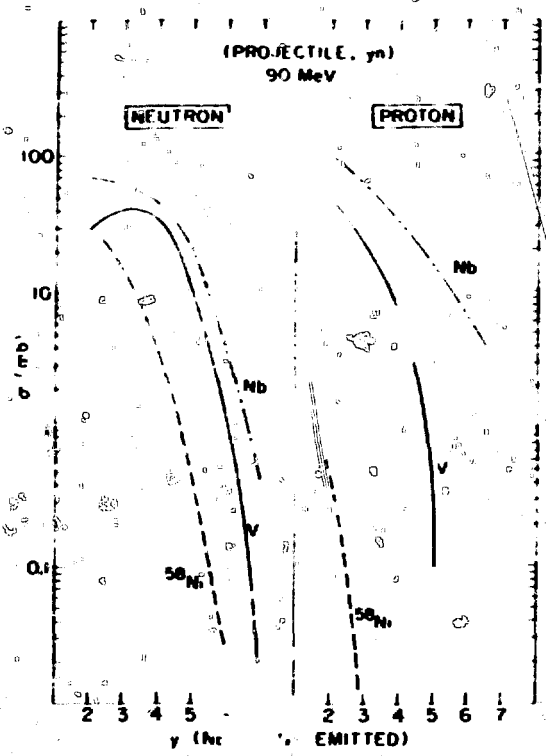

Fig. 2. 90 MeV neutron and proton induced excitation functions (n,yn) and (p,yn) respectively as a function of y, the number of neutrons emitted. Smooth curves are drawn through the calculated points.

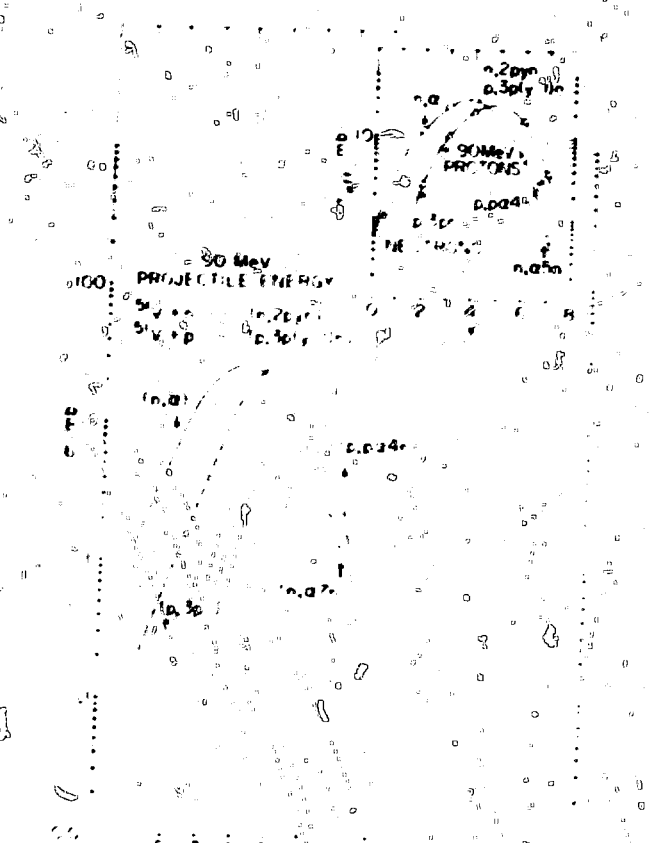
90 Mev
PROJECTILE ENERGY
90Mev
PROTONS
0.024
0.034
0.3p
1
2
3
4
5
6
7
8

[illegible]

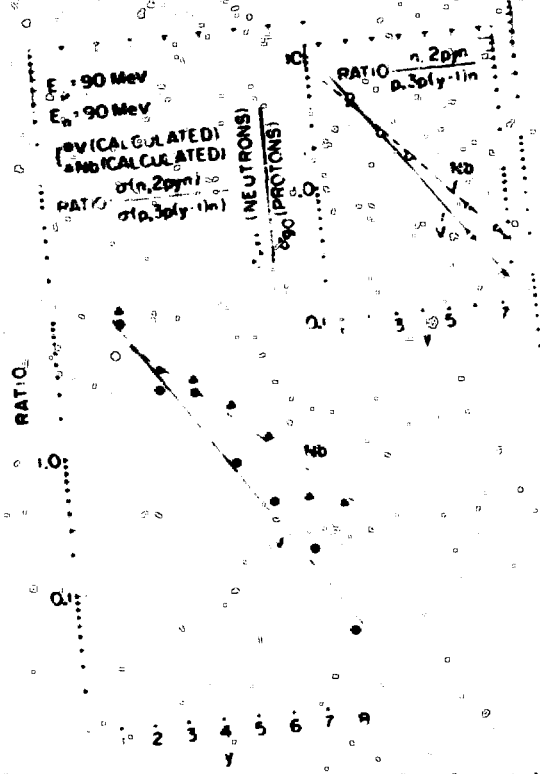

FIG. [illegible] The ratio [illegible] as a function of y, the number of neutrons [illegible] extra. [illegible] times through the [illegible] calculated [illegible] drawn to guide the eye. Insert: measured experimental ratio (Katcoff, et.al; Errors: 10%).

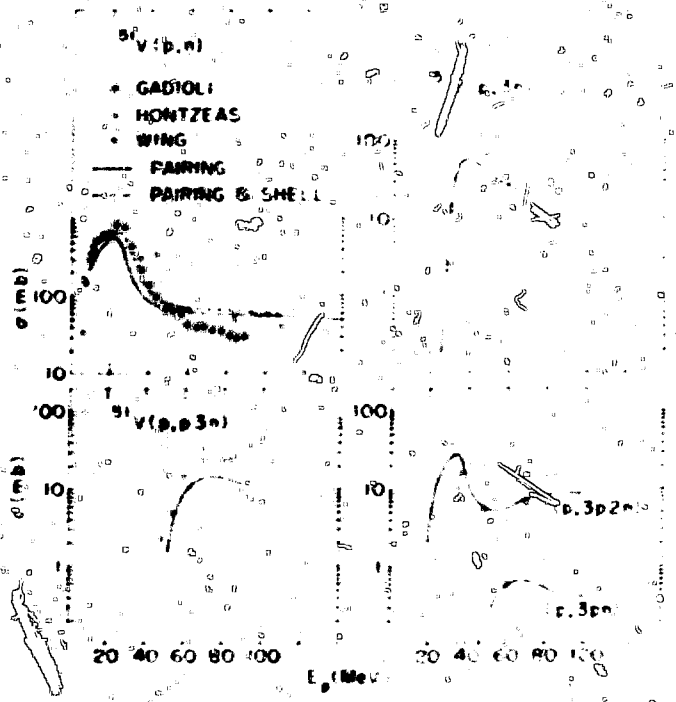

Fig. 3. ^{51}V + p: Comparison of experimental and theoretical excitation functions. Hontzeas' data has uncertainties of about 20% and the rest have 10%.

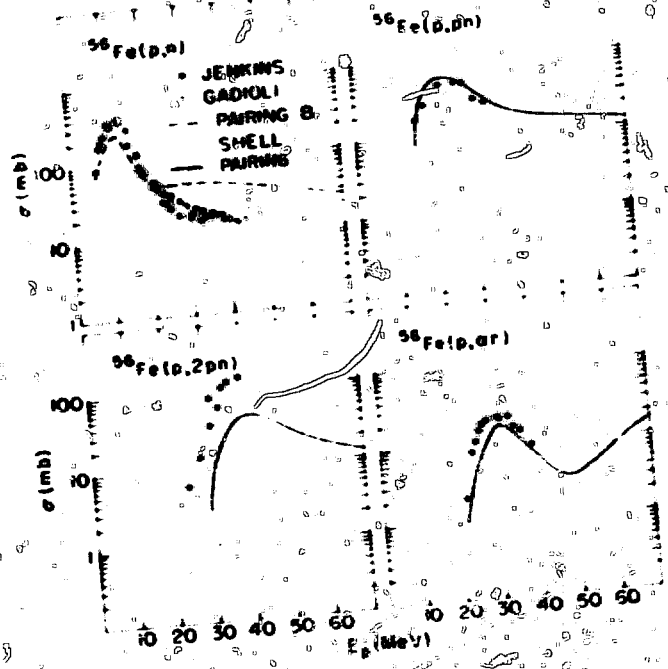

Fig. 6. ^{56}Fe + p: (p,n) excitation function calculated with pairing and shell correction and the rest with pairing only. Over-prediction of (p,n) beyond 25 MeV results in an under-prediction of (p,2pn) cross section. Errors for the experimental data are of the order of 10%.

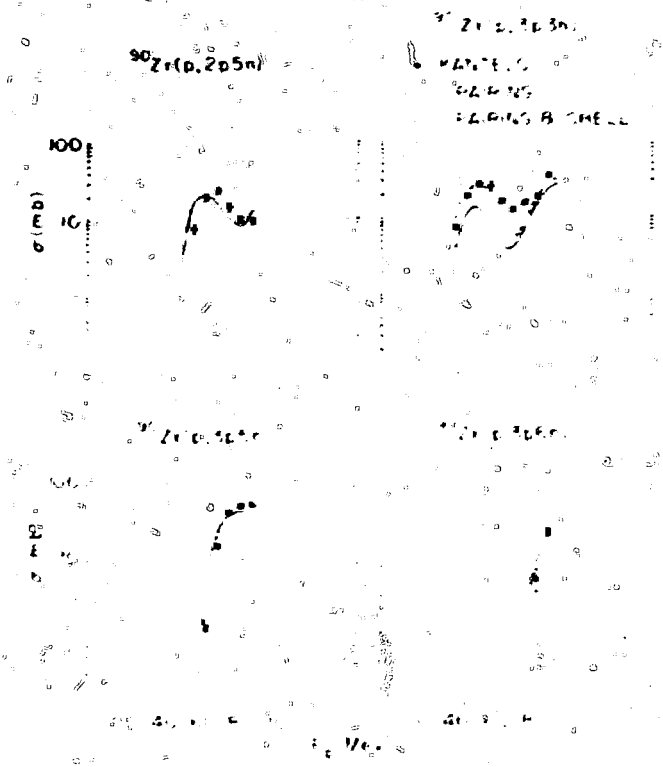

Fig. 8. Same as Fig. 5. Two different sets of calculated results are shown for (p,2pxn) cross section.

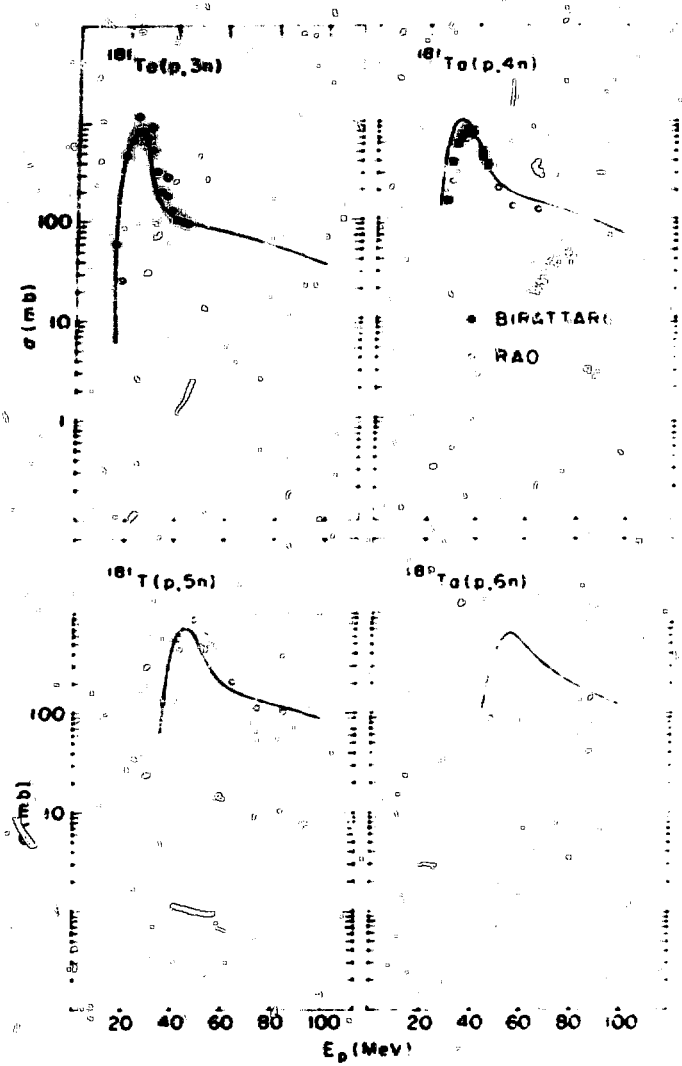

Fig. 10. Comparison of experiment with theoretical prediction for proton induced reactions on ^{181}Ta. Errors: Brittari (152); Rao (252).

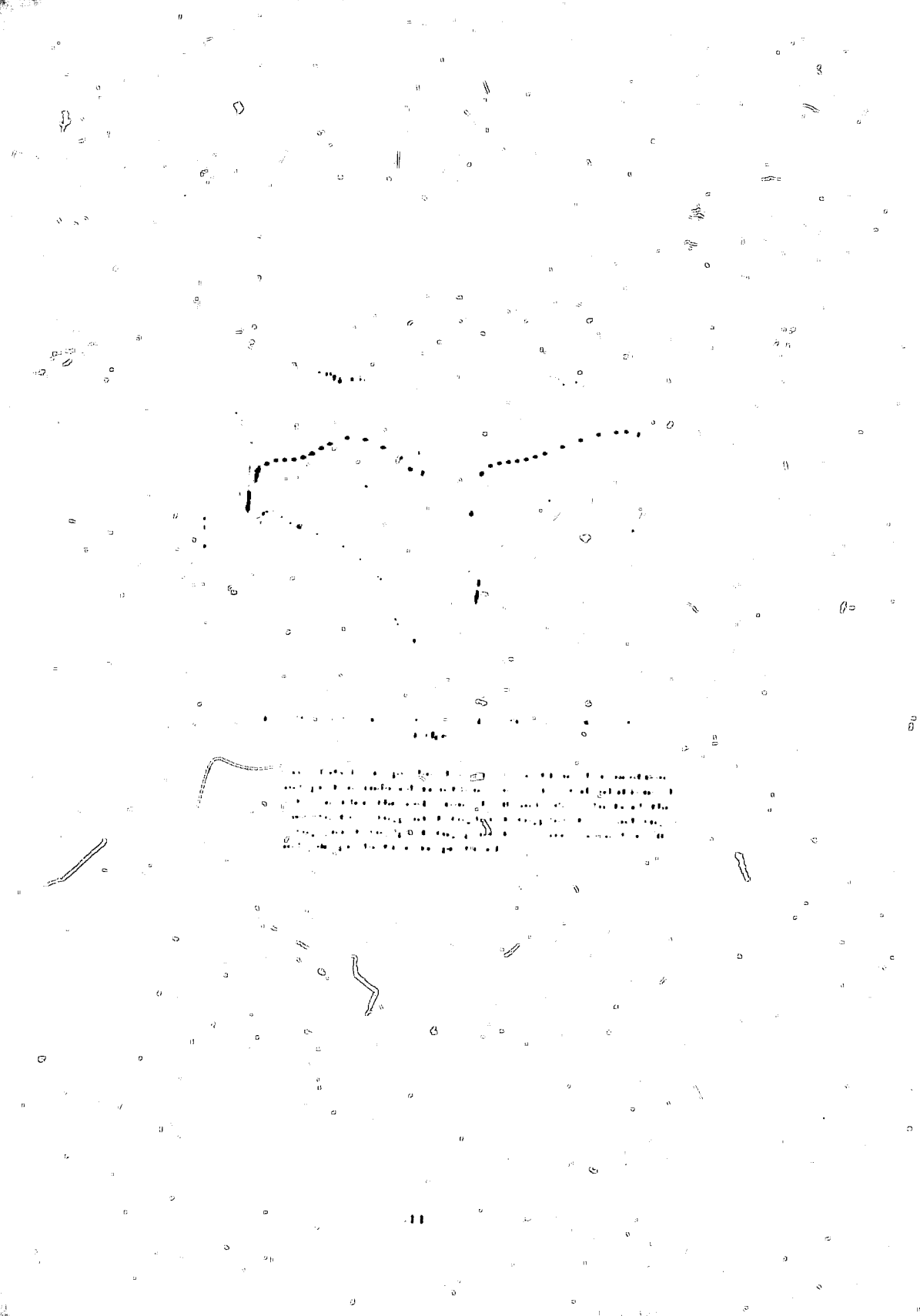

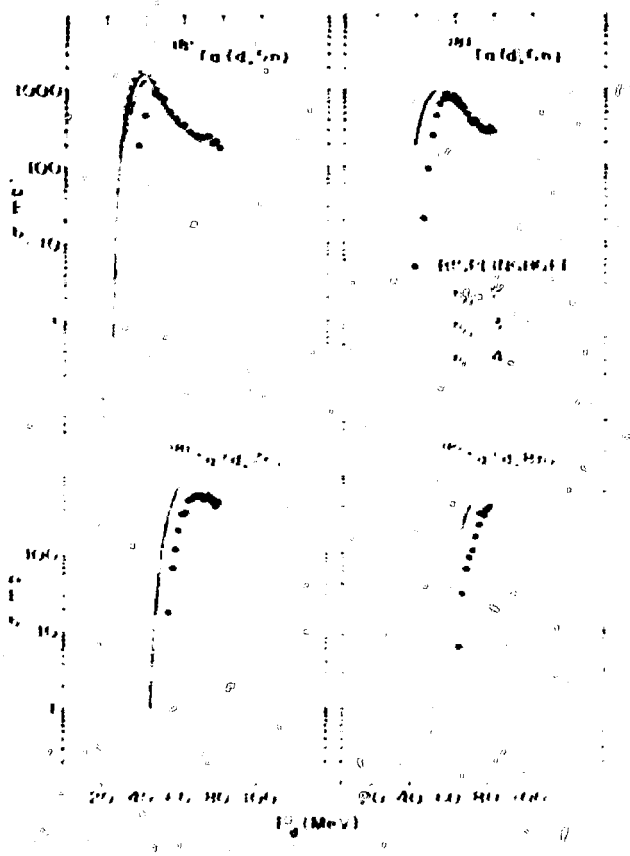

Fig. 13. [illegible]: Comparison of theoretical and experimental excitation functions. Predictions for n = 2, 3 and 4 are shown for the [illegible](d,5n) case; n = 3 results for the rest. Experimental uncertainties are about 10%.

The Intranuclear-Cascade-Evaporation Model for Nonelastic Nuclear Collisions and Its Application in Biomedical and MHD Research

[illegible] and [illegible] G. Alsmiller, Jr.
[illegible] National Laboratory, Oak Ridge, Tennessee

I. INTRODUCTION

The intranuclear-cascade-evaporation model (ICEM) of nuclear reactions [illegible] approach used to describe an absolute [illegible] induced by a variety of incident particles [illegible], heavy ions, etc. [illegible] incident protons and neutrons. The [illegible] applicable to high-energy [illegible] nuclear reactions, but comparisons [illegible] total and differential [illegible] data, this model [illegible] differential nuclear reaction data for a variety of [illegible]. For example, ICEM is currently incorporated into a Monte Carlo radiation transport code [illegible] that has been and [illegible] extensively and successfully for a variety of radiation transport problems, and data obtained from ICEM have often been used [illegible] in the discrete ordinates codes DOT4 and [illegible].

In Section II, a brief description of ICEM is given and comparisons between results obtained with ICEM and experimental cross section data are presented. In Section III transport calculations using [illegible] different cross section data obtained with ICEM are presented and compared with experimental data.

II. THE INTRANUCLEAR-CASCADE-EVAPORATION MODEL

A. Description of the Model

The intranuclear-cascade model is based on the assumption that the reactions of incident particles with complex nuclei can be represented by a sequence of two-particle interactions that take place within a model nucleus. A brief description of the calculational method is given here with details given elsewhere [illegible].

The nucleus is assumed to be spherically symmetric, consisting of a dense central core surrounded by angular regions of diminishing density. The density within each region is assumed to be constant. The energy distribution of the bound nucleons in the nucleus was taken to be a zero-temperature Fermi distribution. The maximum kinetic energies of the protons and neutrons in each

regions are thereby determined from their densities in each region. The single-particle potential for the protons, and similarly for the neutrons, in each region was taken to be $-(E_F + 7)$ MeV, where E_F is the proton Fermi energy in the region and the 7 MeV is an approximation to the separation energy of the neutrons and protons for all nuclei.

In the model an incident particle is made to enter the nucleus, and, if it collides with one of the target nucleons, it is assumed that the collision can be described as a free-particle collision. Free-particle total and differential-scattering cross sections, in conjunction with Monte Carlo techniques, are used to determine the interaction probability and the scattering angle. Relativistic kinematics are used to determine the vector momenta of the scattered and recoil nucleons in the laboratory system. An approximation to the exclusion principle is invoked by comparing the energies of the neutrons and protons after every collision with the neutron or proton Fermi energy of the region in which the collision has taken place. If the energy of either particle is below the Fermi energy, the reaction is "forbidden," the collision is aborted, and the nucleon that initiated the collision is allowed to proceed to its next estimated collision site.

Tracking of each nucleon from an allowed collision is followed to the next collision site where the process is repeated, thus developing a cascade. The history of each nucleon involved in the cascade is traced until the nucleon either escapes or until its energy falls below a cutoff energy (E_{CN} for neutron, E_{CP} for proton), thereafter it is assumed to be trapped within the nucleus. Due to the holes produced in the nucleus as a result of the cascade and to the capture of the low-energy particles, the residual nucleus after all cascade particles have been omitted is usually in an excited state. In the model this excited residual nucleus is allowed to emit further particles (neutrons, protons, deuterons, tritions, etc.) by means of an evaporation theory [illegible]. As part of the evaporation calculation the type of residual nucleus and the kinetic energy of recoil of this residual nucleus for each "history" is also obtained. A record is kept of the information pertinent to each escaping particle, such as the type of particle (neutron, proton, etc.), its vector momentum, etc. Many incident-particle and induced-cascade histories are followed in order to generate statistically significant results.

The ICEM has been implemented by Bertini [illegible] in the code MECC-7 [illegible] and K. Chen [illegible]. Most of the results presented here were obtained using the Bertini model, but a few examples of comparisons between the two models and experimental data are included. The code MECC-7 is available from the Radiation Shielding Information Center, and, as far as the user is concerned is parameter free. That is, the user need specify only the type and energy of the incident particle and the A and Z of the target nucleus to obtain in absolute units all of the differential cross section data available from the model.

5. Differential Cross Section Calculations and Comparison with Experimental Data

Comparisons due to [illegible] between calculated [illegible] total nonelastic cross sections and experimental data for [illegible] elements in the energy range of 3 to 6[illegible] MeV are [illegible] in Fig. [illegible]. The agreement is quite good and [illegible] unreliable in this energy range.

In Figs. 2-4 calculated results [illegible] for neutron production from 1[illegible]-MeV protons on [illegible], and ^{208}Pb, respectively, are presented and [illegible] experimental data of Verbinski and [illegible]. [illegible] are calculated results obtained [illegible] model.

In Fig. 2 ICEM results are [illegible] the cutoff energies E_c [illegible] results are quite insensitive [illegible]. The ICEM results are in reasonable agreement with the [illegible] data over much of the energy range [illegible] differed with the evaporation model [illegible] experimental data. In [illegible] the ICEM [illegible] agreement with the data for [illegible] are in moderate agreement with the experimental data [illegible]. In both Figs. 3 and 4, as in Fig. 2, the [illegible] evaporation model do not agree at all well with the experimental data. Neither the ICEM nor the evaporation model give [illegible] results at the low incident energy considered in the figure. [illegible] of one or the other of these models must be used [illegible] from the comparisons presented that the ICEM is to be preferred.

In Fig. 5 comparisons between calculated and measured differential proton emission spectra for [illegible], and ^{209}Bi are presented. Calculated results are given in the figure from the cascade model of Bertini [illegible] cascade and the cascade model of [illegible] cascade. [illegible] calculated results shown in the figure were started with [illegible] particles only, i.e. no contribution from the evaporation [illegible] included. The [illegible] cascade model reproduces [illegible] and the magnitude of the experimental spectra [illegible] better than does the [illegible] cascade model.

In Fig. 6 comparisons between calculated and measured angular distributions of protons with energy [illegible] protons on [illegible], ^{54}Fe, and ^{209}Bi are [illegible]. [illegible] are again given in the figure from the [illegible] cascade and the [illegible] cascade. Except at wide angles the [illegible] cascade reproduces the magnitude of cross section better than does the [illegible] cascade. At wide angles, where the number of emitted particles is small, both calculations underestimate the measured cross section by a rather large factor.

It should be kept in mind while reviewing Figs. 1 to 6 that absolute comparisons are shown and no attempt has been made to adjust any of the data in the Bertini model to obtain better agreement. All of the comparisons are for incident protons rather than neutrons, but there is no very good theoretical reason to expect the model to be any less valid for incident protons than for incident neutrons.

III. TRANSPORT CALCULATIONS AND COMPARISON WITH EXPERIMENTAL DATA

A. Biomedical Applications

The IEEM of Bertini has been incorporated into a Monte Carlo transport code, HETC, and the code has been used to obtain a variety of results of biomedical interest.

Theus [illegible] have measured the absorbed dose as a function of depth along the axis of a tissue-equivalent phantom when the neutron spectrum produced by 35-MeV ^2H on Be is incident on the phantom. Measurements were carried out with several conical collimators that produce circular fields of radius R at the phantom surface that was 125 cm from the source. The experimental absorbed doses are shown by the solid curves in Fig. 7 for R values of 17, 13, 9, 5, and 3 cm. Calculated results [illegible] that were obtained using the same geometry and tissue-equivalent composition as those used in the experiment, are shown by the histogram values in Fig. 7. In carrying out the calculations, the energy distribution of neutrons from 35-MeV ^2H on Be as measured by Theus [illegible] was used, the neutrons were assumed to be emitted isotropically from a point source, and perfect collimation was assumed; i.e., no scattered neutron contribution from the collimator or photon cotamination was considered. The radial intervals over which the calculations were averaged to obtain an estimate of the center-line absorbed dose are specified in the figure for each collimator size. The error bars shown on the histograms are statistical and represent one standard deviation.

The absolute normalization of the experimental data was not known, but all of the data have the same normalization. To make the comparisons shown in Fig. 7 the normalization was established by making the calculated and experimental values agree at a depth of 5 cm for the R = 9 cm case. The agreement between the calculated and experimental data in all cases is very good.

For neutrons from 35-MeV ^2H on Be, Theus *et al.*[23,24] have also measured the absorbed dose as a function of depth along the center line of the tissue-equivalent phantom when a collimator that produces a square 10-by-10-cm field is used. A comparison between the calculated and experimental data for this case is shown in Fig. 8. To obtain an estimate of the center-line absorbed dose, the calculated results have been averaged over a 6-by-6-cm square about the center line. The calculated results

given in the figure have an absolute normalization. The experimental results have an unknown normalization and have therefore been made to agree with the calculated absorbed dose at a depth of 5 cm. The agreement between the calculated and experimental center-line absorbed dose in the case of a square field (Fig. 8) is approximately the same as that obtained in the case of circular fields (Fig. 7).

In the case of the collimator discussed in the previous paragraph, Todd [illegible] have measured the absorbed dose as a function of distance from the beam center line at depths of 5 and 10 cm in the phantom. In Fig. 9 the calculated absorbed doses are compared with these experimental data. The calculated results are given with absolute units and the experimental results have been normalized to agree with the calculations at the point shown in the figure. The distance from the center line (abscissa in Fig. 9) is measured parallel to the small dimension of the collimator; that is, at the surface of the phantom where the field is 10 cm by 10 cm, the distance from the center line to the edge of the field is 5 cm. The calculated results at depths of 5 and 10 cm shown in the figure were obtained by averaging over the depth intervals of 4 to 6 cm and 9 to 11 cm, respectively. The agreement between the calculated and experimental absorbed doses is quite good even at distances from the center line that are well beyond the collimator field, i.e., at distances from the center line that are irradiated only by scattered radiation.

[illegible]. MFE Radiation Damage: Calculated Spatial Variation of the Damage Energy in the Experimental Volume of a Li(D,n) Source

Using nonelastic differential cross section data, for neutron energy [illegible] 15 MeV, obtained from the ICEM model of Bertini, calculated results of the spatial variation of the damage energy in the experimental volume of a Li(D,n) source when this volume is partially filled with experimental samples have been obtained.

The geometry used in the calculations is shown in Fig. 10. The energy distribution of the neutron source was taken from the measurements of Saltarsh [illegible]. The calculations were carried out with the discrete ordinates code DOT.

Calculations were carried out for no absorber, a 5-cm-thick iron absorber, and a 10-cm-thick carbon absorber (see Fig. 10). In Fig. 11 the damage energy in copper and in niobium is shown as a function of z for several values of r. The results in Fig. 2 are for an incident current of 100 mA of 40-MeV deuterons and are extended over an experimental volume of [illegible] 6000 cm [illegible]. The plotted points in Fig. 11 have no significance other than to distinguish between the various curves. At the smaller radii there is a very substantial variation as a function of depth of the damage energy in both copper and niobium for all absorbers considered. At the larger radii, however, the variation of the damage energy with depth is only of the order of a factor of two for the cases considered. On the other hand, for a fixed depth the damage energy

in both copper and niobium decreases rapidly with increasing radii. The results in Fig. 11 are dependent on the fact that both the magnitude of the neutron flux and the spectral shape of the neutron flux varies with position and with the absorber used. The fact that the damage energy changes rather slowly with depth at the larger r values is presumably due to compensations between the changes in the magnitude of the neutron flux and the changes in the spectral shape of the neutron flux. At a given position in the experimental volume for either copper or niobium, the ratio of the damage energy with no absorber to the damage energy with the iron or carbon absorbers is never greater than three and in most positions is less than two. Calculated results for the hydrogen and helium production in copper and niobium as a function of position in the experimental volume have also been obtained and are given in Ref. 25.

SUMMARY

It is impossible in a short summary paper such as this to cover all facets of the intranuclear-cascade-evaporation model. The comparisons with experimental data that have been presented, however, are, hopefully, sufficient to indicate that the model is not completely unreliable in the energy region of interest here (≲ 50 MeV) and to indicate that transport calculations of interest in biomedical and magnetic fusion energy applications can, at the present time, be carried out.

REFERENCES

1. K. C. Chandler and T. W. Armstrong, "Operating Instructions for the High-Energy Nucleon-Meson Transport Code HETC," ORNL-4744, Oak Ridge National Laboratory (1972).
2. R. W. Roussin, R. G. Alsmiller, Jr., and J. Barish, "Calculations of the Transport of Neutrons and Secondary Gamma Rays Through Concrete for Incident Neutrons in the Energy Range 15 to 75 MeV," Nucl. Eng. Design 24, 250 (1973).
3. R. G. Alsmiller, Jr., F. R. Mynatt, M. L. Grieveson, J. V. Pace, and J. Barish, "The Lateral Spread of High-Energy (≲ 400 MeV) Neutron Beams and Earthshine," Nucl. Instr. Meth. 89, 53 (1970).
4. R. G. Alsmiller, Jr. and J. Barish, "The Calculated Response of ^{6}LiF Albedo Dosimeters to Neutrons with Energies ≲ 400 MeV," Health Phys. 26, 13 (1974).
5. R. G. Alsmiller, Jr. and J. Barish, "Shielding Against the Neutrons Produced When 400-MeV Electrons are Incident on a Thick Copper Target," Particle Accelerators 5, 155 (1973).

[illegible] Kiessling, [illegible] "Calculations Pertaining to the [illegible] of Fast [illegible] Neutrons in Cancer Radiotherapy," Med. Phys. 1.

[illegible] Kiessling, Jr. [illegible], "Calculations Related to the Possible Use of Protons, Neutrons, Negatively Charged Pions, Protons, and Alpha Particles in Radiotherapy," Rad. Res. 65, 365 (1976).

[illegible] Middle Atlantic Neutron Therapy Association (MANTA), Progress Report, Submitted by L. L. Rogers, M.D., Virginia Commonwealth University, Medical College of Virginia, Richmond, Virginia (1977).

[illegible] R. B. Theus, "Neutron Delivery," Proceedings Conference on Particle Accelerator in Radiation Therapy, LA-5125-C, Los Alamos, New Mexico, October 2-5, 1972, p. 62.

[illegible] R. G. Alsmiller, Jr. and J. Barish, "The Spatial Variation of the Damage Energy and Gas Production in the Experimental Volume of a LiTiO,n, Neutron Radiation Damage Facility", ORNL/TM-5554, Oak Ridge National Laboratory (1976) (to be published in Nuclear Technology).

26. M. J. Saltmarsh and R. L. Worsham, Eds., "TNPRTU - An Intense Neutron Generator for Radiation-Induced Damage Studies in the CTR Material Program," ORNL/TM-5233, Oak Ridge National Laboratory (1976).

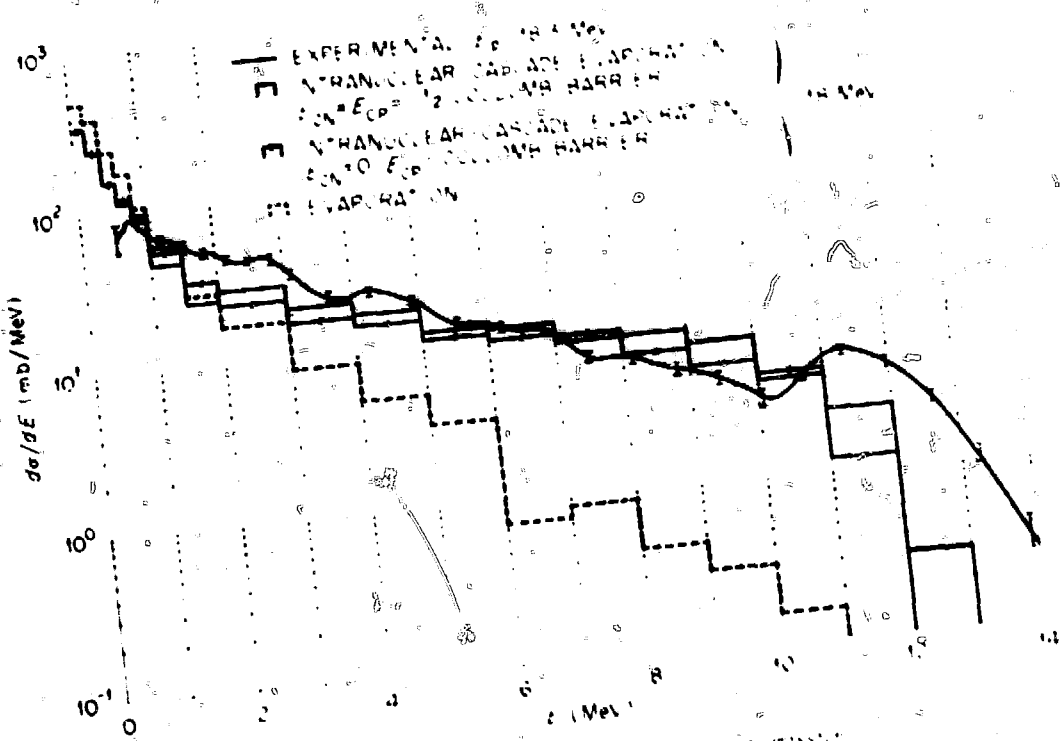

Fig. [illegible] Differential cross section for neutron emission from 18-MeV protons on [illegible]

EXER VENT
INFRA
EVAP RA
EVAP RA
dq/dt m2/Mol

do/dt : mc/yr(1)

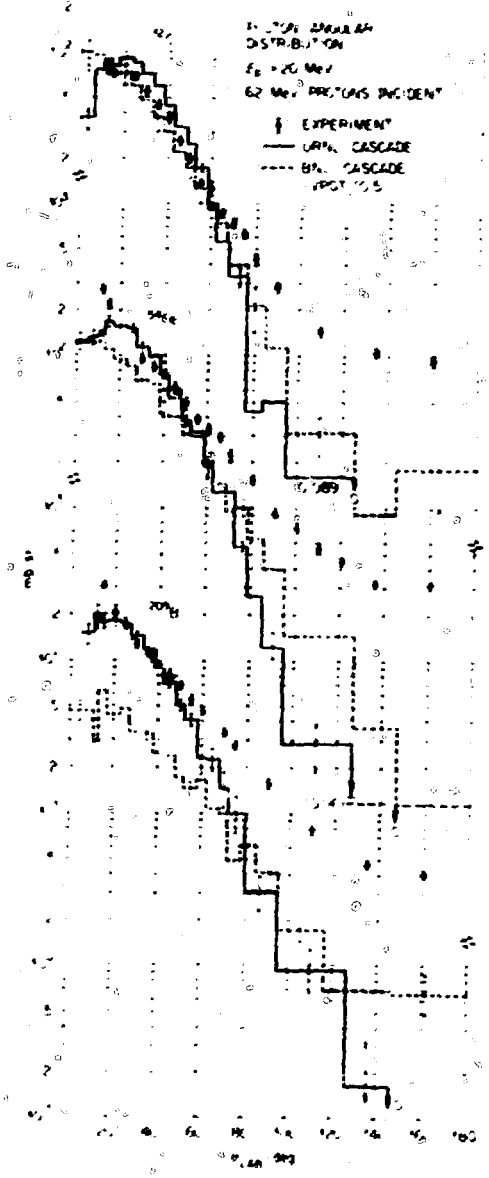
EXPERIMENT

NORMALIZATION
POINT

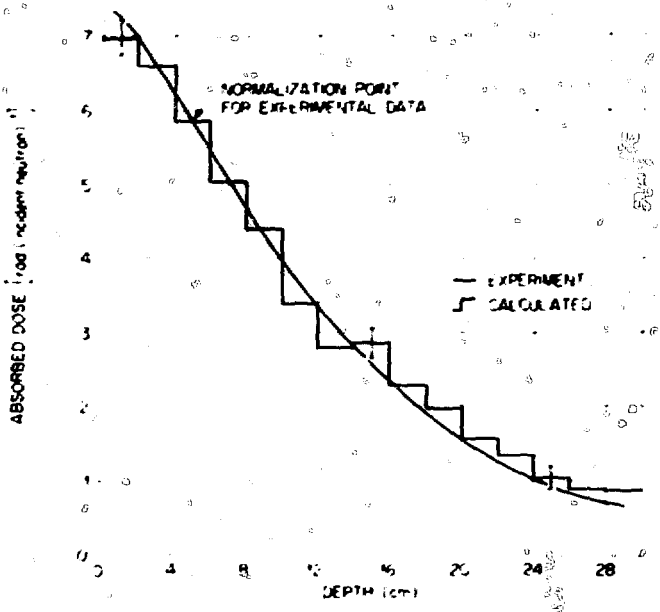

Fig. 8. Center-line absorbed dose vs depth for neutrons from 35-MeV ^2H on Be incident on a tissue-equivalent phantom. The collimator used produced a square 10-by-10-cm field at the surface of the phantom.

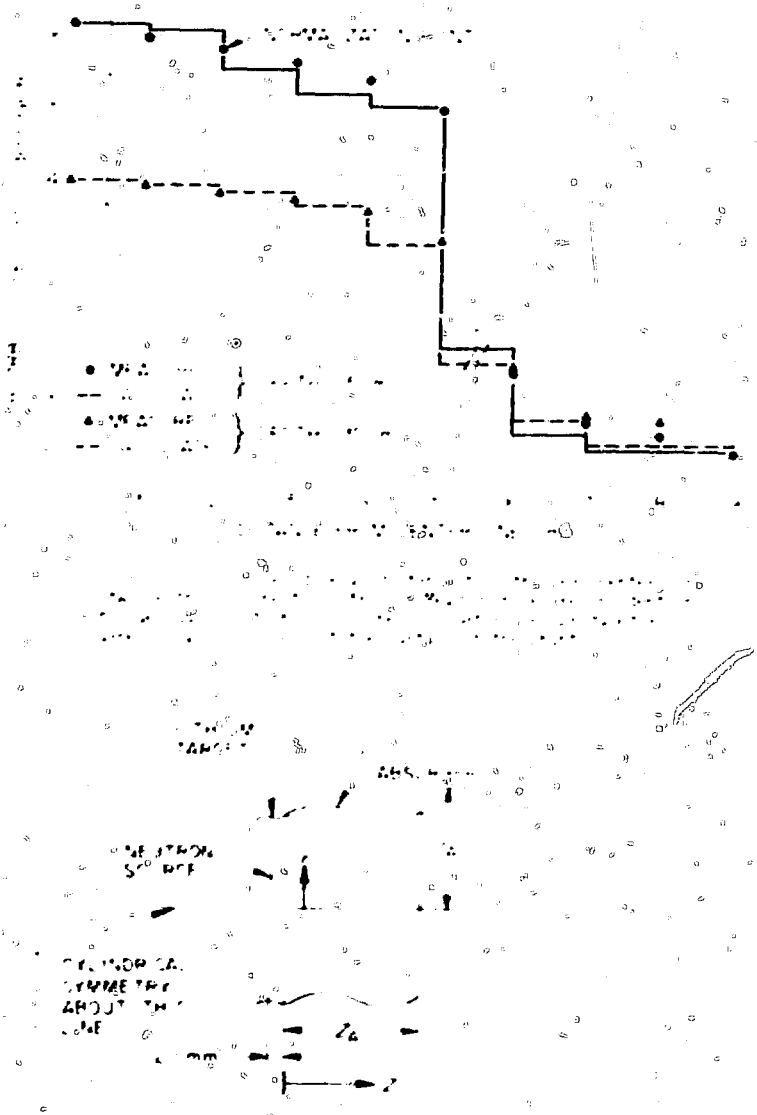

[illegible] energy [illegible] as function in the experimental [illegible] for [illegible] of 20-MeV neutrons incident on the [illegible] target.

[illegible]

[illegible]
Department of Physics, University [illegible]

The purpose of the present [illegible] of [illegible] continuous spectra observed in [illegible] light ions. It seems that the use [illegible] the spectra observed [illegible]

[illegible] in the past two decades [illegible] that there are a number [illegible] but more [illegible] theories [illegible]

[illegible] in fitting the [illegible] individual eigenstates, but only in the mean [illegible] or sections. We further note that all the interference contributions cancel out [illegible] the [illegible] the last of the same is what is obtained by assuming that [illegible] basis state to itself in a total eigenstate of [illegible] this fact is most [illegible]

[illegible] simplest complete set that can be used [illegible] that of the single-particle [illegible] process, assuming that the target [illegible] nature, a subshell closure being in [illegible] state that is excited by a [illegible] process [illegible] the state which may be detected [illegible] the next complication are those of [illegible] nature which may be [illegible] $(l_1 l_2)_1 (l_3 l_4)_1 J_{tot}$. It is easy to see that the [illegible] excited by a one-step process, while the [illegible] states [illegible] two-step process, and so forth. Because [illegible] sample nature of the eigenstates involved, the calculation of the corresponding cross

*Supported in part by the U.S.A.R.D.A.

[illegible] is not very difficult to perform.

[illegible] next consider a (p,n) reaction, assuming for simplicity [illegible] the (p,n) process takes place as the first step. A [illegible] related may simply leave the nuclear region (one-step [illegible]), or it may lose its energy further by inelastically exciting the residual nucleus, before it finally leaves the nuclear region (two-step process). The eigenstates involved in describing [illegible] may be written in exactly the same form as the [illegible] for (p,p'), except that the lpln state $(j_1^1 j_1^1)$ should now be interpreted to mean a neutron-hole-proton-particle state, rather than a lpln state of the same kind of particle.

[illegible] illustrate how the transfer reactions can be [illegible], let us take the (p,n) reaction. A bound state, i.e., one of our eigenstates, formed after a (p,n) process takes place is of a [illegible] nature, which may be denoted as [illegible] in appropriate form factor to [illegible] transition [illegible] is well known and thus a MSDR [illegible] for (p,p') or (p,n) cases. [illegible] of such calculations [illegible] can be a rather time [illegible]

A [illegible] difficulty could have been encountered, [illegible] to a lesser degree, in the (p,p') case as well. The number of possible lpln and [illegible] states can be rather large, and [illegible] calculate cross sections [illegible] can become very time [illegible]. The calculation is greatly simplified, however, if we introduce the assumption that the form factor is independent of the [illegible] of the hole and particle orbits involved in describing the eigenstate. This assumption can be justified because of the fact that we are mainly interested only in the averaged cross sections. One may choose a number of pairs j_1^1 and j_1^1, construct realistic form factors for such pairs, and then take their average.

As has been explained in some detail, the cross section is then separated into two factors: the first carrying all the information concerning the structure of the eigenstate, while the second depending only on the dynamics of the reaction. One may thus write the one-step contribution as

$$\sigma^{(1)}(E_p^{\prime}; \theta^{\prime}) = \sum_{j_1^1} d_1(E_p - E_p^{\prime}) \sigma^{(1)}(E_p^{\prime}; \theta^{\prime}), \qquad (1)$$

with

$$d_1(E_p - E_p^{\prime}) = \sum_{j_1^1 j_1^1; 1} d_{j_1^1 j_1^1; 1} . \qquad (2)$$

In Eq. (2) the sum is to be taken over lpln states within a bin $E_p^{\prime}$. The summand is purely geometrical and easy to calculate.

The two-step cross section can be written similarly as

[illegible]

[illegible]

[illegible]

[illegible] 1pih and 2pih states are complete [illegible] states, the total cross section is obtained simply [illegible] these two cross sections. If it is necessary we may add still higher order contributions as well.

In Fig. 1 we illustrate our fit to the Al(p,p') and Si(p,p') data induced by 62 MeV protons. In Fig. 2 we show a similar fit to data of the Pb(p,n) reaction induced by [illegible] MeV protons. As is seen, very good agreement has been obtained for both cases. It is also seen that the lower the energy of the outgoing particle and the larger the angle of observation, the larger is the (relative) contribution of the two-step processes.

The above fit shows that the MSDR approach is in fact a rather powerful tool in describing cross sections with continuous spectra. One may nevertheless suggest that our approach can only fit the portion of the spectra in which the outgoing particles still retain comparatively high energies. In fact in both Figs. 1 and 2, we did not even attempt to fit data with very low outgoing energies. We believe that the following can be done for these lower energy components.

In the process of obtaining the above MSDR cross sections, we have already calculated the probabilities with which a residual nucleus is left at a given excitation energy E_{ex} and with known values of the spin I and its projection M. We treat these residual states as metastable states from which secondary emission of the particles can take place.

Since the distribution of the three [illegible] quantities, [illegible] and M is known, we can apply, e.g., Hauser-Feshbach [illegible] the [illegible] stage. This process does not interfere with the previously described MSDR processes, and thus the newly obtained [illegible] cross sections can simply be added to the MSDR cross sections. [illegible] that the [illegible] cross section [illegible] interpreted to the experimental data for the [illegible] with [illegible] MeV. The differences have a shape which seems [illegible] the [illegible] cross sections.

References

1. [illegible]
2. [illegible]
3. [illegible]
4. [illegible]

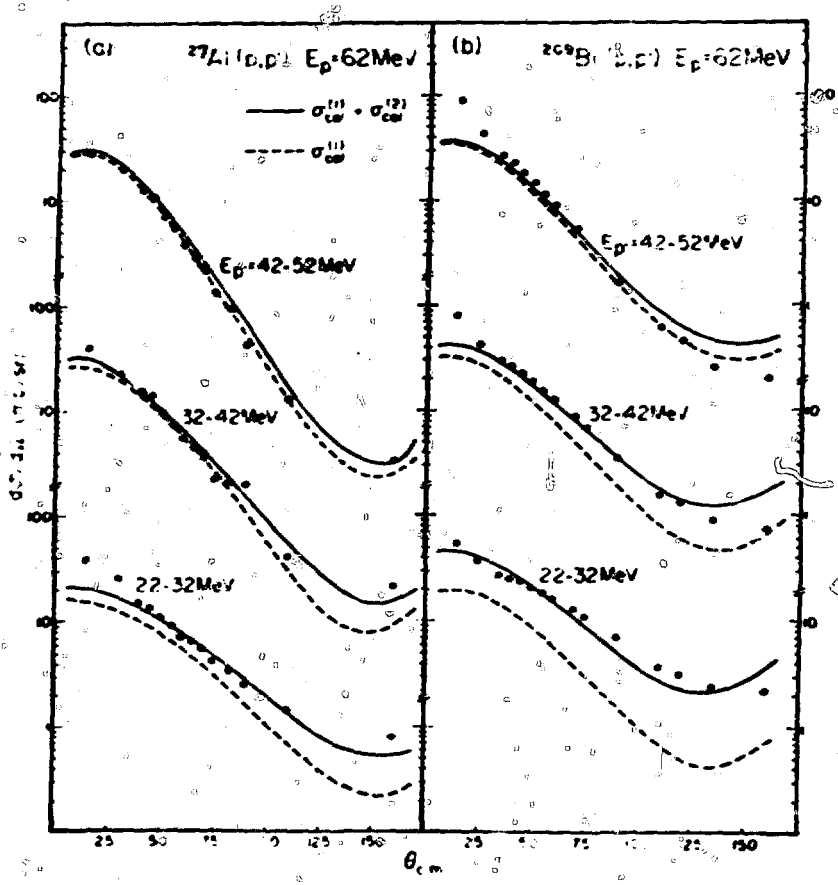

Fig. 5. Comparison of model calculations with experimental data for ^{27}Al(p,p') and ^{209}Bi(p,p') reactions.

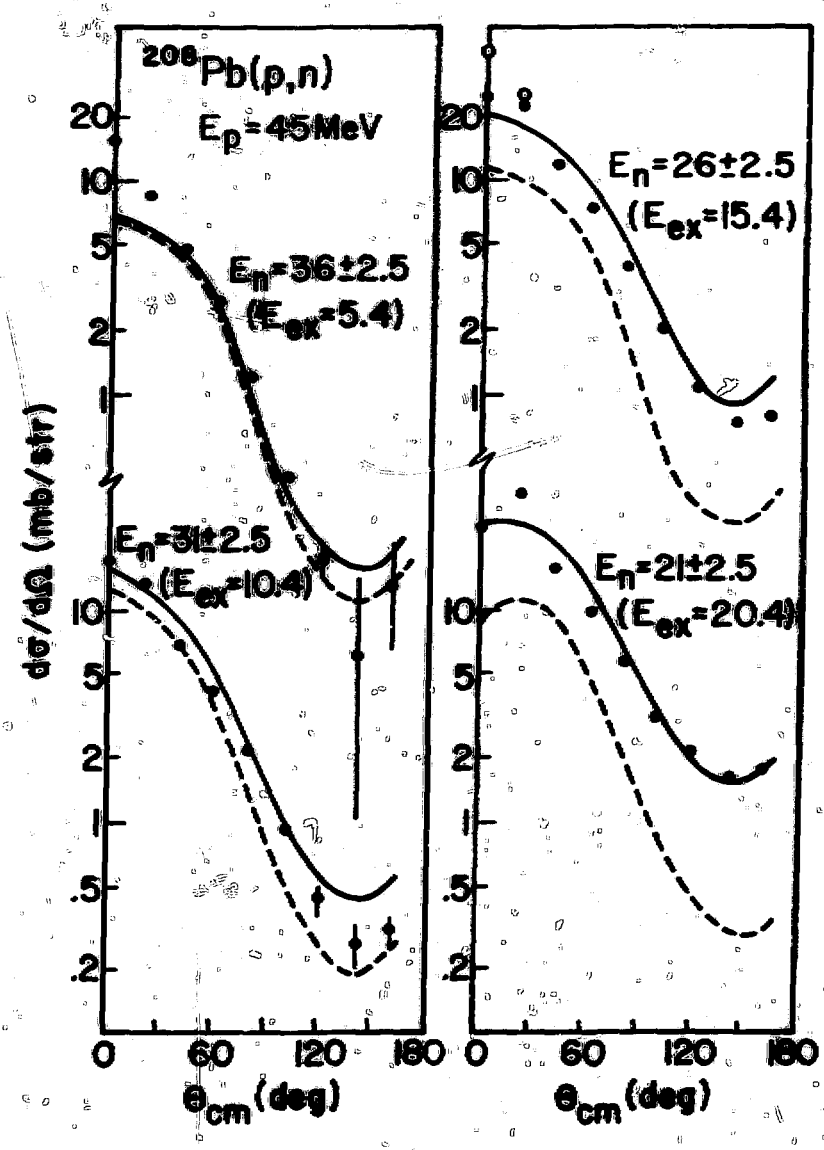

Fig. 2. Comparison of model calculations with experimental data for ^{208}Pb(p,n) reaction.

[illegible]

[illegible]

[illegible]

[illegible]

[illegible]

The calculations on [illegible] have been carried out by one of two alternative methods: the [illegible] Fourier method[1] and the Hartree-Fock-Slater method.[2] The Fourier method was first made [illegible] the implementation[4] of the program known as [illegible]. It was a general-purpose program for the [illegible], and initially operated on a very small computer, [illegible]. It was [illegible] the [illegible] approximations [illegible] could be [illegible]. [illegible] the [illegible] were [illegible] the [illegible] approximations. Angular momentum effects were ignored. The results of the calculations under [illegible] left much to be desired, and therefore, to obtain better fits with experiment, the [illegible] density parameter was adjusted. [illegible] approximate [illegible] detail, [illegible] left [illegible]. This type of adjustment had no [illegible] [illegible].

It was [illegible] recognized that in order to arrive at any [illegible] concerning the theoretical calculations, the [illegible] experimental data must be considerably better than obtainable with [illegible]. A [illegible] Hartree-Fock program, [illegible], was introduced which was demonstrated to be able to reproduce calculations from [illegible] quite satisfactorily. As an example, [illegible] in Figure 4 for the $^{40}Ar(e,e)^{40}Ar$ [illegible]. There are no adjustable parameters used in [illegible] this fit. Good, however, is [illegible] to [illegible] proper calculation of all of the required [illegible] and [illegible] proper calculation of [illegible] the [illegible] and, if it is [illegible] to determine the [illegible] than a single proper [illegible] path of particle [illegible], the entire calculation must be [illegible] for each path. The program was originally written for an IBM 7090 whose small memory made the [illegible] necessary. It has since been modified in various ways to accommodate some of these problems.[7] However, these accommodations require additional approximations that are considered undesirable; [illegible]

*This work was supported in part by the Division of Physical Research U.S. Energy Research and Development Administration, Washington, D. C.

transmission coefficients for the transitions from the initial nuclide in place of the proper transmission coefficients for the transitions from the residual nuclides. There are other approximations in GROGI that are either due to oversights or purposeful and need not be discussed here. Their effect is not precisely known but are not apparently too significant. The value of the program, though, has been amequately demonstrated, and, despite the inconvenience, it is in use in various laboratories.

Since it is a Hauser-Feshbach program, GROGI does take angular momentum into account. However, it does not give information about the angular distributions of the products. To do this simply it is necessary to convert it to a Monte-Carlo program. A recently written program,[8] DELTA, is a Monte-Carlo version of GROGI. Unfortunately, it is very slow. Another recent program,[9] ALICE, is similar to DEF, and purports to take angular momentum into account in a strange way. To wit, the rotational energy is subtracted from the excitation energy. Since Alice gives what is described as "reasonable" results, and, since it has other interesting features, such as pre-equilibrium decay, it has become quite popular. This, in our opinion, is a mistake.

In Figure 2 is an illustration of what is wrong with the method used by ALICE to account for angular momentum. If the excited nuclide has a spin that is along the yrast line, then ALICE says that the effective excitation energy is zero. Consequently the nuclide could not evaporate any particles, nor could it emit any gamma rays except to the ground state. This is patently incorrect. Analogous arguments can be illustrated for other spins. There is no physical basis for the method used in ALICE. The "reasonable" agreement that has been reported must be considered to be an artifact, and the program should be ignored. I offer this as a caveat, not as a discovery, since this fact is increasingly known, and ALICE is apparently no longer considered useful even by the original authors.

Two new programs have been introduced in the past year. The second will be discussed in detail. The first, CASCADE,[10] is a super-version of GROGI. Taking advantage of the very large modern computers, the program follows all of the evaporation paths. It obtains transmission coefficients from a library, and is, therefore, not restricted by the approximations used by GROGI2. The Lang[11] formula with Dilg-Vonach[12] parameters are used by CASCADE for level densities. However, some adjustment of the "spin-cut-off" parameter has been reported to be necessary to obtain good results. Details

are not yet [illegible]
obtainable with [illegible].

JULIAN [illegible]
Except for the [illegible]
various approximations [illegible]
of 1 MeV bins was [illegible]
Transmission coefficients [illegible]
each of the excited [illegible]
is used here and in all other [illegible]
mission coefficients is that [illegible]
dependent of the [illegible]
depend only on the [illegible]
since nothing is known [illegible]
for transitions between [illegible]

The treatment of the [illegible]
and is new and account [illegible]
Finally, in a Monte-Carlo [illegible]
of all transitions are calculated [illegible]
chosen by random [illegible]
another product [illegible]
until further transitions [illegible]
[illegible]. The result is stored, and the [illegible]
[illegible] from the original [illegible]
a large number of times [illegible]
[illegible] statistics. [illegible] the transitional [illegible]
[illegible]. BILLETT, requires an inordinate [illegible]
[illegible] of transmission coefficients, [illegible]
consuming part of the calculation. [illegible]
[illegible] the recalculation by storing the [illegible]
[illegible]. This would require very large [illegible]
relatively slow storage [illegible].

In JULIAN, the Monte-Carlo [illegible]
the following way: A 4x4 matrix is set up which [illegible]
number of cascades. Each cascade initially contains [illegible]
Z, N, E, J and I of the starting nuclide. As the [illegible]
are developed, each cascade contains the Z, N, E, [illegible]
of the stage of development of the cascade. The [illegible]
[illegible] proceeds by first considering the [illegible]
[illegible] Z, N of the highest [illegible] N. The [illegible]
transmission coefficients are calculated [illegible]
probability matrix for a given initial [illegible]
of random numbers, one for each cascade [illegible]
initial Z, N, E, J, the Z, N, E, J [illegible]
nuclides are chosen and replace the initial [illegible]
for a different J, the same transmission [illegible]
[illegible], and only a new probability matrix [illegible]
[illegible]. For a lower energy of that J, [illegible]
[illegible] coefficients may be used since equivalent [illegible]
bins are used. (For transitions to low lying experimental levels which are occasionally used, it is always necessary to recalculate the transmission [illegible]

by proceeding in this way no Z, N, E, J can reappear at a later time, and consequently no sets of transmission coefficients need ever be recalculated. The time of the calculation is roughly proportional to the number of transmission coefficients calculated, but only increases [illegible] as the fifth root of the number of cascades.

When calculating angular distributions, two additional terms are needed in the matrix: V_z, the velocity component in the beam direction, and V_y, the velocity component normal to the beam. Symmetry allows the elimination of the third velocity component. The present version of the program assumes isotropic emission of the evaporated particle; however, only small changes in the [illegible] are necessary to include other distributions. A [illegible] would be required to include the Hauser-Feshbach formula for angular distribution.

The above method permits great flexibility. The [illegible] of a compound nucleus at a specific excitation energy, separate [illegible], or it may consist of a combination of [illegible] different excitation energies, each [illegible] separate [illegible]. Note that an entire excitation function may be calculated at once. One corollary of the latter technique is that the initial matrix can consist of the distribution of products of other reactions, [illegible], pre-equilibrium decay, direct reactions, the [illegible] of high energy reaction. A second corollary is that several excitation functions may be determined simultaneously if all of the nuclides involved are in the same area of the nuclide chart. The spin distribution may be assumed, determined from the reaction forming the compound nucleus, or calculated as the equilibrium distribution of the spins from the level density.

At the present time the program only considers four modes of de-excitation, n, p, α, and γ emission. Other modes are easily added merely by the change of dimension statements and the addition of the appropriate input parameters. Fission as a mode of decay has been included in at least one user in his copy. Other features easily included are planned for emission of products that themselves undergo decay. This is simply accomplished by expanding the matrix each time such a nucleus is evaporated; [illegible] increased accordingly. Finally, the calculation of rare events can be included by adding another row to the matrix to record the probabilities of specific paths.

The input parameters to the program are under the control of the user. These include the optical model parameters, the level densities, the masses, and enhancement factors for gamma emission. Weisskopf gamma emission probabilities are included in the program.

Examples of the output of the program are [illegible] Table I and in Figure [illegible].

Table I

Julian Output—Yields of [illegible]

Target	[illegible]
Projectile	[illegible]
Bombarding Energy	[illegible]
Compound Nucleus	[illegible]
Excitation Energy	[illegible]
[illegible]	[illegible]

Z	N	A	[illegible]	[illegible]	[illegible]
14	14	[illegible]	[illegible]	[illegible]	[illegible]
14	[illegible]	[illegible]	[illegible]	[illegible]	[illegible]
[illegible]	14	27	[illegible]	[illegible]	[illegible]
[illegible]	[illegible]	26	1409	[illegible]	[illegible]
[illegible]	[illegible]	26	1612	5.90	[illegible]
[illegible]	[illegible]	24	[illegible]	[illegible]	[illegible]
[illegible]	11	[illegible]	[illegible]	[illegible]	[illegible]
[illegible]	[illegible]	[illegible]	[illegible]	[illegible]	[illegible]
[illegible]	10	29	[illegible]	[illegible]	[illegible]

[illegible] compound-nuclear [illegible] the [illegible] of the calculations will [illegible]. The results are strongly dependent on the input [illegible] [illegible] for the most part, [illegible] are poorly known. However, [illegible] program that can [illegible] and it makes it possible to [illegible] them with the [illegible] experimental [illegible]. For example, for complex nuclear reactions [illegible] the [illegible] products [illegible] strongly dependent on the [illegible] of the level densities [illegible] the [illegible] the same calculations [illegible] Gilbert-Cameron[illegible] level densities and Hillman-Grover[illegible] level densities. The results using Hillman-Grover level densities [illegible] experimental data[16] (Figure 4) far better than the results using Gilbert-Cameron level densities [illegible] the other

hand, the cross-section distribution of products is strongly dependent on the pairing parameters used in the level densities. This is most easily demonstrated in simple reactions and comparisons have been made for the reaction[17] of ^{16}O with ^{12}C; however, all of the results of the calculation are not available for illustration.

Confidence in the reliability of the method of calculation is necessary before it can be successfully used for predictions of even simple nuclear reactions. JULIAN offers the possibility of such reliability once the input parameters have been determined adequately. There is a large volume of nuclear reaction data of interest to this conference which can be used for that purpose.

REFERENCES

1. V. F. Weisskopf, Phys. Rev. 52, 295 (1937).
2. V. F. Weisskopf and D. H. Ewing, Phys. Rev. 57, 472 (1940).
3. W. Hauser and H. Feshbach, Phys. Rev. 87, 366 (1952).
4. I. Dostrovsky, Z. Fraenkel, and G. Friedlander, Phys. Rev. 116, 683 (1959).
5. J. R. Grover and J. Gilat, Phys. Rev. 157, 802 (1967).
6. M. Hillman, V. R. Wilson, and J. R. Grover, unpublished results.
7. J. Gilat, GROGI2 - A Nuclear Evaporation Computer Code, Description and User's Manual, Brookhaven National Laboratory, BNL-50246, 1970.
8. T. Mayer-Kuckuk, private communication, 1975.
9. M. Blann and F. Plasil, ALICE: A Nuclear Evaporation Code, University of Rochester, COO-3494-10, 1970.
10. F. Puhlhofer, unpublished results.
11. D. W. Lang, Nucl. Phys. 77, 545 (1966).
12. W. Dilg, W. Schantl, H. Vonach, and M. Uhl, Nucl. Phys. A2.7, 269 (1973).
13. M. Hillman and Y. Eyal, Proc. of the European Conference on Nuclear Physics with Heavy Ions, Communications, Caen, France, European Physical Society, 1976, p. 109.
14. A. Gilbert and A. G. W. Cameron, Can. J. Phys. 43, 1446 (1965).
15. M. Hillman and J. R. Grover, Phys. Rev. 185, 1303 (1969).
16. Y. Eisen, I. Tserruya, Y. Eyal, and M. Hillman, unpublished results.
17. J. J. Kolata, R. M. Freeman, F. Haas, B. Heusch, and A. Gallmann, Phys. Lett. 65B, 333 (1976).

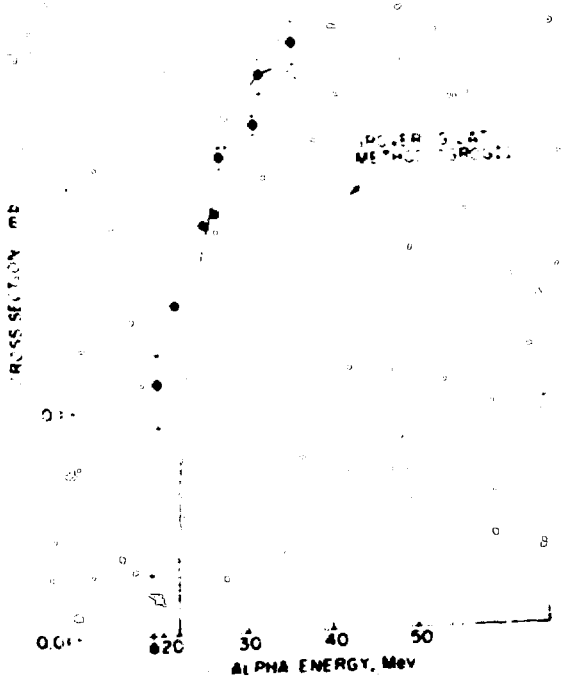
0.01
20
30
40
50
ALPHA ENERGY, Mev

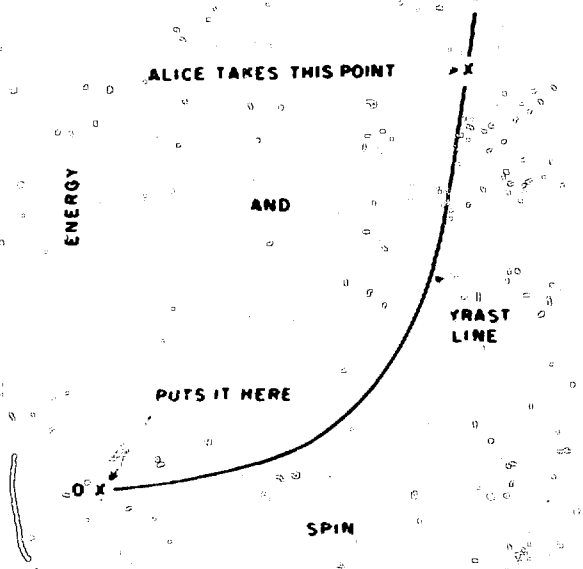

Figure 2 What's wrong with ALICE?

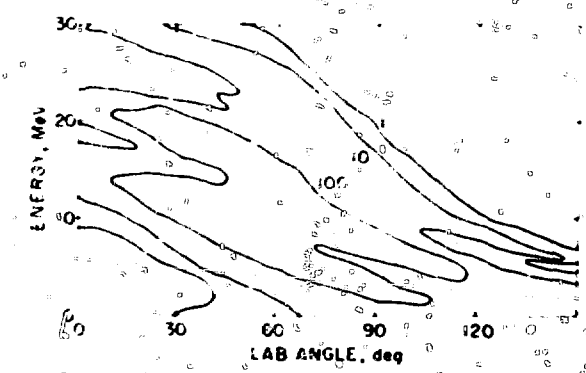

Figure 3 Calculated angular distribution of alpha particles from reaction of 32.6 MeV ^{16}O with ^{12}C.

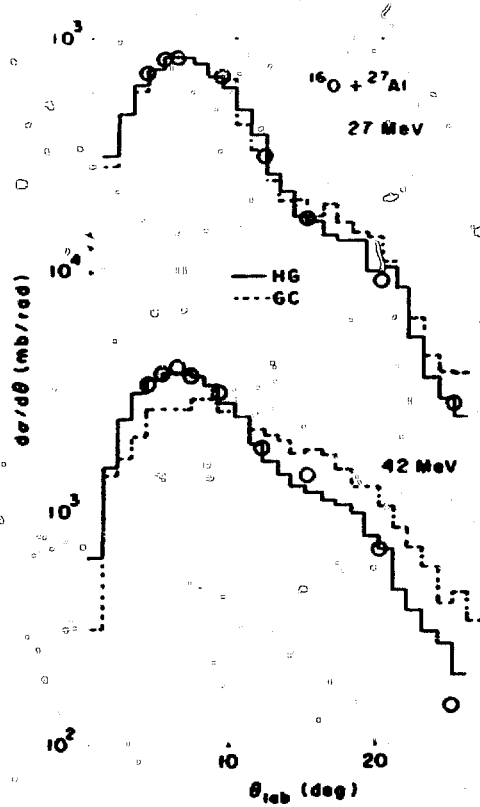

Figure 4 Angular distributions of residual nuclei from reactions of ^{16}O with ^{27}Al.

ELEMENT	QUANTITY	TYPE	REFERENCE MIN	REFERENCE MAX	DOCUMENTATION REF	DOCUMENTATION DATE	LAB	COMMENTS
LI 006	DIFF ELASTIC	EXPT-CORR	6000	1000	77DRL	2/1 977	LAS	AUCHAMPAUGH-VDG.1E3 NDG.TDE
LI 006	DIFF INELAST	EXPT-CORR	6000	1000	77DRL	2/1 977	LAS	AUCHAMPAUGH-VDG.1E3 NDG.TDE
LI 006	NON REACTION	EXPT-CORR	1000	2000	77DRL	2/1 977	LAS	AUCHAMPAUGH-VDG PRELIM.ROUGHLY CORRECT
LI 006	NON REACTION	EXPT-CORR	1000	2000	77DRL	2/1 977	LAS	AUCHAMPAUGH-VDG MIN MEAS NDG
LI 007	DIFF ELASTIC	EXPT-CORR	6000	1000	77DRL	2/1 977	LAS	AUCHAMPAUGH-VDG.1E3 NDG.TDE
LI 007	DIFF INELAST	EXPT-CORR	6000	1000	77DRL	2/1 977	LAS	AUCHAMPAUGH-VDG.1E3 NDG.TDE
LI 007	NON REACTION	EXPT-CORR	1000	2000	77DRL	2/1 977	LAS	AUCHAMPAUGH-VDG PRELIM ROUGHLY CORRECT
LI 007	NON REACTION	EXPT-CORR	1000	2000	77DRL	2/1 977	LAS	AUCHAMPAUGH-VDG MIN MEAS.NDG
BE 009	TOTAL EXPCT	EXPT-CORR	1000	1000	77DRL	2/1 977	LAS	AUCHAMPAUGH-TRNS HIGH RESOL.ALL NDG
BE 009	DIFF ELASTIC	EXPT-CORR	5000	1000	77DRL	2/1 977	LAS	AUCHAMPAUGH-VDG NEL M.1E3.CPD EXPT
BE 009	DIFF INELAST	EXPT-CORR	5000	1000	77DRL	2/1 977	LAS	AUCHAMPAUGH-VDG.NEL M UNPM.CPD EXPT
BE 009	MODEL GAMMAS	EXPT-CORR	1000		77DRL	2/1 977	LAS	AUCHAMPAUGH-VDG.LEPP CS FOR 10 GEV
BE 009	NON REACTION	EXPT-CORR	6000	2000	77DRL	2/1 977	LAS	AUCHAMPAUGH-VDG PRELIM CS GEV RP TPL
BE 009	NON REACTION	EXPT-CORR	1000	2000	77DRL	2/1 977	LAS	AUCHAMPAUGH-VDG MIN MEAS NDG
BE 009	N, EPITOM	DEVE-CORR	1000	1000	77DRL	2/1 977	LOL	WEIGHT DEV.TOTO EXPT.NDG
B 010	TOTAL EXPCT	EXPT-CORR	1000	1000	77DRL	2/1 977	LAS	AUCHAMPAUGH-TRNS HIGH RESOL.ALL NDG
B 011	TOTAL EXPCT	EXPT-CORR	1000	1000	77DRL	2/1 977	LAS	AUCHAMPAUGH-TRNS HIGH RESOL.ALL UNPM
C 012	EVALUATION	EVAL-CORR	1000	2000	77DRL	2/1 977	DRC	WALLAT.CCC OPTMDL CALC CPD EVAL
C 012	TOTAL EXPCT	EXPT-CORR	1000	1000	77DRL	2/1 977	LAS	AUCHAMPAUGH-TRNS HIGH RESOL.ALL NDG
C 012	TOTAL EXPCT	EVAL-CORR	1000	2000	77DRL	2/1 977	DRC	WALLAT.EXPT. PRE CS CALC CPD EVAL
C 012	TOTAL EXPCT	THE-CORR	2000	2000	77DRL	2/1 977	DRC	WALLAT.CCC OPTMDL PRELIM CALC CORR
C 012	ELASTIC SCAT	EVAL-CORR	6000	2000	77DRL	2/1 977	DRC	WALLAT.EXPTS PRE CS CALC CPD EVAL
C 012	DIFF ELASTIC	EVAL-CORR	6000	2000	77DRL	2/1 977	DRC	WALLAT.EXPTS PRE CS OMEV PRE EXPT
C 012	DIFF ELASTIC	EVAL-CORR	6000	2000	77DRL	2/1 977	DRC	WALLAT.EXPT. PRE CS CALC CPD EVAL
C 012	DIFF INELAST	EVAL-CORR	6000	2000	77DRL	2/1 977	DRC	WALLAT.EXPT. PRE CS CALC CPD EVAL
C 012	MODEL-TH	THE-CORR	2000	1000	77DRL	2/1 977	DRC	WALLAT.CCC OPTMDL PRELIM CALC CORR
C 012	N, GAMMA	EVAL-CORR	2000	2000	77DRL	2/1 977	DRC	WALLAT.CCC OPTMDL CALC CORR
C 012	MODEL GAMMAS	EXPT-CORR	1000		77DRL	2/1 977	LAS	AUCHAMPAUGH-VDG.LEPP CS FOR 10 GEV
C 012	N, EPITOM	EVAL-CORR	1000	2000	77DRL	2/1 977	DRC	WALLAT.EXPT. PRE EVAL N
C 012	N, CONTROLS	EVAL-CORR	1000	2000	77DRL	2/1 977	DRC	WALLAT.DOM PRE MEA T. N NDG
C 012	N,ALPHA DEAC	DEVE-CORR	1000	1000	77DRL	2/1 977	LOL	WEIGHT DEV.VERIFICAT.TRN EXPT.
C 012	N,ALPHA DEAC	EXPT-CORR	1000		77DRL	2/1 977	LAS	N.CROSS.SECT.MEA A.E. DE
C 012	N,ALPHA DEAC	EVAL-CORR	2000	2000	77DRL	2/1 977	DRC	WALLAT.DOM EXPT.CHE EXPT N NDG
C 012	N,N ELAST	EVAL-CORR	2000	2000	77DRL	2/1 977	DRC	WALLAT.EXPT. PRE EVAL N
C 012	N,TOT EXPCT	EXPT-CORR	1000	1000	77DRL	2/1 977	LAS	AUCHAMPAUGH-VDG.LEPP CS GEV RP TPL

ELEMENT	QUANTITY	TYPE	[illegible]	[illegible]	[illegible]	[illegible]	[illegible]	[illegible]	[illegible]	COMMENTS
[illegible]	[illegible]	[illegible]	[illegible]	[illegible]	[illegible]	[illegible]	[illegible]	[illegible]	[illegible]	[illegible]

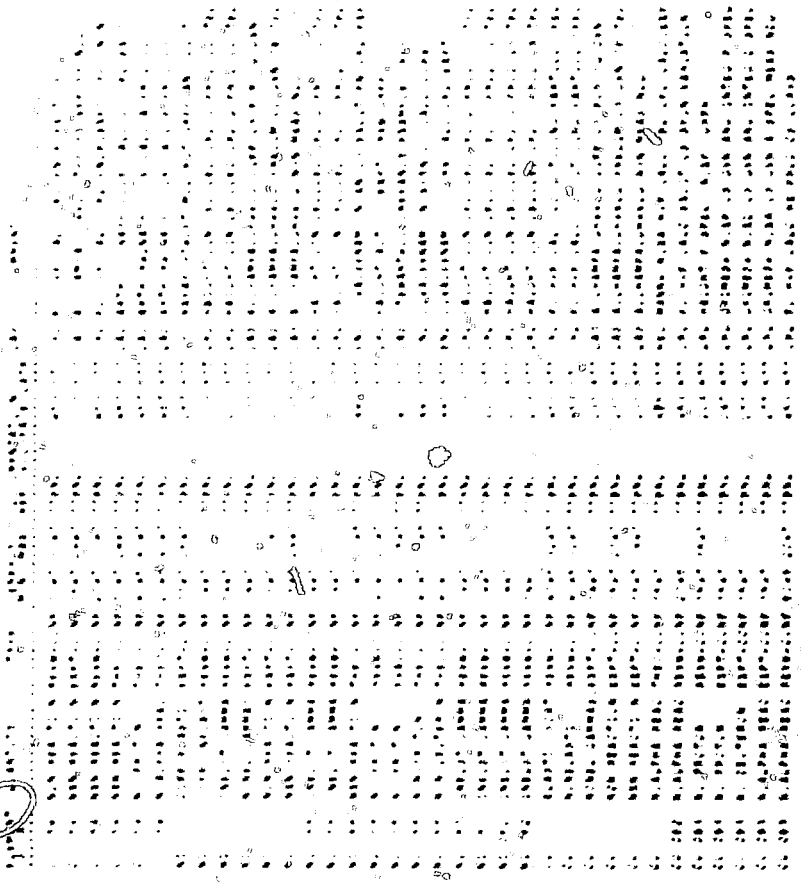

ELEMENT	QUANTITY	TYPE	[illegible]	[illegible]	[illegible]	[illegible]	LAB	COMMENTS
[illegible]								
NB 093	N. DEUTERON	EXPT	[illegible]	[illegible]	[illegible]	[illegible]	[illegible]	[illegible]
NB 093	N.ALPHA REA	EXPT	[illegible]	[illegible]	[illegible]	[illegible]	[illegible]	[illegible]
NB 093	N.ALPHA REAC	EVAL	[illegible]	[illegible]	[illegible]	[illegible]	[illegible]	[illegible]
NB 093	N.N ALPHA	EVAL	[illegible]	[illegible]	[illegible]	[illegible]	[illegible]	[illegible]
MO 092	DIFF ELASTIC	EXPT	[illegible]	[illegible]	[illegible]	[illegible]	[illegible]	[illegible]
MO 092	DIFF ELASTIC	EXPT	[illegible]	[illegible]	[illegible]	[illegible]	[illegible]	[illegible]
MO 092	DIFF INELAST	EXPT	[illegible]	[illegible]	[illegible]	[illegible]	[illegible]	[illegible]
MO 096	DIFF ELASTIC	EXPT	[illegible]	[illegible]	[illegible]	[illegible]	[illegible]	[illegible]
MO 096	DIFF ELASTIC	EXPT	[illegible]	[illegible]	[illegible]	[illegible]	[illegible]	[illegible]
MO 096	DIFF INELAST	EXPT	[illegible]	[illegible]	[illegible]	[illegible]	[illegible]	[illegible]
MO 098	DIFF ELASTIC	EXPT	[illegible]	[illegible]	[illegible]	[illegible]	[illegible]	[illegible]
MO 098	DIFF ELASTIC	EXPT	[illegible]	[illegible]	[illegible]	[illegible]	[illegible]	[illegible]
MO 098	DIFF INELAST	EXPT	[illegible]	[illegible]	[illegible]	[illegible]	[illegible]	[illegible]
MO 100	DIFF ELASTIC	EXPT	[illegible]	[illegible]	[illegible]	[illegible]	[illegible]	[illegible]
MO 100	DIFF ELASTIC	EXPT	[illegible]	[illegible]	[illegible]	[illegible]	[illegible]	[illegible]
MO 100	DIFF INELAST	EXPT	[illegible]	[illegible]	[illegible]	[illegible]	[illegible]	[illegible]
CD 110	DIFF INELAST	REVW	[illegible]	[illegible]	[illegible]	[illegible]	[illegible]	[illegible]
CD 110	INELST GAMMA	REVW	[illegible]	[illegible]	[illegible]	[illegible]	[illegible]	[illegible]
CD 112	DIFF INELAST	REVW	[illegible]	[illegible]	[illegible]	[illegible]	[illegible]	[illegible]
CD 112	INELST GAMMA	REVW	[illegible]	[illegible]	[illegible]	[illegible]	[illegible]	[illegible]
CD 114	DIFF INELAST	REVW	[illegible]	[illegible]	[illegible]	[illegible]	[illegible]	[illegible]
CD 114	INELST GAMMA	REVW	[illegible]	[illegible]	[illegible]	[illegible]	[illegible]	[illegible]
CD 116	DIFF INELAST	REVW	[illegible]	[illegible]	[illegible]	[illegible]	[illegible]	[illegible]
CD 116	INELST GAMMA	REVW	[illegible]	[illegible]	[illegible]	[illegible]	[illegible]	[illegible]
SN	DIFF ELASTIC	EXPT	[illegible]	[illegible]	[illegible]	[illegible]	[illegible]	[illegible]
SN 118	DIFF ELASTIC	EXPT	[illegible]	[illegible]	[illegible]	[illegible]	[illegible]	[illegible]
SN 118	DIFF INELAST	EXPT	[illegible]	[illegible]	[illegible]	[illegible]	[illegible]	[illegible]
SN 120	DIFF ELASTIC	EXPT	[illegible]	[illegible]	[illegible]	[illegible]	[illegible]	[illegible]
SN 120	DIFF INELAST	EXPT	[illegible]	[illegible]	[illegible]	[illegible]	[illegible]	[illegible]
SN 122	DIFF ELASTIC	EXPT	[illegible]	[illegible]	[illegible]	[illegible]	[illegible]	[illegible]
SN 122	DIFF INELAST	EXPT	[illegible]	[illegible]	[illegible]	[illegible]	[illegible]	[illegible]
SN 124	DIFF ELASTIC	EXPT	[illegible]	[illegible]	[illegible]	[illegible]	[illegible]	[illegible]
SN 124	DIFF INELAST	EXPT	[illegible]	[illegible]	[illegible]	[illegible]	[illegible]	[illegible]
HF 181	DIFF ELASTIC	EXPT	[illegible]	[illegible]	[illegible]	[illegible]	[illegible]	[illegible]
TA 181	DIFF ELASTIC	EXPT	[illegible]	[illegible]	[illegible]	[illegible]	[illegible]	[illegible]